ON THE COMBUSTION OF BITUMINOUS COAL CHARS

Thesis by

Ranajit Sahu

In Partial Fulfillment of the Requirements

for the Degree of

Doctor of Philosophy

Department of Mechanical Engineering

California Institute of Technology

Pasadena, California

1988

Submitted April 22, 1988

To Ma and Baba

ACKNOWLEDGEMENTS

It is not possible to thank all the people who have helped me over the last five years. I owe a debt of gratitude to everyone who has made my stay at Caltech so rewarding.

It is customary to first thank one's advisor. I have the double pleasure of thanking both Professor Richard Flagan and Professor George Gavalas — without their help, patience, and understanding the results would have been very different. I owe special thanks to Professor Flagan for having faith in my ability to handle a predominantly experimental project despite my meagre background in the area. His encouragement in the face of adversity helped me more than I can ever thank him for. Dr. Gavalas always managed to rescue me from whatever conceptual 'blind-pore' I kept wandered into. His insight into the subject matter and his willingness to share it with his students are both inspirational. I would also like to thank Professors Rolf Sabersky, Ed Zukoski, Chris Brennen, Glen Cass, Anatol Roshko, and Frank Marble for their encouragement throughout my entire stay at Caltech.

My roommates over the last half decade (yes! that's how it long it has been) deserve special mention. To Randy, Pratim, Hidenori, Steve, Apoorva, Youngil, Mark, Brian, and Duncan — a heartfelt thank you. Raghu and Sandip are tolerating my bad habits even at the present time. Their camaraderie and support has helped make many a hopeless situation seem better.

My friends at Keck labs have made life here more rewarding, exciting, and, yes, almost fun at times. They little know the profound impact they have had on my ability to function as a productive individual. I would be lucky to have such a

group of coworkers again. In no particular order, I owe more than I can ever repay to JinJwang Wu, Brian Wong, Yiannis Levendis, Hung Nguyen, Sonya Kriedenweiss-Dandy, Carol Jones-Adkins, Jennifer Stern, Gidi Sageev, Mark Cohen, and many others. Perhaps more than anyone else, Scott Northrop and I have shared in the joys and sorrows of doing research together on an almost daily basis for the past two years. I could not have asked for a better colleague, co-worker, or friend.

I would like to thank Elton, Joe, and Rich in the shop downstairs for their help in getting my experiments going. Jean and Rayma made going to the library an enjoyable experience, without exception. And, there was no problem for which Joan, Sandy, or Elaine did not have a solution. Thank you all.

To Ma, Baba, Baby and Budhaba in India, to Minu and Lon in Texas and to Tinku in Maine, I express my deepest thanks. Without your love, understanding, and patience, none of this would have happened nor would have meant much.

Finally, last but not the least, I wish to thank Cathy and little Jim for all their love and support during the last year.

ABSTRACT

The combustion of chars from pulverized bituminous coals was experimentally and theoretically investigated. The chars were made by pyrolyzing size-graded PSOC 1451 coal particles in nitrogen at temperatures of 1000-1600K. Sized char particles were then used for further experiments. Low temperature reactivities of such cenospheric chars were measured at 800K on a thermogravimetric analyzer. The effects of initial coal size, char size, pyrolysis temperature, and oxygen concentration were investigated. Single particle combustion experiments were done in both air and 50% oxygen ambients at wall temperatures of 1000-1500K in a drop tube laminar flow furnace. Particle temperatures were measured during the entire course of combustion. From the complete temperature-time histories of such burning particles, the apparent activation energy and pre-exponential factors were inferred, using numerical models and statistical modelling techniques. Questions of particle-particle variability were addressed. The ignition transients of single burning particles were studied and a model that predicted delay times observed experimentally was developed. Char samples were also partially oxidized at temperatures in the range 1200-1500K (particle temperatures) and physically characterized. Methods of characterization included optical and electron microscopy, gas adsorption methods for specific surface area and pore volume distributions, and mercury porosimetry for pore volume distribution measurements. The results of these characterizations were compared with those done on chars oxidized at 500°C.

The combustion of single char particles was numerically modelled. A continuum model for asymptotic shrinking-core combustion was developed using apparent

reaction rates and temperature-dependent properties. Simplified assumptions were made regarding the gas-phase combustion. Parametric sensitivity of this model yielded significant insight into the combustion process. A more general continuum model was then developed. This model treated the internal pore structure more realistically, as inferred from experiments. The steady state diffusion equation was solved inside the particle to determine its theoretical temperature-time history. Good agreement with experiments was found. The model was extended to include the effects of some nonlinear kinetic reaction rate expressions. A discrete model for a cenospheric particle was also developed. This model consists of spherical voids randomly placed in a spherical particle. It simulates the combustion by taking into account the connectivity of the internal pore structure. This connectivity influences the access of reactant to the interior of the particle and, therefore, the extent of internal reaction. The changes in the internal connectivity led to a percolation type behavior in most particles.

TABLE OF CONTENTS

LIST OF FIGURES

Chapter 3

Chapter 4

Chapter 5

Chapter 6

Chapter 7

Chapter 8

Appendix II

Appendix III

Appendix IV

Appendix V

Appendix VII

Appendix VIII

Appendix XI

Appendix XII

LIST OF TABLES

Chapter 2

Chapter 3

Chapter 4

Chapter 5

Chapter 6

Chapter 8

Appendix III

Appendix IV

Appendix V

Appendix X

Appendix XI

Appendix XII

Chapter 1

INTRODUCTION

This dissertation deals with some aspects of the combustion of chars made from some U.S. bituminous coals. Bituminous coals are characterized by fixed carbon contents between 69 and 86%. Of course there are wide variations in the contents of volatile matter, moisture and mineral matter between various bituminous coals. While the primary emphasis was on one coal, PSOC 1451, chars from other coals have been used for comparision purposes. The most common method of coal utilization is in the form of pulverized coal for power generation. The particle size used is in the range 40-200μm. When coal particles are heated, moisture and the volatiles are successively expelled leaving behind a carbonaceous char. The volatiles burn in the gas phase on time scales of the order of less than a millisecond while the char burns out in tens of milliseconds. Thus, char combustion is the controlling factor in the overall process and it determines combustor size.

While gas phase combustion reactions involving the volatiles have been extensively studied, the peculiar problems of char combustion are now receiving greater attention. The latter is a much more difficult problem due to the following causes: heterogeneity of the system, internal morphology characterized by the presence of pores with diameters ranging from few angstroms to few microns, diffusion and reaction in such a media, nonavailability of reliable kinetic data on intrinsic chemical reactions of the carbon at high temperatures, and the presence of ash and mineral matter in the solid which have physical and chemical ramifications on the combustion process. All these problems are for single particle combustion. In a real system, the problems of particle-particle interaction, fluid-particle interaction and

mass transfer have also to be accounted for.

Appendix I lists some of the physical and chemical properties of PSOC 1451 including its proximate and ultimate analyses, heating values, elemental composition, and the composition of its ash. While there are many excellent reviews of coal science in the literature, not all of them deal with bituminous char combustion in sufficient detail. Chapter 2 summarizes the important findings from the recent literature in the area of bituminous char combustion. Apart from char reactivities at low and high temperatures, the chapter also discusses models used to represent the internal structure of such chars and the dispersion of mineral matter and ash in single particles. Finally, single particle combustion models are discussed. No attempt has been made to discuss the combustion behaviour of groups consisting of many particles.

Chapter 3 describes the results of oxidation studies on sized char particles at temperatures around 800K. The experiments were done on a thermogravimetric analyzer. In addition to PSOC 1451, chars from two other bituminous coals, PSOC 176 and PSOC 282 were also used in this study. At these low temperatures, it was shown that the effects of diffusion are minimal and that the observed reactivities represent the true rates. Various experiments were done to test the effect of coal type, char pyrolysis temperature, char particle size, parent coal particle size, oxygen concentration, and other variables on reaction rates. Physical characterization of the chars was done using gas adsorption, capillary condensation, and mercury porosimetry. Surface area values were determined for some samples at intermediate conversions. Heating values were determined as a function of carbon conversion

for PSOC 1451 chars. The intrinsic kinetic rates were then determined from the apparent reactivities and the measured surface area values. It was shown that, after accounting for the effects of ash, the intrinsic rate was fairly constant over a wide range of carbon conversion. Appendix X describes in detail the experimental conditions used.

Single particle combustion experiments done in the laminar flow drop tube reactor are described in Chapter 4. These experiments were done at wall temperatures in the range 1000K-1500K. Some experiments were done in air and others in an ambient of 50% oxygen. Complete temperature-time burn histories for each particle were recorded. This was repeated for many particles in a given sample. It was observed that particles from the same sample often produced temperature-time signatures that were quite different. This was primarily due to the different initial particle sizes and shapes. While there are other particle-particle differences, the initial size and shape variations are undoubtedly major causes of later combustion variability. Based on this hypothesis, a statistical model was developed and used to derive the apparent kinetic rates of combustion at these high temperatures. Appendix VIII gives the listings of the programs used in the data acquisition, inversion and modelling. The temperature-time traces for each of the various runs is given in Appendix XII.

Physical characterization experiments of char samples that were partially oxidized at high temperatures in air are described in Chapter 5. The various methods of characterization include optical and electron microscopy, gas adsorption to determine BET specific surface areas, capillary condensation to determine pore volume

distributions of the micro and transition pores, and mercury porosimetry to find the pore volumes of the macro and transition pores. The physical changes occurring in the particles as conversion increases are discussed in great detail in the chapter. The final section compares the changes at high temperatures to those occurring when the conversion is carried out at low temperatures. The temperature of the particles as they burned was also measured at different conversions. Appendix II describes in some detail the design and construction of a two color optical pyrometer employed for particle temperature measurement. The construction of the high temperature reactor is described in Appendix IV. Computer programs used for data acquisition and inversion for the gas adsorption experiments are given in Appendix V. Appendix VI gives similar listings for the programs used for mercury porosimetry data analysis. Finally, programs used to acquire data from the pyrometer and convert the data to particle temperature measurements are given in Appendix VII.

The temperature-time traces from single particle combustion experiments led naturally to questions regarding the ignition transients observed at the earlier stages of combustion. It was observed that while the particle temperature was constant, the light intensity signal from the particles continued to increase. This was attributed to the growth of hot spots on the particle surface. A model that describes the growth of such a spot was developed and its predictions were compared to the experimentally observed delay times. Good agreement was found. This is described in Chapter 6.

Continuum models depicting the combustion of single particles are described in Chapter 7. The simplest model assumes that all the reaction takes place on

the external surface of the particle with the apparent kinetic rates derived earlier. This diffusion limited regime is typical of combustion of large particles at high temperatures and at high oxygen concentrations. While the model does not treat the details of the internal morphology, it does account for the presence of ash in the particle. The gas phase outside the particle is modelled in a simple manner assuming it to be quasi-steady with respect to the solid combustion. The next level of complexity involves accounting for the presence of pores inside the particle. Starting with initially monodisperse spherical pores, a general model that accounts for internal diffusion and reaction is formulated. The internal porosity and specific surface area are allowed to change. The chemical reactions are described by their intrinsic rates. The reaction rate is assumed to be linear with respect to local oxygen concentration. This model is then extended to allow a more realistic description of the internal morphology consisting of pores of three sizes corresponding to micro, transition and macro pores, observed experimentally. The parametric sensitivities of all the models are discussed. The last section deals with the inclusion of nonlinear kinetic expressions in the reaction rates. Two forms corresponding to Langmuir-Hinschelwood and Power law functions of the local oxygen concentration are considered. Appendix IX lists the computer codes of the different models.

While assuming that the interior of a char particle is homogenous and capable of continuum description is a convenience, it is often an over-simplification. There are cases when the internal morphology cannot be described as a continuum due to the presence of voids whose sizes are comparable to the particle radii. A discrete simulation model was developed to describe, in general terms, the combustion of

cenospheric chars like those of PSOC 1451. While most simulation models of this nature are based on lattice geometries, the present model described in Chapter 8, is closer to describing the physical reality. Spherical pores were randomly placed inside a spherical particle leading to void overlap. This model takes into account the connectivity of the pores inside the particle and the connectivity of pores to the outside. The access of oxygen to the interior is constrained by this connectivity. Particle void fraction and conversion are tracked as they change with burn time. Interesting percolation behaviour of the void structure was observed. Examples of the percolation traces are shown in Appendix XI.

Specific surface areas and pore volume distributions obtained by gas adsorption techniques are widely used to characterize porous particles in many different areas including coals and chars. However, there are many questions regarding the applicability of techniques, models, and inversion paradigms commonly used. The suitability of such techniques is discussed in Appendix III. Four solids having different internal morphologies were chosen. Also, three different gases were chosen as the adsorptives. The applicability of the various adsorptive-adsorbate combinations is discussed. The next question involves inversion routines to generate pore volume distributions from the raw data. The standard inversion methods are described and critically analyzed. Finally, methods used specially for microporous solids are studied.

Chapter 9 briefly summarizes the major conclusions of the thesis.

Chapter 2

INTRODUCTION TO BITUMINOUS COAL CHAR COMBUSTION

2.1 Introduction

Coal has always been a major source of energy for electricity generation. Since the 1960's, however, it began losing ground as the primary fuel for power generation. Oil and natural gas prices were cheap and nuclear power was poised for rapid growth. In the 1970's the situation suddenly changed. Oil and gas prices had sky rocketed and safety concerns regarding the nuclear power industry were thwarting its projected growth. All this, coupled with the realization that oil and gas supplies are rapidly dwindling, has created renewed interest in utilization of the vast coal reserves in the world. Of course, coal, like oil, is also a non-renewable source of energy. Eventually, nuclear, solar or some other renewable energy source will be required. But, in the short term, coal and energy conservation offer the best alternatives for meeting our energy demands.

At the very outset it should be recognized that 'coal' is a generic term and the solids it refers to are often more dissimilar than alike. This is due to the conditions under which coal was formed. At various times in geological history, due to land subsidence and water inundation, plant debris was gradually covered by silts which shielded it from further degradation. As this debris was buried under increasingly thick inorganic sediments, it was progressively compacted by overburden pressures and chemically altered by heat. Whenever this happened, coal was formed. The fact that coal is so widely distributed shows that it did not require a particular types of debris. It formed from whatever plant life happened to flourish at the time. But the variety of this vegetation and the diverse conditions under which it accumulated and decayed had a profound effect on the kinds of coal that developed

from it.

Numerous attempts have been made to organize various types of coal into comprehensive classification schemes primarily to assess their suitability for different applications. *Rank*, as applied to coal, carries the same meaning as extent of maturation and is therefore a qualitative measure of its carbon content. Bituminous coals and anthracites are classified as being high rank while lignites and subbituminous coals are considered to be low rank. However, rank should not be confused with *grade*, which refers to quality. The widely accepted ASTM classification by rank is shown in Table 2.1. For lower rank coals, heating value rather than fixed carbon content is used to classify the coals.

For practical purposes, the chemical composition of coal is always defined in terms of its proximate analysis which determines its moisture, volatile matter, ash, and fixed carbon contents. Upon heating, moisture and the volatiles are lost leaving a solid *char* which contains the carbon and mineral matter. At higher temperatures the char burns. Thus coal combustion involves the combustion of the volatiles in the gas phase and the combustion of the char. For pulverized combustion, in which coal is generally ground to sizes below 200μm, char combustion controls the overall burn time and, therefore, the combustor size.

The scope of this chapter will be limited to combustion and modelling of single bituminous coal or char particles. Reactivity measurements at high and low temperatures and various approaches used to model the internal morphology of char particles will be discussed. Attempts to predict the effects of ash on the combustion of single particles are receiving greater attention now but as yet there is no

consensus on the best approach. Some experimental work on the effects of ash and mineral matter will be reviewed. Finally, some complete models of single particle combustion will be discussed.

Excellent reviews in the general area of pulverized coal combustion are available in the literature. Field and co-workers (1967) described all aspects of combustion of pulverized coal including fluid mechanical, thermal, and chemical kinetic effects. Although most of the material is derived from their own research at the BCURA, they give a succint review of various topics prior to the mid 1960's. A few years later, Mulcahy and Smith (1969) published a review dealing exclusively with chemical kinetic aspects of pulverized fuel combustion. Laurendeau (1978) describes in great detail much of the progress made in the 1970's in the area of heterogenous kinetics of coal char combustion. His review gives a complete discussion of the mechanisms and rates of the relevant gas-solid reactions. Mass transfer and diffusion are also discussed. Smith (1982) summarizes the field of char kinetics including a comprehensive attempt to gather the reactivity data for all types of carbons over a wide range of temperatures. He proposed an intrinsic chemical rate expression suitable for all chars. Essenhigh (1981) gives an extensive review of most aspects of coal combustion, with a scope much larger than any of those previously mentioned. Recently, Smoot and Smith (1985) have also published a valuable addition to the field of coal combustion. While most of the references mentioned above deal with the solid phase in greater detail than the gas phase combustion, Libby and Blake (1979) examine the latter in greater detail.

2.2 Low Temperature Kinetic Studies

Although temperatures in the practical combustion systems of interest here are generally high, reactivity studies at lower temperatures can give valuable insight into the various physio-chemical processes occuring during combustion. The influence of diffusion resistance in the gas phase can be minimized by suitable choice of temperature, oxygen partial pressure, and particle size making possible direct observations of chemical effects. In many cases pore diffusion does not limit the reaction rate, at least for the larger feeder pores. Therefore, it is possible, in principle, to determine the intrinsic reactivity of the carbonaceous matter from such experiments. Care must be taken to properly account for the presence of ash or mineral matter in the coal or char since, at lower temperatures, the influence of ash on the chemical kinetic effects can be quite important. The growth and development of the internal morphology (pore growth) is also important at lower temperatures.

The Thermogravimetric Analyzer (TGA) is most commonly used for low temperature reactivity studies. The TGA is convenient because it directly gives the rate of mass loss of a given sample under a specified programmable temperature loading. From the rate of mass loss data the apparent reactivities are easily calculated. Finally, knowing the surface area of the sample and the diffusion limitations of the particular experiment, it is possible to estimate the intrinsic chemical reactivity. Table 2.2 summarizes some of the work in the area of low temperature reactivity measurement. Low temperature reactivity measurements in the present study are discussed in Chapter 3.

In a major study Jenkins *et al.* (1973) investigated the role of coal rank, pyrol-

ysis temperature, and mineral matter on the reactivity of chars from 21 US coals. For coals pyrolyzed in N_2 at 600-1000°C they found that while reactivity increases with the decreasing coal rank, possibly due to the catalytic effects of mineral matter, it decreases with increasing pyrolysis temperature. They also correlated reactivity with the calcium and magnesium contents in the char. Since reactivity was not well correlated with other known catalysts like iron, they speculated that the form and distribution of mineral matter has an important influence on the reactivity. The role of the internal structure of the chars in determining their reactivities was shown by Dutta and Wen (1977). They found that in the chemical kinetic regime, the reactivity depended more on the degree of gasification and the pore characteristics of the char than it did on the parent coal. In another important study Mahajan *et al.* (1978) supported the earlier findings of Jenkins *et al.*. While the latter had used the maximum weight loss as the reactivity parameter in their work, Mahajan *et al.* suggested that the time to reach a particular fractional burnoff, say 50%, be used as a parameter to correlate reactivity data of different chars. This unification of reactivity data was further proof that the changes in the pore structure with burnoff greatly influences reactivity. More recently, Morgan *et al.* (1987) have shown that reactivity depends on the maceral content of the chars. Vitrinites are more reactive than inertinites. An important conclusion of their work was that there is maceral segregation in the different size fractions of char. Therefore, char size, in addition to influencing diffusion conditions, also determines intrinsic chemical reactivity.

2.3 High Temperature Kinetic Studies

At higher temperatures, the combustion of particles in the pulverized size range is

usually strongly diffusion limited. There are two major diffusion limitations. The first is the diffusion across the particle boundary layer. The second is pore diffusion. Since the chemical rate is a sensitive function of the particle temperature, the combustion rate is governed by the amount of oxidant that reaches the char surface and then penetrates into the interior of the particle. In most cases, the reaction occurs only in the larger pores and most of the internal area in the smaller pores is not utilized. The particle density and size are both reduced. Since diffusion is such an important aspect of high temperature combustion, it must be treated in any determination of the intrinsic chemical rate parameters. Smith and Tyler (1974) have outlined a first order procedure for determining the intrinsic reactivities.

A number of experimental techniques have been used to measure reactivity at high temperatures. The thermogravimetric analyzer can be used up to 1300K. Most workers have used the laminar flow drop tube reactor. The flow is generally kept laminar to minimize complications in the data interpretation due to fluid mechanics. The heat source can be a flame, plasma, or some type of electric heating. The limitations of using a flame (vitiated combustion) as the heat source are obvious. The temperature depends on the fuel/oxidant mixture ratios and flame stability considerations. The chemistry in the gas phase around the particle is difficult to characterize due to the presence of various radicals and other species. Plasma heating also introduces reactive species. Electric heating allows greater control of the temperature and gas composition. Shock tubes have been used in some studies to determine high pressure reactivities.

The reactivity can be measured either gravimetrically, involving a direct mea-

sure of the carbon mass loss, or inferred from the gas phase composition by monitoring the carbon oxides. In most of the earlier measurements, the particle temperature was calculated from the carbon mass loss data by using an energy balance and making appropriate assumptions regarding the nature of the heterogenous reaction at the particle surface. More recent studies have employed nonintrusive optical techniques for independent determination of the particle temperature. Table 2.3 summarizes the high temperature reactivity studies of the last two decades. The present work in this area is presented in Chapters 4, 5, and 6.

Direct comparison of the reaction rates or the activation energies from different studies is not possible since the nature of the chars is quite different. While it is certainly true that the influence of char type on the reactivity at higher temperatures is much less than at lower temperatures, Smith (1982) found that the reactivities of different chars at a given temperature varied by as much as four orders of magnitude. His attempt to unify the known reactivities of various carbons over a wide range of temperatures met with limited success. This may be due to the intrinsically different nature of the carbons and their reactivity with oxygen, or due to the different pore structures of the carbons, or both. The chemical influences of ash were not investigated. The measurement of reaction order is also open to question. Mechanisms that have been theoretically proposed for the carbon-oxygen reaction (Nagle and Strickland-Constable, 1962; Essenhigh, 1981) have not been entirely validated (Laurendeau, 1978; Tseng and Edgar, 1985), probably due to incomplete control over experimental conditions. As experimental techniques improve, better understanding will doubtless emerge. The recent simultaneous op-

tical measurements of particle size, velocity, and temperature reported by Mitchell (1987) represent a significant step in this direction.

2.4 Description of Internal Morphology

The description of the internal structure of a char particle is critical to any model that attempts to describe its combustion behaviour. The reaction rate depends on the available internal surface area, which, in turn, depends on the diffusion of reactant into the solid structure. The estimation of the overall porosity and the particle density are also determined by the particular pore structure model. It is quite clear from experiments that pore sizes in pulverized coal or char combustion range from tens of microns to few Angstroms. They are also irregular in shape. However, for reasons of mathematical tractability, simple geometrical pore shapes like cylinders, spheres, and slits are often assumed. A comprehensive pore model should be able to describe the overall features of the pore distribution, *i.e.* porosity, average pore radius, and pore surface area, as well as the evolution of the pore structure with reaction. Mechanisms of pore formation, growth, and coalescence must be described. Of course, the reaction kinetics are closely coupled with the problem of pore diffusion since the reaction rate is dependent on the local concentration of oxidant at each location inside the particle. Few general models are available that describe these features satisfactorily. Some of the important models will be briefly described below.

Petersen (1957) proposed a simple model of reaction and diffusion in a single cylindrical pore and then extended it to a network of similar pores with random intersections. However, his model predicted values of effective diffusivity that were

an order of magnitude lower than the experimentally observed values. Johnson and Stewart (1965) and later Feng and Stewart (1973) calculated diffusivities using a capillary model containing a size distribution of randomly oriented pores. Cross linking of the pores was assumed. Their models contain adjustable parameters that must be evaluated from experiments. The 'calibrated' models predict reasonably accurate values of diffusivity. Szekely and Evans (1970) describe two simple models of porous solids. Their pore model consists of parallel, regularly spaced cylindrical pores of uniform size. While this may describe some situations in heterogenous catalysis, it is not a suitable model for chars. Their grain model consists of spherical solid particles of uniform radii arranged in a lattice with fixed center separation. Using a population balance method, Hashimoto and Silveston (1973) proposed the first sophisticated model of a porous solid. They also review the relevant catalysis literature regarding homogenous and shrinking core models. Their model includes the effects of pore growth, creation of new pores, and pore coalescence. Surface area, porosity, and mean pore radius were predicted as a function of the extent of reaction. By adjusting the model parameters, they were able to obtain good agreement with experiments. Simons (1982) proposed a pore tree model for chars, postulating that feeder pores that were connected to the external surface branched into smaller and smaller pores as the radius increased. This branching sequence creates a pore network that resembles a tree-like structure. This model cannot predict the change of surface area and other pore structure parameters at the local level that is essential for a predictive model. Gavalas (1980) and Bhatia and Perlmutter (1980) independently proposed similar random pore models for solids

with cylindrical pores. The model by Gavalas consists of infinitely long cylinders whose radii are drawn from a certain size distribution. The axes of the cylinders are randomly oriented creating pore intersections in a natural manner. Bhatia and Perlmutter consider the random overlap of a set of cylindrical surfaces of different radii. Although their formulation is different, their results closely resemble those obtained by Gavalas.

2.5 Mineral Matter and Ash

In addition to the engineering considerations of deposit formation, fouling, and environmental pollution (Raask, 1985), the presence of mineral matter and its transformation to ash strongly influences the combustion of coal or char.

The application of such methods as low temperature ashing and x-ray diffraction has increased our understanding of ash. Of the hundred or so different minerals that can occur in coal, about 15 are abundant enough to have major influence (Harvey and Ruch, 1984). Different investigations have shown that the presence of CaO in the ash tends to enhance reactivity (Hippo and Walker, 1975). Hippo and Walker (1975) also showed that MgO enhances reactivity when present in concentrations less than 1%. Surprisingly, they found that iron, sodium or potassium do not correlate well with reactivity. Padrick (1984) observed enhancement in the hydrogasification rate when iron-bearing compounds were added to the coal. Pohl (1984) comments on the reactivity enhancement of graphite in the presence of sodium. But, he reports that sodium must be distributed on the molecular level to be effective. These obswervations suggest that the sodium in real coals may be segregated, reducing its effectiveness as a catalyst. Huffman and Huggins (1984) have concluded

from Mossbauer spectrometry that iron undergoes a number of reactions at high temperatures under both oxidizing and reducing conditions, suggesting that iron compounds may act as catalysts if present in sufficient amounts. The other important effect of iron compounds is on ash emissivity (Raask, 1985) which profoundly affects the radiation balance of the particle and its temperature.

2.6 Modelling of Single Particle Combustion

Although many models have been proposed to describe the combustion of single particles, a few of them will be described here.

The simpler models assume that the particle is impervious to the reactant and that the reaction is lumped at the particle surface. Caram and Amundson (1977) proposed such a boundary layer model for slab and spherical geometries. They also give an excellent review of some previous models. Two heterogenous reactions at the carbon surface ($C+O_2 \rightarrow CO_2$; $2C+O_2 \rightarrow 2CO$) and one homogeneous reaction in the gas phase involving oxidation of carbon monoxide were considered. The particle was assumed to be in radiation equilibrium with similar particles. Transport properties were assumed to be independent of temperature. From such a simple model, they nevertheless concluded that Stefan flow was a negligible factor in spherical geometry. More importantly, they found that while larger particles (5mm) burned according to the double-film theory, smaller ones (50μm) burned consistent with single-film theory predictions. In the latter, the primary reaction at the surface produces carbon monoxide which is later oxidized to carbon dioxide far from the particle. Thus there is no flame in the particle boundary layer. Caram and Amundson also predicted the existence of multiple steady states in the solution of the differential

equations, some of which were interpretaed as ignition and extinction phenomena. Mon and Amundson (1978) extended the previous work to include the effect of radiative exchange with a wall or enclosure and also assumed varying diffusivities of the gas phase components. They concluded that, for particles in the pulverized coal size range burning in air, CO oxidation always takes place outside the boundary layer and that the only important heterogenous reaction at the particle surface is $2C + O_2 \rightarrow 2CO$.

Srinivas and Amundson (1980, 1981a, 1981b) investigated the effects of intraparticle transport. Although the earlier papers (1980, 1981a) treated the internal structure as invariant (*e.g.* porosity and surface area as constant) with respect to combustion, this assumption was later relaxed (1981b). They found that the pore structure and its evolution significantly influences all aspects of combustion including burn time, ignition, and extinction. The validity of previous boundary layer models (Caram and Amundson, 1977; Mon and Amundson, 1978) was thus doubtful under any condition.

Thus the internal particle structure must be incorporated into any realistic model although properly formulated shrinking core models could still describe combustion at high temperatures. For these, reaction rates were a crucial input parameter. Sotirchos and Amundson (1984) combined the previous approaches of the boundary layer and the intraparticle models into a single model. Internal surface area, porosity, and diffusivity were functions of the local conversion. They also included the effects of intraparticle thermal gradients. As before, internal pore structure and growth were dominant parameters.

Bhatia and Perlmutter (1980, 1981) proposed a random pore model to describe the internal particle geometry. Their model for the kinetic regime (1980) later extended to diffusion dominated combustion (1981) predicted experimentally observed maxima in the reaction rate. Independently, Gavalas (1980) proposed a similar random pore model, capable of realistically describing particles with cylindrical pores. His model for the kinetic regime gave similar results to that of Bhatia and Perlmutter (1980). Gavalas (1981) extended his model to describe the combustion in diffusion dominated and intermediate regimes. Sotirchos and Burganos (1986) recently included Gavalas's random pore model in their unsteady particle combustion model. They found that pore structure, pore structure evolution, and radiant exchange significantly influences the ignition and extinction behaviour of single particles. Other models describing char combustion include those of Lee *et al.*(1984) and Simons (1979a,1979b).

None of the models described above attempt to include the presence of ash in any manner. Some attempts to incorporate the presence of ash in continuum models is described in Chapter 7.

References

1. Bhatia, S.K. and Perlmutter, D.D., *AIChEJ*, **26**, 1980, 379.
2. Bhatia, S.K. and Perlmutter, D.D., *AIChEJ*, **27**, 1981, 247.
3. Caram, H.S. and Amundson, N.R., *Ind. Eng. Chem. Fundam.*, **16**, 1977, 171.
4. Dutta, S., and Wen, C.Y., *Ind. Eng. Chem., Proc. Des. Dev.* **16**, 1977, 31.
5. Essenhigh, R.H., In 'Chemistry of Coal Utilization' 2^{nd} suppl. vol. (M.A.Elliott, ed) Wiley, New York, 1981.
6. Feng, C. and Stewart, W.E., *Ind. Eng. Chem. Fundam.*, **12**, 1973, 143.
7. Field, M.A., *Combustion and Flame*, **13**, 1969, 237.
8. Field, M.A., Gill, D.W., Morgan, B.B., Hawksley, P.G.W., 'Combustion of Pulverized Coal', BCURA, Leatherhead, 1967.
9. Gavalas, G.R., *AIChEJ*, **26**, 1980, 577.

45. Gavalas, G.R., *Comb. Sci. Tech.*, **24**, 1981, 197.

10. Hamor, R.J., Smith, I.W., Tyler, R.J., *Combustion and Flame*, **21**, 1973, 153.
11. Harvey, R.D. and Ruch, R.R., Proceedings of the Division of Fuel Chemistry, American Chemical Society, **29**, 1984, 2.
12. Hashimoto, K. and Silveston, P.L., *AIChEJ*, **19**, 1973, 259.
13. Hippo, E.J. and Walker Jr., P.L., *Fuel*, **54**, 1975, 245.
14. Huffman, G.P. and Huggins, F.E., Proceedings of the Division of Fuel Chemistry, American Chemical Society, **29**, 1984, 56.
15. Jenkins, R.G., Nandi, S.P., Walker Jr., P.L., *Fuel*, **52**, 1973, 288.
16. Johnson, M.F.L. and Stewart, W.E., *J. Catalysis*, **4**, 1965, 248.

17. Knill, K.J., Chambers, A.K., Parkash, S., Ungarian, D.E., Zacharkiw, R., Presented at the Spring Meeting of the Canadian and Western States Section of the Combustion Institute, 1986.

18. Laurendeau, N.M., *Prog. Energy Combust. Sci.*, **4**, 1978, 221.

19. Lee, S., Angus, J.C., Edwards, R.V., Gardner, N.C., *AIChEJ*, **30**, 1984, 583.

20. Lester, T.W., Seeker, W.R., Merklin, J.F., *Eighteenth Symposium (international) on Combustion*, 1981, 1257.

21. Libby, P.A., Blake, T.R., *Combustion and Flame*, **36**, 1979, 139.

22. Mahajan, O.P., Yarzab, R., Walker Jr., P.L., *Fuel*, **57**, 1978, 643.

23. Mitchell, R.E., *Comb. Sci. Tech.*, **53**, 1987, 165.

24. Mon, E. and Amundson, N.R., *Ind. Eng. Chem. Fundam.*, **17**, 1978, 313.

25. Morgan, P.A., Robertson, S.D., Unsworth, J.F., *Fuel*, **66**, 1987, 210.

26. Mulcahy, M.F.R. and Smith, I.W., *Rev. Pure and Appl. Chem.*, **19**, 1969, 81.

27. Nagle, J. and Strickland-Constable, R.F., *Proc. 5^{th} Conf. on Carbon*, **1**, 1962, 154.

28. Padrick, T.D., Proceedings of the Division of Fuel Chemistry, American Chemical Society, **29**, 1984, 270.

29. Petersen, E.E., *AIChEJ*, **3**, 1957, 443.

30. Pohl, J.H., Proceedings of the Division of Fuel Chemistry, American Chemical Society, **29**, 1984, 295.

31. Raask, E., 'Mineral Impurities in Coal Combustion', Hemisphere, New York, 1985.

32. Radovic, L.R., and Walker Jr., P.L., *Fuel*, **62**, 1983, 849.

33. Simons, G.A., *Comb. Sci. Tech.*, **20**, 1979a, 107.

34. Simons, G.A., *Comb. Sci. Tech.*, **20**, 1979b, 117.

35. Simons, G.A., *Nineteenth Symposium (international) on Combustion*, 1982, 1067.

36. Smith, I.W., *Combustion and Flame*, **17**, 1971, 303.

37. Smith, I.W., *Fuel*, **57**, 1978, 409.

38. Smith, I.W., *Nineteenth Symposium (international) on Combustion*, 1982, 1045.

39. Smith, I.W. and Tyler, R.J., *Comb. Sci. Tech.*, **9**, 1974, 87.

40. Smoot, L.D. and Smith, P.J., 'Coal Combustion and Gasification', Plenum, New York, 1985.

41. Sotirchos, S.V. and Amundson, N.R., *AIChEJ*, **30**, 1984, 537.

42. Sotirchos, S.V. and Burganos, V.N., *Chem. Eng. Sci.*, **41**, 1986, 1599.

43. Srinivas, B. and Amundson, N.R., *The Canadian J. Chem. Eng.*, **58**, 1980, 476.

44. Srinivas, B. and Amundson, N.R., *The Canadian J. Chem. Eng.*, **59**, 1981a, 60.

45. Srinivas, B. and Amundson, N.R., *The Canadian J. Chem. Eng.*, **59**, 1981b, 728.

46. Szekely, J. and Evans, J.W., *Chem. Eng. Sci.*, **25**, 1970, 1091.

47. Tseng, H.P., and Edgar, T.F., *Fuel*, **64**, 1985, 373.

48. Wells, W.F., Kramer, S.K., Smoot, L.D., Blackham, A.U., *Twentieth Symposium (international) on Combustion*, 1984, 1539.

49. Young, B.C. and Smith, I.W., *Eighteenth Symposium (international) on Combustion*, 1981, 1249.

Class and Group	Fixed Carbon[a] (%)	Volatile Matter[a] (%)	Heating Value[b] (Btu/lb)[d]
I. Anthracite			
1. Metaanthracite	>98	<2	
2. Anthracite	92-98	2-8	
3. Semianthracite	86-92	8-14	
II. Bituminous			
1. Low Volatile	78-86	14-22	
2. Medium Volatile	69-78	22-31	
3. High Volatile A	<69	>31	>14000
4. High Volatile B			13000-14000
5. High Volatile C			10500-13000[c]
III. Subbituminous			
1. Subbituminous A			10500-13000[c]
2. Subbituminous B			9500-10500
3. Subbituminous C			8300-9500
IV. Lignite			
1. Lignite A			6300-8300
2. Lignite B			<6300

a Calculated on dmmf basis.

b Calculated on mmf basis with bed moisture content.

c If agglutinating then HVC, else Subbit. A.

d 1 Btu/lb = 478.55 J/kg.

Table 2.1 ASTM Coal classification by rank.

Authors	Method	Temperature	% O_2	Pressure	Char Type
Jenkins *et. al.* (1973)	TGA	500°C	21	1 atm	From 21 US Coals pyrolyzed in N_2 at 600-1000°C
Dutta *et. al.* (1977)	TGA	424-576°C	21	1 atm	From 2 US Bituminous Coals pyrolyzed in N_2 at 1024°C and 4 process chars
Mahajan *et. al.* (1978)	TGA	405°C	21	1 atm	From 16 US Coals pyrolyzed in N_2 at 1000°C
Radovic *et. al.* (1983)	TGA	550-750K	21	1 atm	Process Chars
Tseng *et. al.* (1985)	TGA	425-900°C	0.5-100	1 atm	From 1 US Bituminous Coal pyrolyzed in N_2 at 1000°C
Knill *et. al.* (1986)	TGA	< 500°C	0-100	1 atm	From hydropyrolysis of sub-bituminous Canadian coals at 600-800°C
Morgan *et. al.* (1986)	TGA	450-650°C	21	1 atm	From hydropyrolysis of a British coal at 1400°C

Table 2.2 Low Temperature Reactivity Studies

Authors	Method	Temperature	% O_2	Pressure	Char Type
Field (1969)	Drop Tube	1200-1720°C	5, 10	1 atm	low rank UK Coal (N_2 at 1600K)
Smith (1971)	Drop Tube	1200-1900K	21	1 atm	NZ Bit. Coal (air at 1500K)
Hamor *et al.* (1973)	Drop Tube	900-2200K	10, 20	1 atm	Aust. Brown Coal (air at 1600K)
Smith *et al.* (1974)	Drop Tube	630-1812K	10, 20	1 atm	Aust. Brown Coal (air at 1600K)
Dutta *et al.* (1977)	TGA	834-1106°C	0.2-2	1 atm	US Bit. Coals (N_2 at 1024°C)
Smith (1978)	See Ref.	See Ref.	See Ref.	1 atm	Different Porous Chars
Young *et al.* (1981)	Drop Tube	1000-1800K	5-30	1 atm	Petro. coke
Lester *et al.* (1981)	Shock Tube	1700-2200K	10-50	5.5-10 atm	US Bit. Coals.
Wells *et al.* (1984)	Drop Tube	1300-1700K	21	1 atm	Process Chars
Knill *et al.* (1986)	Drop Tube	1100°C	21	1 atm	Can. bit. coals (600-800°C)
Mitchell (1987)	Drop Tube	1300-1800K	0-30	1 atm	Bit. coals/chars

Table 2.3 High Temperature Reactivity Studies

Chapter 3

PHYSICAL PROPERTIES AND OXIDATION RATES OF CHARS MADE FROM THREE BITUMINOUS COALS

Published in *Fuel*, **67**, 1988, 275-283.

Abstract

Intrinsic oxidation rates of coal chars derived from three bituminous coals were measured at 800 K and the effects of char formation temperature, conversion, coal particle size and char particle size on the rates were evaluated. Characterization of the various samples by BET surface area, mercury porosimetry, mercury and helium densities, heating values and in some cases elemental analyses were carried out to better understand the roles and interactions of the various parameters. Optical microscopic observations were also made to verify assumptions wherever possible. The results show that apparent and intrinsic rates as well as heating values are reduced with increasing char formation temperature. N_2-BET surface areas increase by an order of magnitude with conversion and exhibit maxima in the range of temperatures considered (1000 K to 1600 K). Of similar sized chars derived from different sizes of coal particles, those from the smaller coal size fractions had higher apparent reaction rates.

3.1 Introduction

The relationship between char reactivity and its physical or chemical properties is a subject of long standing. Several authors have reported on the dependence of the rates of char gasification by O_2, H_2O, and CO_2 on rank or chemical composition of the parent coal,[1–3] mineral matter,[1,2,4,5] and thermal pretreatment.[1,2,4,5] These experimental studies have, in most instances, employed sufficiently low temperatures and have taken other suitable precautions in order to minimize or eliminate intraparticle and external diffusion limitations. In the absence of diffusional effects the reaction rate divided by the surface area of the char, e.g. the N_2-BET surface area, provides what is known as the "intrinsic rate" or "intrinsic reactivity." It is well known that both total surface area and reactivity vary with the rank of the parent coal and its thermal pretreatment, although both surface area and reactivity have not always been measured.

Once a char has been prepared under specified and carefully controlled conditions, the gasification rate becomes a function of temperature, gas composition, and char conversion only. From the standpoint of process design, the dependence on conversion is as essential as the dependence on gas composition. Rates of char gasification by O_2, H_2O, and CO_2 have been reported as functions of conversion by several authors.[6–9,28] The rate versus conversion curves normalized by the maximum or the initial rate were found, in some cases, to be insensitive to reaction temperature but to vary with the reactant gas. Few workers measured surface area as well as reaction rate as functions of conversion to determine whether or not that ratio remained constant, although the assumption of constant ratio has been widely

employed in modelling work. In a recent investigation[10] oxidation rates of chars from an anthracite and a bituminous coal (hva) were found to be approximately proportional to the surface area determined by CO_2 adsorption at 273K at all conversions. The constancy of the intrinsic rate permitted the analysis of the data by the random pore model.

In addition to their inherent interest, studies as the ones quoted above are useful in the interpretation of gasification or combustion rates under conditions pertinent to applications. At temperatures typical of practical processes, the reactions of char are quite strongly influenced by external heat and mass transfer and by internal pore diffusion. The interpretation and extrapolation of high temperature data must somehow take into account pore diffusion and pore growth. Some progress has been made in this area[11,12] but the problem is far from having been satisfactorily treated, especially in regard to swelling coal chars. It is hoped, nevertheless, that in many cases the conversion dependence of pore structure characteristics and relative reaction rates measured under diffusion-free conditions can be approximately applied to high temperature reaction conditions.

In this paper we report oxidation rates and physical properties of bituminous coal chars subjected to devolatilization for two seconds at 1000-1600K. The focus is on the variation of surface area, reaction rate, and intrinsic reaction rate with conversion under diffusion-free conditions. Other physical properties reported include pore volume distribution, elemental composition and heating value. The effects of devolatilization temperature and particle size of the char and the parent coal are also examined.

3.2 Experimental Procedure

3.2.1 Char Formation

Chars were made from three bituminous coals with the compositions given in Table 3.1. At first the coals were ground in a mechanized mortar and pestle grinder in air for approximately 30 seconds and then sieved on a mechanical shaker for 10 minutes and classified into the following size fractions: less than 45μm, 45 - 53μm, 53 - 90μm, 90 - 104μm, 104 - 125μm and greater than 125μm.

Chars were then generated from the 45 - 53μm and 104 - 125μm size fractions of coal. These size fractions are narrow enough to minimize the effects of coal size variability while providing adequate sample quantities. The mean sizes 49μm and 114μm were different enough to examine the effects of coal size on subsequent char combustion.

The coals were pyrolysed in an electrically heated drop tube furnace. The furnace consists of an alumina tube having 5 cm. internal diameter heated by Kanthal heating elements placed in a radiation cavity 20 cm. long. Coal particles were entrained in a stream of nitrogen at rates of 2 g/hr using the syringe pump feeder arrangement described by Senior[13] and were injected into the radiation cavity of the furnace through a wide bore (1 cm) water cooled injector. Furnace wall temperatures were measured by thermocouples attached to the outside of the alumina tube. Gas temperatures were measured using a suction pyrometer. Based on both wall and gas temperatures the particle temperature was deduced from a steady state thermal energy balance. The carrier gas flow rate was adjusted to achieve residence times of 2 seconds. The devolatilization loss for the coals ranged between 30-50 %,

depending on the temperature, and varied from coal to coal.

The chars were collected on a filter. To eliminate any tars that might have condensed, the chars were washed repeatedly with tetrahydrofuran and then dried at room temperature for 1 hour. Finally the tar-free chars were sieve-classified into the following size fractions: less than 45μm, 45 - 53 μm, 53 - 90 μm, 90 - 104 μm, 104 - 125 μm, 125 - 147 μm and greater than 147 μm.

3.2.2 Rate Measurements with TGA

A DuPont model 920 electrodynamic balance was used to measure the weight loss of a char sample oxidized at 800 K. In all cases the samples were heated in nitrogen at 50 K/min until the final temperature of 800 K was reached at which instant oxygen was admitted. The flow rates of the initial nitrogen stream and the oxidizing stream (17 % oxygen by volume) were kept at 100 cm^3/min STP for all runs. This low flowrate was used to avoid entrainment of the extremely low density samples. The sample was placed on a platinum pan and its temperature was monitored with a thermocouple placed directly above. The mass loss, rate of mass loss, and the sample temperature were continuously recorded by a computerized data acquisition system. The initial sample masses were in the range 5 - 10mg.

3.2.3 Surface Area and Helium Density Measurement

Surface areas were measured by a pseudo-static technique by acquiring gas adsorption isotherms using continous addition of adsorbate gas (N_2 at 77 K) as described by Northrop *et al.*[14] BET and capillary condensation analyses were carried out on the resulting isotherms. Calibration of the apparatus was carried out using various standardized samples of alumina and graphite. Helium densities were determined

on vacuum-dried samples by helium displacement at room temperature. Sample quantities of at least 0.8 g were used to obtain reliable density values.

3.2.4 Mercury Porosimetry

Pore volume distributions were determined by mercury penetration. An Autoscan porosimeter, Model 33 was used. Low pressure penetration (101 kPa) was implemented to fill the interparticle voids and intraparticle voids with openings larger than 7 μm. High pressure, to a maximum of 227 MPa (30000 psi), was used to penetrate pores having diameters larger than 6 nm. The Washburn equation[15] was used to calculate pore volume distribution as a function of pore radius from pressure and intrusion volume measurements under the assumption of cylindrical pores.

3.3 Results and Discussion

3.3.1 Physical Characteristics

Apparent densities, σ_A; mercury densities, σ_{Hg}, corresponding to the solid plus pores below 6 nm in diameter; and helium densities, σ_{He}, for the uncombusted chars are listed in Table 3.2. Total porosity, ϵ_A, and porosity of pores below 64 Å , ϵ, can be estimated from the density values. Pore diffusivities for the initial materials were calculated based on mercury porosimetry, nitrogen capillary condensation and helium density data. Values of mean pore radii r_p were determined from the porosimetry plots or calculated from the microporosity values. Figure 3.1 shows the volume and surface area distributions for the 1200 K and 1600 K chars of PSOC-1451. These were obtained from mercury intrusion and nitrogen capillary condensation measurements. An interesting feature of the pore volume and area distributions

is that chars obtained by devolatilization at higher temperatures (1600 K) developed trimodal distributions while the low temperature (1200 K) chars developed bimodal ones. As is evident from the surface area curves in the same figure, pores below 100 Å in diameter account for most of the area while contributing very little to the total volume. On the other hand the presence of the pores above 1000 Å in diameter is manifested in the volume distribution. Therefore the presence of different pore ranges can be inferred by examining both the volume and surface area distributions. For the 1200 K char the distribution is bimodal showing appreciable pore volume in the macropore region and significant surface area in the micropore region. The same peaks are also evident for the 1600 K char. In addition there is a distinct peak around 500 Å showing development of accessible porosity in the transitional region. The 1000 K and 1400 K chars for this coal exhibit characteristics similar to the 1200 K char. Chars of the other coals also exhibited similar behaviour. The total pore volume penetrated by mercury, V_{Hg}, along with the pore size distribution is a good indication of the extent of connectivity of the macro and the transitional pores. The corresponding pore area, A_{Hg} is calculated assuming cylindrical pores. Also listed are initial BET surface areas, heating values and elemental composition, expressed as mass fractions, for some of the chars. Data for partially combusted PSOC-176 1600 K char at 80% conversion are also tabulated. The apparent density of the partially combusted char has diminished while its porosity and the pore volume have increased.

3.3.2 Heating Values

Higher heating values (HHV) were measured using the 1341 Parr oxygen bomb

calorimeter. The results obtained were reproducible to within 250 J/g or about 1%. The values obtained for the PSOC-1451 coal and chars are plotted in Figure 3.2 as a function of charring temperature both on a total weight basis and on a dry ash-free basis. For both cases the heating values decrease with the increase in pyrolysis temperature. The reduction of heating value is obviously related to the loss of hydrogen at higher devolatilization temperatures as shown by the elemental analysis values listed in Table 3.2. Dulong[16] gives an empirical relationship between coal heating value and C,H,O and S content. Experimental values agree very well with Dulong's formula as shown in the figure. There appears to be some disagreement for the 1600 K char. This might be due to a small error in the C:H ratio measurement.

3.3.3 Rate Calculations

The variation of sample mass with time in the TGA experiments was normalized with its value at the moment oxygen was admitted. There was some mass loss due to tar release as the sample was heated. The chars formed at relatively low temperature (1000 K and 1200 K) lost considerable mass during this period. For the 1400 K and 1600 K chars, almost all the volatiles were expelled during char formation, so that the loss during the heat up period was less than 3%.

In Figure 3.3 the apparent reaction rate ρ_m is plotted versus carbon conversion. The conversion, X, at any given time is the mass of carbon reacted divided by the mass of initial carbon.

$$X = \frac{m_{initial} - m}{m_{initial} - m_{ash}} \tag{3.1}$$

The apparent reaction rate normalized per unit instantaneous mass, m, of carbon,

ρ_m, is defined as

$$\rho_m = \frac{1}{m - m_{ash}} \frac{dm}{dt} \tag{3.2}$$

The mass of ash, m_{ash}, was measured in each run by carrying out oxidation until there was no further mass loss.

Another common way to plot the data is also shown in Figure 3.3 where ρ_{m_0} is defined by normalizing with respect to the initial mass.

$$\rho_{m_0} = \frac{1}{m_{initial} - m_{ash}} \frac{dm}{dt} \tag{3.3}$$

Plotted in this fashion the reaction rate exhibits a distinct maximum at a certain conversion that varies with char type, and particle size.

Figure 3.4 shows the reaction rate ρ_m, as a function of conversion for two sizes of the 1600 K char of PSOC-1451. The two curves are indistinguishable, consistent with the absence of diffusion limitations concluded from the calculations given in the discussion below. Optical microscope photographs of PSOC-176 1600 K char at conversions of 0, 65 and 90% show that the particle size is independent of conversion as would be expected for regime I reaction.

3.3.4 Surface Areas

The surface area, A_T, for the PSOC-176 1600 K char is shown in Figure 3.5 as a function of conversion. The area reported corresponds to the carbonaceous matter in as much as the surface area of the ash was measured to be only 2 - 3m^2/g, in good agreement with values reported by Smith and Tyler[17]. It can be seen that the surface area increases rapidly with conversion and at about 60% conversion, reaches a maximum value of 450m^2/g which is almost higher by an order of magnitude than

the initial value $50m^2/g$. At higher conversions the area stays constant or decreases slightly. Similar trends have been observed for other coals[18]. Surface areas of the three chars are plotted as a function of char pyrolysis temperature in Figure 3.6. The top three curves give the areas of the chars after partial oxidation to 50% conversion while the fourth curve shows the variation of the uncombusted area of the PSOC-176 char; areas for the other two 1600 K uncombusted chars are also shown. The area of the PSOC-176 char at zero conversion increases with pyrolysis temperature. There are two competing effects that affect surface area. While volatiles and tars released at higher temperatures leave a larger pore volume accessible to nitrogen, thermal annealing and structural reorganisation of the carbon matrix at higher pyrolysis temperatures leads to closing of pore mouths and pore coalescence thus reducing surface area. Which effect will dominate is not predictable *a priori*. In the present case experimental evidence suggests that for PSOC-176 the former does. The surface areas of partially combusted PSOC-176 and 1451 chars initially increase with pyrolysis temperature, reach a maximum and then drop. The high surface area of the PSOC-176 char indicates that it has more small pores accessible to N_2 at 77 K. In contrast,the surface area of the PSOC-282 char is approximately constant initially but later increases with pyrolysis temperature. Reduction of areas at higher charring temperatures may result from closure of the finer pores due to structural ordering of the carbon that increases with temperature of exposure. This hypothesis is supported by X-ray diffraction studies on semi-anthracite reported by Smith and Tyler[17]. The anomaly presented by the 1000 K char is probably due to the presence of heavy tars in the material.

3.3.5 Diffusion Limitations

Three distinct processes must be examined to insure that the measured rates are free of diffusional limitations. They are diffusion in the boundary layer between the flowing oxidizer stream and the bed of particles, diffusion through the particle bed, and pore diffusion inside the particles. Each shall be examined briefly.

1. Bed Boundary Layer Diffusion: As a very simple approximation, the flow of oxidizer over the pan was modelled as flow past a flat plate, neglecting the effects of the pan walls, pan leading edge and the confining reactor tube walls. For the conditions of the experiment, the Reynolds number (based on average velocity at the reactor temperature and pan length) is about 1.5 and hence the flow is laminar. The time for diffusion across the boundary layer is negligible compared to the characteristic reaction time computed as ρ_m^{-1} (see Table 3.3). Therefore it is safe to assume that there is no limitation imposed by diffusion in the bed boundary layer.
2. Bed Diffusion : Although sample quantities were small and spread uniformly over the pan, the effect of bed diffusion could become important at high temperatures. A modified Thiele modulus based on bed parameters and the apparent reaction rate can be formulated[23] as shown below

$$K = \dot{N}\frac{H^2}{C_0 D_B} \tag{3.4}$$

where $\dot{N}$ is the apparent reaction rate per unit bed volume (g/cm^3-s), C_0 is the oxygen concentration in the ambient (g/cm^3), H is the bed thickness (cm) and D_B is the bed diffusion coefficient (cm^2/s), given by Satterfield[24] as

$$D_B = \frac{D_m \epsilon_0}{\tau} \tag{3.5}$$

where D_m is the molecular or bulk binary diffusion coefficient of oxygen in nitrogen at the proper temperature, ϵ_0 is the void fraction of the bed normally in the range 0.35 - 0.4 and τ is the bed tortuosity, commonly taken equal to 2. Bed diffusion is negligible[23] for K < 1. For the 45 - 53 μm size fraction of the PSOC-1451 1600 K char the sample size was 5 mg. and its apparent particle density was 0.98 g/cm^3. The apparent rate was 25x10^{-4} g/cm^3-s. The pan area was 0.3 cm^2. Hence, the thickness of the bed, H, was 0.017 cm. Assuming a mean particle size of 50 μm, the average bed depth was only 3.4 particles. At 800 K the value of D_m is 1.88 cm^2/s and, therefore, D_B is 0.33 cm^2/s, assuming ϵ_0 to be 0.35. At an oxygen mole fraction of 0.17 C_0 is 6.03x10^{-5} g/cm^3. The resulting Thiele modulus, K, is 3.64x10^{-4}, hence bed diffusion does not significantly influence the reaction in these experiments.

3. Pore Diffusion : The present chars are extremely porous, having pore openings with length scales ranging from few microns down to few angstroms. The type of diffusion taking place covers the range from bulk diffusion in the macropores to Knudsen diffusion in the smaller meso and micropores with a combination of the two in pores of intermediate size. It is essential, therefore, to know the pore size distribution of the material before the pore diffusional resistance can be assesed. In the present study all micro and meso pore diameters were smaller than the mean free path of oxygen, approximately 0.3μm for the experimental conditions and thus, the diffusivity was that corresponding to Knudsen diffusion[25],

$$D_K = 9.7\text{x}10^3 r_p \left(\frac{T}{M}\right)^{0.5} \tag{3.6}$$

For the pores that have diameters comparable to the mean free path of oxygen, the transition regime diffusivity was applied i.e.[26],

$$\frac{1}{D_p} = \frac{1}{D_m} + \frac{1}{D_K} \tag{3.7}$$

Finally the total effective diffusivity was calculated by adding the contributions from the different pore sizes and the resulting values varied from 0.02 to 0.2.

3.3.6 Reaction Rate

As shown in Figure 3.3, ρ_m increases sharply during the first 3-4% carbon conversion. The principal reason for this phenomenon is that the gas composition over the bed gradually changes from pure nitrogen to a final mixture of 17% O_2 in nitrogen. Jenkins *et al.*[1] also suggest that oxygen complex formation at the surface and char activation may also be important at this early stage of conversion. After this initial delay the oxygen concentration reaches a steady value and the apparent rate increases slowly with conversion until the completion of combustion.

Following the proceedure outlined by Smith[19] an effectiveness factor η defined as the ratio of actual reaction rate to the rate found in the absence of restrictions due to pore diffusion can be calculated as:

$$\eta\phi^2\frac{(m+1)}{2} = \frac{\gamma^2\rho_m\sigma_A(m+1)}{4D_eC_s} \tag{3.8}$$

where ϕ is the pore Thiele modulus and γ is the characteristic length defined as the ratio of particle volume to external area. Thus the right side of equation (3.8) can be calculated and η can be calculated by the relationships between η and $\eta\phi^2(\mathrm{m}+1)/2$ given by Mehta and Aris[20]. The effectiveness factors calculated for the uncombusted

chars using suitable diffusion parameters are equal to unity, in agreement with findings by Knill and others[21] for similar conditions. This calculation also shows that there are no pore diffusion limitations. The order of magnitude increase in the surface area after partial combustion indicates the opening of a vast micropore network. A worst case calculation assuming that all pores have diameters of 10 Å, yielded an effectiveness factor η which was still close to unity.

Since the particles oxidize in the kinetically controlled regime I as shown earlier, an intrinsic reaction rate ρ_i can be defined by

$$\rho_i = \frac{\rho_m}{A_T} \tag{3.9}$$

Table 3.3 shows the intrinsic rate of PSOC-176 1600 K char at various degrees of conversion. Values for the areas were taken from Figure 3.5 and values of the apparent rate from Figure 3.3. It can be seen that after approximately 5% of conversion the intrinsic rate becomes essentially independent of conversion providing a justification for employing the N_2-BET surface area A_T for the defination of ρ_i. Approximately constant intrinsic rates after the first 5% conversion were obtained for the PSOC-1451 chars as well. The small increase in the rate at the highest conversions could be attributed to experimental error particularly in the area measurement of very small samples. It could also be due to the decrease in the particle conductivity with increasing porosity, causing local hot spots with high reaction rates.

The fact that the intrinsic rate is nearly constant with conversion makes possible the comparison of the intrinsic reactivities of chars at any conversion for which surface area values are available. In the present study all rates have been compared

at 50% conversion. Figure 3.7 shows the apparent reaction rate at 50% conversion for the three chars for two size cuts, 104-125μm and 45-53μm . It is evident that the reaction rates of all chars increase with decreasing pyrolysis temperature, possibly due to the residual volatile matter of higher reactivity or to less complete structural ordering which leaves a larger number of sites available for reaction with oxygen. The figure also shows that the apparent rate is independent of char particle size.

The effect of parent coal size on the apparent combustion rate was investigated for PSOC-1451 chars for the two size cuts 45-53 and 90-104 μm, both produced from coal size cuts 53-90 μm, and from coal fines below 45 μm in diameter. This effect of parent coal size can be quite important as the fractionation of coal leads to selective segregation of the different maceral types in certain sizes[22]. The presence of macerals of different chemical compositions affects the morphology, structure and reactivity of the char. Figure 3.8 shows the oxidation rates of chars derived from different size fractions of the parent coal. The oxidation rates of the char fraction derived from smaller coal particles appear to be 10-20% higher. This fraction was characterized by a more pronounced cenospheric structure and higher mineral matter content, the latter possibly causing some catalytic enhancement of the oxidation rate.

Intrinsic reaction rates for two size cuts of the three chars are presented in Figure 3.9. The intrinsic rate for two of the chars decreases with pyrolysis temperature, most probably due to the increased structural ordering of the carbon matrix with temperature. The rate of the PSOC-1451 char decreases the least, suggesting minimal structural changes. It is interesting to note that the intrinsic rates of the

three chars are equal at the lowest devolatilization temperature but deviate as much as 30% at higher devolatilization temperatures. One reason may be that structural ordering at the lower temperature is minimal in all three chars while as the temperature increases changes become more pronounced and differentiated among the chars. The fact that the intrinsic rate follows similar trends with the heating value of the chars suggests that the loss of hydrogen at higher devolatilization temperatures reduces the number of active sites for oxidation. This is in agreement with results reported by Khan[27] showing a correlation between hydrogen content and rate of oxidation.

3.4 Conclusions

Increasing the pyrolysis temperature of three bituminous coals from 1000 K to 1600 K resulted in (i) decrease of the H:C ratio of the resulting char by a factor of 2 to 2.5 (ii) decrease of the heat of combustion of the char by 10-15% (iii) change in the pore volume and pore surface distributions from bimodal to trimodal with the creation of porosity in the mesopore range. The apparent oxidation rate (at 800K) decreased by about 50% as the pyrolysis temperature increased from 1000 K to 1600 K.

The N_2-BET surface areas of the char increased from 10-50 m^2/g in the first few percent of conversion to 300-500 m^2/g at the highest conversions measured. The surface area at 50% conversion varied irregularly with the pyrolysis temperature.

The intrinsic char oxidation rate defined in terms of the N_2-BET surface area was approximately the same for all coals pyrolysed at 1000 K but varied with the parent coal for the higher pyrolysis temperatures. The intrinsic reaction rate after

the first 5% of conversion was found to be approximately independent of conversion for all chars examined.

Char particles in the same size fraction obtained from coal of different size fractions differ in properties. The cenospheric char produced from the smaller coal particles was 10-15% more reactive than the char of equal size produced from the larger coal particles.

3.5 Acknowledgements

This work was supported by the US Department of Energy under their contract DE-AC2284FC70915. Thanks are due to Mr. P. S. Northrop for help in constructing and testing the BET apparatus and for carrying out some of the surface area measurements. The authors are also grateful to the reviewers for their useful suggestions and comments.

References

1. Jenkins, R.G., Nandi, S.P. and Walker Jr., P.L. *Fuel*, **52**, 1973, 288
2. Linares-Solano, A., Mahajan, O.P., and Walker Jr., P.L. *Fuel*, **58**, 1979, 327
3. Hippo, E and Walker Jr., P.L. *Fuel*, **54**, 1975, 245
4. Ashu J.T., Nsakala Y.N., Mahajan O.P. and Walker Jr., P.L. *Fuel*, **57**, 1978, 250
5. Razouk, R.I., Saleeb, F.Z., and Youssef, A.M. *Carbon*, **6**, 1968, 325
6. Dutta, S., and Wen, C.Y. *IEC Process Des. Dev.*, **16**, 1977, 20
7. Dutta, S., and Wen, C.Y. *IEC Process Des. Dev.*, **16**, 1977, 31
8. Mahajan, O.P., Yarzab, R., and Walker Jr, P.L. *Fuel*, **57**, 1978, 643
9. Tseng H.P. and Edgar T.F. *Fuel*, **63**, 1984, 385
10. Su, J.-L., and Perlmutter, D.D. *AIChE J.*, **31**, 1985, 973
11. Smith, I.W. *Fuel*, **57**, 1978, 409
12. Gavalas, G.R. *Comb. Sci. Tech.*, **24**, 1981, 197
13. Senior, C.L. and Flagan, R.C. Twentieth Symposium (International) on Combustion, the Combustion Institute, 1984, 921
14. Northrop, P.S., Gavalas G.R., Flagan R.C. *Langmuir*(in press)
15. Lowell, S. and Shields J. E. 'Powder Surface Area and Porosity' Chapman and Hall, 1984, 94
16. In 'Chemistry of Coal Utilization' 2nd suppl. vol. (ed) M.A.Elliot ,Wiley, 1981.
17. Smith I.W. and Tyler R.J. *Fuel*, **51**, 1972, 312
18. Northrop, P.S. *Personal Communication*
19. Smith I.W. and Tyler R.J. *Comb. Sci. Tech.*, **9**, 1974, 87

20. Mehta, B.N. and Aris, R. *Chem. Eng. Sc.*, **26**, 1971, 1699

21. Knill, K.J., Chambers, A.K., Parkash S., Ungarian D.E., Zacharkiw, R. Presentation at 1986 Spring Meeting of the Canadian and Western States Section of the Combustion Institute.

22. Berkowitz, N. 'An Introduction to Coal Technology' Academic Press, 1979

23. Weisz, P.B., Hicks, J.S. *Chem. Eng. Sci.*, **17**, 1962, 265

24. Satterfield, C.N. 'Mass Transfer in Heterogeneous Catalysis.' M.I.T. Press, Cambridge, Mass. 1970

25. Wheeler, A. *Adv. in Catalysis*, **3**, 1951, 249

26. Ruthven, D.M. 'Principles of Adsorption and Adsorption Processes' Wiley, 1984, 133

27. Khan, M.R. *ACS Div. Fuel Chem. Preprints*, **32**, No. 1, 1987, 298

28. Tseng H.P. and Edgar T.F. *Fuel*, **64**, 1985, 373

List of Symbols

SYMBOL	DESCRIPTION	UNITS
A_{Hg}	specific Mercury area[N_2-BET]	m^2/g
A_T	specific total area	m^2/g
C_g	ambient oxygen concentration	g/cm^3
C_s	oxygen concentration at particle surface	g/cm^3
d	particle diameter	cm
D_B	bed diffusivity	cm^2/sec
D_K	Knudsen diffusivity	cm^2/sec
D_m	molecular diffusivity	cm^2/sec
D_p	pore diffusivity	cm^2/sec
H	bed thickness	cm
K	modified bed Thiele modulus	
m	true order of reaction	
M	molecular weight	g/g-mole
n	apparent order of reaction	
N	bed density	g/cm^3
p_{O_2}	ambient partial pressure of oxygen	
r_p	mean pore radius	cm
T_g	ambient temperature	K
T_p	particle temperature	K
V_{Hg}	specific mercury pore volume	cm^3/g
X	burn-off	

γ	characteristic particle dimension	cm
ϵ_0	bed void fraction	
ϵ	porosity below 6 nm.	
ϵ_A	total porosity	
η	effectiveness factor	
ρ_m	apparent reaction rate	g/g-sec
$\rho_{m,D}$	diff. controlled apparent reaction rate	g/g-sec
ρ_i	intrinsic reaction rate	g/cm^2-sec
σ_A	apparent density	g/cm^3
σ_{Hg}	mercury density	g/cm^3
σ_{He}	true (helium) density	g/cm^3
τ	tortuosity	
ϕ	Thiele modulus	
χ	ratio of ρ_m to $\rho_{m,D}$	

COALS	282	176	1451
RANK	Bit. HVB	Bit. HVB	Bit. HVA
MOISTURE (%)	5.7	0.8	2.5
ASH (%)	6.8	6.5	13.5
CARBON (%)	75.0	78.4	71.5
HYDROGEN (%)	5.3	5.4	4.7
OXYGEN (%)	8.7	5.5	7.0
NITROGEN (%)	1.7	1.3	1.3
SULFUR (%)	1.6	2.9	1.3
VOLATILE MATTER (%)	35.7	40.2	33.5
HEATING VALUE (DRY BASIS) cal/g	7407	7910	6965

Table 3.1 Properties of the three bituminous coals devolatilized to produce the chars used in the experiments.

TYPE OF COAL OR CHAR		σ_A (g/cm^3)	σ_{Hg} (g/cm^3)	σ_{He} (g/cm^3)	ϵ_A % <7μm	ϵ % <32 Å	PORE V_{Hg} (cm^3/g)	PORE S_{Hg} (m^2/g)	S_{BET} (m^2/g)	C (%)	H (%)	C/H	HEATING VALUE (cal/g)
PSOC 282	COAL	0.66	1.07	—	~ 38	—	0.75	15.7	—				7407
	1000 K	0.6	1.35	1.63	63	17	0.96	11.9	—				
	1200 K	0.52	1.4	1.59	67	12	0.90	13.8	—				
	1400 K	0.61	1.55	1.53	60	~ 0	1.0	15.1	—				
	1600 K	0.63	1.55	1.84	66	16	0.94	15.0	15.3				
PSOC 176	COAL	1.25	1.4	1.25	11	~ 0	0.08	6.8	9.5				7910
	1000 K	0.68	1.4	1.34	49	~ 0	0.74	12.9	17.5				
	1200 K	0.60	1.43	1.39	57	~ 0	1.47	16.37	20				
	80% CONV. AT 500° C	0.48	1.76	—	~ 72	—	1.53	14.7	—				
	1400 K	0.65	1.68	1.63	61	~ 0	1.62	26.93	31				
	1600 K	0.76	1.8	1.85	51	3	0.81	28.02	56				
PSOC 1451	COAL	1.18	1.42	—	17	—	0.14	7.9	—				6965
	1000 K	1.084	1.8	1.28	18	~ 0	0.4	14.8	—	66.8	2.8	1.9	6242
	1200 K	1.0	1.8	1.50	33	~ 0	0.43	11.6	—	69.9	1.8	3.1	6123
	1400 K	0.9	1.86	1.50	40	~ 0	0.57	11.4	—	71.0	1.1	5.6	5965
	1600 K: 53-90μm FROM FINES	0.76	1.85	1.85	59	~ 0	0.78	20.9	—	73.4	0.9	6.8	5594
	1600 K: 53-90μm FROM 53-90μm	0.98	1.81	1.85	47	2	0.46	14.7	27.8				
	1600 K: 53-90μm FROM 90-125μm	1.26	1.9	1.85	32	~ 0	0.40	14.5	—				
	1600 K: 125-147μm FROM 90-125μm	0.92	1.5	1.85	47	19	0.35	14.9	—				

Table 3.2 Properties of coals and chars.

CONVERSION %	APPARENT RATE ρ_m (g/g-sec)	INTRINSIC RATE ρ_i (g/cm^2-sec)
5	1.9×10^{-3}	7.0×10^{-10}
10	2.06×10^{-3}	7.2×10^{-10}
15	2.34×10^{-3}	7.1×10^{-10}
20	2.52×10^{-3}	7.15×10^{-10}
25	2.67×10^{-3}	7.11×10^{-10}
30	2.84×10^{-3}	7.1×10^{-10}
35	2.96×10^{-3}	7.12×10^{-10}
40	3.15×10^{-3}	7.3×10^{-10}
67	3.64×10^{-3}	7.9×10^{-10}
90	3.71×10^{-3}	8.0×10^{-10}

Table 3.3 Variation of rates with conversion for PSOC-176, 1600K char.

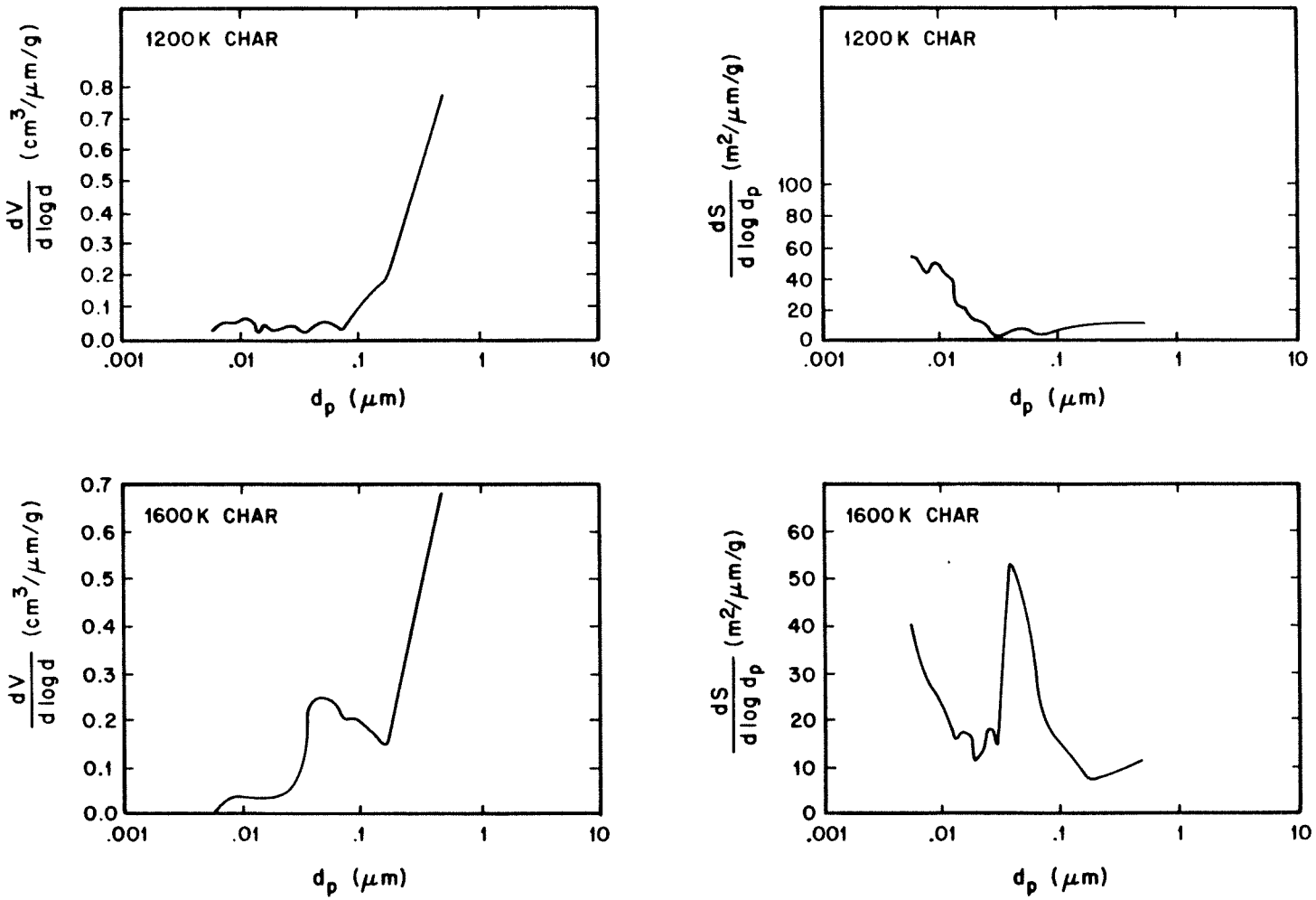

Figure 3.1 Pore volume and surface area distributions for PSOC-1451 chars (a) 1200 K (b) 1600 K

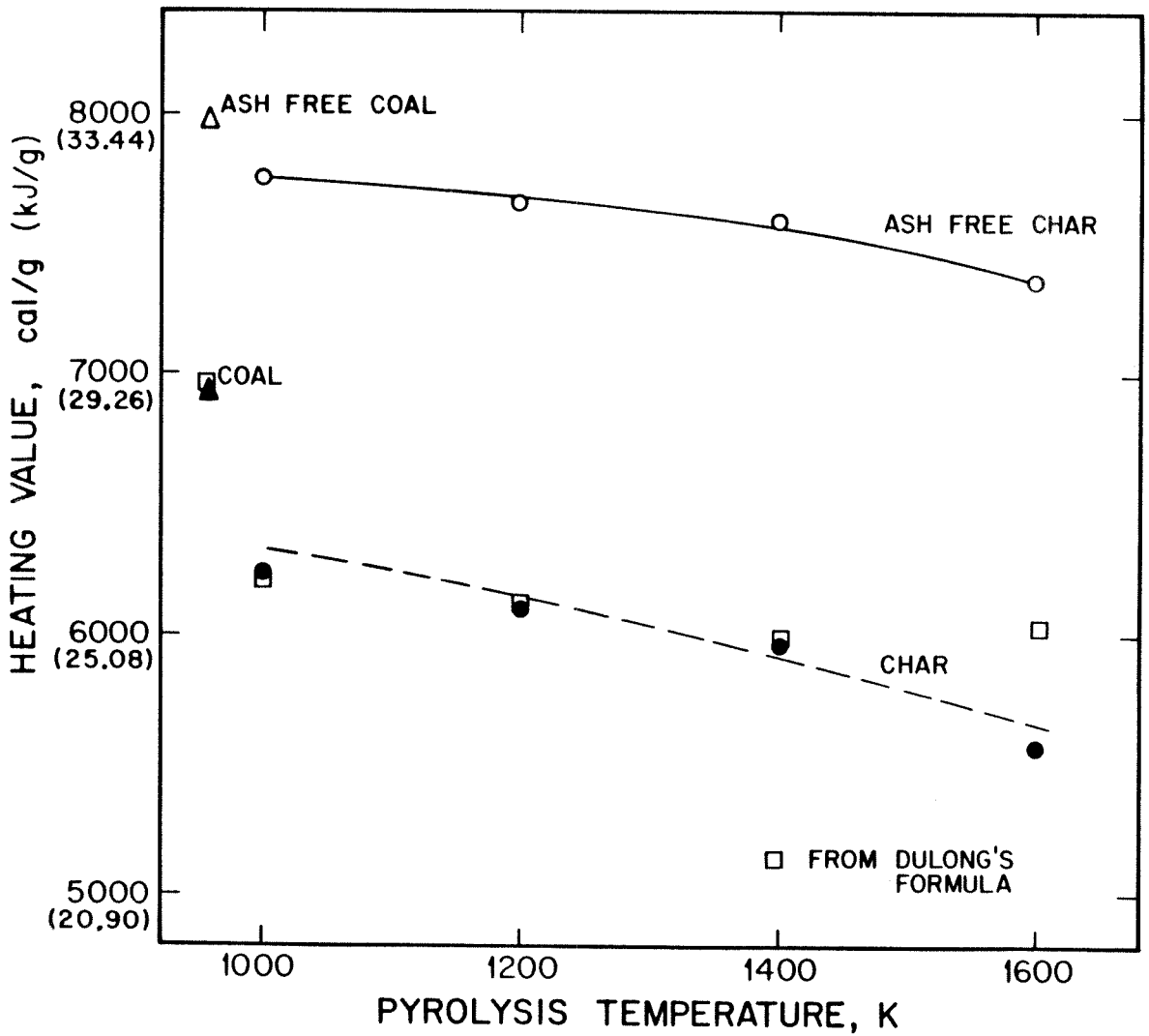

Figure 3.2 Heating Values of PSOC-1451 coal and chars versus pyrolysis temperature.

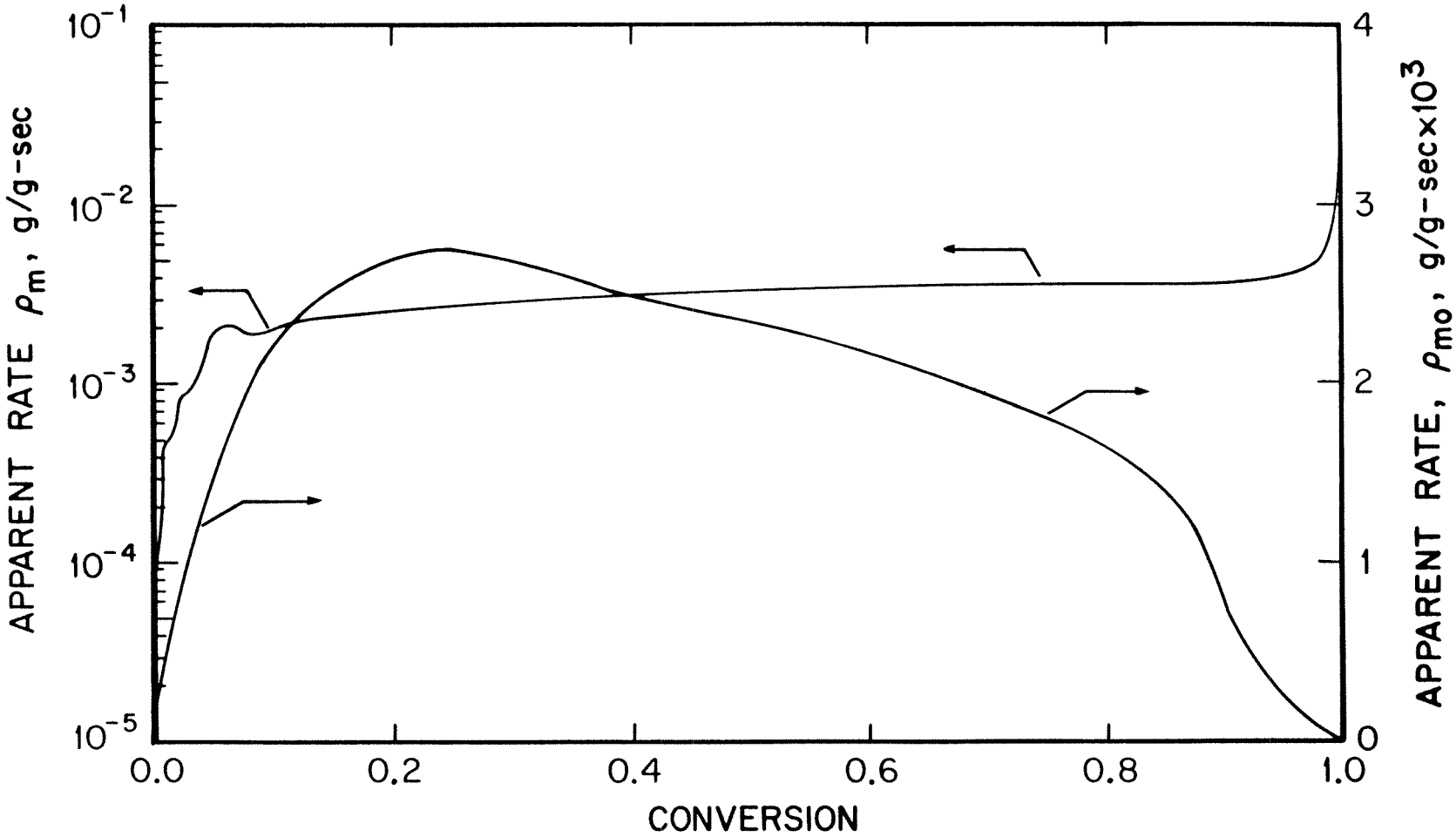

Figure 3.3 Apparent rates, ρ_m and ρ_{m_0} versus conversion, X, for PSOC-176 1600 K char.

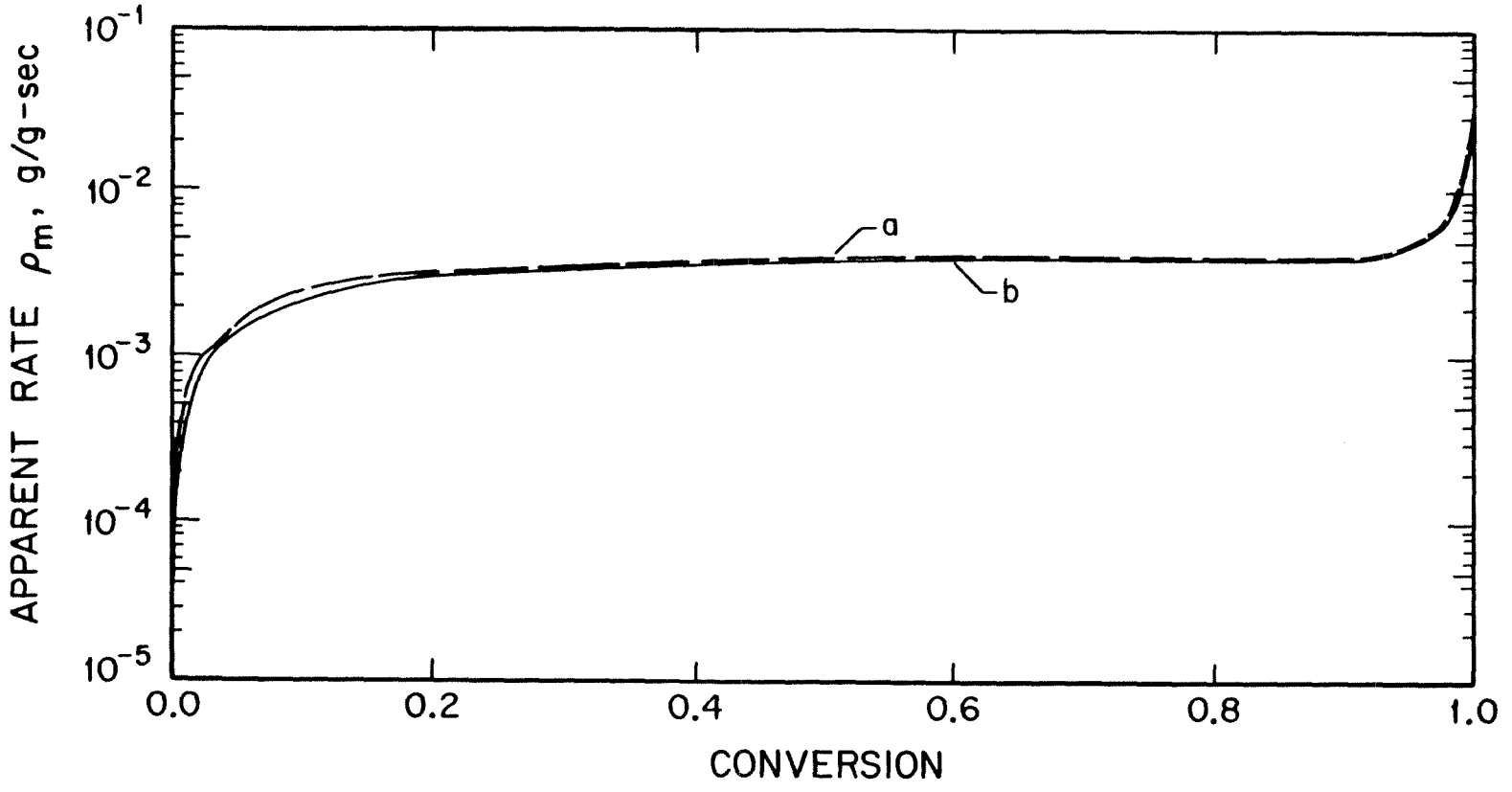

Figure 3.4 Apparent rates, ρ_m versus conversion, X, for PSOC 1451 1600K char, (a)45-53 and (b)104-125 μm.

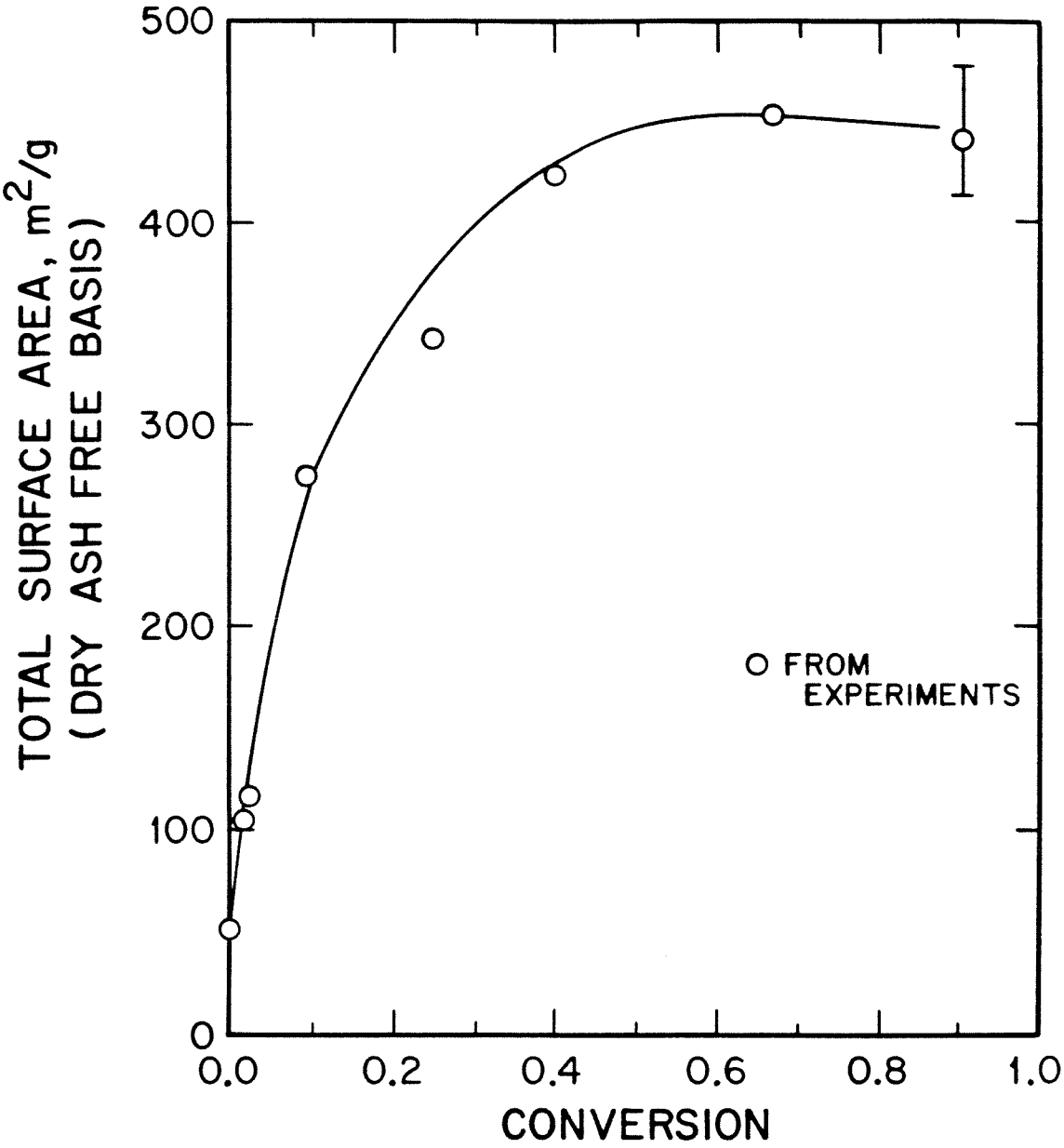

Figure 3.5 Surface areas of PSOC-176 1600 K char versus conversion. Line is smooth fit.

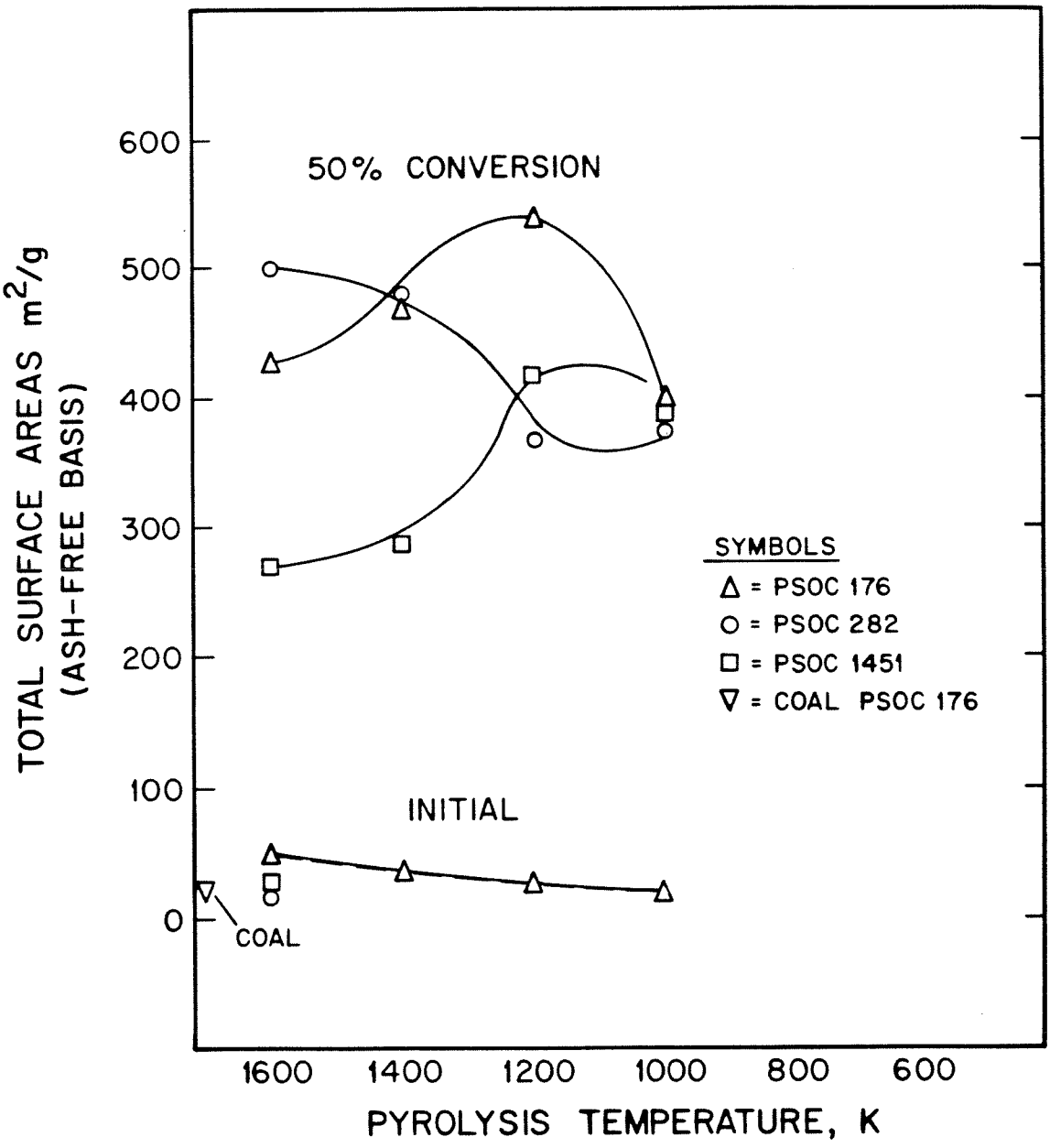

Figure 3.6 Initial surface areas and surface areas after 50% conversion for all chars versus pyrolysis temperature.

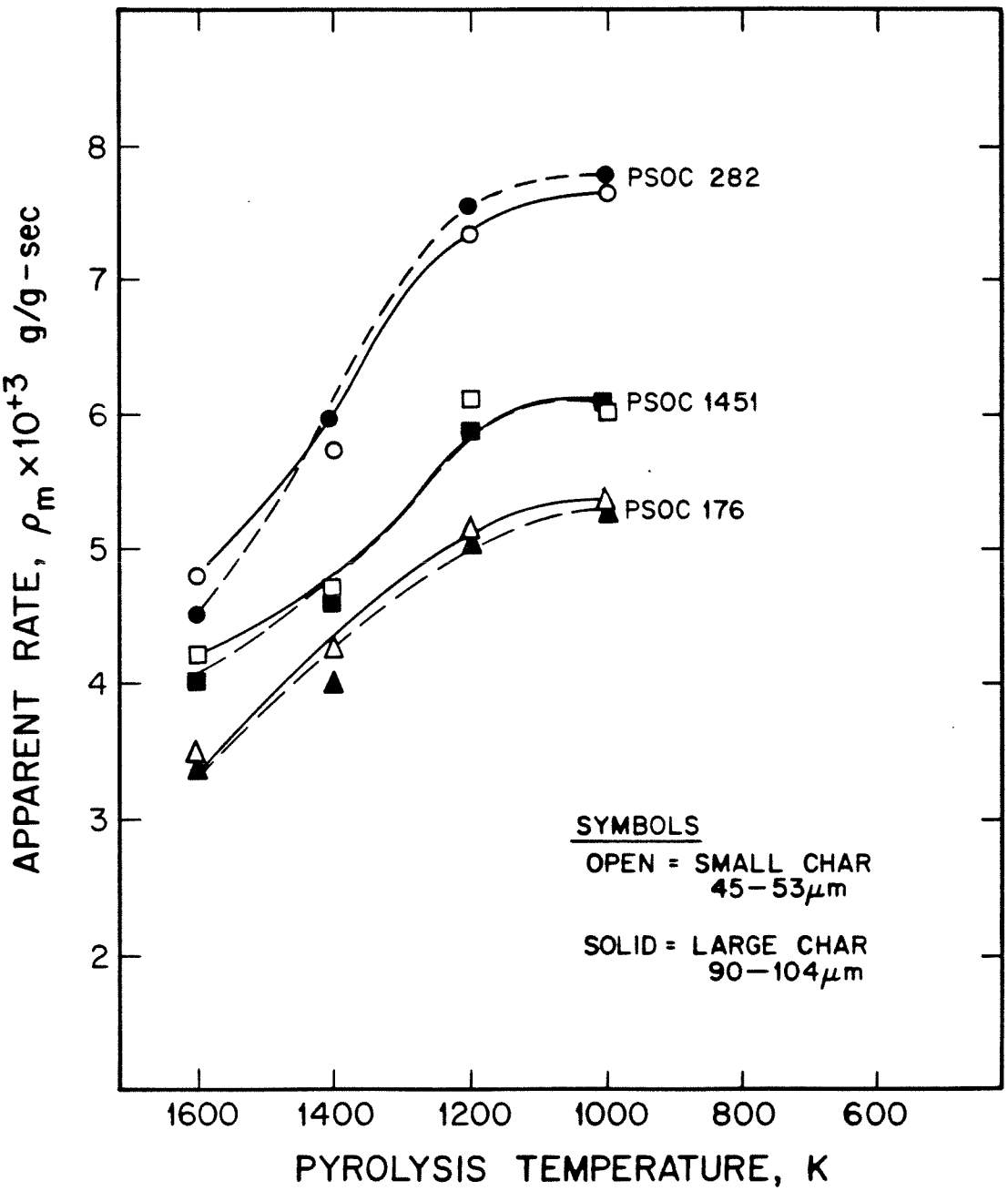

Figure 3.7 Apparent reaction rates at 50 % conversion for 45-53 and 104-125 μm sizes of all chars versus pyrolysis temperature.

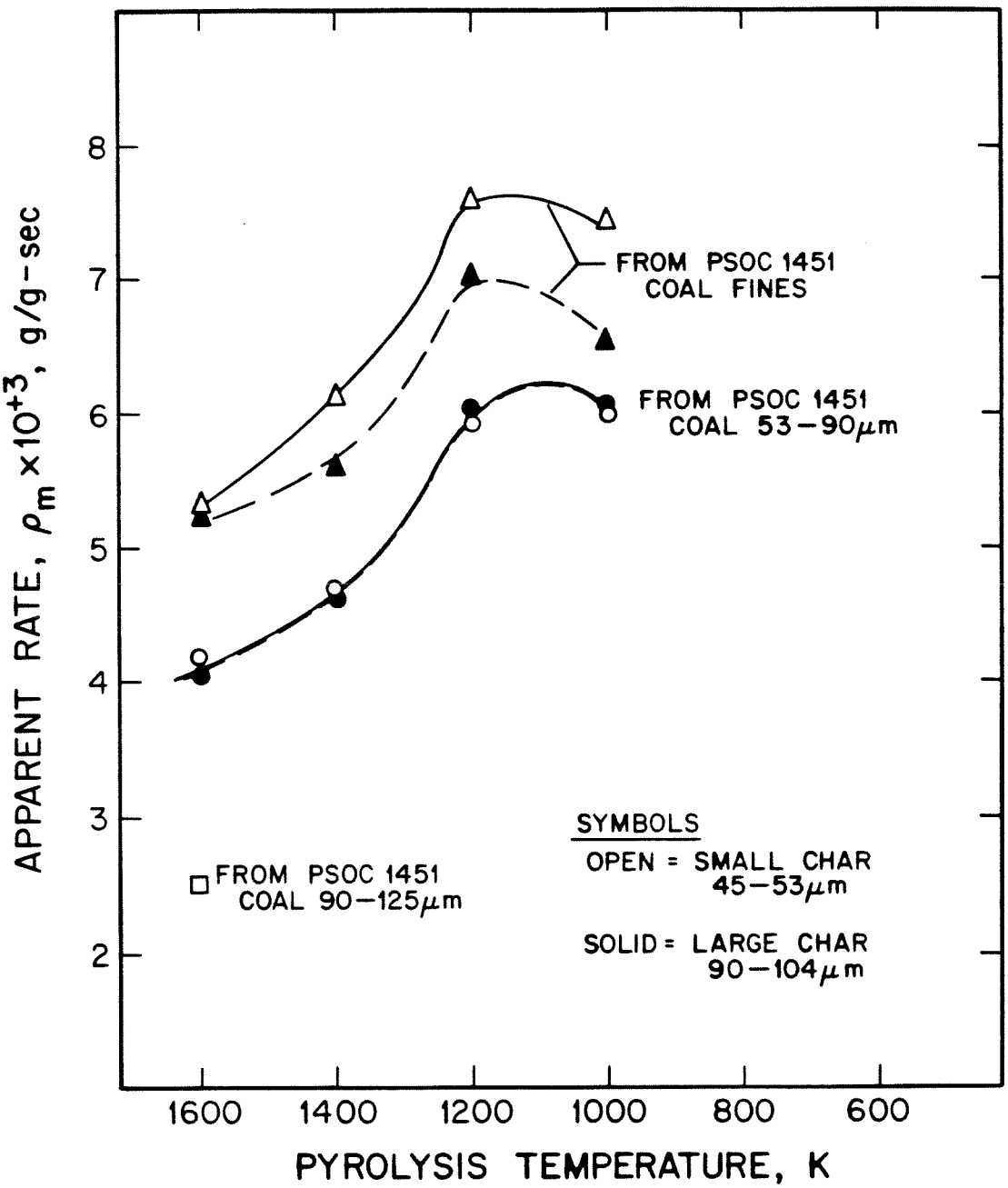

Figure 3.8 Apparent reaction rates at 50 % conversion for 45-53 and 104-125 μm char sizes derived from PSOC-1451 coal sizes (a) less than 45 μm (b) 53-90 μm versus pyrolysis temperature.

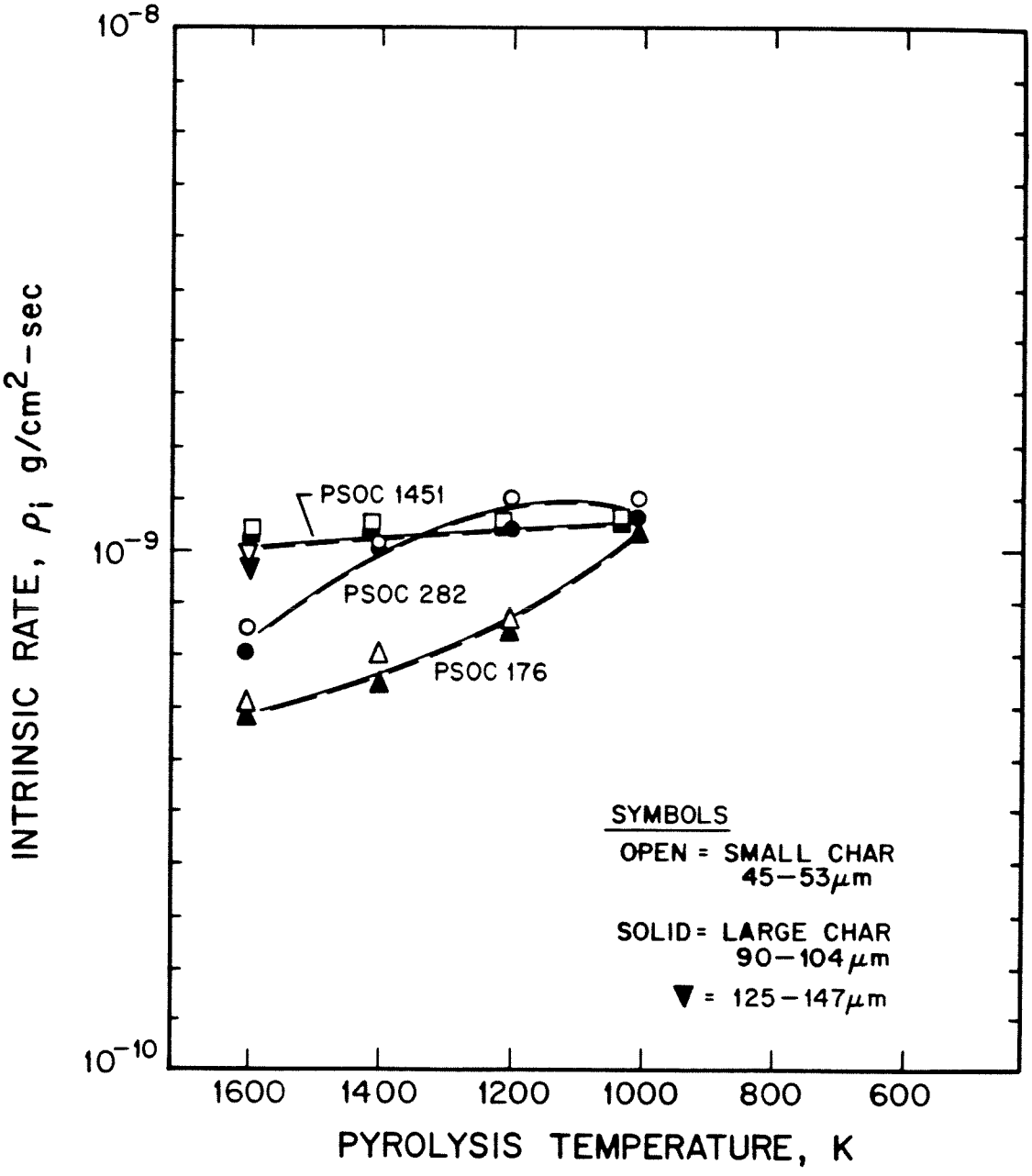

Figure 3.9 Intrinsic reaction rates at 50 % conversion for 45-53 and 104-125 μm sizes of all chars versus pyrolysis temperature.

Chapter 4

CHAR COMBUSTION: MEASUREMENT AND ANALYSIS OF PARTICLE TEMPERATURE HISTORIES

Accepted for publication in

Combustion Science and Technology

Abstract

Single particle combustion experiments were carried out with 50 - 100μm char particles derived from one lignite and one HVA bituminous coal. Reactor wall temperatures in the range 1050 K to 1450 K and oxygen partial pressures of 0.21 and 0.5 were used. The complete temperature-time histories of individual burning particles were measured using two-color optical pyrometry techniques. Apparent combustion rate parameters of the chars were then estimated using a model of single particle combustion and taking into account the random particle-to-particle property variation.

4.1 Introduction

The entrained flow reactor is the standard experimental system for the measurement of pulverized char combustion rates. Measurements that can be carried out in this system include (*i*) carbon conversion and characterization of physical properties (size, density, etc.) of partially burned char withdrawn at the reactor outlet or at intermediate axial positions using a cooled probe (*ii*) reactor wall temperature and gas temperature at various axial locations. The measurement techniques and procedures for data analysis have been described in the well known papers of Field (1969) and Smith and coworkers (Hamor and Smith, 1973). In analyzing their data these authors estimated particle temperatures by a steady-state energy balance using the measurements of reaction rates and gas and wall temperatures. Ayling and Smith (1972) used two-color pyrometry to determine directly the temperature of a stream of burning particles and found fair agreement between measured and calculated temperatures. Such measurements and calculations involve averages over many particles which, even when carefully sized, can differ considerably in shape, density, mineral content and other properties. This averaging is quite reasonable from the engineering point of view but it introduces an as yet unexplored uncertainity in the reported apparent or intrinsic reaction rate parameters.

More recently various workers have been able to measure the temperature of individual burning particles by two-color pyrometry (McLean *et al.*, 1981; Mitchell and McLean, 1982; Timothy *et al.*, 1982; Jorgensen and Zuiderwyk, 1985). The key element in this technique is the introduction of an extremely dilute stream of particles into the reactor so that the optical volume sampled by a pyrometer

equipped with a very sensitive detector, contains a single particle. The measurements involve either a particle at a particular location along the furnace, *i.e.* at a particular instant during its burning history (McLean *et al.*, 1981; Mitchell and McLean, 1982), or the complete temperature-time history of the particle (Timothy *et al.*, 1982; Jorgensen and Zuiderwyk, 1985). The interpretation of single particle temperature-time traces using some suitable particle combustion model requires specification of particle properties. As mentioned earlier, these properties vary considerably from particle to particle and this variation poses a major problem in the analysis of the data. The experimental technique of Mitchell and McLean (1982) provides simultaneous information about particle size and particle temperature at a fixed location but is not applicable in its present form to the measurement of a complete temperature-time trace.

In this paper we report measurements of temperature-time traces of single char particles derived from a narrow sieve cut. A particle combustion model is then used to analyze the temperature traces and estimate the apparent combustion rate parameters. The analysis uses a simple approach to account for the random particle-to-particle property variation.

4.2 Experimental Procedure

4.2.1 Char Formation

Chars were made from one high-volatile A bituminous coal (PSOC 1451) and one lignite coal (PSOC 1443). The coals were ground in a mechanized mortar and pestle grinder in air for approximately 30 seconds and then sieved on a mechanical shaker for 10 minutes into the following size fractions: less than 45μm, 45 - 53μm,

53 - 74μm, 74 - 104μm, 104 - 125μm and greater than 125μm. Chars were then generated from the 53 - 74μm size fraction of coal.

The coals were pyrolysed in an electrically heated drop tube furnace. The furnace consists of an alumina tube of 5 cm. internal diameter heated by Kanthal heating elements placed in a radiation cavity 20 cm. long. Coal particles were entrained in a stream of nitrogen at rates of 2 g/hr using the syringe pump feeder arrangement described by Senior and Flagan (1984) and were injected into the alumina tube through a wide bore (1 cm) water cooled injector. Furnace wall temperatures were measured by thermocouples attached to the outside of the alumina tube. Gas temperatures were measured using a suction pyrometer. The carrier gas flow rate was adjusted to achieve residence times of 2 seconds. The devolatilization loss for the coals ranged between 30-50%, depending on the coal type.

The chars were collected on a filter. To eliminate any tars that might have condensed, the chars were washed repeatedly with tetrahydrofuran and then dried at room temperature for 1 hour. Finally the tar-free chars were sieve-classified into the following size fractions: less than 45μm, 45 - 53 μm, 53 - 90 μm, 90 - 104 μm, 104 - 125 μm, 125 - 147 μm and greater than 147 μm. A few chemical and physical characteristics of the coals are given in Table 4.1. Some properties of the derived chars are shown in Table 4.2.

4.2.2 Optical Pyrometry

The temperature of the burning char particles was measured by two-color optical pyrometry in the near infrared. The radiation from the burning particles was focussed onto a bifurcated optical fibre and transmitted to two silicon photodetectors

via medium band (70nm) filters centered at 800 and 1000nm. The voltage signals from each channel were read by a high speed, computerized data acquisition system. Details of pyrometer construction are given elsewhere (Levendis and Flagan, 1987). By using Planck's law of radiation the temperature of each particle can be deduced from the ratio of the two signals as a function of time. The system was calibrated at the melting point of pure platinum (2045 K). The pyrometer was aligned along the direction of flow of the particles and thus was able to 'see' each particle for its entire burning history.

4.2.3 Experimental Conditions

Experiments were carried out with char particles of different sizes at various wall temperatures and in different ambients. For the bituminous coal (PSOC 1451), char sizes 45-53 and 104-125 μm were used. Both fractions were derived from sieving the char produced from the 53-74 μm coal fraction. Char sizes of 45-53 μm and 53-74 μm were derived from 45-63 μm and 63-75 μm fractions of raw lignite, respectively. Ambients were air and 50% O_2 for the bituminous char and air for the lignite char. Wall temperature was varied from 1000 K to 1500 K. In all cases the gas velocity was roughly 0.1 m/s, so the particles burned within a few millimeters after igniting. Since the distance between the point of injection and the detector was 0.3 m., the detector effectively saw 'stationary' particles.

4.3 Experimental Results

4.3.1 Temperature versus Time Traces

Intensity-time traces were measured for at least twenty particles for each set of

experimental conditions. Figures 4.1a-d show the intensity-time traces and the calculated temperature-time traces for a few particles. The temperature-time traces show widely different qualitative behaviour from particle to particle. While some burn at almost constant temperature (Figure 4.1a), many particles show temperature maxima (Figure 4.1b) or even monotonic behavior, both increasing (Figure 4.1c) and decreasing (Figure 4.1d). This variability is particularly pronounced in the case of the bituminous char. Temperature traces for lignite char showed maxima at intermediate times in most cases.

4.3.2 Data Analysis

The observed variability of the temperature-time traces is due partly to experimental error and partly to the variability in the initial properties of individual particles: size or shape, density, pore structure, maceral and mineral content. Pyrometry measurements on uniform spherical particles of synthetic char (Levendis, 1987) using the same reactor and pyrometer have yielded much more uniform traces of intensity and temperature. Most of the observed variation in the traces of the bituminous and lignite chars must, therefore, be due to differences in the properties of individual particles.

The obvious approach to estimating combustion rate parameters from a set of temperature traces is to postulate a spherical particle having average size, density etc. and to assign to that particle a single temperature-time trace obtained by averaging the measured individual traces. This straightforward approach would entail loss of the detailed information contained in the individual traces. Moreover, calculating an 'average' trace is not very meaningful because of the different

burnout times of the individual traces. In this study we have followed a different approach whereby the rate parameters are estimated from the individual temperature traces treating the properties of individual particles as random variables. While the particle-to-particle variation involves several properties, the level of experimental accuracy and the need for mathematical tractability suggests a highly simplified approach. We assume that the properties of the i^{th} particle are characterized by two random variables: its initial radius, r_{0i}, assuming spherical shape, and the apparent Arrhenius pre-exponential factor A_{ai}. The apparent reaction rate is assumed to be of the form

$$R_a = A_a e^{-E_a/RT} p_s^m \tag{4.1}$$

This is based on the external surface area of the particle. The reaction order, m, is assumed to be one, but other types of kinetics can be treated without difficulty.

Using an effective radius (i.e. assuming spherical particles) is a clear necessity in view of the impracticability of carrying out mathematical calculations for particles of irregular and unknown shape. The second random variable A_a is assumed to account for particle-to-particle variations in reactivity and porosity, the latter affecting A_a (and not E_a) as discussed by Gavalas (1981). Variations in mineral and maceral content affect E_a as well as A_a. Nevertheless, the accuracy of the data does not warrant using more than one or two parameters that vary from trace to trace. Therefore, we have treated E_a as an unknown parameter common to all traces. The other properties of the particle, namely density, heat capacity, and mineral content are treated as known constants. Under these assumptions, the temperature

of the i^{th} particle may be expressed as

$$T_i(t) = f(t; E_a, A_{a_i}, r_{0_i}) + \epsilon_i(t) \tag{4.2}$$

where $\epsilon_i(t)$ is the error in the measurement of the temperature. The dependence on the known properties (e.g. particle density and heat capacity) is not shown explicitly. The function f is defined by some suitable combustion model. The model that has been used in the present study is discussed briefly in the following section.

The analysis of the data proceeds as follows. For each trace we define a quantity

$$J_i = \sum_{j=1}^{n} [f(t_j; E_a, A_{a_i}, r_{0_i}) - T_i^{exp}(t_j)]^2 + w(\bar{r}_0 - r_{0_i})^2 \tag{4.3}$$

where the first term represents the deviation of experimental and calculated temperatures over a suitable discrete set of times and the second term represents the deviation of the random radius from the known mean radius (the mean of the appropriate sieve size cut). The weighting coefficient w must be chosen in accordance with the expected error in the temperature measurement ($\epsilon_i(t)$) and the spread in particle size. It is given by $\sigma_T^2/\sigma_{r_0}^2$ where σ_T is the standard deviation in the particle temperature measurement and σ_{r_0} is the standard deviation in the initial radius measurement. The error in the temperature measurement can be calculated from the spread observed over many calibration runs. It was taken as $\sigma_T \sim 50$K. The experimental error in the radius measurement was calculated by two independent means: (i) from optical size measurements over many particles (ii) from ASTM sieve standards for wire mesh sieves. Both methods give similar results, $\sigma_{r_0} \sim 12\mu m$. The values of A_{a_i} and r_{0_i} that minimize J_i are denoted by $A_{a_i}^*$ and $r_{0_i}^*$. We also denote

by J_i^* the minimum value of J_i. The three quantities A_{ai}^*, r_{0i}^*, and J_i^* are clearly functions of E_a.

We now calculate the minimum with respect to E_a of the quantity

$$Q = \sum_{i=1}^{N} J_i^*(E_a) \tag{4.4}$$

obtained by summing over all N traces. If we denote by $\hat{E}_a$ the minimizing value of E_a then the quantities

$$\hat{r}_{0i} = r_{0i}(\hat{E}_a) \tag{4.5}$$

$$\hat{A}_{ai} = A_{ai}(\hat{E}_a) \tag{4.6}$$

are the best estimates of radius and pre-exponential factor for the i^{th} particle. A mean preexponential factor can then be defined by the arithmetic mean

$$\bar{A}_a = \frac{1}{N} \sum_{i=1}^{N} \hat{A}_{ai} \tag{4.7}$$

A mean particle size is not needed since this can be directly determined by simple observation. However, comparision of the range of $\hat{r}_{0i}$ values with the directly observed range of particle sizes provides a general consistency check.

The cumulative sum Q of the J_i's over all particles versus activation energy is shown in Figure 4.2: Figures 4.2a and 4.2b show the minimization with respect to E_a for the bituminous char and lignite char, respectively. The estimated apparent rates for these two chars are given by

$$R_a = 107.1 \exp\left(-17000/RT\right) \quad \text{gcm}^{-2}\text{s}^{-1}\text{atm}^{-1} \tag{4.8}$$

$$R_a = 20.8 \exp\left(-14000/RT\right) \quad \text{gcm}^{-2}\text{s}^{-1}\text{atm}^{-1} \tag{4.9}$$

The estimated apparent activation energy for the bituminous char is in good agreement with that reported by Field (1969) but lower than the value of 21400 cal/gmole that follows from the collective correlation given by Smith (1982). The apparent activation energy for the lignite char is somewhat lower than the value of 16300 cal/gmole that is obtained from Australian brown coal chars reported by Smith and Tyler (1974). The values for preexponential factors reported here are arithmetic means over many traces. The spread of these factors was rather large, as shown in the histograms given in Figures 4.3a and 4.3b. A similar, though smaller spread of values was obtained for the estimated particle diameters. The average of the diameter estimates was 45μm for the lignite char and 57μm for the bituminous char. Taking into account the irregular shape of the particles, the estimated equivalent sphere diameters are in fair agreement with the sieve sizes (45-53μm) and the sizes observed by microscopy.

4.4 Particle Combustion Model

4.4.1 Model Description and Comparision with Experimental Data

The particle combustion model described by Loewenberg *et al.* (1987) was employed for the calculations after being extended to include the effects of ash. The ash is initially uniformly distributed throughout the particle, but as the carbonaceous material is oxidized, the exposed ash particles accumulate on the surface as a porous layer of increasing thickness. Scanning electron microscopy of individual particles at various conversions has shown the accumulation of ash but does not exclude the possibility of some ash loss to the gas phase. The ash layer is assumed to add a mass transfer resistance in series with the resistance across the film or boundary layer

around the particle. However, it does not create an additional thermal resistance. To calculate the resistance to mass transfer, the ash layer is regarded as a stagnant packed bed with effective diffusivity equal to the bulk gas phase diffusivity multiplied by the ash layer void fraction (~0.4) and divided by a tortuosity factor (~2).

The complete particle combustion model includes a detailed description of intraparticle diffusion and pore growth. However, the calculations reported here used a limiting form of the model wherein the reaction takes place in a thin outer shell (Gavalas (1981); Loewenberg *et al.* (1987)). Simulations have shown that this limiting form of the model is adequate for the range of particle temperatures encountered in the experiments. In this case the mass and energy balances can be written as

$$\frac{d}{dt}\left[m_c + m_{ash}\right] = -4\pi r^2 R_a \tag{4.10}$$

$$\frac{d}{dt}[\{m_c C_{pc} + m_{ash} C_{p_{ash}}\}T] = 4\pi r^2 \{R_a \Delta H - e_c - e_r\} \tag{4.11}$$

where r is the radius of the particle including the ash layer; m_c, C_{pc} and m_{ash}, $C_{p_{ash}}$ are mass and heat capacity of the total carbon and the total ash within the particle; R_a is the apparent rate; ΔH is the heat of the combustion reaction; and e_c, e_r are heat fluxes from the particle by conduction and radiation, respectively. The radiative term was based on a constant overall emissivity without provision for any effects of the accumulating ash. The apparent rate R_a depends on the intrinsic kinetics as well as on the pore structure of char (Gavalas (1981); Loewenberg *et al.* (1987)). From the standpoint of parameter estimation, however, all that is needed is a functional form as given by Eq.(4.1) where A_a and E_a are treated as apparent rate parameters.

Equations (4.10) and (4.11) are coupled to the equations of diffusion and heat transfer from the particle surface to the free stream. The latter equations, which include Stefan flow and temperature dependent properties are given in Lowenberg *et al.* (1987). The coupled system of equations is solved to yield the radius and temperature of the particle and the oxygen partial pressure p_s at the surface of the particle, all as functions of time.

Sample comparisions between calculated and experimental temperatures are shown for two particles in Figures 4.4a and 4.4b. For each particle the calculated curve was obtained using the optimal parameters $\hat{E}_a$, $A_{a_i}(\hat{E}_a)$, and $r_{0_i}(\hat{E}_a)$. The fits are good, indicating the ability of the simple model to describe particle combustion using the estimated rate parameters.

4.4.2 Parametric Studies

Calculations were carried out to determine the effect of various properties on the particle temperature. Figure 4.5a shows that the predominant effect of increasing initial particle size is to increase the burn time and slightly decrease the maximum temperature. The increase in burn time varies approximately as the square of the particle radius as expected from the 'shrinking core' particle combustion. Increasing the apparent density of the particle (Figure 4.5b) increases only the burn time and does not affect the maximum temperature reached. The presence of ash affects the shape of the temperature trace dramatically (Figure 4.5c). At high conversions, the particle consists mainly of ash so that its thermal inertia is higher and, hence, its temperature does not fall as quickly as it would have if ash was not present. The effect of carbon emissivity (Figure 4.5d) is straightforward: for a fixed wall

emissivity, a particle with higher carbon emissivity burns at a lower maximum temperature due to increased radiative loss. However, the decrease in temperature is not dramatic and the burn time increases only marginally. The most dramatic effect on the temperature-time traces are caused by changing the reaction rate parameters. For example, the effects of the frequency factor at constant activation energy are shown in Figure 4.5e.

4.5 Conclusions

Single particle temperature-time traces measured by optical pyrometry show considerable variability due to different size, shape, pore structure and mineral content of individual particles. A novel technique is introduced to analyze the traces by treating size and preexponential factor of each particle as random variables. This technique was used in conjunction with a particle combustion model assuming that the heterogenous reaction is limited to a thin surface layer of the particle in order to estimate the apparent kinetic parameters. The estimated values of the apparent preexponential factor varied significantly from particle to particle. Using the estimated parameters provided good agreement between calculated and experimental temperature-time traces.

4.6 Acknowledgements

This work was supported by the U.S. Department of Energy under contract DE-AC2284FC70915. The authors also wish to thank Dr. Yiannis Levendis for help with the pyrometry experiments.

References

1. Ayling, A.B., and Smith I.W. (1972). Measured temperature of burning pulverized fuel particles and the nature of the primary reaction product. *Combust. Flame* **18**, 173.

2. Field, M.A. (1969). Rate of combustion of size-graded fractions of char from a low-rank coal between 1200K and 2000K. *Combust. Flame* **13**, 237.

3. Gavalas, G.R. (1980). Analysis of char combustion including the effect of pore enlargement. *Comb. Sci. Tech.* **24**, 197.

4. Hamor, R.J., and Smith, I.W. (1973). Kinetics of combustion of a pulverized brown coal char between 830 and 2200K. *Combust. Flame* **21**, 153.

5. Jorgensen, F.R.A. and Zuiderwyk, M. J. (1985). Two-Color pyrometer measurement of the temperature of individual combusting particles. *J. Phys. E: Sci. Instrum.* **18**, 486.

6. Levendis, Y.A. and Flagan, R.C. (1987). Combustion of uniformly sized glassy carbon particles. *Comb. Sci. Tech.* **53**, 117.

7. Loewenberg, M., Bellan, J., and Gavalas, G.R. (1987). A simplified description of char combustion. *Chem. Eng. Comm.* in press.

8. McLean, W.J., Hardesty, D.R., and Pohl, J.H. (1981). Direct observations of devolatilizing pulverized coal particles in a combustion environment. *Eighteenth Symposium (International) on Combustion, the Combustion Institute*, 1239.

9. Mitchell, R.E., and McLean, W.J. (1982). On the temperature and reaction rate of burning pulverized fuels. *Nineteenth Symposium (International) on*

Combustion, the Combustion Institute, 1113.

10. Senior, C.L. and Flagan, R.C. (1984). Synthetic chars for the study of ash vaporization. *Twentieth Symposium (International) on Combustion, the Combustion Institute*, 921.
11. Smith, I.W. and Tyler, R.J. (1974). The reactivity of a porous brown coal char to oxygen between 630 and 1812K. *Comb. Sci. Tech.* **9**, 87.
12. Smith, I.W. (1982). The combustion rates of coal chars: a review. *Nineteenth Symposium (International) on Combustion, the Combustion Institute*, 1045.
13. Timothy, L.D., Sarofim, A.F., and Beer, J.M.,Nineteenth Symposium (International) on Combustion, the Combustion Institute, 1982, 1123.

	PSOC 1451		PSOC 1443	
RANK	HVAB		SUB-BIT C/ LIGNITE	
SAMPLE LOCATION	PENNSYLVANIA		TEXAS	
SEAM NAME	PITTSBURG		LOWER WILCOX	
PROXIMATE ANALYSIS (%) (AS REC'D)				
MOISTURE	2.54		28.54	
ASH	13.32		15.31	
VOLATILE MATTER	33.56		44.17	
FIXED CARBON	50.58		11.98	
ULTIMATE ANALYSIS (%)	AS REC'D	DRY	AS REC'D	DRY
ASH	13.32	13.67	15.31	21.43
CARBON	70.05	71.88	40.62	56.84
HYDROGEN	4.55*	4.67	2.92*	4.09
NITROGEN	1.33	1.36	0.76	1.06
SULFUR	1.33	1.36	0.53	0.74
CHLORINE	0.07	0.08	———	———
OXYGEN (DIFF.)	6.81*	6.99	11.32*	15.84
* EXCLUDES MOISTURE				
FREE SWELLING INDEX	7.5		0.0	

Table 4.1 Properties of parent coals.

Coal Rank	HVA Bituminous	Lignite
C(wt %)	78.3	59.6
H(wt %)	0.96	0.43
Ash(wt %)	19.1	36.4
Surface Area (m^2/g)	175*	235
Density (g/cm^3)	0.5	1.1
Pore Volume (cm^3/g)	0.4	0.5
Particle Diameter (μm)	45-53, 90-104	45-53, 61-74

* after 5% conversion at 450°C

Table 4.2 Properties of the Chars.

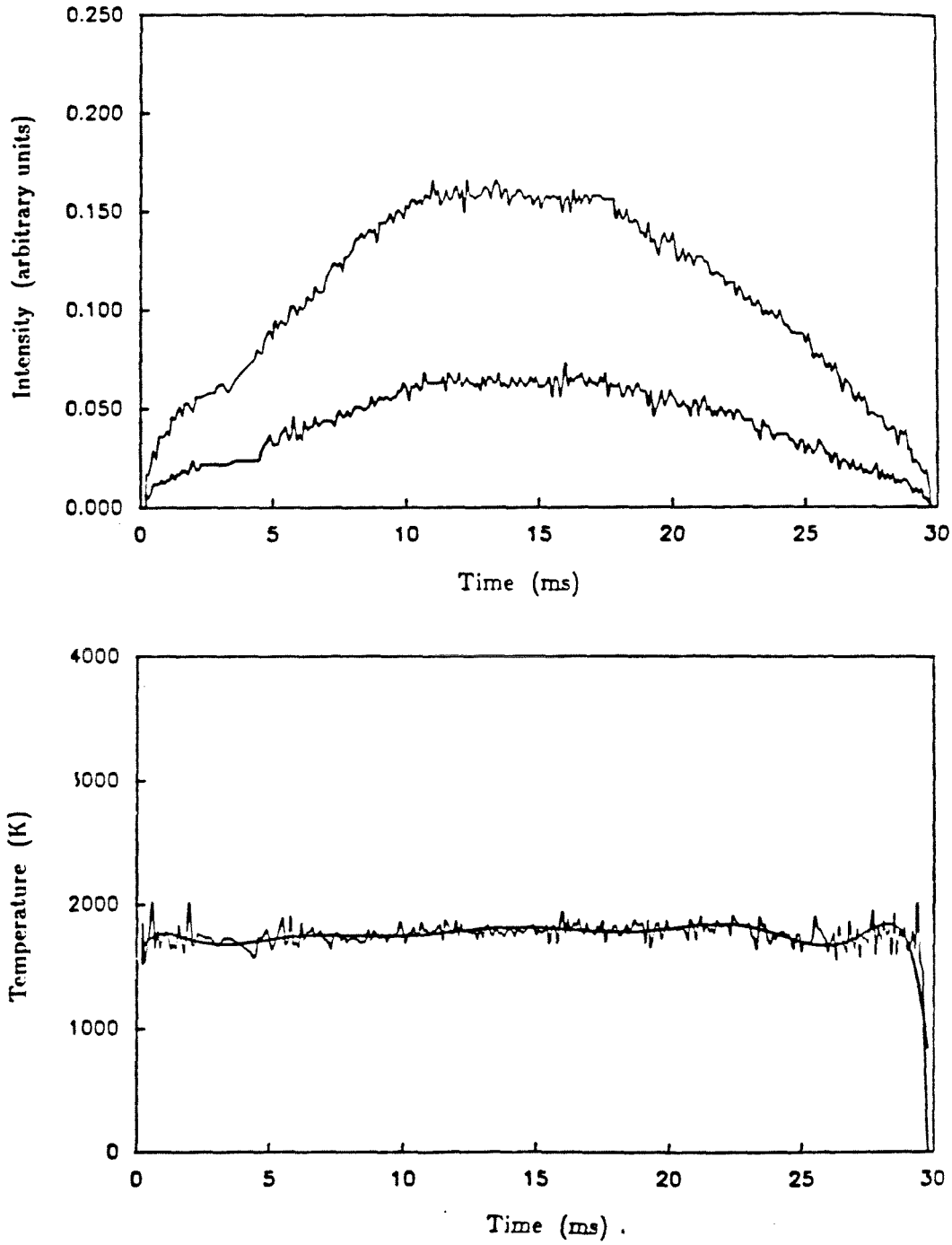

Figure 4.1a Intensity vs. Time and Temperature vs. Time during the combustion of one bituminous char particle in air at reactor wall temperature of 1450K.

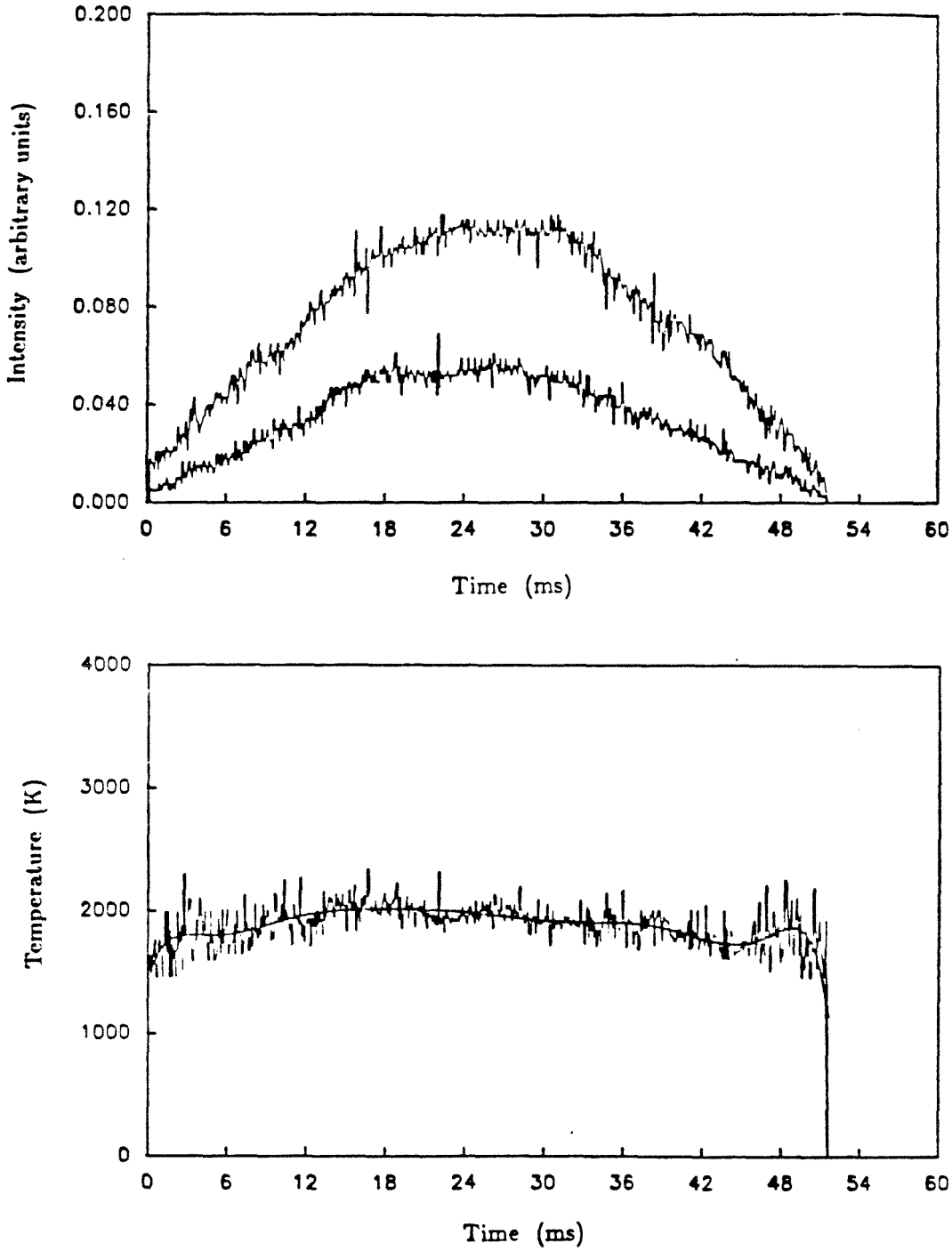

Figure 4.1b Intensity vs. Time and Temperature vs. Time during the combustion of one bituminous char particle in air at reactor wall temperature of 1450K.

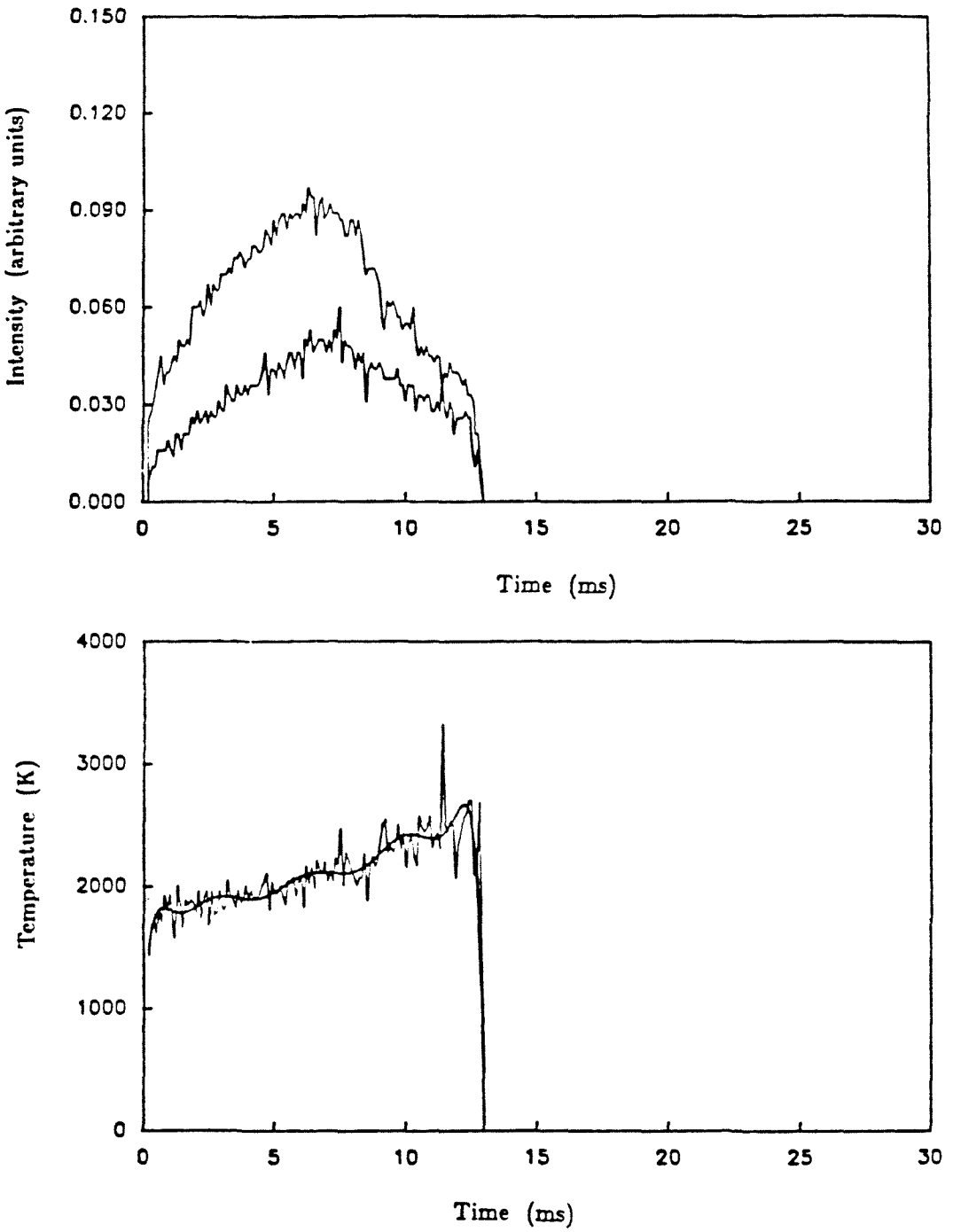

Figure 4.1c Intensity vs. Time and Temperature vs. Time during the combustion of one bituminous char particle in air at reactor wall temperature of 1450K.

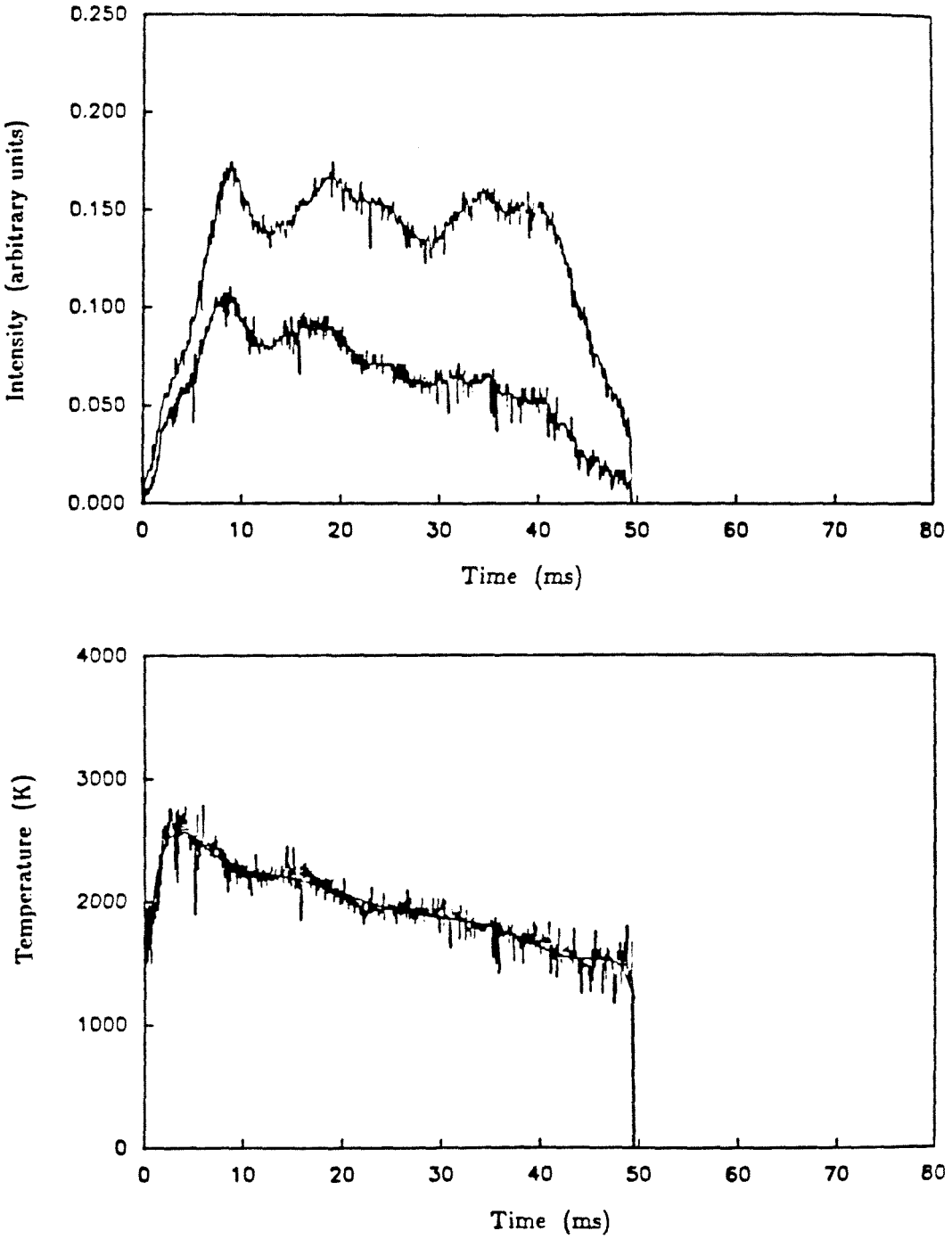

Figure 4.1d Intensity vs. Time and Temperature vs. Time during the combustion of one bituminous char particle in air at reactor wall temperature of 1450K.

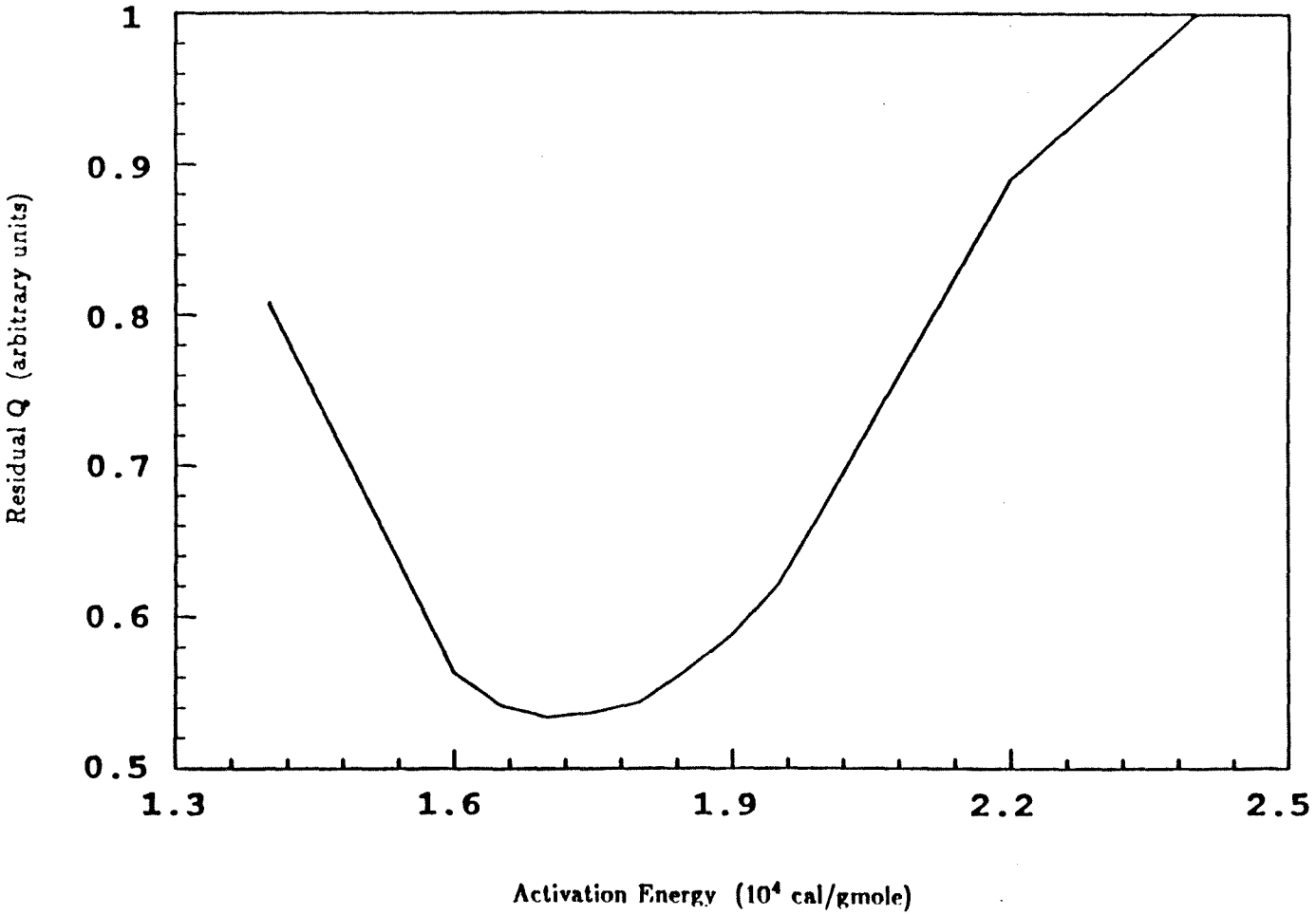

Figure 4.2a Minimization of the sum of residuals with respect to activation energy for bituminous char.

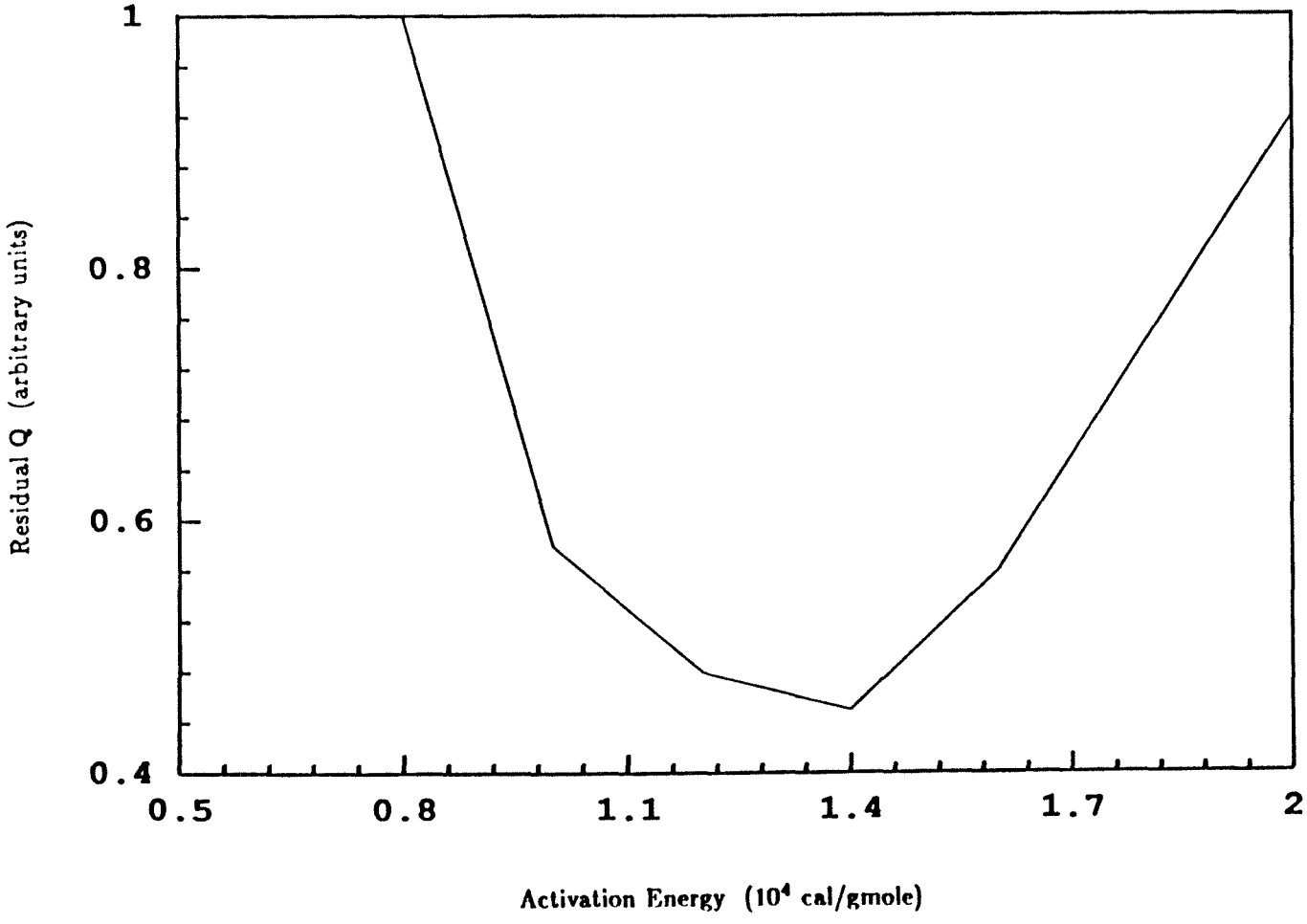

Figure 4.2b Minimization of the sum of residuals with respect to activation energy for lignite char.

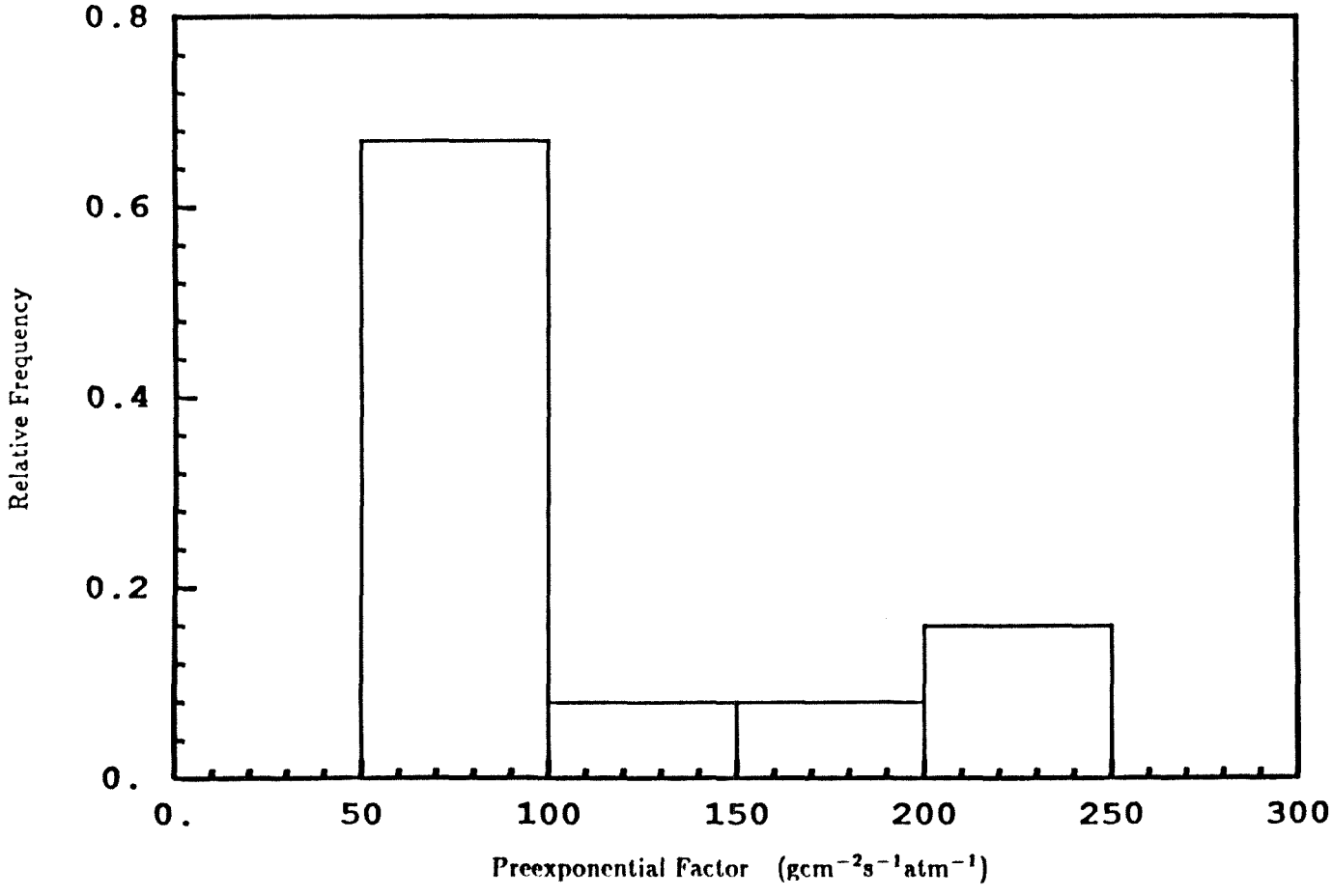

Figure 4.3a Histogram of pre-exponential factors for bituminous char.

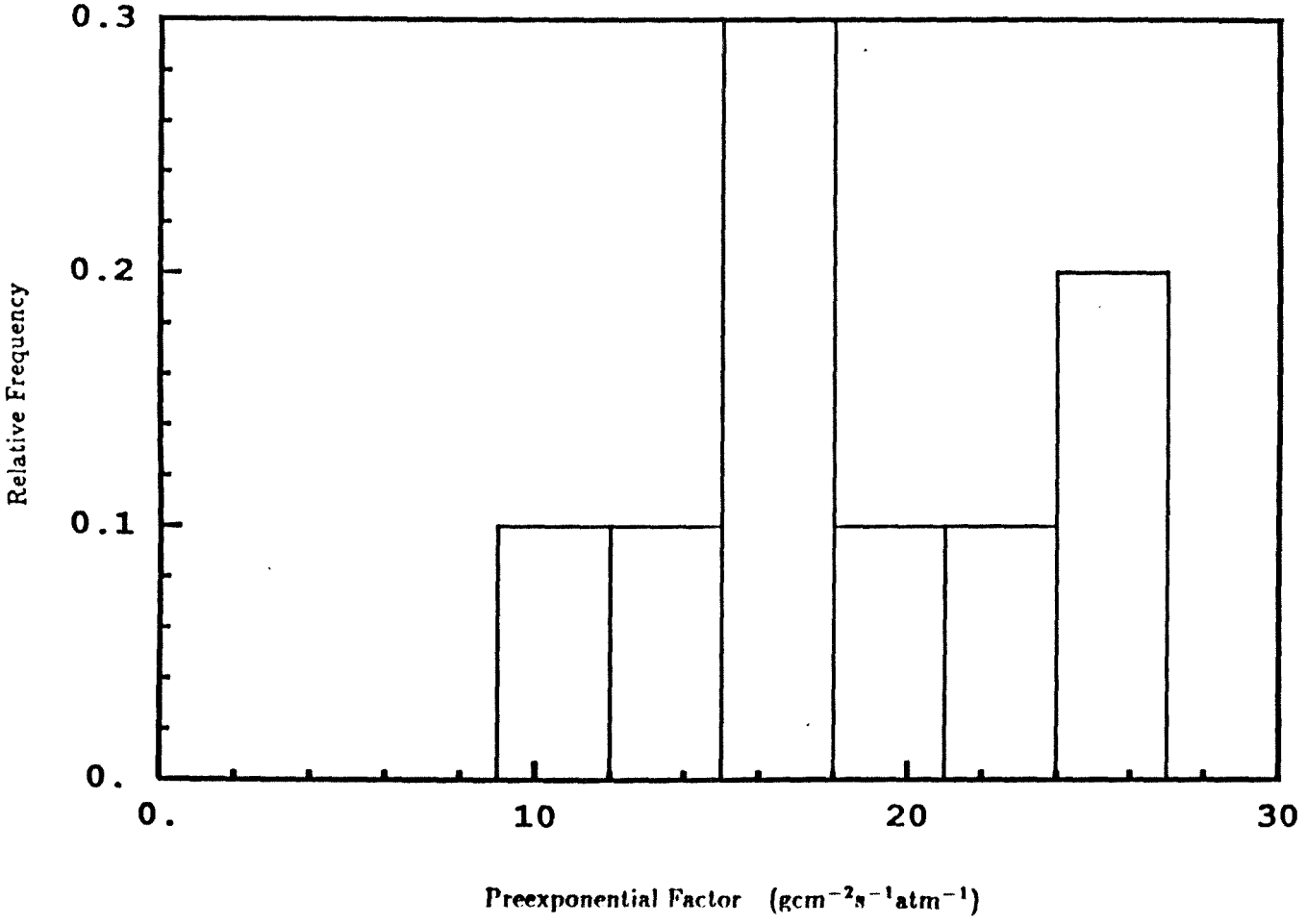

Figure 4.3b Histogram of pre-exponential factors for lignite char.

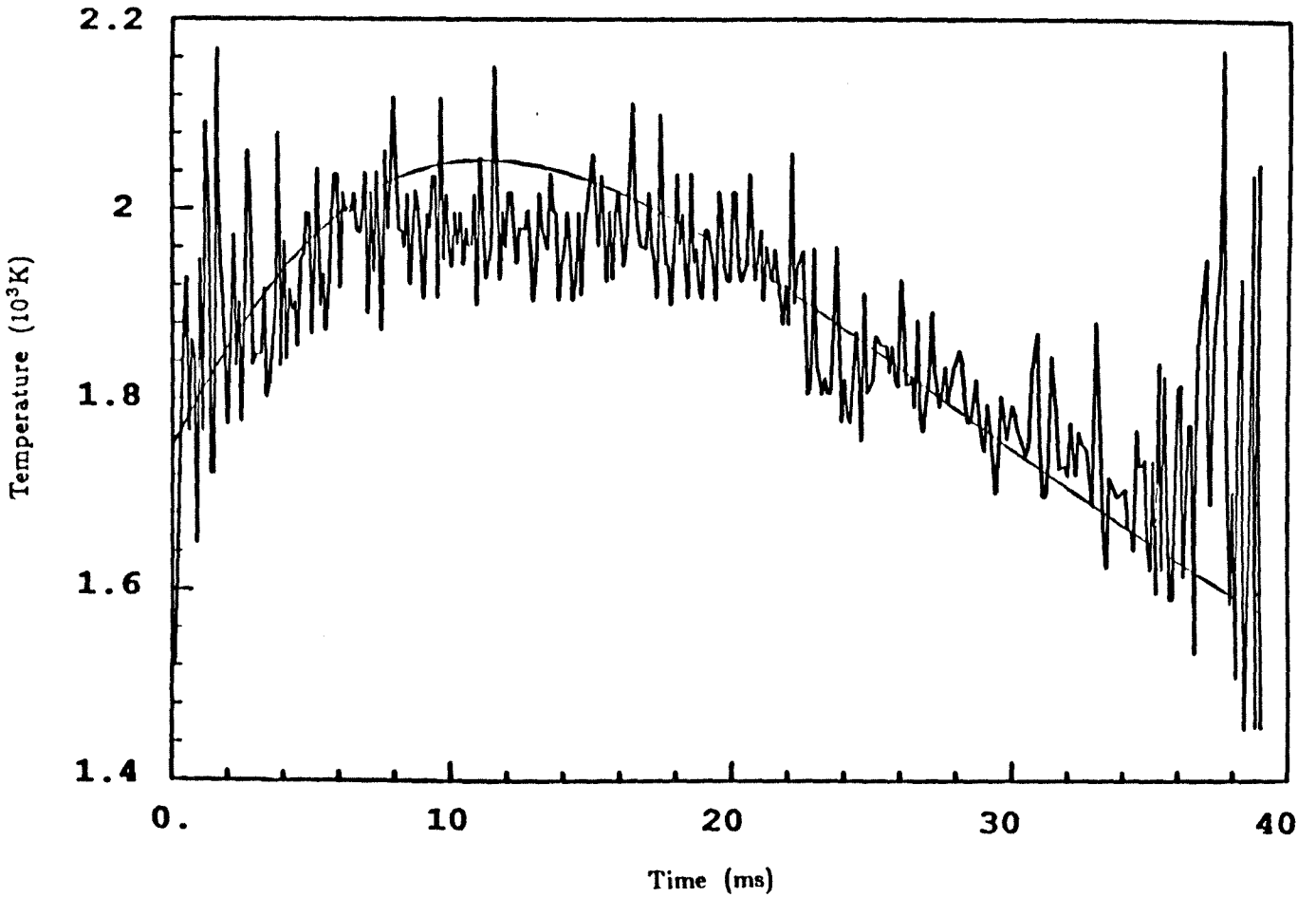

Figure 4.4a Comparision of experimental and calculated temperature-time history for a bituminous char particle.

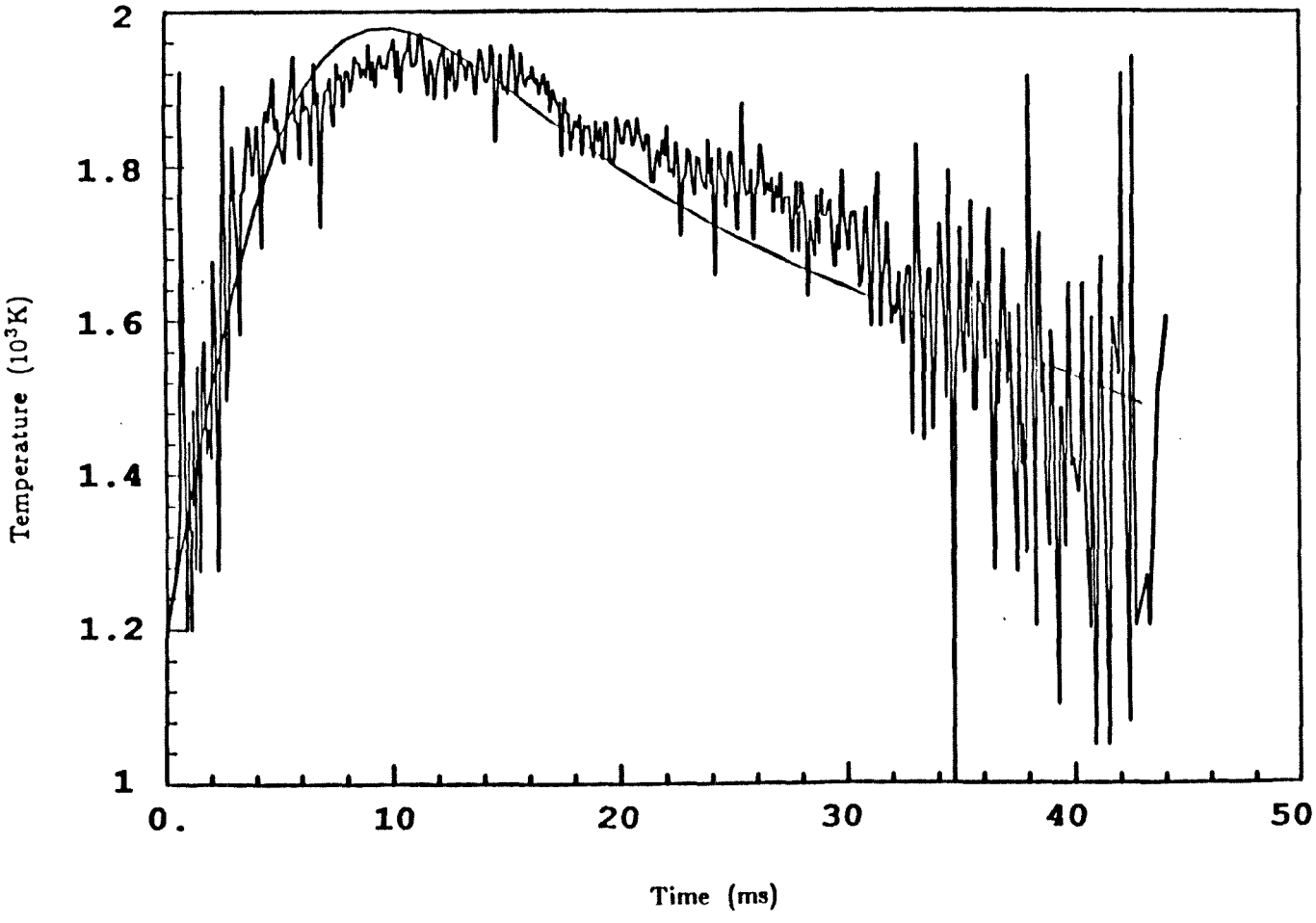

Figure 4.4b Comparision of experimental and calculated temperature-time history for a lignite char particle.

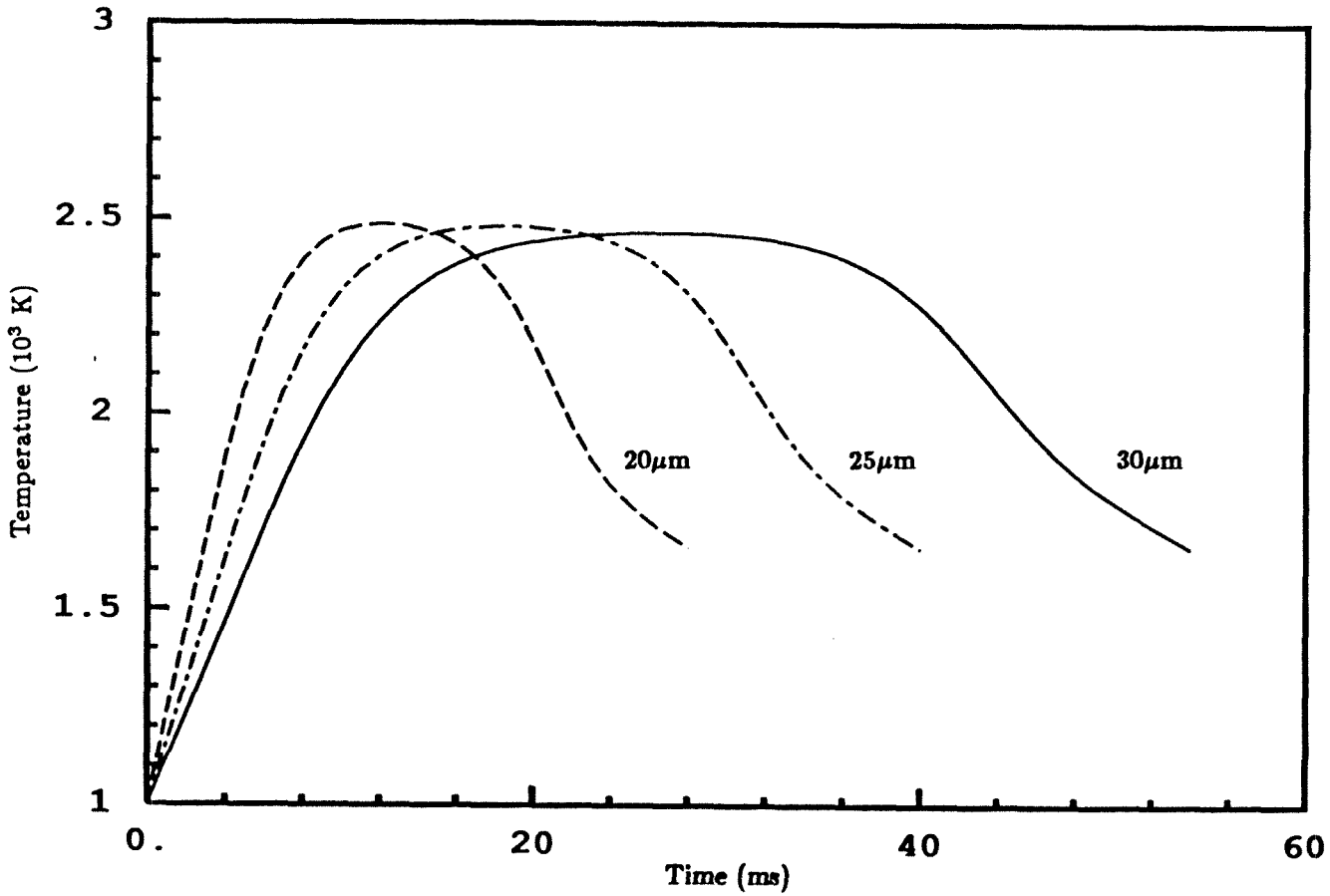

Figure 4.5a The effect of initial particle size as predicted by the model.

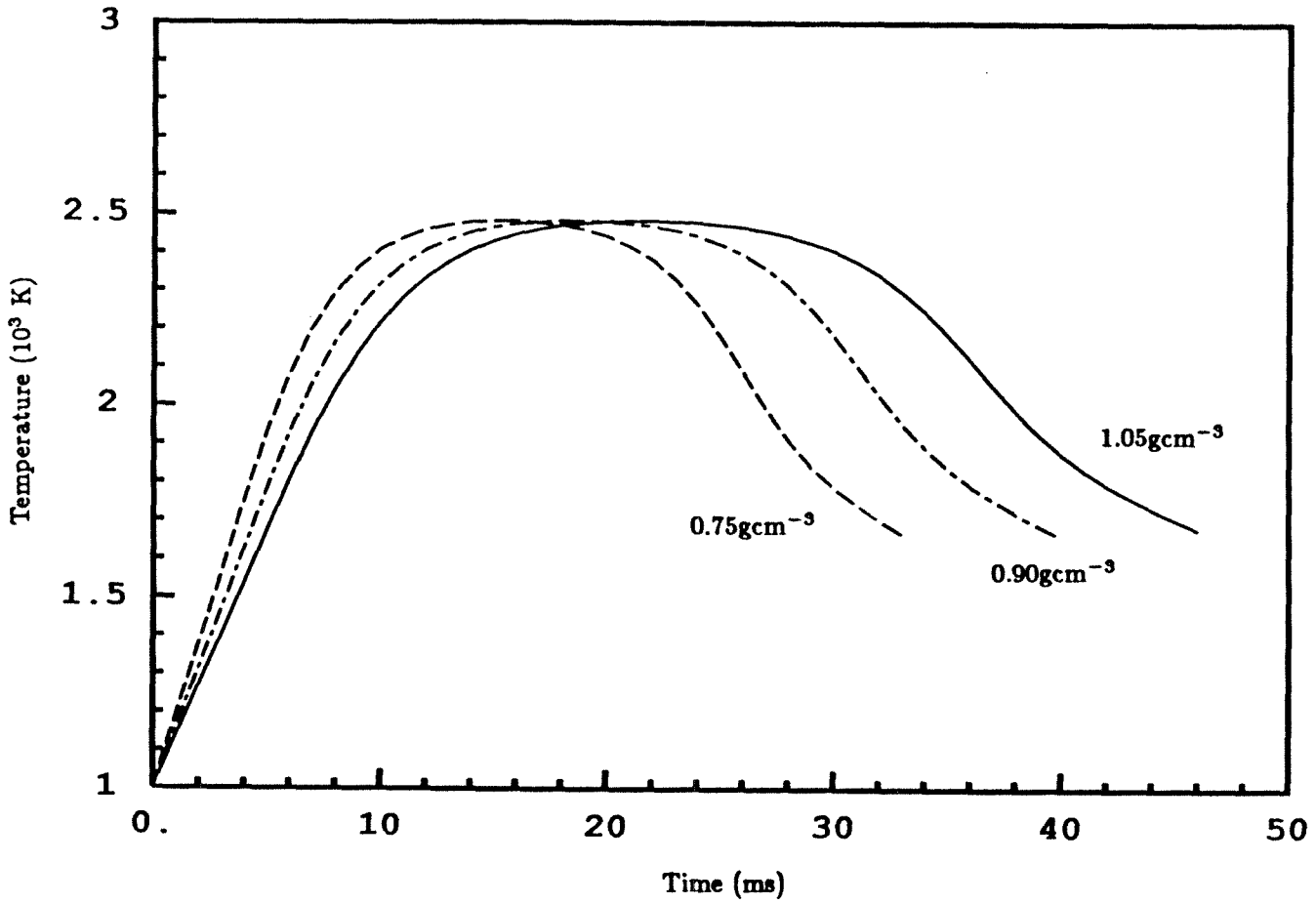

Figure 4.5b The effect of apparent particle density as predicted by the model.

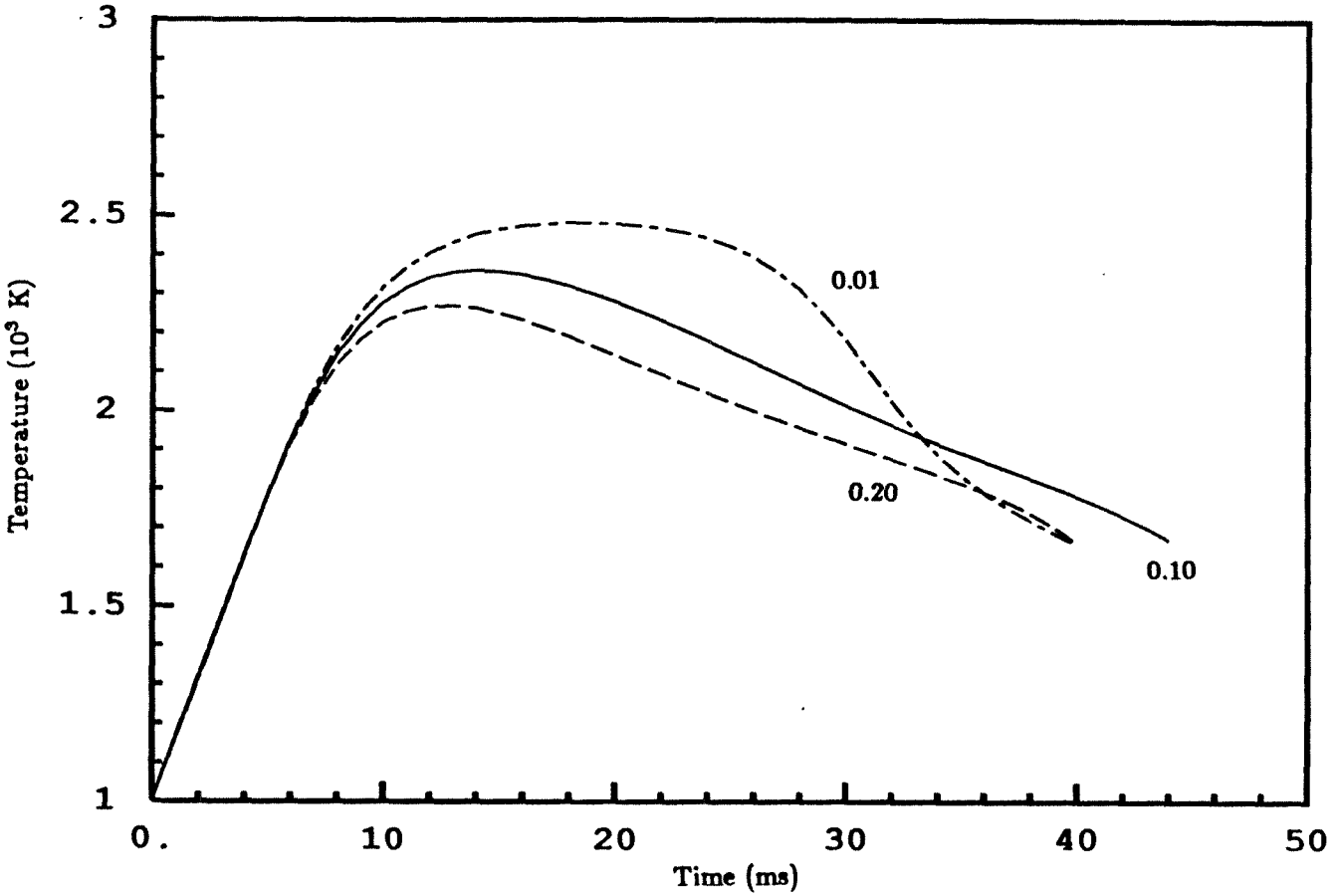

Figure 4.5c The effect of initial ash content as predicted by the model.

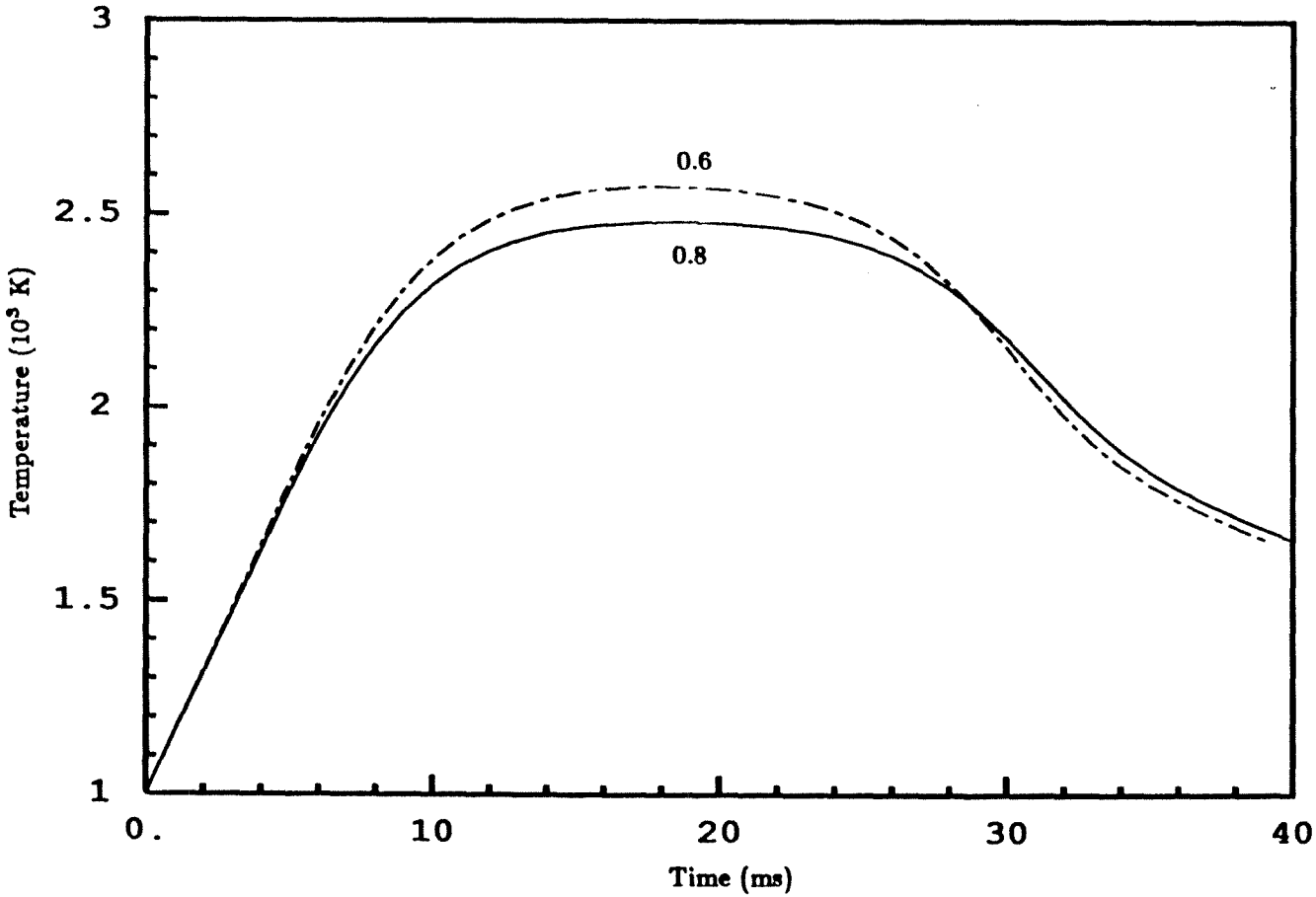

Figure 4.5d The effect of carbon emissivity as predicted by the model.

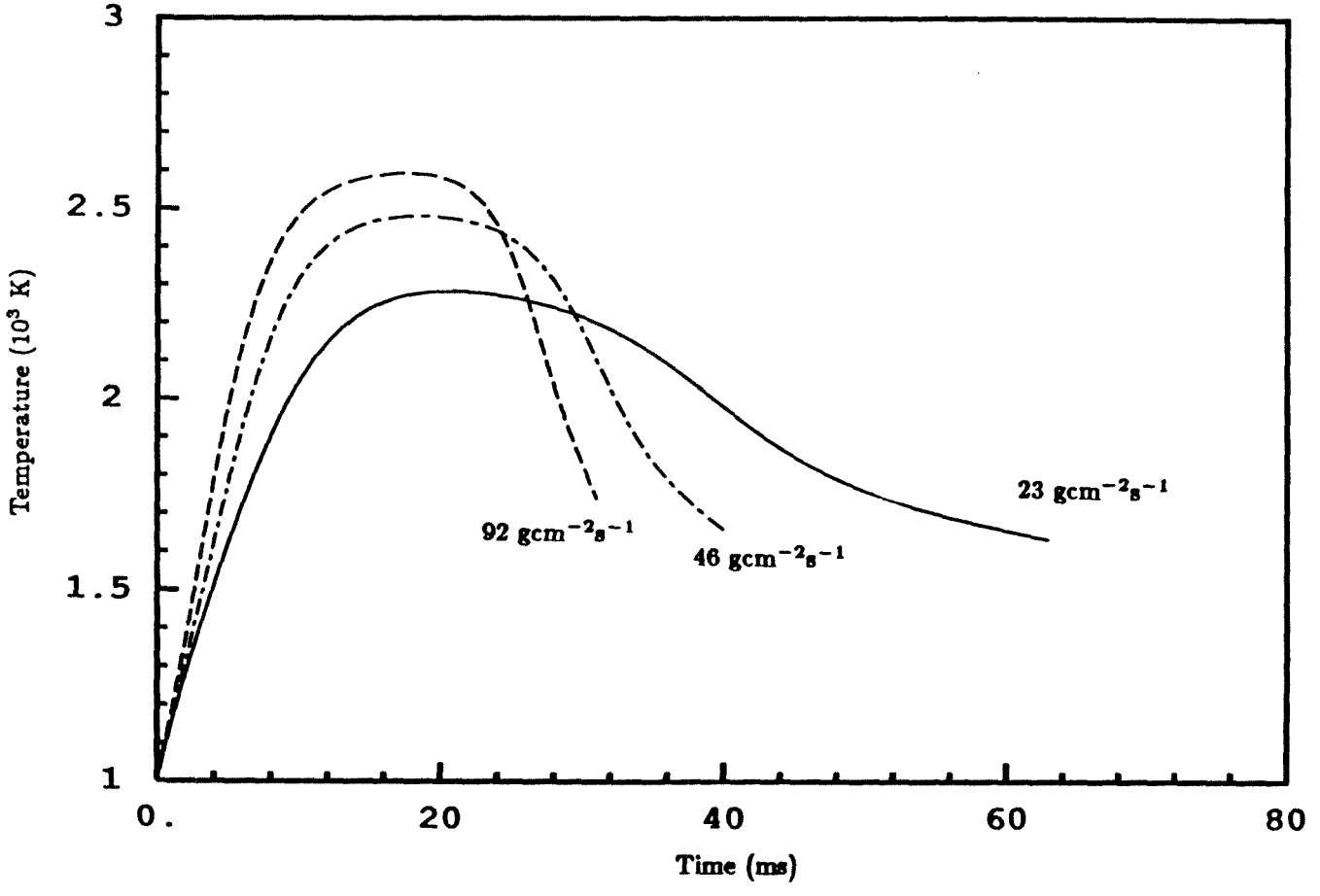

Figure 4.5e The effect of pre-exponential factor as predicted by the model.

Chapter 5

COMBUSTION OF CHARS AT HIGH TEMPERATURES

5.1 Introduction

Particle temperatures in large pulverized coal combustion systems are often greater than 1000K and may be in excess of 2000K. Many of the published measurements of coal or char combustion rates were made at temperatures much lower than this (Essenhigh, 1981; Tseng and Edgar, 1984). The low temperature data are useful and can be obtained with relative ease, but, given the complex nature of coal or char and the combustion process, it is not obvious that low temperature combustion data can be used to predict behavior at higher temperatures.

The entrained flow reactor is the most common experimental system for the study of high temperature pulverized char combustion. Measurements typically made in combustion experiments include (*i*) carbon conversion and characterization of physical properties (size, density, etc.) of partially burned char withdrawn at the reactor outlet or at intermediate axial positions using a cooled probe (*ii*) reactor wall temperature and gas temperature at various axial locations (Field, 1969; Hamor and Smith, 1973).

Prior to understanding combustion behavior, it is imperative that the physical and structural changes of the char be well characterized. This chapter describes experiments that were carried out to physically characterize bituminous chars combusted at high temperatures. These results are then compared to those from similar experiments done on the same chars combusted at lower temperatures.

5.2 Experimental Procedure

5.2.1 Char Formation

Chars were made from PSOC 1451. The chemical and physical properties of this coal are summarized in Table 5.1. The coal was ground in a mechanized mortar and pestle grinder in air for approximately 30 seconds and then sieve classified on a mechanical shaker for 10 minutes. Chars were generated from the 53 - 74μm size fraction of the coal.

The coal was pyrolysed in an electrically heated drop tube furnace. The furnace consists of an alumina tube of 5 cm. internal diameter heated by Kanthal Super 33 heating elements placed in a radiation cavity 20 cm. long. Coal particles were entrained in a stream of nitrogen at rates of 2 g/hr using a syringe pump feeder and were injected into the alumina tube through a wide bore (1 cm) water cooled injector. The furnace wall temperature was maintained at a temperature of approximately 1650K, in order to achieve gas temperatures of 1600K. Furnace wall temperatures were measured by thermocouples attached to the outside of the alumina tube. Gas temperatures were measured using a suction pyrometer. Based on wall and gas temperatures the particle temperature was deduced from a steady state thermal energy balance. The carrier gas flow rate was adjusted to achieve residence times of about 2 seconds. The mass loss during devolatilization of the coals ranged from 30-40%, depending on the coal particle size.

The char particles were collected on a filter. To eliminate any tars that might have condensed, the chars were washed repeatedly with tetrahydrofuran and then dried at room temperature for 1 hour. Finally, the tar-free chars were sieve-classified

into the following size fractions: less than 45μm, 45 - 53μm, 53 - 90μm, 90 - 104μm, 104 - 125μm, 125 - 147μm and greater than 147μm. The 45-53μm and 90-104μm char size fractions were used for the combustion studies described in this chapter.

Combustion experiments were performed in the high temperature flow reactor shown in Figure 5.1. Preheater wall temperatures of 1475K and 1675K were used to heat the primary air stream. However, due to heat losses in the section between the pre-heater and the reactor, the gas temperature at the entrance to the reactor was lower. The particle temperature was measured by a split-beam two-color optical pyrometer. Particle temperatures were generally higher than the gas temperature at the same axial location. For each value of the pre-heater wall temperature, partially burned particles were collected for analysis at three axial locations using a moveable water-cooled, N_2-quenched collection probe. The residence time upstream of the collection point in the reactor was also estimated in each case by knowing the velocity of the laminar carrier gas flow. The collected samples were then analyzed as described in a later section.

5.2.2 Experimental Conditions

Experiments were carried out using two sizes of char particles at two reactor temperatures. Char sizes of 45-53 and 90-104μm were used. The first two sets of experiments were performed at a preheater wall temperature of 1475K using the two char sizes. For the third set of experiments, the preheater temperature was 1675K, and the initial char size was 90-104μm. In the first two sets of experiments the gas velocity was roughly 0.7 m/s. In the last set it was about 0.9 m/s. In all cases the particles travelled several centimeters before burning out. Partially

burned samples were collected at three different axial locations. While every effort was made to collect samples of widely differing conversions, *a priori* control of conversion at the sampling locations was not possible. The quantities of char collected were small since the original samples were themselves small due to the narrow size cuts chosen.

5.2.3 Particle Temperature Determination

The particle temperatures as a function of axial location were measured in a dilute stream using the two-color pyrometer. The detector optics was mounted on a 3-degree of freedom translator so that any volume in the test section could be probed. The pyrometer was focussed at the center of the particle stream on the axis of the reactor. The whole assembly was moved vertically to the desired axial location. The view volume of the detector optics was about 0.4 to 0.8 millimeters at its narrowest. At the flow rates used, the particle residence time in the view volume was 0.3 to 0.6 ms. Since the view volume was so small, and the particle stream so dilute, the probability of more than one particle occupying the view volume at the same time was negligible. A high-speed data accquistion system was used to gather the temperature data. Average particle temperatures were determined by observing many particles at each location. The pyrometer was calibrated using a Type S thermocouple bead placed in the hot gas flow within the view volume of the detector optics.

Table 5.2 shows the average particle temperatures measured in each case. The spread of measurements as well as the average is shown. The temperature data are consistent with model predictions that the temperature of the particles remains

reasonably constant over the burnout period. The drop in temperature at the highest conversions is attributed to heat losses from the test section since it was not completely insulated. The particle temperatures of the 1675K preheater wall temperature samples are smaller than the 1475K case because they were collected further downstream than the latter and thus suffered more heat losses. Given the uncertainities in calibration and measurement, it is impossible to infer minor trends with conversion. The data suggest that the particle temperature was approximately constant throughout the combustion process for each case.

5.2.4 Collection of Partially Oxidized Chars

A water-cooled probe was used to collect the partially oxidized material. The particles were quenched with a large flow of nitrogen to ensure that oxidation did not take place in the probe and on the filter downstream. A schematic diagram of the collector is shown in Figure AIV.6 (Appendix IV).

5.3 Conversion Determination

The single most important variable in characterizing the partially oxidized samples is the carbon conversion or burnoff. The conversion is most commonly determined gravimetrically from mass measurements made before and after combustion. Assuming that there are no sampling losses the extent of conversion is easily estimated. However, in most cases sampling losses are unavoidable so this method is relatively inaccurate.

In the present system, while most of the particle stream was captured, there were thermophoretic losses at the cold entrance region of the collector. These losses

are difficult to estimate. Therefore, the ash was used as a tracer to estimate the quantity of carbon represented by a particular char sample. This assumes that the ash is not lost due to devolatilization during char formation. Even at combustion temperatures, volatilization is minimal, amounting to less than a few percent of the ash (Flagan and Friedlander, 1978). Since the chars were made at 1600K, ash volatilization is expected to be a very small correction. Thus the ash-tracer technique is well suited for measuring carbon conversion in chars used in this study. The drawbacks of this method are that the char sample must be destroyed to determine the ash content and that, for reasons of accuracy, the sample size should be as large as possible. Therefore, all char characterization tests were performed on the sample *before* its ash content was determined by incineration and subsequent weighing. Rapid heating rates were used in char ashing to prevent graphitization of the carbon. This is necessary since the resulting graphitic structure is difficult to oxidize except at very high temperatures. Graphitic residues left with the ash could lead to erroneous carbon conversion values.

Let the mass fractions of ash in the unburned and partially burned chars be x_0 and x respectively. Let the total masses in the beginning and at the end of partial combustion be m_0 and m respectively. Since, the mass of ash is assumed to be constant, we have

$$m_0 x_0 = m x \tag{5.1}$$

Also, the mass of carbon burnt, m_{loss} is

$$m_{loss} = m_0 - m \tag{5.2}$$

The experimental carbon conversion, X_{expt}, is defined as the mass of carbon burnt

divided by the initial mass of carbon. Thus,

$$X_{expt} = \frac{m_{loss}}{m_0(1 - x_0)} \tag{5.3}$$

Combining equations (5.1), (5.2) and (5.3), and eliminating m and m_0, we have,

$$X_{expt} = \frac{x - x_0}{x(1 - x_0)} \tag{5.4}$$

Thus, knowing the mass fractions x and x_0, conversion X_{expt} can be calculated.

5.4 Experimental Methods and Results

5.4.1 Optical Microscopy

Particle size was determined visually under the optical microscope. Since the particles were generally irregular, the following procedure was used: the length along the major axis and the greatest length along its perpendicular were measured. The average particle size was computed as the arithmetic mean of these lengths. This was randomly repeated for 25 particles in each sample. Figure 5.2 shows the distributions of the average particle sizes for the unburned 90-104μm sieve cut char. This figure clearly shows that char sizes were bigger than expected from the particular sieve size cut. Similar size distributions were also measured for one group of the partially burned samples (1675K wall, 90-104μm parent size). They are shown in Figures 5.3-5.5 in order of increasing carbon conversion. The size distribution shifts to smaller sizes at higher conversions. However, the decrease in particle size is smaller than would be expected from diffusion limited combustion conditions. Thus, there must be some internal combustion to explain the observed carbon loss. This will be discussed more fully later on. Figure 5.6 shows the variation of the average particle size as a function of conversion.

Observations using the optical and electron microscopes have shown that the bituminous char is cenospheric, *i.e.* it is almost spherical and contains large bubble-like voids (Lightman and Street, 1967). The free swelling index (FSI) of the parent coal (7.5) also indicates its propensity to swell on devolatilization. An indicator of the irregularity of shape of a particle is its aspect ratio, which is defined as the ratio of the major to the minor dimension. The average aspect ratio for the unburned 90-104 μm bituminous char particles is 1.18. Since this is not too different from unity, it shows that the char of this size is indeed roughly spherical. However, aspect ratio measurements on the partially burned chars do not show any systemic variation. This also indirectly supports the contention that there is internal combustion. The argument is as follows: Let each particle be an ellipse. Further, let the external surface recede at a constant velocity all around the particle, as would be expected for diffusion limited combustion. The aspect ratio of the particle should then increase monotonically. Since this is not observed, there must be some penetration of oxidant into the particle causing internal reaction.

5.4.2 Electron Microscopy

Figure 5.7 is an electron micrograph of an unburned char particle from the 90-104μm sieve cut. It is a typical cenosphere. The outer surface is smooth though quite convoluted. In addition to the large pore in the upper part of the figure, other pore mouths are clearly visible. Some mineral matter agglomerates are also seen on the surface of the particle. Figure 5.8 is a higher magnification picture of the lower part of the same particle. The smooth nature of the surface is again clearly visible. At the top right hand corner of this figure, pore mouths about 1μm in diameter are

seen. Fine mineral matter is also dispersed on the particle surface.

Figures 5.9 and 5.10 show two different magnifications of a particle converted to 17.4% at the 1475K preheater wall temperature. The striking changes even at such small conversions should be noted. The particle surface is very convoluted now, with deep recesses, and shows the enlarged mouths of the bigger pores. On the small scale, however, the surface is still very smooth. Large ash agglomerates are clearly seen. The effect that such an ash agglomerate might have on reactant access to the interior of the particle is unknown. However, 5-8μm diameter pore mouths, beyond the ash, are seen in Figure 5.10. It seems plausible that the ash particle grows by physical agglomeration as the carbon surface recesses with combustion, thus bringing together the smaller ash particles. The ash itself appears fairly loosely bound and there is no evidence of ash melting. Figure 5.11 shows another particle converted to 17.4% at 1475K. From this picture it seems that there is hardly any change from the unburned material, but the morphology on the blind side is hard to guess. A closer look at the particle (Figure 5.12) shows that loose physical agglomeration of ash has taken place like in Figure 5.10. Yet another particle converted to 17.4% is shown in Figure 5.13. Although not much ash is visible, the hollow nature of the particle is striking. Clearly, in such a particle, there is little difference between the external and internal surfaces as far as reactant access is concerned. The pores in the interior surface are also visible.

Figures 5.14 and 5.15 show two particles, from the 45-53μm size fraction burned to 46.6% conversion at a preheater wall temperature of 1475K. The presence of large voids in the particle is obvious. Ash also appears in forms similar to those in the

larger particles. In general, the smaller particles are not as rounded as the bigger ones. They also have more ash. The ash bridge on the particle in figure 5.14 is an interesting feature.

The ash in the char may catalyze combustion (Walker and Nichols, 1957) and/or limit access of oxygen to the particle surface. The catalytic effects of ash are expected to be more important at lower temperatures than at higher temperatures. However, the physical effects of ash are important at higher conversions at all temperatures. It appears from examination of the micrographs that much of the ash remains associated with the particle. While some ash may be lost due to fragmentation or attrition, this is probably of minor importance at these conversions as indicated by the absence of separate ash fragments on the filter.

5.4.3 Surface Area Measurement

Adsorption isotherms on all samples were obtained using nitrogen at 77K as the adsorptive gas. The Brunauer-Emmett-Taylor (BET) theory (Brunauer *et al.*, 1938) was then used to infer specific surface areas of unburned and partially oxidized samples from these isotherms. The procedure and details are described later (Appendix III).

Although most of the pore volume in these porous chars is present in the macro and larger transition pores, it is well known that the micropores account for most of the surface area. The areas normalized per unit total mass are shown in Table 5.3. Since the weight percent ash is also given in the same table, the area per unit carbon mass can also be easily obtained.

In all cases, there is a significant decrease in the area compared to the unburned

material at very low conversions. This can only be attributed to closure of the small pores due to thermal annealing at these high temperatures (Smith, 1972). For the 45-53μm char, the trend with respect to conversion appears to be anomalous. But this is most probably due to an erroneous data point at 5.6% conversion. In the other cases, the surface area, after the initial drop, appears to rise with conversion, reaches a maximum (90-104μm, 1675K wall temperature case) and then decreases again. The final drop is due to pore coalescence at the higher conversions. While the trends are correct, the actual values may not be exact because sample sizes were small in most cases.

5.4.4 Pore Volume Distribution: Capillary Condensation

Pore volume distributions for pores with radii between 20 and 200 Å were obtained from measurement of capillary condensation of nitrogen in the pores of the chars. This corresponds to relative pressures of 0.35 to 0.975 of the isotherms. Since multilayer adsorption occurs over the entire range of pressures, the pore radii and volumes had to be adjusted accordingly. The algorithm given by Yan and Zhang (1986) was used for the calculations. Details of the inversion are given in Appendix III.

Results are given in Figure 5.16 for one case and tabulated in Table 5.3 for all cases. As before, the total volume in this range of pore sizes is appreciably smaller after few percent conversion at high temperatures compared to the unburned material indicating thermal annealing effects in pores of this range. The effect of conversion is best illustrated by Figure 5.16. The pore volume distributions shown are for the 90-104μm parent material converted at 1675K wall temperature. There

is very little decrease of the volume with conversion and no shift of the distribution at all. This shows that pores of this size do not participate in combustion because of diffusion limitations. The figure also shows that the char has very few pores with radii in the range 30-50Å radius. However, minor growth of the smaller pores creates some pores of this size at the higher conversions.

5.4.5 Pore Volume Distribution: Mercury Porosimetry

Mercury porosimetry experiments were performed on an Autoscan-33 porosimeter capable of applying pressures up to 33000 psig. This means that the smallest pores that can be detected are around 32Å in radius. The raw data were in the form of cumulative volume versus applied pressure. Although both intrusion and extrusion curves can be interpreted to derive pore sizes, the intrusion branch was used in our experiments. The many problems of data interpretation including hysteresis and pore geometry are discussed by Lowell and Shields (1979). The pore radius penetrated at a given pressure is calculated from the Washburn equation:

$$r_p = \frac{2\gamma\cos\theta}{P} \tag{5.5}$$

where r_p is the pore radius, γ is the surface tension of mercury normally taken to be 480 ergs/cm^2, θ is the angle of contact between mercury and the char, and P is the applied pressure. The contact angle is conventionally assumed to be 140°. This equation assumes that the pores are cylindrical in shape. Thus, while the results may not have any intrinsic value in describing the present char which is cenospheric, their value as a comparative tool is well accepted. Figure 5.17 shows an example of the raw data derived from a porosimetry run. The abscissa is the volume

in cubic centimeters and the ordinate is the pressure in psig. The intrusion and extrusion curves are both shown. The former is shown in two parts, the scale being expanded at lower pressures for better accuracy in that range. This cumulative curve (intrusion branch) was numerically differentiated to give the pore volume distribution shown in Figure 5.18 for the 90-104μm size fraction of the unburned material. A dead volume correction was applied before the numerical differentiation.

The distribution for the unburned material shows that there is significant transition porosity (200-1000Å radius) as well as macroporosity in this char. Pores larger than 1.76μm in radius are penetrated at pressures below 60 psig and are assumed to be interparticle spaces rather than internal porosity. Of course, it is not possible to rule out the presence of cracks and voids of these sizes or even larger ones within particles. Indeed electron micrographs do show the presence of voids of this size in the particles. Thus, at these low pressures it is impossible to resolve the controversy regarding the relative contributions of the inter and intraparticle voids to the total voidage, particularly in a material that has large voids.

Figure 5.19 shows the pore volume distribution of the 90-104μm parent char after 65.9% conversion at 1675K preheater wall temperature. Comparing with figure 5.18, it is clear that there is less transitional porosity in the burned char. This indicates that these pores are accessible to oxygen at these temperatures. There is some resulting increase in the macroporosity. Table 5.3 shows the pore volumes in the ranges 32-500Å and 500-17600Å. 32Å is normally taken as the micro-transitional boundary and 500Å is the transitional-macropore boundary in the literature. Due to sample size limitations, porosimetry was done on samples having the highest

conversion in each group. In the 1675K 90-104μm group we see that while the transitional pore volume decreases, the macroporosity increases showing oxygen accessibility in the transitional range. The same trend is observed in the sample with big particles burned at 1475K wall temperature.

5.4.6 Conclusions from High Temperature Combustion

This section will summarize the observations from all the characterization experiments described earlier. Although there is a noticeable decrease in the particle size with conversion at high temperatures indicating the possibility of diffusion-limited combustion, this decrease by itself is insufficient to account for the total carbon loss. Thus there is internal burning in these char particles which is not surprising considering that there are macropores as large as 8μm in diameter visible on the char surface. These obviously act as feeder pores allowing oxygen to penetrate into the particle. The only question that remains to be answered is the extent of the oxygen penetration.

Capillary condensation and mercury porosimetry together indicate quite clearly that while pores above 200Å in radius do grow during combustion, those smaller than this size remain unaffected. Thus pores below 200Å are diffusion limited. This is also indirectly seen from the small values of surface area present in the samples. Since most of the surface area is in the micropores below 200Å in radius, it is clearly not accessible. One cause of the lack of penetration into pores of this size may be that their pore mouths are closed by some thermal annealing mechanism as the particle is heated to these temperatures. That thermal annealing occurs is indicated in the drop in the surface area value compared to that of the unburned

material.

The presence of ash on the surface of the burned materials is quite evident from the electron micrographs. The ash appears to be present as loosely bound globules of very small size that are drawn together as the carbon surface below them recedes. There is no evidence to show ash melting at the temperatures used.

5.5 Comparison of High and Low Temperature Combustion

Table 5.4 shows data on chars burned to various conversions at 500°C. There are two major sets of data corresponding to the 104-125μm and 90-104μm size fractions. Porosimetry experiments were done on the bigger samples for reasons of greater sample availability. However, since the sizes are similar, the results should also be indicative of the 90-104μm size fraction.

The main difference between high and low temperature combustion is seen in the surface area values. Table 5.4 and Figure 5.20 show the change of the surface area with conversion at 500°C. The areas at the lower temperature are at least an order of magnitude larger than those from the high temperature experiments. This indicates that most or all of the micropores are accessible at low temperatures and that diffusion is not a factor. Thus combustion takes place in the kinetic limited regime. Figure 5.20 shows the surface area normalized with total and carbon masses. The rapid initial rise in the surface area is due to the opening of the pore mouths. Thereafter, the rise is smaller, reaching a maximum at some carbon conversion and finally the area decreases due to pore coalescence.

Pore volume distributions from capillary condensation are shown in Figure 5.21. This shows that the volume in this range increases with conversion and drops

slightly at the last point. This reinforces the conclusion that even these small pores are accessible to oxygen, unlike burning during high temperatures (Figure 5.16).

The pore volume data from porosimetry on the 104-125μm samples show that pore volumes in all size ranges increase with conversion. The pore volume distribution of a char converted to 70.6% at 500°C is shown in Figure 5.22. Comparing with the pore volumes of the unburned material (Figure 5.18) and that burned at 1675K wall temperature (Figure 5.19) to a similar conversion we see that although the total volume is not very different, there is little volume in the small pores (indicating their growth) and somewhat more porosity in the larger pores and cracks. Figure 5.23 is a plot of the pore volumes versus conversion at low temperature.

Thus the major difference between the combustion of the char at low and high temperatures is the absence of diffusion limitations in the micropores and their resulting accessibility to the oxidizer at lower temperatures. There is also no evidence of thermal annealing at the low temperature.

References

1. Brunauer, S., Emmett, P. H. and Teller, E., J. Am. Chem. Soc., **60**, 1938, 309-319.
2. Essenhigh, R. H., in **Chemistry of Coal Utilization**, 2^{nd} Supp. Vol., edited by M. A. Elliot. pp 1153-1312 John Wiley and Sons, New York, 1981.
3. Field, M.A., Combust. Flame, **13**, 1969, 237.
4. Flagan, R.C., and Friedlander, S.K., in **Recent Developments in Aerosol Science** edited by D.T.Shaw. pp 25-59 John Wiley and Sons, New York 1978.
5. Hamor, R.J., and Smith, I.W., Combust. Flame, **21**, 1973, 153.
6. Lightman, P., and Street, P. J., Fuel, **47**, 1968, 7-28.
7. Lowell, S., and Shields, J.E., **Powder Surface Area and Porosity**, Chapman and Hall, 1979.
8. Smith, I. W., Fuel, **51**, 1972, 312-321.
9. Tseng, H. P., and Edgar, T. F., Fuel, **63**, 1984, 386-393.
10. Walker P. L., Jr., and Nichols, J. R., Ind. Carbon and Graphite Conf., London, 1957, 334-347.
11. Yan, J., and Zhang, Q., Part. Charact. **3**, 1986, 20-25.

Rank	HVAB	
State	Pennsylvania	
Seam	Pittsburgh	
Proximate Analysis (%)		
Moisture	02.54	
Ash	13.32	
Volatile Matter	33.56	
Fixed Carbon	50.58	
Ultimate Analysis (%)	As rec'd	Dry
Ash	13.32	13.67
Carbon	70.05	71.88
Hydrogen	4.55*	4.67
Nitrogen	1.33	1.36
Sulfur	1.33	1.36
Chlorine	0.07	0.08
Oxygen(diff.)	6.81*	6.99
*excludes moisture		
Free Swelling Index	7.5	
Dry Heating Value	29114 J/g	

Table 5.1 Properties of raw coal.

Wall Temperature	Sieve Cut	Conversion	Particle Temperature
K	μm	%	K
1475	45-53	5.6	1425±44
		46.6	1446±60
		63.1	1457±44
1475	90-104	10.3	1465±44
		17.4	1441±59
		30.4	–
1675	90-104	11.7	1363±27
		46.7	1406±29
		65.9	1379±10

Table 5.2 Particle temperature measurements.

Wall Temp.	Sieve Cut	Run No.	N_2 Mass	Hg Mass	Ash	Conv.	Avg. Size	Aspect Ratio	N_2 BET Area	Vol. (Hg)			Vol. (N_2)
										32-500Å	500-17600Å	32Å -∞	20-200Å
K	μm		g	g	%	%	μm		m^2/gtot	cc/gtot	cc/gtot	cc/gtot	cc/gtot
1475	45-53	345	0.1031		25.5	0			11.3				0.062
		330	0.1400		28.7	5.6			7.8				0.018
		331	0.0716		34.3	46.6			5.2				0.016
		329	0.0829	0.1027	37.4	63.1			8.7	0.0994	0.1931	0.3112	0.024
1475	90-104	248	0.0747	0.1800	19.5	0			12.6	0.1279	0.1991	0.3988	0.040
		341	0.0836		21.3	10.3			4.7				0.018
		342	0.0778		22.7	17.4			5.5				0.014
		340	0.0550	0.1063	25.9	30.4			12.4	0.0851	0.2218	0.3222	0.034
1675	90-104	248	0.0747	0.1880	19.5	0	114.0	1.177	12.6	0.1279	0.1991	0.3988	0.040
		337	0.0693		21.6	11.7	111.7	1.140	6.4				0.026
		332	0.0520		31.3	46.7	109.3	1.186	10.2				0.028
		336	0.0506	0.0639	41.6	65.9	100.9	1.166	5.3	0.0905	0.2845	0.4405	0.027

Table 5.3 Characterization of PSOC 1451 1600K chars burned at high temperatures.

Run No.	Char Size	Conv.	N_2 Mass	Hg Mass	Ash	N_2 BET Areas		Vol. (N_2) 20-200 Å radius		Vol. (Hg) 32-500Å	Vol. (Hg) 500-17600Å	Vol. (Hg) 32Å -∞
	μm	%	g	g	%	m^2/gtot	m^2/gC	cc/gtot	cc/gC	cc/gtot	cc/gtot	cc/gtot
239	104-125	0	0.1323	0.0856	19.0	12.4	15.3	0.0413	0.0510	0.1279	0.1991	0.3988
232		14.2	0.0801	0.0616	21.5	146.1	186.0	0.1042	0.1327	0.1185	0.2477	0.4630
233		27.3	0.0752	0.0568	24.4	190.2	251.5	0.1252	0.1656	0.1165	0.2729	0.4729
234		39.9	0.0842	0.0639	28.1	148.5	206.4	0.1550	0.2155	0.1298	0.3306	0.7001
236		57.7	0.0613	0.0503	35.7	181.1	281.5	0.1896	0.2948	0.1558	0.3547	0.7357
235		70.6	0.0590	0.0427	44.4	200.0	359.7	0.1881	0.3383	0.1616	0.3961	0.8109
248	90-104	0	0.0747		19.5	12.6	22.7	0.0400	0.0497			
346		4.6	0.0694		20.2	21.7	27.2	0.0473	0.0593			
249		7.0	0.0711		20.5	87.2	110.0	0.0774	0.0973			
348		32.4	0.0792		26.4	150.3	204.0	0.0597	0.0810			
349		41.2	0.0666		37.0	189.2	267.0	0.0812	0.1289			
350		65.7	0.0541		41.4	201.5	344.0	0.1041	0.1776			
247		72.5	0.0419		44.6	163.0	306	0.5205	0.9395			
345	45-53	0	0.1031		25.5	11.3	15.1	0.0619	0.0831			

Table 5.4 Characterization of PSOC 1451 1600K chars burned at 500°C.

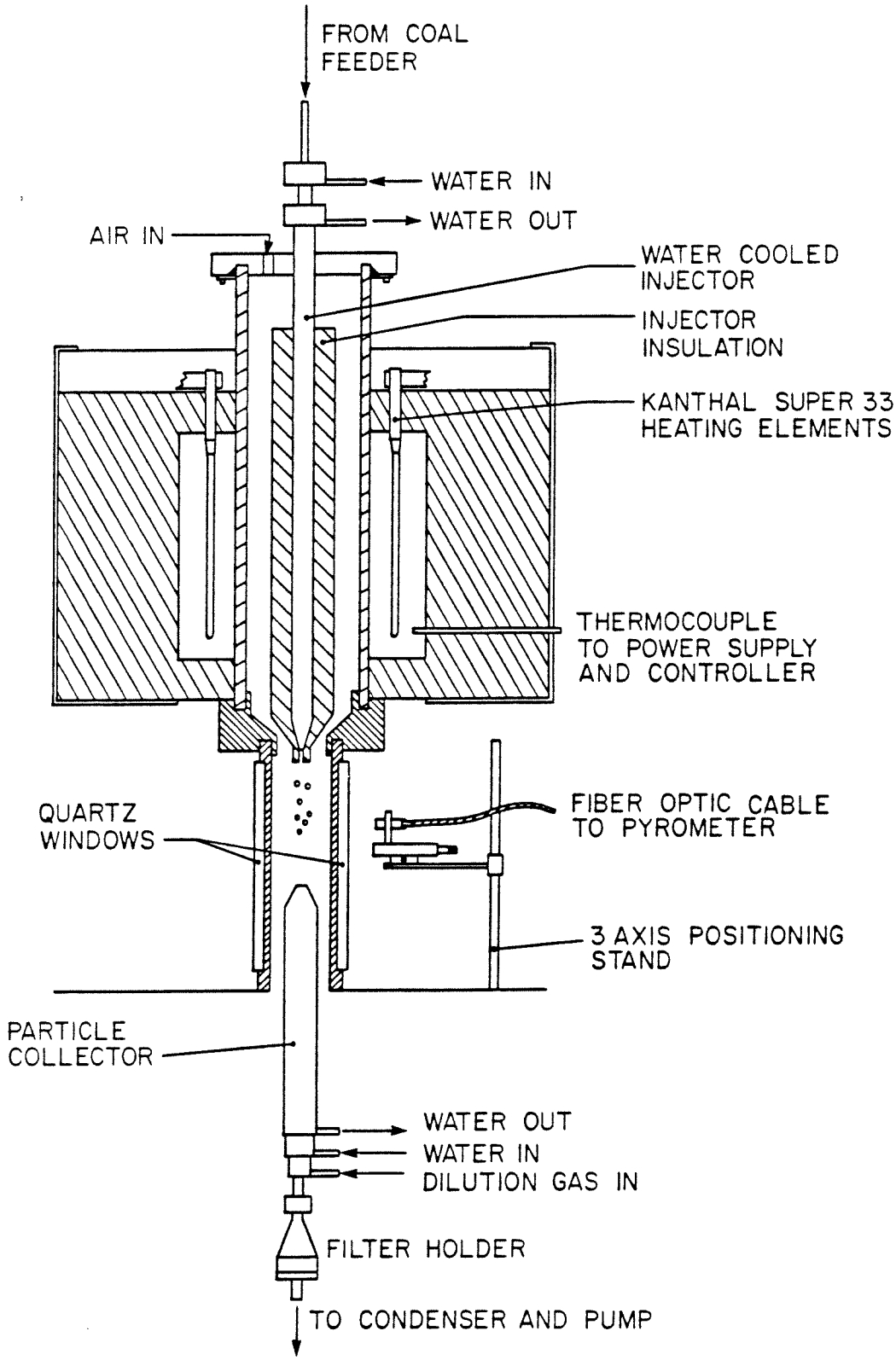

Figure 5.1 Schematic of the high temperature flow reactor.

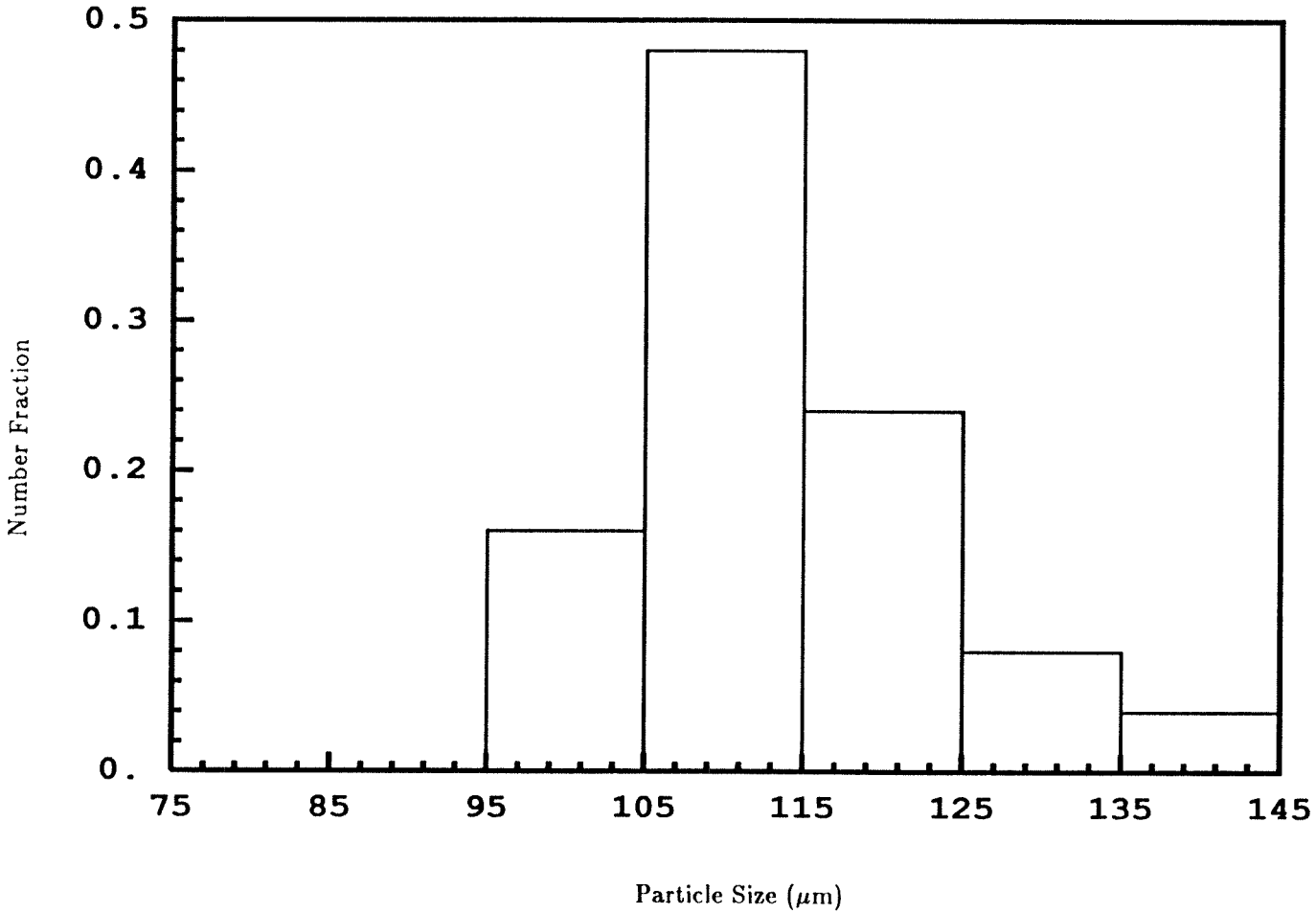

Figure 5.2 Particle size distribution of unburned 90-104μm sieve cut PSOC 1451 1600K char.

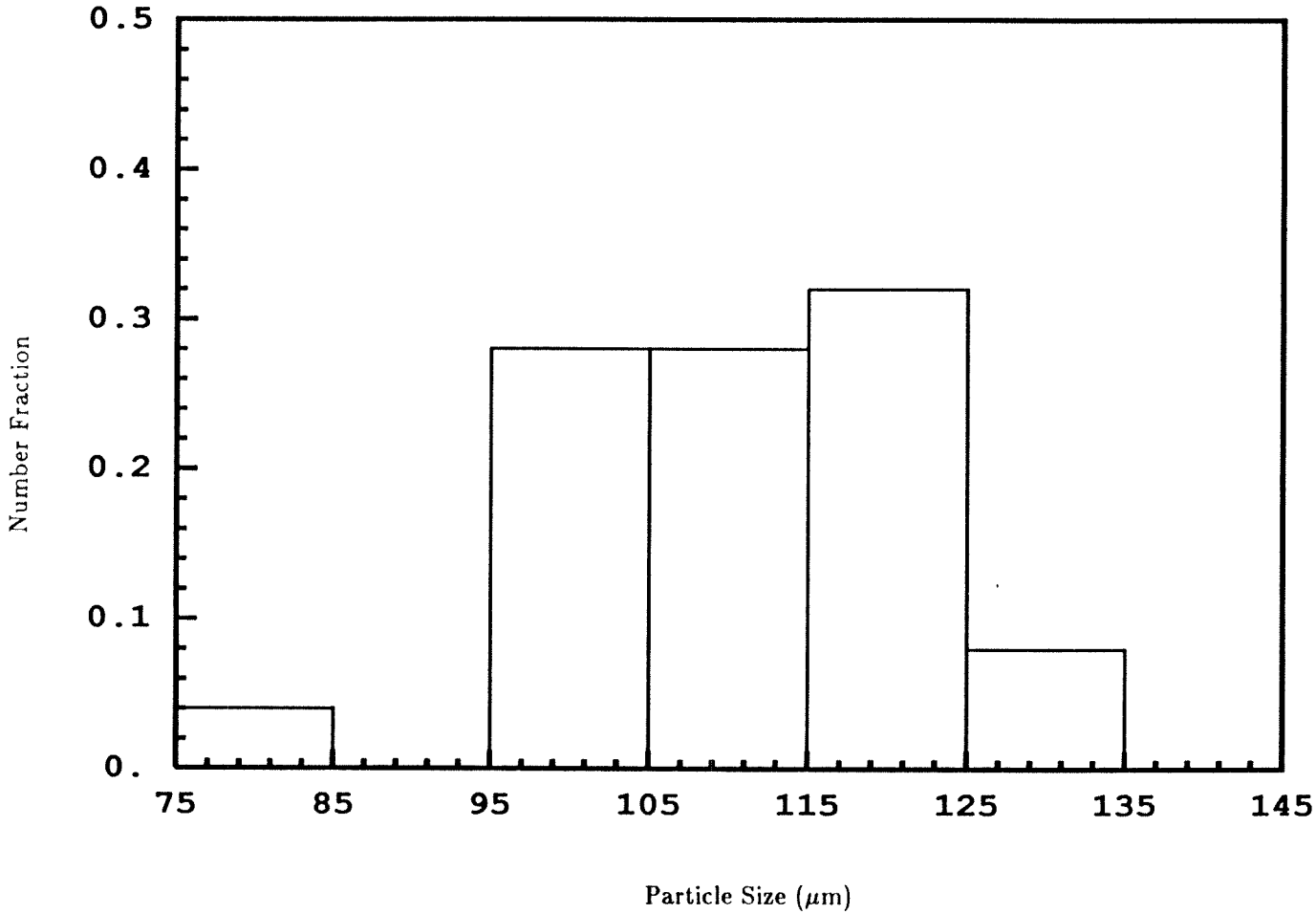

Figure 5.3 Particle size distribution of 90-104μm sieve cut PSOC 1451 1600K char after 11.7% conversion at 1675K.

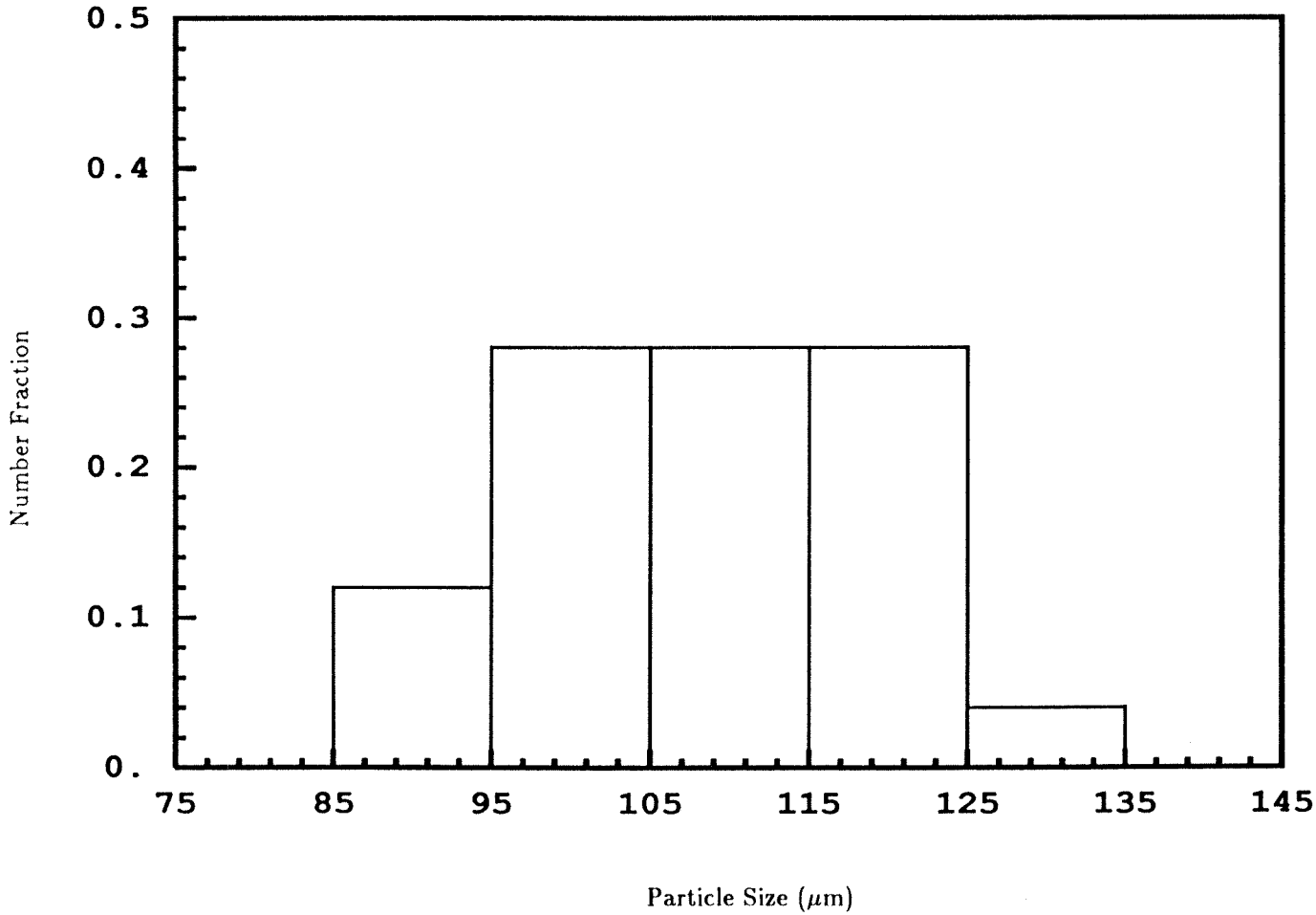

Figure 5.4 Particle size distribution of 90-104μm sieve cut PSOC 1451 1600K char after 46.7% conversion at 1675K.

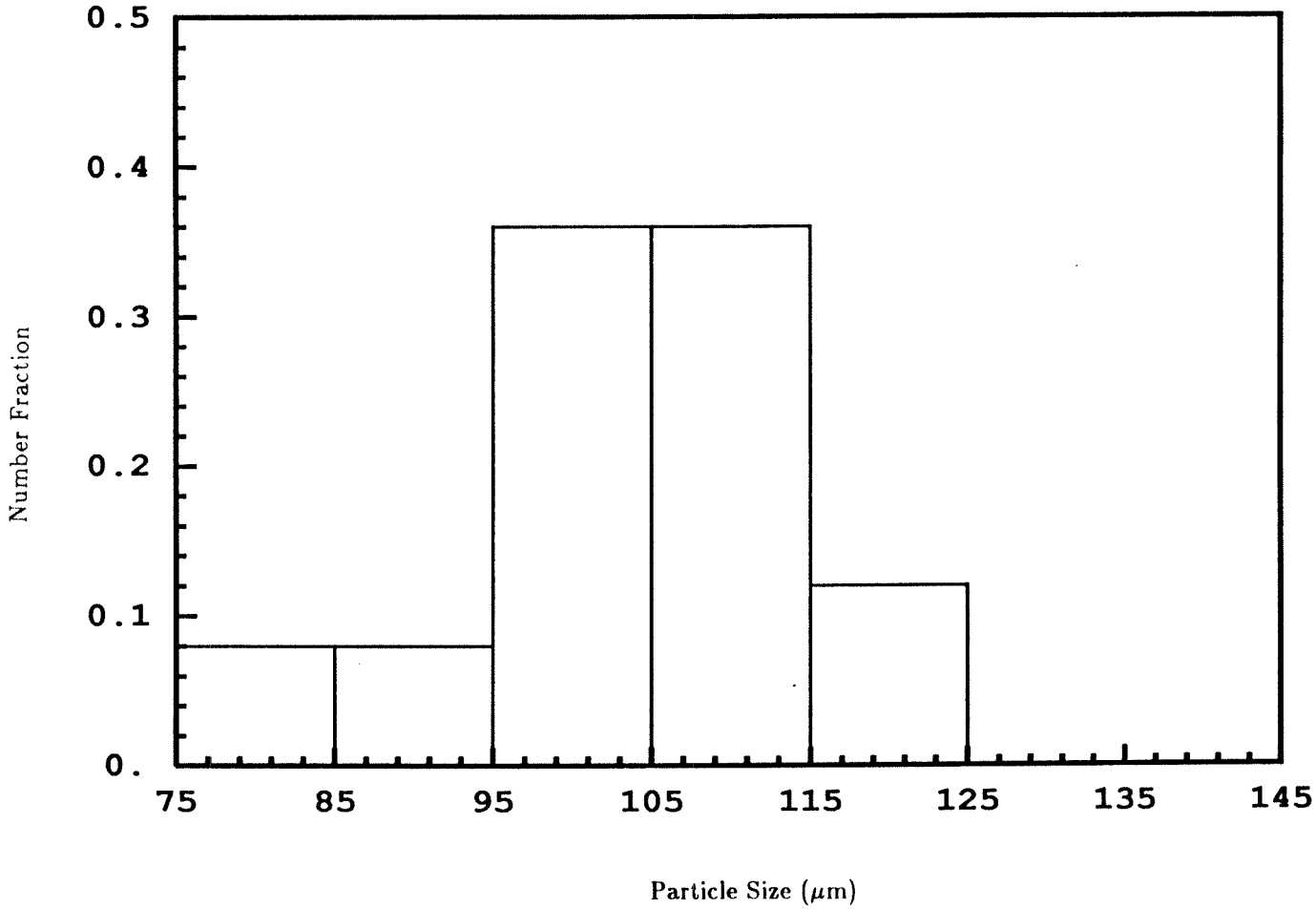

Figure 5.5 Particle size distribution of 90-104μm sieve cut PSOC 1451 1600K char after 65.9% conversion at 1675K.

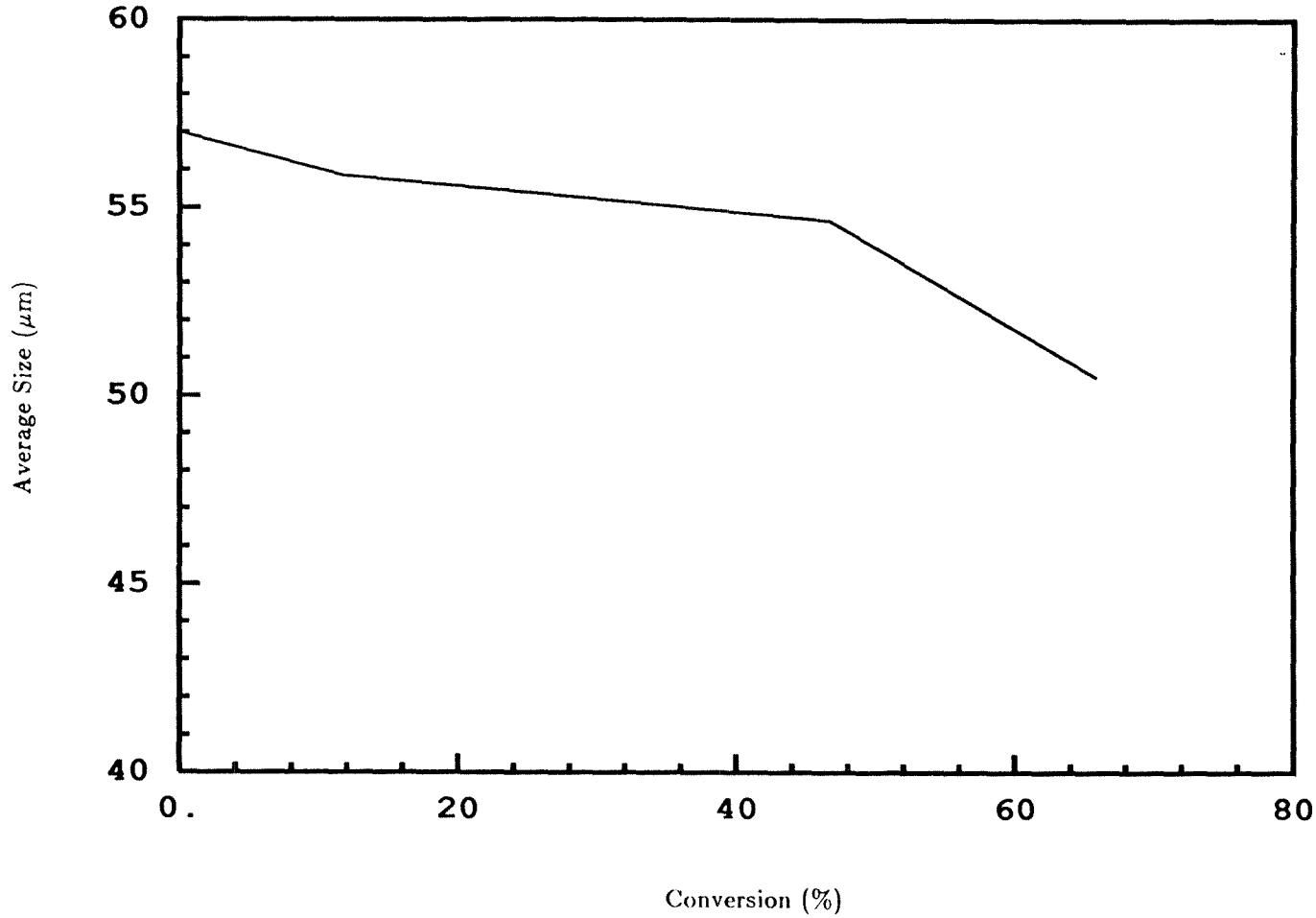

Figure 5.6 Variation of particle size as a function of conversion for PSOC 1451 1600K char burned at 1675K.

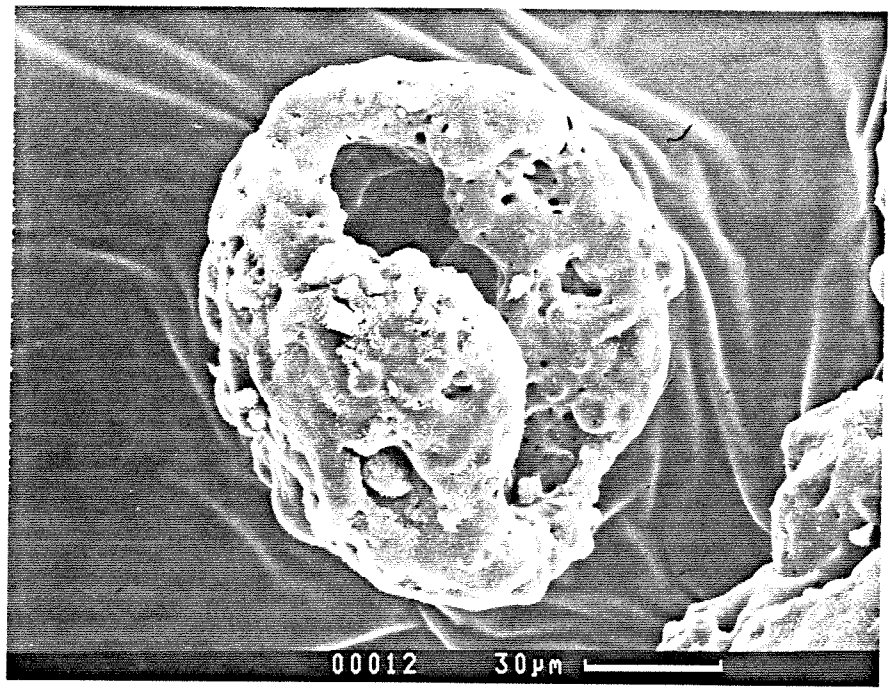

Figure 5.7 Electron micrograph of an unburned PSOC 1451 1600K 90-104μm char particle.

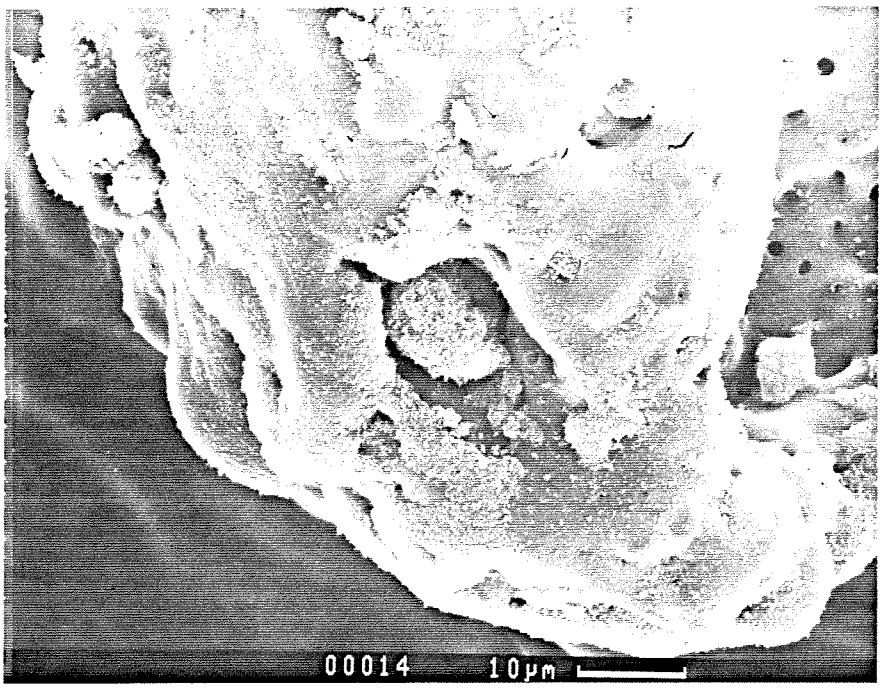

Figure 5.8 Magnified electron micrograph of the particle in Figure 5.7.

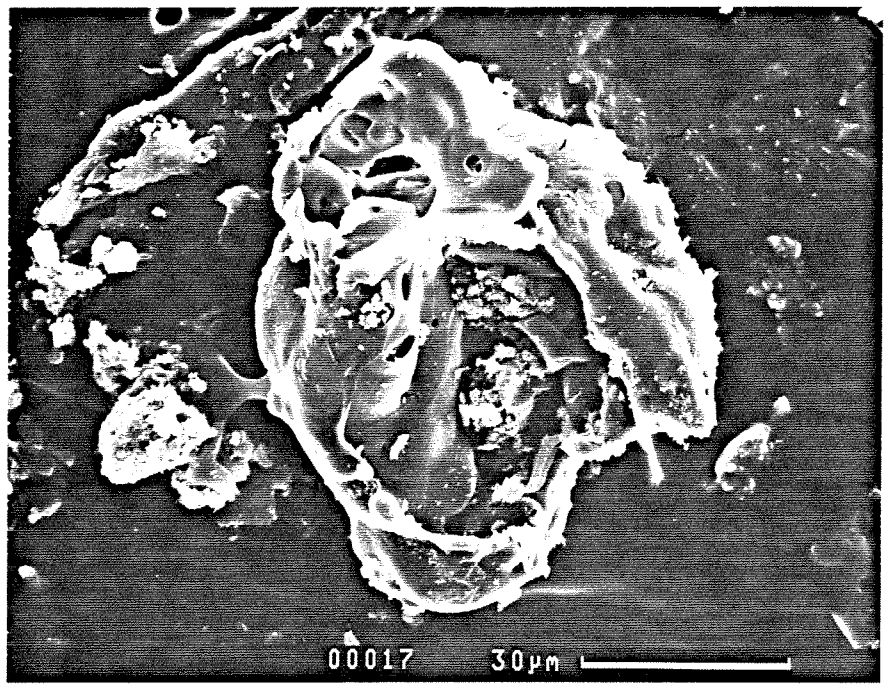

Figure 5.9 Electron micrograph of a PSOC 1451 1600K char particle after 17.4% conversion at 1475K.

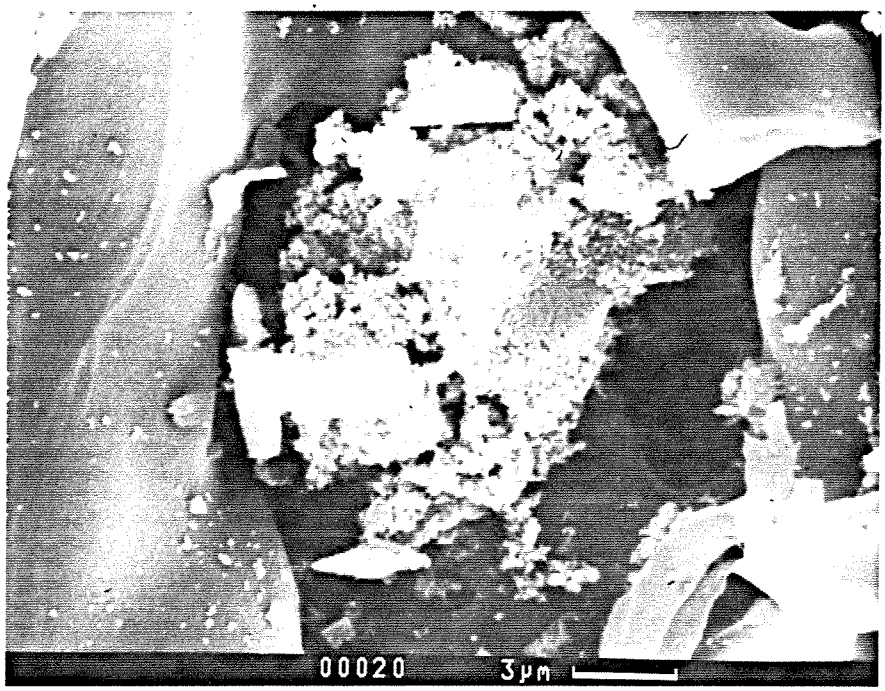

Figure 5.10 Magnified electron micrograph of the particle in Figure 5.9.

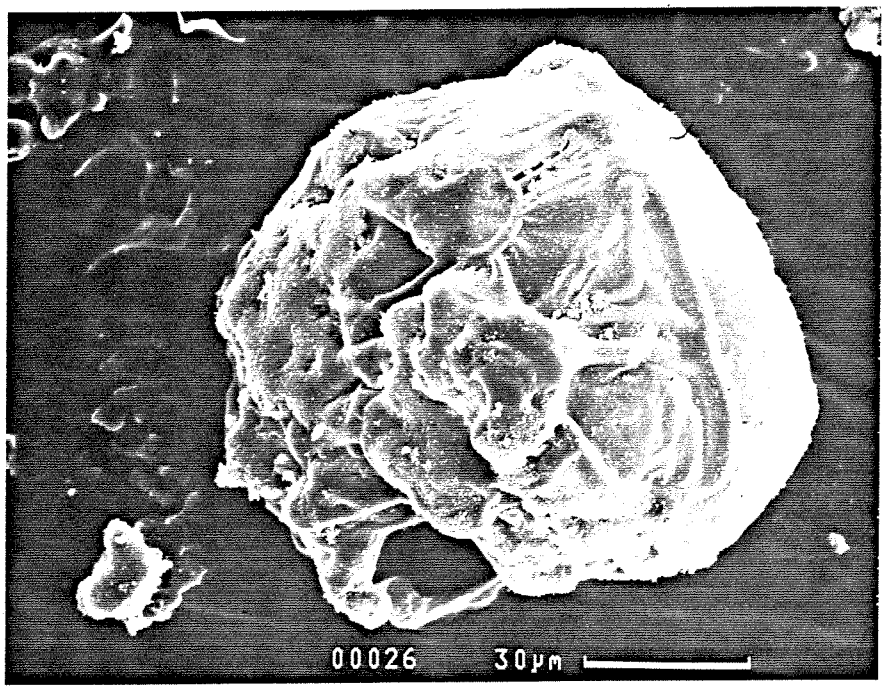

Figure 5.11 Electron micrograph of a PSOC 1451 1600K char particle after 17.4% conversion at 1475K.

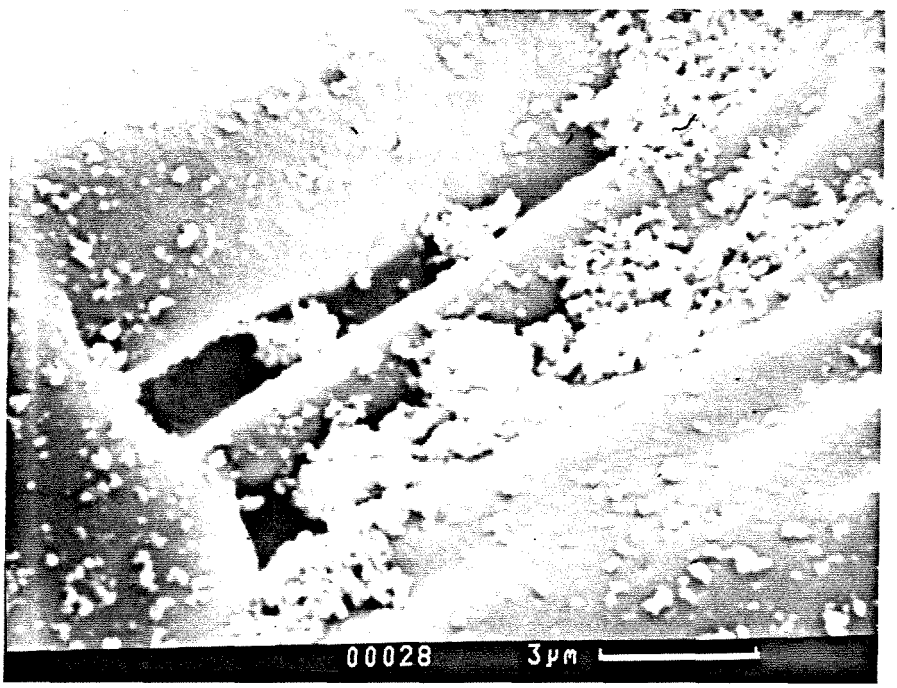

Figure 5.12 Magnified electron micrograph of the particle in Figure 5.11

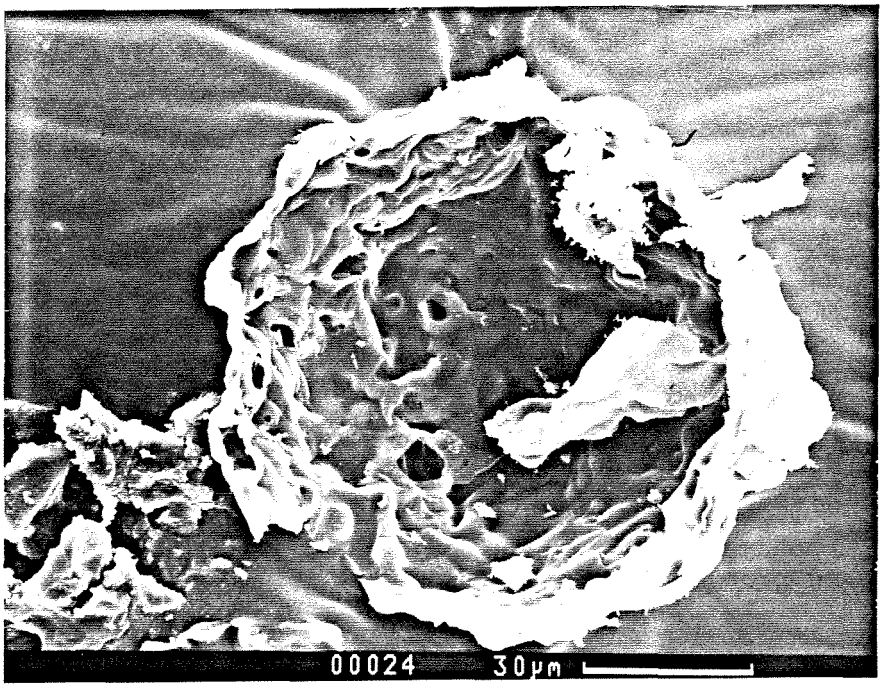

Figure 5.13 Electron micrograph of a PSOC 1451 1600K char particle after 17.4% conversion at 1475K.

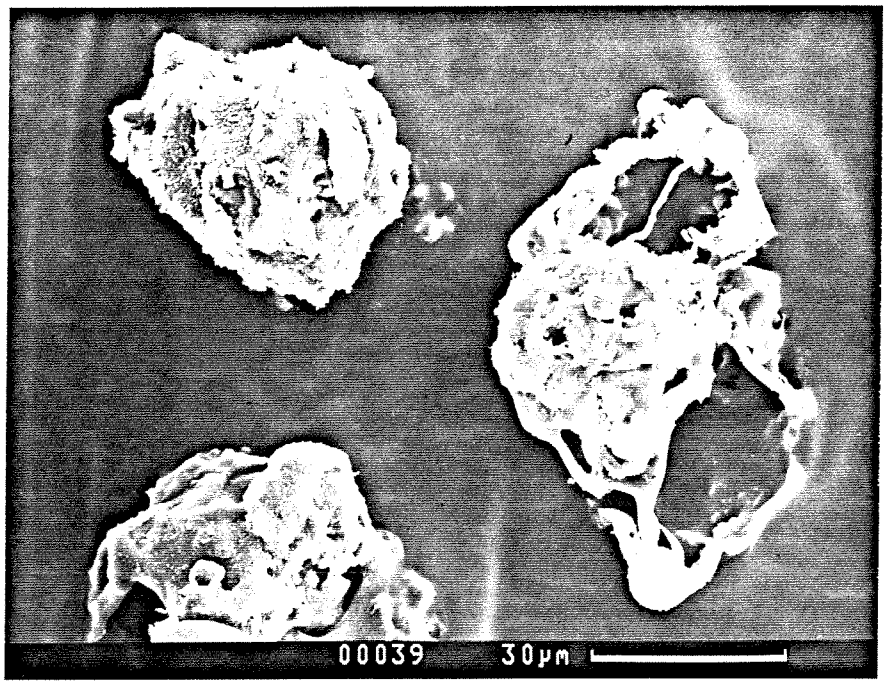

Figure 5.14 Electron micrograph of a PSOC 1451 1600K char particle after 46.7% conversion at 1475K.

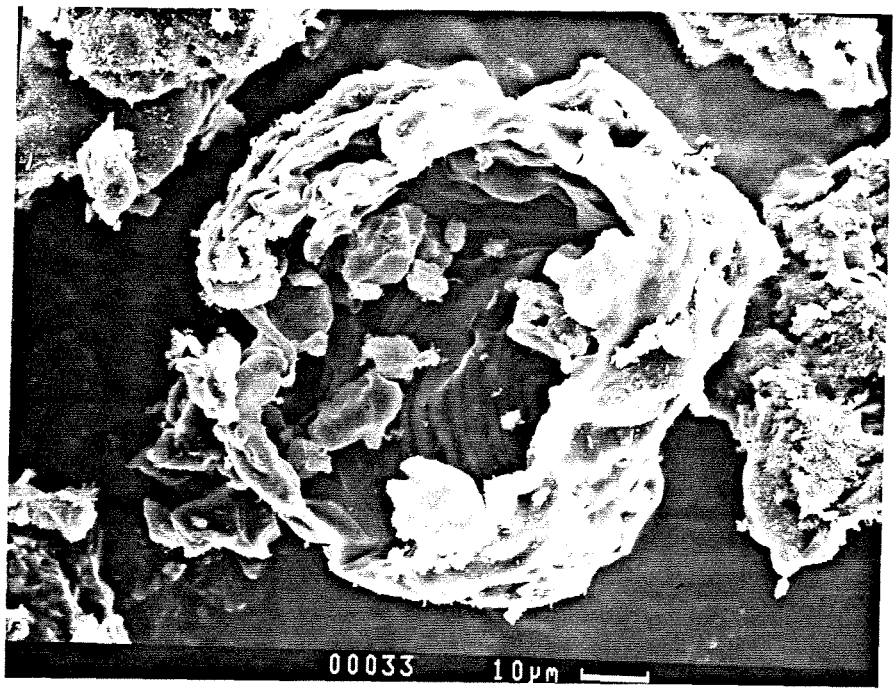

Figure 5.15 Magnified electron micrograph of the particle in Figure 5.14.

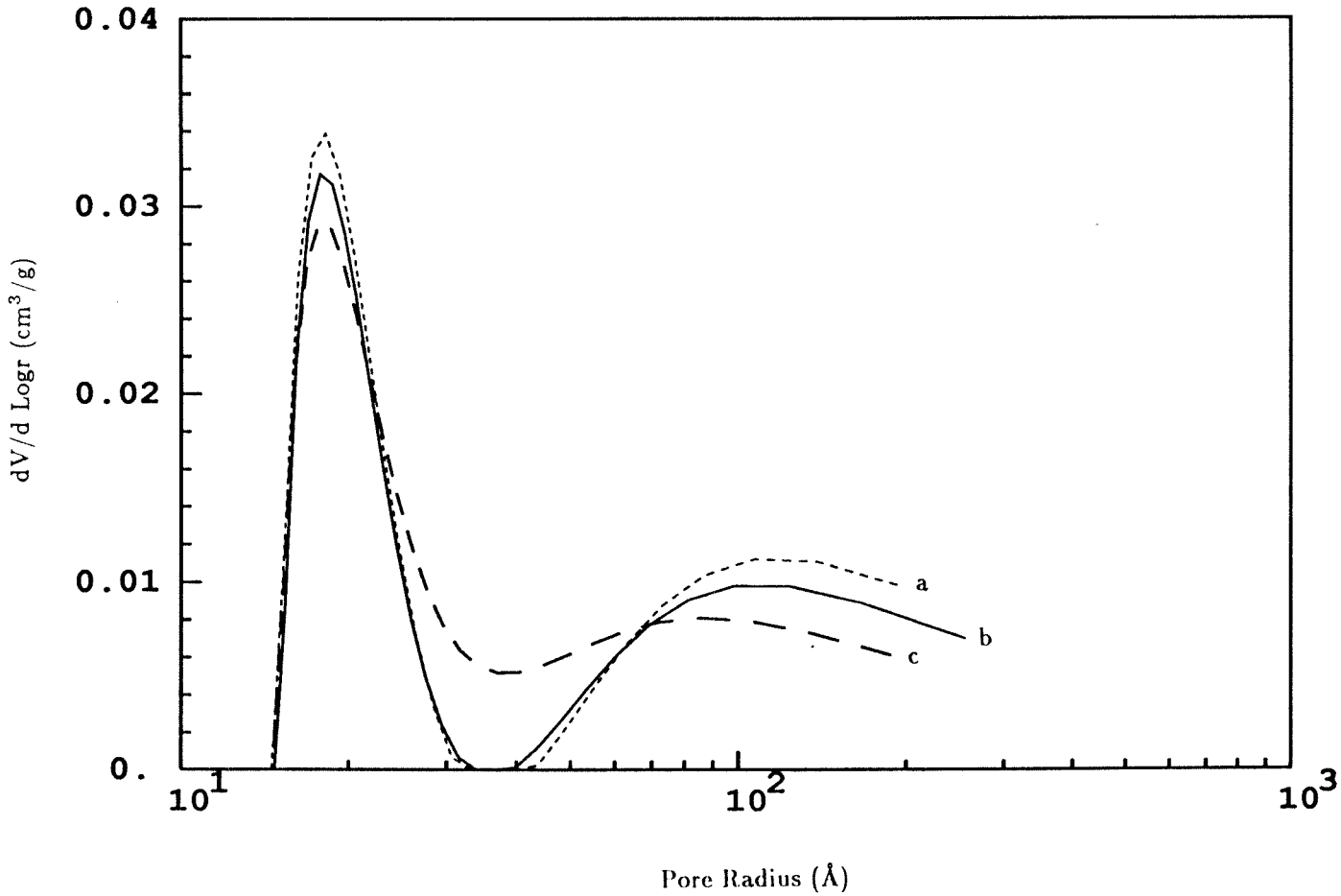

Figure 5.16 Pore volume distributions from capillary condensation on PSOC 1451 1600K 90-104μm char at (a) 11.7% conversion (b) 46.7% conversion (c) 65.9% conversion.

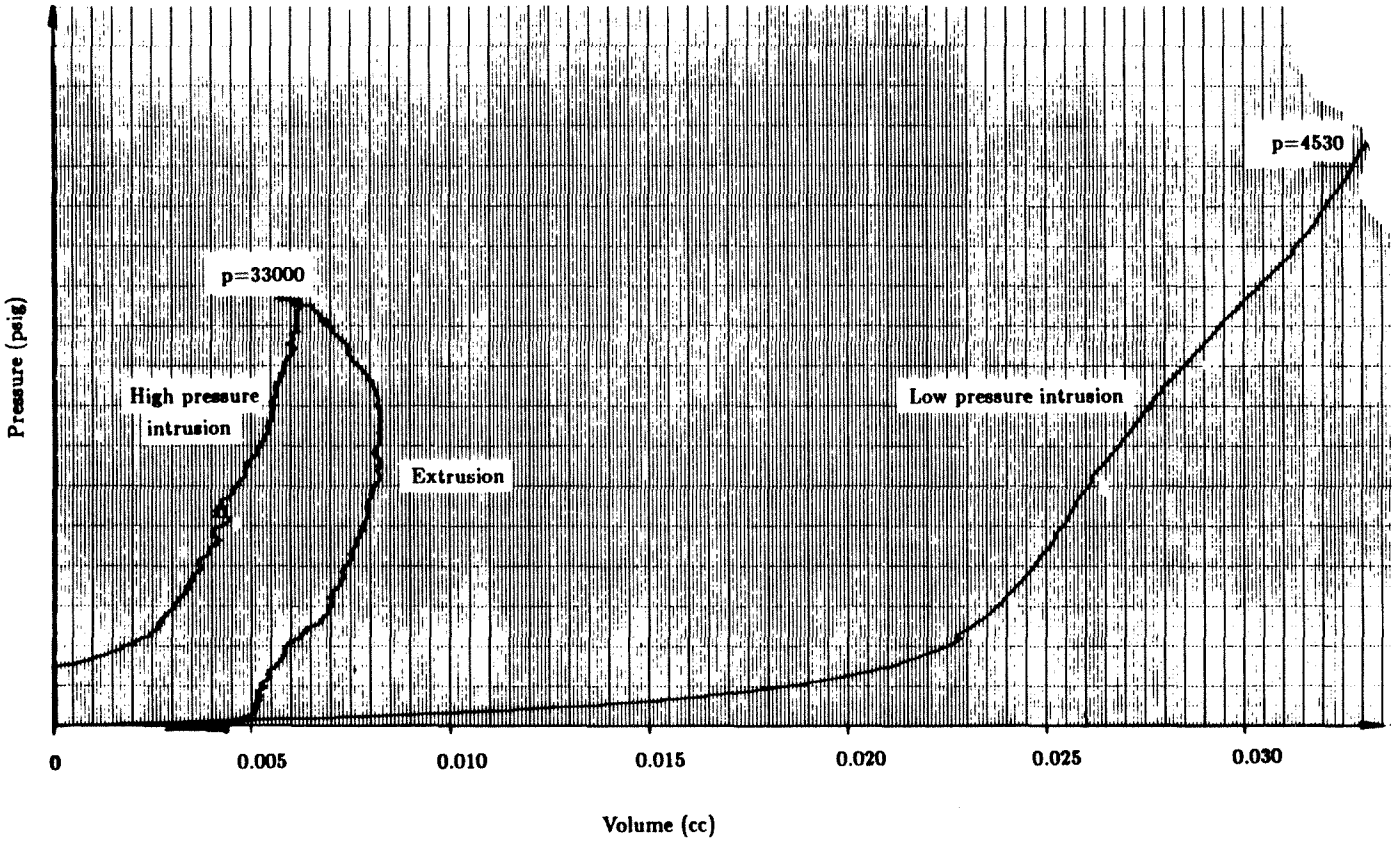

Figure 5.17 Intrusion pressure versus volume from a mercury porosimetry run on unburned PSOC 1451 1600K 90-104μ char.

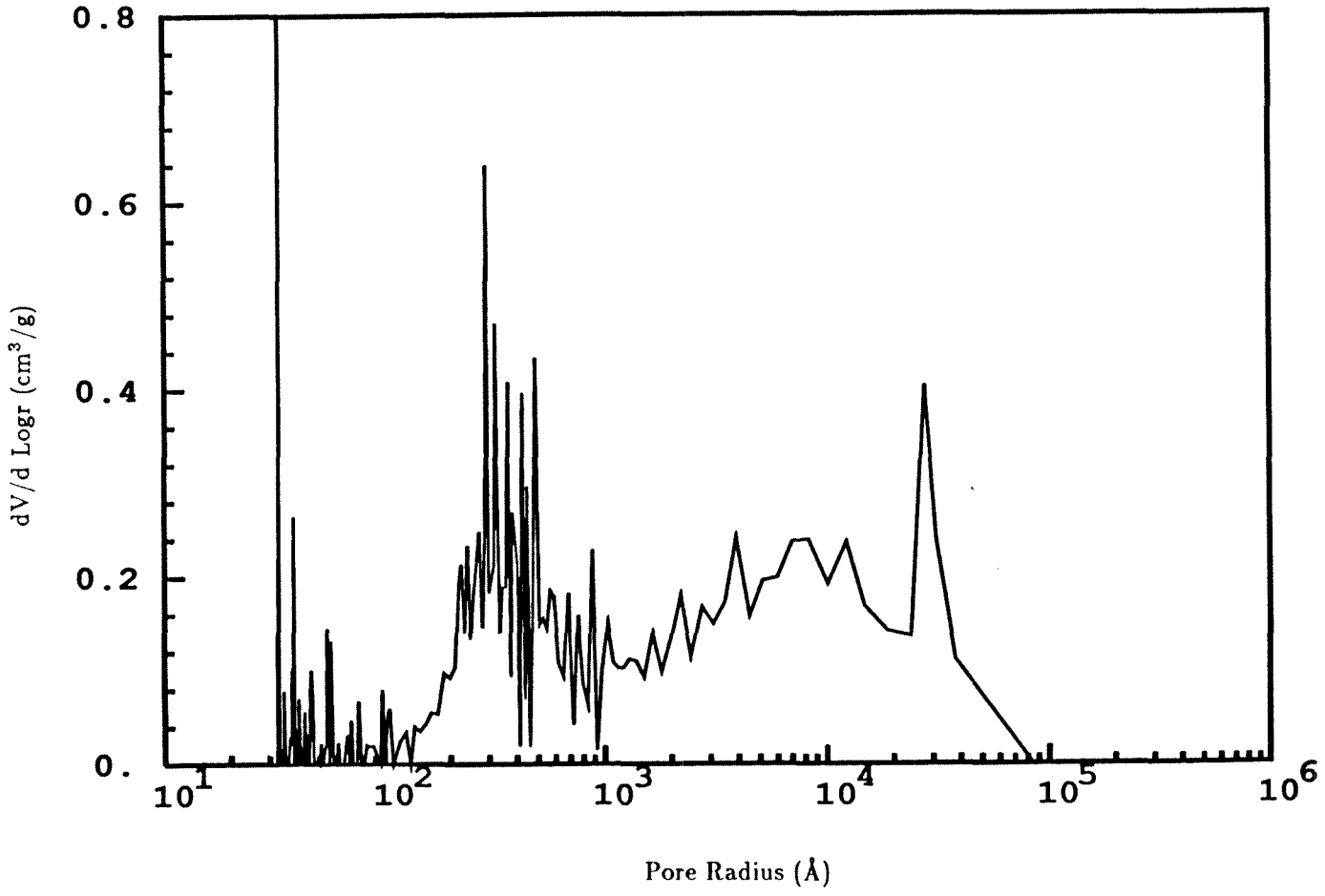

Figure 5.18 Pore volume distribution from a mercury porosimetry run on unburned PSOC 1451 1600K 90-104μ char.

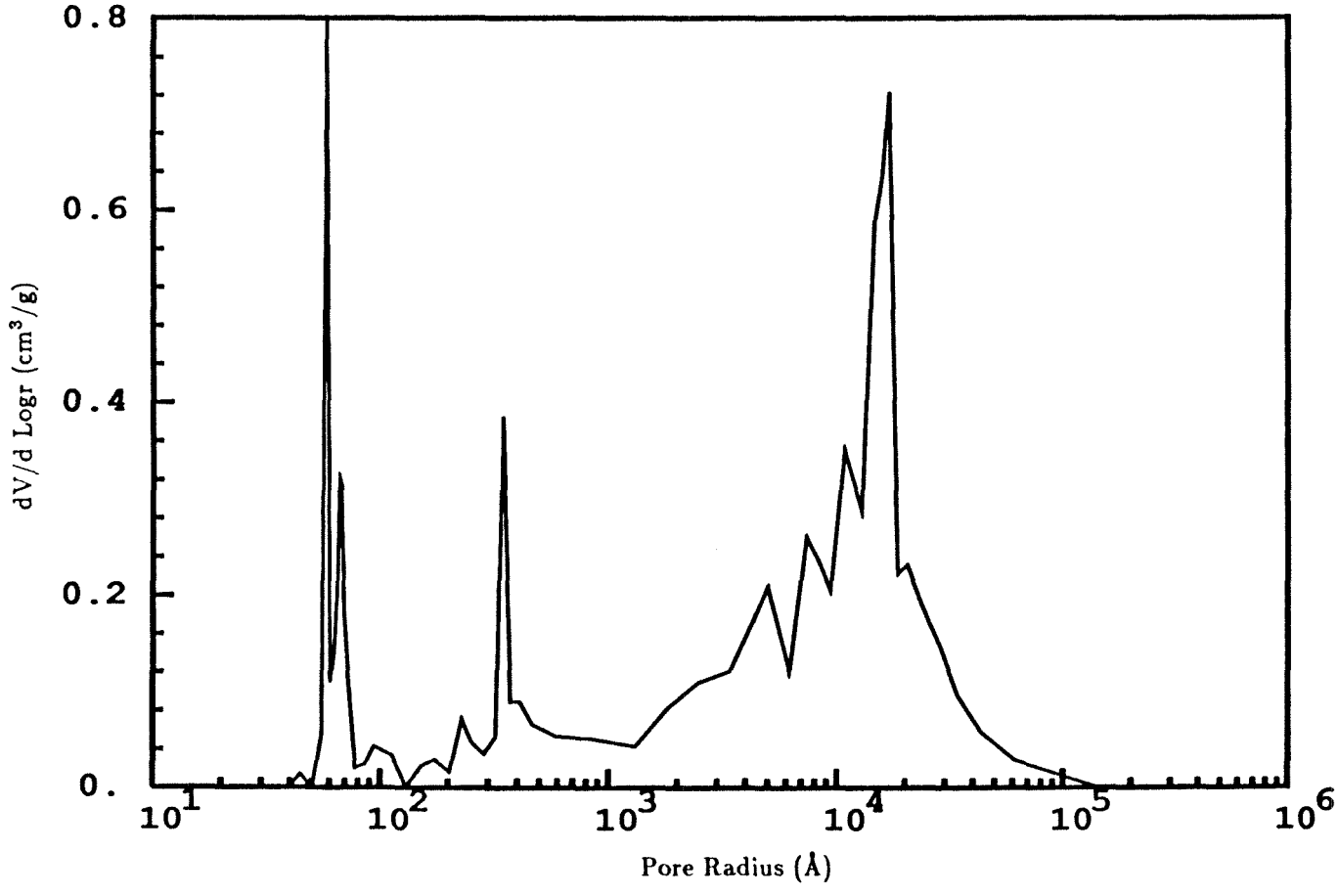

Figure 5.19 Pore volume distribution from mercury porosimetry on PSOC 1451 1600K 90-104μ char after 65.9% conversion at 1675K.

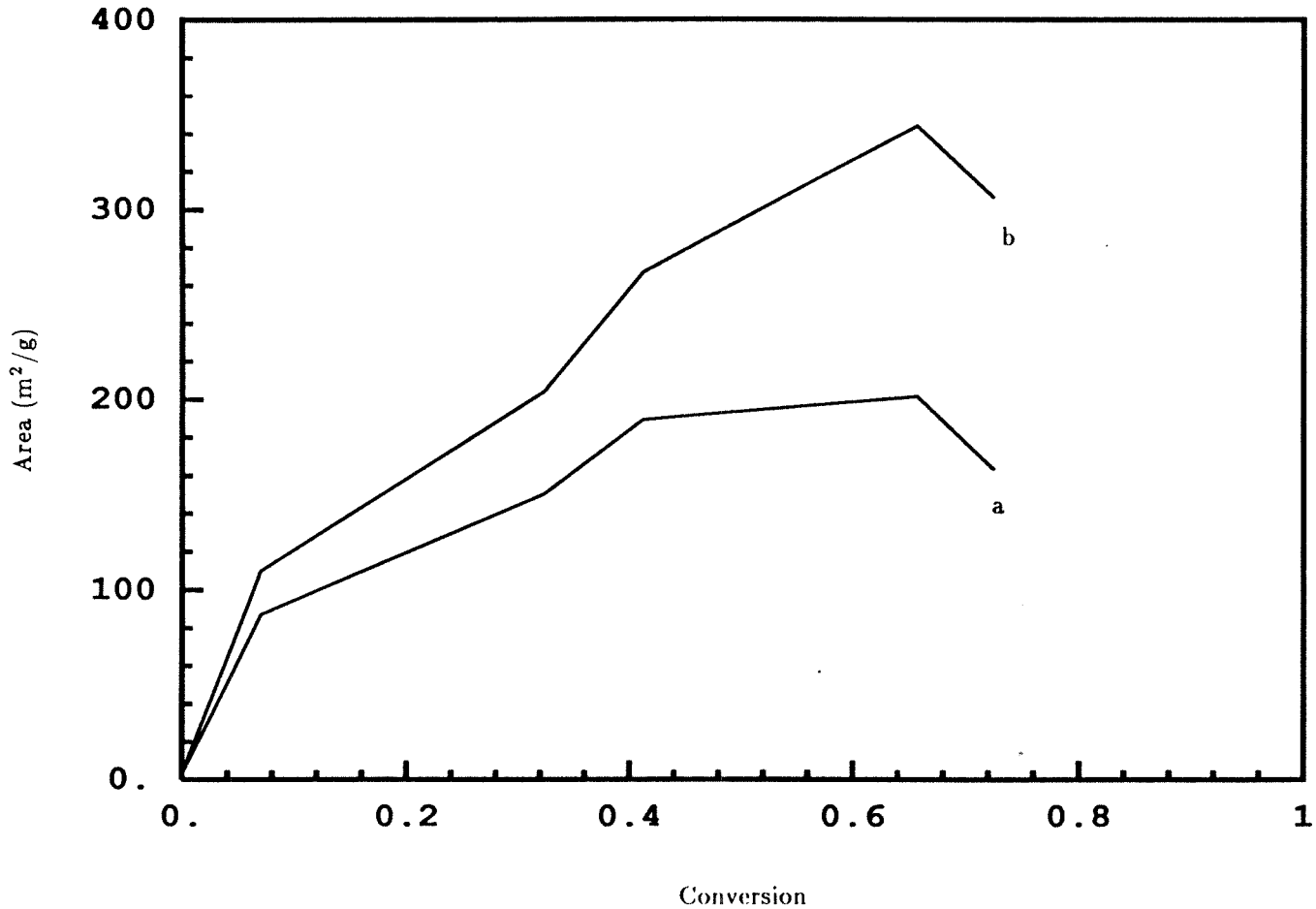

Figure 5.20 N_2 BET surface area versus conversion on PSOC 1451 1600K 90-104μ char burned at 500°C. (a) Normalized with total mass (b) Normalized with carbon mass.

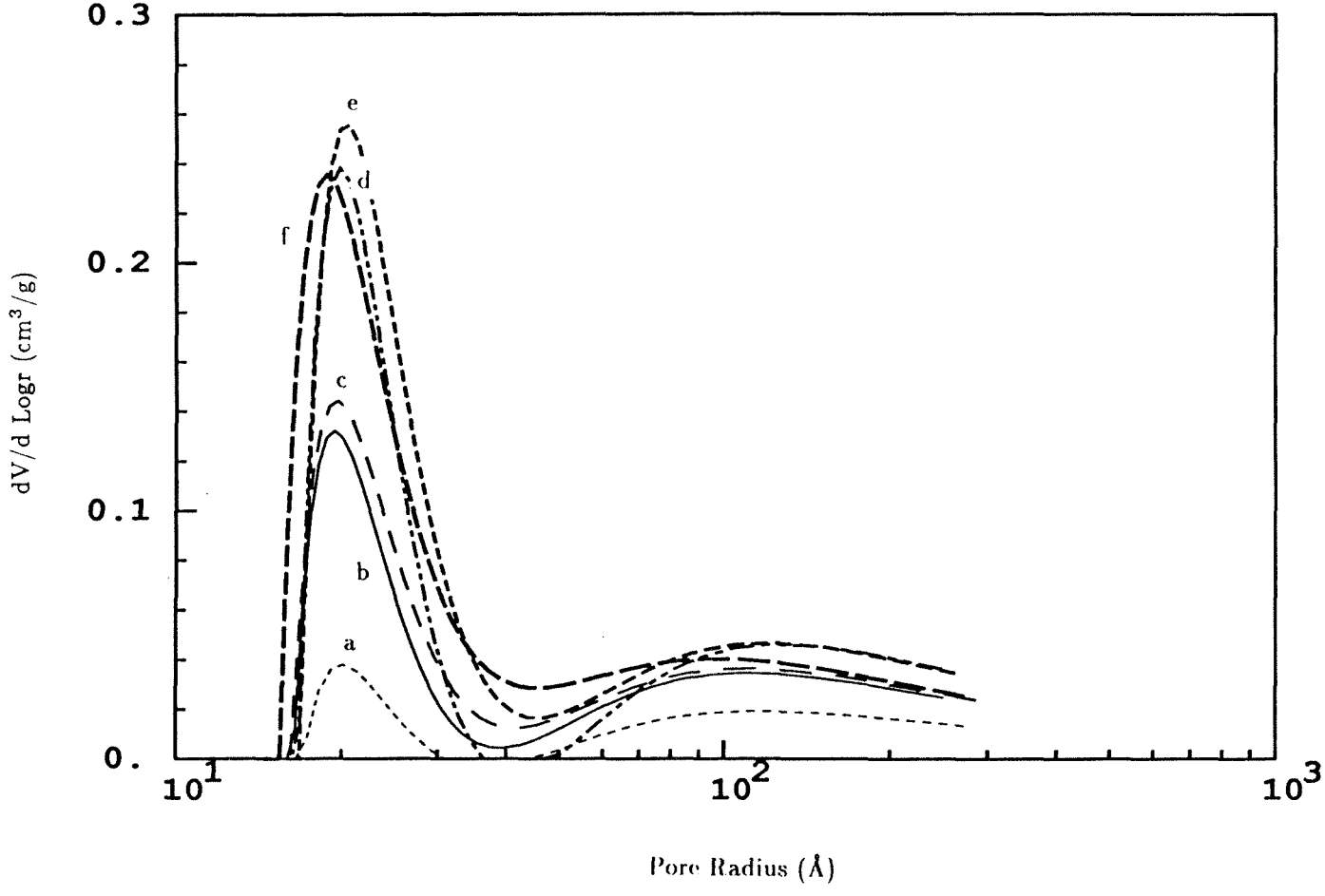

Figure 5.21 Pore volume distributions from capillary condensation on PSOC 1451 1600K 104-125μm char at (a) 0% conversion (b) 14.2% conversion (c) 27.3% conversion (d) 39.9% conversion (e) 57.7% conversion (f) 70.6% conversion.

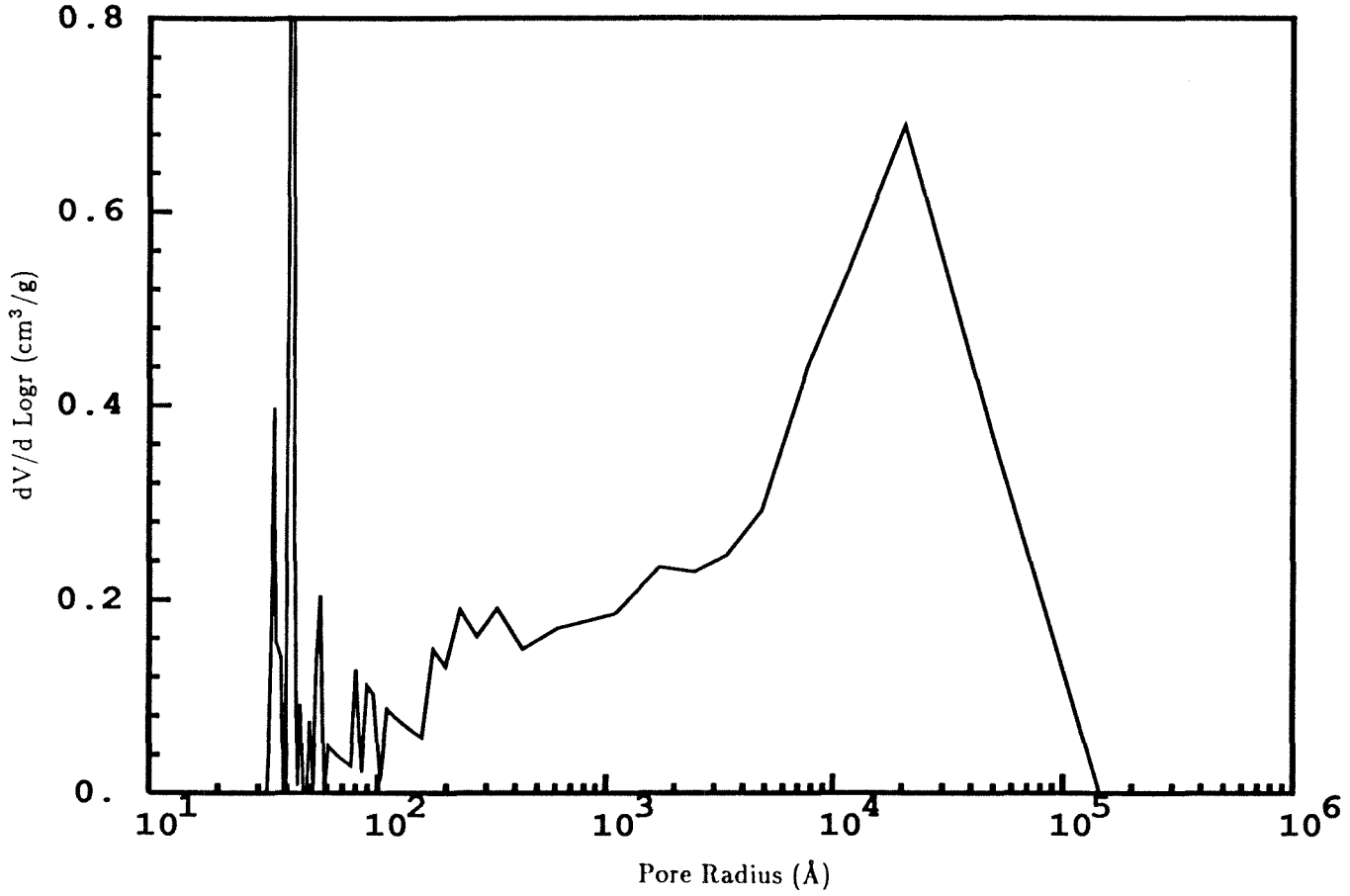

Figure 5.22 Pore volume distribution from mercury porosimetry on PSOC 1451 1600K 104-125μ char after 70.6% conversion at 500°C.

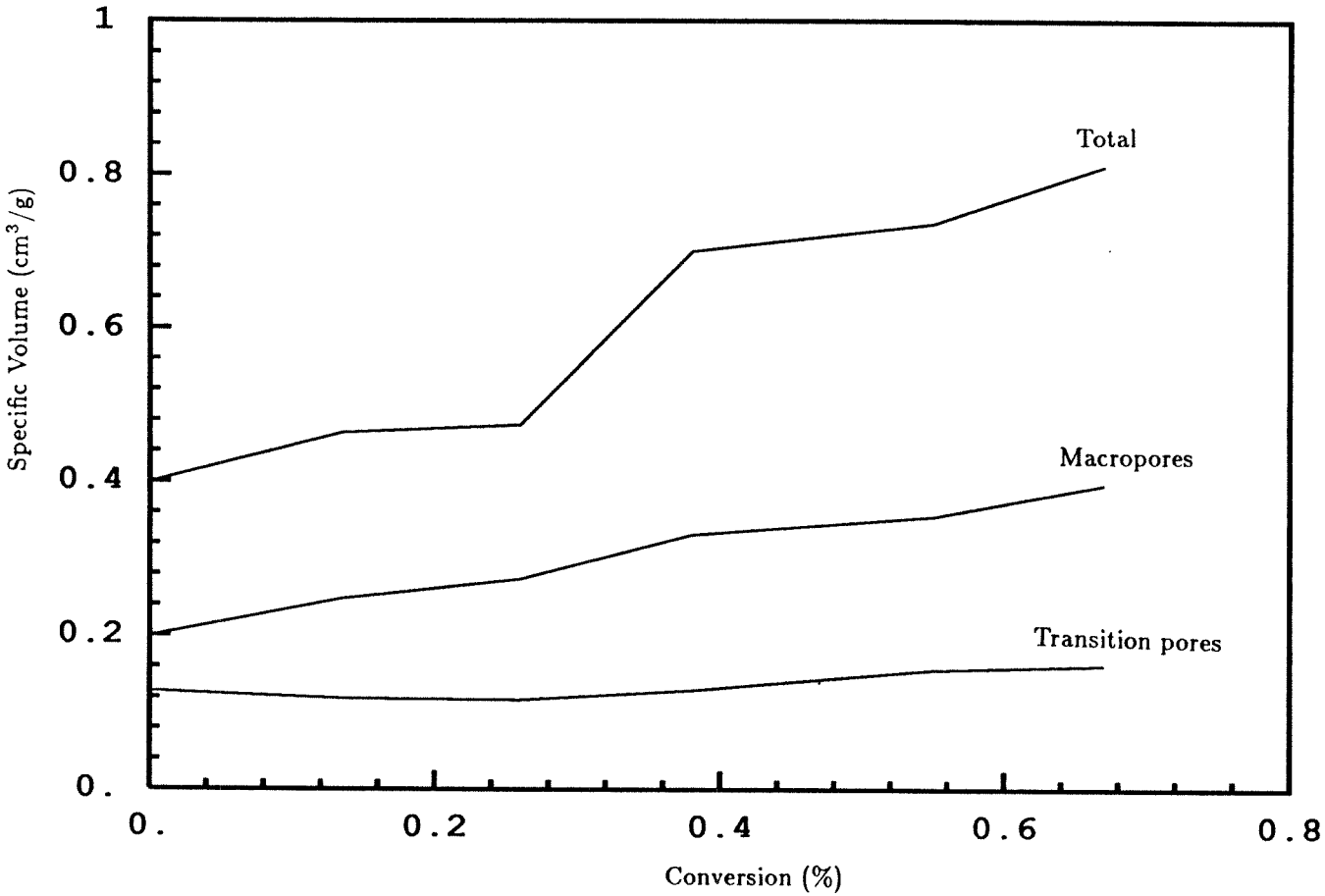

Figure 5.23 Pore volume versus conversion of PSOC 1451 1600K 104-125μ char burned at 500°C.

Chapter 6

IGNITION TRANSIENTS IN THE COMBUSTION OF SINGLE CHAR PARTICLES

Submitted to *Fuel*

Abstract

The temperature-time history of single char particles burning at temperatures above 1500 K have been measured by two-color near infrared pyrometry techniques. Two coal chars and a synthetic char consisting of spherical glassy carbon particles of uniform size were used in the experiments. The results indicate that in the regime of lean combustion and low-to-medium temperatures, the char particles do not ignite over their whole external surface, but exhibit preferential ignition at specific sites. These *hot-spots* probably involve regions where the material exhibits strong inhomogeneities, either on or below the surface. Following ignition, the reaction may propagate over the particle surface. At elevated combustor temperatures and/or high oxygen partial pressures, ignition spreads quickly over the entire particle surface and the importance of the *hot-spots* diminishes. A simple model is used to estimate the rate of growth of a *hot-spot* under various experimental conditions.

6.1 Introduction

The structural complexity of coal is well-documented. The organic components have been mixed with sedimentary strata, compacted, variably subjected to decay and chemically altered by geological processes[1]. In addition to the organic components, the coal microstructure incorporates small and large pores and a plethora of minerals. The particles produced during the grinding process have irregular shapes, and contain cracks and loosely bound material on the surface. Because of this variable surface morphology and the physical and chemical inhomogeneities, there is no reason to expect the particles to ignite and burn uniformly over their surface. In the customary mathematical analysis of char combustion the particles are assumed to have spherical shape and spatially uniform properties, density, pore structure etc. Real particles of course, have irregular shapes and gross spatial inhomogeneities (pores, cracks, minerals) but these irregularities cannot be described mathematically in any reasonable fashion. Nevertheless it is quite clear that these irregularities in char particles cause significant particle-to-particle variations in particle temperature and burnout time. Variations in ignition behavior due to these irregularities can also be expected.

Efforts to understand the ignition mechanism of coal particles date back to Semenov[2]. Thereafter studies on the ignition of clouds of particles,[3,4] and packed beds of particles[5] have been conducted but studies concerning the ignition behavior of single particles are rare. Ignition of coal particles has been assumed to be either homogeneous[6] where emitted volatiles ignite first or heterogeneous[7] where ignition occurs at the particle surface. Recent studies on ignition of single coal particles[8]

suggest that ignition swiches from being homogeneous to heterogeneous as the reactor temperature increases. The ignition of char particles is heterogeneous, in view of the absence of volatiles. Ignition occurs with[9] or without[10] a temperature jump and the measured ignition temperature has been observed to increase with decreasing particle size.[9]

Previous modelling work has utilized steady or unsteady energy balances assuming that the particle ignites uniformly over its surface.[9–12] In this paper we shall present experimental observations that suggest that ignition does not occur uniformly over the particle surface but, rather, occurs in small localized regions. Reaction fronts then propagate over the particle surface. A theoretical description of a reaction front propagation is developed.

6.2 Experimental

The coal chars used in the combustion experiments were derived from the two high volatile bituminous coals, listed in Table 6.1, by devolatilization at 1600 K, for 2 s, and in nitrogen. Experiments were also conducted with glassy carbon chars for comparison purposes. These glassy carbons were synthesized from polymer materials[13] in the form of mineral-free, homogeneous, uniformly sized spheres. The char particles were sized by sieving, with the aid of a mechanical shaker. The size and surface morphology of the particles were examined by optical and scanning electron microscopy (SEM). Physical properties and chemical composition of the particles were measured as described elsewhere.[13,14]

Both coal pyrolysis and char combustion were performed in an externally heated, laminar flow, drop-tube furnace capable of reaching centerline temperatures

of 1600 K. Pyrolysis was performed in a stream of pure nitrogen and combustion in O_2-N_2 mixtures at oxygen partial pressures varying between 0.21 (air) and 1.0 atm. Particle temperatures were monitored with a two-color pyrometer, with broad band filters centered in the near-infrared at 800 and 1000 nm, respectively, and employing silicon photocell detectors. Details of the combustion apparatus and the pyrometer are given elsewhere.[13] For the present experiments, only one particle at a time was introduced into the combustion chamber making it possible to record the two-color radiation intensity traces throughout the combustion life of a single particle. Employing a Planck-law analysis, temperature-time profiles were derived from the ratio of the two intensity signals.

6.3 Results and Discussion

Typical intensity-time traces and the corresponding calculated temperatures for the two coal chars are shown in Figures 6.1-6.3. The combustion atmosphere and wall temperatures were as indicated in the figures while the gas temperature was 1100 K for all cases. Since the oxidation took place at furnace temperatures (centerline and wall) lower than the temperatures used for the pyrolysis process, no devolatilization is anticipated during the char combustion experiments. In Figure 6.1, the particle temperature is approximately constant throughout combustion, but the emission intensities rise through a large fraction of the burn time (region 1) and then decrease throughout the remaining time (region 2). The behavior in region 2 can be attributed to the decreasing particle cross section as the char particle shrinks during the final stages of combustion. In short, the increase in intensity in region 2 is a purely geometrical effect.

The behavior in region 1, where the intensity increases while the temperature remains approximately constant is more difficult to explain. We first ascertained that this behavior is not an artifact generated by the pyrometer electronics. This possibility can be eliminated by the following observations: (a) The silicon photocell detectors used, *Hamamatsu S1336-5BQ*, are very fast, having a nominal rise time of 0.2 μs, and exhibit a linear response. (b) The 'slew' rate of the amplifiers is very fast, 2 V/μs. (c) The response of the two channels of the pyrometer was verified to be the same, by swapping the filters. (d) Radiation intensity traces obtained by Sarofim and coworkers[16,17] exhibit similar behavior, even though a totally different system was used for data acquisition. The pyrometer used in their work employed photomultiplier tubes (PMT) that exhibited a rise time of 15 ns. (e) The peak occurred at different times for different particles and, moreover, a late peak occurred only for particles burning in air, in contrast to particles burning at high O_2 partial pressures, where the intensity rise is almost instantaneous. Thus, it can be safely concluded that the intensity increase must be a characteristic of the combustion behavior of the chars.

It is proposed that the gradual increase in intensity at constant temperature is caused by the spread of the reacting region from one or more localized ignition sites at the particle surface. The intensity of the radiation that is received by the detectors depends on three parameters: (i) the *luminosity* of the light source that is directly related to its temperature; (ii) the *size* of the light source, and (iii) the *distance* between the source and the detector. The distance did not vary significantly in our experiments since, at the furnace flowrates used, a particle travels at most 2 to

4 mm during its burntime (velocity $\approx 10^{-1}$ mm/ms), which is much smaller than the distance between the particle and the detector ($\approx$ 300 mm). Hence, the detectors see a particle that is almost stationary during its entire combustion history. Further, if distance were responsible for the intensity variation at constant temperature, the intensity traces would monotonically decrease, since the particles travel away from the detector. Such behavior was not observed for any particles. The second parameter, luminosity at some fixed wavelength, is a function of temperature via the temperature dependence of Planck's law and by the temperature dependence of the emissivity. However, if the temperature of the particle remains constant, as observed, the luminosity of the particle should also remain constant. Therefore, the recorded intensity variations must be due to variations in the radiating area of the particle projected in the direction of the detector. The increase in the radiating area could be attributed to either an increase in the total area, radiating uniformly, or an increase of the radiating fraction of a roughly constant physical area. In view of prior devolatilization, the total area could not increase by swelling. Therefore, the area of the particle that is radiating increases with time in region (1). It is proposed that a few reactive regions on the char surface ignite first, and thereafter combustion fronts propagate over the rest of the particle. Thus, the radiating area of the particle can increase without an associated increase in temperature, if the ignited regions or *hot-spots* have roughly the same temperature. Progressive ignition on the particle surface has also been observed by photographic techniques.[17]

The higher reactivity in localized regions on the particle surface could result from a number of causes. One possibility is local mineral concentrations that cat-

alyze and accelerate reaction. Previous investigations[18] have shown that the reactivity is greatly enhanced in the presence of impurities, particularly magnesium and calcium. Reactive spots could also be due to localized macro- and transitional pores that serve as *feeders* to the micropores and enhance reactivity. In Figure 6.4a the scanning electron micrograph of a char particle reveals an irregular particle shape, various surface cavities, and large pores and protrusions that usually appear (by the degree of darkness in BSE-SEM) to be rich in ash and could contribute to localized ignition.

Whatever the cause of the localized ignition, particles of the same char would be expected to become fully ignited more rapidly in oxygen-enriched atmospheres than at lower oxygen levels because the combined effect of the oxygen availability and the resulting higher temperatures accelerate the reaction. Hence, the observed delay times, i.e., the duration of region (1), should be short. This is seen by comparing Figures 6.1-6.3. Clearly, the rate of intensity increase in region (1) increases with oxygen level. The short delay observed in the high O_2 level experiments was usually associated with the period of increasing temperature. Ignition in pure oxygen was almost instantaneous.

Combustion of spherical synthetic char particles such as that shown in Figure 6.4b provides a sharp contrast to coal char combustion. These particles are highly uniform and are mineral-free, hence catalytic effects are minimal. These particles are not expected to have important reactive sites. Instead of undergoing localized ignition, such a particle may be uniformly heated close to the ignition temperature before rapid reaction begins. Once ignited, the particle would rapidly be engulfed

in flame. This was confirmed in the experiments whenever it occurred. Combustion of the synthetic chars, proceeded rapidly. Any delay in reaching peak intensities was associated with rising temperatures. The temperature and intensity profiles for combustion of a typical synthetic char particle is shown in Figure 6.5.

Some coal char particles exhibited another interesting phenomenon that is shown in Figure 6.6. The intensities undergo roughly periodic fluctuations. In Figure 6.6a, the intensity in each channel fluctuates periodically for three complete cycles while following an overall decreasing trend. The temperature of the particle is almost constant over that period of time. We attribute these oscillations to the tumbling motion of the particle that changes the projected burning area that is viewed by the detector. Another set of measurements is shown in Figure 6.6b. In this case the periodically varying signal is superimposed on an increasing trend suggesting that tumbling is taking place while *hot-spots* are growing.

Pyrometry traces were also obtained for a lignite char. These are not shown here but they exhibit similar ignition delay times as those observed for the chars of the two bituminous coals. Similar pyrometry results on lignite have also been obtained by others.[15,16]

6.4 Analysis of the Growth of a Hot Spot

In this section we examine the growth of a single local ignited region in an attempt to explain the gradual intensity rise while the particle temperature remains constant. We postulate that a hot, burning region propagates on the comparatively cooler particle surface without delving into the reasons of how such a region was ignited in the first place. The burning region, assumed circular and locally two-dimensional

(Figure 6.7), dissipates heat to the surroundings and the rest of the particle while spreading on the surface at the same time. Using a quasi-one-dimensional analysis and thermal balance arguments, we calculate the growth of the burning region and determine the time required for the ignited region to engulf a hemisphere of the entire particle. This time turns out to be larger than the experimental ignition delay time indicating that ignition involves several rather than one spot on the particle surface.

Assuming the burning region to be a spherical sector, its area A_s is given as:

$$A_s = 2\pi r_p^2 \left(1 - \sqrt{1 - (r/r_p)^2}\right) \tag{6.1}$$

where r and r_p are the radii of the burning region and the particle, respectively. The area of a differential element is then given by:

$$dA_s = 2\pi r \frac{r_p}{\sqrt{r_p^2 - r^2}} dr \tag{6.2}$$

The growth of the burning region is controlled by the balance between heat generation and heat dissipation:

$$\tilde{d}\sigma_a c_p (T_s - T_p) \frac{dA_s}{dt} = Q_G - Q_D \tag{6.3}$$

where Q_G and Q_D are the heat generation and dissipation terms, respectively, c_p the heat capacity and σ_a the apparent density. The thickness, $\tilde{d}$, and the temperature, T_s, of the burning region are assumed to be constant. The temperature T_s is taken equal to the temperature measured by pyrometry. The thickness, $\tilde{d}$, is estimated by the procedure followed in reaction-diffusion problems in the limit of large Thiele modulus. It is given by:

$$\tilde{d} = \frac{r_p}{\phi} \tag{6.4}$$

where r_p is the particle radius and ϕ is the Thiele modulus of the particle[19] given as:

$$\phi = \frac{r_p}{3}\left[A_T \sigma_a R_i C_s^{m-1} D_e^{-1}\right]^{1/2} \tag{6.5}$$

A_T is the pore surface area per unit mass, averaged over the course of combustion, obtained from BET measurements or other equivalent techniques; σ_a is the apparent density of the solid; R_i is the intrinsic reaction rate coefficient; C_s is the oxygen concentration at the particle surface; m is the true reaction order, taken as unity in the present calculations, and D_e is the effective diffusivity in the porous particle. Thus the value of ϕ can be estimated using information about the porous structure of the particle and measured combustion rates.

The heat generated by the burning region can be expressed as:

$$Q_G = A_i \exp(-E_i/\mathrm{R}T_s) C_s A_T \tilde{d} A_s \sigma_a \Delta H \tag{6.6}$$

where E_i is the activation energy of the reaction, A_i is the pre-exponential factor, and C_s is the oxygen concentration at the particle surface. ΔH is the heat of combustion at temperature T_s assuming that the heterogeneous reaction at the surface produces CO exclusively.

Heat dissipation consists of three contributions: conduction into the core of the particle, convection to the surrounding gas, and radiation to the furnace walls. The convection to the ambient gas can be calculated from:

$$\frac{k_{gas}}{r_p}(T_s - T_{gas}) A_s \tag{6.7}$$

where k_{gas} is the thermal conductivity of the gas at the film temperature. This assumes that the Nusselt number is 2, since the Reynolds number, based on the

slip velocity between the particle and the gas is very small. The radiation to the furnace enclosure is:

$$\sigma(\epsilon_s T_s^4 - T_w^4)A_s \tag{6.8}$$

where σ is the Stefan-Boltzmann constant and ϵ_s and ϵ_w are the emissivities of the *hot-spot* and the wall respectively.

Conduction from the surface layer to the interior of the particle is a complicated unsteady two-dimensional problem coupled with the overall propagation problem. For the purpose of this analysis we assume that heat conduction occurs only perpendicular to the surface in an unsteady fashion. The heat flux from an element of the burning region is then given by:

$$\frac{k_c(T_s - T_p)}{\sqrt{\alpha_{eff}(t - \acute{t})}} \tag{6.9}$$

where k_c, α_{eff} are the thermal conductivity and the effective thermal diffusivity of the particle core, t is the current time, and $\acute{t}$ is the time at which burning first reached the surface element in question. The conduction heat flux over the entire burning region is then given by:

$$(T_s - T_p)\int_0^r \frac{k_c d\acute{A}_s}{\sqrt{\alpha_{eff}(t - \acute{t})}} \tag{6.10}$$

where now $\acute{A}_s$ is the area of the burning region at time $\acute{t}$ and r is the radius at time t.

Combining Eqs. (6.3),(6.6)-(6.8) and (6.10) we obtain the heat balance equation for the burning region:

$$\begin{aligned} A_i \exp(-E_i/\mathrm{R}T_s)C_s A_T \tilde{d} A_s \sigma_a \Delta H \;&=\; \sigma_a \tilde{d} c_p (T_s - T_p)\frac{dA_s}{dt} \\ +\frac{k_{gas}}{r_p}(T_s - T_{gas})A_s + \sigma(\epsilon_s T_s^4 - T_w^4)A_s &+ \frac{k_c(T_s - T_p)}{\sqrt{\alpha_{eff}}}\int_0^r \frac{d\acute{A}_s}{\sqrt{t - t_{\acute{t}}}} \end{aligned} \tag{6.11}$$

In equation (6.11), the time t for the front to propagate to radius r is given by

$$t = \int_0^r \frac{d\hat{r}}{S(\hat{r})} \tag{6.12}$$

where $S(r) = dr/dt$ is the velocity of propagation of the burning region. Similarly $t_{\acute{r}}$ is given by Eq. (6.12), replacing r in the upper limit of the integral with $\acute{r}$. Thus Eq. (6.11) is an integro-differential equation in $r(t)$ which must be solved numerically. Once $r(t)$ has been computed, the total time taken by the burning region to cover the hemispherical surface of the particle (visible to the detector) can be found as that value of t for which $r(t) = r_p$. This time, which will be denoted as t_b, should be the upper bound of the experimentally observed delay time, t_D, that elapses before the peak in the pyrometer signals occurs. For the present calculations the temperature of the burning region was taken equal to the temperature deduced from the pyrometer traces, assumed constant, and the temperature of the rest of the particle was assumed equal to the combustor wall temperature. The total surface area of the layer was deduced from BET area measurements on partially combusted samples, assuming that the burning region had the same average surface per unit mass as that of the char after partial burning. Details of the variation of total surface area with burnout are not included in the present analysis but are given elsewhere[14]. The effective conductivity was estimated using the correlation of Butt[20], while the heat capacity by a relationship given by Kelley[21]. The intrinsic kinetics used were determined for the present chars from other experiments[22] employing the same experimental setup and analyzing the results using the capillary model of Gavalas[23] to describe the evolution of pores. For the PSOC-1451 1600 K char the activation energy, E_i was estimated to be 34000 cal/mole and the pre-exponential factor A_i

was 8.6x10^5 cm/s. Smith's kinetics[24] (E_i = 42800 cal/mole and A_i = 1.46x10^6 cm/s) give similar values.

Figure 6.8 shows the calculated variation of t_b with oxygen partial pressure. The predicted ignition transient times are higher by a factor of almost five compared to those observed experimentally. For the case of the particle shown in Figure 6.1, the experimentally observed delay time is 12 ms while the thoeretically determined delay time (corresponding to an oxygen partial pressure of 0.12) is around 60 ms. This suggests that there are more than one such spots propagating over the particle surface. As expected, t_b decreases with increasing oxygen partial pressure and with decreasing particle size.

The speed of propagation of the spot increases rapidly as the radius expands, reaches a maximum and falls off as the particle radius is reached. This is shown in Figure 6.9. If several *hot-spots* are growing simultaneously as suggested by the experimental ignition delay times then only the first part of the speed versus radius curve is physically significant. The values assumed for the emissivities of both the particle and the wall had negligible effects in the calculation, indicating the minor importance of the radiation heat loss in the cases examined. Likewise, the apparent particle density does not seem to be an important factor. Finally, t_b is inversely proportional to the pore surface area of the char.

6.5 Conclusions

The ignition behavior of coal chars at various oxygen partial pressures and combustion chamber temperatures has been observed by means of near-infrared optical pyrometry techniques. It has been concluded that at mild combustion conditions

(combustor temperatures around/or below 1300 K and oxygen partial pressures at/or below 0.21), the char particles undergo preferential ignition at localized reactive sites leading to the development of *hot-spots*. The reaction zones take a finite time to engulf and ignite the whole particle. These reactive sites can be due to of mineral matter catalysis, enhanced porosity or favorable surface morphology. At elevated combustor temperatures and/or high O_2 concentrations the ignition proceeds almost instantaneously because of temperature-dependent kinetics. A energy balance was used to estimate the time required for the spreading of a local *hot spot*. Comparision of the estimated times and measured ignition times suggest that several spots are spreading over the particle surface simultaneously.

6.6 Acknowledgements

This work was supported by the U.S. Department of Energy University Coal Programs Grant Number DE-FG22-84PC70775.

References

1. Neavel, R. C.: *Chemistry of Coal Utilization* (M. A. Elliot, Ed.) Wiley-Interscience, New York, 1981.
2. Semenov, N. N.: Chemical Kinetics and Chain Reactions, Clarendon Press, Oxford, 1935; original publication in USSR in 1934.
3. Palmer, K. W.: Dust Explosions and Fires, Chapman and Hall, London, 1973.
4. Essenhigh, R. H.: *Chemistry of Coal Utilization*, 2^{nd} suppl. vol. (M. A. Elliot, Ed.) Wiley, New York, 1981.
5. Hardman, J. S., Lawn, C. J. and Street P. J.: Fuel 62, 632 (1983).
6. Borio, R. W.: ASME Paper No. 74 WA/FU-2 (1974).
7. Howard, J. B. and Essenhigh, R. H.: *Eleventh Symposium (International) on Combustion*, p. 399, The Combustion Institute, 1967.
8. Gomez C. O. and Vastola F. J.: Fuel 64, 558 (1985).
9. Bandyopadhayay S. and Bhaduri D.: Comb. Flame 18, 411 (1972).
10. Thomas, G. R., Stevenson, A. J. and Evans, D. G.: Comb. Flame 21, 133 (1973).
11. Annamalai, K and Durbetaki P.: Comb. Flame 29, 193 (1977).
12. Libby, P. A.: Comb. Flame 38, 285 (1980).
13. Levendis, Y. A. and Flagan, R. C.: Comb. Sci. Tech. 53, p117 (1987).
14. Sahu, R., Levendis, Y. A., Flagan, R.C., and Gavalas, R. G.: Fuel, in print.
15. Altrichter, D. M.: *Optical Determination of Time-Temperature Profiles for Single Coal Particle*, Master's Thesis, MIT, 1981.

16. Timothy, L. D., Sarofim, A. F. and Béer, J. M.: *Nineteenth Symposium (International) on Combustion* p. 1123, The Combustion Institute, 1982.

17. Sarofim, A. F. and Béer. (1986), personal communication.

18. Jenkins, R. G., Nandi, S. P. and Walker, Jr. P. L.: Fuel 52, 288, (1973).

19. Hill, Jr. C. G.: An Introduction to Chemical Engineering Kinetics and Reactor Design, Wiley, New York, p. 447, 1977.

20. Butt, J. B.: A.I.Ch.E.I VII, 106 (1965).

21. Kelley, K. K.: US Bureau of Mines, Bull. 476, 1949.

22. Sahu, R., Northrop, P. S., Flagan, R. C. and Gavalas, R. G.: Presented at AIChE 1987 Annual Meeting, Nov 15-20, 1987.

23. Gavalas, G. R.: Comb. Sci. Tech. 24, 197 (1981).

24. Smith, I. W. Comb. Flame 17, 303 (1971).

Notation

SYMBOL	DESCRIPTION	UNITS
A_i	pre-exponential factor	g/cm^2s
A_s	surface area of spherical sector	cm^2
A_T	specific total surface area	cm^2/g
c_p	heat capacity of carbon	J/g K
C_s	surface oxygen concentration	g/cm^3
$\tilde{d}$	oxygen diffusion zone	cm
$\acute{d}$	thermal diffusion zone	cm
D_e	effective diffusivity	cm^2/s
e	particle porosity	
E_i/R	reduced activation energy	K
k_p	conductivity of carbon	W/cm K
k_c	effective conductivity	W/cm K
k_{gas}	conductivity of gas	W/cm K
$p_{O_2,s}$	oxygen partial pressure at particle surface	atm
r	radial distance	cm
r_p	particle radius	cm
R_i	intrinsic reaction rate coefficient	cm/s
S	flame front velocity	cm/s
t_b	theoretical flame propagation time	ms
t_D	experimentally observed delay time	ms
T_p	particle temperature	K

T_g	ambient temperature	K
T_s	*hot-spot* temperature	K
T_w	combustor wall temperature	K
α_{eff}	effective thermal diffusivity	cm^2/s
δ	flame front propagation zone	cm
ΔH	heat release	J/g
ϵ_s	emissivity of *hot-spot*	
ϵ_w	emissivity of wall	
σ_a	apparent density	g/cm^3
σ	Stefan-Boltzmann constant	W/cm^2K^4

COALS	176	1451
RANK	Bit. HVB	Bit. HVA
MOISTURE (%)	0.8	2.5
ASH (%)	6.5	13.5
CARBON (%)	78.4	71.5
HYDROGEN (%)	5.4	4.7
OXYGEN (%)	5.5	7.0
NITROGEN (%)	1.3	1.3
SULFUR (%)	2.9	1.3
VOLATILE MATTER (%)	40.2	33.5
HEATING VALUE (DRY BASIS) cal/g	7910	6965

Table 6.1 Properties of parent coals.

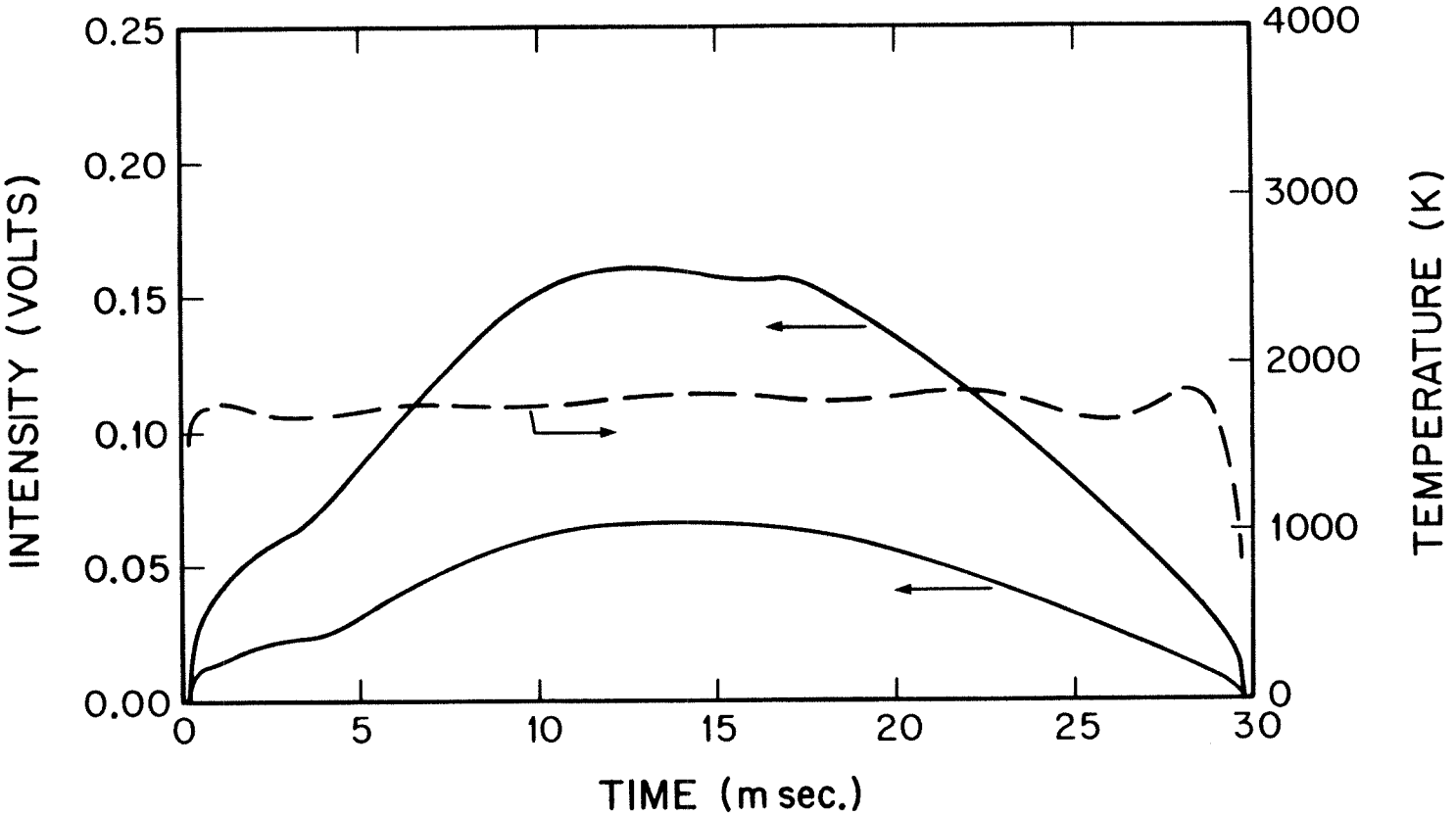

Figure 6.1 Intensity signals and particle temperature profiles of a PSOC-1451 100μm coal char particle burning at a combustor wall temperature of 1300 K and p_{O_2} = 0.21.

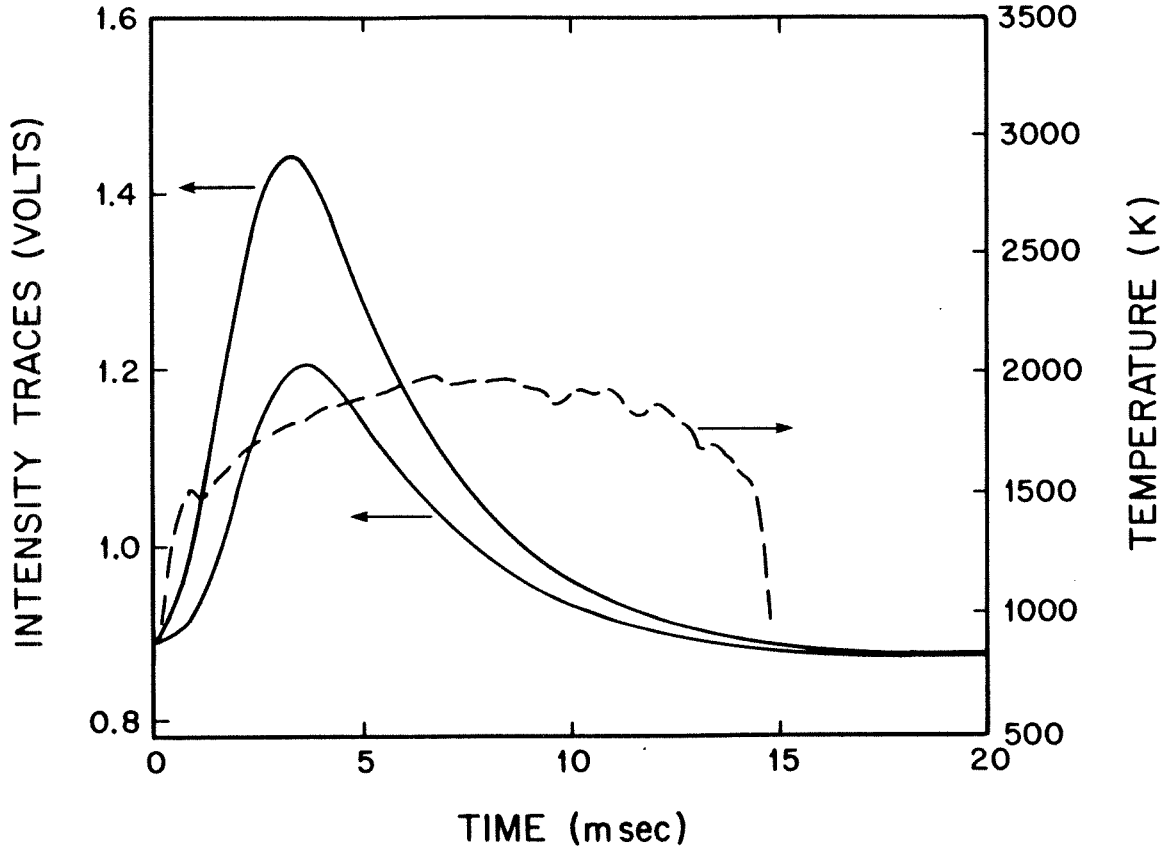

Figure 6.2 Intensity signals and particle temperature profiles of a PSOC-176 50μm coal char particle burning at a combustor wall temperature of 1300 K and p_{O_2} = 0.50.

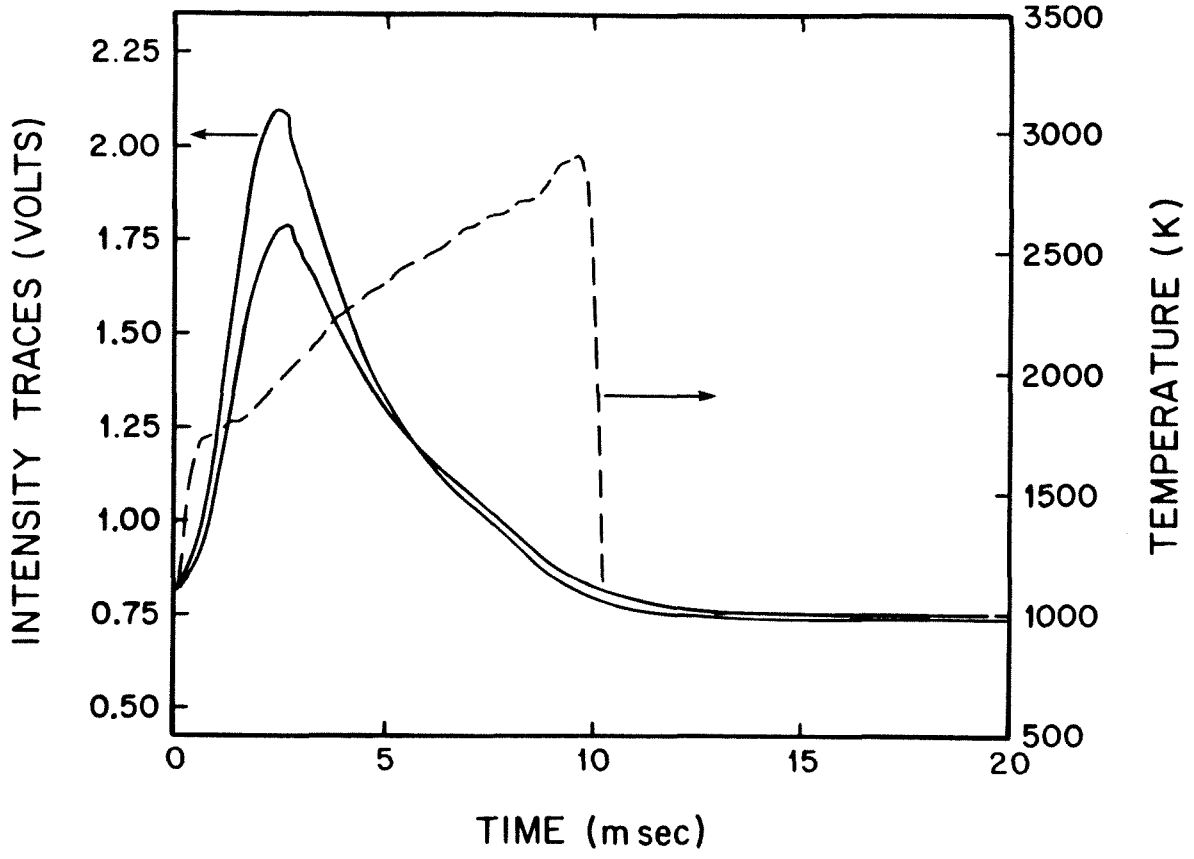

Figure 6.3 Intensity signals and particle temperature profiles of a PSOC-176 50μm coal char particle burning at a combustor wall temperature of 1300 K and $p_{O_2} = 1.0$.

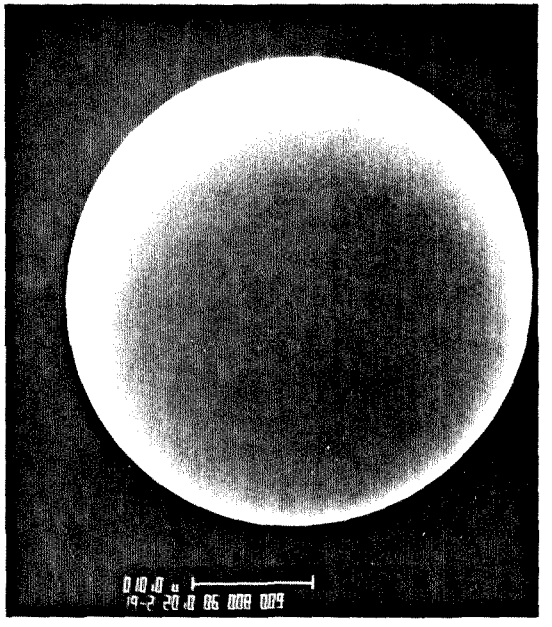

a b

Figure 6.4 SEM micrographs depicting (a) a PSOC-1451 particle pyrolyzed at 1600 K. and (b) a glassy carbon particle.

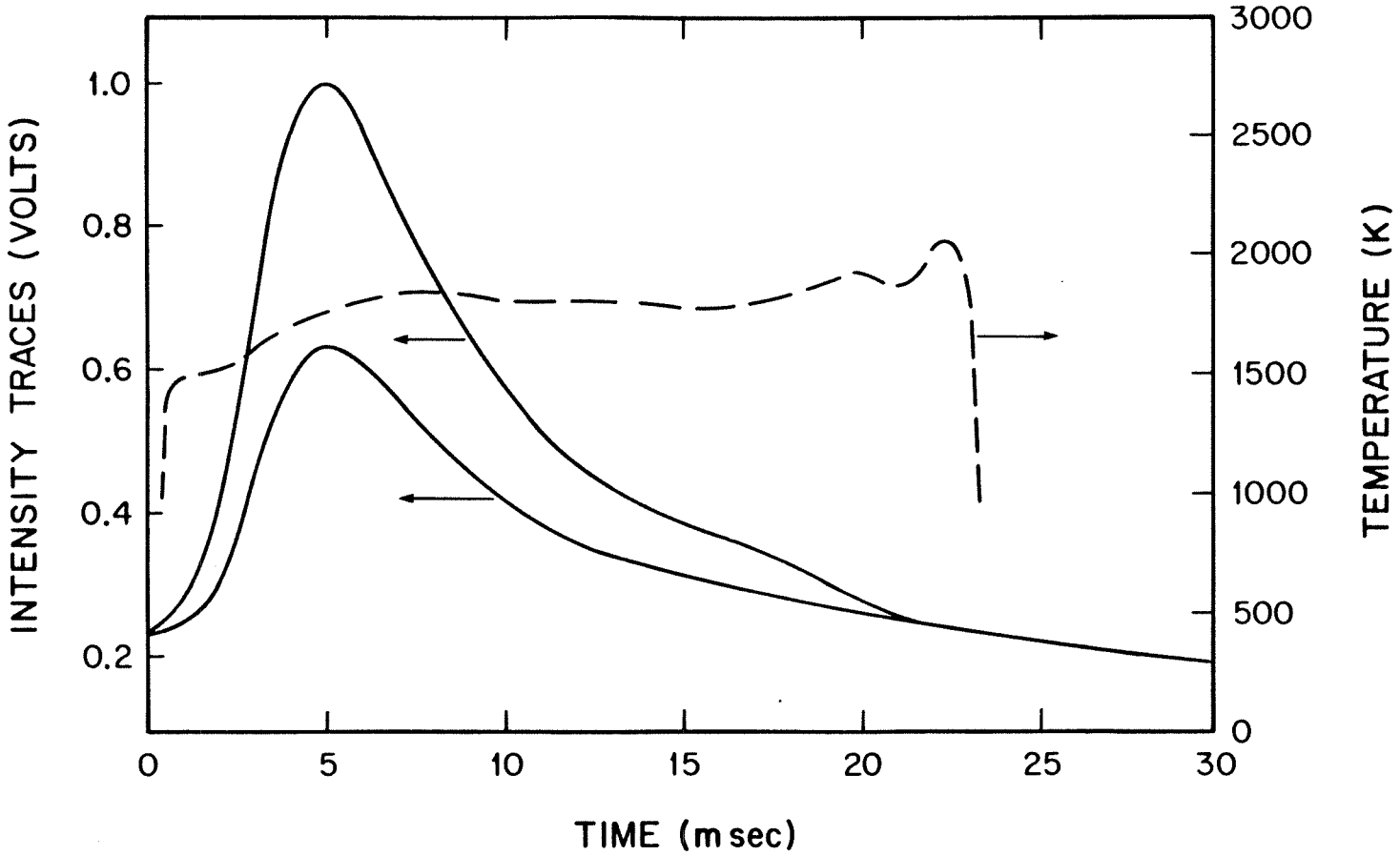

Figure 6.5 Intensity signals and particle temperature profiles of a 45μm glassy carbon particle burning at a combustor wall temperature of 1500 K and $p_{O_2} = 0.40$.

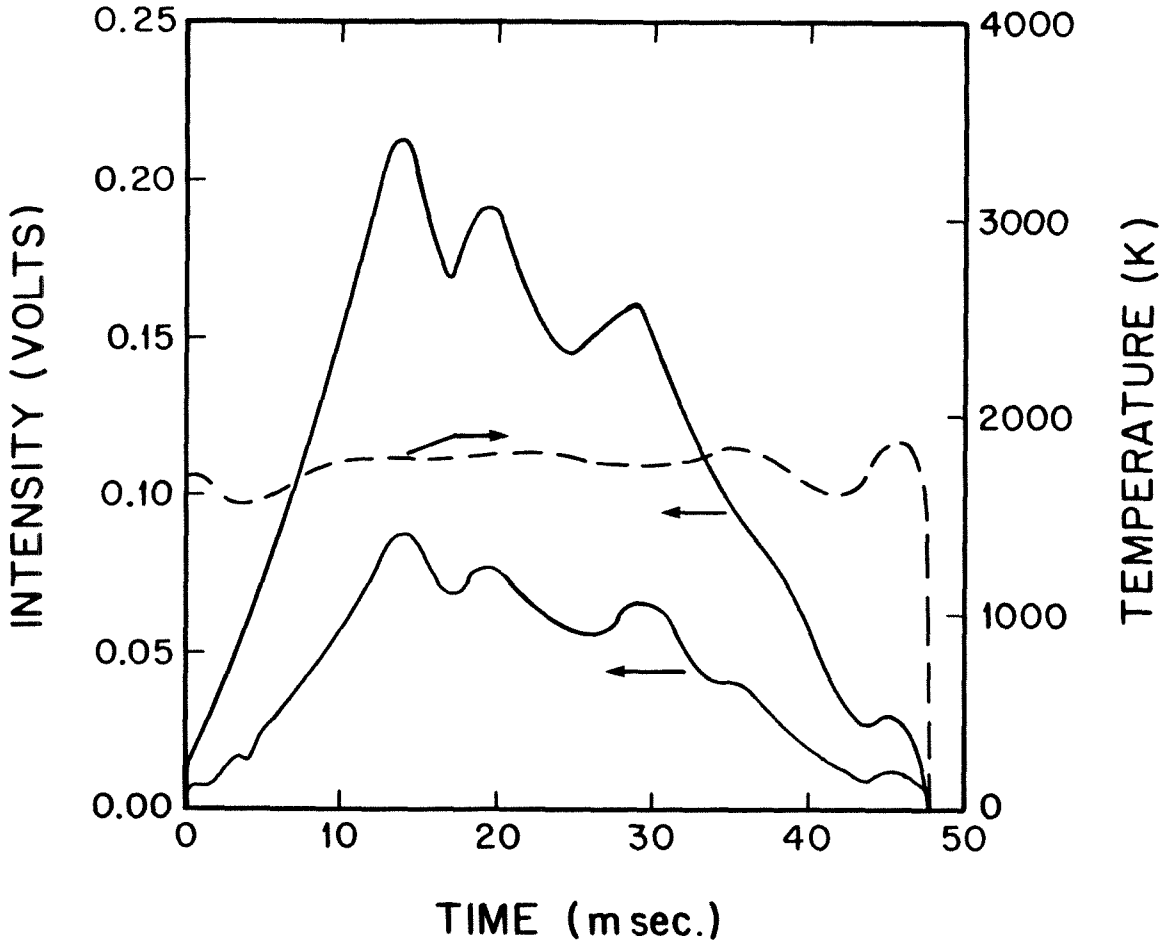

Figure 6.6a Intensity signals and particle temperature profiles of a PSOC-1451 100μm coal char particle burning at a combustor wall temperature of 1300 K and p_{O_2} = 0.21. Particle exhibits tumbling behavior.

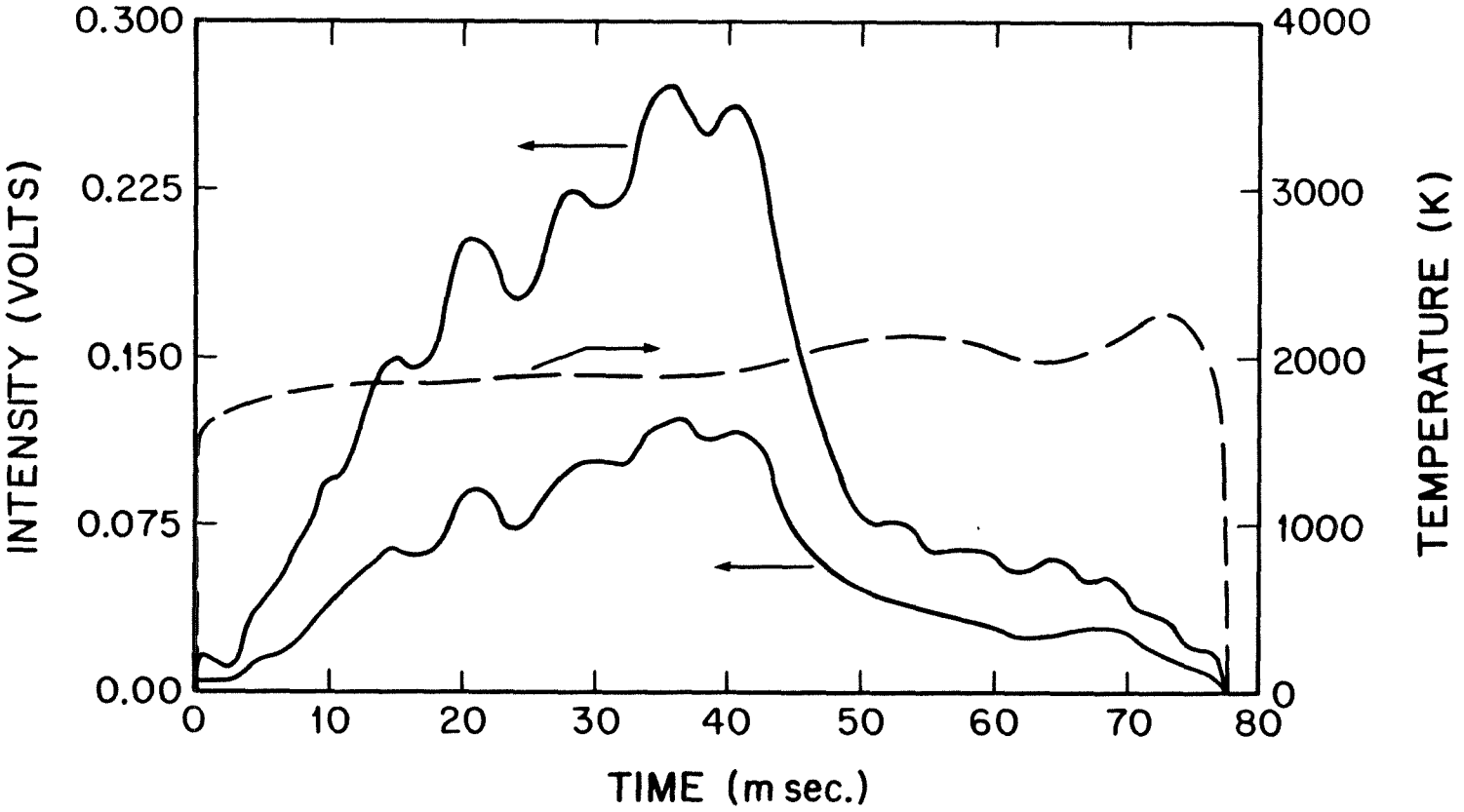

Figure 6.6b Intensity signals and particle temperature profiles of a PSOC-1451 100μm coal char particle burning at a combustor wall temperature of 1300 K and p_{O_2} = 0.21. Particle exhibits tumbling behavior.

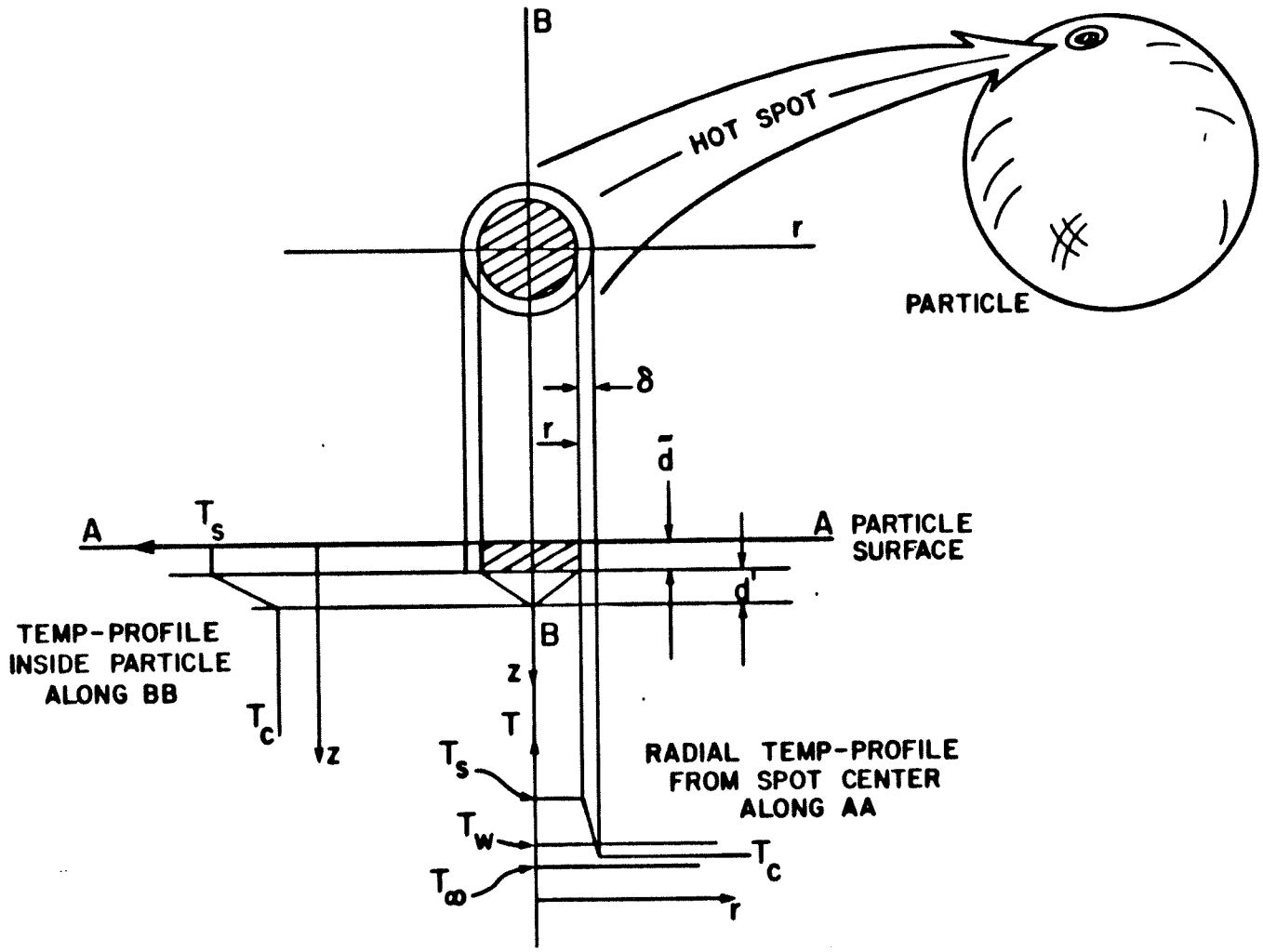

Figure 6.7 Schematic representation of the *hot spot* assumed in the model.

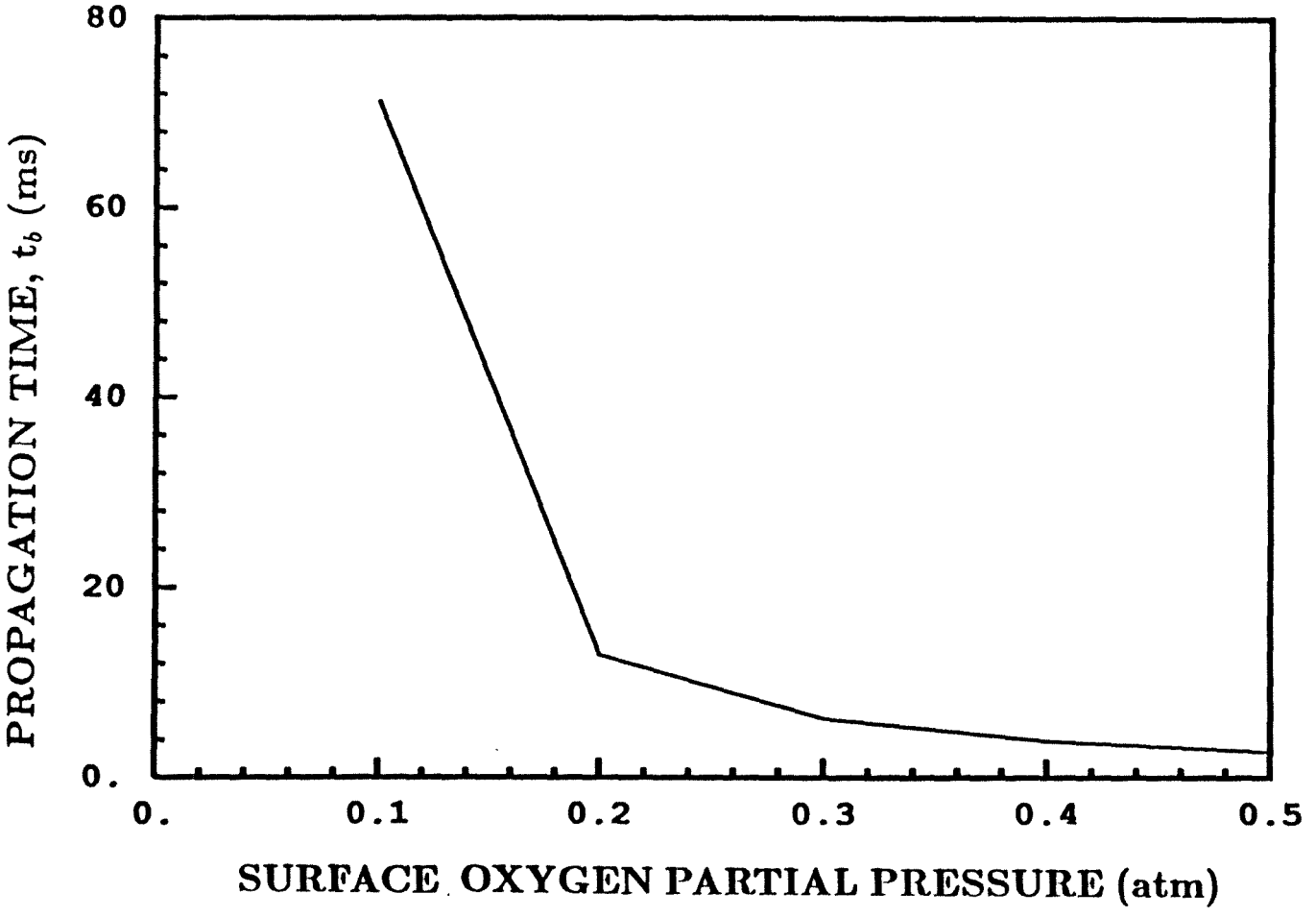

Figure 6.8 Results of the mathematical modelling: the effect of oxygen partial pressure on the flame spreading delay time t_b.

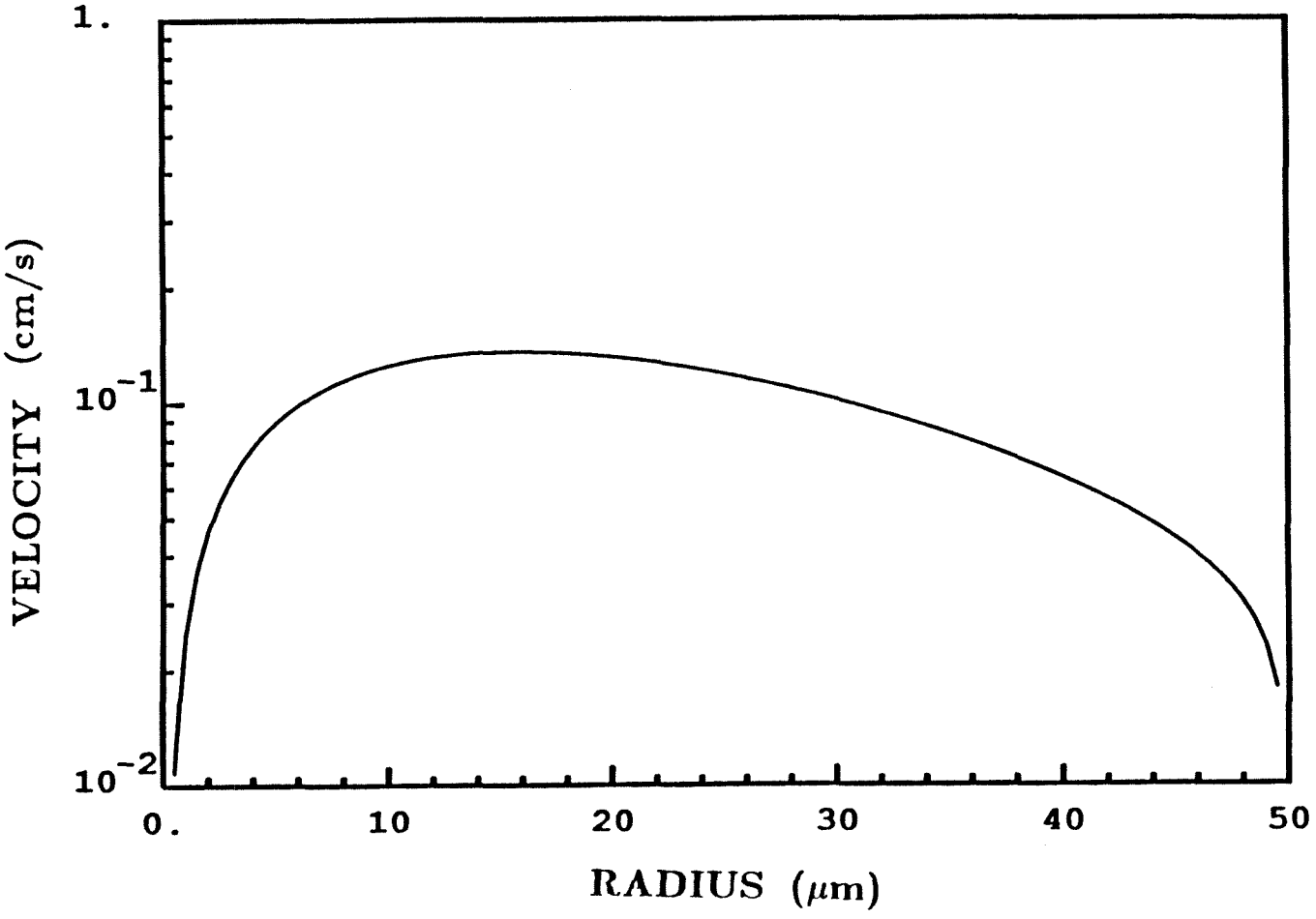

Figure 6.9 Results of the mathematical modelling: velocity of propagation of the burning region as a function of its radius.

Chapter 7

CONTINUUM MODELLING

7.1 Introduction

This chapter will describe, in detail, the models that were developed to describe char particle combustion. All the models assume that the particle is spherical and has internal spherical symmetry. The internal morphology is assumed to be a continuum of fine pores, thereby allowing diffusion and reaction inside the particle to be described by differential equations. Models that consider larger discrete pores are described in the next Chapter.

Most of the attention has been focussed on the changes in the internal solid structure of the particle and its effect on combustion variables. Reasonable assumptions were made regarding the description of the solid morphology. Pore structure parameters were estimated from gas adsorption and mercury porosimetry data. Thermodynamic and transport properties were assumed to be functions of temperature within the particle and in the gas phase. The reactions in the gas phase were not considered.

The simplest model which assumes that all the reaction occurs at the particle surface and none inside is described in detail in the next section. While this may seem too restrictive at first, it is applicable to many situations of combustion at high temperatures and high oxygen concentrations since, in these situations, there is very little penetration of oxygen into the particle as will be shown later. The computational burden is light, and the model can describe fairly accurately the proper temperature-time histories observed in the experiments.

Section 7.3 describes the general model involving a simplistic internal geometry which is later extended in Section 7.4 to more realistic internal morphologies. The

diffusion equation inside the particle is solved to accurately predict the internal oxygen concentration profiles which then determine the carbon flux, void fraction, specific surface area, etc.

The influence of nonlinear reaction kinetics such as the Langmuir-Hinschelwood and Power law are discussed briefly in the last section.

The effects of parametric variations are discussed in detail in all cases. Limitations and applicability of the various models are stated as necessary.

Computer code listings for all the major programs are given in Appendix IX. The programs were written in standard Fortran 77 and the actual simulations were done on IBM and compatible personal computers.

7.2 Asymptotic Model with Lumped Surface Reaction

The simplest model of char combustion considered is a homogenous particle that reacts only at its exterior surface. The solid particle is assumed to be spherical and to contain internal voids and ash particles distributed uniformly throughout its entire volume. Details of the internal morphology, such as pore volume distribution and ash size and distribution, are not important in this model since the reaction is assumed to occur only at the particle surface. However, the presence of the voids changes the particle density. Let the volume fraction of the voids and ash in the particle be ϵ and ϵ_A respectively. Assuming that the densities of carbon and ash are ρ_C and ρ_A, a mass balance gives,

$$\rho_a = \epsilon_A(\rho_A - \rho_C) + \rho_C(1 - \epsilon) \tag{7.1}$$

where ρ_a is the apparent density of the particle.

The reaction at the particle surface is assumed to be the heterogenous reaction, $2C+O_2 \rightarrow 2CO$ since it has been shown that, at high temperatures, the heterogenous reaction leading to CO_2 formation is not as important (Mitchell, 1986). Also, the reaction of carbon with water vapor has been neglected since the amounts of water vapor in the experimental systems used in this study were negligible.

Once the carbon monoxide is formed, it is assumed to oxidize in the gas phase, far from the particle. Thus, in this model details of the gas phase combustion are not considered. The gas phase is also assumed to be quasi-steady with respect to solid phase combustion.

The particle is also assumed to be isothermal. The reaction rate used in this model is based on the external area of the particle, *i.e.* it is the apparent rate. All thermodynamic and transport properties are assumed to be temperature dependent. This is a significant improvement over models that assume constant or average property values over wide ranges of temperature variation.

Assumptions regarding the effects of ash on combustion are based on experimental observations from electron microscopy as discussed in Chapter 5. As the carbon is oxidized, the ash particles are exposed at, then accumulate on the surface. The thickness of the ash layer increases as combustion proceeds, and it is assumed that none of the ash is lost. This porous ash layer presents a diffusional resistance to the oxygen transport in series with the gas phase diffusional resistance. The presence of ash also manifests itself in the energy balance of the particle, increasing its thermal inertia and altering its radiative properties. A detailed study of the radiative properties of the combined carbon-ash layer has not been undertaken.

Instead, an overall emissivity of the particle is used.

In an early version of the model, the effect of ash was accounted for differently. Instead of forming a porous layer on the particle, patches of ash were assumed to cover parts of the surface of the carbon. Reaction was allowed to take place only on those parts not blocked by the ash. The fraction of surface blocked was equal to the ash mass fraction in the particle. The computer code for this model is also given in Appendix IX.

7.2.1 Equations

The particle mass balance can be written in terms of the apparent reaction rate as:

$$\frac{dm_C}{dt} = -A_a e^{-E_a/RT_p} Y_{1*} 4\pi r^2 \tag{7.2}$$

where m_C is the mass of carbon, A_a and E_a are the apparent Arrhenius reaction rate parameters, R is the universal gas constant, Y_{1*} is the mass fraction of oxygen at the carbon surface, r is radius of the carbon sphere (Figure 7.1), and T_p is the particle temperature. The negative sign implies that mass decreases with time. The reaction kinetics are assumed to be first order with respect to surface oxygen concentration. The value of Y_{1*} is determined as follows: at first the oxygen mass fraction outside the ash layer, Y_{1p}, is determined and then by properly accounting for diffusion in the ash layer, we get Y_{1*}.

The particle energy balance can be written as:

$$\frac{d}{dt}\{m_C H_C + m_A H_A\} = \text{Energy Generation Rate} - \text{Energy Loss Rate} \tag{7.3}$$

where m and H are the mass and enthalpy, respectively. The subscripts C and A

denote carbon and ash. The energy generation rate is given by

$$-\frac{dm_C}{dt}\Delta H_{comb}(T_p) \tag{7.4}$$

where ΔH_{comb} is the enthalpy of combustion of the heterogenous reaction at the particle temperature. The rate of mass loss can be rewritten using the carbon mass flux per unit external area at the particle surface, N_p, as

$$-\frac{dm_C}{dt} = 4\pi r_p^2 N_p \tag{7.5}$$

The energy generation term can be written in terms of the enthalpies and the mass fluxes of the gas phase components (O_2=1: CO=2: N_2=3) as

$$-4\pi r_p^2 \sum_{i=1}^{3} N_i H_i \Big|_{r=r_p} \tag{7.6}$$

In equation (7.6), N_i and H_i are, respectively, the mass flux away from the particle and specific enthalpy of the gas phase component i. From stoichiometry we have

$$N_{1p} = -\frac{4}{3}N_p, \quad N_{2p} = \frac{7}{3}N_p, \quad N_{3p} = 0 \tag{7.7}$$

There are two heat loss terms accounting for conduction and radiation. The heat loss by conduction is given by

$$e_{cond} = -4\pi r_p^2 k \left.\frac{dT}{dr}\right|_{r=r_p} \tag{7.8}$$

where k is the thermal conductivity of the gas phase. The heat loss due to radiation from the particle to its surroundings is given by

$$e_{rad} = 4\pi r_p^2 \sigma\{\epsilon_o T_p^4 - \epsilon_\infty T_\infty^4\} \tag{7.9}$$

where σ is the Stefan-Boltzmann constant of radiation, ϵ_o is the emissivity of the particle, ϵ_∞ is the emissivity of the wall or radiating environment far from the particle, and T_∞ is the temperature of the wall. The unsteady term on the left hand side of equation (7.3) can be expanded using the chain rule. Also the enthalpy H of either carbon or the ash can be written as

$$H = H_0 + \int_{T_0}^{T_p} c_p dT \tag{7.10}$$

where H_0 is the enthalpy at some reference temperature T_0. Using the chain rule, equation (7.10) and equation (7.5), the unsteady term in equation (7.3) becomes

$$(m_C c_{pC} + m_A c_{pA}) \frac{dT_p}{dt} - 4\pi r_p^2 N_p H_C \tag{7.11}$$

Therefore combining equations (7.11),(7.6),(7.8) and (7.9), the particle energy balance becomes

$$\begin{aligned}(m_C c_{pC} + m_a c_{pa}) \frac{dT_p}{dt} = 4\pi r_p^2 \Bigg[& N_p H_C - \sum_{i=1}^{3} N_i H_i \Big|_{r=r_p} \\ & + k \frac{dT}{dr}\Big|_{r=r_p} - \sigma\{\epsilon_o T_p^4 - \epsilon_\infty T_\infty^4\} \Bigg]\end{aligned} \tag{7.12}$$

Defining

$$e_p \equiv \left[-k \frac{dT}{dr} + \sum_{i=3}^{3} N_i H_i \right]_{r=r_p} \tag{7.13}$$

and

$$\gamma_p \equiv \frac{e_p}{N_p} \tag{7.14}$$

the energy balance becomes

$$(m_C c_{pC} + m_A c_{pA}) \frac{dT_p}{dt} = 4\pi r_p^2 \left[N_p H_C - N_p \gamma_p - \sigma\{\epsilon_o T_p^4 - \epsilon_\infty T_\infty^4\} \right] \tag{7.15}$$

Transport in the gas phase is described by the Stefan-Maxwell equations:

$$\frac{dY_i}{dr} = \sum_j \frac{(Y_i N_j - Y_j N_i)}{\rho_g \mathcal{D}_{ij}} \tag{7.16}$$

where Y_i is the mass fraction of species i, N_i is the mass flux of i, ρ_g is the density of gas and $\mathcal{D}_{ij}$ is the diffusivity of component i in component j. Here, in our 3-component system: species 1 = O_2, 2 = CO, and 3 = N_2. Since these molecules are similar in size, the binary diffusion coefficients $\mathcal{D}_{ij}$ are assumed equal. This simplifies (7.16) to

$$N_i = -\rho_g \mathcal{D} \frac{dY_i}{dr} + NY_i \tag{7.17}$$

where N is the total mass flux $\sum_i N_i$ which satisfies

$$r^2 N = r_p^2 N_p \tag{7.18}$$

where the subscript p denotes values at the surface of the particle. Loewenberg *et al.* (1987) have shown that the equations (7.17) for the various species can be combined to give

$$\frac{d(Y_1/4 + Y_2/7)}{dY_3} = \frac{Y_1/4 + Y_2/7}{Y_3} \tag{7.19}$$

From this, along with boundary conditions at r→∞ and the fact that $\sum_i Y_i = 1$, Y_2 and Y_3 are obtained in terms of Y_1 as given below:

$$Y_3 = \frac{3/28 Y_1 + 1/7}{1/Y_{3\infty}(Y_{1\infty}/4 + Y_{2\infty}/7) + 1/7} \tag{7.20}$$

$$Y_2 = 1 - Y_1 - Y_3 \tag{7.21}$$

where the subscript ∞ denotes values far from the particle.

The energy balance for the gas phase is:

$$r^2\{-k\frac{dT}{dr} + \sum_i N_i H_i\} = r_p^2 e_p \tag{7.22}$$

From the stoichiometric relations (7.19) and overall mass balance (7.18),

$$r^2 k\frac{dT}{dr} = r_p^2\left(\frac{N_p}{3}(h(T) - e_p)\right) \tag{7.23}$$

with $h(T) = \{7H_2 - 4H_1\}/3$. The boundary conditions are:

$$r = r_p : T = T_p; r \to \infty : T \to T_\infty \tag{7.24}$$

Integrating (7.23) gives

$$r_p N_p = \int_{T_\infty}^{T_p} \frac{k dT}{\gamma_p - h(T)} \tag{7.25}$$

This is an algebraic expression for mass flux at the surface. Combining (7.25) with the mass balance for oxygen (7.23) yields

$$r^2 \rho_g \mathcal{D}\frac{dY_1}{dr} = r_p^2 N_p\{Y_1 + \frac{4}{3}\} \tag{7.26}$$

Dividing (7.26) by (7.23) gives

$$\frac{\rho_g \mathcal{D}}{k}\frac{dY_1}{dT} = \frac{Y_1 + 4/3}{h(T) - \gamma_p} \tag{7.27}$$

Assuming that the temperature and mass fraction of oxygen far from the particle are T_∞ and $Y_{1\infty}$ equation (7.27) can be integrated to yield

$$ln\frac{Y_{1\infty} + 4/3}{Y_{1p} + 4/3} = \int_{T_\infty}^{T_p} \frac{k dT}{\rho_g \mathcal{D}\{\gamma_p - h(T)\}} \tag{7.28}$$

This is a quadrature for the energy flux at the particle surface. Equations (7.25) and (7.28) were solved numerically to obtain the particle temperature and the oxygen mass fraction at the external surface of the ash layer as a function of time.

Once the oxygen mass fraction outside the ash layer, Y_{1p}, is obtained, its mass fraction, Y_{1*}, at the carbon surface can be determined. The ash layer is assumed to be at the same temperature as the particle. Let h_{mgas} and h_{mash} be the mass transfer coefficients in the boundary layer outside the particle and in the ash layer respectively. Then, the mass balance across the various layers can be written as

$$\begin{aligned} 4\pi r^2 A_a e^{-E_a/RT_p} Y_{1*} &= 4\pi r^2 h_{mash}(Y_{1p} - Y_{1*})\frac{\mathcal{F}M_{O_2}}{RT_p} \\ &= 4\pi(r+t)^2 h_{mgas}(Y_{1\infty} - Y_{1p})\frac{\mathcal{F}M_{O_2}}{RT_g} \end{aligned} \tag{7.29}$$

where, t is the thickness of the ash layer, $\mathcal{F}$ is a stoichiometric factor relating the number of grams of carbon to the number of grams of oxygen, M_{O_2} is the molecular weight of oxygen and T_g is the boundary layer film temperature. Eliminating Y_{1p} from (7.29) we get

$$Y_{1*} = \frac{XY_{1\infty}}{(M+1)(X+1)-1} \tag{7.30}$$

where M and X are given by the relations below:

$$X = \frac{h_{mgas}}{h_{mash}}\left(1+\frac{t}{r}\right)^2 \tag{7.31}$$

$$M = \frac{A_a e^{-E_a/RT_p}}{h_{mash}\frac{\mathcal{F}M_{O_2}}{RT_p}} \tag{7.32}$$

The mass transfer coefficients, assuming spherical geometry and negligible Reynolds number, are given by

$$h_{mgas} = \frac{\mathcal{D}}{r+t} \tag{7.33}$$

and

$$h_{mash} = \frac{\epsilon_A \mathcal{D}}{\tau_A t} ln\left(1+\frac{t}{r}\right) \tag{7.34}$$

In equation (7.34), the void fraction, ϵ_A, and tortuosity, τ_A, in the ash layer are assumed to be 0.35 and 2, respectively. The bulk diffusivities $\mathcal{D}$ in the gas and the ash layers are calculated at the film and particle temperatures respectively. The thickness of the ash layer, t, is calculated from a mass balance of the total ash in the particle, assuming that none of it is lost.

$$t = \left[r^3 + \frac{x_0(r_0^3 - r^3)}{1 - 0.35} \right]^{0.33} - r \tag{7.35}$$

where, x_0 is the initial volume fraction of ash in the particle and 0.35 is the void fraction in the ash layer. The mass fraction Y_{1_*} is then used in the carbon flux calculation.

7.2.2 Parametric Sensitivity

Since so many different parameters have to be known in advance as inputs to the model, it is important to find out the effect of some of the major parameters on crucial combustion variables such as particle temperature and burnout time.

Figure 7.2 shows the temperature-time histories for three different initial particle radii. While the bigger particles appear to burn at slightly lower temperatures due to increased radiative heat loss, the burnout times scale approximately as the square of the size. The radiating area also explains the increase in particle temperature with time. As the particle becomes smaller, the radiation loss decreases. The ash volume fraction was arbitrarily assumed to be 1% for all three cases. Wall temperature was kept at 1600K and the apparent densities of all particles were assumed to be 0.9 g/cc (900 kg m^{-3}). The ambient was air. The initial particle temperature was 1000K. Emissivities of the wall and the particle were taken to be

0.8 at all temperatures. The apparent activation energy was 17000 cal/mole (71.4 kJ/mole) and the pre-exponential factor was 46 g $cm^{-2}s^{-1}$ (460 kg $m^{-2}s^{-1}$) in all three cases.

The influence of the apparent density of the particle is shown in Figure 7.3 for combustion of 25μm radius particles. It has no effect on the maximum particle temperature, but the burn time increases linearly with density as expected. Figure 7.4 shows the effect of wall temperature keeping all other parameters the same. Not unexpectedly, the particle burns faster and at higher temperatures if the wall is hotter. This is due to higher radiant heat transfer to the particle. Particle emissivity is not a very influential parameter for the combustion of such small particles, as seen in Figure 7.5. Decreasing the emissivity from 0.8 to 0.6 increased the maximum temperature by only 4%, with hardly any change in the burntime.

The apparent reaction kinetics profoundly influence combustion. For a constant apparent activation energy of 17000 cal/mole, calculations for variation in the pre-exponential factor from 23 to 92 g $cm^{-2}s^{-1}$ are shown in Figure 7.6. The burn time decreases with increasing frequency factor as expected. At high rates, the particle burns isothermally over a significant part of its history, with a relatively brief initial rise and final burnout phase. At lower rates, however, there is no isothermal region. Instead, the temperature begins to fall immediately after the initial heatup period.

Figure 7.7 shows the dramatic influence of ash on the combustion. Since the final mass of the particle does not go to zero, the ash residue eventually reaches a steady-state temperature in radiative and conductive equilibrium with its surroundings. In reality, this steady-state may not be physically attainable since frag-

mentation of the particle would most likely have occured before this. The density of the ash was taken as 2 g/cc and the carbon density was 1.5 g/cc. The fact that all three curves have similar heatup characteristics deserves special comment. While particles with higher ash contents should have more thermal inertia, this is not the case since the value of specific heat of the ash is not very different from that of carbon over the temperature range of interest. Figure 7.8 shows the effect of ash density. As expected, higher density implies a higher thermal inertia and consequently a higher burnout time. In order to emphasize this effect, the initial ash volume fraction was assumed to be 20%.

7.3 General Case: Monodisperse Internal Voids

The model described in the previous section does not treat the problem of diffusion and reaction inside the particle. Only at very high temperatures or at high oxygen concentrations, can reaction be assumed to proceed only at the exterior surface of the char particle. Under these special conditions, the particle is pore diffusion limited and the penetration of oxygen is limited to a fairly thin outer shell of the particle.

In general, however, internal reaction within the pores of the particle must be accounted for. This requires a suitable model for the internal structure of the particle. Pore sizes in coal char may vary over four orders of magnitude (Chapter 5). However, as a first step in modelling this internal structure, a relatively simple pore model will be used. As in any continuum model, the porosity will be assumed to be homogenous within the particle. However, as combustion proceeds, variations in the radial distribution of pores will develop. In this model, the initial porosity

is assumed to be due to monodisperse spherical voids present in the particle. The radius of the void and the void volume fraction (or porosity) are the two parameters that characterize the initial porosity. Let a_0 be the initial radius of the spherical voids and let there be λ voids per unit particle volume. Then, accounting for pore overlap (Gavalas, 1985), the initial void fraction in a solid of infinite extent is

$$\epsilon_{init} = 1 - e^{-\lambda \frac{4}{3}\pi a_0^3} \tag{7.36}$$

The void fraction of a finite particle will be larger due to edge effects.

In the present analysis, temperature has been assumed to vary with time but to be constant throughout the particle. The maximum difference between the external particle temperature and that at its center is estimated to be 25-50K (Field, 1967). Thus, the particle can reasonably be taken to be spatially isothermal.

The presence of ash has been neglected in this model because: (*i*) the bituminous char does not have as much ash as many other coals and chars and thus it is not as significant; and (*ii*) the main purpose of the modelling effort was to test the effect of the internal structure as the particle burns. Without knowing the various details of how the ash behaves inside the particle, its inclusion in any model but the very simplest (like the one in the previous section) would be meaningless. Moreover, it would obscure those parts of the model that do correspond to physical reality. At the present moment our knowledge of ash behavior do not justify its inclusion in this model.

Since the reaction can take place inside the particle, the kinetic parameters used in the model are the intrinsic Arrhenius parameters derived from single particle experiments described in Chapter 4. These are based on the total surface area per

unit mass of the particle (*e.g.* N_2-BET area). The reaction kinetics will be assumed to be first order with respect to local oxygen concentration.

The overall scheme of the solution is as follows. The steady state diffusion equation is solved within the particle to determine the oxygen concentration as a function of radius. Since the problem is linear in oxygen concentration, the diffusion equation can be solved with an arbitrary boundary concentration at the exterior surface of the particle. Once the concentration profile is determined, it is scaled such that the external concentration matches the concentration determined from the transport outside the particle. This scaling is possible due to the linearity of the reaction rate.

7.3.1 Equations

The diffusion equation inside the particle is

$$\frac{1}{r^2}\frac{\partial}{\partial r}\left(r^2 \mathcal{D}_e \frac{\partial c}{\partial r}\right) = \frac{1}{\rho_C} A_i e^{-E_i/RT_p} S(r) c \tag{7.37}$$

where c is the oxygen concentration, $\mathcal{D}_e$ is the effective diffusion coefficient, ρ_C is the density of carbon, A_i and E_i are the intrinsic Arrhenius parameters, and S is the internal surface area per unit volume. The boundary conditions for this equation are

$$r = 0 : \frac{\partial c}{\partial r} = 0 \tag{7.38a}$$

and

$$r = r^* : c = c^* \tag{7.38b}$$

The first condition is from spherical symmetry. r^* and c^* are the external radius and oxygen concentration respectively. c^* is determined from the gas phase equations

and is the matching condition at the boundary.

Based on the oxygen concentration inside the particle, the local carbon recession q is determined by

$$q(r,t) = \int_0^t \frac{A_i e^{-E_i/RT_p(t)} c(r)}{\rho_c} dt' \tag{7.39}$$

This important equation determines the depth of carbon burned at any given radial location as a function of time. It is assumed that the void radius grows by the amount q with time. Thus, knowing q, the void fraction ϵ can be determined as

$$\epsilon(r) = 1 - e^{-\lambda \frac{4}{3}\pi\left[a_0^3 + q(r)\right]} \tag{7.40}$$

Once the void fraction is known, the local surface area, S, is given by

$$S(r) = \left[1 - \epsilon(r)\right] 4\pi\lambda\left(a_0 + q(r)\right)^2 \tag{7.41}$$

This surface area is then used in the reaction rate term of the diffusion equation (7.37).

In calculating the external radius of the particle, the effect of surface crumbling must be taken into account. Once the void fraction at the surface reaches a critical value, the surface becomes too porous to retain its structural integrity. The char particle then crumbles, shedding some carbon and decreasing in radius to the point where the void fraction is below the critical value. This becomes the fresh surface and the cycle repeats. The fragments of carbon burn in the gas phase tranferring some or all heat to the particle. If the model is run at fine enough time intervals the magnitude of the shedding is small and the radius appears to decrease smoothly. The time resolution is based on the penetration of oxygen and depends on the

porosity at the exterior surface. Therefore, the radius of the particle is calculated as follows:

$$\begin{aligned} &\text{for} \quad \epsilon_{ext} < \epsilon_{crit} : r^* = r_0 - q(ext) \\ &\text{for} \quad \epsilon_{ext} \geq \epsilon_{crit} : r^* = r^*_{old} - \left.\frac{d\epsilon/dt}{d\epsilon/dr}\right|_{ext} \Delta t \end{aligned} \tag{7.42}$$

where the subscript ext refers to the external surface of the particle and ϵ_{crit} denotes the critical value of the void fraction at which crumbling starts. ϵ_{crit} was assumed to be 0.8 in the model.

The effective diffusivity in equation (7.37) was calculated from the void fraction using

$$\mathcal{D}_e(r) = \frac{1}{\tau} D\epsilon(r) \tag{7.43}$$

where, τ is a tortuosity factor, commonly taken as 2, and D is the bulk diffusion coefficient at the particle temperature.

Clearly, the above equations are strongly coupled with each other and with the external gas phase equations. The particle energy equation and all the gas phase transport equations derived in the previous section can be applied to this formulation. The particle was radially discretized into fifty shells of equal radial thickness. Conditions were assumed to be uniform inside each shell. As the radius decreased with time, the number of remaining shells correspondingly decreased. The position of the external surface was calculated as a function of time by interpolating between shells. Hence, the resolution in calculating the radius was not limited by the number of shells chosen.

The overall carbon flux for the particle was the sum of all the fluxes at the various radii. This flux, in conjunction with the gas phase, determined the new external oxygen concentration. This was used to recalculate new internal profiles of

the various quantities. This iterative process was continued until convergence was achieved at each time step. Then the overall energy balance was used to calculate the new particle temperature and a new particle radius was also calculated. This was repeated over as many time steps as needed to achieve preset final conversion values.

7.3.2 Parametric Sensitivity

Figure 7.9 shows the size of the particle as a function of time. A typical particle, having an initial radius of 25μm and an initial void fraction of 0.1 consisting of 0.1μm diameter voids, was used. The density of the solid carbon was assumed to be 2.0g/cc. The initial particle and wall temperatures were both 1500K and the critical void fraction was 0.8. The wall and the particle emissivities were 0.9 and 0.8 respectively. The figure shows three distinct regions. At first, the external radius of the particle decreases very slowly because the surface void fraction is below the critical void fraction and the radius can only change by reaction. When the surface void fraction does reach the critical value, crumbling starts and the radius reduces as a faster rate. As the particle burns, however, oxygen penetrates further and more of the outer shell reaches the critical value and is shed. This causes the radius to decrease faster. Finally, when the particle becomes quite small, there is complete oxygen penetration and it burns in the kinetic limited regime. The shedding thickness becomes smaller and the radius decrease is arrested. Eventually, the entire particle reaches the critical void fraction and disintegrates. This happens when the radius is around 3μm. Therefore the final radius is not zero. Figure 7.10 shows the variation of conversion versus time. The particle temperature is

shown in Figure 7.11. The heat up period, the almost isothermal phase, the rapid decrease and finally the kinetic regime are all shown. In the kinetic regime the particle is in thermal equilibrium with its environment. In fact the kinetic regime is seen because of the preceeding temperature drop. Figure 7.12 shows the variation of the surface oxygen partial pressure. The initial surface partial pressure, 0.145, is lower than that in the free stream, 0.21, because of the diffusional resistance in the particle boundary layer. During the heat up period, the reaction rate increases and the oxygen concentration drops. For most of the burning period, the oxygen concentration at the surface is quite low, indicating near diffusion limited conditions. Finally, as the particle size decreases, the external concentration rises, approaching the ambient partial pressure. The flux of carbon from the particle is shown in Figure 7.13. The fluctuations are due to the numerical method employed and the choice of each time step interval. The temporal resolution in various runs was 0.1 milliseconds. Figure 7.14 shows the surface and total void fractions of the particle as a function of time. Since the critical void fraction is chosen as 0.8, the surface void fraction increases to 0.8 and then remains constant throughout most of the combustion. The drop at the start of the kinetic regime is due to computational inaccuracies. The total void fraction starts from the value of the initial void fraction (0.1). At first it rises because the radius is not changing and there is some reaction. As soon as shedding begins, it starts decreasing because the particle loses its most porous external shell. However, the thickness of the outer layer that crumbles decreases with time, and the particle void fraction decreases to a relative minimum. Eventually, the particle size becomes small enough that oxygen

penetrates throughout the particle. The accelerating reaction then increases the particle void fraction monotonically till the critical void fraction is reached when the entire particle crumbles.

The effect of particle radius on the combustion temperature plot is shown in Figure 7.15. The burn times again scale approximately as the square of the size because of the aforementioned shrinking core type of behavior. The peak temperature is almost the same for the two particle sizes examined. The initial void fraction and void radius, were, in both cases, 0.1 and 0.05μm, respectively. The wall and initial particle temperatures were both 1500K. The intrinsic pre-exponential factor was 10^5 kg $m^{-2}s^{-1}$ and the intrinsic activation energy was 179740 J/mole (43000 cal/mole). Figure 7.16 shows that the carbon density affects only the burn time and not the peak temperature. The lower density particle also heats more rapidly due to its low thermal inertia. The influence of carbon emissivity is shown in Figure 7.17. Again, the change in the temperature is small and the higher the emissivity, the lower the final particle temperature. In both cases the wall emissivity was assumed to be 0.9. In Figure 7.18, the influence of the pre-exponential factor is demonstrated. The nature of the variation is as expected. The initial rate of rise is not commensurate with the rise in reaction rate, but the duration of time the particle spends in the final kinetic regime is dramatically increased with decreasing reaction rate. The curves in Figure 7.19 show the effect of initial void size. The initial void fraction in all cases was 0.1, so the number concentration of voids decreased with increasing void size. The specific surface area increases as the void size decreases, so the net reaction rate also increases. Since the radiative heat loss is the same in

all cases, the particles with the smaller voids tend to reach higher temperatures and consequently burn out faster. The influence of the initial void fraction is shown in Figure 7.20. The initial void size in all cases was 0.05μm in radius. The smaller the void fraction, the larger the particle mass and therefore the longer the burn time. The particle temperature does not vary significantly with void fraction. In all the cases discussed above, the energy released by the core particle and the burning fragments was completely fed back to the particle. However, not all the energy of combustion is necessarily available for the remaining particle. Burning fragments expelled from the particle may burn far from the particle. To simulate such a situation, various fractions of energy released by the exterior crumbling shell were fed back to the particle and the effect on its combustion behavior noted. Figure 7.21 shows two cases involving no (0%) and 50% feedback. The particle burns at almost 100K high in the second case. The final comparision (Figure 7.22) involves various wall temperatures. The heat up period is longer when the wall is cool, but the latter part of the combustion is similar in both cases.

Figures 7.23-7.29 show the oxygen concentration profiles inside the particle as a function of time for different values of reaction rate, initial void size and initial void fraction. Figure 7.23 shows the case with a pre-exponential factor of 10^5 kg $m^{-2}s^{-1}$, initial void radius of 0.05 μm, and initial void fraction of 0.1. The first profile is labelled 0 ms. It shows that after the first time step, the radius of the particle is still 25 μm and the external oxygen partial pressure is 0.12. There is no penetration below 10 μm radius, implying that the oxygen is confined to an outer layer 15 μm thick. The profiles are drawn every 2 ms and labelled every 10 ms for clarity.

Twenty milliseconds after the start of combustion, the profile shows that the particle radius is around 18 μm and the penetration depth is only 3 μm. The surface partial pressure is 0.025. As combustion continues, the external concentration rises, and the radius decreases. The penetration depth remains around 3 μm. At about 42 ms after the start of combustion, the concentration at the center of the particle becomes non-zero for the first time and the particle is in the kinetic regime. Although there is some drop in concentration inside the particle, the penetration of oxygen is not limited to a layer on the outside. Figures 7.24 and 7.25 show similar profiles for a lower and a higher pre-exponential factor, respectively. When the reaction rate is lower, there is better penetration of oxygen into the particle and also the concentration at the exterior is higher. The opposite is true for the high reaction rate (Figure 7.25). The influence of the initial void fraction on the profiles are shown in Figures 7.26, 7.23 and 7.27 which have initial void fractions of 0.05, 0.1 and 0.15 respectively. All three cases have the same initial void size and reaction rate. The higher the void fraction, the greater the void surface area (this is only true for small void fractions; at much larger void fractions, void coalescence actually reduces the area) and effectively, higher the reaction rate. Hence, there is better penetration of oxygen at lower void fractions. The influence of initial void size are shown in Figures 7.28, 7.23 and 7.29 respectively. All three cases have the same initial void fraction (0.1) and reaction rate. Clearly, for a given void fraction there are more numbers of smaller voids leading to larger surface areas and therefore higher reaction rates. Therefore there is very little penetration and the surface concentrations are the least for the smallest void sizes (Figure 7.28).

7.4 General Case: Polydisperse Internal Voids

In general coal chars have a distribution of void sizes. We now extend the spherical void model to a more realistic representation of the internal structure. Three different void sizes, corresponding to micro, transition, and macro pores were used. The sizes of the voids and the void fraction for each size were determined from mercury porosimetry. (see Chapters 5 for examples). The surface area and diffusion calculations were modified to account for the presence of the different size voids. All other equations are essentially unchanged from the ones given in the previous sections.

Input data for the internal pore morphology assumed in this model were the average radii of pores in the micro, transition, and macro ranges, assumed to be 0.001μm, 0.01μm, and 0.1μm, respectively. The void fractions in the three pore types were also specified. At first, the void number density, λ_i, was determined. This is the number of voids of a particular type per unit particle volume. The number densities were then held constant while the pore radii were allowed to grow by reaction. Let $\epsilon_{i,0}$ be the initial void fractions of the macro (i=1), transition (i=2), and micro (i=3) pores. If $a_{i,0}$ are the initial radii, then let

$$\omega_{i,0} \equiv \frac{4}{3}\pi\lambda_i a_{i,0}^3 \qquad i = 1,2,3 \tag{7.43}$$

Assuming overlap of micro pores with the other two types we have

$$\epsilon_{3,0} = 1 - e^{-\omega_{3,0}} \tag{7.44}$$

Also, assuming overlap of transition pores with macro pores but not with micro pores we have

$$\epsilon_{2,0} = e^{-\omega_{3,0}} - e^{-\omega_{2,0}-\omega_{3,0}} \tag{7.45}$$

Finally assuming no overlap of the macro pores with the other two types we get

$$\epsilon_{1,0} = e^{-\omega_{2,0}-\omega_{3,0}} - e^{-\omega_{1,0}-\omega_{2,0}-\omega_{3,0}} \tag{7.46}$$

Equations (7.44), (7.45), and (7.46) successively determine λ_3, λ_2 and λ_1 respectively. Once the void number concentrations are known, the void fractions at any time can be determined by knowing the surface recession, q. Let

$$\omega_i \equiv \frac{4}{3}\pi\lambda_i(a_{i,0}+q)^3 \qquad i = 1,2,3 \tag{7.47}$$

Then the void fractions are given by

$$\begin{aligned} \epsilon_3 &= 1 - e^{-\omega_3} \\ \epsilon_2 &= e^{-\omega_3} - e^{-\omega_2-\omega_3} \\ \epsilon_1 &= e^{-\omega_2-\omega_3} - e^{-\omega_1-\omega_2-\omega_3} \end{aligned} \tag{7.48}$$

The total void fraction, ϵ, is given by

$$\epsilon = \epsilon_1 + \epsilon_2 + \epsilon_3 \tag{7.49}$$

The surface area, $S(q)$, is given by

$$S(q) = (1-\epsilon)4\pi \sum_{i=1}^{3} \lambda_i(a_{i,0}+q)^2 \tag{7.50}$$

The result of varying the different void fractions in the various sizes is shown in Figure 7.30. The total initial void fraction is kept constant in all cases. Figure 7.31 shows the specific surface area of the particle as a function of carbon conversion. The shape of the curves is very similar to those obtained experimentally, including the maximum observed at some intermediate conversion. This is an indicator of the

capability of such a model to describe accurately the combustion behavior of single particles.

7.5 General Case: Polydisperse Voids and Nonlinear Kinetics

The condition of first order Arrhenius kinetics was relaxed to test the effects of various non-linear reaction rate expressions on the combustion history. The presence of ash was neglected in these formulations.

The introduction of non-linearity makes the problem more difficult to solve numerically. Various shooting and adaptive-grid techniques were used to make the numerical aspects tractable, accurate, and efficient since scaling was no longer possible. Computation times increased by about one order of magnitude.

The first non-linear expression used was of the Langmuir-Hinschelwood type. The intrinsic reaction rate was assumed to be of the form

$$R = A_i e^{-E_i/RT_p} \frac{c}{1 + Cc} \tag{7.51}$$

where c is the oxygen concentration and C is a constant. The effect of varying C is shown in Figure 7.32. The results are also compared to the temperature-time history obtained from linear kinetics in Figure 7.33.

Figure 7.34 shows the internal oxygen concentration profiles when the intrinsic reaction rate is of the form

$$R = A_i e^{-E_i/RT_p} c^m \tag{7.52}$$

where m is between 0 and 1. If m is smaller than 0.8, the problem becomes numerically stiff and difficult to solve. However, in those cases it is seen from the figure that the penetration of oxygen is confined to a very thin shell on the outside of the

particle. In such situations, the asymptotic formulation given in Section 7.2 can be used without much error.

References

1. Field, M.A., Gill, D.W., Morgan, B.B., and Hawksley, P.G.W., **Combustion of Pulverized Coal**, 314 (1967).
2. Gavalas, G.R., Loewenberg, M., Bellan, J., and Clayton, R.M., Structure and Combustion of Cenosphere Particles, Presented at the Annual AIChE Meeting, Chicago (1985).
3. Loewenberg, M., Bellan, J. and Gavalas, G.R., Chem. Engg. Comm., **58**, 89 (1987).
4. Mitchell, R.E., Experimentally Determined Overall Burning Rates of Coal Chars, Presented at the combined Canadian and Western States Section Technical Meeting of the Combustion Institute, Banff, Canada (1986).

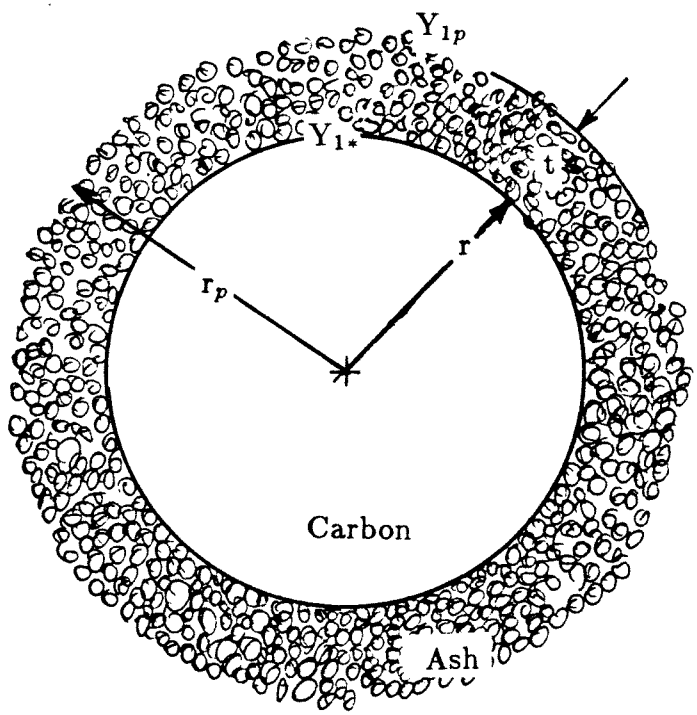

Figure 7.1 Schematic diagram of a single char particle with ash.

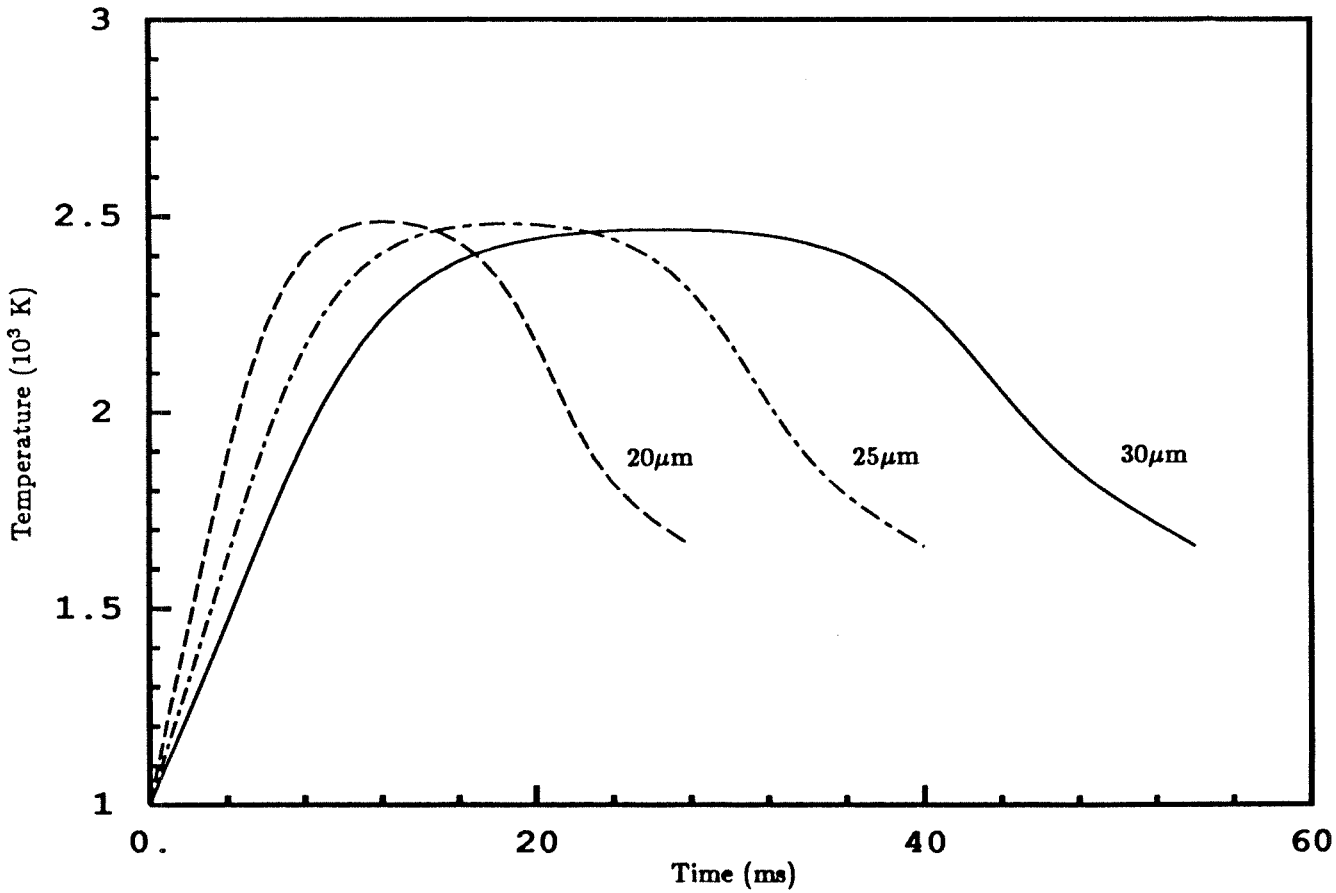

Figure 7.2 Asymptotic Model: Effect of initial particle radius, r_p. ϵ_A=0.01, ρ_A=2000 kg m^{-3}, T_∞=1600 K, T_{pi}=1000 K, ρ_a=900 kg m^{-3}, $p_{O_2,\infty}$=0.21, $\epsilon_\infty=\epsilon_0$=0.8, E=71060 J/mole, A_a=460 kg m^{-2} s^{-1}

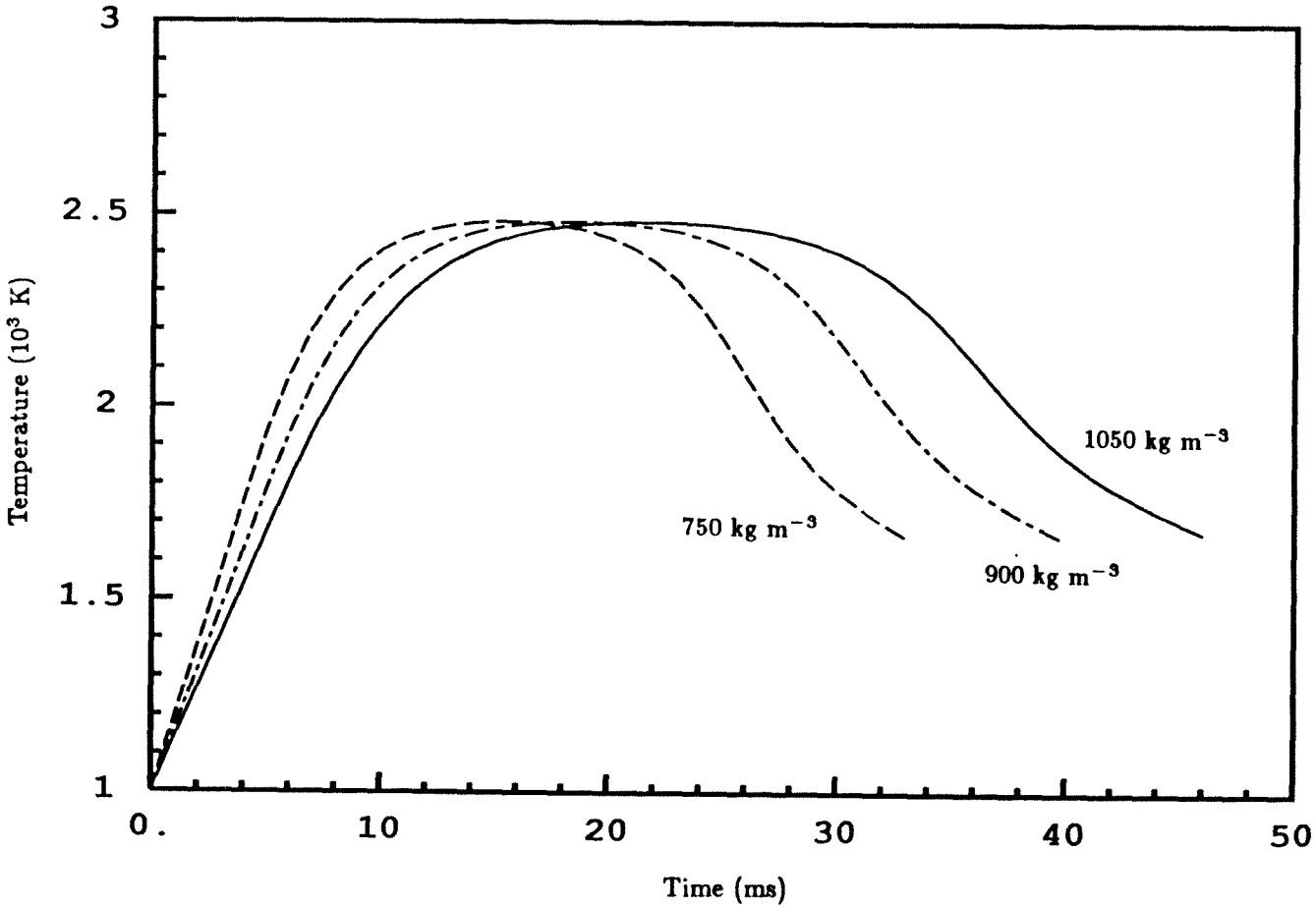

Figure 7.3 Asymptotic Model: Effect of apparent particle density, ρ_a. r_p=25 μm, ϵ_A=0.01, ρ_A=2000 kg m^{-3}, T_∞=1600 K, T_{pi}=1000 K, $p_{O_2,\infty}$=0.21, ϵ_∞=ϵ_0=0.8, E=71060 J/mole, A_a=460 kg m^{-2} s^{-1}

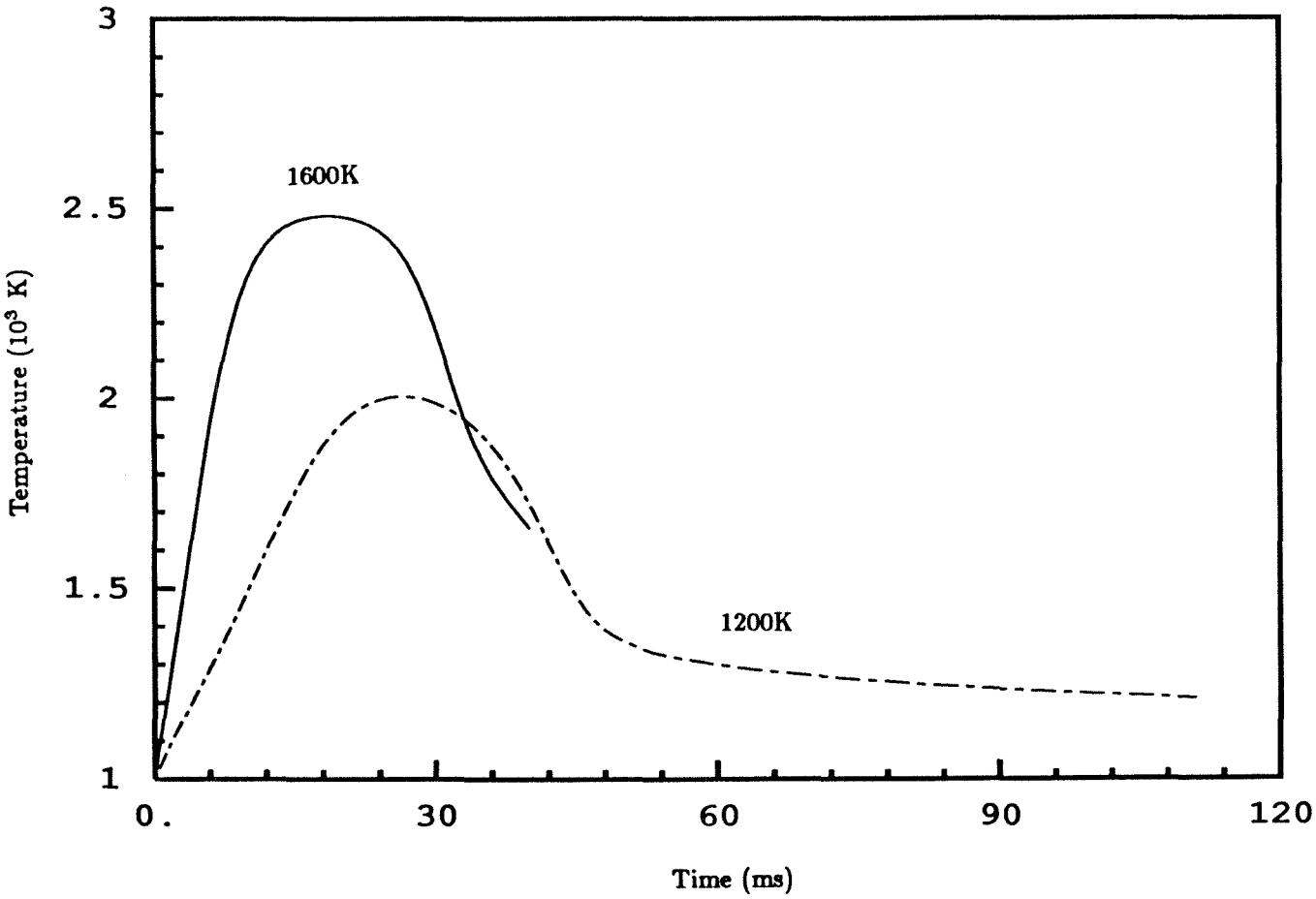

Figure 7.4 Asymptotic Model: Effect of wall temperature, T_∞. r_p=25 μm, ϵ_A=0.01, ρ_A=2000 kg m^{-3}, ρ_a=900 kg m^{-3}, T_{pi}=1000 K, $p_{O_2,\infty}$=0.21, $\epsilon_\infty=\epsilon_0$=0.8, E=71060 J/mole, A_a=460 kg m^{-2} s^{-1}

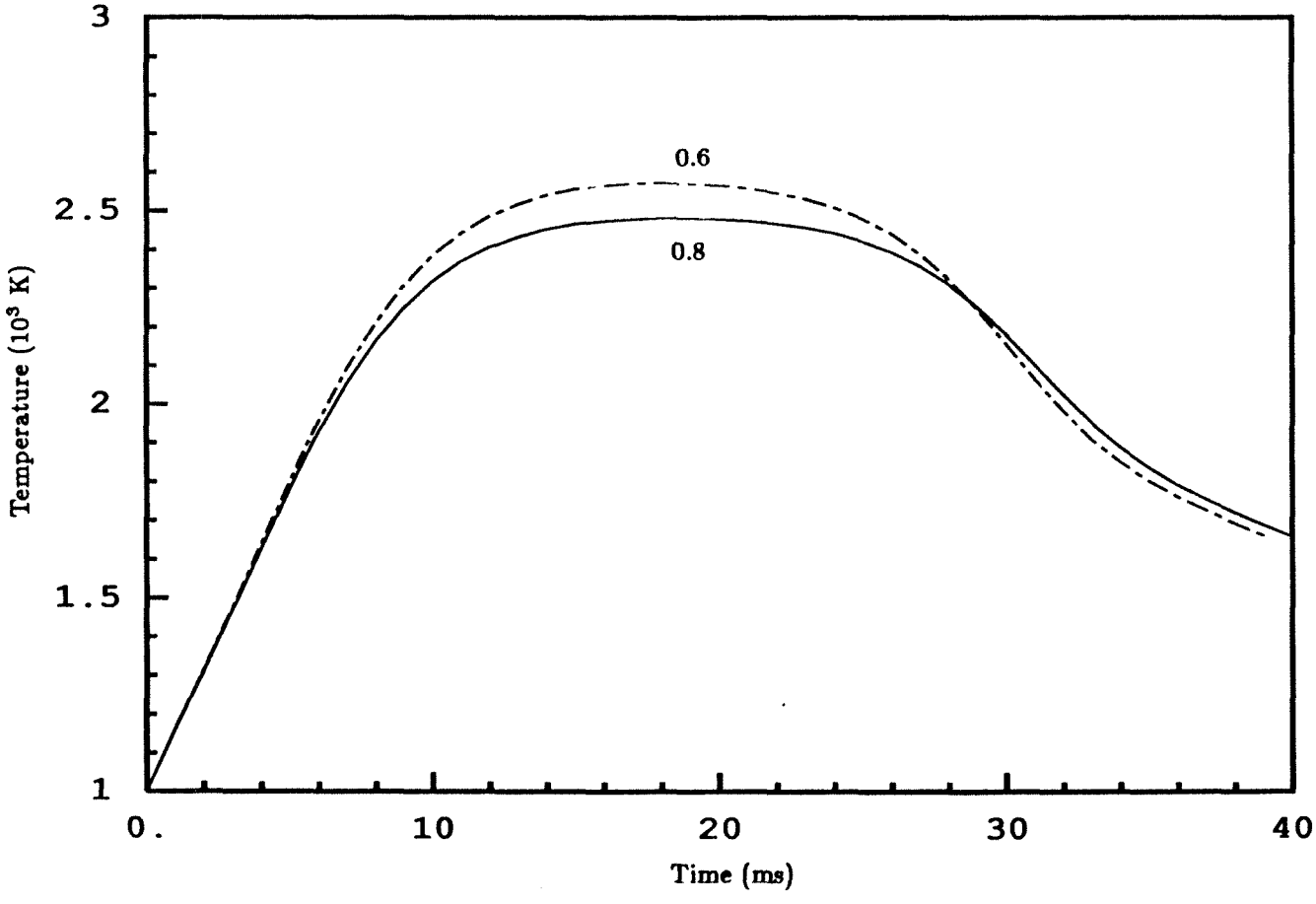

Figure 7.5 Asymptotic Model: Effect of particle emissivity, ϵ_0. r_p=25 μm, ϵ_A=0.01, ρ_A=2000 kg m^{-3}, ρ_a=900 kg m^{-3}, T_{pi}=1000 K, $p_{O_2,\infty}$=0.21, ϵ_∞=0.8, T_∞=1600 K, E=71060 J/mole, A_a=460 kg m^{-2} s^{-1}

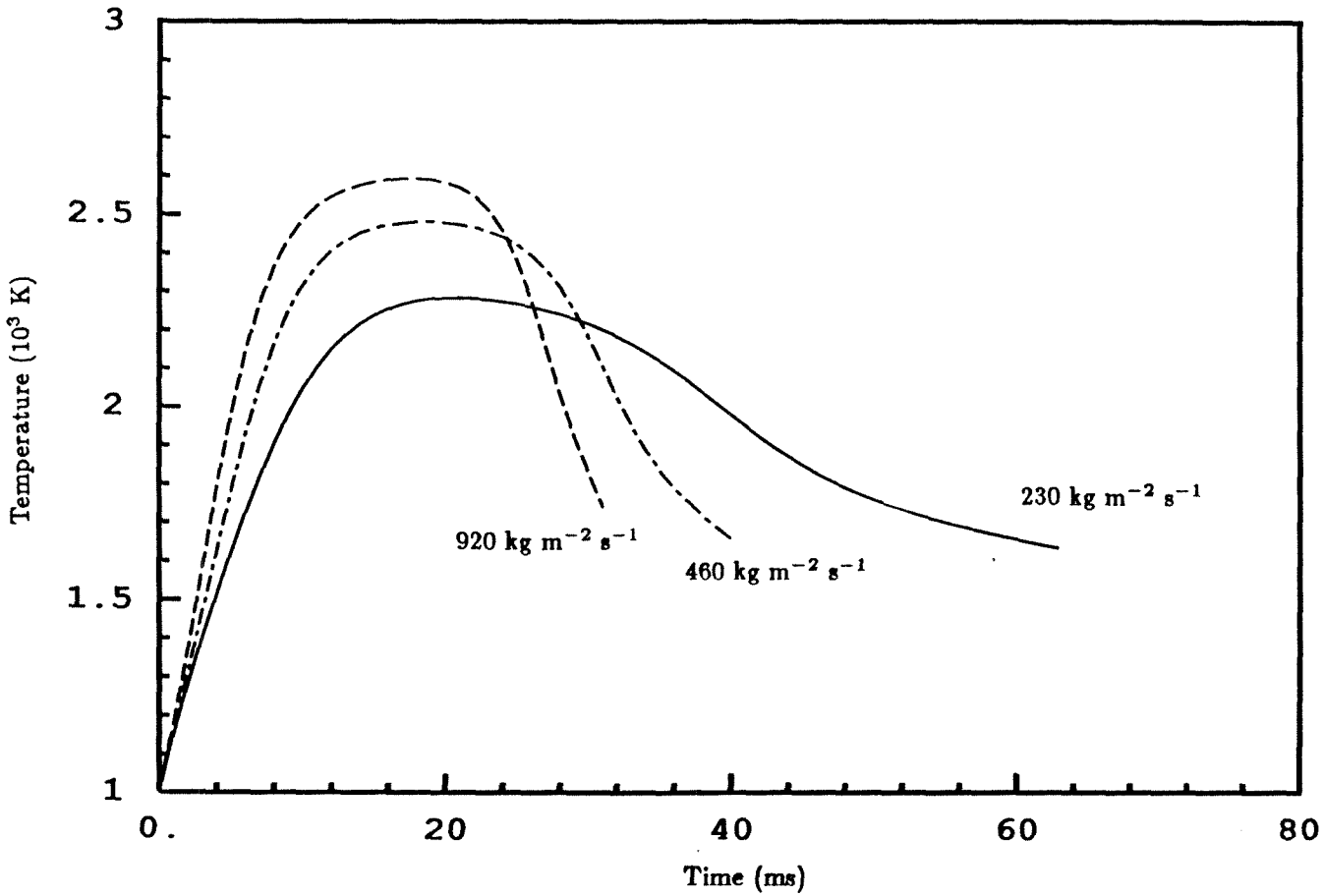

Figure 7.6 Asymptotic Model: Effect of the apparent Arrhenius pre-exponential factor, A_a. r_p=25 μm, ϵ_A=0.01, ρ_A=2000 kg m^{-3}, ρ_a=900 kg m^{-3}, T_{pi}=1000 K, $p_{O_2,\infty}$=0.21, ϵ_∞=ϵ_0=0.8, T_∞=1600 K, E=71060 J/mole,

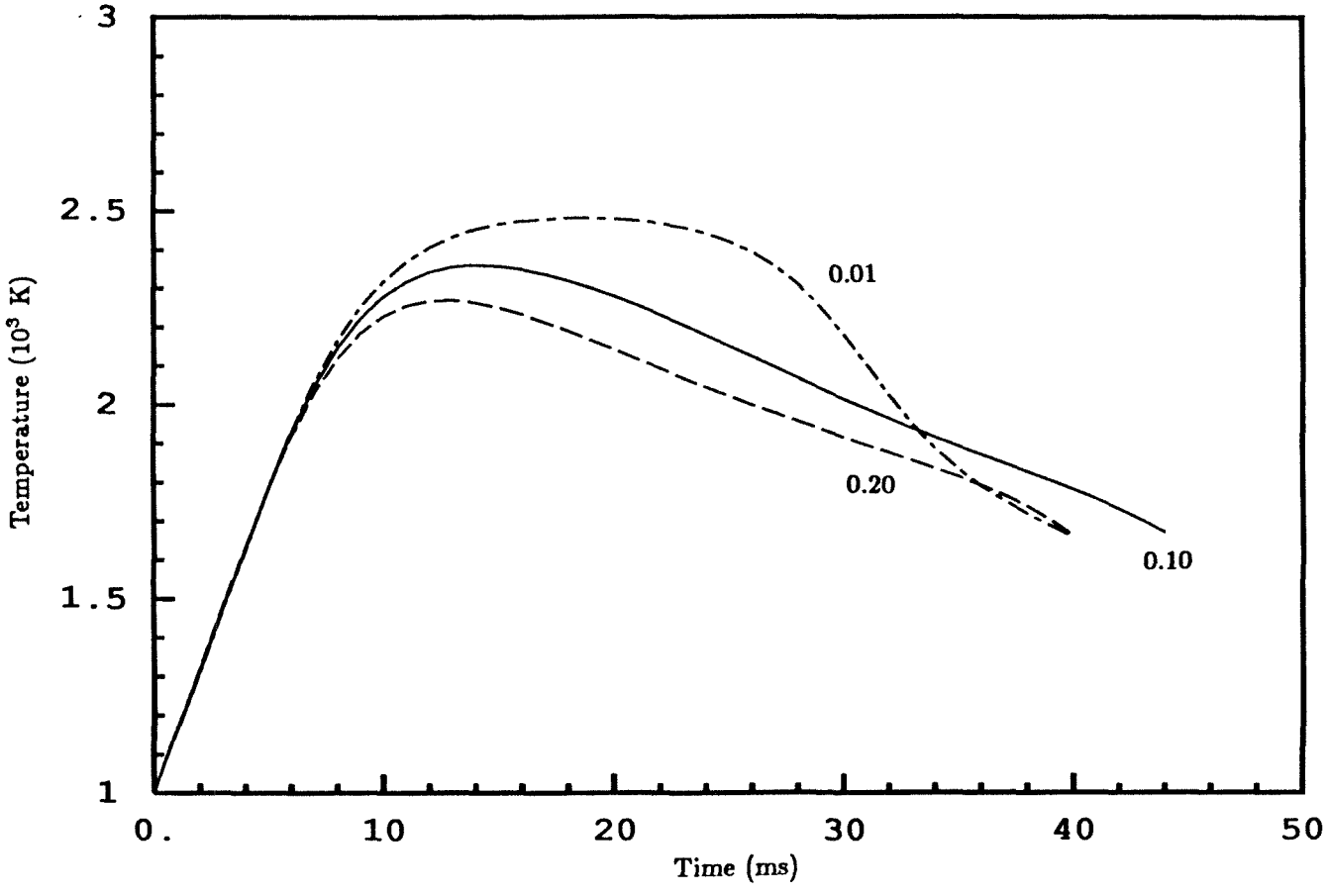

Figure 7.7 Asymptotic Model: Effect of initial ash volume fraction in the particle, ϵ_A. r_p=25 μm, ρ_A=2000 kg m^{-3}, ρ_a=900 kg m^{-3}, T_{pi}=1000 K, $p_{O_2,\infty}$=0.21, $\epsilon_\infty=\epsilon_0$=0.8, T_∞=1600 K, E=71060 J/mole, A_a=460 kg m^{-2} s^{-1}

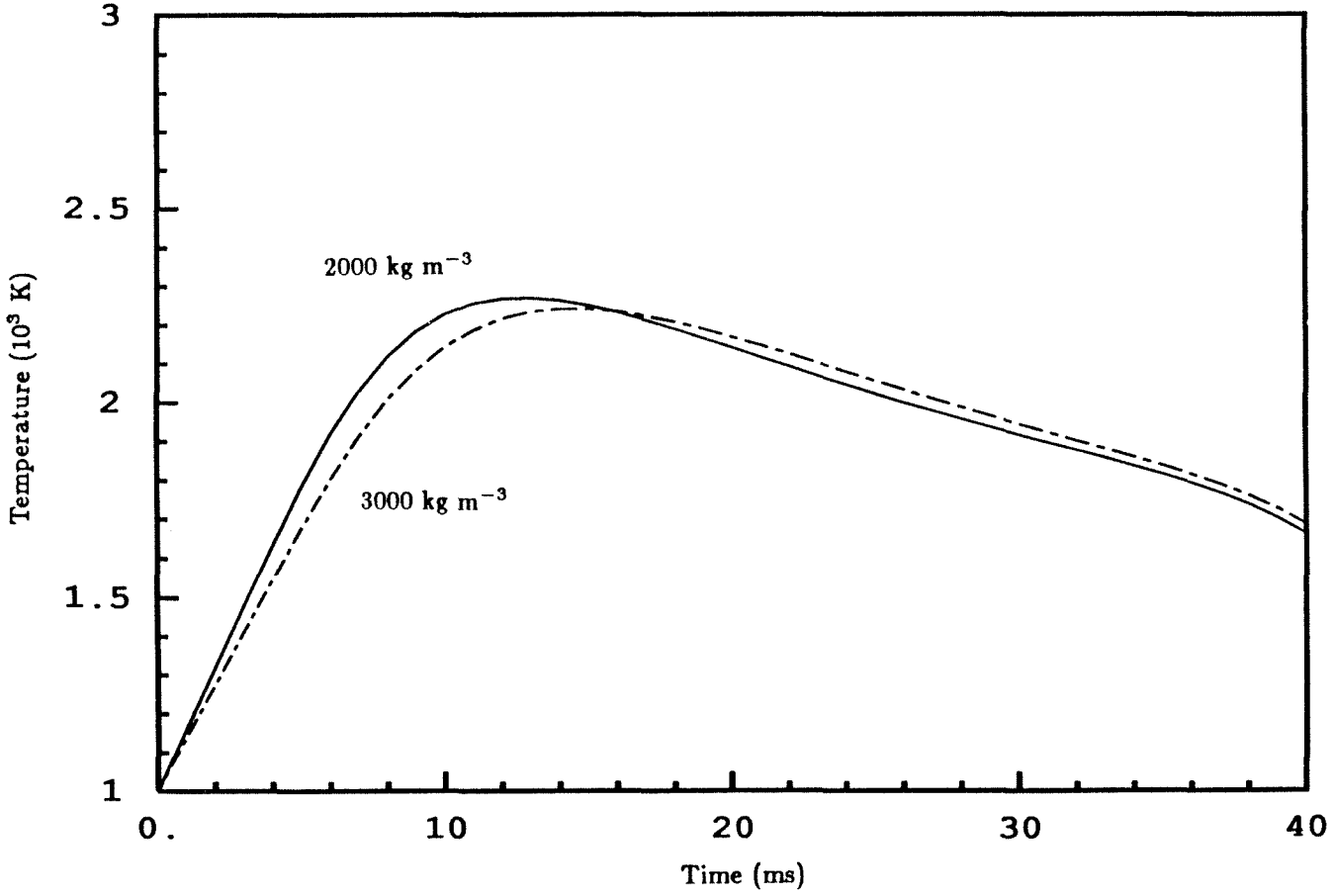

Figure 7.8 Asymptotic Model: Effect of ash density, ρ_A. ϵ_A=0.2, r_p=25 μm, ρ_a=900 kg m^{-3}, T_{pi}=1000 K, $p_{O_2,\infty}$=0.21, ϵ_∞=ϵ_0=0.8, T_∞=1600 K, E=71060 J/mole, A_a=460 kg m^{-2} s^{-1}

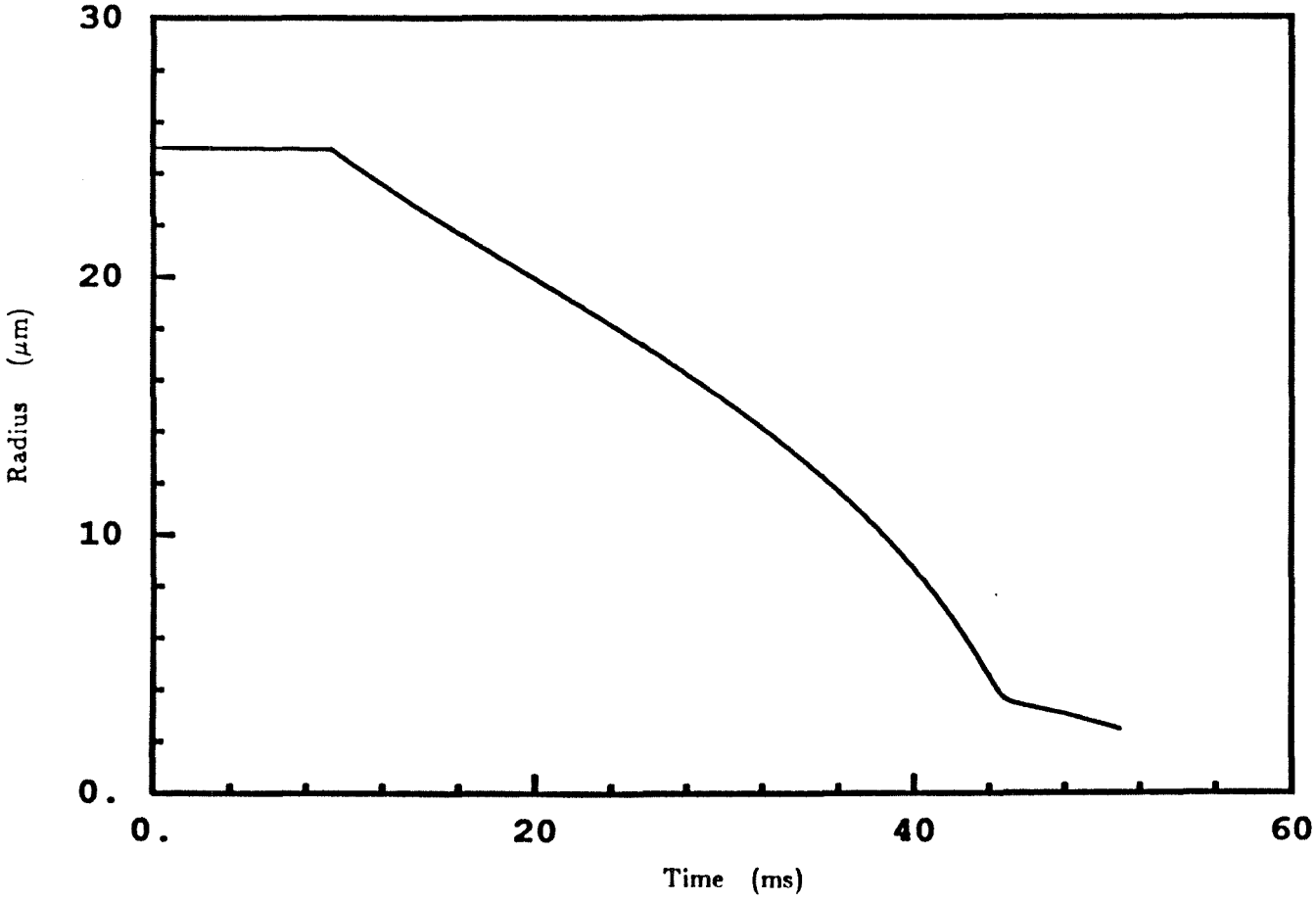

Figure 7.9 General Model with initially monodisperse voids: Particle radius versus time. r_p=25 μm, ϵ=0.1, a_0=0.05 μm, ρ_C=2000 kg m^{-3}, T_{pi}=T_∞=1500 K, ϵ_{crit}=0.8, ϵ_∞=0.9, ϵ_0=0.8, $p_{O_2,\infty}$=0.21, E=179740 J/mole, A_i=10^5 kg m^{-2} s^{-1}, 0% feedback.

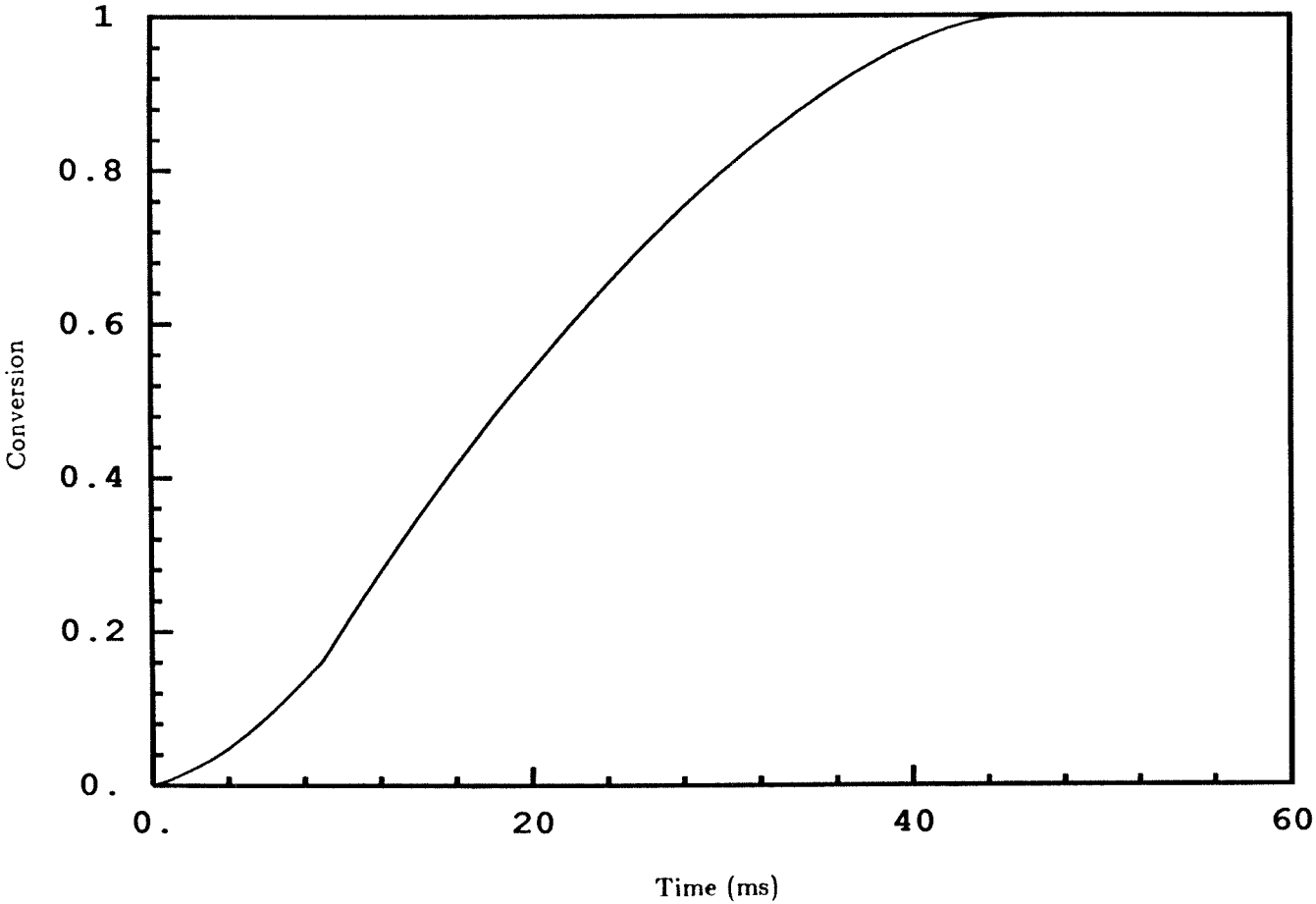

Figure 7.10 General Model with initially monodisperse voids: Carbon conversion versus time. Parameters as in Figure 7.9.

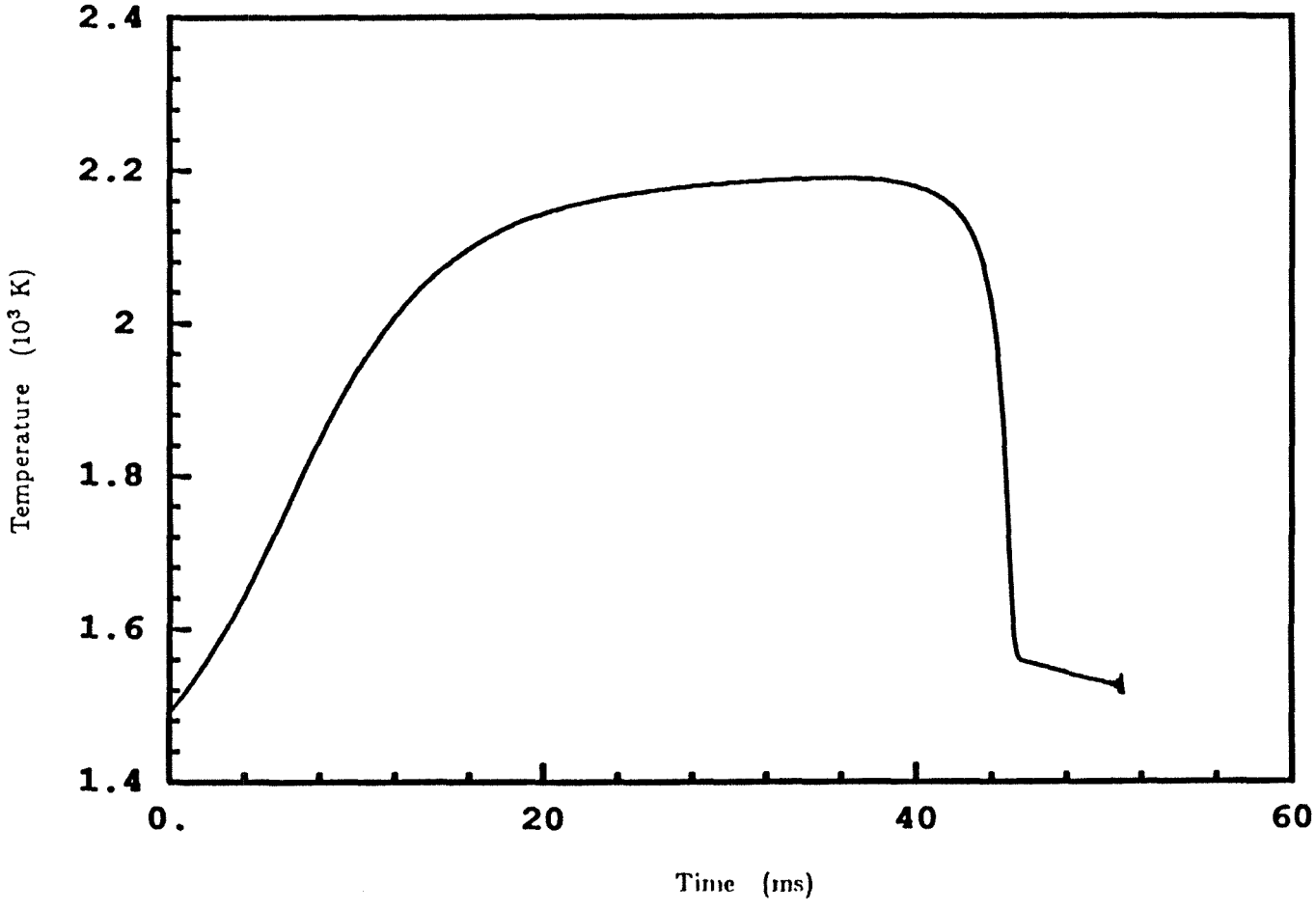

Figure 7.11 General Model with initially monodisperse voids: Particle temperature versus time. Parameters as in Figure 7.9.

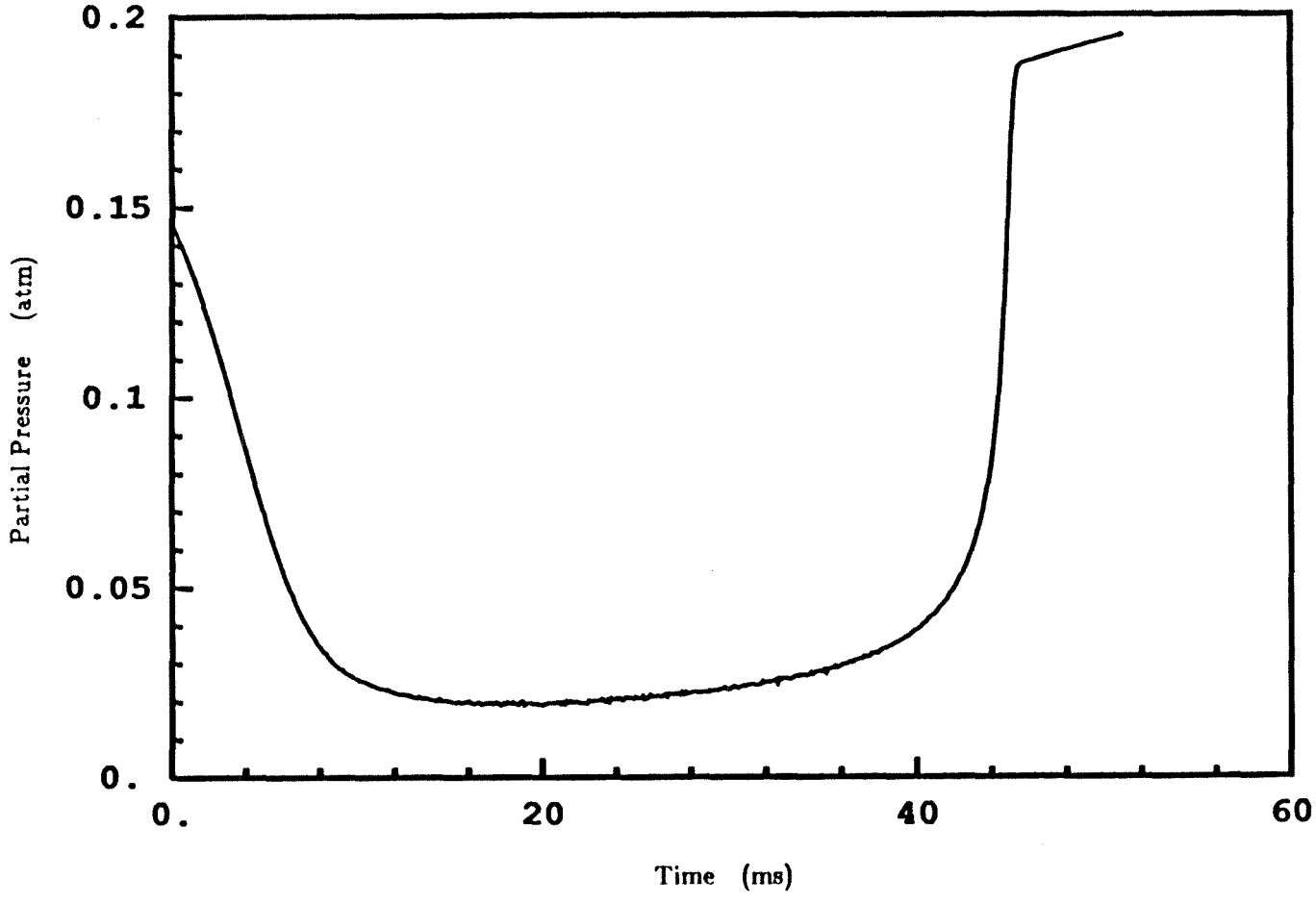

Figure 7.12 General Model with initially monodisperse voids: Oxygen partial pressure at the particle surface versus time. Parameters as in Figure 7.9.

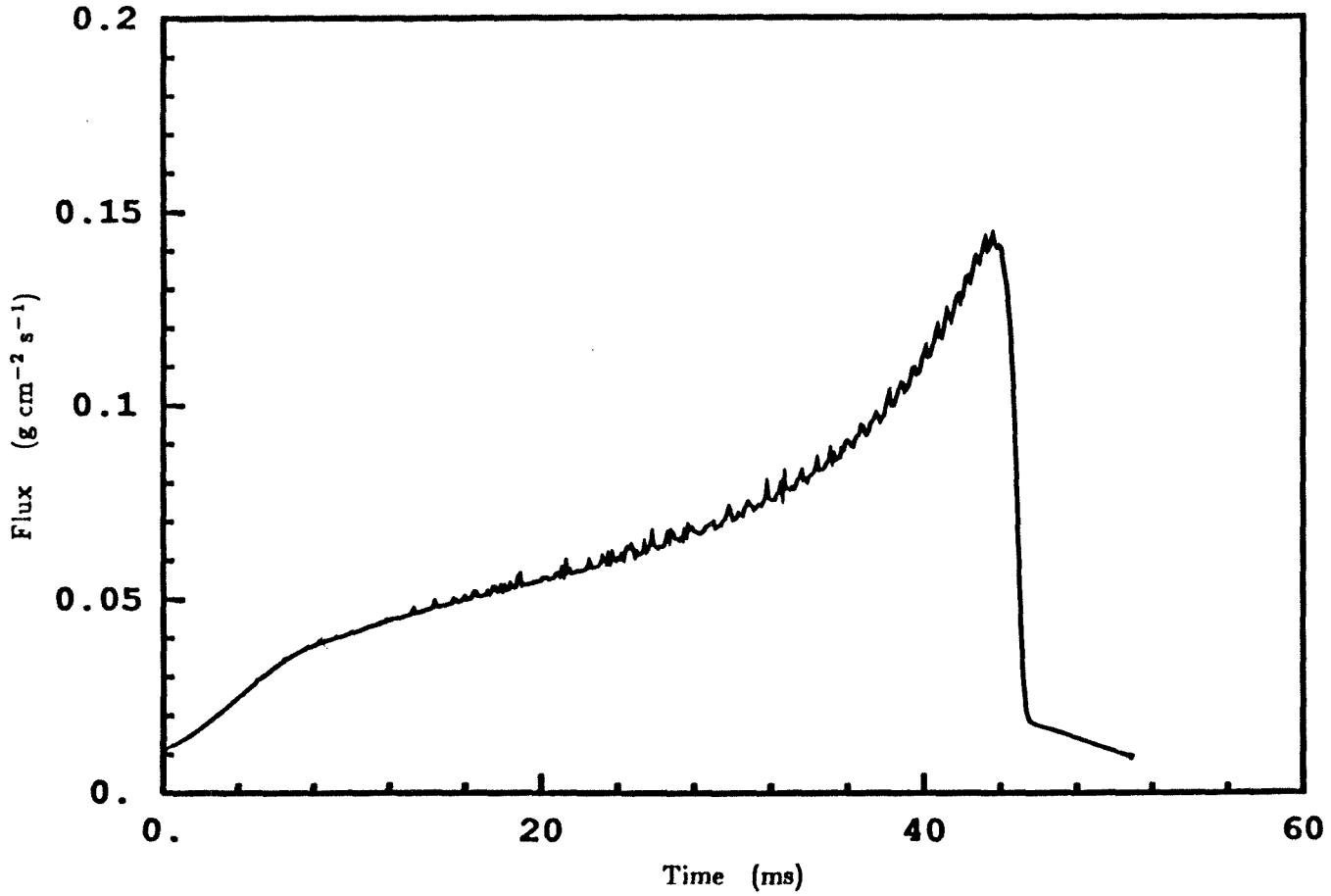

Figure 7.13 General Model with initially monodisperse voids: Carbon flux versus time. Parameters as in Figure 7.9.

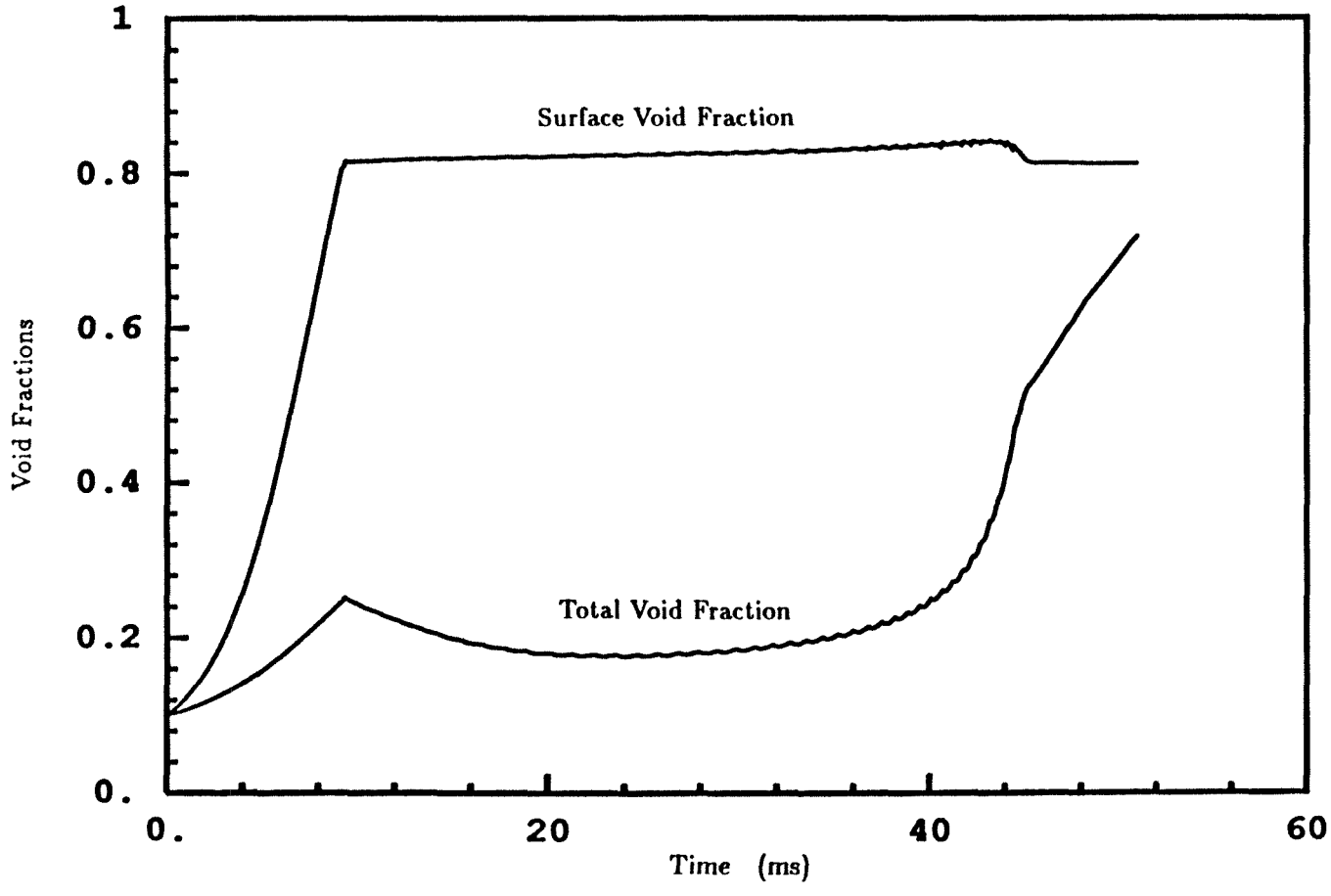

Figure 7.14 General Model with initially monodisperse voids: Total and Surface void fractions versus time. Parameters as in Figure 7.9.

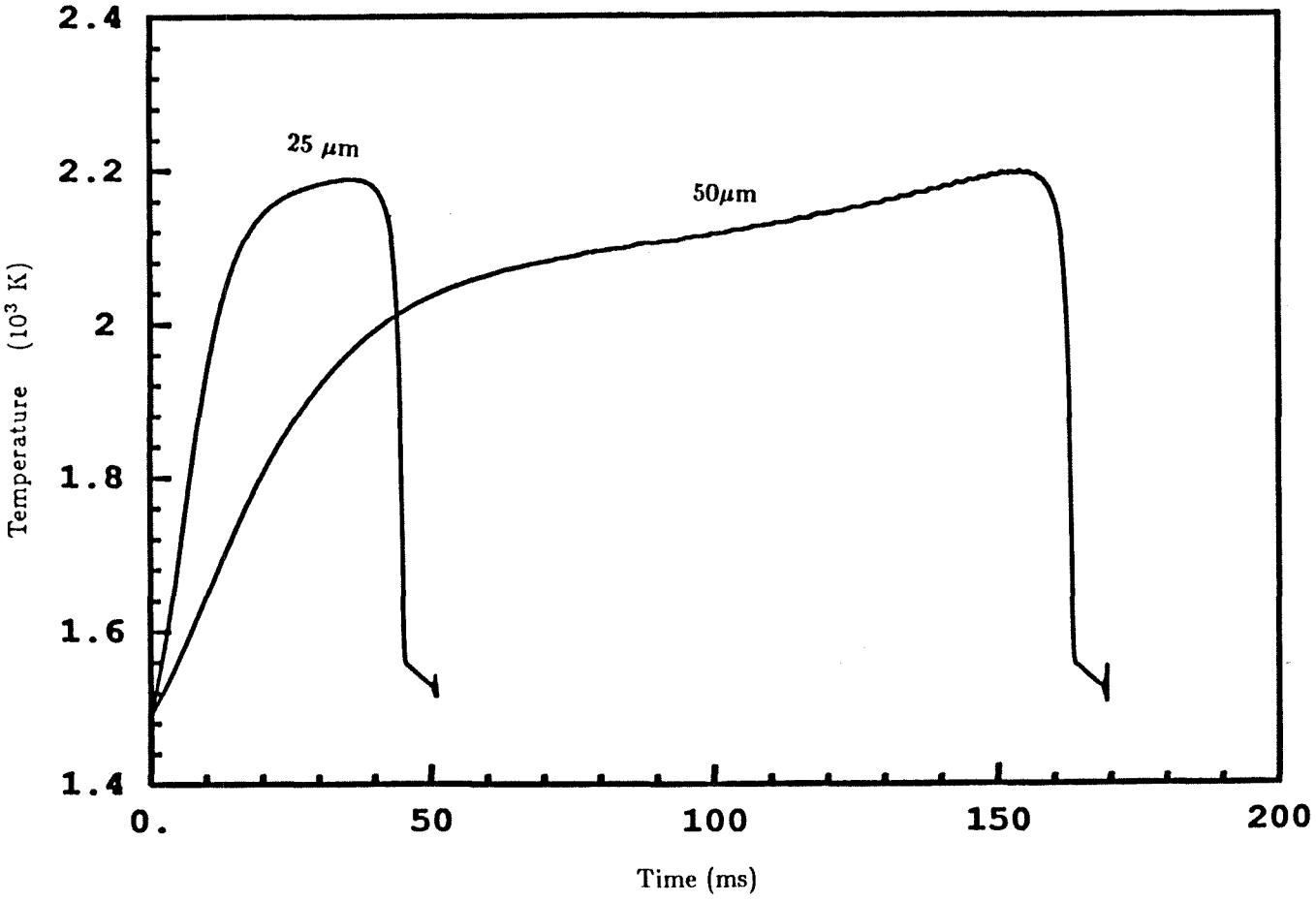

Figure 7.15 General Model with initially monodisperse voids: Effect of initial particle radius, r_p. Parameters as in Figure 7.9.

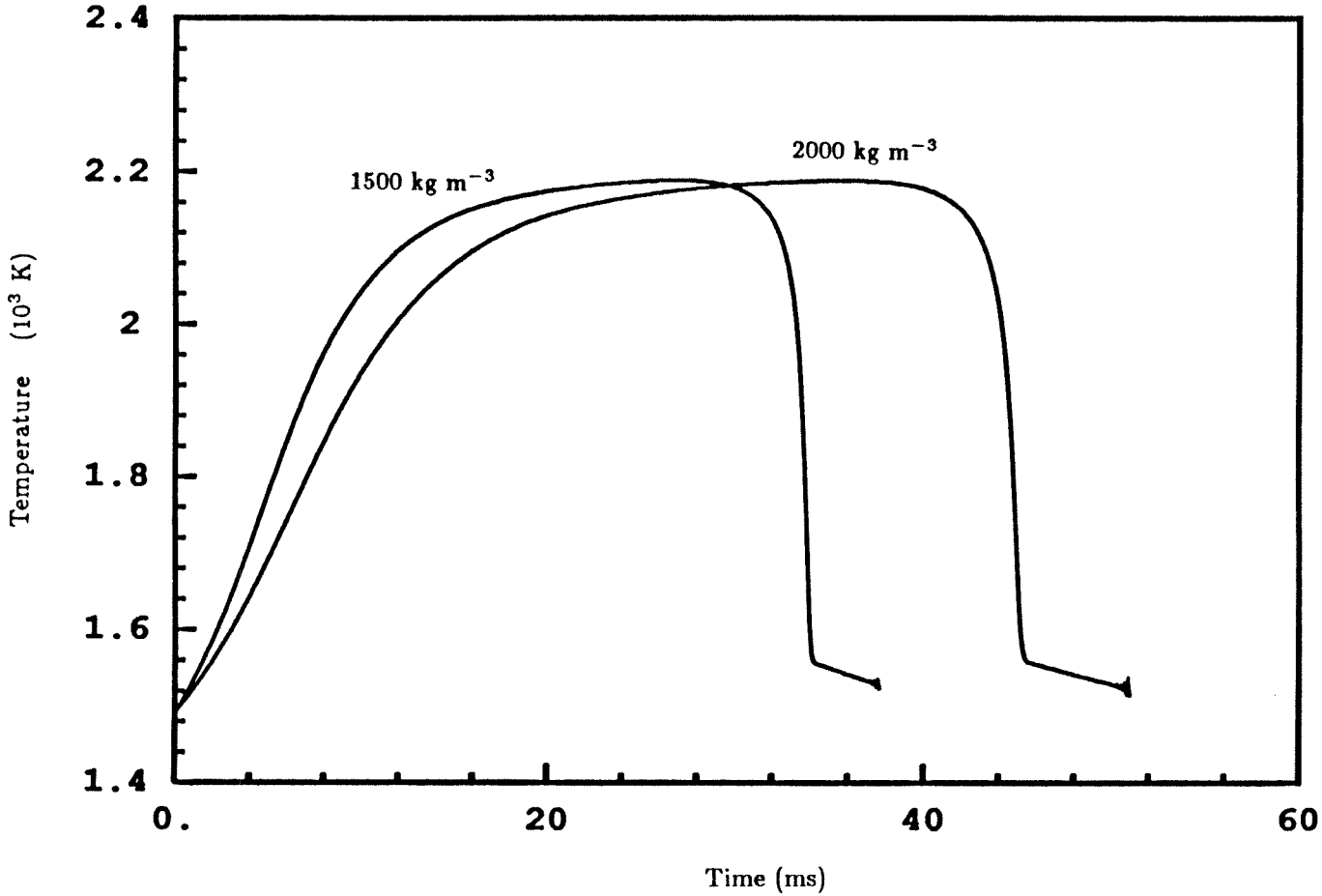

Figure 7.16 General Model with initially monodisperse voids: Effect of carbon density, ρ_C. Parameters as in Figure 7.9.

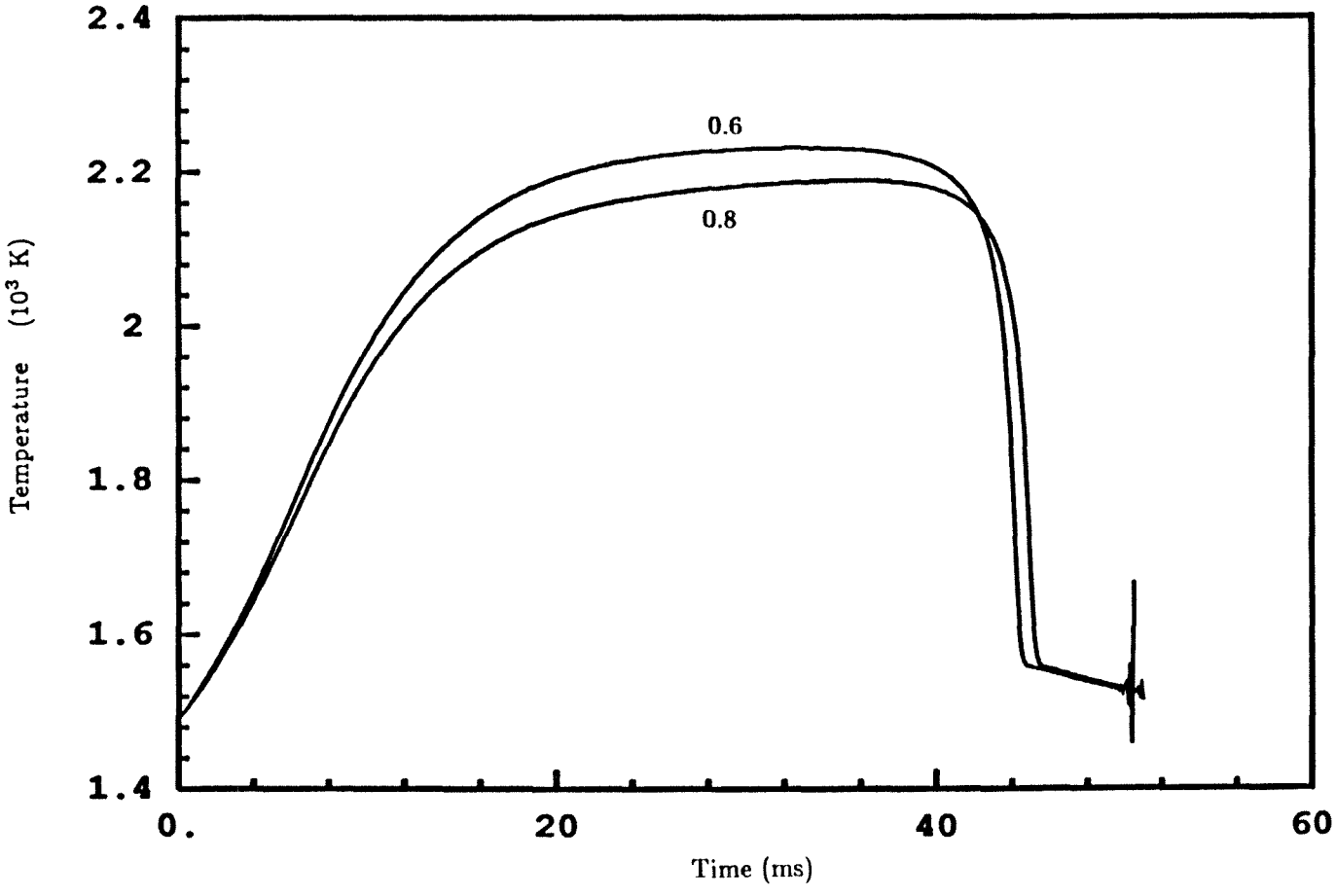

Figure 7.17 General Model with initially monodisperse voids: Effect of particle emissivity, ϵ_0. Parameters as in Figure 7.9.

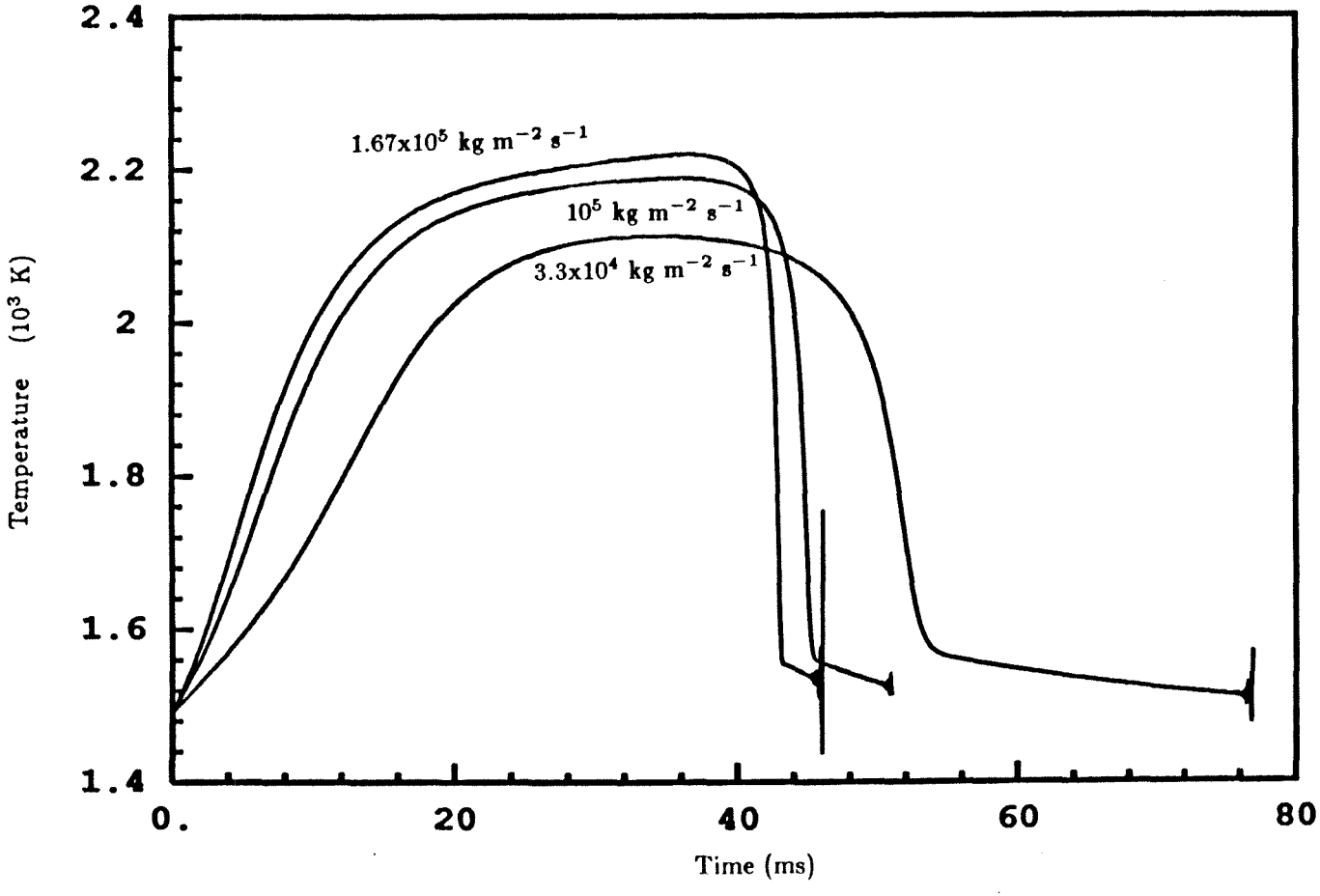

Figure 7.18 General Model with initially monodisperse voids: Effect of intrinsic Arrhenius pre-exponential factor, A_i. Parameters as in Figure 7.9.

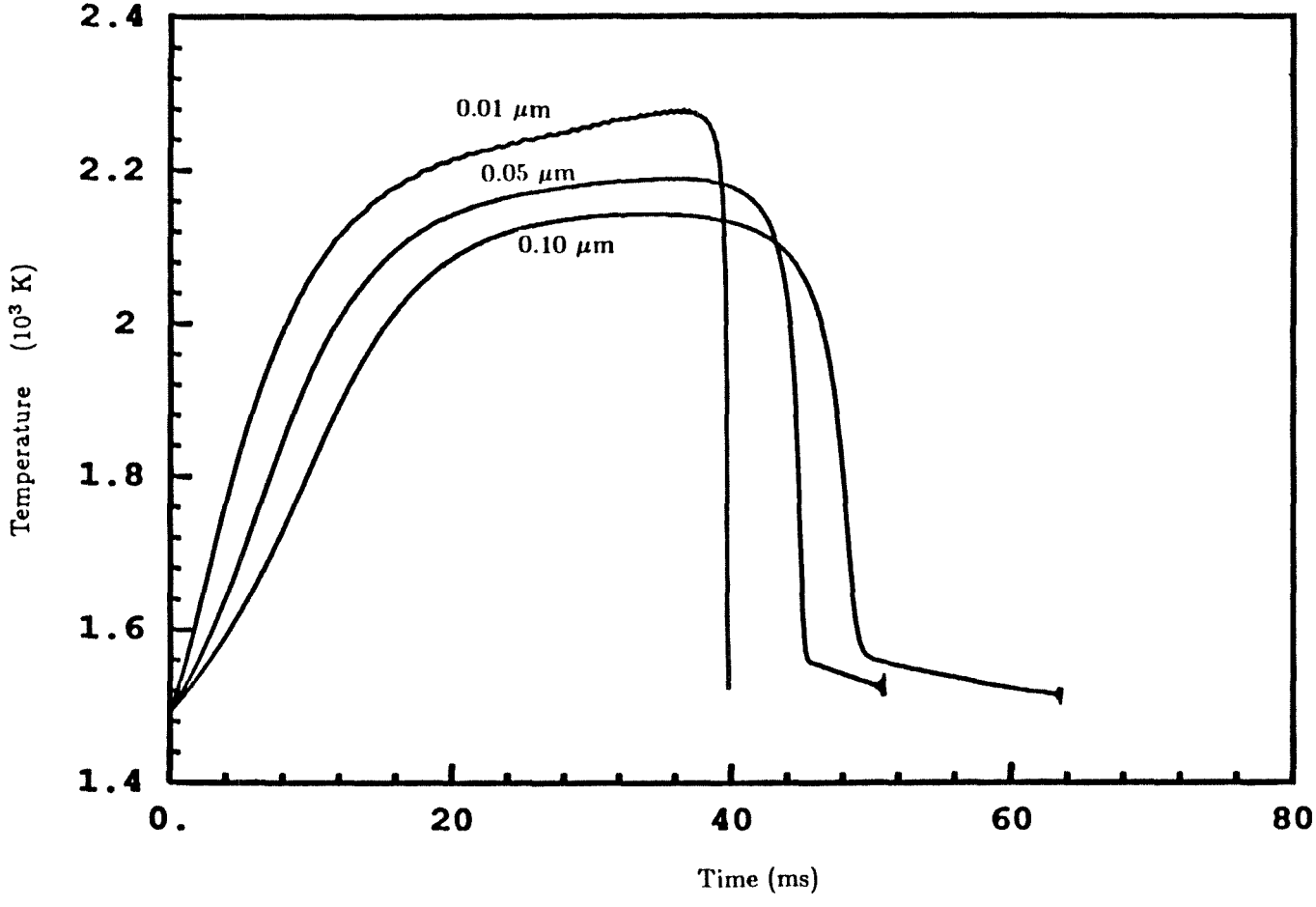

Figure 7.19 General Model with initially monodisperse voids: Effect of initial void radius, a_0. Parameters as in Figure 7.9.

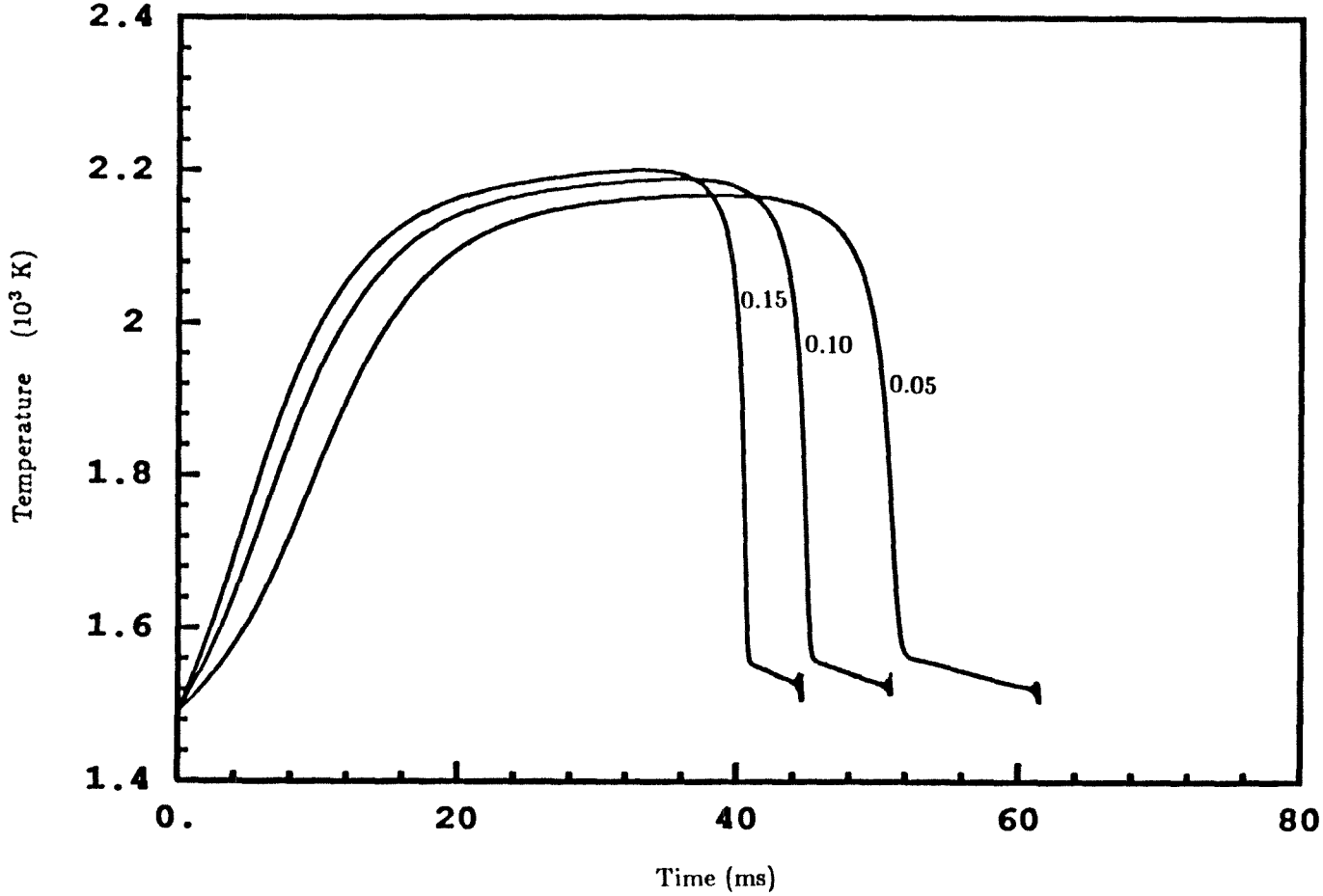

Figure 7.20 General Model with initially monodisperse voids: Effect of initial void fraction, ϵ. Parameters as in figure 7.9.

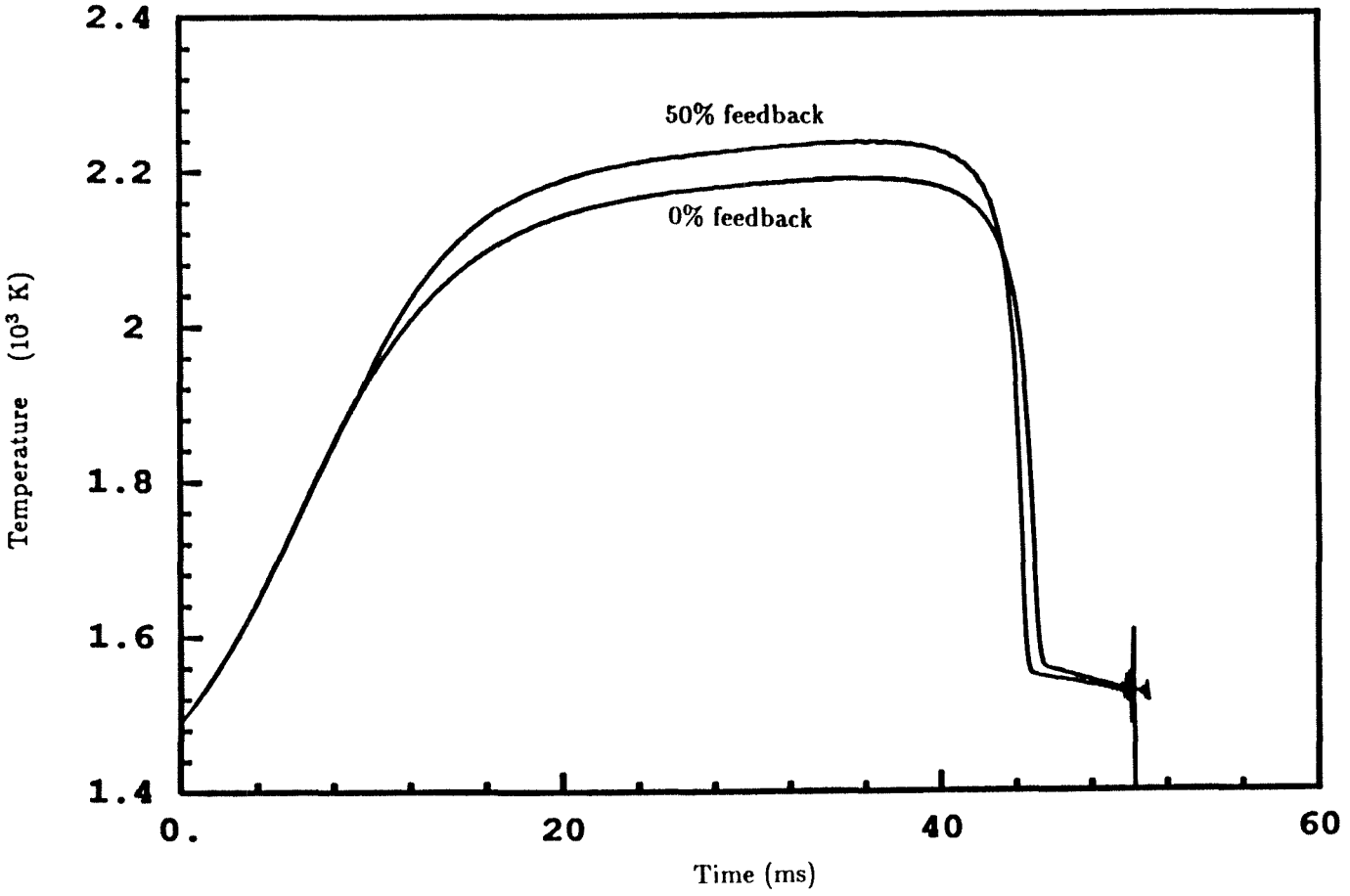

Figure 7.21 General Model with initially monodisperse voids: Effect of energy feedback. Parameters as in Figure 7.9.

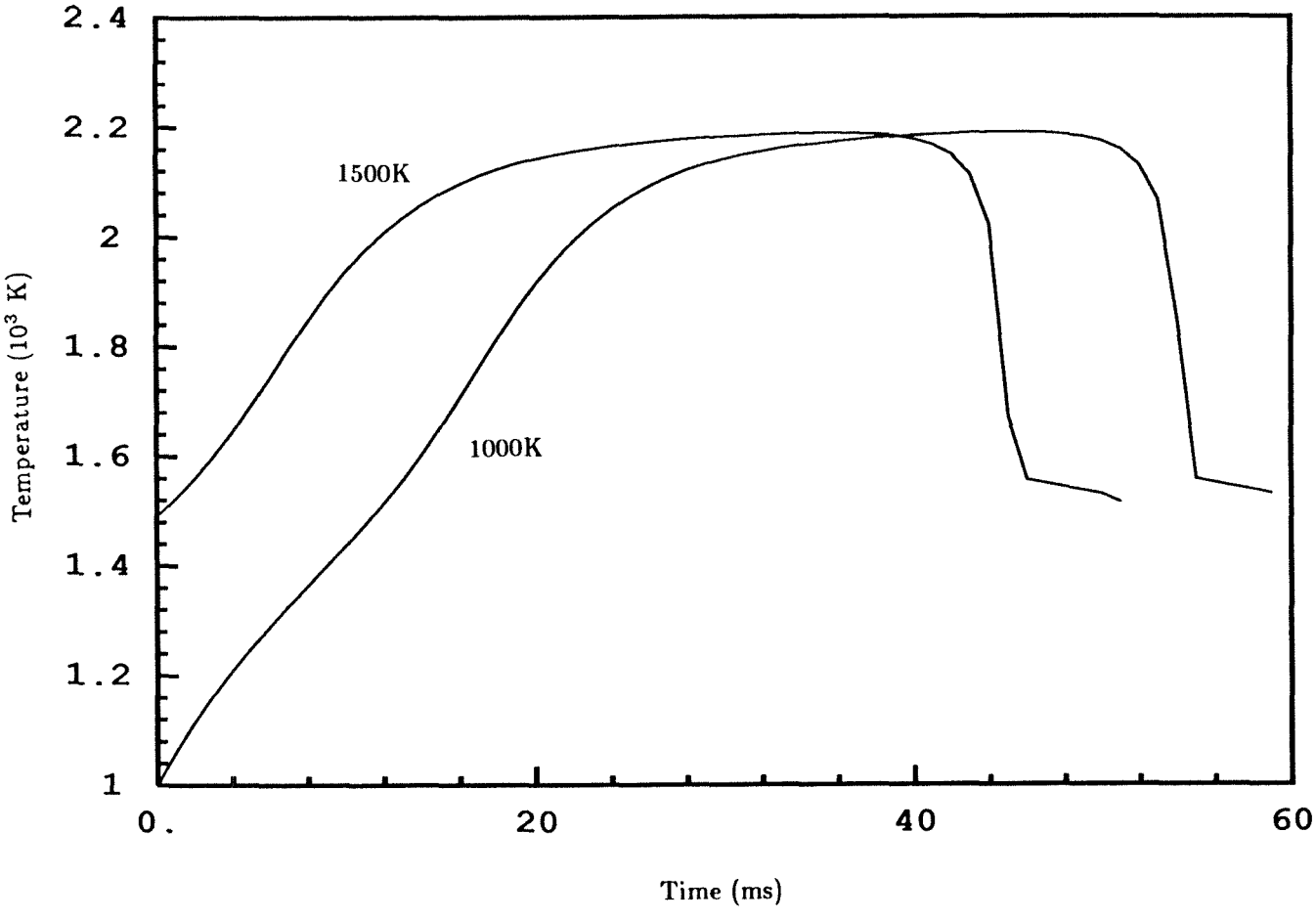

Figure 7.22 General Model with initially monodisperse voids: Effect of wall temperature, T_∞. Parameters as in Figure 7.9.

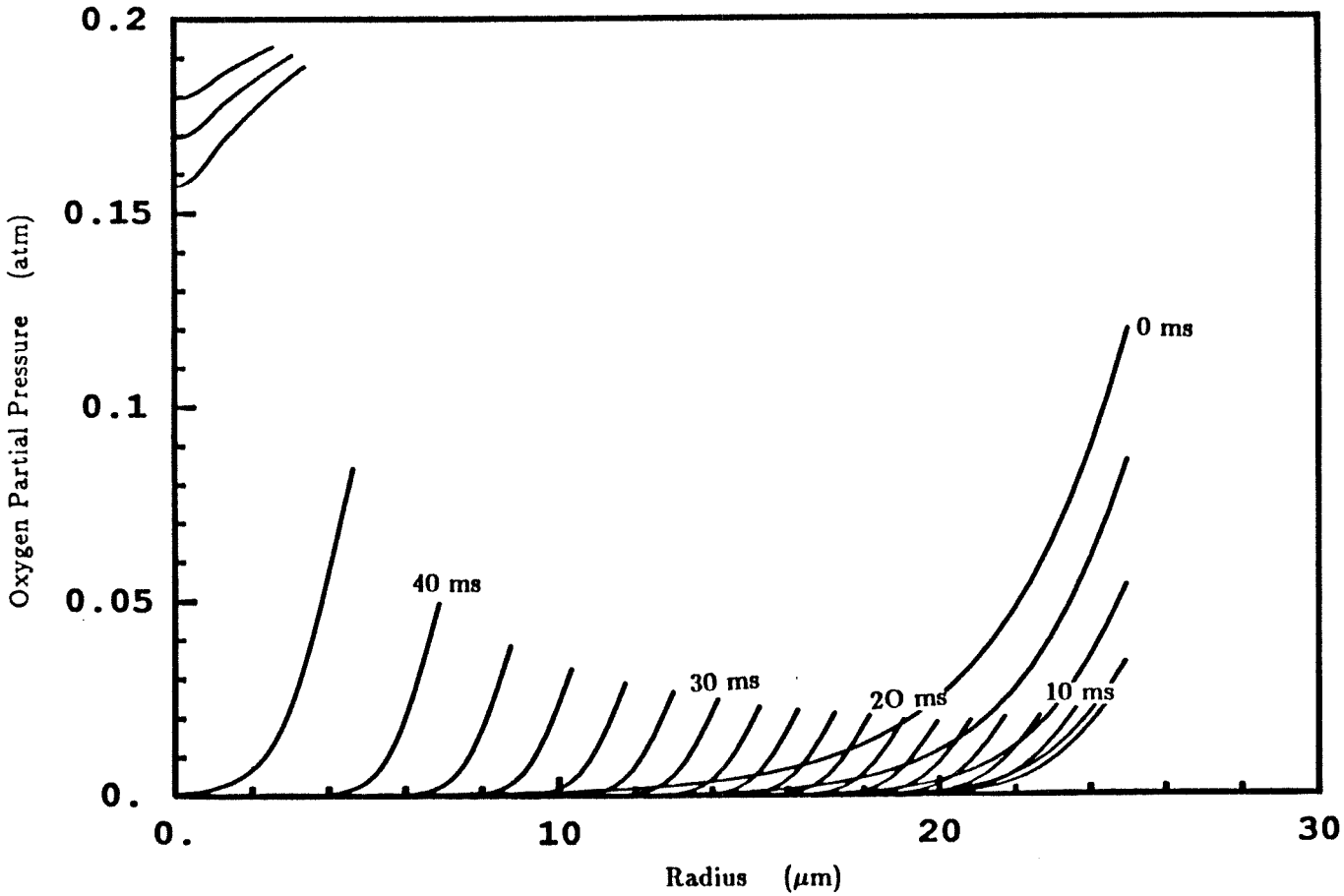

Figure 7.23 General Model with initially monodisperse voids: Internal oxygen partial pressure profiles at various times for $A_i=10^5$ kg m^{-2} s^{-1}. Other parameters as in Figure 7.9.

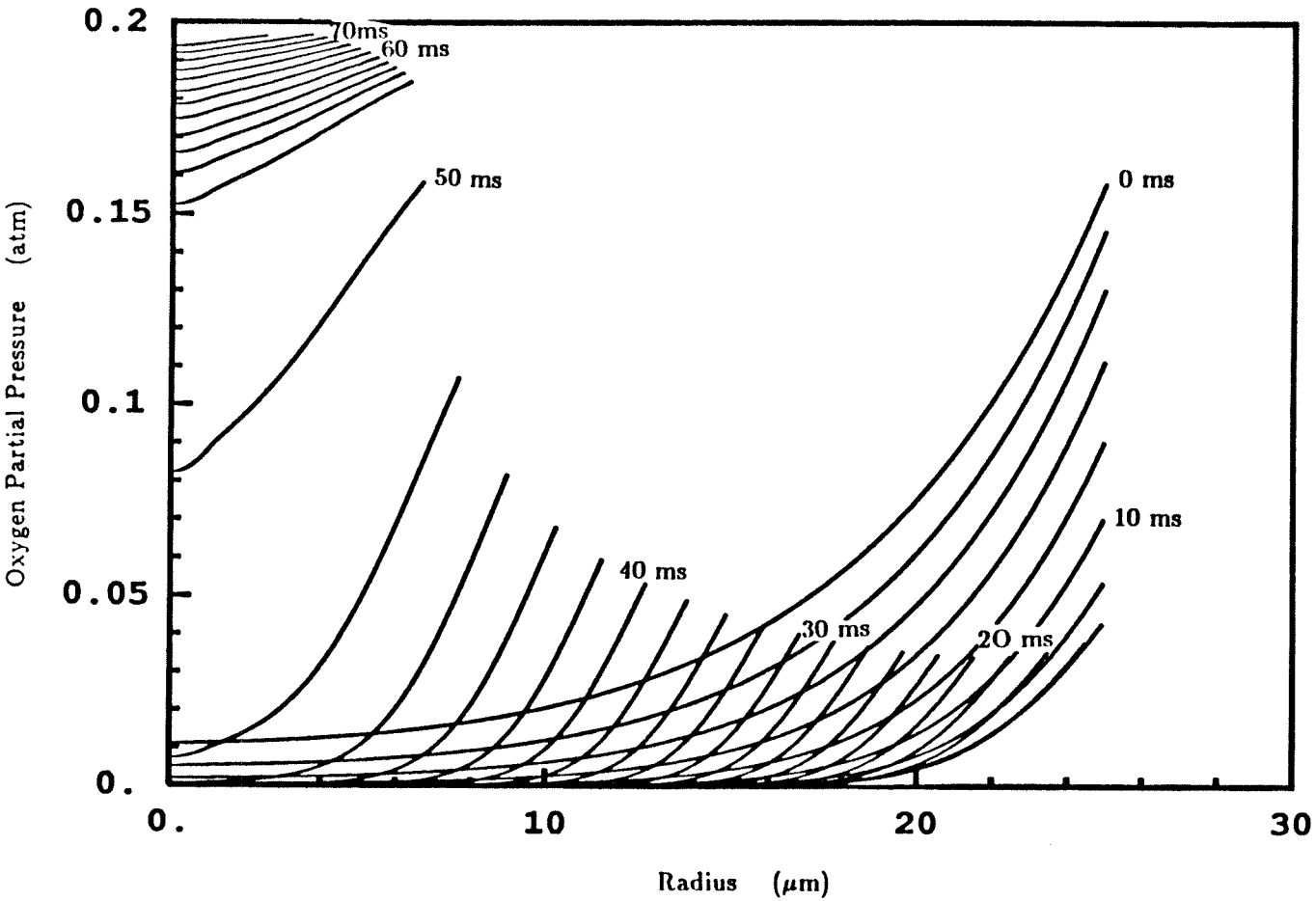

Figure 7.24 General Model with initially monodisperse voids: Internal oxygen partial pressure profiles at various times for A_i=3x10^4 kg m^{-2} s^{-1}. Other parameters as in Figure 7.9.

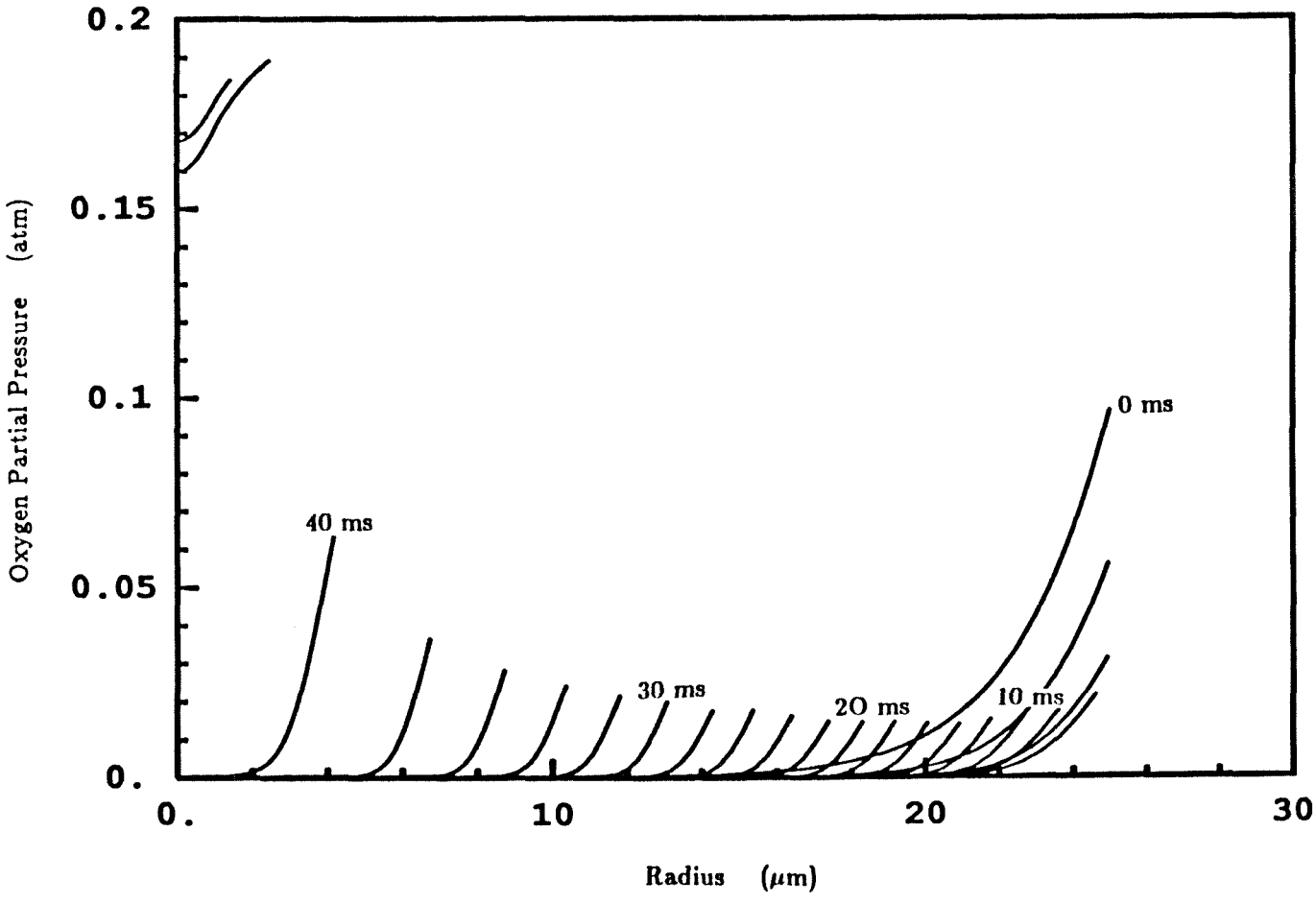

Figure 7.25 General Model with initially monodisperse voids: Internal oxygen partial pressure profiles at various times for A_i=1.67x10^5 kg m^{-2} s^{-1}. Other parameters as in Figure 7.9.

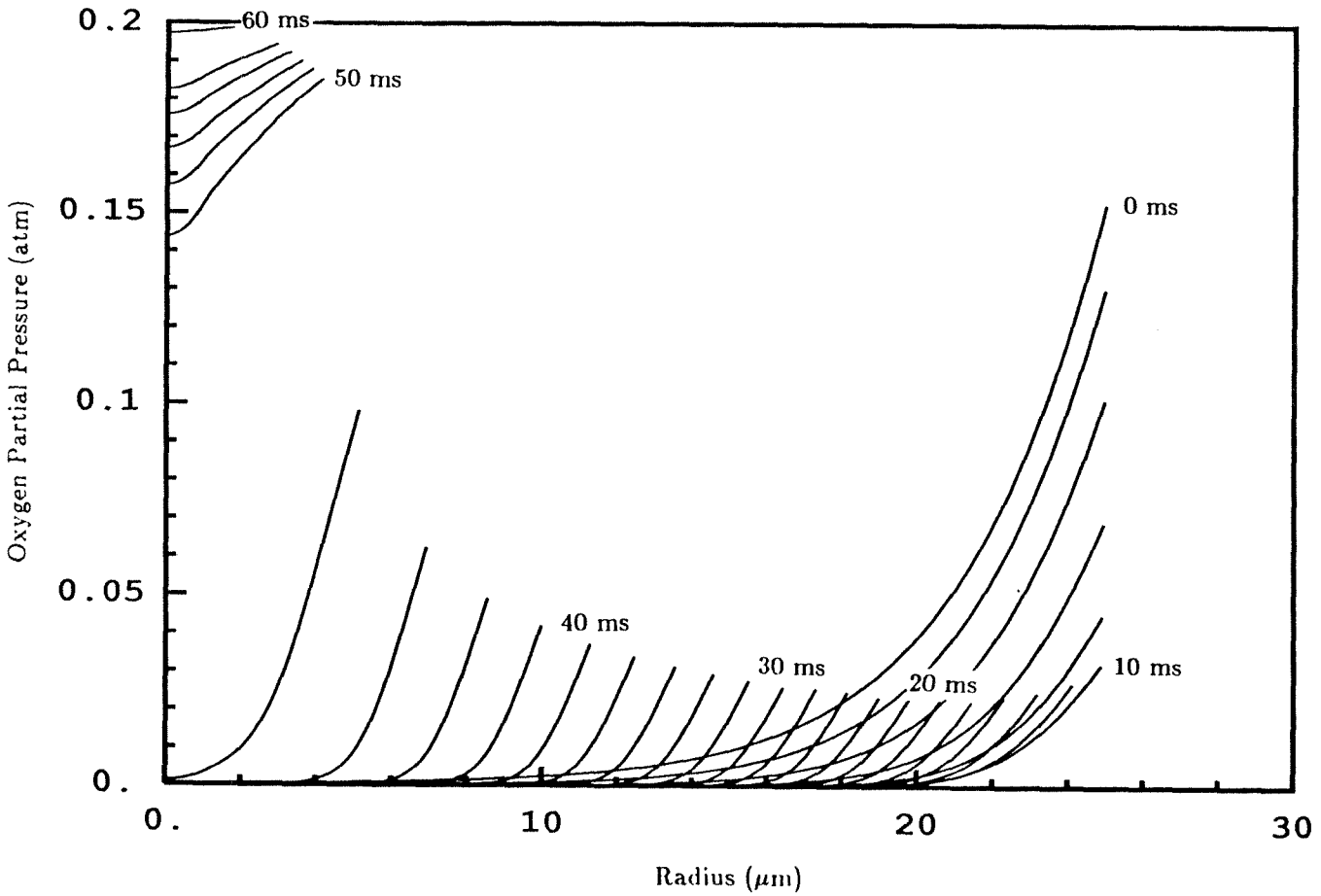

Figure 7.26 General Model with initially monodisperse voids: Internal oxygen partial pressure profiles at various times for ϵ=0.05. Other parameters as in Figure 7.9.

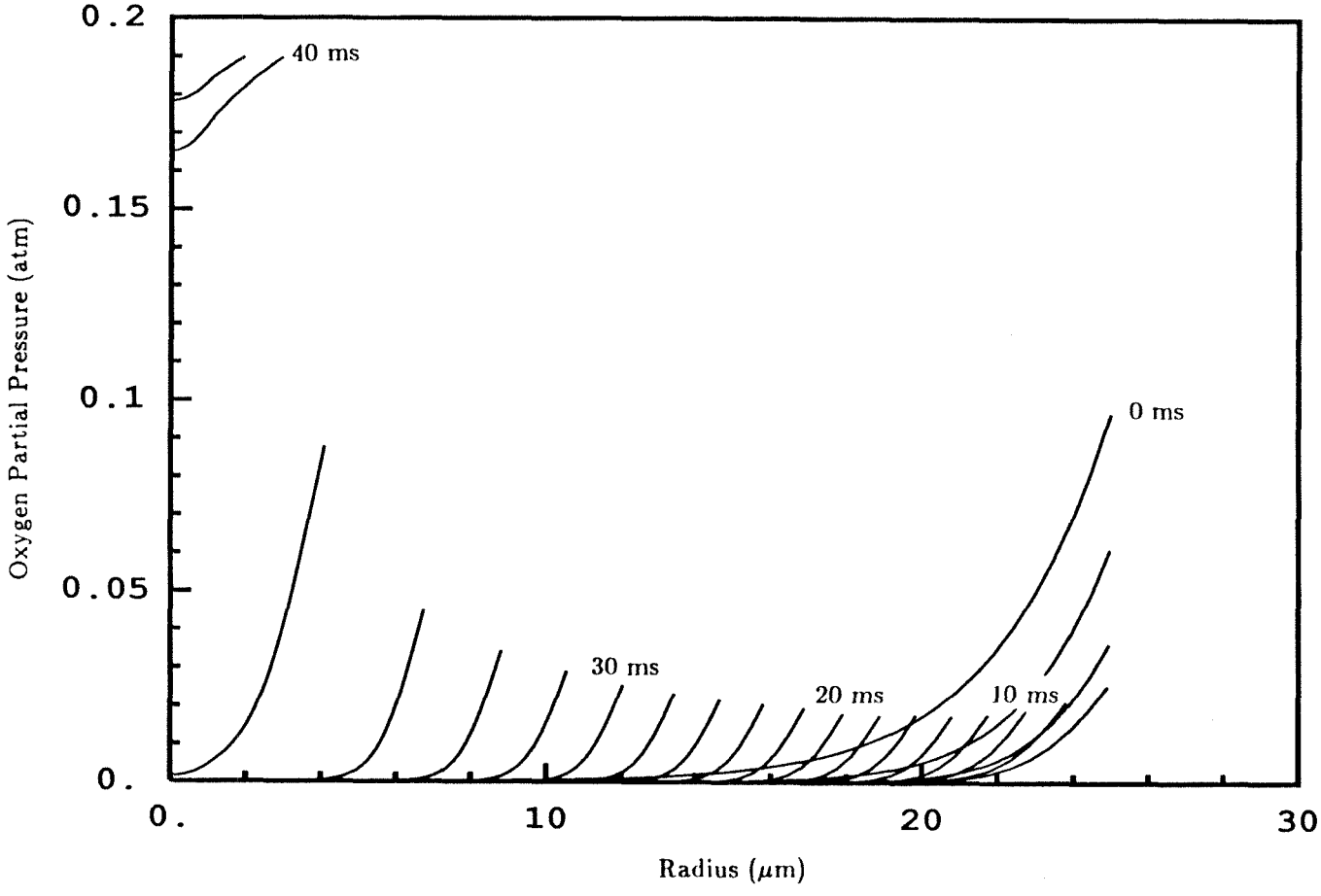

Figure 7.27 General Model with initially monodisperse voids: Internal oxygen partial pressure profiles at various times for ϵ=0.15. Other parameters as in Figure 7.9.

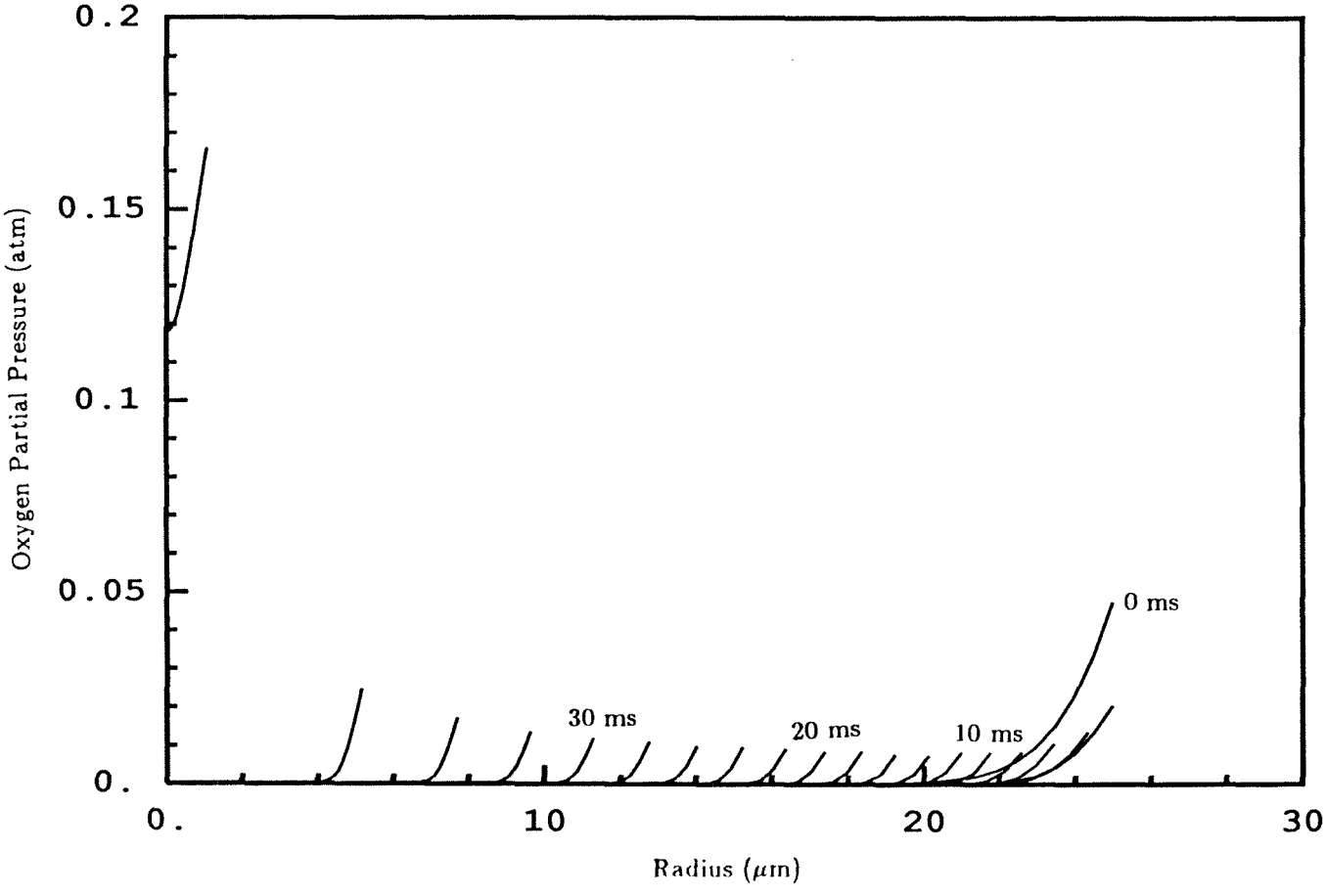

Figure 7.28 General Model with initially monodisperse voids: Internal oxygen partial pressure profiles at various times for a_0=0.01 μm. Other parameters as in Figure 7.9.

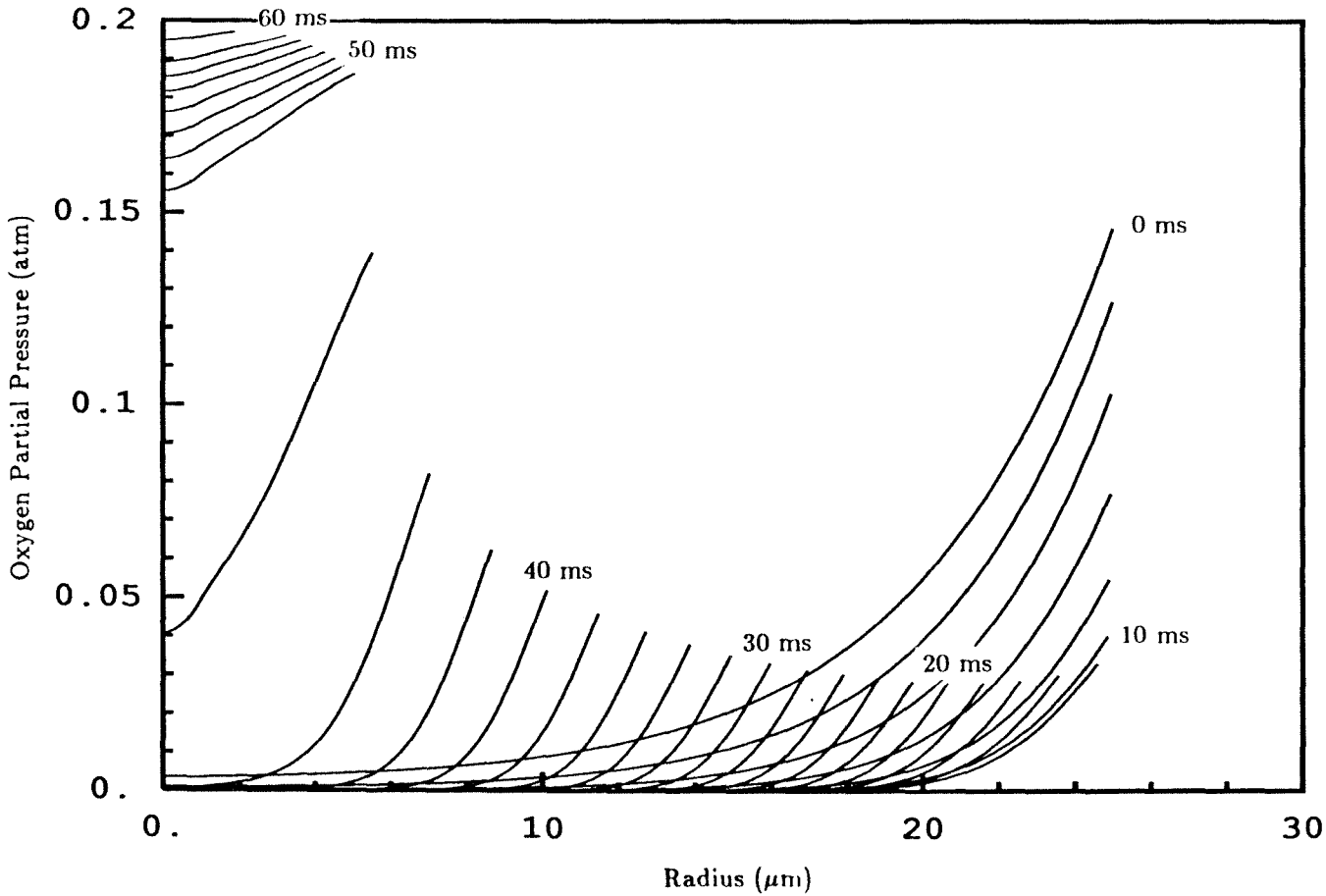

Figure 7.29 General Model with initially monodisperse voids: Internal oxygen partial pressure profiles at various times for a_0=0.1 μm. Other parameters as in Figure 7.9.

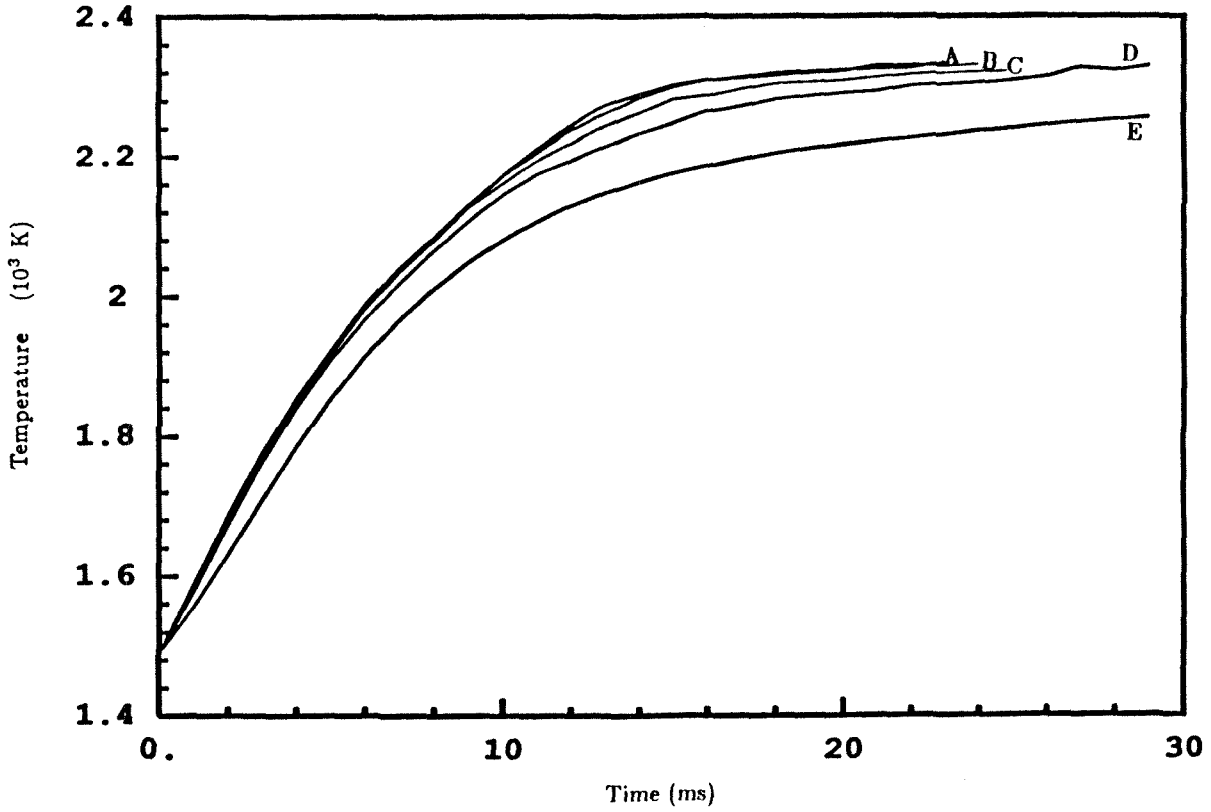

Figure 7.30 General Model with initially polydisperse voids: Effect of void fraction distribution in the three void radii 0.1 μm, 0.01 μm, and 0.001 μm respectively. Case A: 0.05, 0.09, 0.03; Case B: 0.10, 0.04, 0.03; Case C: 0.10, 0.05, 0.02; Case D: 0.10, 0.06, 0.01; Case E: 0.10, 0.07, 0.00. Total initial void fraction in all cases = 0.17. Other parameters as in Figure 7.9.

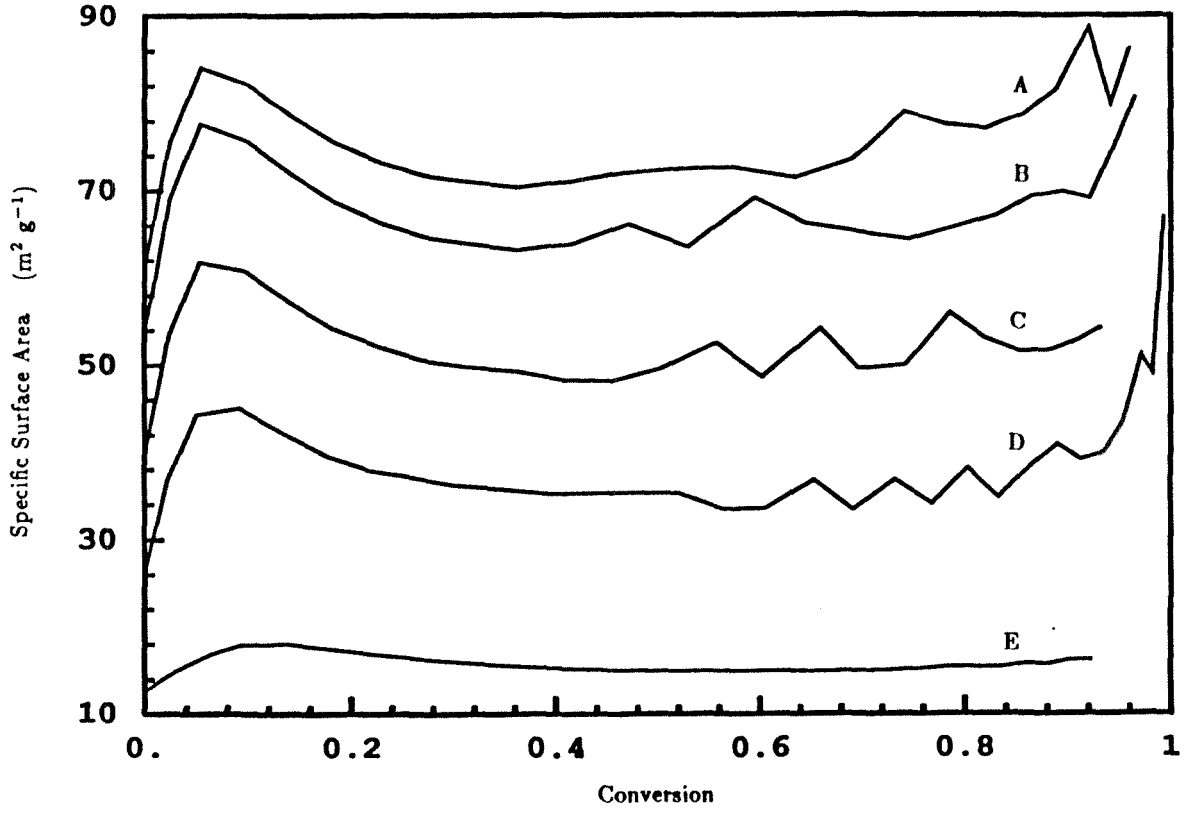

Figure 7.31 General Model with initially polydisperse voids: Specific surface area versus carbon conversion for cases with varying void fractions in the different void sizes. Case A: 0.05, 0.09, 0.03; Case B: 0.10, 0.04, 0.03; Case C: 0.10, 0.05, 0.02; Case D: 0.10, 0.06, 0.01; Case E: 0.10, 0.07, 0.00. Total initial void fraction in all cases = 0.17. Other parameters as in Figure 7.9.

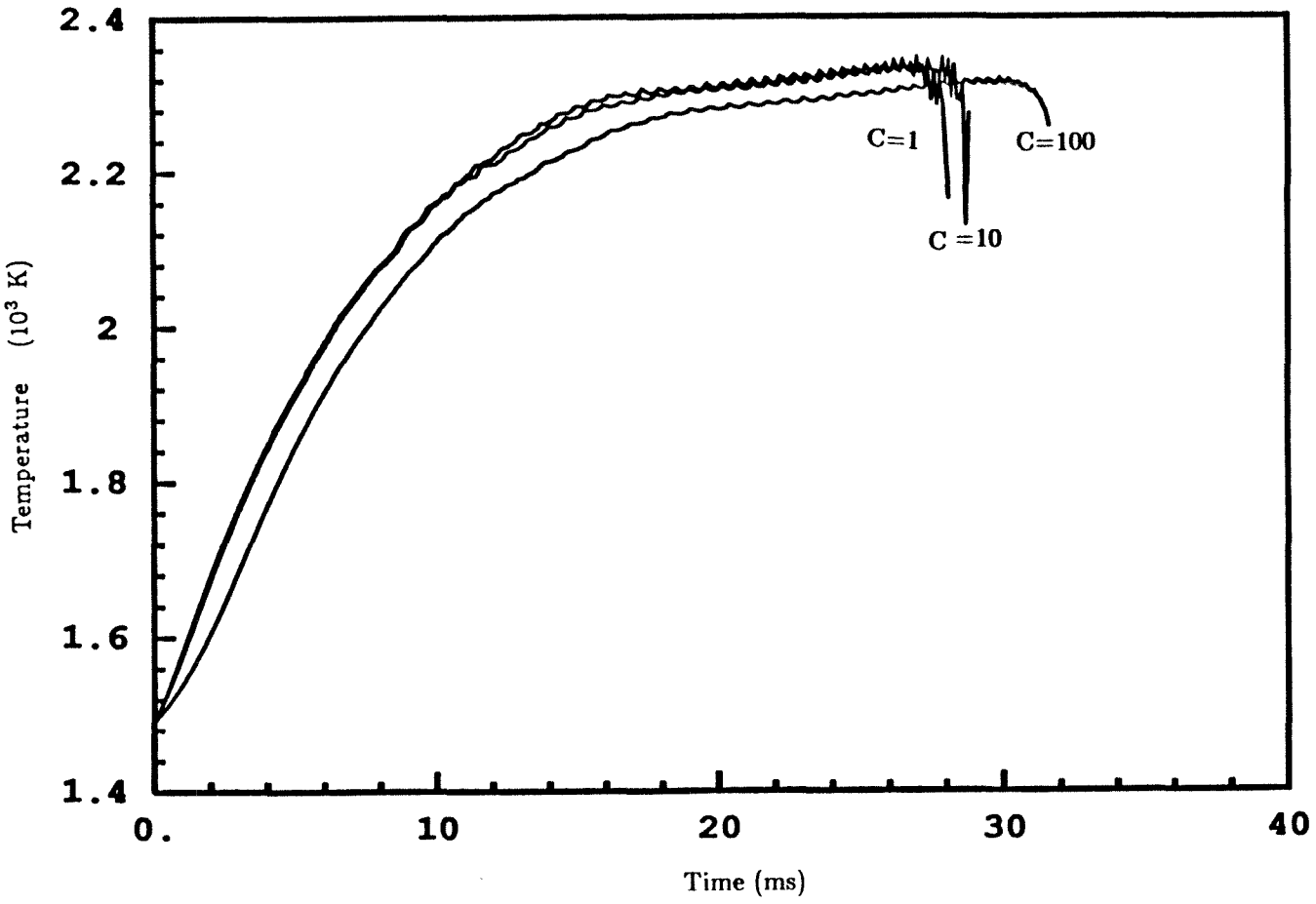

Figure 7.32 General Model with initially polydisperse voids: Effect of the parameter C in the Langmuir-Hinschelwood reaction rate expression. Other parameters as in Figure 7.30 Case A.

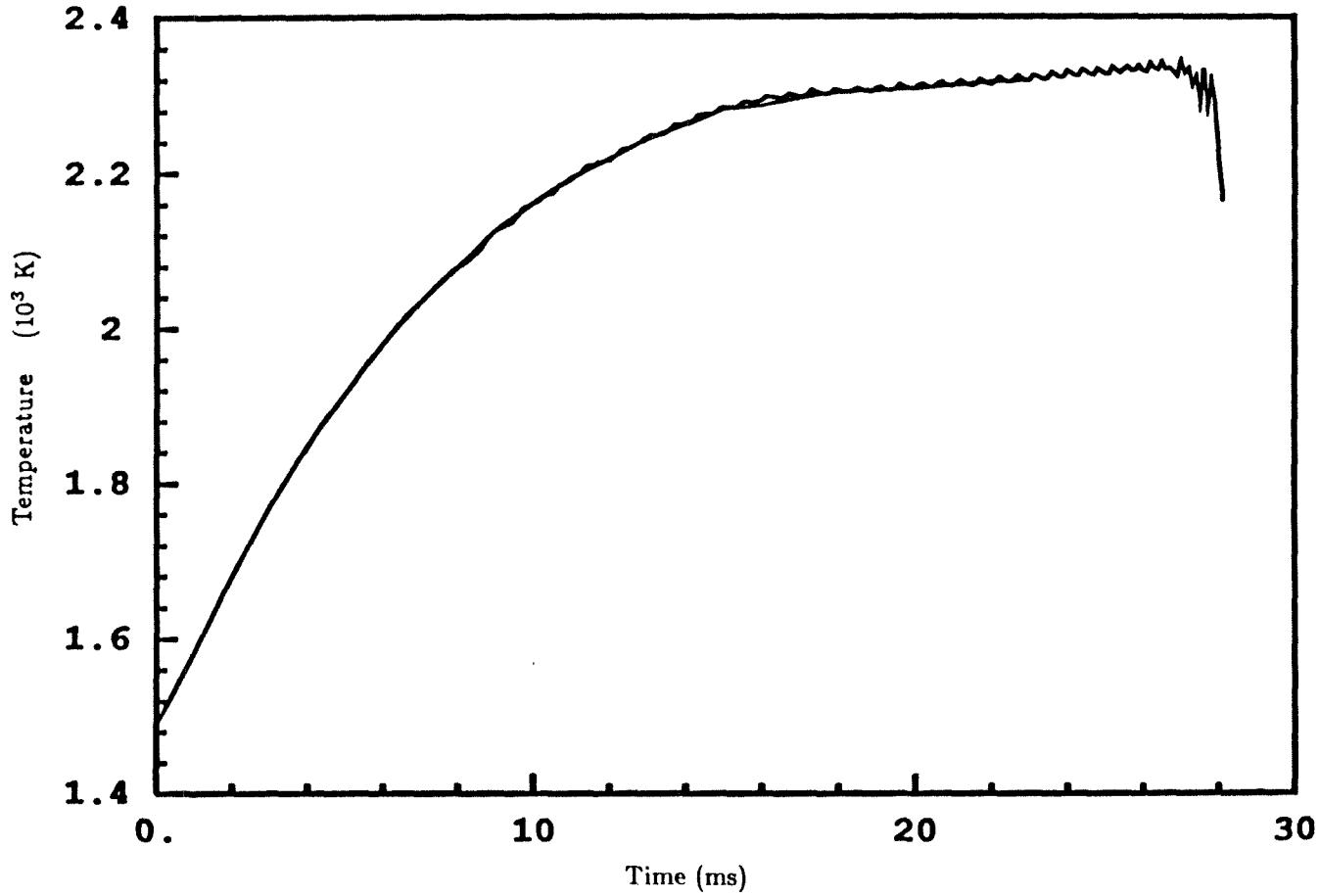

Figure 7.33 General Model with initially polydisperse voids: Comparision of the linear rate with the Langmuir-Hinschelwood rate with C=1.

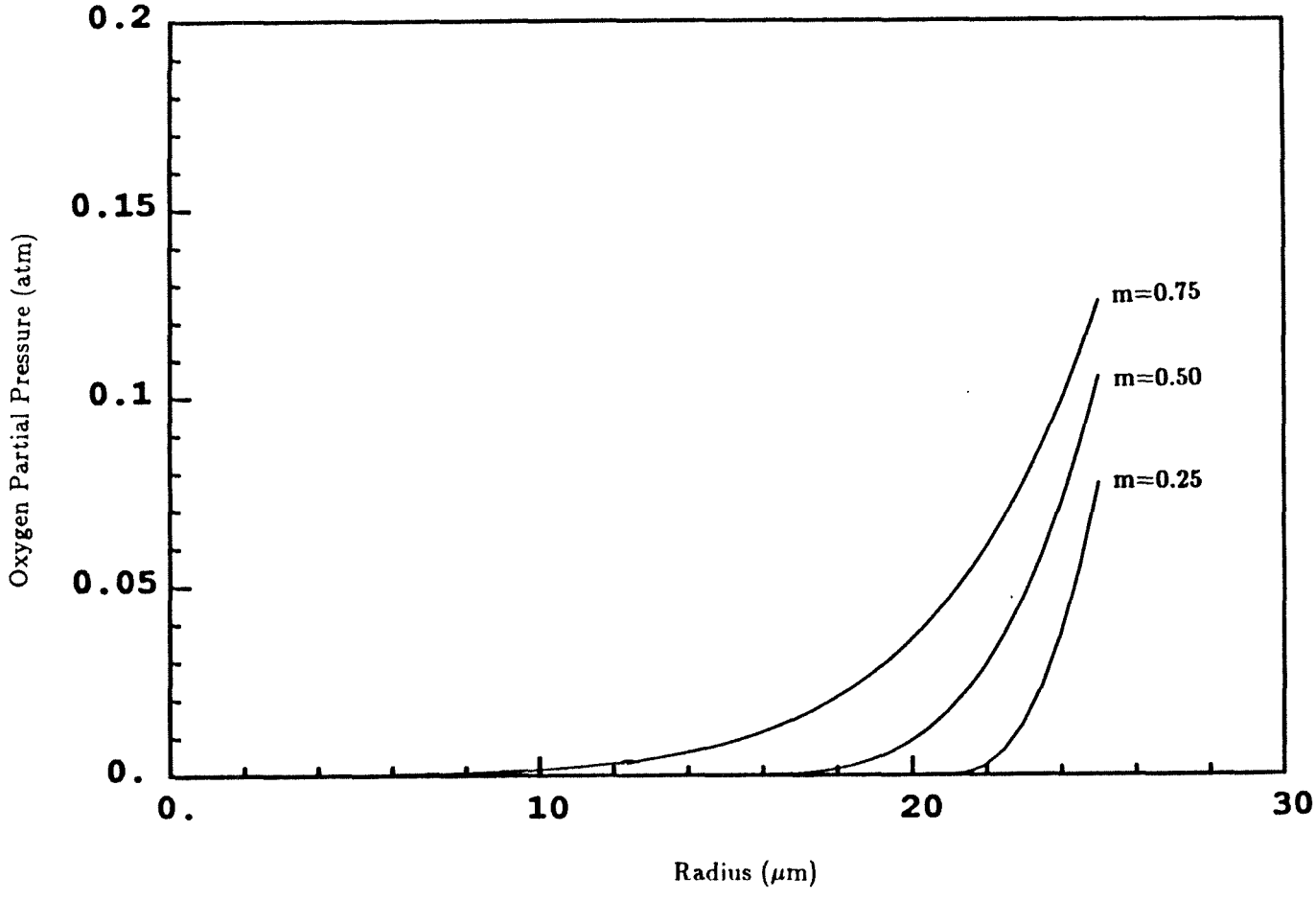

Figure 7.34 General Model with initially polydisperse voids: Internal oxygen partial pressure profiles at t=0 for different powers in the power law reaction rate expression. Other parameters as in Figure 7.30 Case A.

Chapter 8

DISCRETE SIMULATION OF CENOSPHERIC COAL-CHAR COMBUSTION

Submitted to *Combustion and Flame*

Abstract

A phenomenological model of structural transformations during pulverized coal char combustion is presented. The random geometry of the voids is modelled realistically by means of a random assemblage of spheres in a spherical particle. Pore connectedness and growth are accounted for as the combustion proceeds. The percolation behaviour of the void space is dramatically demonstrated. The effects of different initial voidfractions and of the random nature of the structure itself, at a given initial voidfraction are shown. This sheds some light on our ability to realistically model the solid. The limitation of shrinking core models of combustion of cenospheric chars are demonstrated. In this initial application, the model is limited to isothermal combustion with no diffusional limitations.

8.1 Introduction

Recent theoretical research in coal combustion and gasification has emphasized the role of intraparticle reaction, diffusion, and pore morphology evolution. Two approaches have been taken. In the first approach [1-8], the carbonaceous matter is treated as a continuum and the material and energy balances governing the combustion process are formulated as differential equations. These equations contain coefficients, such as specific surface area and internal diffusivity, which are generally functions of carbon conversion and vary with time and intraparticle position. The relations between surface area, diffusivity and conversion were either based on the random pore model [1,5,6], treated as directly measurable properties [2-4], or derived using results from percolation theory [7,8]. Regardless of the particular form or origin of these functional relationships, the use of local average properties presumes that the largest length scale characteristic of the porous structure is much smaller than the characteristic length associated with concentration gradients. It is not necessary, for our present purposes, to define these length scales more precisely except to note that the characteristic length of the porous structure could be considerably larger than the pore diameter itself. It is easy to verify that the relation between the length scales necessary to justify the continuum description is not satisfied under conditions of pulverized combustion where the oxygen penetration depth of a few microns is on the same order of magnitude as the largest length scale characteristic of the porous structure. Chars of softening coals often possess a sponge-like structure containing large voids, several micrometers in diameter, as well as smaller pores all the way down to one nanometer. For such chars

the continuum description is particularly unsuitable.

In the second approach that has been used to describe intraparticle processes in combustion, the porous structure is represented by a lattice where, for example, the presence or absence of a bond signifies the solid and the void phases respectively. This approach, sometimes known as 'discrete simulation', has been used by several authors particularly as a means of exploring the role of connectivity and the onset of fragmentation. Sandmann and Zygourakis [9] have developed a detailed discrete simulation approach to describe char gasification. The char particle is represented by a two-dimensional lattice whereon voids of different sizes are constructed according to some geometric rule to simulate mercury porosimetry data. To simulate pure kinetic control, they assumed that all voids are accessible and grow at the same rate in discrete increments. In another limiting case examined, only those voids accessible to the external particle surface were allowed to grow, all at the same rate. This diffusion-reaction regime would be applicable to a material having a macropore-micropore structure where the Thiele modulus for the micropores is very high but that for the macropores is low.

Sahimi and Tsotsis [10] have represented the porous structure on a three-dimensional lattice, using a percolation cluster to represent a char particle. Only those solid sites accessible to the particle surface were allowed to react, at an uniform rate. Their simulations provide detailed information about fragmentation as well as the rate of conversion history of a burning particle.

Kerstein and Edwards [11] followed a similar modelling approach but used a two-dimensional lattice. The discrete simulation studies [9-11] do not consider the

effect of intraparticle diffusion. Sahimi and Tsotsis [12] have extended their model to include the effect of diffusion, simulated by random walks of the oxidizer molecules towards the particle.

The near percolation structure used to represent the char particle in papers [10-12] is not suitable for representing a material with macropore-micropore morphology or one having a more complex pore structure. Nevertheless, this limitation can be overcome by adopting the approach of Sandmann and Zygourakis [9]. Thus representation of the pore structure on a three-dimensional lattice in conjunction with random walks to describe diffusion provides, in principle, a very general and flexible approach to modelling char gasification and combustion.

The use of the lattice is computationally attractive because it allows use of efficient searching and sorting routines. Many results from graph theory and percolation theory developed for lattices are also applicable. However, quantitative applications and predictions would have to employ three-dimensional and relatively fine grids involving large-scale computations.

In this paper we present an alternative non-lattice representation of the porous structure which is computationally simpler although not quite as general as the lattice representation.

8.2 Pore Structure Model

As a model of a cenospheric char particle, consider a spherical char particle with spherical voids randomly distributed throughout its volume. The voids may overlap and, therefore, be connected to one another, or they may be isolated. Thus, connectivity to other voids and the external particle surface are built into the geometry.

Two voids overlap when their center separation is less than the sum of their radii. Similarly, a void is connected to the outside when the distance between its center and the instantaneous external surface is less than its radius. Figure 8.1 illustrates the initial geometry, and that corresponding to a later time when considerable reaction has already occurred. Voids that are connected together form clusters. A cluster is connected to the outside if any one of its constituent voids is connected to the outside. A cluster may be multiply-connected to the outside via more than one void.

The size of the initial particle, the initial number, volume, and size distribution of the voids and the initial random distribution of the void centers are parameters in this geometry. We have chosen a particle size of 50μm in diameter. For simplicity the initial void sizes are taken to be monodisperse and 5μm in diameter. This assumption is easily relaxed to introduce a variety of void sizes, but the essential results of the model are captured by assuming an initially monodisperse set of voids. Initial voidfractions are then varied by changing the number of void centers in the particle.

The particle combustion is modelled as follows. Analogous to Gavalas [1] we postulate a surface recession velocity, q, such that every surface that is connected to the outside, either directly or indirectly (being part of a cluster that is connected to the outside) recedes by the amount $\delta = q\Delta t$ in time, Δt. The effects of temperature and reaction rates are lumped into the parameter q. In the simplest case we have assumed that q is constant with time and with radius. Physically this corresponds to an isothermal, homogeneous particle burning with no diffusional re-

sistances. The motivation for this study was to determine the structural dynamics of a burning cenospheric char particle. Hence, as a first approximation we minimized the complications introduced by diffusion, composition inhomogeneities, and the energy balance. However, diffusion can be taken into account by varying q with radius.

It is clear that, if we take discrete steps of magnitude δ, the smaller we take δ the better the temporal resolution of the simulation. That is, when δ is small the surface area of an accessible cluster will change smoothly without abrupt jumps. However making δ too small increases the simulation time considerably. We have taken q to be 0.05 μm/time step and the simulations have been carried out till δ/R_0 was 0.25. Since the particle was burning internally, this was sufficient to reach void fractions as high as 0.95.

The main variable that is measured at each step is void fraction. By randomly distributing a large number (typically 3000 or more) of probe points in the particle and counting that fraction which lies in the voids we can measure the void fraction and conversion very accurately. As the exterior of the particle also recedes at the rate q, the particle radius is defined accurately at all times. We also record some other geometrical parameters defined in the next section that shed light on the dynamics.

The simulation is terminated after a given number of time steps. The values of conversion at the end of the runs were in the range 0.8-1.0. For some of the runs clearly fragmentation must have occurred. This paper will not address the challenging questions posed by fragmentation.

It is clear that the results will depend on the quality of the random number generator used. We have used a generator in the IMSL library after rigorously testing its output for independence of sequence entries and repartisation. To avoid the possibility of creating N-tuples for some starting seed numbers the random numbers were re-randomised by randomly mixing two strings [13].

8.3 Model Parameters

The voidfraction is defined as the volume fraction of voids in a particle. It is denoted by ϵ. This parameter is directly obtained from the simulation by counting the number of probe points. The carbon conversion is calculated knowing the initial and final void fractions and radii of the particle. This assumes that there is no mineral matter or ash in the particle. The final radius of the particle is the external radius of the particle at the termination time step. The conversion in percent is given by

$$c = 100 \left[1 - \frac{R_f^3(1-\epsilon_f)}{R_0^3(1-\epsilon_0)} \right] \tag{8.1}$$

where R_f^3 and R_0^3 are the final and initial radii of the particle and ϵ_f and ϵ_0 are the final and initial voidfractions. The density of the solid phase is assumed to stay constant throughout the process. Another interesting parameter is the conversion rate. This is the instantaneous slope of the conversion versus time curve, i.e., the rate of mass loss. The relation between number of steps in the simulation and real time for an isothermally burning particle is

$$t = \aleph \frac{MqN}{R\rho} \tag{8.2}$$

where t is time, M is the molecular weight of carbon, N is the number of steps,

q is the surface recession velocity (μm/step), ρ is the particle density, R is the reaction rate in moles-sec/cm^2 (assumed invariant with temperature) and $\aleph$ is an unit conversion constant.

For a particle whose temperature is uniform but varies with time, the relation is given by the following integral

$$t = \aleph \int_0^T \frac{Mq}{R(\tau)\rho} \frac{dN}{d\tau} d\tau \tag{8.3}$$

where T is the particle temperature and $\frac{dN}{d\tau}$ is derived from an energy balance.

A preliminary effort has been made to model the effects of diffusion by varying the parameter q with radius. An exponential function was chosen such that the value of q was 0.05μ/step at the instantaneous surface of the particle and 0.005μ/step at the particle center. However, results pertaining to diffusion will not be given in this paper.

Apart from the above, another important variable is the size of the largest void cluster. Due to overlap and given the fact that the clusters do not grow in geometrically regular shapes we denote size by the number of void centers in a given cluster. As will be seen later this parameter shows interesting percolation properties. One other important variable is the radial distribution of voidfraction as a function of conversion. This clearly shows the depth of the combustion zone on the particle surface. If this depth is small, modelling of the process by a 'shrinking core' model can be justified. Hence, our model helps to identify those types of solid structures that can be modelled with traditional and simple models.

8.4 Results

Table 8.1 shows the run numbers, number of initial voids and initial void fractions of the various runs. There are five groups of runs with around 50 (group E), 70 (group C), 100 (group B), 165 (group A) and 215 (group D) voids in the particle initially for each run. Due to the random nature of specifying the voids it was not possible to have exactly the same number of voids in the particle for each run in a given group. Moreover, void overlap leads to additional variation in the initial void fraction. However we believe that the variances in the initial number of voids within a group do not significantly affect our conclusions. We shall study in detail those runs where in fact there are exactly the same number of initial voids (e.g. runs D1,D2,D13,D14,D17,D18 — all having 216 voids initially). The other runs are given for the sake of completeness.

Table 8.2 compares the initial voidfractions obtained from the simulation and those calculated using the method given in Gavalas [1]. The void fractions calculated from theory are higher because the theory assumes an infinitely large particle and thus tends to overestimate the effects of voids whose centers are near or just outside the outer surface of the particle.

Figure 8.2 is a plot of the void fraction versus number of steps for run D14. Plots for the other runs are similar. At first the rate of increase of the void fraction from the initial voidfraction, accelerates with conversion. The rate then levels off and decreases slowly till the termination of the simulation. Initially, only those few voids that are connected to the outside can grow. As time progresses, the number of voids connected to the outside increases due to the capture of inaccessible voids by

the growing externally-connected clusters. Some other voids also become externally connected as the particle radius decreases. Eventually, most of the voids become externally connected and, therefore, can grow. The void fraction then grows rapidly. Finally, void collapse becomes dominant and the rate of growth of void fraction decreases. Void collapse occurs when the surface of a given void no longer exists, having been merged with other neighboring voids.

Figures 8.3 and 8.4 show conversion and conversion rate plotted against time, respectively. There is a slight maximum in Figure 8.4. The location and height of this maximum varies from run to run and, in some cases there is only a monotonic decrease as in Figure 8.5. This is consistent with previous experimental and theoretical observations of the variation of the reaction rate with time (or conversion). Since there are no composition heterogenities in the model solid, this variation is due to pore growth and collapse. The fact that different realizations show different behaviour underscores the importance of the random nature of the pore structure and its effects on the combustion.

Figure 8.6 shows the ratio of the number of voids in the largest cluster (XLAR) to the total number of voids (RTOT) as a function of the void fraction. The percolation of the void cluster through the particle occurs at various void fractions and finally all voids belong to one large cluster by 60% void fraction. This ratio of the number of voids in the largest cluster to the total number of voids can be thought of as a percolation probability. However, although all runs showed similar behaviour, there are important differences. The discrete jumps in the curve are capture events when growing clusters merge, creating larger clusters. Thus, in this

example at 40% void fraction nearly 70% of the voids already belong to the largest cluster. However, in Figure 8.7 (run D13) at 40% void fraction nearly 90% of the voids belong to the largest cluster. The only difference between runs D13 and D14 is that they are different members (realizations) of the same ensemble. There are similar examples in the other groups of runs where major differences are observed simply by changing only the random ordering of the voids in the particle.

The strong influence of the initial random nature of the solid and the importance of connectivity and growth of the solid in the combustion process cannot be overemphasized. Given this variability between 'similar' particles we have to be careful in defining and using 'average' values. In Figures 8.6 and 8.7 we see that the major transition takes place at a given void fraction. Figures 8.8 and 8.9 plot the void fraction when the percolation probability is 80% and 50% respectively as a function of the total number of voids in each run. Although there is variability the average values point to a definite trend. The variability also does not exceed the 1σ limits which are plotted in the figures. From those figures it seems that the asymptotic (when the number of voids $\rightarrow \infty$) void fractions when the percolation probability is 80% and 50% are 0.4 and 0.32 respectively.

The solid fraction is shown in Figure 8.10 as a function of the radius of the particle from run D14 at two different instants as it is burning. The curve A is at the start of the run and shows that except for deep inside the particle there are voids scattered throughout the particle such that the solid fraction at any radius is around 75% – 95%. The curve is jagged because the particle was divided into 50 spherical shells in order to calculate the radial solid fraction and reflects numerical noise.

Curve B corresponds to 70% conversion when combustion has penetrated quite deep into the particle leaving deep pits in the external surface. These pits account for the greatly reduced solid fraction at larger radii. A pictorial representation of this particle is shown in Figure 8.1. In this instance the assumption of a shrinking core model would not be valid. That was the general observation in most of the runs.

8.5 Discussion and Conclusions

Some additional comments are necessary regarding the percolation behaviour demonstrated by the void space with change in conversion. It should be quite evident that the process described here does not correspond to a simple percolation process in which the changes occur homogeneously through the domain under consideration. Here, only those voids connected to the outside grow and therefore this connectivity driven growth alters the phenomena and does not permit direct comparision with results from percolation theory (like critical voidfractions and critical exponents). Sahimi and Tsotsis have discussed this issue in considerable detail for their lattice representation.

The assumption of an initially monodisperse set of voids is oversimplified. It is clear that the model can readily be applied to other pore size distributions since, from the second step of the simulation onwards, the voids become poly disperse due to the extenal connectivity-growth constraint. Far more important is the role of multiple scales of voids that are present in an actual particle. A real particle typically has voids whose length scales differ by as much as four orders of magnitude. The number of the smallest voids is also very large. While, in principle, our model

can be extended to simulate such a case the computational cost and time make such an approach impractical. Renormalisation to account for the various length scales is a more elegant approach but it is still an open problem particularly for the non-lattice random geometry described here. The connectivity problem further complicates the issue.

Our calculations did not include diffusion and as such they are restricted to the following to physical situations. The first is a solid with a narrow pore size distribution burning in the kinetics controlled regime. The second is a bimodal macropore-micropore solid with large Thiele modulus for the micropores and small Thiele modulus for the macropores. In this case, the micropores need not be described explicitly, although their effect is manifested via an apparent rate expressed per unit macropore surface area. Chars of softening coals contain macropores, as large as 5μm in diameter, and micropores. However they sometimes contain transitional pores as well. Under conditions of pulverized combustion the micropore Thiele modulus is large but the macropore Thiele modulus is not always small. To describe this situation more realistically, diffusion has to be incorporated in any such discrete model.

References

1. Gavalas G.R., *Comb. Sci. and Tech.* 24:197 (1981)
2. Sotirchos S.V., and Amundson N.R., *AIChE J* 30:537 (1984)
3. Sotirchos S.V., and Amundson N.R., *AIChE J* 30:549 (1984)
4. Sotirchos S.V., and Burganos V.N., *Chem. Eng. Sci.* 41:1599 (1986)
5. Loewenberg M., Bellan J., and Gavalas G.R., *Chem. Eng. Comm.* 58:89 (1987)
6. Su J.L., and Perlmutter D.D., *AIChE J* 31:973 (1985)
7. Reyes S., and Jensen K.F., *Chem. Eng. Sci.* 41:333 (1986)
8. Reyes S., and Jensen K.F., *Chem. Eng. Sci.* 41:345 (1986)
9. Sandmann C.W.,jr. and Zygourakis K., *Chem. Eng. Sci.* 41:733 (1986)
10. Sahimi M., and Tsotsis T.T., *Chem. Eng. Sci.* 43:113 (1987)
11. Kerstein A.R., and Edwards B.F., *Chem. Eng. Sci.* 42:1629 (1987)
12. Sahimi M., and Tsotsis T.T., *Phys. Rev. Let.* 59:888 (1987)
13. Press W.H., Flannery B.P., Teukolsky S.A., and Vetterling W.T. *Numerical Recipes : The art of scientific computing* Cambridge University Press, Cambridge, 1986, p. 191.

RUN # / GROUP	1	2	3	4	5	6	7	11	12	13	14	15	16	17	18
A	(169) 0.1187	(162) 0.1105	(158) 0.1173	(169) 0.1120	(171) 0.1277	(167) 0.1158	(163) 0.1270								
B		(104) 0.0814			(106) 0.0814			(104) 0.0845	(105) 0.0852	(107) 0.0861	(107) 0.0734	(104) 0.0826	(106) 0.0907	(107) 0.0911	(104) 0.0879
C	(67) 0.0519	(72) 0.0588	(71) 0.0607	(69) 0.0594	(73) 0.0569	(75) 0.0575	(66) 0.0569								
D	(216) 0.1434	(216) 0.1609	(215) 0.1539			(214) 0.1516	(214) 0.1586	(215) 0.1466	(215) 0.1358	(216) 0.1479	(216) 0.1394		(214) 0.1413	(216) 0.1678	(216) 0.1627
E								(51) 0.0434	(54) 0.0362	(54) 0.0328	(55) 0.0469	(52) 0.0359	(52) 0.0348	(53) 0.0348	(53) 0.0294

Table 8.1 Initial conditions for various runs. The number in brackets is the initial number of voids in the particle and the other number shows the initial void fraction.

RUN NUMBER	INITIAL VOIDFRACTION (SIMULATION)	INITIAL VOIDFRACTION (THEORETICAL)
D1	0.1434	0.1943
D2	0.1609	0.1943
D3	0.1539	0.1935
D6	0.1516	0.1927
D7	0.1586	0.1927
D11	0.1466	0.1935
D12	0.1358	0.1935
D13	0.1479	0.1943
D14	0.1394	0.1943
D16	0.1413	0.1927
D17	0.1678	0.1943
D18	0.1627	0.1943

Table 8.2 Comparision of the initial void fractions as calculated from theory and from the simulation for Group D runs.

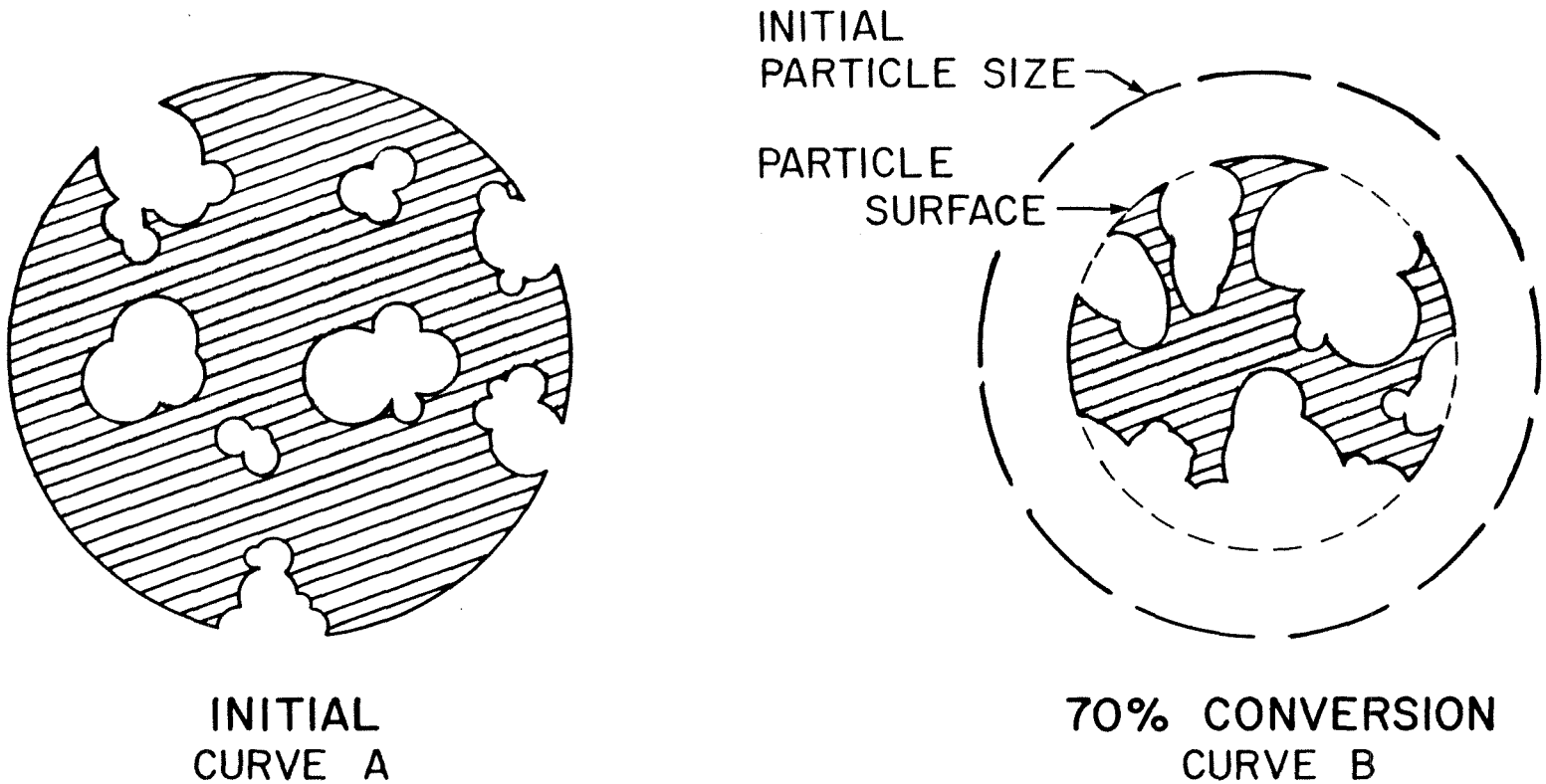

Figure 8.1 Geometry of the simulation showing the voids and clusters in the particle initially (A) and after significant conversion (B). The hatched area is solid carbon.

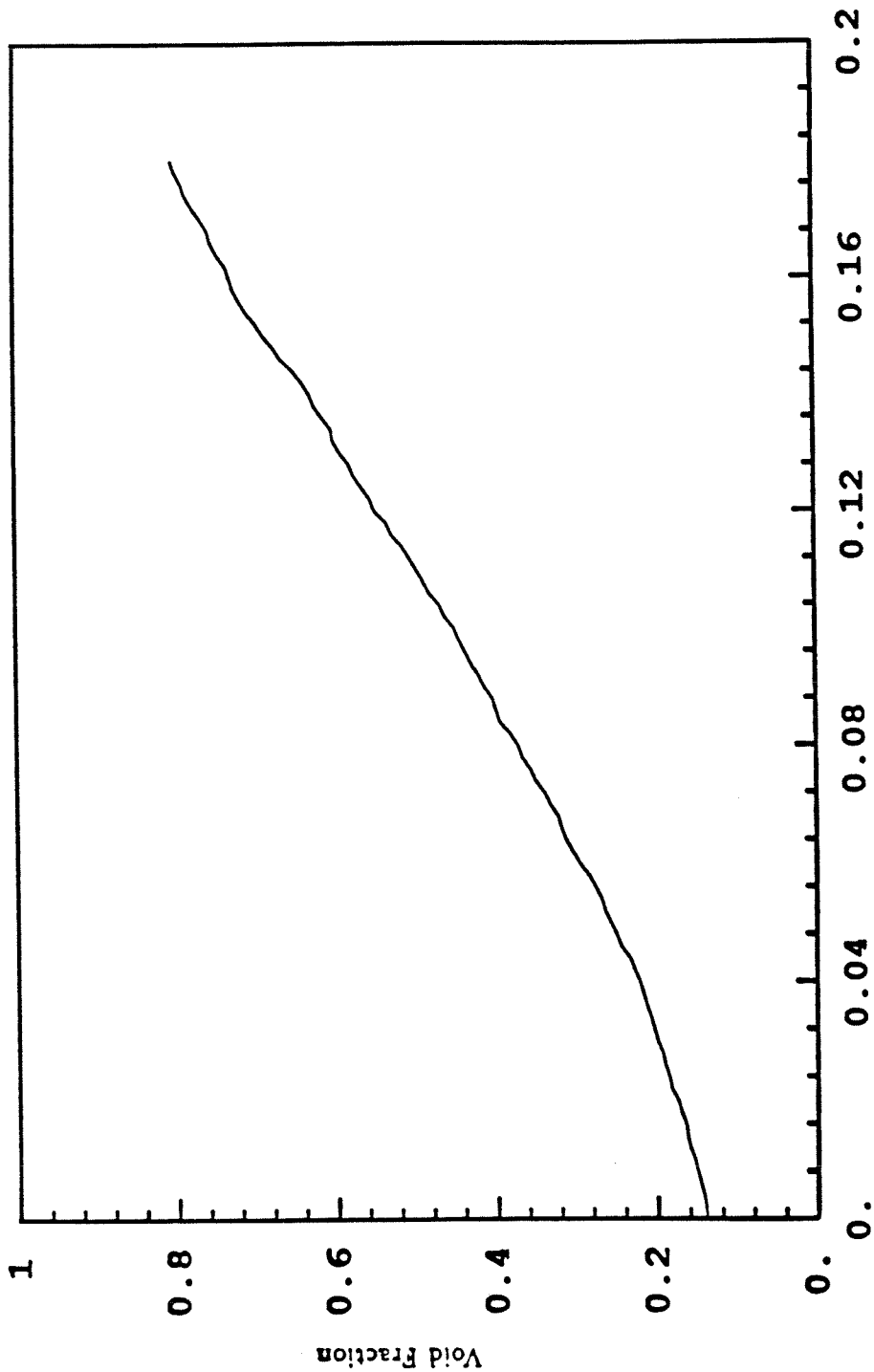

Figure 8.2 Void fraction versus δ/R_0 for run D14.

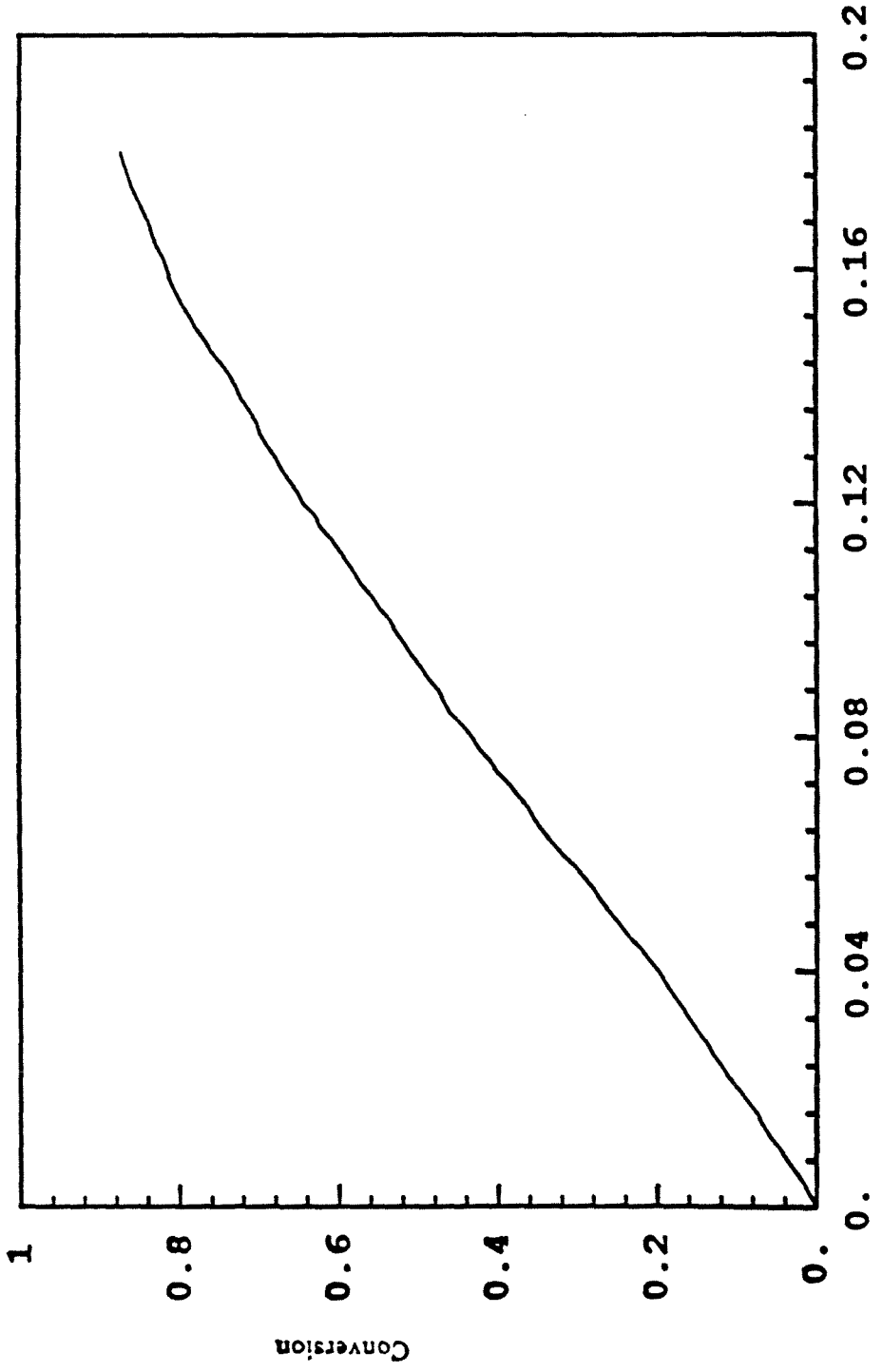

Figure 8.3 Carbon conversion versus δ/R_0 for run D14.

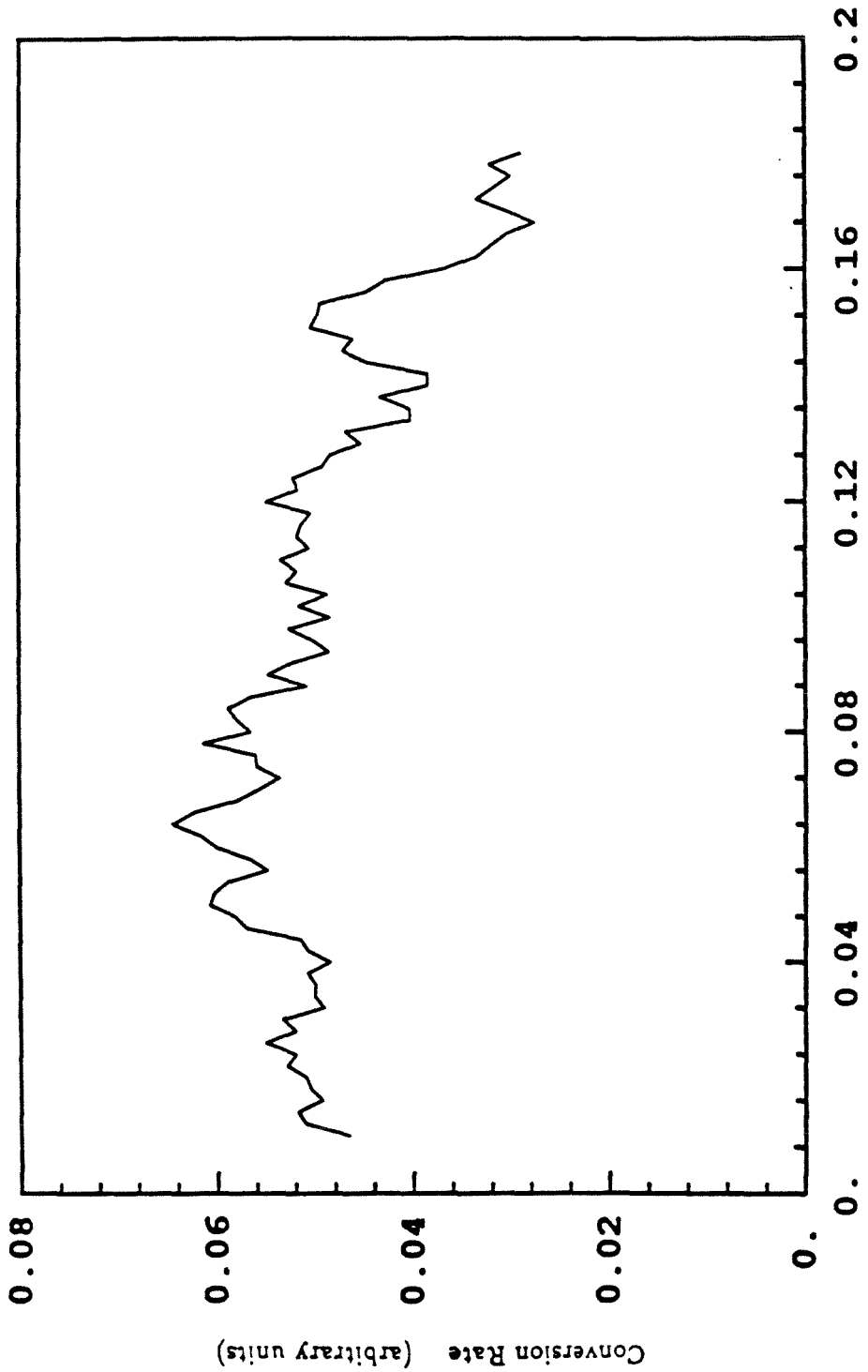

Figure 8.4 Carbon conversion rate versus δ/R_0 for run D14.

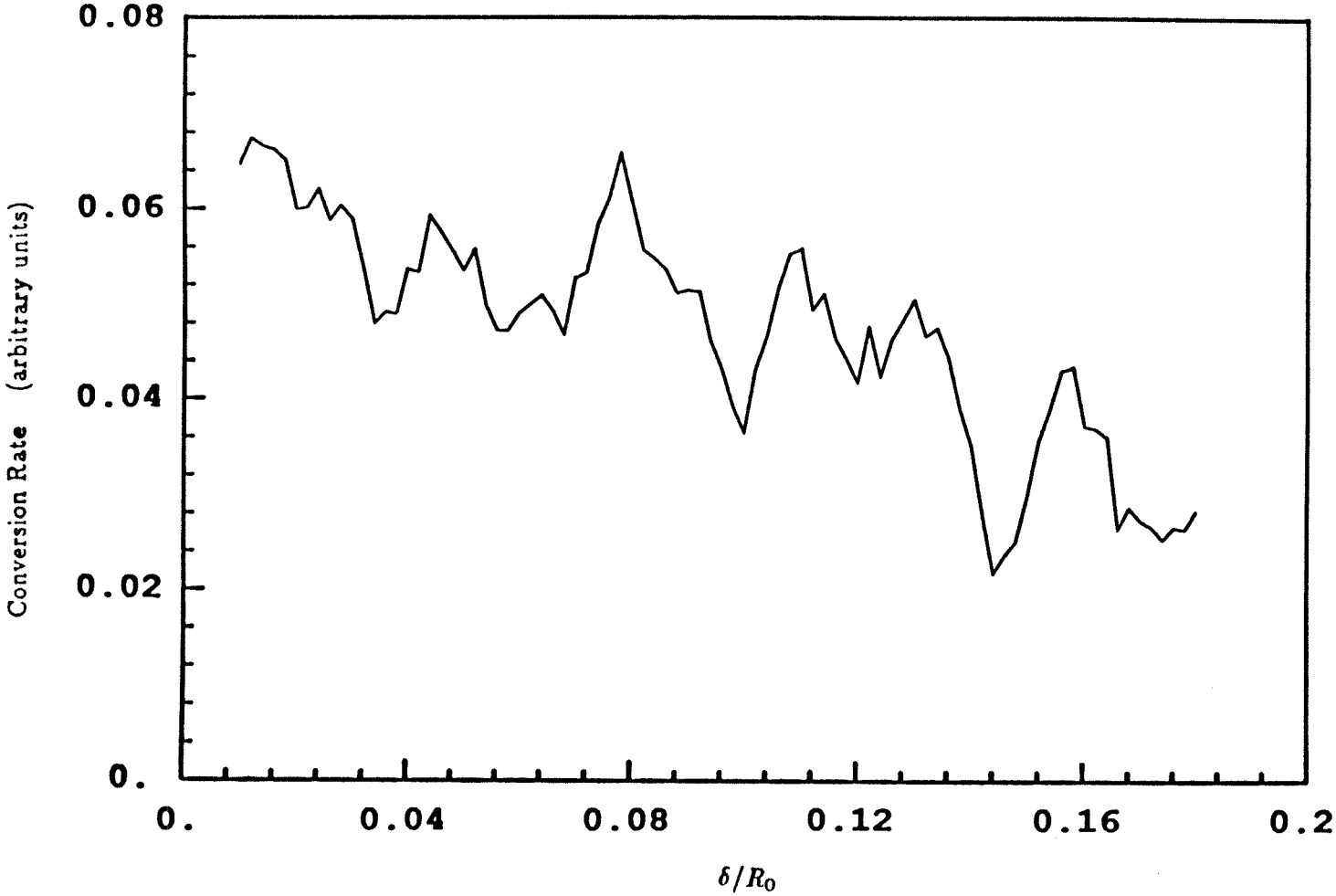

Figure 8.5 Carbon conversion rate versus δ/R_0 for run D3.

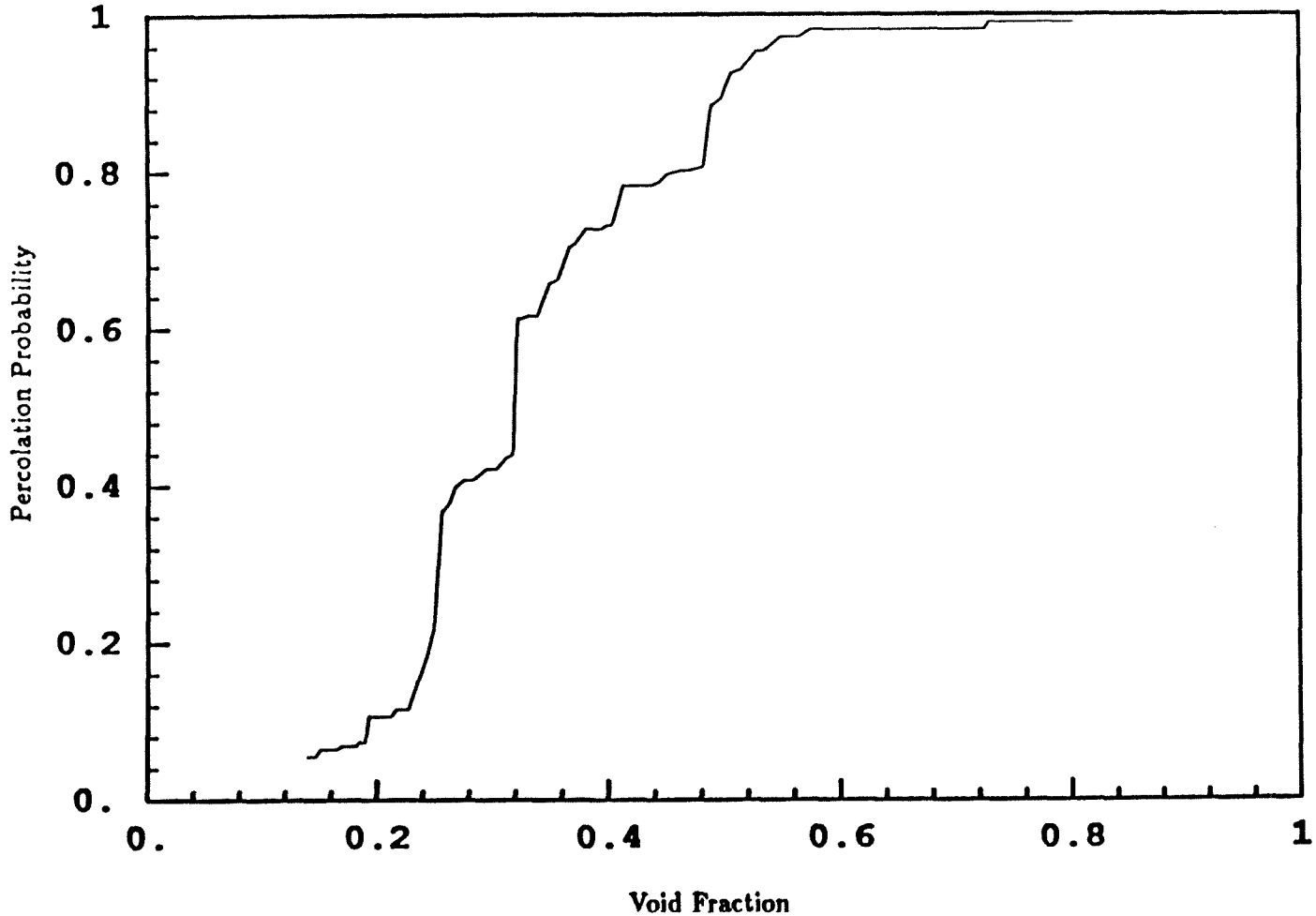

Figure 8.6 Percolation probability versus void fraction for run D14.

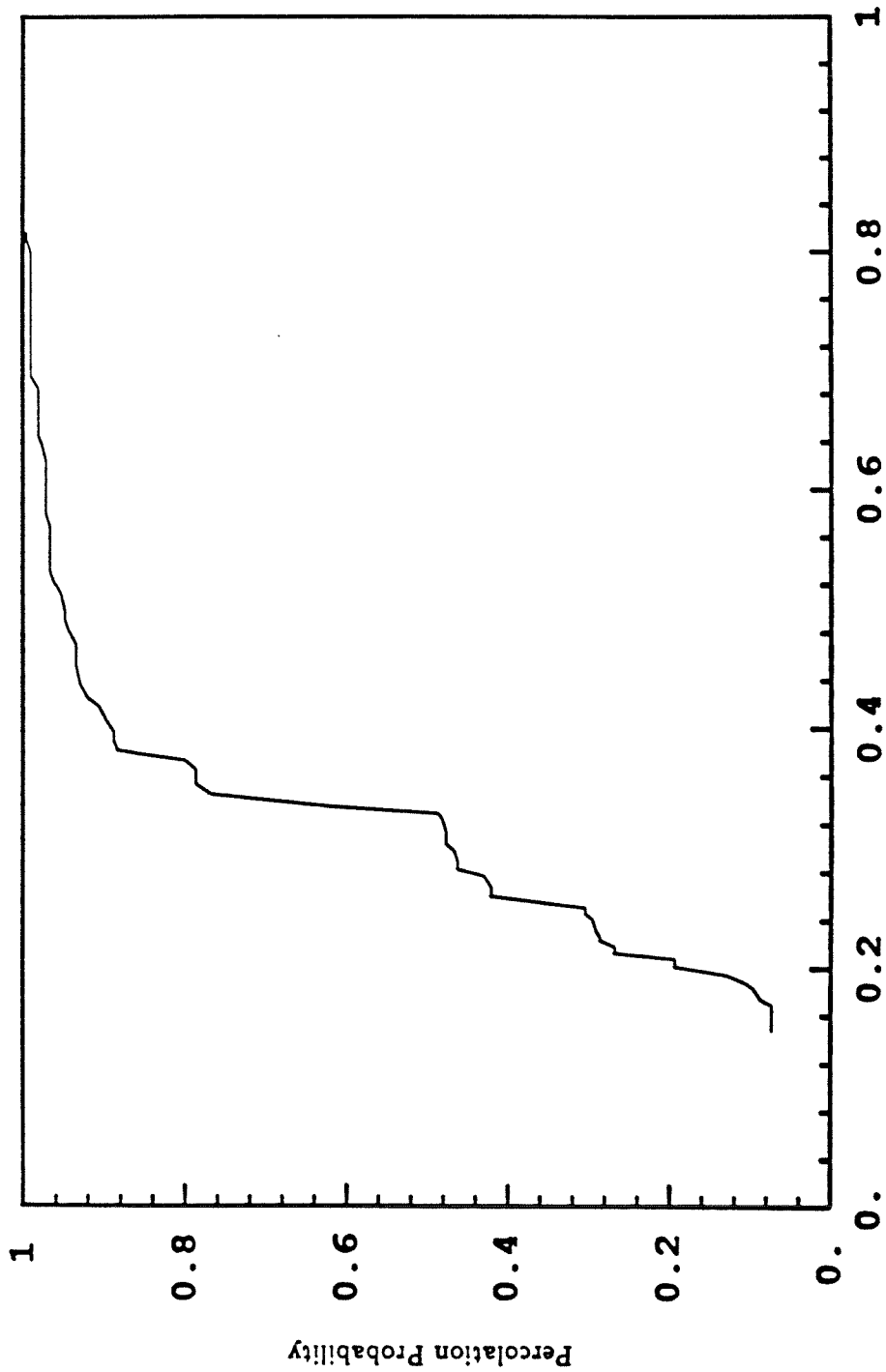

Figure 8.7 Percolation probability versus void fraction for run D13.

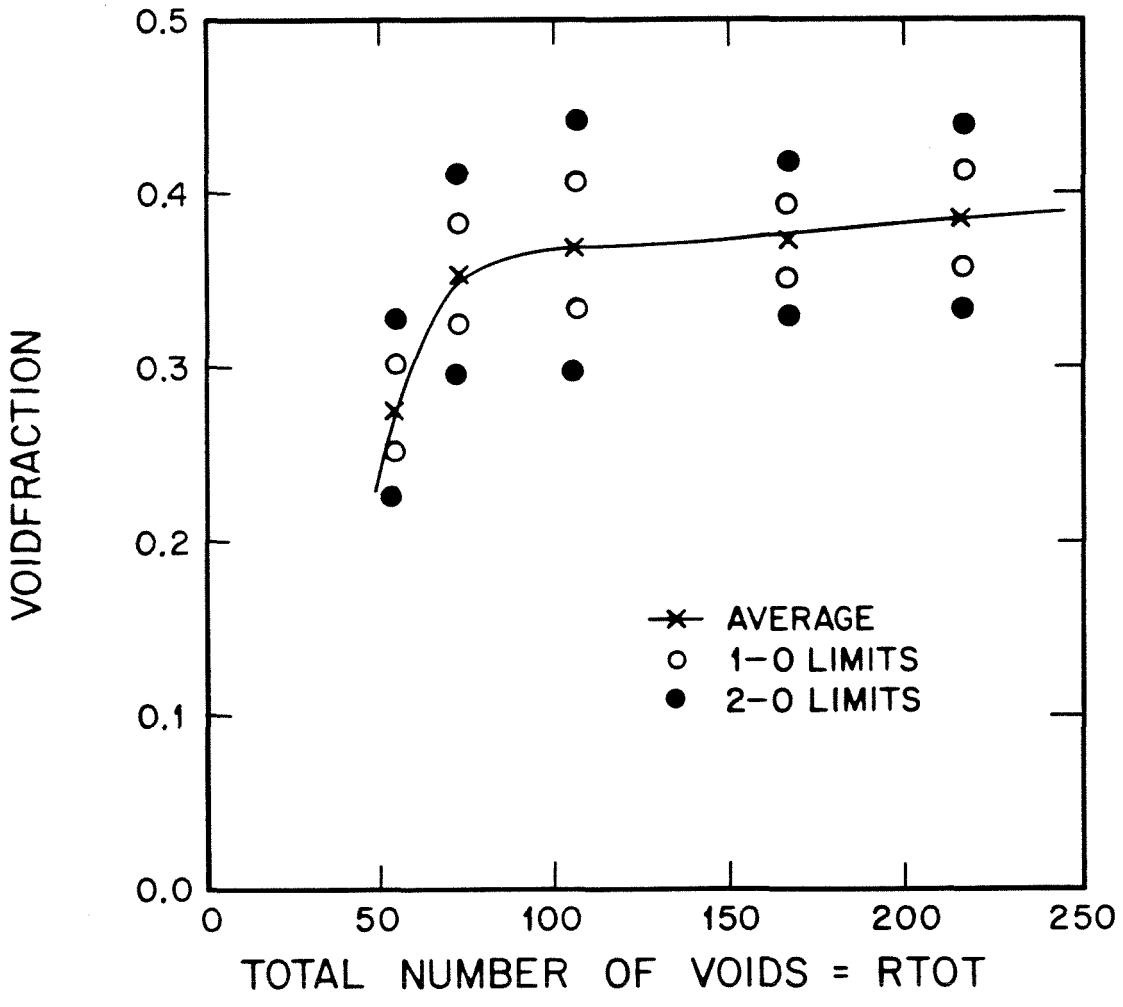

Figure 8.8 Void fraction versus number of initial voids for percolation probability = 80%.

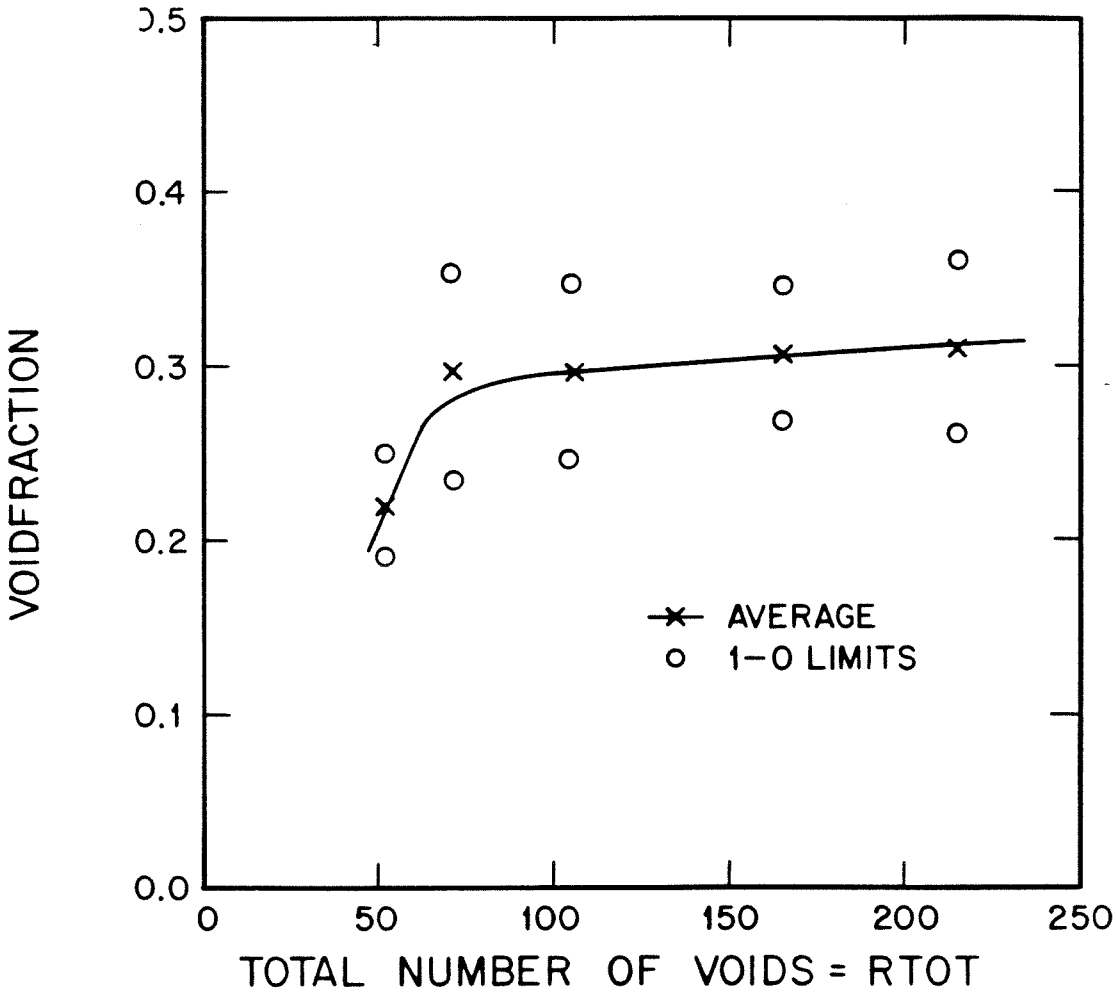

Figure 8.9 Void fraction versus number of initial voids for percolation probability = 50%.

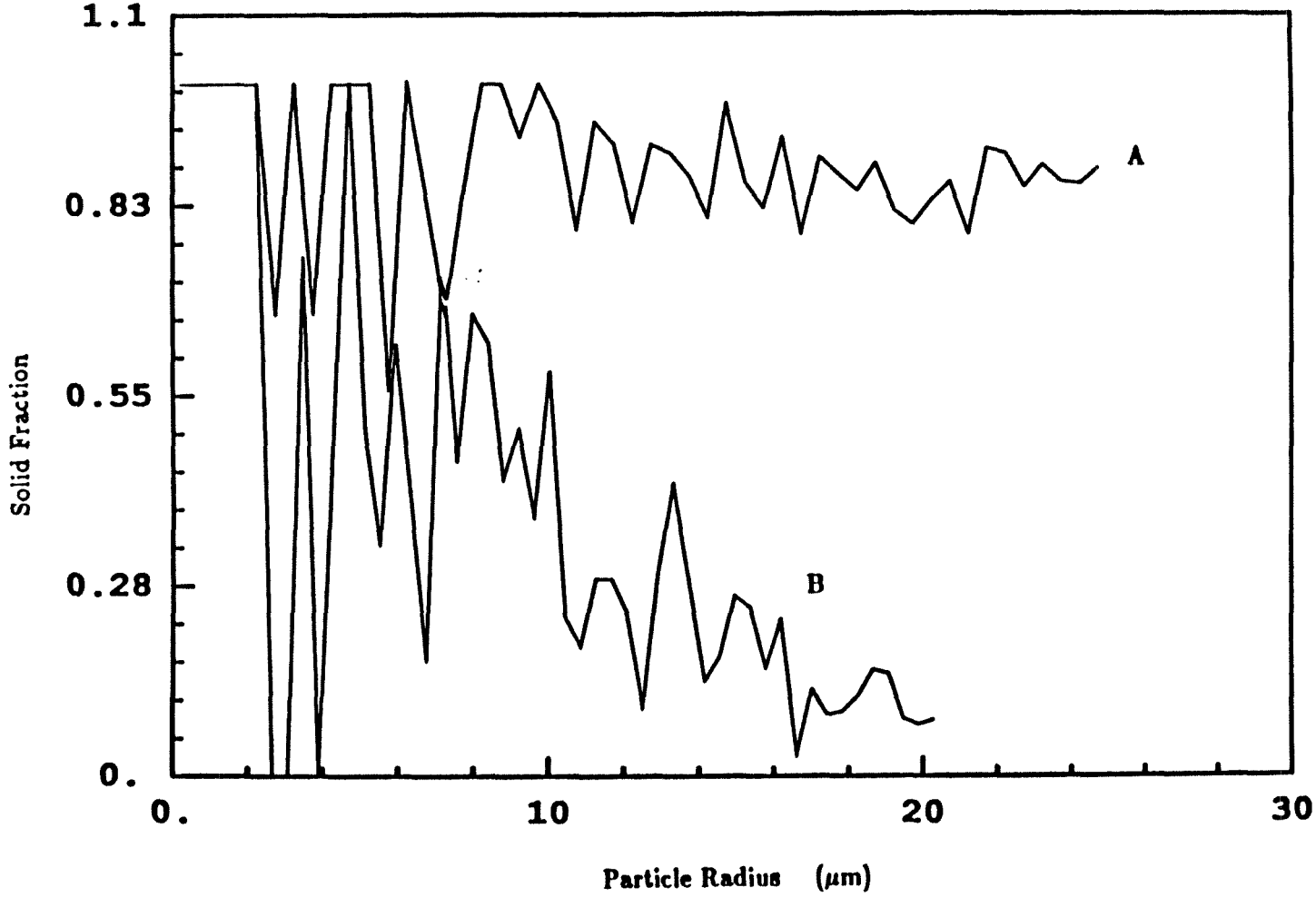

Figure 8.10 Solid fraction versus radius of the particle at two different conversions. A: 0% conversion. B: 70% conversion.

Chapter 9

CONCLUSIONS

Factors that govern the low and high temperature reactivities of coal chars were examined. The size of the parent coal particles had a significant influence. The cenospheric char produced from the smaller coal particles was 10-15% more reactive than char of equal size produced from larger coal particles. This is partly due to maceral segregation in the coal particle as a function of their size. Chars were formed by pyrolyzing the coals in nitrogen at temperatures ranging from 1000K to 1600K. Increasing the pyrolysis temperature reduced the H:C ratio in the char by a factor of almost 2.5 and the heat of combustion by 10-15%. The apparent oxidation rate (at 800K) decreased by as much as 50% as the pyrolysis temperature was increased. The pore size distribution in the chars changed from being bimodal at a pyrolysis temperature of 1000K, to trimodal at 1600K. Transitional porosity was evident at the higher pyrolysis temperatures. The impact of carbon conversion on char reactivity was investigated. The N_2-BET surface areas of the bituminous chars increased from 10-50 m^2/g in the first few percent of conversion to 300-500 m^2/g at the highest measured conversions, but the intrinsic oxidation rate defined in terms of the N_2-BET area was found to be almost constant after the initial 5% of conversion for all of the chars examined. The intrinsic rate was same for chars from different coals pyrolyzed at 1000K but showed significant variations as the pyrolysis temperature was increased. Care was taken to account for diffusion effects in the interpretation of the reactivity results. It was shown that at 800K, diffusion is not

important.

Single particle experiments were performed in a drop-tube reactor at wall temperatures ranging from 1050K to 1450K. Complete temperature-time histories were measured for individual particles. These traces show considerable variability due to the different size, shape, pore structure and mineral content of individual particles. Even though narrow size fractions of char were used, it was not possible to eliminate such variability. A novel technique was, therefore, used to analyze the traces by treating size and pre-exponential factor of each particle as a random variable. This technique was used in conjunction with an asymptotic combustion model to determine the apparent Arrhenius kinetic parameters. Using the estimated parameters provided good agreement between calculated and experimental temperature-time traces.

Chars were also partially oxidized to various conversions at high temperatures. Physical characterization of these partially oxidized samples showed that while there is some decrease in the particle size, that reduction is insufficient to account for the total carbon conversion. Thus, there is internal combustion as well. Capillary condensation and mercury porosimetry indicate that while pores greater than 200Å in radius grow during combustion, those smaller than this size remain unaffected. The surface area, which is mostly present in the micropores, is almost constant. The micropores may be inaccessible due to pore mouth closure induced by a thermal annealing mechanism. The above results from high temperature conversion are in marked contrast to those obtained from characterization of samples converted at lower temperatures ($\sim$ 500°C). The latter indicate that there is complete penetra-

tion of oxygen into the particle at the lower temperatures. Surface areas increase significantly with early conversion as the smallest pores become accessible.

The ignition behaviour of chars was observed from the temperature-time traces of single particles. Comparing the temperature traces with the intensity traces, it was concluded that under mild oxidation conditions (wall temperatures below 1300K and oxygen partial pressures at/or below 0.21), the char particles undergo localized ignition at reactive sites leading to the development of hot-spots. These hot spots then grow, taking a finite time to engulf the whole particle. A model was proposed to explain this behaviour. Delay times predicted by the model agree closely with experimentally observed delay times.

Continuum and discrete models of single particle combustion were developed. While the continuum models assume that the reaction-diffusion problem inside the particle can be formulated in terms of differential equations which are then solved subject to appropriate boundary and initial conditions, the discrete models take into account the non-homogenous and non-symmetric nature of the actual particles. Results of parametric variations of the continuum models indicate the relative importance of different parameters like particle size, density, reaction rate, emissivity, and ash content on the burn time of each particle. Burn times predicted by the various models are similar to those observed experimentally. By proper adjustment of the key parameters, good agreement was obtained between the experimental and theoretical temperature-time traces. The discrete models show the importance of void connectivity inside the particle. While the discrete models did not consider intraparticle diffusion, they pointed out the existence of percolation in the void space

with increase in carbon conversion.

The total surface area and pore volume distribution obtained from gas adsorption experiments are widely used to characterize porous materials. A critical analysis of the various experimental methods used and the results obtained therefrom, was performed. Algorithms commonly used to invert pressure-volume raw data into pore volume distributions with respect to pore radius were critically examined. The suitability of different gas-solid pairs was also analyzed. Special methods used to probe microporous solids were also studied.

Appendix I

PROPERTIES OF PSOC 1451 COAL

SAMPLE HISTORY	
Penn State Number	PSOC 1451
Collected By	Pennsylvania State University
Collection Date	May 1, 1985
Reported Rank	High Volatile A Bituminous (HVAB)
Sample Type	Channel Whole Seam
Seam Name	Pittsburgh
Alternate Seam Name	# 8
Total Seam Thichness	6 ft. 5 in.
Thickness of Seam Sampled	6 ft. 5 in.

SAMPLE LOCATION	
Country	USA
State	Pennsylvania
County	Washington
Township	North Strabane
Nearest Town	Linden
Coal Province	Eastern
Coal Region	Appalachian
Coal Field	Main Bituminous
Map Reference	
Latitude	80D 8M 20S
Longitude	40D 14M 00S
Quadrangle	Washington East (7.5 ft.)

GEOLOCICAL AND MINE INFORMATION	
System (Age)	Pennsylvanian
Group	Monongahela
Overburden Lithology	Shale
Overburden Thickness	230 ft.
Floor Lithology	Shale
Mine name	Mathies
Mining Method	Underground
Mine Production	700,000 tons/year
Mine Life Expectancy	15 years

CHEMICAL DATA				
	As Rec'd	Dry	DAF	DMMF(Parr)
Proximate Analysis				
% Moisture	2.54			
% Ash	13.32	13.67		
% Volatile Matter	33.56	34.43	39.88	38.81
% Fixed Carbon	50.58	51.90	60.12	61.19
Ultimate Analysis				
% Ash	13.32	13.67		
% Carbon	70.05	71.88	83.26	85.08
% Hydrogen	4.55*	4.67	5.41	5.53
% Nitrogen	1.33	1.36	1.58	1.61
% Sulfur	1.33	1.36	1.58	
% Chlorine	0.07	0.08	0.09	0.09
% Oxygen(diff.)	6.81*	6.99	8.10	7.71
* Excludes Moisture				
Elemental Analysis				
% Carbon		71.64		85.16
% Hydrogen		4.64		5.52
% Nitrogen		1.36		1.61
% Organic Sulfur		0.53		0.63
% Chlorine		0.08		0.09
% Oxygen(diff.)		5.95		7.00
% Mineral Matter		15.87		
Calorific Value (BTU/lb)				
MM-Containing	12528	12855		
MM-Free(Parr)	14682	15135		
Net DMMF		14713		
Ash Free		14891		
Atomic Ratios				
Atomic H/C				0.780
Atomic O/C				0.068

ASH COMPOSITION Ashing at 750°C			
Major Compounds		Trace Elements	
SiO_2	54.40 %	Ba	540 ppm
Al_2O_3	24.50 %	Be	7 ppm
TiO_2	1.14 %	Cr	150 ppm
Fe_2O_3	9.16 %	Cu	80 ppm
MgO	0.85 %	Mn	140 ppm
CaO	2.97 %	Ni	65 ppm
Na_2O	0.61 %	Rb	100 ppm
K_2O	2.02 %	Sr	590 ppm
P_2O_5	0.34 %	V	200 ppm
SO_3	2.30 %	Zn	85 ppm
		Zr	240 ppm

PETROGRAPHIC DATA	
	Dry Weight (%)
Vitrinite	73.7
Inertinite	8.0
Liptinite	2.8
Mineral matter	15.5

PHYSICAL PROPERTIES	
Hardgrove Grindability	38.9
Free Swelling Index	7.5
Gieseler Plasticity Data	
Maximum Fluidity	8525
Max. Fluidity Temp.	433
Initial Softening Temp.	390
Solidification Temp.	470
Fluid Temperature Range	80

ASH FUSION ANALYSIS		
	Reducing	Oxidizing
Initial Deformation Temperature	2435°F	2570°F
Softening Temperature	2580°F	2640°F
Hemisphere Temperature	2670°F	2690°F
Fluid Temperature	2685°F	2700°F

Appendix II

OPTICAL PYROMETER DESIGN

AII.1 Objective

To elucidate the kinetics of char oxidation, it is necessary to know the relationship between the particle mass loss rate and its temperature. In this report, we describe a two-color optical pyrometer designed to measure the temperature of individual burning particles.

AII.2 Theory

From Planck's law for spectral distribution of radiation from a black body at temperature T, the intensity of radiation in the wavelength range [λ,λ+dλ] is given by

$$i_{\lambda,b} = \frac{2C_1}{\lambda^5\left(e^{C_2/\lambda T} - 1\right)} \qquad (AII.1)$$

where C_1 and C_2 are the first and second radiation constants. The temperature of an emitting object can be estimated by measuring its absolute emission intensity at one wavelength (typically 650 nanometers) or by measuring the relative emission intensities at two or more different wavelengths. The former approach, called brightness pyrometry, requires knowledge of the emissivity and geometry of the emitting object. The latter method is better suited to the measurement of temperatures of burning particles of microscopic size since it only requires that the particles be gray, *i.e.*, that their emissivity not vary significantly over the wavelength range examined. The different wavelengths can be selected with monochromators or narrow bandpass filters. The signal recorded by a detector is determined by the contributions of all wavelengths that reach the detector, *i.e.*,

$$s_i = \int_{\lambda_l}^{\lambda_h} \epsilon_\lambda \mathcal{F}_\lambda i_{\lambda b} d\lambda \qquad (AII.2)$$

where s_i is the response of the i^{th} detector, ϵ_λ is the emissivity, and $\mathcal{F}_\lambda$ is the wavelength dependent response function of the optical system and detector. λ_l and λ_h are the low and high wavelengths allowed by the filter. The ratio of two such signals is used to estimate the temperature of the object being observed. In the special case of extremely narrow band pass measurements centered about λ_1 and λ_2, this ratio reduces to

$$R = K\left(\frac{e^{C_2/\lambda_2 T} - 1}{e^{C_2/\lambda_1 T} - 1}\right) \qquad (AII.3)$$

where K is the calibration constant into which the optical inefficiencies and emissivity factors have have been lumped. K is determined by calibrating the instrument at a known temperature (e.g. melting point of a pure metal like platinum). It is then assumed to be independent of temperature. This last assumption is permissible only if the source is a gray body. There is also a geometrical factor in the intensity expression if the source distance from the detector is rapidly changing. This is not necessary in the present case as the burning particle is quasi-static in relation to the detector given the short burning time and relatively slow particle velocity.

AII.3 System Specifications

The size of particles to be burnt is in the range 50-300μm. Expected burning temperatures are in the range 1000 K to 2500 K. Particle flow velocity is around 10 cm/s, corresponding to a cold gas flow rate of around 2 l min^{-1} heated to 1500 K. The viewing dimension of the optics, 330μm was chosen to accommodate the largest particles expected. Based on the above flow rate, particle residence time in the view

volume is close to 4 ms. This sets the lower limit of the frequency response of the signal processing and real-time data acquisition systems.

AII.4 Wavelength Selection

Black bodies emit radiation whose spectral behaviour is governed by Planck's law. While coal or char particles are not expected to be black emitters, to a first approximation they shall be assumed to be gray bodies. The spectral response of a black body is shown in Figure AII.1 for various temperatures. The intensity maxima and the temperature are related by Wien's displacement law. Clearly, in order to attain maximum sensitivity, wavelengths that are smaller than the wavelength at maximum intensity, λ_{max} should be selected. The smallest λ_{max} occurs at the highest temperature. This then sets a natural upper limit for the choice of wavelengths. However, it should be mentioned that it is definitely possible to use wavelengths higher than λ_{max} if loss of resultant signal strength is compensated later in the signal processing stage.

In the present case, since T_{max} was 2500 K, λ_{max} was calculated to be 1.16μm. The second criterion for choosing wavelengths is that the two wavelengths chosen be sufficiently apart to minimize experimental error and to enhance the sensitivity in temperature measurement. This implies, of course, that the smaller wavelength be quite small. The lower limit, however, is set by the intensity of the signal at the lowest design temperature, at that wavelength, that can be detected. Apart from the black body radiation, it must be kept in mind that the signal is attenuated in passing through the various optical elements before reaching the detector where it can be amplified. The last consideration regarding wavelength choice is the commercial

availability of suitable filters. Based on all these considerations, wavelengths around 1000nm and 800nm were chosen. The filters chosen had bandwidths of 70nm and their spectral responses are shown in Figures AII.2 and AII.3.

AII.5 Detector Selection

This is governed by the following considerations:

(i) Maximum sensitivity (Amps/Watts) at the desired wavelengths.

(ii) It is desirable that the detector have similar sensitivity at both wavelengths.

(iii) Low dark current.

(iv) Reasonably large detector area.

(v) Linearity of response over wide input power signals.

The detector selected was the Hamamatsu S1336-5BQ. Its spectral response characteristics are shown in Figure AII.4.

AII.6 Preamplifier Selection and Design

As soon as the optical signal is converted at the detector to a feeble voltage signal, it is essential that this small voltage signal be amplified carefully (without amplifying the noise) before it can be processed and stored. For a variety of reasons that will become clear shortly, it is desirable to have the detector and the preamplifier physically close to each other and hence the design of the detector-preamplifier package is of paramount importance. For small signals, having the detector and the preamp separated means that additional wiring has to carry the signal to the amplifier and apart from noise, the stray capacitance induced in the wiring may seriously limit the frequency response of the circuit.

The amplifier gain is a crucial parameter. The gain has to be determined from considerations below and then a suitable amplifier capable of that gain along with the desired frequency bandwidth has to be selected.

The gain is decided based on detectability of the signals. It is convenient to have signals that are at least tens of millivolts so that they can be detected easily and also input directly into the data acquisition system. It is therefore necessary to determine the optical signal strength of a typical burning particle.

For a 50μm particle with emissivity one, burning at 1000 K, the radiant energy reaching the detector after filtering at 800 nm is $1.12\text{x}10^{-4}$ watts. The detector sensitivity is 0.6 amps/watt and therefore the detector signal will be 6.72x^{-5} amps. Accounting for various optical losses we expect microamp signals. Therefore, a gain of at least 1000 is necessary to convert this into a millivolt signal (an op-amp converts amps to volts). Of course, signal levels are more manageable at higher temperatures.

The detector amplifier circuit is shown in Figure AII.5. The single most important parameter of the detector is its junction capacitance, C_{jn}, which is 65 picofarads for the S1336-5BQ. R_F, the feedback resistance and C_F, the feedback capacitance of the amplifier will now be determined. An amplifier has to be chosen at this point. If the gain, frequency bandwidth, and noise criteria cannot be simultaneously satisfied then a different amplifier has to be used and the process repeated. As a start the LF357 amplifier is chosen.

Determination of R_F

The gain bandwidth of the LF357 amplifier is 12MHz (although its specifications

mention 20MHz, a conservative value is chosen). Since the time resolution required is of the order of milliseconds, it is necessary to have a frequency bandwidth of around 10kHz. Now

$$\text{Available Gain} = \frac{\text{Gain bandwidth}}{\text{Frequency bandwidth}} \qquad (AII.4)$$

$$\text{Available Gain} = \frac{12\text{MHz}}{10\text{kHz}} \qquad (AII.5)$$

Thus the available gain is 1200. The impedance of the junction capacitance at 10kHz, Z_{jn} is 240kΩ. Also

$$\text{Gain} = \frac{R_F}{Z_{jn}} \qquad (AII.6)$$

Therefore, R_F is 1200x240kΩ or 288MΩ. A conservative value of 100MΩ is chosen for R_F.

Determination of C_F

Once the feedback resistance has been fixed, the breakpoint frequency, f_1 and the gain amplitude A_2 (Figure AII.6) can be determined as follows:

$$f_1 = \frac{1}{2\pi R_F C_{jn}} \qquad (AII.7)$$

$$A_2 = \frac{\text{Gain bandwidth}}{f_1} \qquad (AII.8)$$

Thus f_1 and A_2 are calculated to be 24.5Hz and 480000 respectively. The frequency f_2 is defined as

$$f_2 = f_1\sqrt{A_2} \qquad (AII.9)$$

and therefore f_2 is 17.3 kHz. The frequency f_3 is chosen such that it is larger than or equal to the frequency bandwidth but smaller than f_2. Let f_3 be 10 kHz. Finally

C_F is defined as follows

$$C_F = \frac{1}{2\pi R_F f_3} \qquad (AII.10)$$

Putting in the appropriate values for R_F and f_3, C_F is computed to be 0.16 picofarads.

Noise Considerations

The electronic noise in the circuit can be expressed in the following form

$$\text{Noise} = 2ei + 4kT/R_F + i_n^2 + e_n^2/R_F^2 \qquad (AII.11)$$

The units of each term are in amp^2/Hz. The last two terms are device noise terms while the first two are unavoidable intrinsic noise factors. Neglecting the device terms, minimum noise is achieved when the first two terms are set equal and is only a function of temperature.

$$iR_{F\,min} = 2kT/e \qquad (AII.12)$$

The device noise terms are tabulated in the specifications. In the present design the choice of R_F ensures that the overall noise is manageable.

AII.7 Additional Features

In addition to the preamplifier, the circuit includes a programmable gain amplifier with gain factors of 10 and 100 for further signal enhancement. A divide circuit is also present in case the signal ratio is desired directly. Finally, a log-ratio circuit is also present. Of course, signal processing can always be done via software after the raw intensity signals have been acquired. To help conserve the system memory, the data acquisition system is enabled only if the signal on a particular channel

(selected by the user) exceeds a certain reference signal. This is done in the trigger circuit. Actual data acquisition is done by a Data Translation DT-2801A board at upto 20kHz rates and the digital signal is input directly into the memory of a Zenith 148 PC converted for data acqisition purposes. Then the signal is read by software and processed. A schematic of the pyrometer is shown in Figure AII.7 and the circuit is shown in Figure AII.8. Device specifications for the essential chips used in the circuit can be obtained from the respective manufacturers' catalogues: DIV 100, LOG 100, and PGA 102 (Burr Brown); LF 356, LF 357, and LM 393 (Motorola).

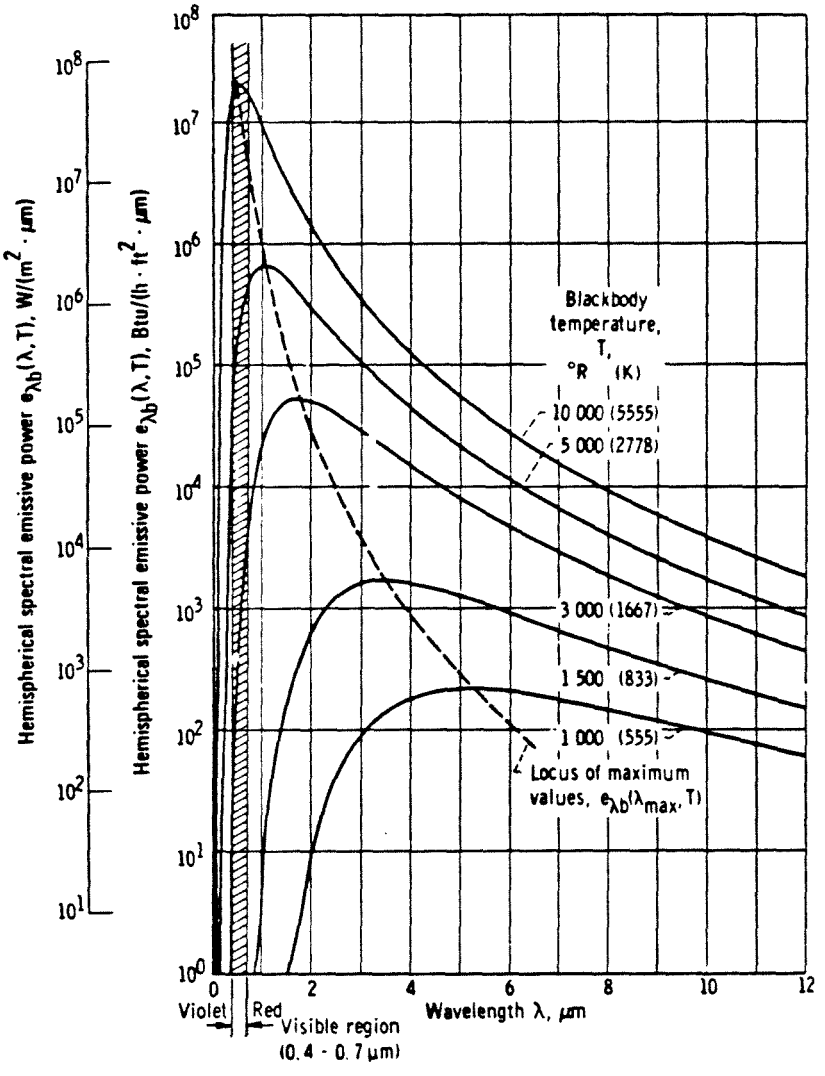

Figure AII.1 Spectral response of a black body.

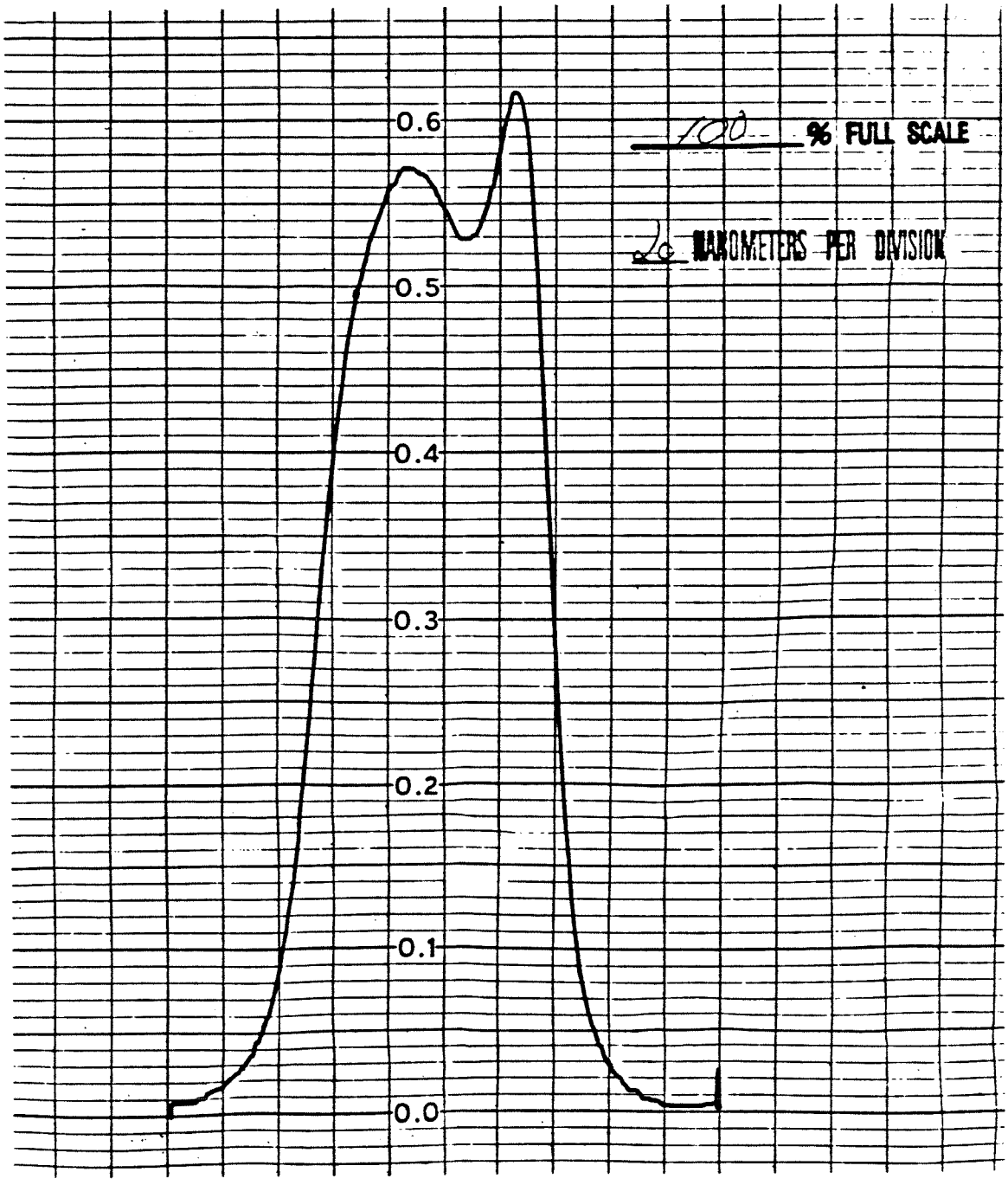

Figure AII.2 Spectral response of the 1000nm filter.

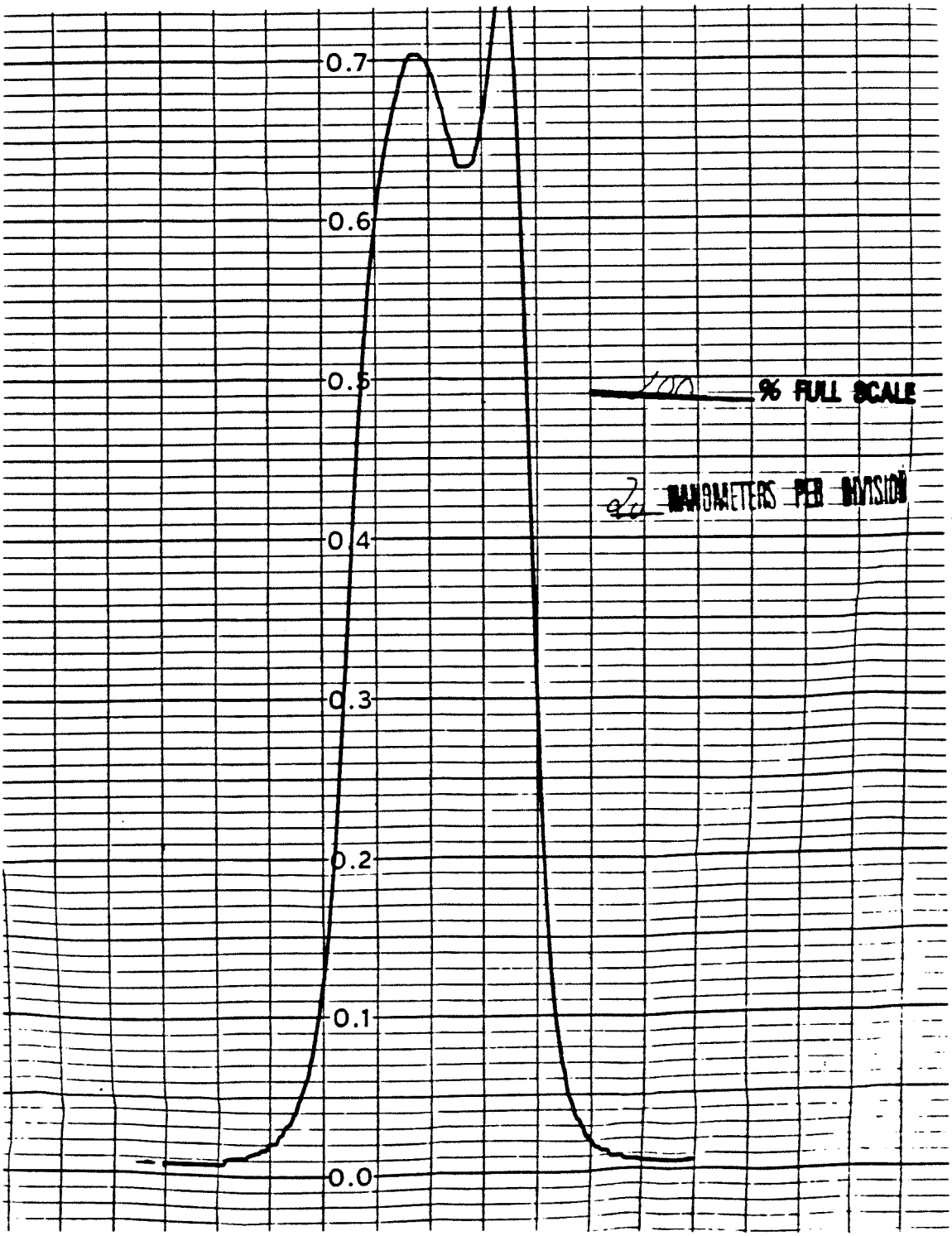

Figure AII.3 Spectral response of the 800nm filter.

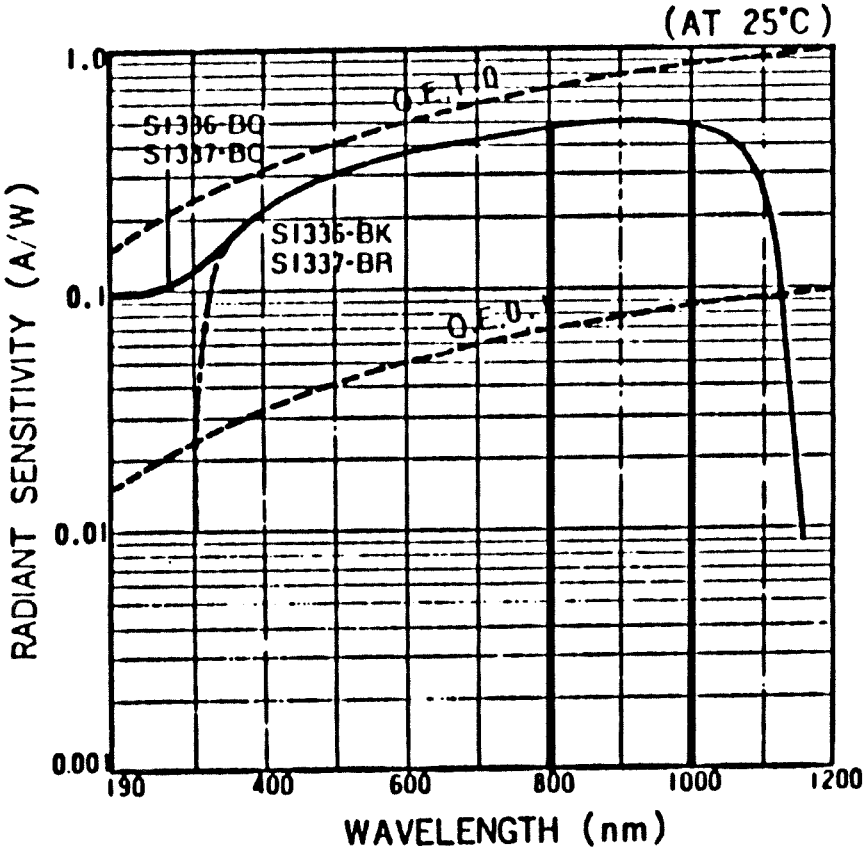

Figure AII.4 Spectral response of the Hamamatsu S1336-5BQ detector.

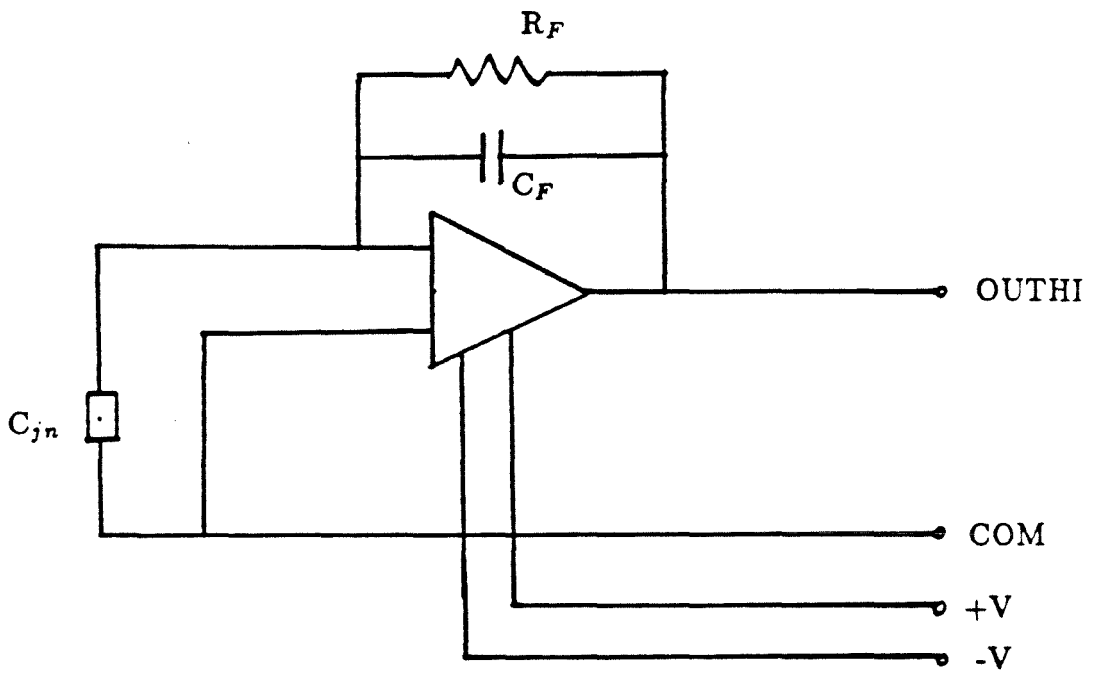

Figure AII.5 Circuit diagram of the detector preamplifier.

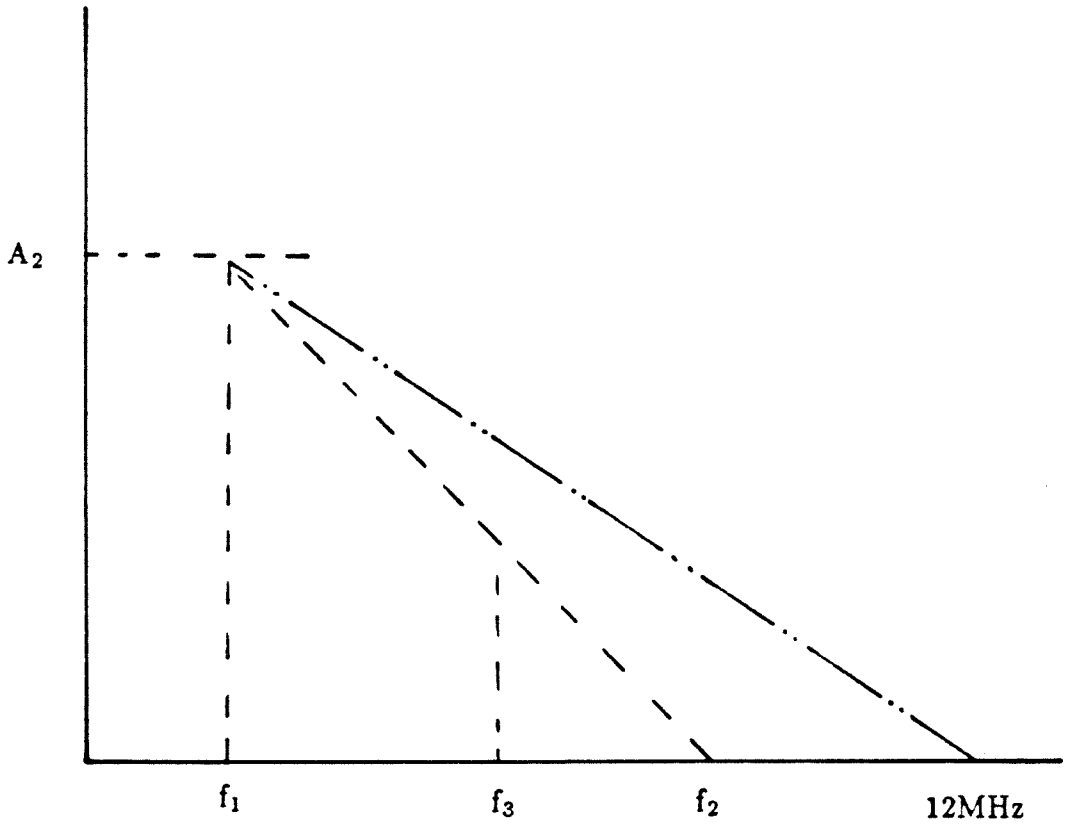

Figure AII.6 Determination of C_F.

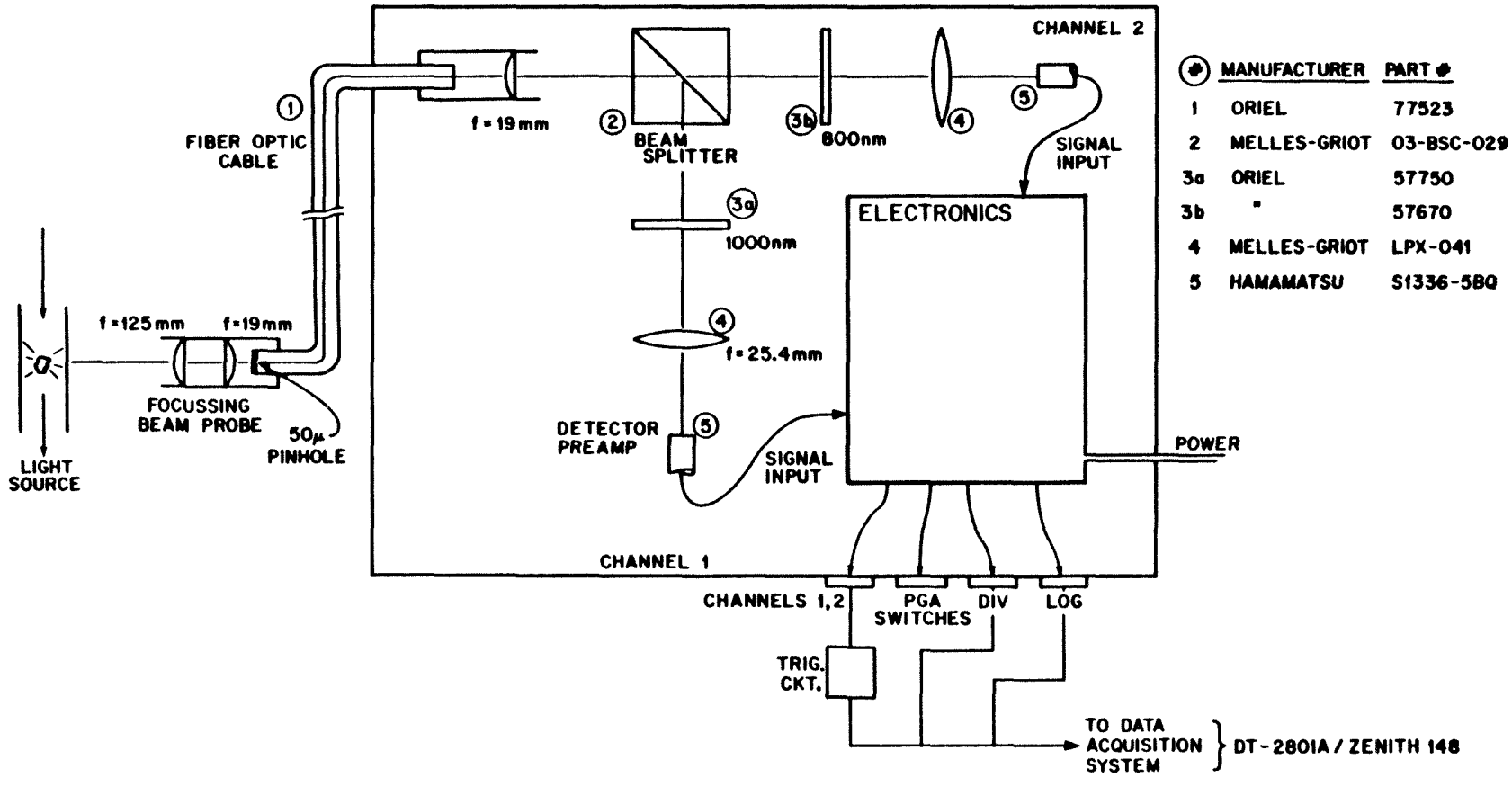

Figure AII.7 Schematic layout of the pyrometer.

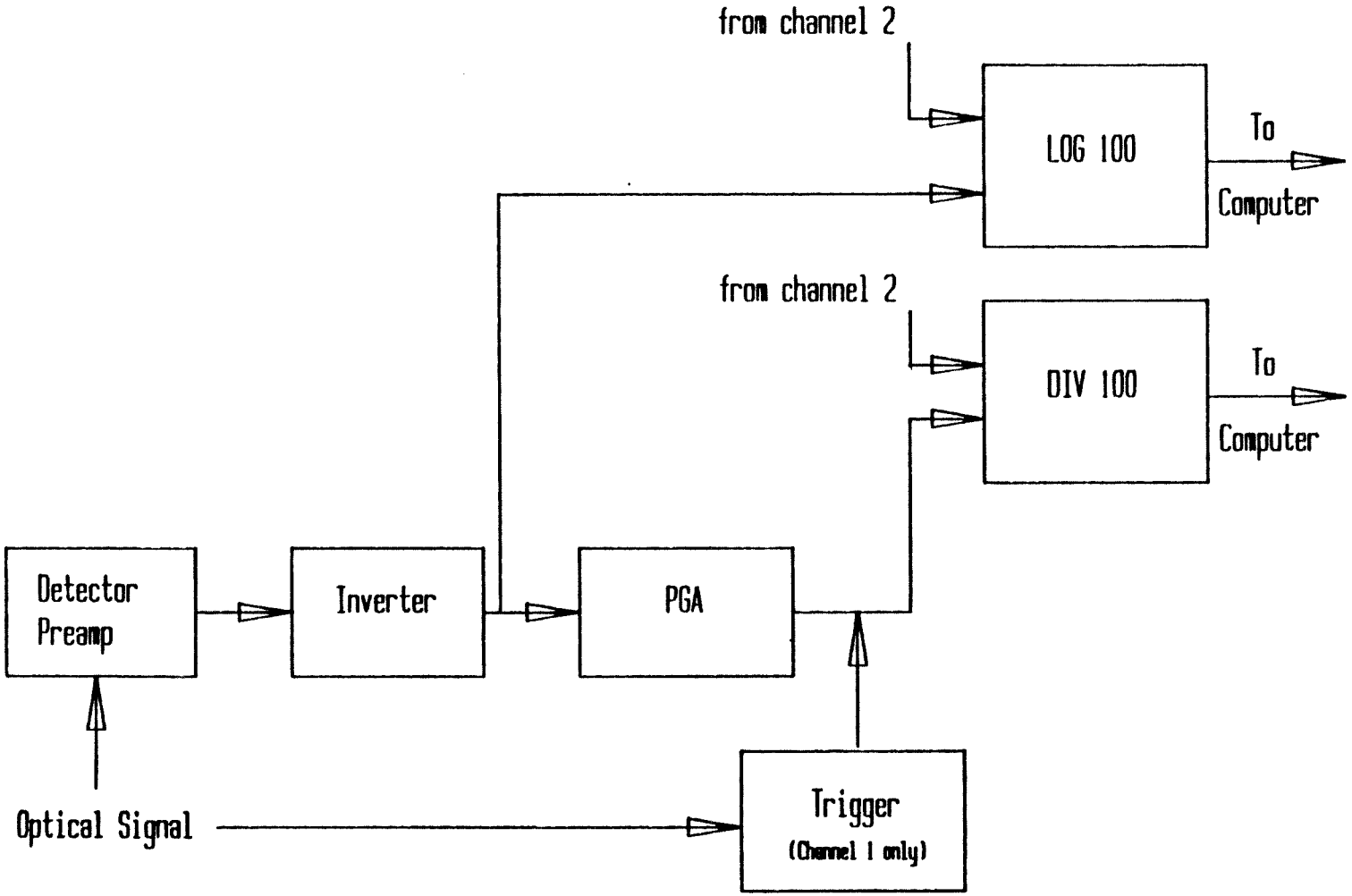

Figure AII.8 Pyrometer electronics circuit diagram.

Appendix III

A CRITICAL ANALYSIS OF GAS-SOLID PHYSISORPTION

To be submitted to the *Journal of Colloid and Interface Science*

Abstract

The internal morphology of three porous solids (γ-alumina, a partially oxidized synthetic char and PSOC-190 coal) was studied in detail using gas adsorption. Four gases (nitrogen, argon, carbon dioxide and Freon-21) were used to observe specific adsorbent-adsorbate interactions in each solid. BET surface areas and C values were determined in each case. Several methods of determining pore volume distributions (Cranston-Inkley, Yan-Zhang and Brunauer's Modelless method) in the meso and macropore range from the isotherms were examined and compared. The pore volume distribution in the micropore range was interpreted according to the M-P and Medek methods. Micropore volumes were obtained from the Dubinin-Radushkevich-Kaganer method.

AIII.1 Introduction

The use of gas adsorption to probe the internal structure of porous solids is presently an accepted and widely used experimental technique. One reason for this is that the measurement of the extent of adsorption of a gas on a solid under a given set of conditions is relatively easy. Also, physical adsorption is reversible (except for porous solids which exhibit hysteresis) and non-destructive.

The amount of gas adsorbed on a solid surface depends on the temperature of the system, the partial pressure of the particular adsorptive, and of course, the nature of the solid. Ordinarily, the extent of adsorption is measured as a function of pressure of the adsorptive at a fixed temperature. For this reason, the resulting plot is known as an isotherm.

Since physical adsorption is rather non-specific, various gas- solid pairs give similar isotherms. Brunauer *et al.*(1) identified five basic types of isotherms. Porous solids usually give type III isotherms, but also psuedo-type I and more rarely type V. For types III and V, enhanced adsorption at relative pressures greater than 0.4 is attributed to capillary condensation of adsorbate in the small pores of the solid. This is the region of the isotherm where information about pore size distribution can be obtained.

It has been found that desorption isotherms do not coincide with adsorption isotherms for porous materials. This phenomenon of hysteresis is attributed to different physical states of the gas-solid system which occur during the processes of evaporation and condensation. Hysteresis may be used to obtain information about pore shape; however, it is debatable as to how accurate this information is, insofar

as actual pores are rarely, if ever, describable by regular geometrical shapes.

Since the dynamics of adsorption and the exact nature of solid surfaces on the molecular level are not well understood, interpretation of experimental data is rather open to question. Even more questionable is the interpretation of data in the regime of capillary condensation. A variety of simplifying assumptions have been made in the attempt to develop models which attempt to elucidate the nature of the underlying porous structure of the solid (Wheeler (7), Brunauer, *et al.* (14), Kaganer (16)). In these models, some ideal pore shape is assumed *a priori.* Pores are often assumed to be cylindrical or slit-shaped. In spite of the overly simplistic structures assumed, some models do, at least qualitatively, describe the particle morphology. The purpose of this paper is to examine a few of these models and apply them to isotherms of several gas-solid pairs. The models will be evaluated in light of what is known about the solid and the gas. An attempt will be made to correlate the properties of the adsorbate and adsorbent with the most suitable model.

Given the complexity of any solid surface it is not surprising that the interaction of different gases with the same solid may lead to divergent interpretations as to the underlying solid structure. With sufficient information about the adsorbing gas, however, it should be possible to draw conclusions about the fundamental nature of the solid consistent with all observations. Thus, it may be preferable to infer the pore morphology of a given solid based on its interactions with a number of different gases rather than a single one. Some attempts in that direction shall be made in the present study.

The analysis of particle morphology in the microporous region is extremely difficult because of the presence of strong overlapping pore potentials from pore walls. Also, the concept of rigid pore geometry is unrealistic at molecular dimensions. Moreover, little is known about actual potential distributions in a real solid. Some of the more common methods for analysing the pore structure in this regime are compared in the present analysis and conclusions as to their suitability are drawn therefrom.

AIII.2 Experimental Procedure

All isotherms were obtained using a system into which a continous flow of adsorbate was introduced (Northrop, *et al.* (2)). The adsorptive was admitted through a 10μ diameter orifice. The flow rate was very carefully calibrated for a given set of conditions by monitoring the pressure increase in a well defined volume. Generally, flow rates were kept at about 1.0 cm^3/min (STP).

During the experimental run, the system pressure was periodically recorded with the aid of a computerised data acquisition system. The pressure was measured with an MKS Baratron 270A Digital pressure gage whose output signal was recorded in a Zenith 152 computer converted for data acquisition purposes.

After the run was completed, the "dead-volume" of the system including the sample tube was measured using helium, assuming that the ideal gas law holds. Knowledge of the system dead-volume and pressure at a given time allowed calculation of the amount of adsorptive in the gas phase. The difference between the amount of adsorptive which had passed through the orifice and the amount remaining in the gas phase was the amount adsorbed at that time. The system can also

be used to obtain desorption isotherms; however, only the adsorption branch was obtained and used in this series of experiments. For further details on apparatus and procedure consult ref. (2).

Experiments were performed using four different adsorbates on three porous adsorbents. The gases used were: nitrogen at 77K, argon at 77K, carbon dioxide at 195K, and Freon-21 at 273K. Carbon dioxide at 298K was also used to obtain data for the Dubinin-Radushkevich-Kaganer (DKR) theory. The solids examined were: a γ-alumina, a partially oxidized synthetic char, and a raw coal (PSOC-190). The unique interactions of each adsorptive-adsorbent pair are important in determining the type of isotherm for that pair. Table AIII.1 lists some of the properties of the adsorptives used.

AIII.3 Inversions

Though the primary interest is in adsorption on porous materials, it will be useful to first consider multilayer adsorption on flat surfaces. Many models have been developed to explain physical adsorption on a free surface. For example, Halsey and Hill (3), Young and Crowell (4) and Sircar (5) have presented such models. However, none of these has been as successful as the theory developed by Brunauer, *et al.* (6).

The BET theory is based on the assumptions of a homogeneous surface and no adsorbate-adsorbate interaction. These assumptions are difficult to justify, yet the model gives a good fit to experimental data for a wide variety of gas-solid pairs over a limited range of relative pressures. Furthermore, the theory predicts the amount of adsorbate required to form a layer one molecule thick over the surface. Knowledge

of the molecular cross-sectional area allows calculation of an overall surface area. The model also gives a measure of the strength of the gas-solid interaction through the C value. C is defined by $exp\{(\epsilon - \epsilon_v)/RT\}$, where ϵ is the energy of adsorption per mole of adsorbate, and ϵ_v is the energy of vaporization per mole. The BET surface area and C value are useful for comparison between experiments; hence, they will be given for all gas-solid pairs (Table AIII.2).

Capillary condensation occurs in porous solids below the vapor pressure of the adsorbate. The reason for this is that a pressure difference exists across the curved meniscus of the condensed vapor. The relationship between the size of the capillary and pressure is given by the Kelvin equation:

$$\ln(P/P^0) = 2\gamma\bar{V}\cos\theta/\mathrm{LRT} \qquad (AIII.1)$$

where γ is the surface tension, $\bar{V}$ is the molar volume, θ is the angle of contact, R is the gas constant and T is the absolute temperature. L is a measure of the width of a pore; for a cylinder, it is the radius, while for a slit it is half the distance between walls.

Wheeler (7) considered a model for capillary condensation which included multilayer adsorption. He deduced a relation between specific pore volume V(r) and the volume of nitrogen desorbed over a small segment on the desorption branch of the isotherm v(r):

$$v(r) = \frac{(r - t(r))^2}{r} V(r) + dt/dr \int_r^{r_0} \frac{2r' - t(r')}{r'^2} V(r')dr' \qquad (AIII.2)$$

where r is the radius of the pore, and t is the thickness of the adsorbed layer of gas. The first term on the right accounts for liquid evaporated from the pore cores, while the second term represents the amount of gas desorbed from free surfaces.

The thickness of the layer was obtained from what is known as a t-curve(8). This is simply a plot of volume of adsorptive divided by BET surface area at monolayer coverage versus relative pressure for a non-porous substance. Thus, it is a relation between the thickness of the adsorbed layer and the relative pressure. It has been pointed out that a t-curve of a material with a similar C value must be used to obtain the proper t values (9).

In principle, both the Kelvin radius and the average thickness of adsorbate can be calculated for a given relative pressure. The appropriate values can then be used in the integral equation (AIII.2). However, Wheeler was not able to come up with an iterative scheme for calculating V(r).

Several authors have developed methods for calculating V(r). Among them are Pierce(10), Dollimore and Heal(11), and Cranston and Inkley(12). The inversion method of Cranston and Inkley was difficult to carry out when it was first introduced, however the calculations are quite easy with any type of computer. For a finite adsorption step from pressure P_1 (corresponding to radius r_1) to P_2 (radius r_2) the amount of nitrogen adsorbed is

$$v_{12} = \int_{r_1}^{r_2} \frac{(r' - t_1)^2}{r'^2} V_{r'} dr' + (t_2 - t_1) \int_{r_2}^{\infty} \frac{V_{r'} (2r' - t_1 - t_2)}{r'^2} dr' \qquad (AIII.3)$$

where t_1 and t_2 are the adsorbed layer thicknesses at the respective pressures and $V_{r'}$ is the volume of pores with radii in the interval r_1 to r_2. It has been shown (12) that V_{12} can be approximated by

$$V_{12} = R_{12} \left(v_{12} - 4 (t_2 - t_1) \sum_{r_2 + \frac{\Delta r}{2}}^{r_{max}} \frac{(r - 1/2 (t_1 + t_2))}{2r^2} V_r \Delta r \right) \qquad (AIII.4)$$

where

$$R_{12} = \frac{r_2 - r_1}{\int_{r_1}^{r_2} \left[(r - t_1)^2 / r^2\right] dr} \qquad (AIII.5)$$

Yan and Zhang (13) have also developed a means of calculating pore volume distribution based on Wheeler's model. The volume of pores of mean radius r_i is given by

$$\Delta V_i = R_i \left(\Delta v_i - 2\Delta t_i \sum_{j=1}^{i-1} \frac{\Delta V_j}{\bar{r}_j} + 2\bar{t}_i \Delta t_i \sum_{j=1}^{i-1} \frac{\Delta V_j}{\bar{r}_j^2} \right) \qquad (AIII.6)$$

$$i = 1, 2, \cdots, n$$

where i refers to the pore group and the overbar denotes average values. They have shown that this method gives essentially the same results as the Cranston-Inkley method. In fact, the only difference is that R_{12} is essentially a log mean of r_1 and r_2, while r_i is an arithmetic mean. Yan-Zhang's method is more compact, however.

A rather different line of thought was used by Brunauer (14) to develop his "modelless" theory. This model is based on the thermodynamic identity

$$\gamma dS = \mu da \qquad (AIII.7)$$

This equation relates change in surface area (dS) of the adsorbate to the free energy change (da) through the surface tension γ and the chemical potential μ. Integration yields

$$S = \frac{1}{\gamma} \int A_n da = \frac{1}{\gamma} \int \mathrm{RT} \ln(P/P^0) dn \qquad (AIII.8)$$

where R is the ideal gas constant, T is the absolute temperature, P^0 is the vapor pressure, dn is the incremental number of moles of adsorbate and A_n is the free energy of adsorption. The method is called modelless because it uses the hydraulic

radius as a characteristic length parameter for the cores instead of the more usual core 'radius'. (The core is the volume of the pore which is not occupied by adsorbed gas.) The hydraulic radius is defined as follows:

$$r_h = V/S \qquad (AIII.9)$$

where V is the volume of adsorbate and S is the wetted surface area.

Again, both the gas evaporating from the cores and the gas desorbing from open surfaces must be accounted for. Unfortunately, one must assume a shape for the pores to calculate the free surface area.

An example of the calculations is as follows: for relative pressure from 1 to 0.95, $V_1 = (n_{1.0} - n_{0.95})\nu$ where ν is the molar volume of liquid. Then, S_1 is obtained from equation (AIII.8). The definition of hydraulic radius is then used to obtain a measure of average core size in this range of relative pressures. For the next step, $V_2 = (n_{0.95} - n_{0.90})\nu - V_2'$. The second term is the correction for gas which is desorbing from the free surface. If the pores are assumed to be parallel slits, $V_2' = (t_1 - t_2)S_1 10^{-4}$, for t in Å, S in m^2 and V in cm^3. The correction for cylindrical pores is more complicated but it does not change the result significantly.

As it stands, the modelless method describes the size and volume distributions of the cores. In order to compare its results with those of other inversions, the pore size and pore volume distributions are needed. However, in going from cores to pores some assumption regarding geometry must be made; hence, the resulting method is no longer modelless. In the present analysis the statistical thickness calculated at the appropriate partial pressure was added to the core hydraulic radius to determine the pore radius. The core volume was also increased by an amount $S_i t_i$

to determine the pore volume. These modifications were made in order to facilitate comparision of the now 'modelless' method with the other schemes.

The procedures above pertain to pores in which capillary condensation takes place. The lower limit of applicability of the Kelvin equation (AIII.1) occurs at a relative pressure of about 0.4, which corresponds to a radius of 16 Å. Below this, the concept of bulk surface tension becomes difficult to justify. Of course, smaller pores may be present in the solid. Thus, it is necessary to consider analyses which deal with these micropores.

One such method is known as the MP method(15). This theory is rooted in the concept of the t-curve described above. A v-t curve is a plot of the liquid volume uptake versus a statistical thickness which is obtained from a t-curve. It is imperative that a t-curve of a similar C value be used.

A v-t plot for a non-porous adsorbent will be a straight line with a slope equal to the surface area (8). A microporous adsorbent will show a downward deviation at lower relative pressures, as shown later. The reason for this is the following: at the lowest pressures, adsorption occurs over the entire surface. As more adsorption occurs, some of the micropores become filled with adsorbate. Thus, less surface is available for adsorption. This is reflected in the v-t curve by a decrease in slope, and hence, apparent surface area.

Actually, surface area in pores of this size cannot be strictly defined because the pore dimensions are similar to the size of individual molecules. Whether the pore is cylindrical or slit-shaped, the total area "covered" by a molecule will be quite different from that which it covers on a free surface.

Dubinin and Radushkevich originally developed a theory for micropore volume analysis of carbonaceous solids; however, Kaganer (16) extended it to surface area analysis. The following assumptions are made concerning microporous materials:

1. The potential distribution is of the form

$$N = N_0 \exp(-KE_0{}^2) \qquad (AIII.10)$$

where N is the number of moles of gas adsorbed, N_0 the total number of moles at monolayer coverage, E_0 is the energy of adsorption of the reference adsorbate and K is a constant characteristic of the system.

2. All adsorbates can be scaled to a single reference adsorbate

$$N = F(E/\beta) \qquad (AIII.11)$$

where $\beta = E/E_0$.

The work required to isothermally compress a gas from P to P^0 is

$$E = \mathrm{RT} \ln(P^0/P) \qquad (AIII.12)$$

Simple substitution of (AIII.11) and (AIII.12) into (AIII.10) gives

$$N = N_0 \exp(-K(\mathrm{RT})^2 \ln^2(P^0/P)/\beta^2) \qquad (AIII.13)$$

or, taking logarithms,

$$\log N = \log N_0 - 2.303K(\mathrm{RT}/\beta)^2 \log^2(P^0/P) \qquad (AIII.14)$$

A plot of $\log N$ vs. $\log^2(P^0/P)$ should give a straight line, from which the number of moles at monolayer coverage can be obtained. Given a molecular cross-sectional area, the total surface area for the sample can be calculated. Again, it is

debatable as to what to use for the value of the the area of a molecule sitting on a particular surface.

Medek (17) extended this theory to determine pore size distributions. Working from Dubinin's equation (AIII.10), he assumed that the potential inside of a pore could be expressed as $\phi = kr_{eq}^{-3}$, where k is a constant and r_{eq} is the equivalent radius of the pore. Substitution into (AIII.10) yields:

$$N/N_0 = \exp\left(-(\kappa/E)^n r_{eq}^{-3n}\right) \qquad (AIII.15)$$

where κ is related to k and the exponent n is close to 2 (but treated as a parameter in the Medek analysis). This expression can be differentiated to get the distribution.

AIII.4 Results

AIII.4.1 Isotherms

The isotherms for nitrogen (N), argon (A), carbon dioxide at 195K (C) and Freon (F) on γ-alumina are shown in Figure AIII.1. They are plotted as a function of relative pressure (P/P^0, where P^0 is the vapor pressure of adsorptive at the system temperature) so that they can be compared on a single plot. All isotherms on the γ-alumina are typical Type IV isotherms. This indicates that the solid is porous, with most pores being in the meso- to macro-pore range (i.e. more than 16 Å in diameter). The similarity between the nitrogen and argon isotherms is to be expected since both molecules are similar in size. The small difference in shapes is due to the slight difference in the relative rates of gas admission in the two cases. Carbon dioxide (196K) and Freon also produce similar isotherms. Since these molecules are larger, the total molar amounts adsorbed are smaller. Multiplication

of the respective molar volumes shows that the total pore volume is nearly 0.40 cm^3/g in all four cases. The isotherm for carbon dioxide on γ-alumina at 298K is shown in Figure AIII.2. It appears as though there is Type I behavior followed by further adsorption. It is possible that at very low relative pressures, carbon dioxide is adsorbed only by the most active sites. At higher pressures, there is more general adsorption.

The nitrogen, argon and carbon dioxide at 195K isotherms on oxidized char are classic examples of pseudo-Type I isotherms (see Figure AIII.3). This shows that the char contains a very large number of micropores. Once these micropores are filled, there is very little subsequent adsorption. Surprisingly, the amount of argon adsorbed is significantly greater than the amounts of the other gases, contrary to the expectation that nitrogen and CO_2 should be adsorbed to a greater extent due to their smaller minimum molecular dimensions and significant quadrupole moments. While the Freon also produces a Langmuir type of isotherm, it is evident that there are two distinct regimes of adsorption (as manifested by the different slopes). This suggests that the char-Freon interaction is site specific and points to the existence of two distinct types of active sites. Given the larger size of the Freon molecule molecular sieve effects may affect its penetration into the very smallest pores. The pore volumes of the char are (in cm^3/g) 0.039 (N_2), 0.033 (CO_2), 0.05 (Freon) and 0.06 (Ar). Incorporating effects of multilayer adsorption in the Freon case will reduce its pore volume but no simple explanation can explain the anomalous argon result. Figure AIII.2 shows the resulting isotherm for carbon dioxide at 298K on the partially oxidized char.

The nitrogen and argon isotherms on PSOC-190 (Figure AIII.4) showed rather unusual behavior. At the lowest pressures there was very little adsorption. However when the relative pressure reached a critical value (0.04 for N_2 and 0.08 for Ar) adsorption increased significantly. The reason for this appears to be lack of equilibration time in the dynamic adsorption apparatus used in this study. At some higher partial pressure there was significant adsorbate uptake at constant partial pressure indicating the establishment of a pseudo-steady state. This is not due to pressure drop in the bed as the particle size was 425μ and the bed was free flowing. Equilibration is not a limiting factor for CO_2 or Freon possibly due to their more complex interactions with the surface. CO_2 adsorbed most strongly on the coal. Freon gave a typical type IV isotherm.

AIII.4.2 BET Plots

The BET plots for nitrogen (N), argon (A), carbon dioxide at 195K (C), and Freon (F) on γ-alumina are shown in Figure AIII.5. All are quite linear, and give reasonably consistent surface areas. The areas were calculated using molecular cross-sectional areas obtained from Lowell and Shields (18), and Gregg and Sing (19). The computed specific areas for this method are 207 m^2/g (N), 174 m^2/g (A), 200 m^2/g (C) and 205 m^2/g (F).

Figure AIII.6 shows the BET plots for the same adsorbates on oxidized char. It is interesting to note the similar shapes of the nitrogen, argon and carbon dioxide plots. The upward deviation at higher relative pressures is due to the fact that there is so little additional adsorption in this region. Once the micropores of the solid are filled with adsorbate, the solid appears virtually non-porous. The specific

areas were found to be: 400 m^2/g (N), 573 m^2/g (A), 430 m^2/g (C) and 433 m^2/g (F).

In Figure AIII.7 the BET plots on the coal are shown. The specific areas were: 23.1 m^2/g (N), 22.8 m^2/g (A), 147.5 m^2/g (C) and 151.6 m^2/g (F).

The *C* values for these isotherms (as calculated from the BET plots) are shown in Table AIII.2.

AIII.4.3 Pore Volume Distributions

The inversions described above (Cranston-Inkley, Yan-Zhang and Modelless — hereinafter referred to as CI, YZ and ML, respectively) were applied to each of the isotherms to determine the pore volume distributions in each case. Pore volume distributions were chosen instead of pore surface area distributions due to the following reasons: (a) Fundamentally, the concept of surface area in porous (or microporous) solids is nebulous on close scrutiny. Surface areas are useful only as a comparison between different materials; therefore, their intrinsic value has been questioned by many researchers (20). (b) Geometrical assumptions, often simplistic, must be made to derive surface area distributions from the experimental data. (c) Most inversions naturally lend themselves to pore volume distribution determinations.

In this section, all plots are in the form dV/dlog r vs. log r. The reason for this is that it is easy to visually integrate to obtain total void volume, and to view the contributions of different size intervals to the total porosity.

The CI and YZ distributions in all cases showed virtually identical results, as shown in Figures AIII.8a-d. As discussed earlier, both methods are essentially the same. In order to observe the effect of the calculation, two approximations for the

thickness have been used in each method: (a) a polynomial function of the relative pressure ($C \sim 130$) and (b) the Halsley expression ($C \sim 100$). For a given expression of thickness, the two methods gave indistinguishable results (Figures AIII.8a,c or Figures AIII.8b,d). This shows that the method of calculation of mean radius (log mean vs. arithmetic mean) is unimportant. Figure AIII.9 shows thickness as a function of relative pressure for these two approaches. Note that the appropriate range of relative pressure is 0.4 to 0.95. The use of the Halsey thickness resulted in total pore volumes which were about 5% lower than those from the polynomial approximation. The reason for this is that the Halsey thickness was slightly smaller than that calculated by the polynomial approximation.

Pore volume distributions were obtained for the different adsorptives on two different solids using the CI method (see Figures AIII.10a,b). The char did not show appreciable volumes in this range of pore sizes, so they will not be considered here. For alumina (Figure AIII.10a), the distributions from the nitrogen and Freon isotherms were strikingly similar. Counterintuitively, the distribution from argon is different. While total pore volumes (equal to area under the curve) are similar, the argon distribution is skewed toward larger pore sizes. The argon was admitted at a higher relative rate than the nitrogen; hence, there was less time for equilibration of the gas with the liquid in the pores. Thus, adsorption took place at higher relative pressures. This shows the importance of allowing adequate times for equilibration. The similarity of the nitrogen and Freon results may seem surprising. However, if the pores are sufficiently large, and if the interaction with the surface is similar, the result is reasonable. Freon has a higher dipole moment, yet it appears to have

little influence on the surface interaction. This may indicate that the nature of the adsorption is rather non-specific, and that the adsorbent is relatively passive. It is also possible that the Freon interaction is very strong on a local level. This interaction may be so localized that there is no overall orientation effect.

The pore volume distributions for PSOC-190 are shown in Figure AIII.10b. Here, the nitrogen and argon distributions differ for the same reasons as described above. Freon, on the other hand, gives a much larger total pore volume. It appears as though Freon has a strong specific interaction with the coal. This may lead to orientation of the adsorbate, which in turn may lead to enhanced adsorption.

The modelless method was applied only to the nitrogen isotherms. The resulting distributions are shown along with those of CI (Figures AIII.11a-c). Recall that the hydraulic core radii calculated by the method were augmented by the adsorbed layer thickness as calculated by the Halsley equation (3). The pore radii in the two methods cannot be directly compared because CI has assumed a cylindrical pore geometry, while the modelless method uses the hydraulic radius. Since the hydraulic radius of a cylinder is half of its radius, the radii from the modelless method could be multiplied by two to obtain some comparison.

AIII.4.4 Microporosity Analysis

The v-t plots for nitrogen adsorption on the porous solids are shown in Figure AIII.12. The slope for the alumina (for t=3 to 5 Å) gave an area of 211 m^2/g, which was quite close to the BET area. The v-t plot gave an area of 34 m^2/g for the PSOC-190. This area was significantly higher than the corresponding BET area. This is an unusual case where the two methods do not agree even though the

v-t plot does not show significant microporosity.

The area for the char had to be estimated from the slope of a line passing through the origin tangent to the plot. This resulted in an area of 750 m^2/g, which was not even close to the nitrogen BET area. These plots show that only the char has significant microporosity. Therefore, the MP analysis was applied only to the char.

The MP method result is shown in Figure AIII.13. According to this analysis, the vast majority of pores have radii between 3.5 and 5 Å. This seems quite reasonable in light of the original isotherm.

The DRK Theory was applied to the isotherms of carbon dioxide at 298K (see Figure AIII.14). Strictly speaking, this theory was developed for carbonaceous solids with micropores. Since the assumptions are not too stringent, the theory was applied to the alumina as well. The plot for PSOC-190 (C) was quite linear; those for γ-alumina (A) and oxidized char (O) were less so. The region of lower log N was used in the calculation of specific area. The areas calculated by this method were: 161 m^2/g for alumina, 1400 m^2/g for char, and 162 m^2/g for PSOC-190. The values for γ-alumina and PSOC 190 are similar to those calculated from the BET method for CO_2. The value for char is significantly greater.

The Medek method was applied to these isotherms in addition to several others. Figures AIII.15a-b show the results for CO_2 and Freon on the porous solids. The form of the curve is the same in all cases; only the magnitude and position of the maxima are different.

AIII.5 Discussion

For the materials studied, the continuous flow method gives isotherms similar to those obtained by the traditional method in a fraction of the time. Any discrepancy is due to the non-equilibration of the gas phase with the adsorbed phase.

The adsorptives were selected because of their different molecular characteristics. Nitrogen, generally regarded as the "standard adsorbate", is non-polar and axially symmetric. Argon, another commonly used adsorptive, is also non-polar, but is spherically symmetric. Carbon dioxide has a strong quadrupole, and is easily polarizable. Freon is larger than the others, and possesses a permanent dipole. In some orientations, however, its minimum dimension is comparable with that of nitrogen or argon.

In spite of these differences, there was little effect on the overall form of the isotherm for a given adsorbent. The only significant exceptions were Freon on char and CO_2 on PSOC-190. The former was probably due to slow diffusion of large Freon molecules into the small micropores, as explained above. The latter was likely due to specific adsorbate-adsorbent interaction, a small minimum dimension, and high absolute temperature.

The areas calculated for the microporous char are rather questionable. The models used assume that the adsorbate molecule sits on a locally flat surface. However, when a molecule is in a pore which has a diameter on the order of molecular dimensions, it will cover a much larger area. The discrepancy between the nitrogen and argon areas shows that the way in which the molecules are packed into the pores is also an important consideration.

It was interesting to see that the DRK model gave an area for γ-alumina that was consistent with the other methods. As described previously, the model was developed from a theory of micropore adsorption. The alumina has few micropores, but it is rich in oxygen. It is possible that the carbon dioxide interaction with oxygen-containing groups is similar in magnitude to its interaction with the walls of a micropore. That the total area obtained is close to the others may be fortuitous.

As mentioned above, the Medek method gave curves which appeared to be self-similar for all adsorbents and adsorptives. Furthermore, it showed significant microporosity for the alumina, which is rather questionable. It seems as though this method simply transforms a given isotherm into a log normal curve.

Alumina is one of the most studied and relatively "well-characterised" material of all the solids considered in this study. According to the present experimental findings, conclusions can be drawn regarding its morphology by applying a unified analysis of surface area, pore volume and pore volume distribution. The BET surface area was around 200 m^2/g for all gases except argon, which gave a lower value, possibly due to non-equilibration effects. The v-t plot gave a surface area which was very close to the BET values; it also indicated an absence of micropores. While the Medek method gave a micropore distribution, its validity is doubtful.

Considering the similarity of the nitrogen and Freon CI pore size distributions, they are likely to give a reasonable picture of the true porosity. The modelless method is difficult to interpret without having some idea about pore shape. Unfortunately, it is difficult to infer anything about pore shape without a desorption isotherm.

The partially oxidized synthetic char is not a common material, but it gives isotherms similar to many other microporous substances, like molecular sieves or activated charcoals. In this case, the micropores were large enough so that diffusion was not a problem. Not surprisingly, the microporous nature of the material precluded the use of CI and YZ. The MP method gave what appears to be a reasonable distribution. The Medek method gave distributions with much larger pore volumes and radii.

The PSOC-190 is a typical bituminous coal. As with many raw coals, reliable determination of particle morphology is difficult at best. The existence of micropores which are of the order of molecular dimensions causes molecular sieve effects to be extremely important. Also, diffusion into pores of this size may be via an activated process. To counter these effects, an adsorptive with small minimum molecular dimension and high critical point is generally used for determining the isotherm. CO_2 at 196 or 298K is usually the adsorptive(21) of choice for these coals (Figure AIII.3). However, applying the BET analysis to the CO_2 at 196K isotherm, it is seen that, while the adsorptive uptake is quite high, the C value is quite small (Table AIII.2). Since the C value indicates the strength of the gas-solid interaction, the only possible conclusion that can be drawn is that CO_2 adsorbs strongly on itself. Care must be taken to interpret surface areas in this case.

AIII.6 Conclusions

Examination of the isotherms shows that the form of the isotherm is essentially independent of the type of adsorptive (for small enough molecules) for a given solid.

The BET areas were generally consistent with areas calculated by other methods for non-microporous solids. When micropores are present, the agreement was not as good. Of course, interpretation of area on this level is frought with uncertainty.

The equivalent methods of CI and YZ appear to be the most suitable means of obtaining pore size distributions in the mesopore range. The modelless method is also quite useful; however, additional information regarding pore shape must be obtained or assumed in order to formulate a reasonable picture of the internal structure.

The MP analysis is the method of choice for pore size distributions in the micropore range. The Medek method is somewhat questionable.

AIII.7 Acknowledgements

This work was supported by DOE Grant No. DE-AC2284FC70915.

References

1. Brunauer, S., Demming, L.S., Demming, W.S., and Teller, E., *J. Amer. Chem. Soc.*, **62**, 1723, (1940).
2. Northrop, P.S., Flagan, R.C., and Gavalas, G.R., *Langmuir*, **3**, 300, (1987).
3. Halsey, G.D., *J. Chem. Phys.*, **16**, 931, (1948).
4. Young, D.M., and Crowell, A.D. "Physical Adsorption of Gases", Butterworths, London, 1962.
5. Sircar, S., *Adsorption Science and Technology*, **2**, 23, (1985).
6. Brunauer, S., Emmett, P.H., and Teller, E., *J. Am. Chem. Soc.*, **60**, 309, (1938).
7. Wheeler, A. Catalyst Symposium, Gibson Island AAAS Conference (1946).
8. Lippens, B.C., deBoer, J. H., *J. Cat.*, **4**, 319, (1965).
9. Lecloux, A., and Pirard, J.P., *J. Colloid Interface Sci.*, **70**, 265, (1979).
10. Pierce, C., *J. Phys. Chem.*, **57**, 149, (1953).
11. Dollimore, D., and Heal, G.R., *J. Appl. Chem.*, **14**, 109, (1964).
12. Cranston, R., and Inkley, F., *Adv. in Cat.*, **9**, 143, (1957).
13. Yan, J., and Zhang, Q., *Part. Charact.*, **3**, 20, (1986).
14. Brunauer, S., Mikhail, R.S., and Bodor, E.E., *J. Colloid Interface Sci.*, **24**, 451, (1967).
15. Mikhail, R.S., Brunauer, S., and Bodor, E.E, *J. Colloid Interface Sci.*, **26**, 45, (1968).
16. Kaganer, *Zhur. Fiz. Khim.*, **33**, 2202, (1959).
17. Medek, J., *Fuel* , **56**, (1977).

18. Lowell, P., and Shields, L., **Powder Surface Area and Porosity**, Chapman and Hall, NY (1984).

19. Gregg, S.J., and Sing, K.S.U., "Adsorption, Surface Area and Porosity", Academic Press, New York, 1982.

20. Debelak, K.A., and Schrodt J.T., *Fuel* , **58**, (1979).

21. Anderson, R. B., Bayer, J., and Hofer, L.J.E., *Fuel*, **44**, 443, (1965).

ADSORBATE	SHAPE	σ ($\mathring{A}^2$)	α $10^{24}(cm^3)$	μ	q	V_{liq} (cm^3/g mol)	γ (dynes/cm)
N_2	SPHERO–CYLINDRICAL	16.2	1.73	NO	YES	34.65	8.5
Ar	SPHERICAL	14.2	1.62	NO	NO	28.53	14.2
CO_2	SPHERO–CYLINDRICAL	19.5	2.59	NO	YES	36.36	25.7
FREON-21	IRREGULAR	40.0	7.4	YES	YES	73.15	18.0

Table AIII.1 Properties of the adsorptive gases.

ADSORBATE : NITROGEN

	A_{BET} (m^2/g)	C_{BET}	V_{C-1} (cm^3/g)	V_{M-L} (cm^3/g)	A_{V-1} (m^2/g)	A_{DRK} (m^2/g)
γ-ALUMINA	207	260	0.409		211	
OXIDIZED SYN-CHAR	400	LARGE	0.009		508	
PSOC-190 COAL	23	100	0.043		34	

ADSORBATE : ARGON

	A_{BET} (m^2/g)	C_{BET}	V_{C-1} (cm^3/g)	V_{M-L} (cm^3/g)	A_{V-1} (m^2/g)	A_{DRK} (m^2/g)
γ-ALUMINA	174	52.5	0.546			
OXIDIZED SYN-CHAR	573	LARGE	0.026		714	
PSOC-190 COAL	23	46	0.06			

ADSORBATE : CO_2 AT 196 K

	A_{BET} (m^2/g)	C_{BET}	V_{C-1} (cm^3/g)	V_{M-L} (cm^3/g)	A_{V-1} (m^2/g)	A_{DRK} (m^2/g)
γ-ALUMINA	200	113	0.166			161
OXIDIZED SYN-CHAR	430	LARGE	0.099		579	1400
PSOC-190 COAL	148	14.3	0.08			162

ADSORBATE : FREON-21

	A_{BET} (m^2/g)	C_{BET}	V_{C-1} (cm^3/g)	V_{M-L} (cm^3/g)	A_{V-1} (m^2/g)	A_{DRK} (m^2/g)
γ-ALUMINA	205	47	0.377			
OXIDIZED SYN-CHAR	433	14	0.206		446	
PSOC-190 COAL	152	8.5	0.162			

Table AIII.2 Summary of adsorptive-adsorbate interactions.

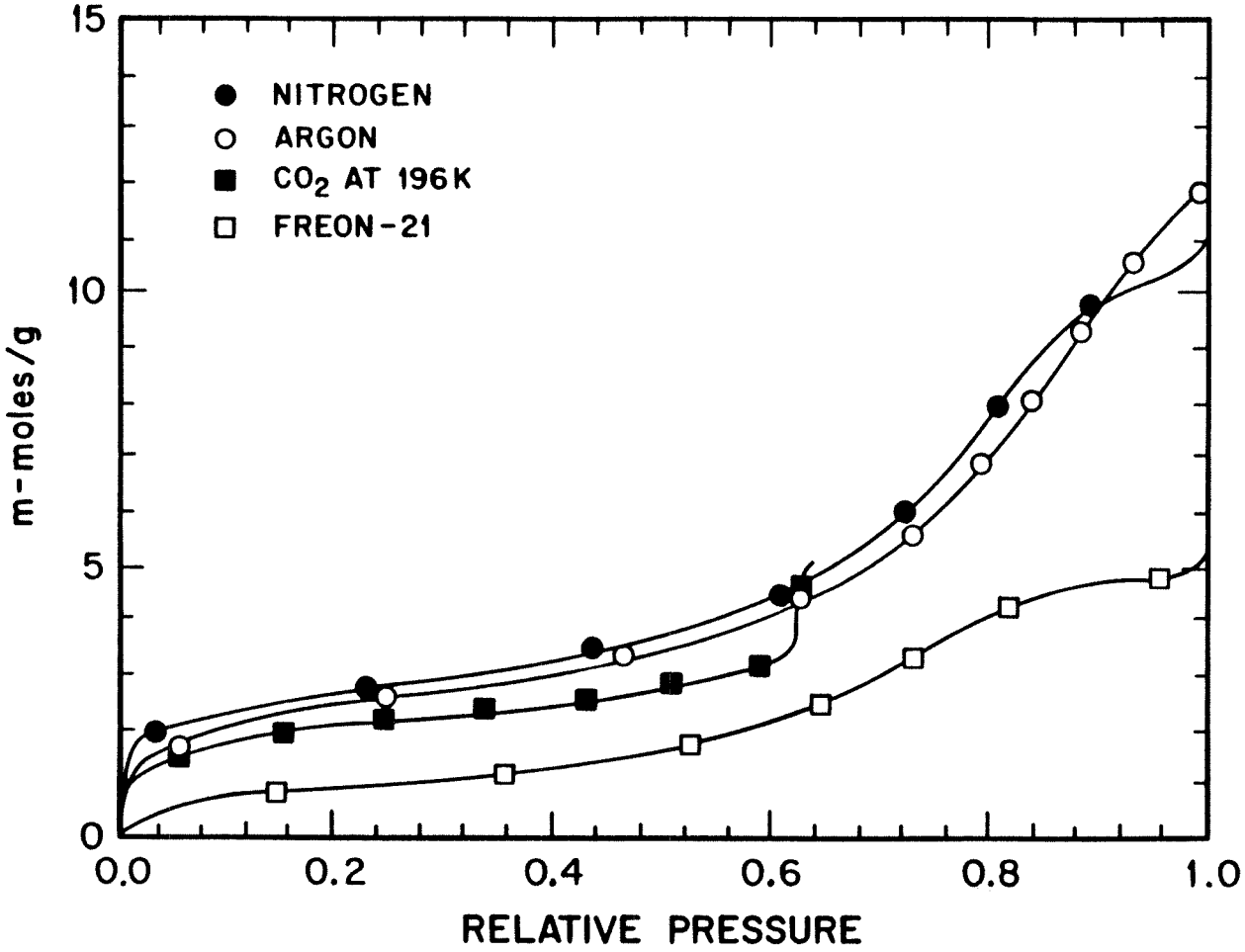

Figure AIII.1 Nitrogen, Argon, CO_2 (196K), and Freon-21 isotherms on γ-alumina.

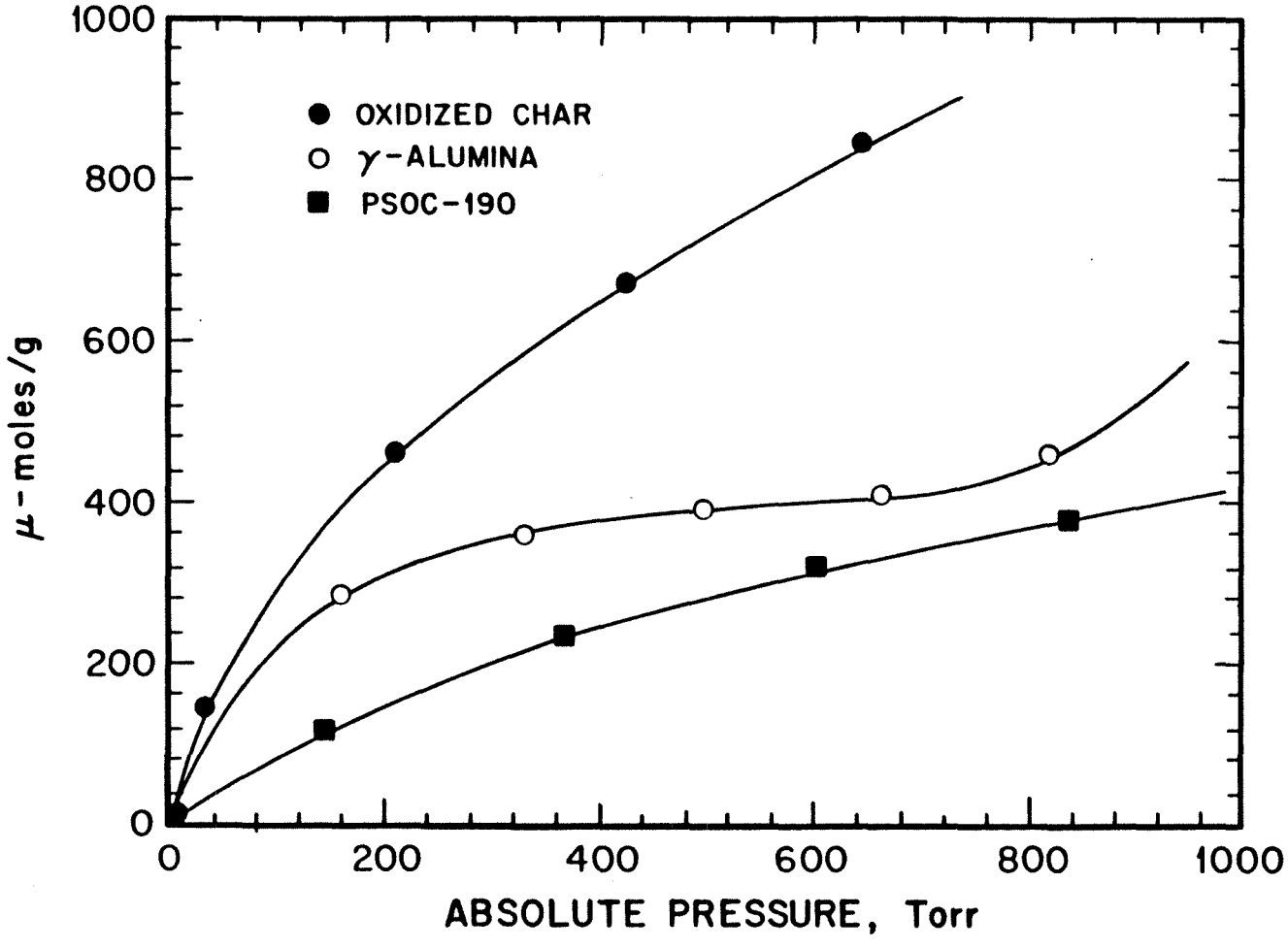

Figure AIII.2 CO_2 isotherms at 298K on γ-alumina, oxidised char and PSOC-190.

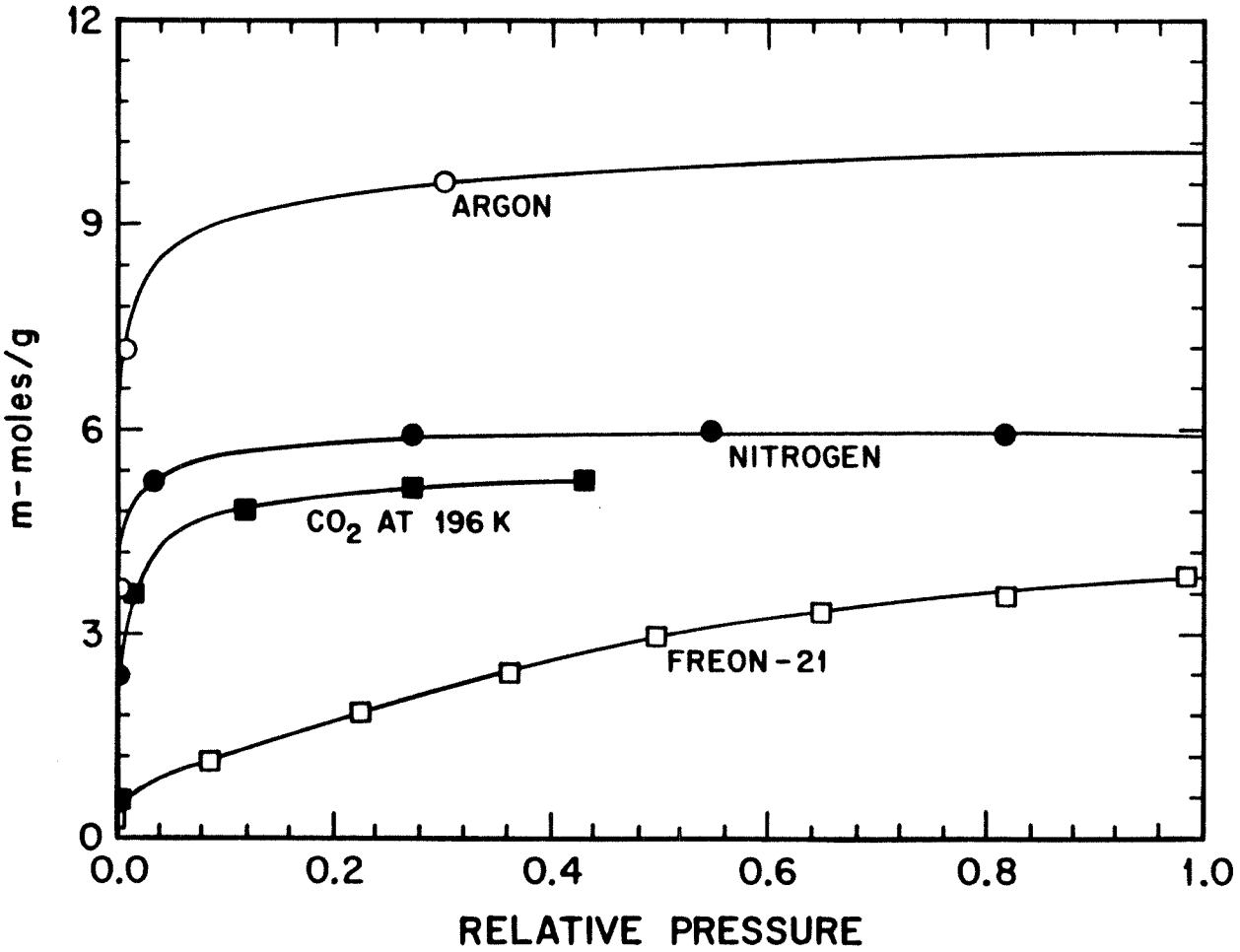

Figure AIII.3 Nitrogen, Argon, CO_2 (196K), and Freon-21 isotherms on oxidized char.

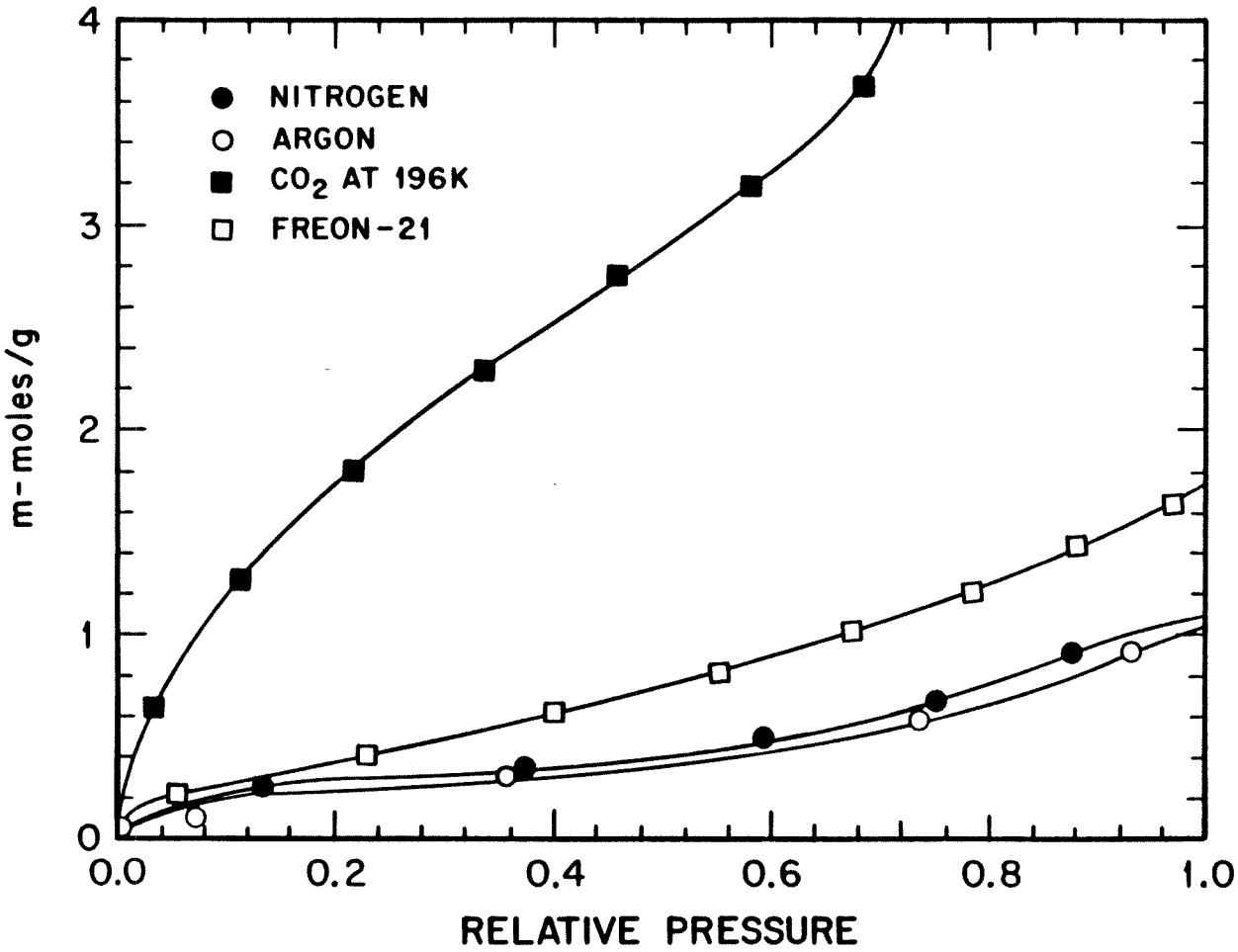

Figure AIII.4 Nitrogen, Argon, CO_2 (196K), and Freon-21 isotherms on PSOC-190 Coal.

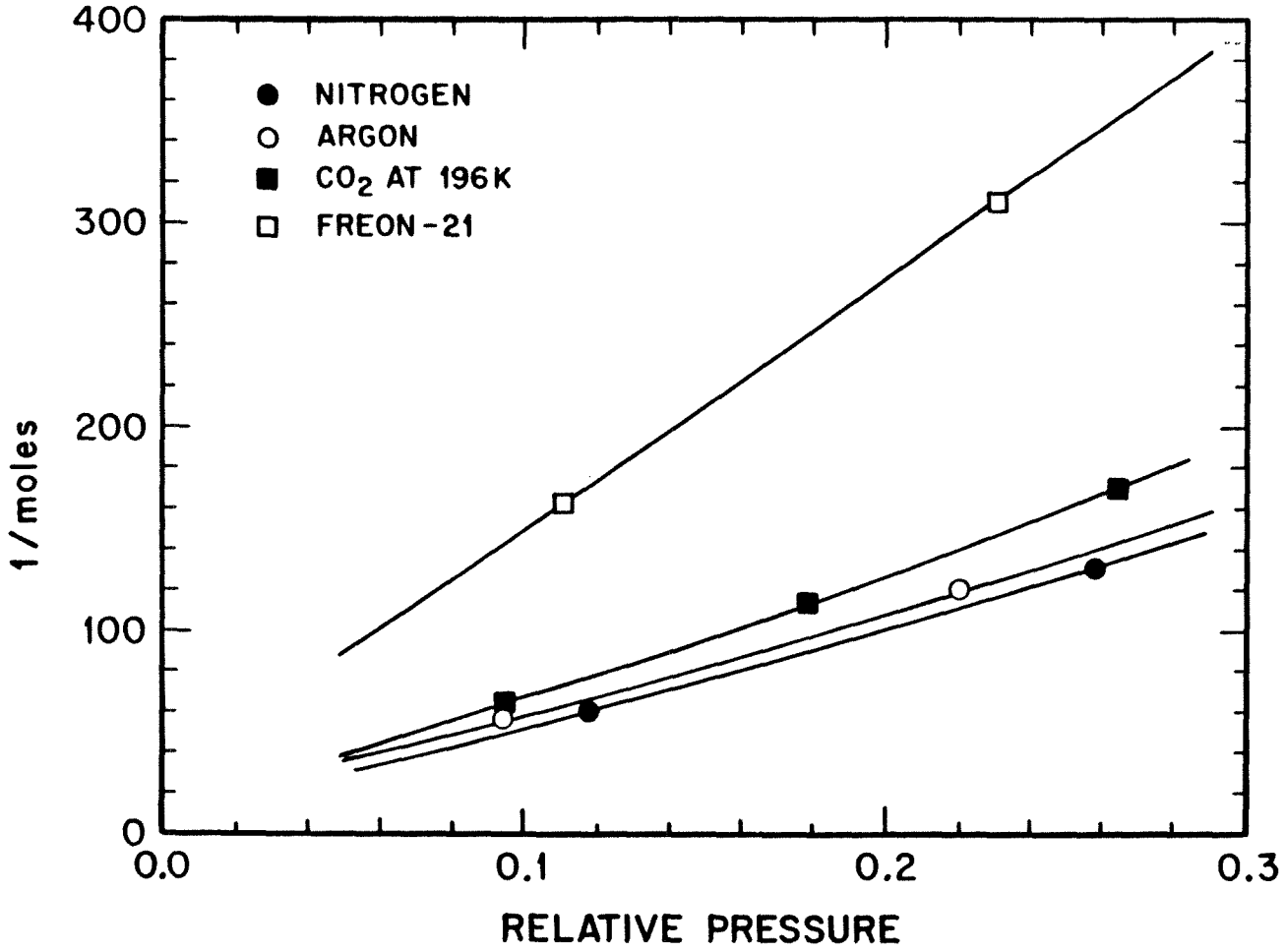

Figure AIII.5 BET plots for γ-alumina

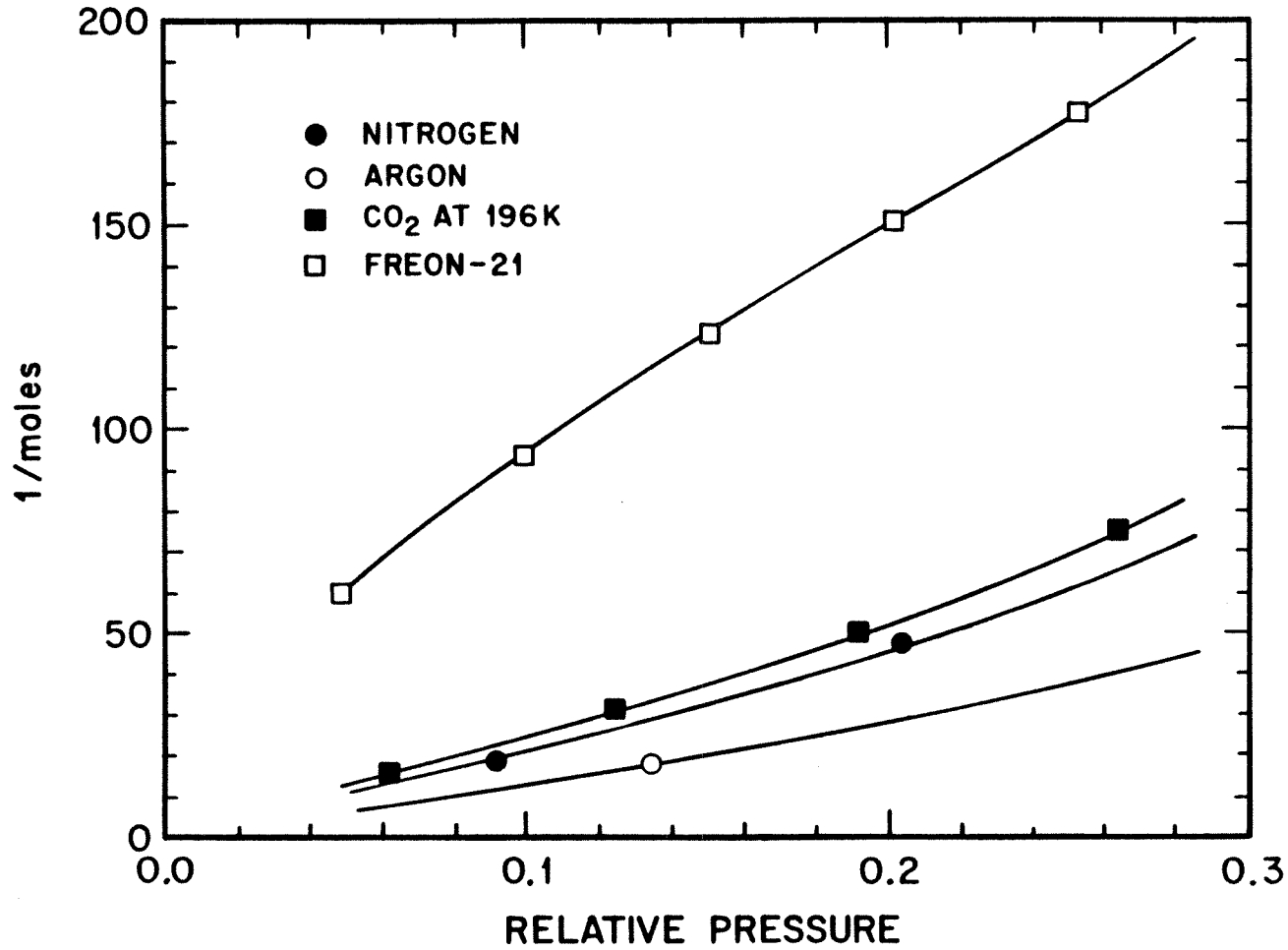

Figure AIII.6 BET plots for oxidised char.

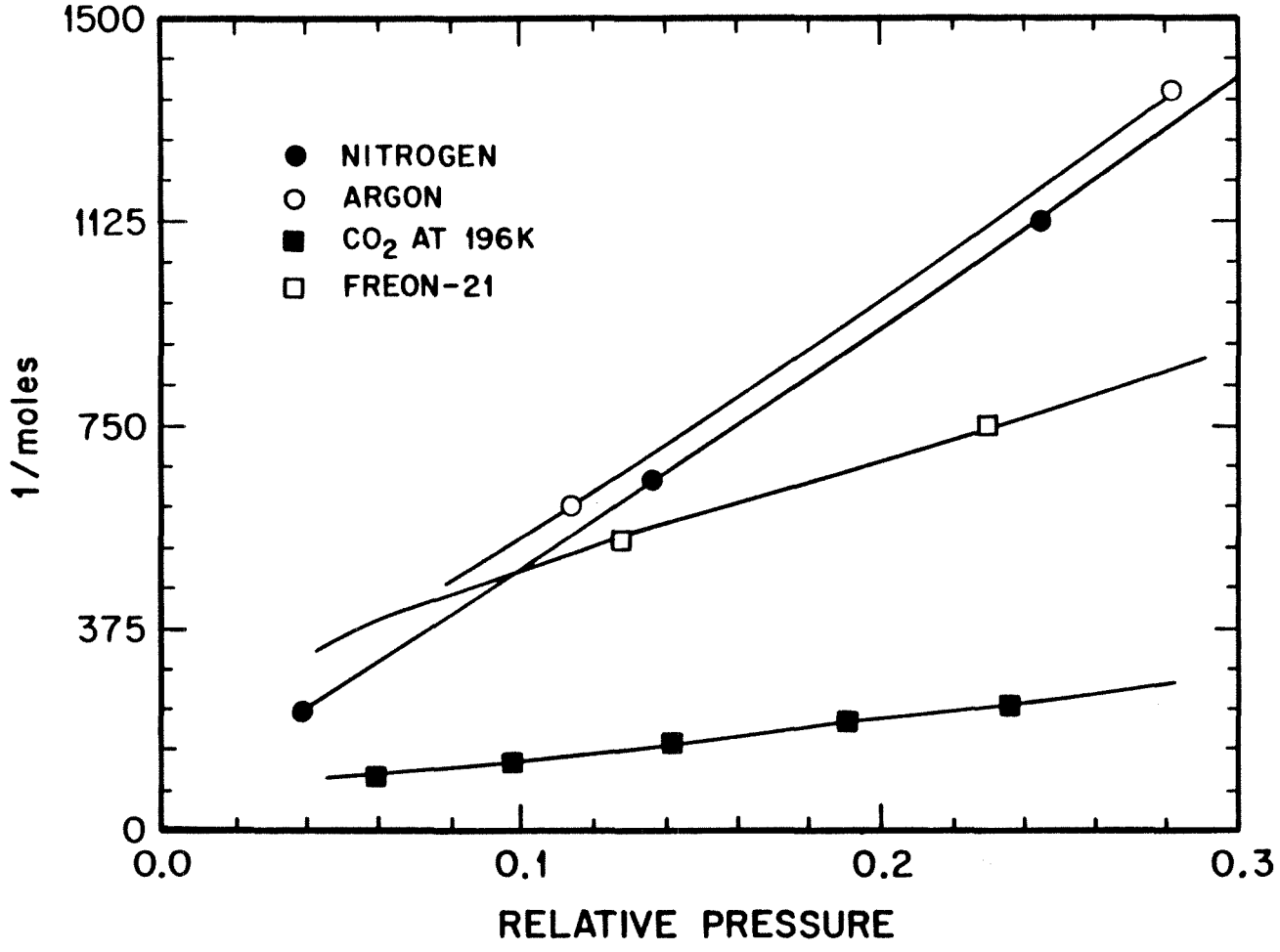

Figure AIII.7 BET plots for PSOC-190 coal.

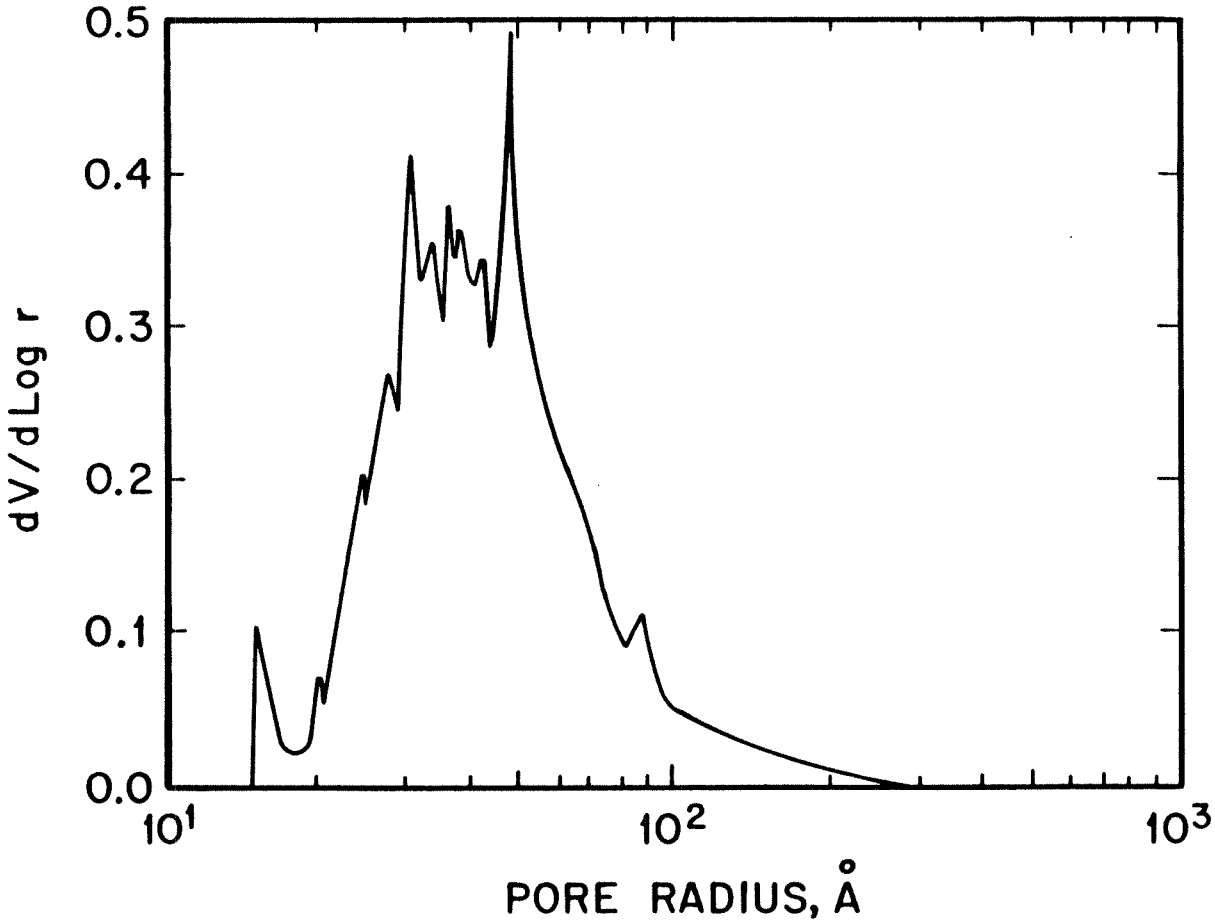

Figure AIII.8a Pore volume distribution of γ-alumina from nitrogen — Cranston-Inkley inversion with polynomial thickness.

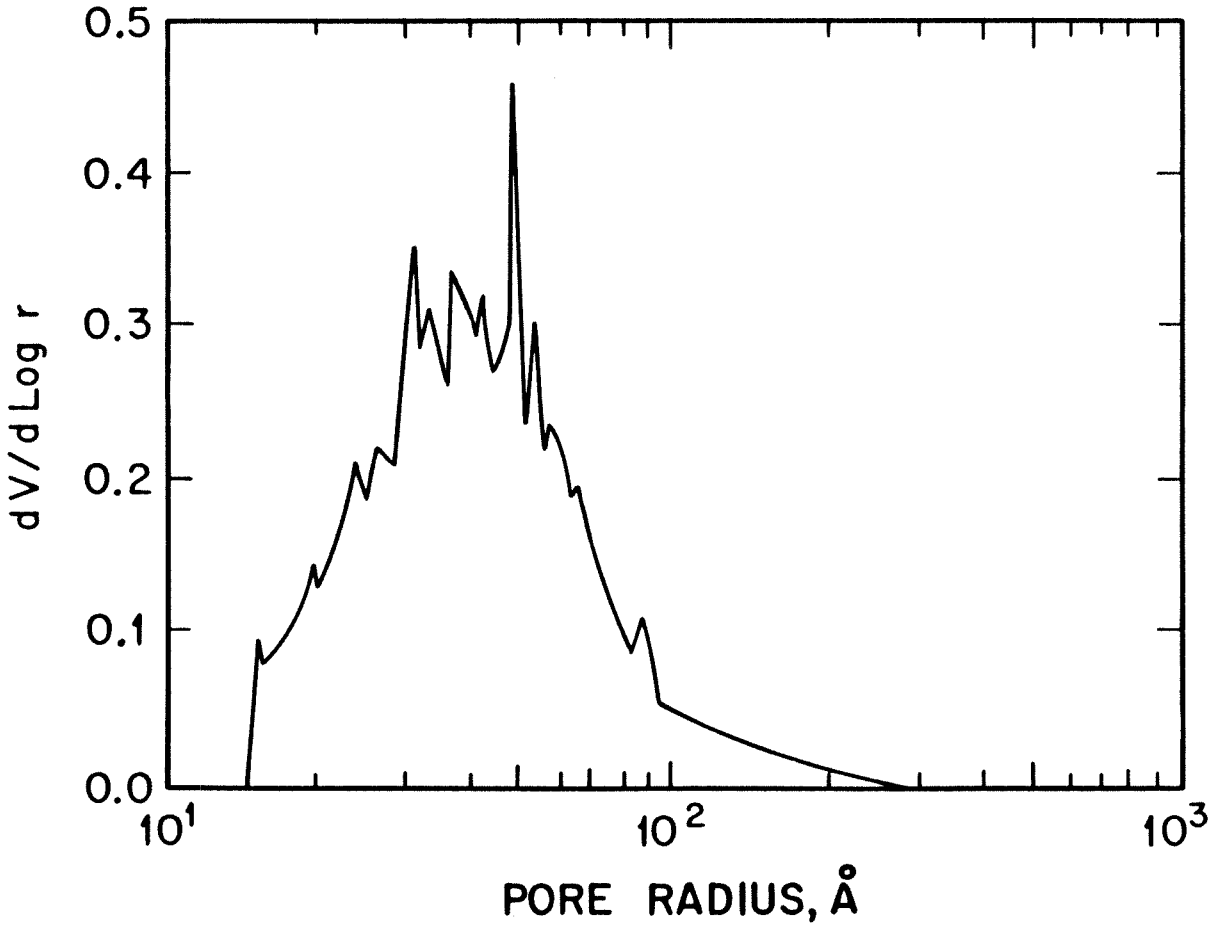

Figure AIII.8b Pore volume distribution of γ-alumina from nitrogen — Yan-Zhang inversion with polynomial thickness.

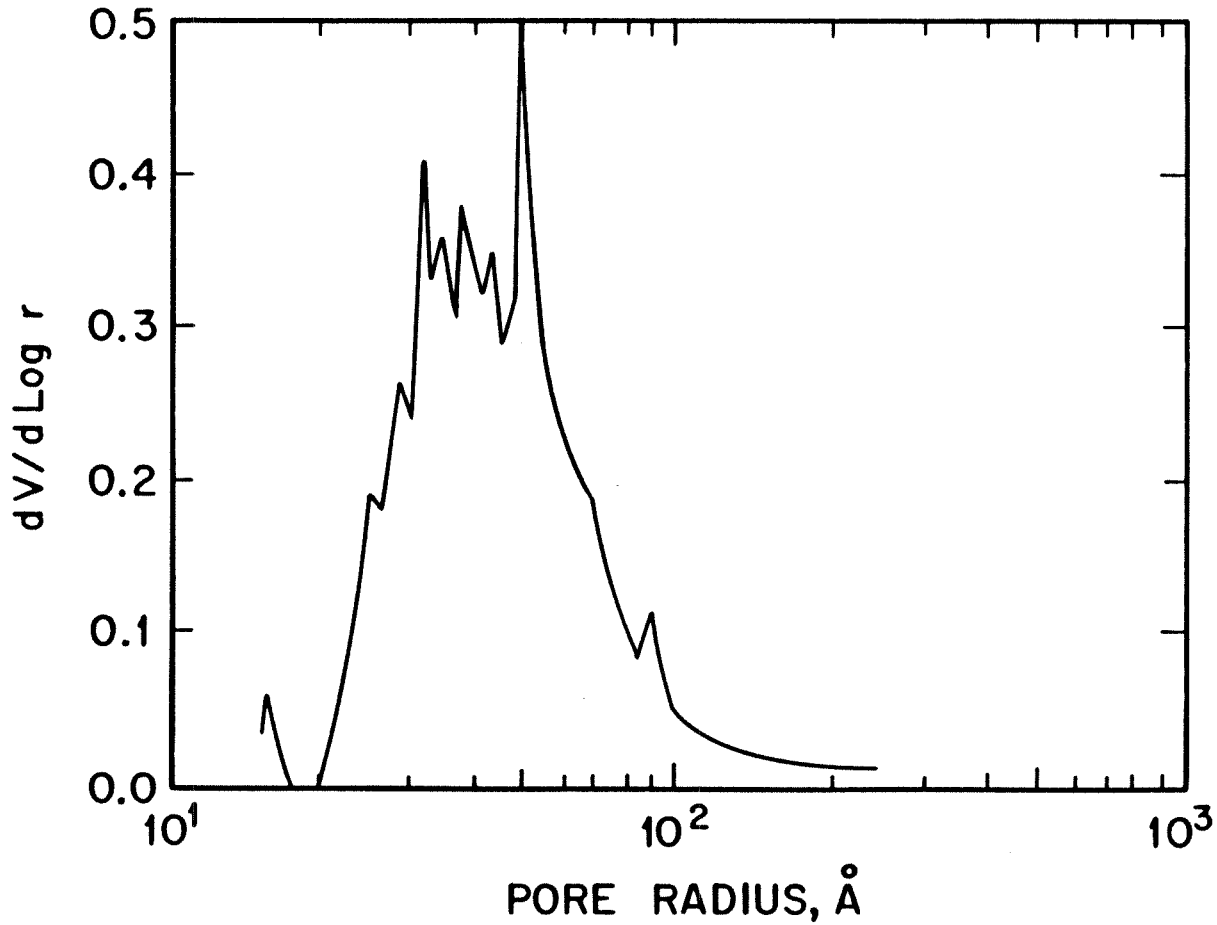

Figure AIII.8c Pore volume distribution of γ-alumina from nitrogen — Cranston-Inkley inversion with Halsley thickness.

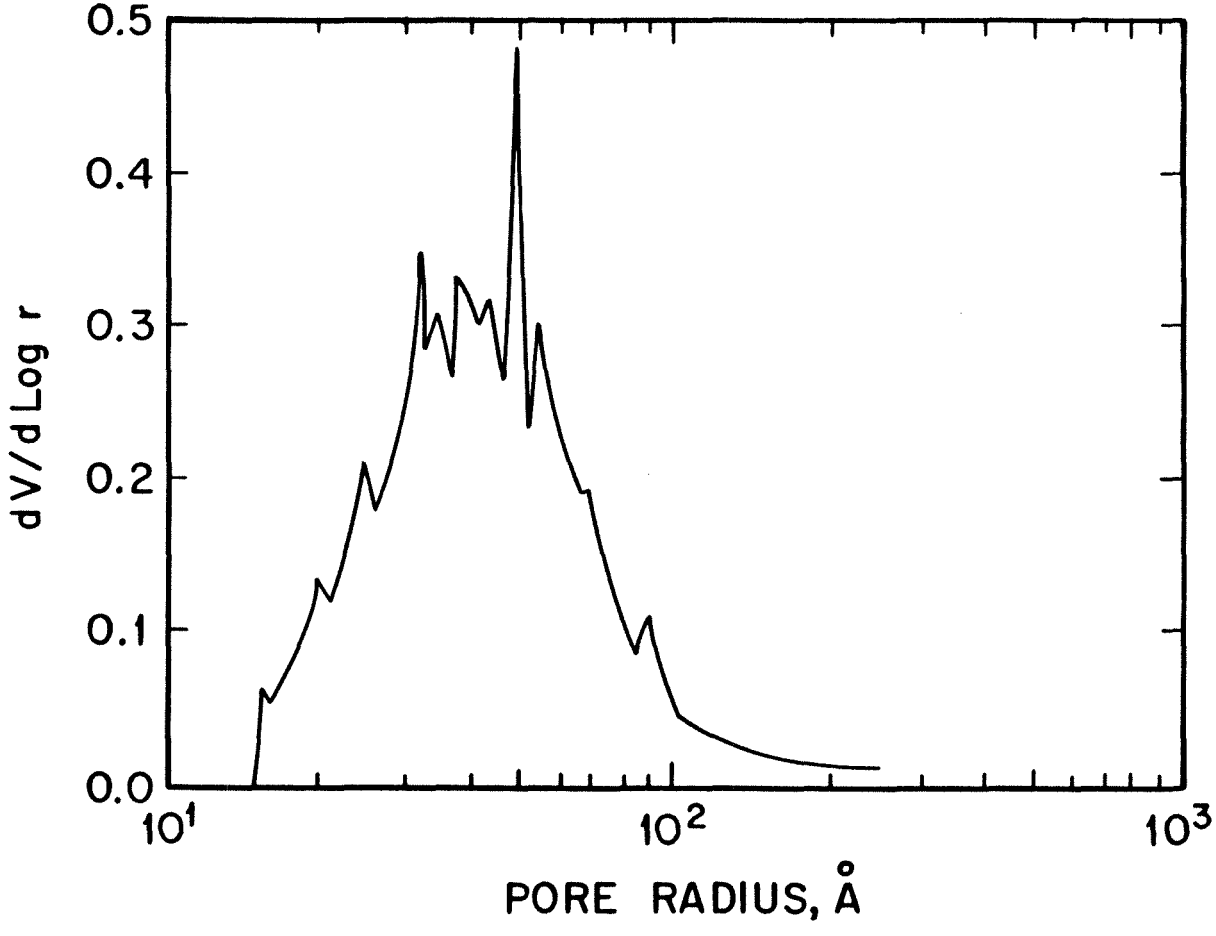

Figure AIII.8d Pore volume distribution of γ-alumina from nitrogen — Yan-Zhang inversion with Halsley thickness.

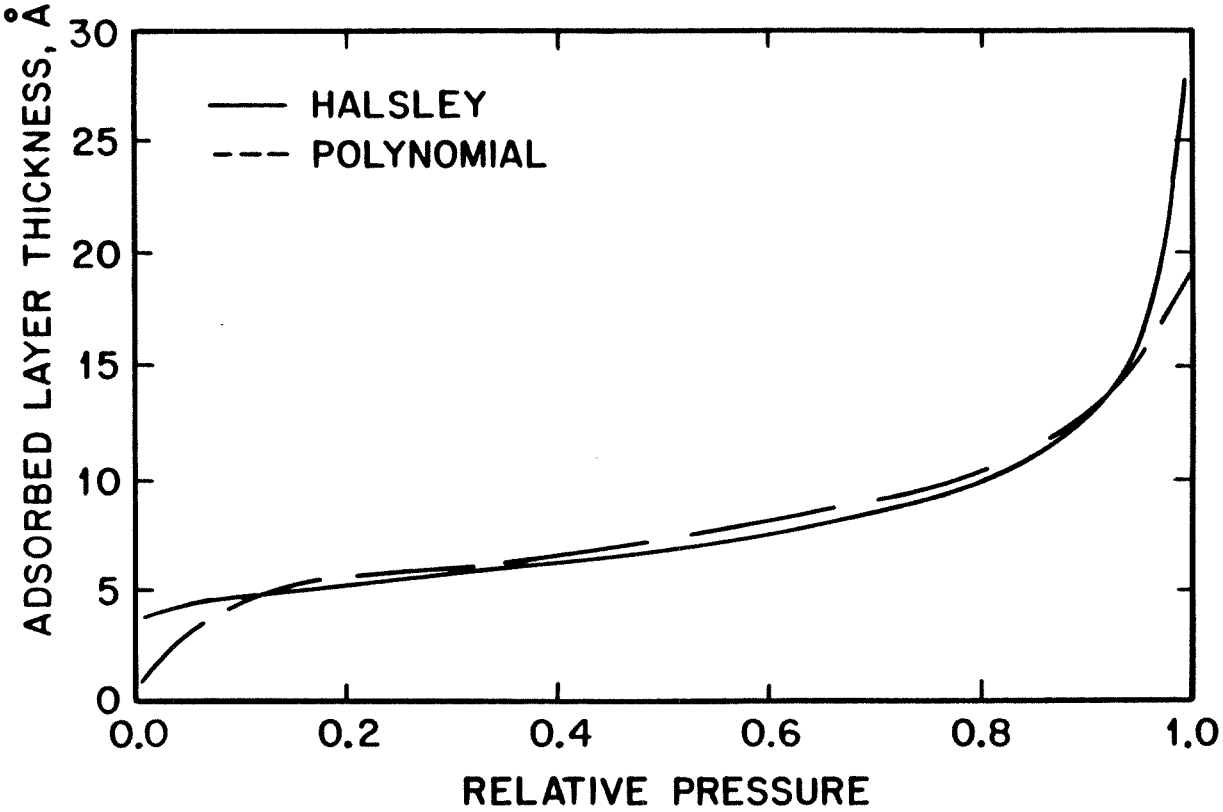

Figure AIII.9 Comparision of polynomial and Halsley thicknesses as a function of relative pressure.

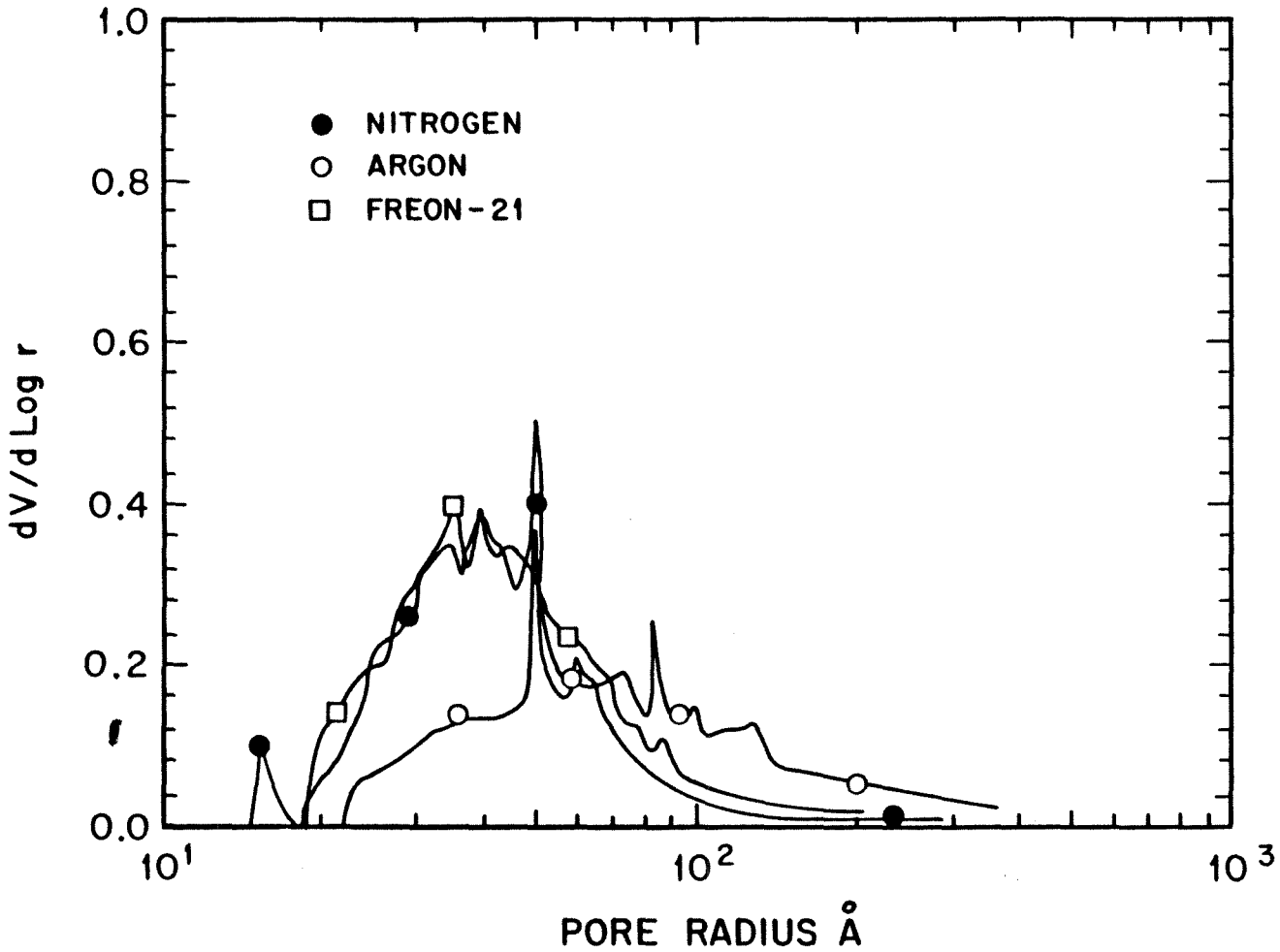

Figure AIII.10a Pore volume distributions of γ-alumina from different adsorptive gases using the Cranston-Inkley inversion.

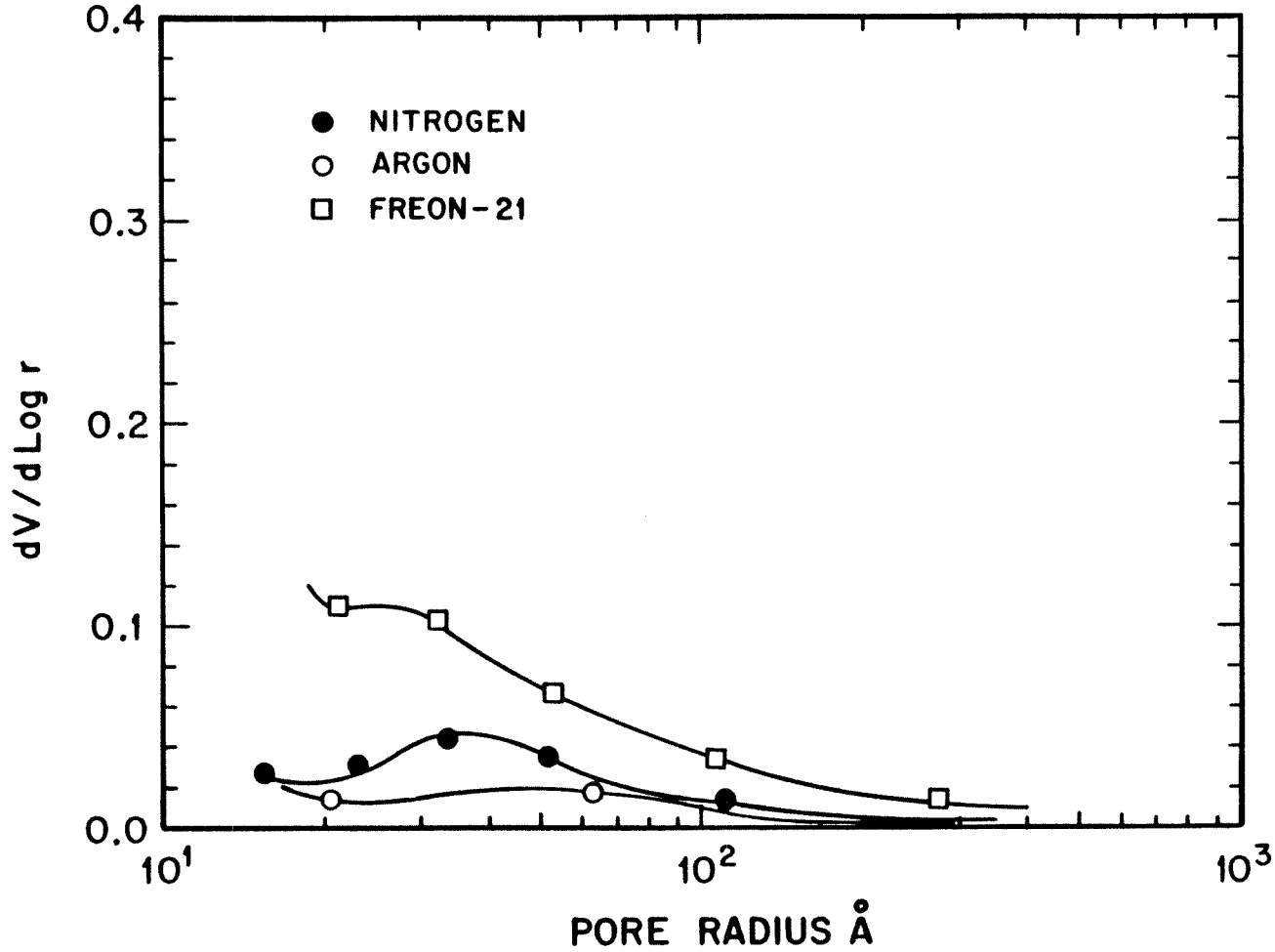

Figure AIII.10b Pore volume distributions of PSOC-190 coal from different adsorptive gases using the Cranston-Inkley inversion.

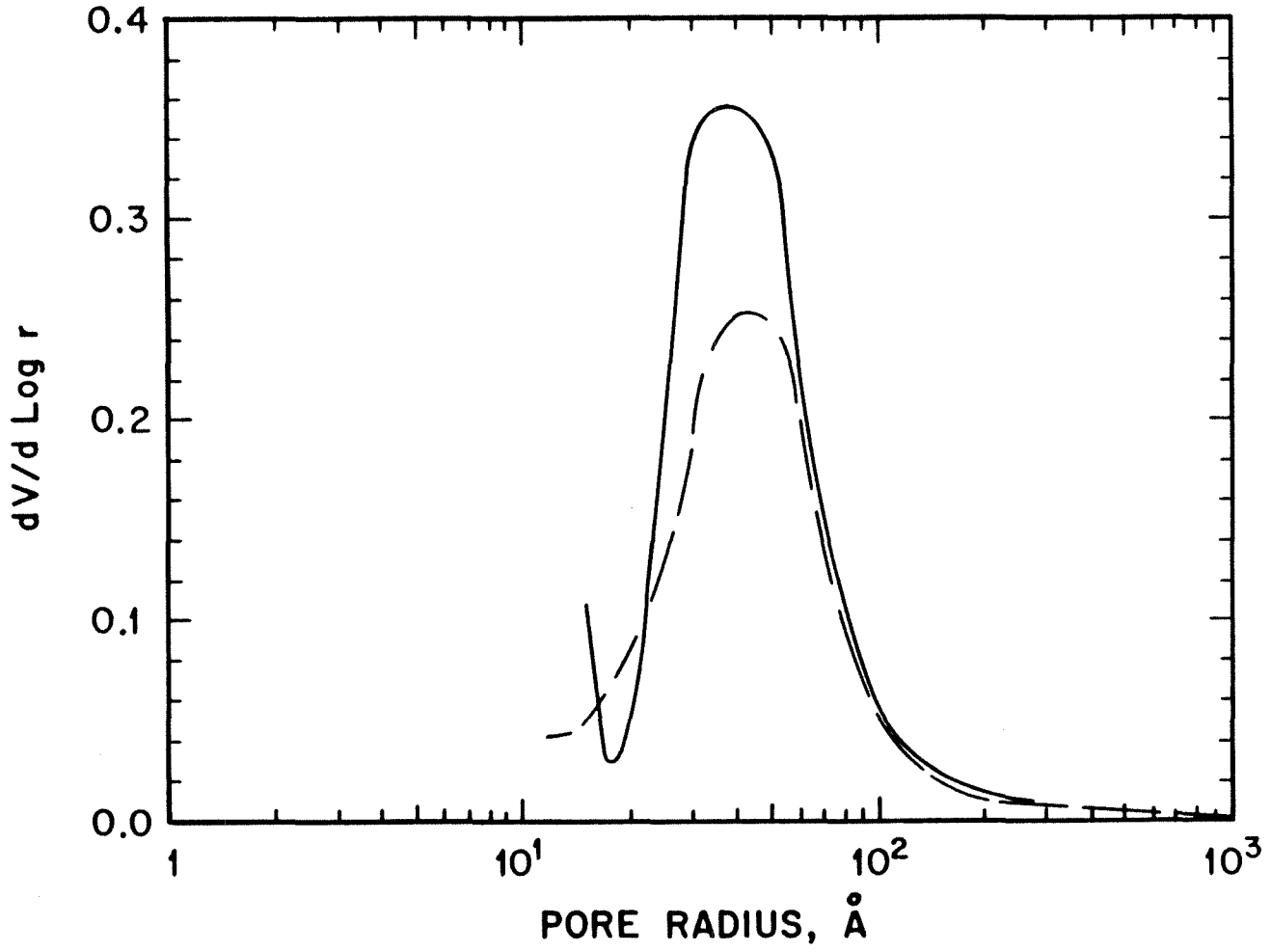

Figure AIII.11a Comparision of pore volume distributions of γ-alumina by nitrogen using the Cranston-Inkley (—) and Modelless Inversions (- - -).

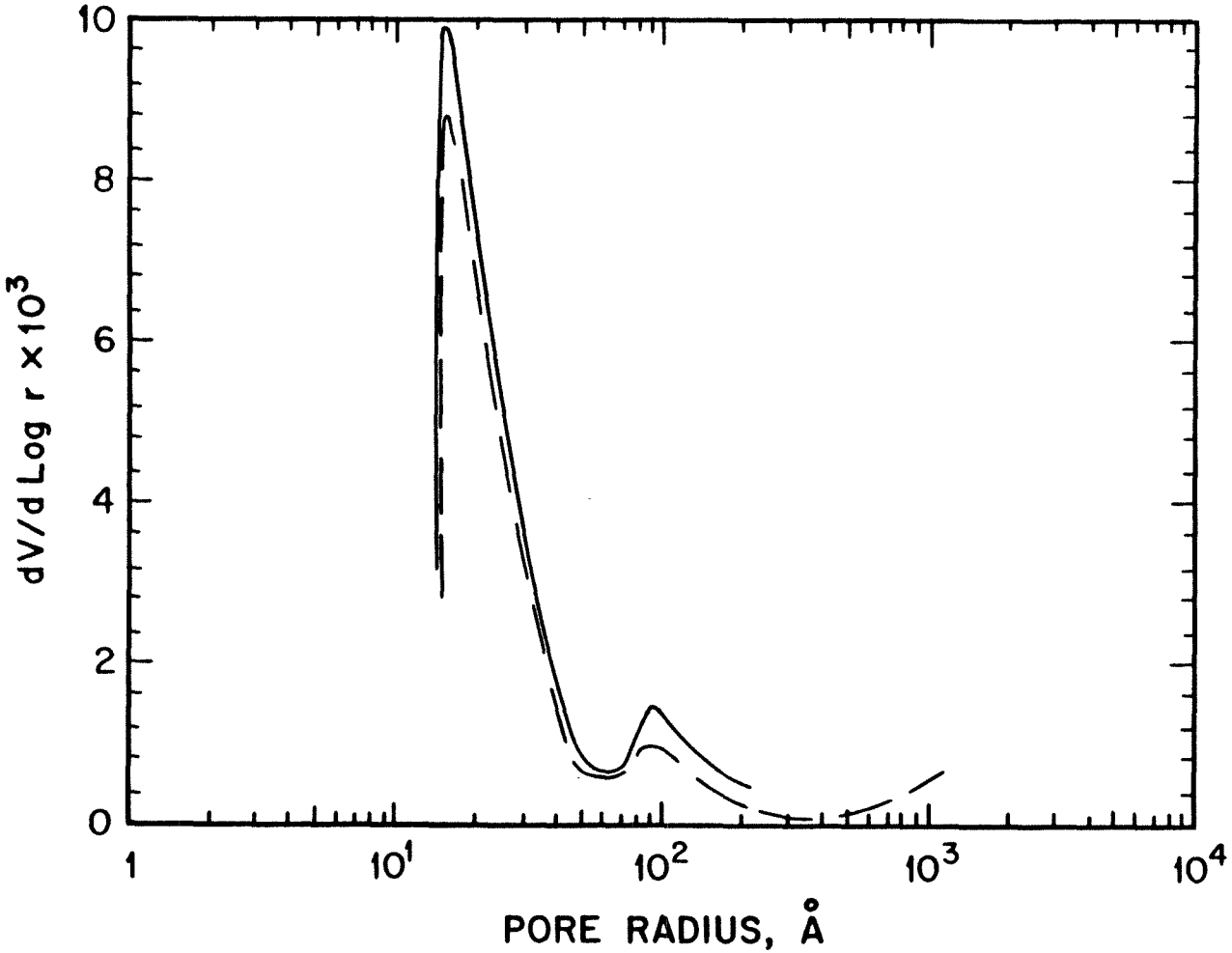

Figure AIII.11b Comparision of pore volume distributions of oxidized char by nitrogen using the Cranston-Inkley (—) and Modelless Inversions (- - -).

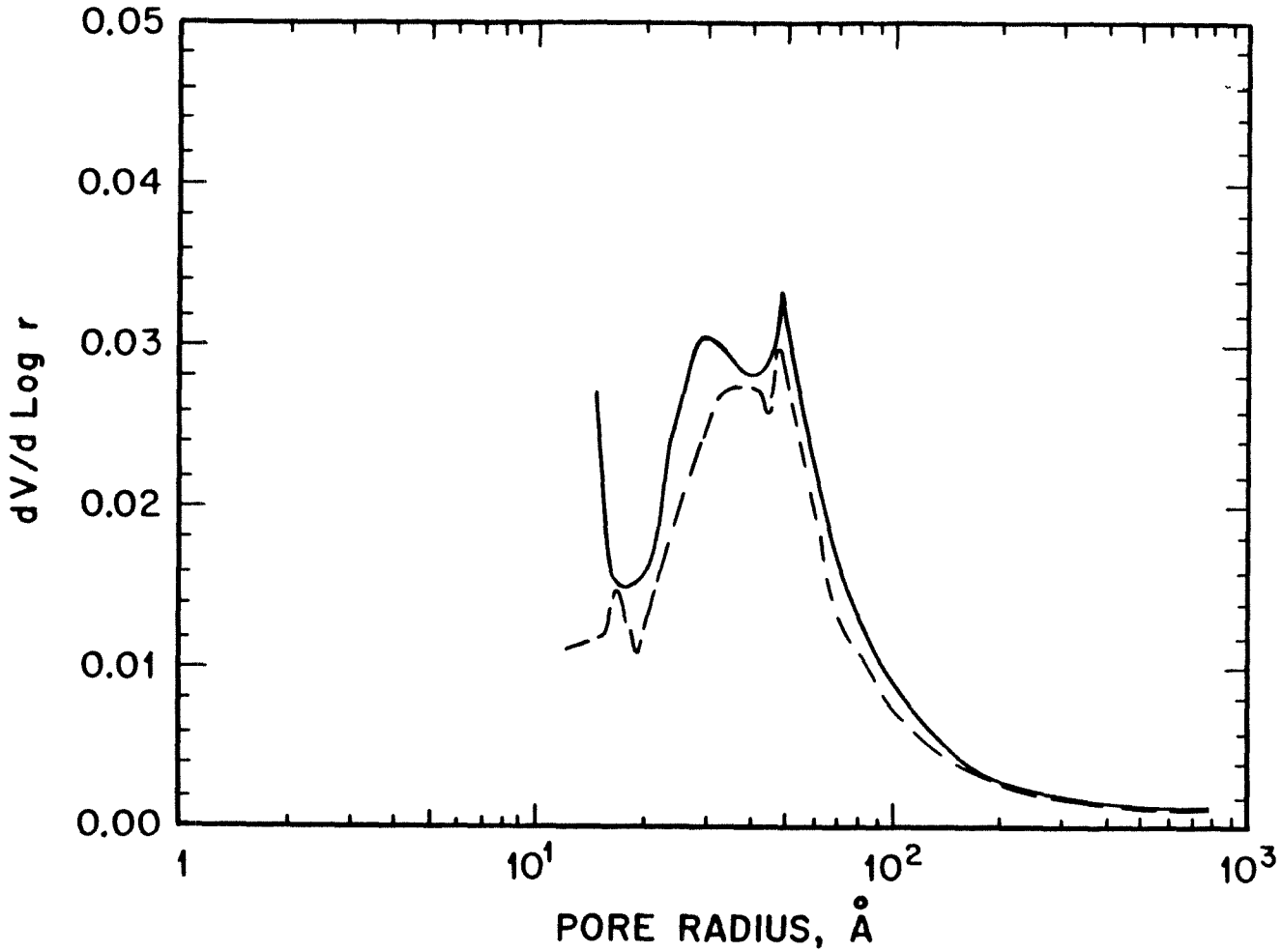

Figure AIII.11c Comparision of pore volume distributions of PSOC 190 coal by nitrogen using the Cranston-Inkley (—) and Modelless Inversions (- - -).

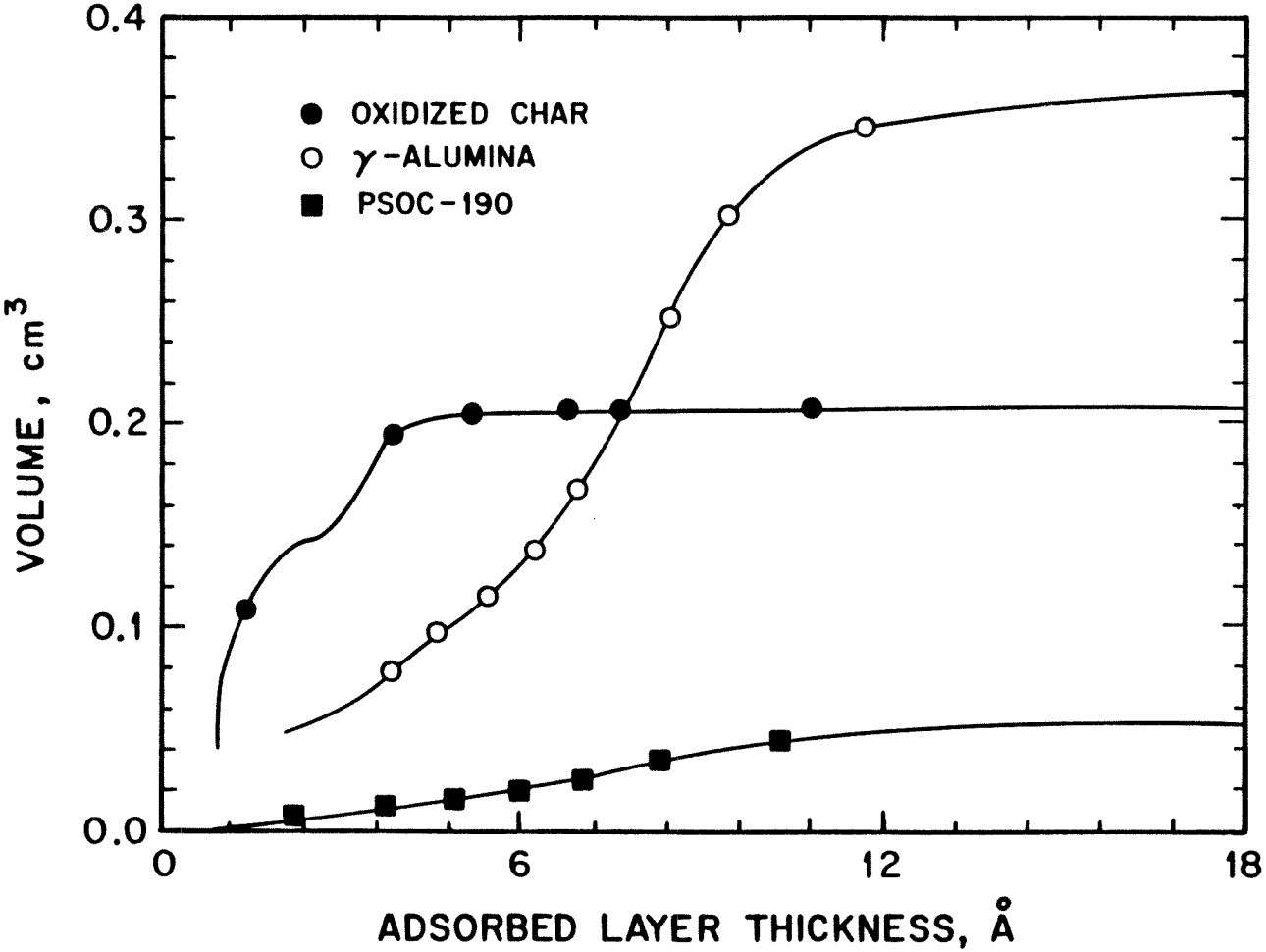

Figure AIII.12 V-t plots with nitrogen.

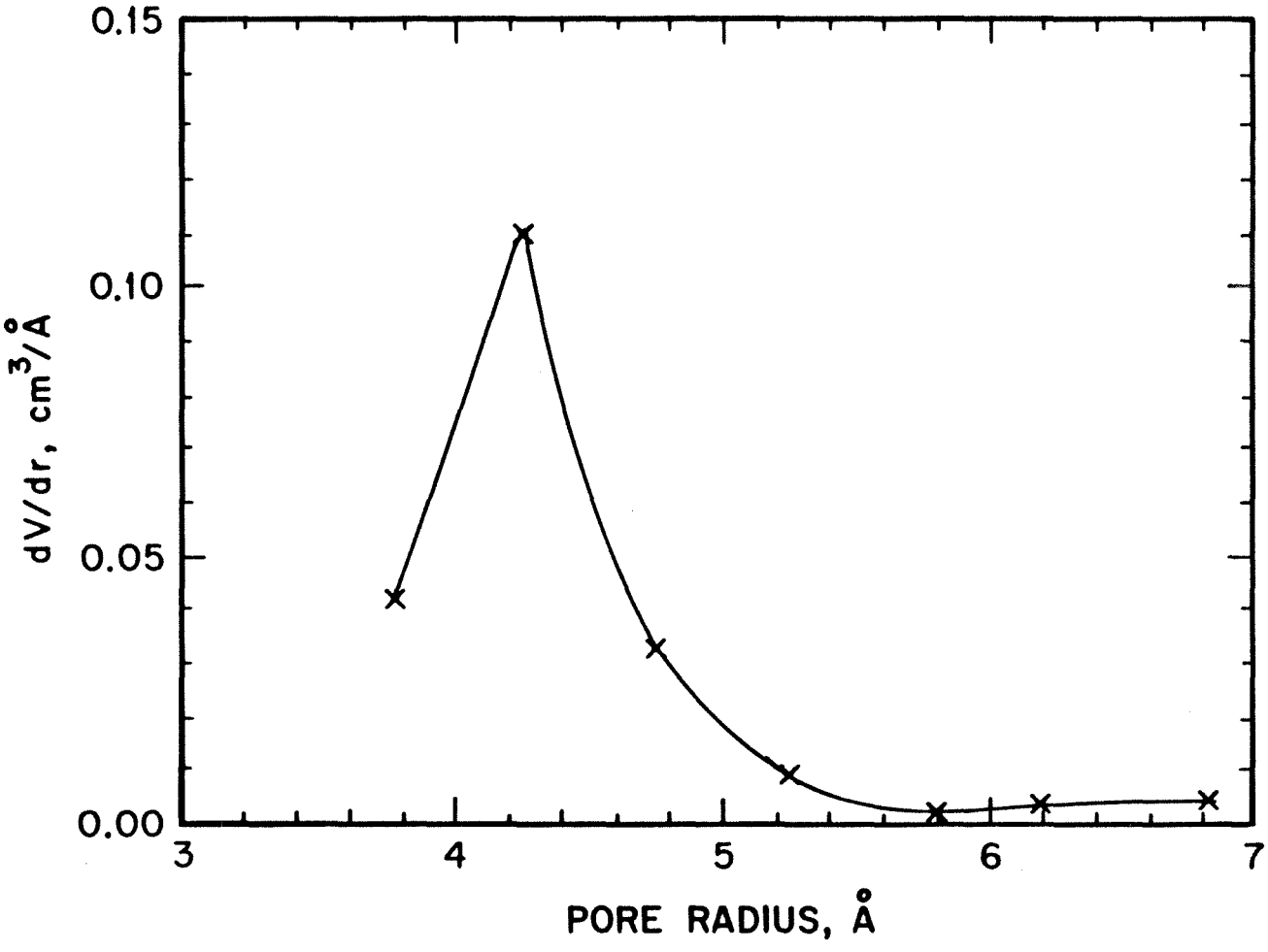

Figure AIII.13 MP distribution with nitrogen on oxidised char.

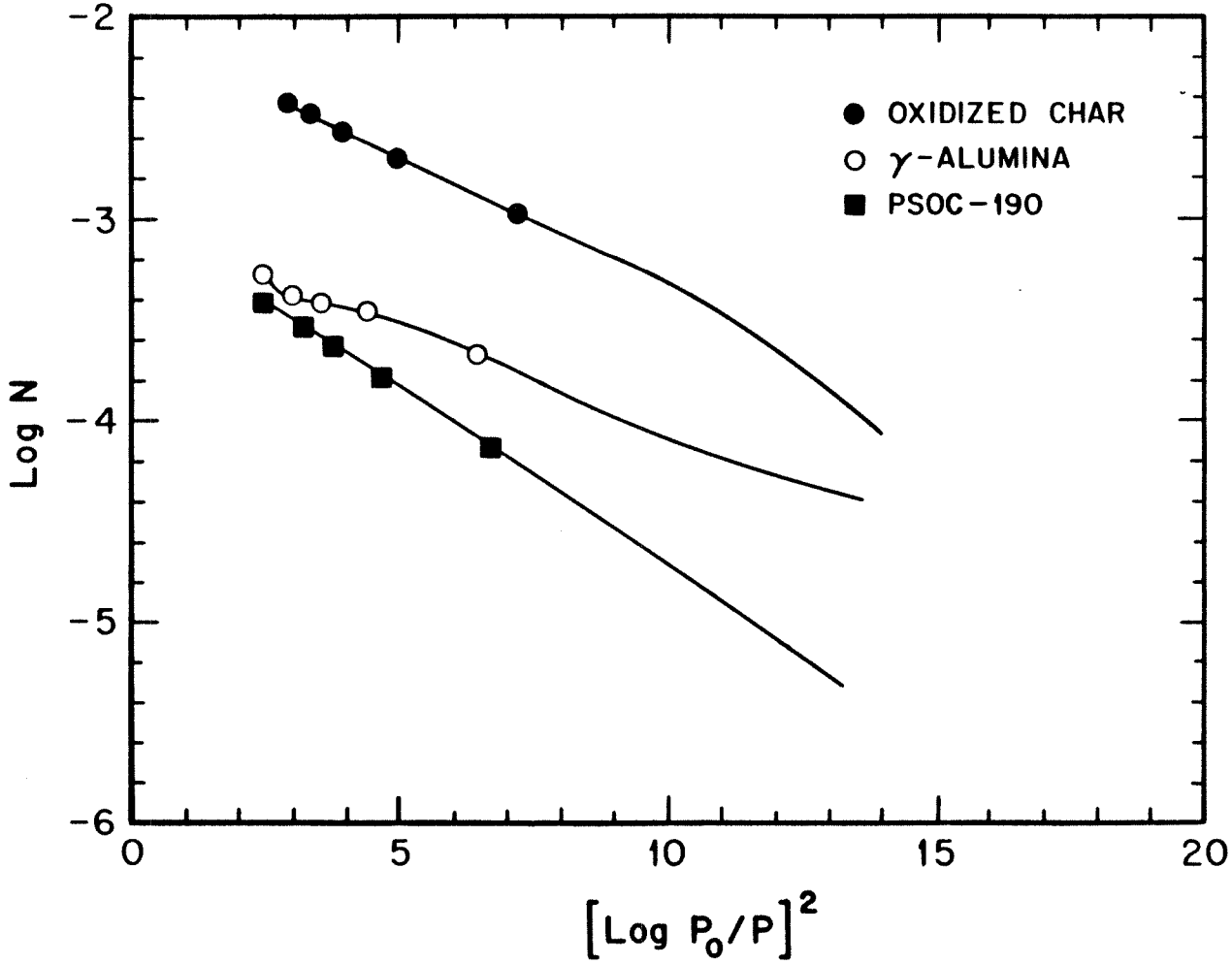

Figure AIII.14 DRK plots with nitrogen.

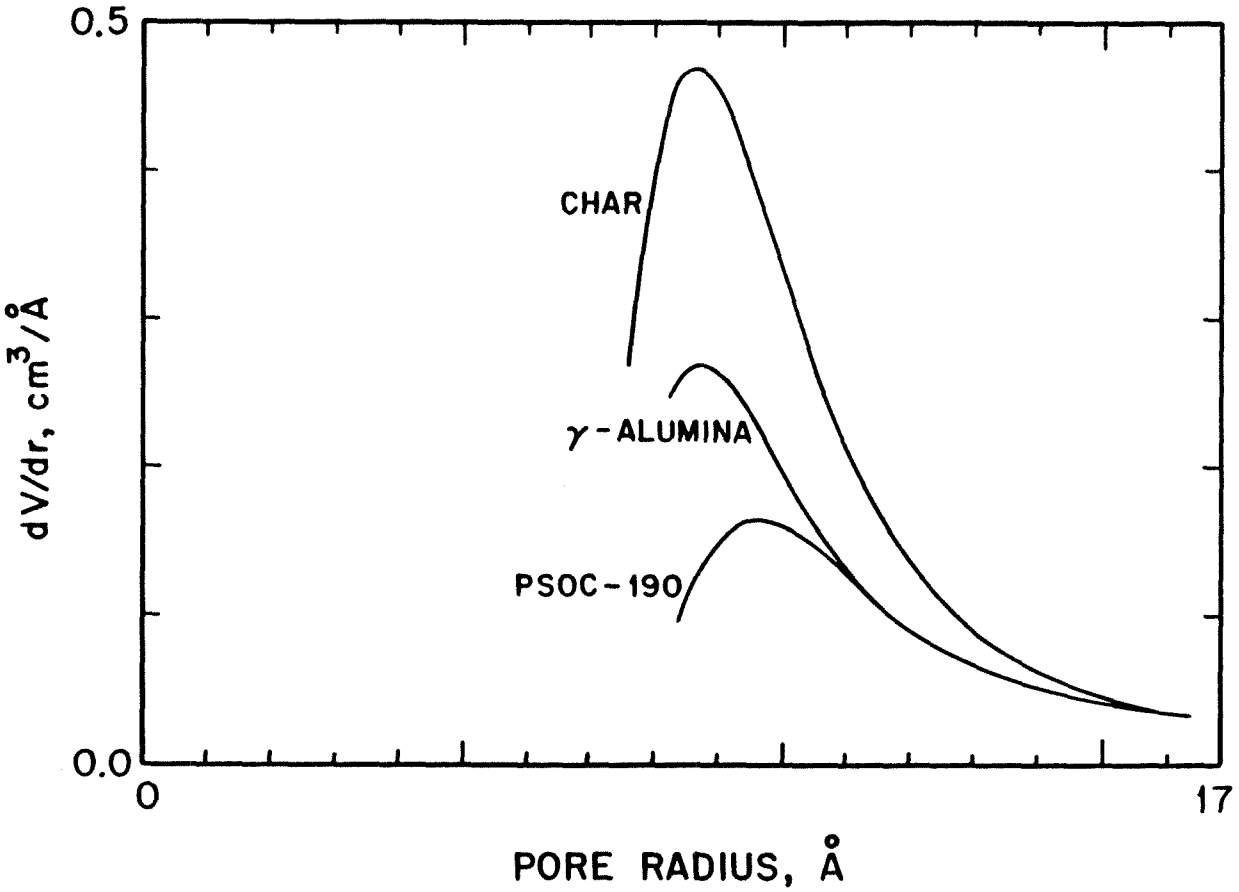

Figure AIII.15a Pore volume distributions of several solids using CO_2 at 196K and the Medek Inversion.

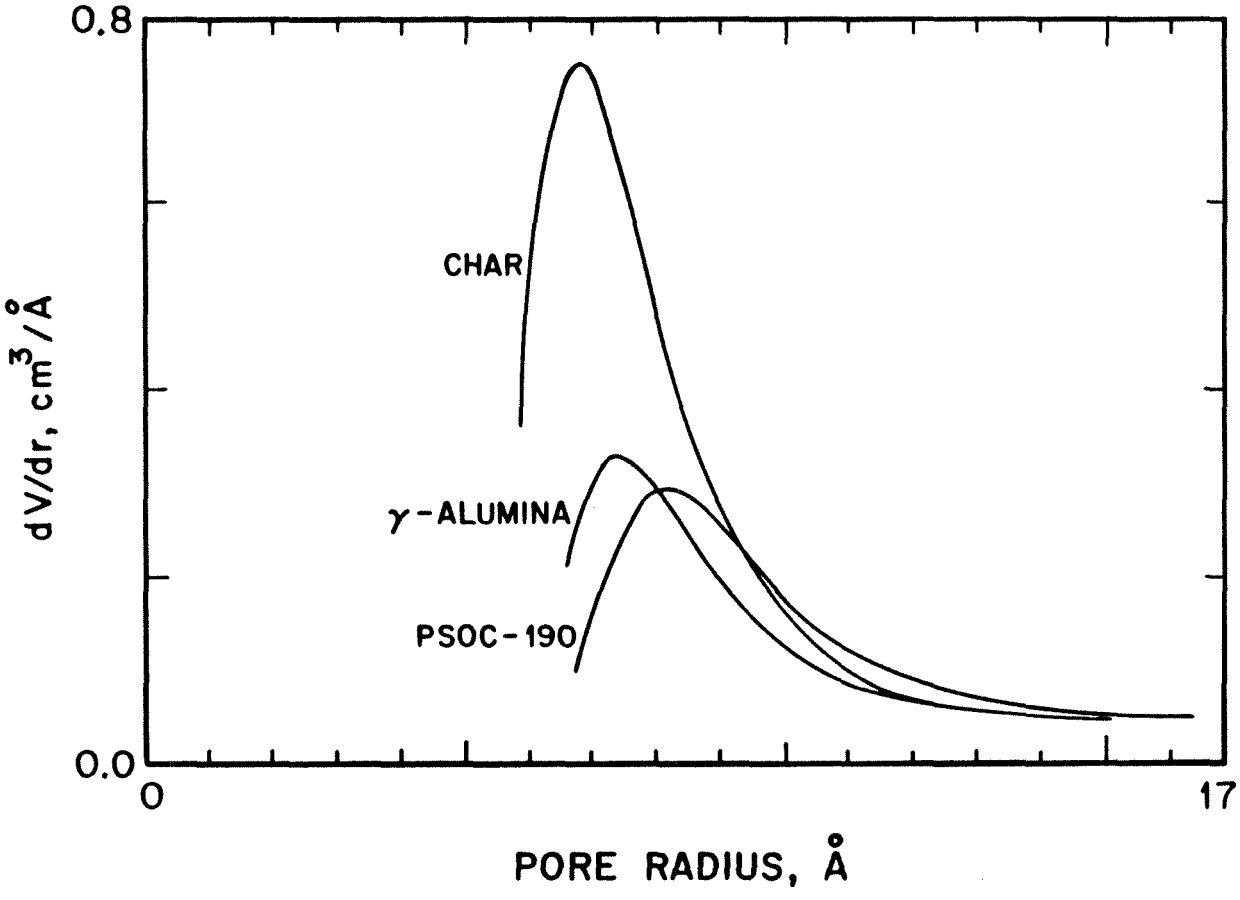

Figure AIII.15b Pore volume distributions of several solids using Freon and the Medek Inversion.

Appendix IV

HIGH TEMPERATURE REACTOR

EQUIPMENT DETAILS

AIV.1 Introduction

This appendix provides details, specifications, and other information on the construction of the high temperature reactor. Manufacturers' names, addresses and part numbers are also given.

The major components of the reactor are as follows: the structural frame, the air preheater furnace, power supply for the furnace, temperature controller, air preheater tube, test section, particle feeder, water-cooled particle injector, and particle collector probe. In addition, the following supporting equipment was used: the optical pyrometer, suction pyrometer, disappearing filament pyrometer, and the data acquisition system. Other minor parts include the vacuum pump, condenser unit, slide, various pressure gages, flowmeters, thermocouples, valves, cooling water lines and air lines.

The details of the electronic design of the pyrometer are described in Appendix II. The part numbers of the optical equipment will be given in this Appendix. The overall layout schematic of the system is shown in Figure AIV.1.

AIV.2 Structural Frame

The furnace and the test section are mounted on a steel frame that was designed and fabricated at Caltech. It is shown in Figure AIV.2. The structural members are angle iron, the various dimensions of which are shown in the figure. The joints are arc-welded for integrity. Levelling screws are provided to align the structure.

AIV.3 Air Preheater Furnace

This furnace was purchased from Applied Test Systems, Butler, PA 16003. It

is a series 3310 tube type furnace with a maximum temperature rating of 3000°F (1650°C). Its tube and external diameters are 4.5in (114.3mm) and 16in (406.4mm) respectively. Its height is 21in (533.4mm) inclusive of the insulation layers at the top and bottom. It uses 8 Kanthal Super 33 heating elements (Kanthal Corporation, Bethel, CT 06801) These 3/6 style elements are capable of prolonged service at temperatures as high as 3200°F (1760°C). The elements are 11in (279.4mm) long. The eight elements are connected in two parallel banks of four elements each.

The furnace has a single heating zone 11in (279.4mm) in length. The power required to run the furnace is 5.25kW at 58 volts (90.5amps). The insulation around the radiation cavity is a low "K" factor cast ceramic fiber, capable of service to 3000°F (1650°C). There is a thin stainless steel shell on the outside of the furnace with one thermocouple port via which the Type B control thermocouple (Pt-6%Rh/Pt-30%Rh) can be introduced into the heating zone.

The approximate heat-up time of the furnace, from room temperature to 1600°C is about 45 minutes.

AIV.4 Furnace Power Supply

The furnace power supply was procured from NWL Transformers, Bordentown, NJ 08505. The schematic of the transformer and the regulating system is shown in Figure AIV.3. The unit consists of a 8kW, single phase, 60Hz transformer with a Thyristor phase angle controller. For safety purposes, the unit is equipped with a current limiting device. The level of the output power is determined by the signal from the temperature controller (0-5V, D.C.). The magnitude of this signal depends on the difference between the control thermocouple signal and the desired

set temperature.

The whole unit is housed in a NEMA I enclosure designed to operate with natural convection cooling. Additional fan cooling is not necessary.

AIV.5 Temperature Controller

The temperature controller was purchased from Omega Engineering Inc., Stamford, CT 06907 (Part Number CN-2001A B-DC1). It is a microprocessor-based controller that accepts the voltage signal from the Type B thermocouple and generates a 0-5 volt D.C. signal. The magnitude of this signal depends on the difference between the thermocouple output and the furnace set temperature. The controller signal is sent to the power supply.

AIV.6 Air Preheater Tube

Primary air at room temperature is heated in the furnace heating zone before entering the test section. It flows through the heating zone in a cast ceramic tube made by the Carborundum Company, Keasbey, NJ 08832 (Matl: Refrax 20). It is 36in (914.4mm) long. Its internal and external diameters are 4in (101.6mm) and 4.5in (114.3mm) respectively. This tube is capable of withstanding high temperatures while maintaining reasonably high thermal conductivity at those temperatures. Moreover, since its radial thermal conductivity is much higher than its axial conductivity, there is not much heat loss to the outside.

AIV.7 Test Section

The actual test section, in which the char is mixed with the hot primary air and combusted, is a cylindrical hollow tube 12in (304.8mm) long with a 2in (50.8mm)

internal diameter. The wall thickness is 0.5in (12.7mm). It is made of light weight, high temperature (up to 1650°C), fibrous ceramic: ZAL 15 (85% alumina; 15% silica), supplied by Zircar Fibrous Ceramics, Florida, NY 10921. This material is very easily machinable.

In order to have optical access to the test section, two ground and polished plate quartz windows, 9in (228.6mm) long, 0.75in (19mm) wide, and 0.25in (6.4mm) thick are mounted in the walls of the ceramic tube diametrically opposite each other. The windows allow the light signal from the burning char particles to fall on the pyrometer detector and thereafter their temperature can be determined. The quartz plates were supplied by U.S. Fused Quartz (Brea, CA 92621). They are glued to the ceramic using high temperature alumina cement from Zircar Fibrous Ceramics (see address above).

AIV.8 Particle Feeder

This fluidized entrainment apparatus was designed and built at Caltech. A schematic diagram is shown in Figure AIV.4. The char sample to be injected into the furnace is put in a glass test-tube 6in (152.4mm) long with an internal diameter of 0.5in (12.7mm). The tube is then sealed from the top with an aluminum adaptor that allows entrainment air to be injected into the test-tube. This air flow rate is adjusted to give desired char feed rate. The entrained char then leaves the tube via a 0.125in (3.175mm) outer diameter steel tube that leads it directly into the test section. Since the level of the char in the test-tube decreases with time, the tube is mounted on a simple apparatus that moves it up at the desired rate so as to keep the level of char constant with respect to the lower edge of the entrainment tube.

This apparatus consists of a screw, powered by a small motor (0-120V, 1.5amp, 2000rpm) via pulleys and belts. The motor rpm is reduced significantly by two reduction gears with a combined ratio of 1:60. Motor speed control is achieved by controlling the input voltage using a simple transformer. All the small parts for this apparatus were obtained from Winifred M. Berg, Fort Rockaway, NY, 11518. The base and adaptor were machined at Caltech.

AIV.9 Particle Injector

The narrow tube carrying the char particles is introduced to the test section by passing it concentrically down the air preheater ceramic tube. To keep the char at room temperature, the injector tube is water cooled by a double water jacket. The length of the water cooled injector is 42in (1066.8mm). Its outer wall is then insulated using ZAL 15 insulating board cut to the proper geometry. Cooling water is introduced directly at the pressure of the mains, without using a pump. Since the volume of water needed is not significant, a open loop system is used, the waste water being returned to the drain. Diagrams of the injector are shown in Figures AIV.5a-c.

AIV.10 Particle Collector Probe

This is a triple jacket probe with an outer diameter of 1.0in (25.4mm) and an internal diameter of 0.5in (12.7mm). It can be moved to any axial location inside the test section tube in order to collect partially burned char at various carbon conversions. The two outer jackets carry cooling water. The innermost jacket provides a path for a quenching gas (nitrogen or argon) to be introduced along with the char so

that the chemical reaction is terminated immediately upon entry of the char into the probe. The quenching gas and the sample are drawn into the probe by suction provided by a vacuum pump. The char is collected on a glass fibre filter 47mm in diameter (Gelman, Type A/E). This filter sample is then removed and analyzed. The length of the probe is 22in (558.8mm). It is attached to a rack and pinion type axial slide. A diagram is shown in Figure AIV.6. The steel tubes for the probe and the injector were obtained from Tube Sales, Los Angeles, CA 90040.

AIV.11 Pyrometers

The design of the Optical Pyrometer has been described earlier. The optical rails, carriers, lens holders, and posts were obtained from Newport Corporation, Fountain Valley, CA 92708. The lenses, beam splitter, and precision pin holes were from Melles Griot, Irvine, CA 92714. The filters, beam probes, and optical fibres were brought from Oriel Corporation, Stratford, CT 06497. The linear positioning slides were manufactured by Daedal Corporation (Harrison City, PA 15636). Two such stages (Model 4804 M) were used at right angles to give precise control in the X and Y directions. A 24in (609.6mm) vertical slide was built at Caltech and used as the adjustable Z axis. The various parts, part numbers and the suppliers are listed in Table AIV.1.

The suction pyrometer was designed and built at Caltech. It uses a Type S thermocouple (Omega Engineering Inc.)

The disappearing filament pyrometer was used to find the temperature of a fairly dense stream of particles. This was used to verify the temperature obtained from the optical pyrometer.

AIV.12 Additional Minor Equipment

These include the vacuum pump, condenser unit, pressure gages, flow meters, thermocouples, valves, cooling water lines, air and gas lines, and the exhaust hood.

The condenser unit was fabricated and built to extract any condensed moisture in the line before it passed through the vacuum pump. Various flow meters were used to monitor the flow rates of the primary, entrainment, and dilution gas streams. Matheson flow meters (Dwyer Instruments Inc., Anaheim, CA 92806) as well as pressure drop flow meters were used. The latter were used for their flexibility. Pressure gages were from Dwyer (Magnahelic type). While 0.25in *poly-flo* lines were used for the gas lines, water lines were of copper. The exhaust hood was fabricated at Caltech.

AIV.13 Data Acquisition

The light intensity signals from the burning char particles were converted to voltage signals in the optical pyrometer. After suitable noise filtering and amplification, these signals were sent to the data acquisition system. This consists of a Zenith 148 Personal Computer with 640K RAM and two 360K floppy drives. The computer was equipped with a 8087-2 math co-processor for speed. For data acquisition purposes, it was equipped with an A/D converter and a Data Translation DT-2801A board rated at 20kHz. Data from the pyrometer was dumped via DMA into the computer's RAM and later retrieved for analysis. Finally, software programs written in Fortran-77 were used to convert the data into temperature measurements. Suitable calibration data was used at this point.

PART NAME	PART NUMBER	MANUFACTURER
Filters	57670, 57750	Oriel Corp.
Beam Probes	77646	Oriel Corp.
Fused Silica Lens	41254	Oriel Corp.
Plano-Convex Lens	01 LPX 219	Melles Griot
Plano-Convex Lens	01 LPX 113	Melles Griot
Plano-Convex Lens	01 LPX 041	Melles Griot
Cube Beam Splitter	03 BSC 029	Melles Griot
Precision Pin Holes	04 PIP 013	Melles Griot
Optical Rails	MRL-6, MRL-12	Newport Corp.
Carriers	MTC, MTF	Newport Corp.
Lens Holders	LH1-P, LH1-1	Newport Corp.
Lens Mounts	LM-1	Newport Corp.
Posts	MSP-1	Newport Corp.
Post Holders	MPH-1	Newport Corp.
Silicon Photodiodes	S1336-5BQ	Hamamatsu Corp.
Linear Slides	4804 M	Daedal Corp.

Table AIV.1 Details of the Optical Pyrometer components.

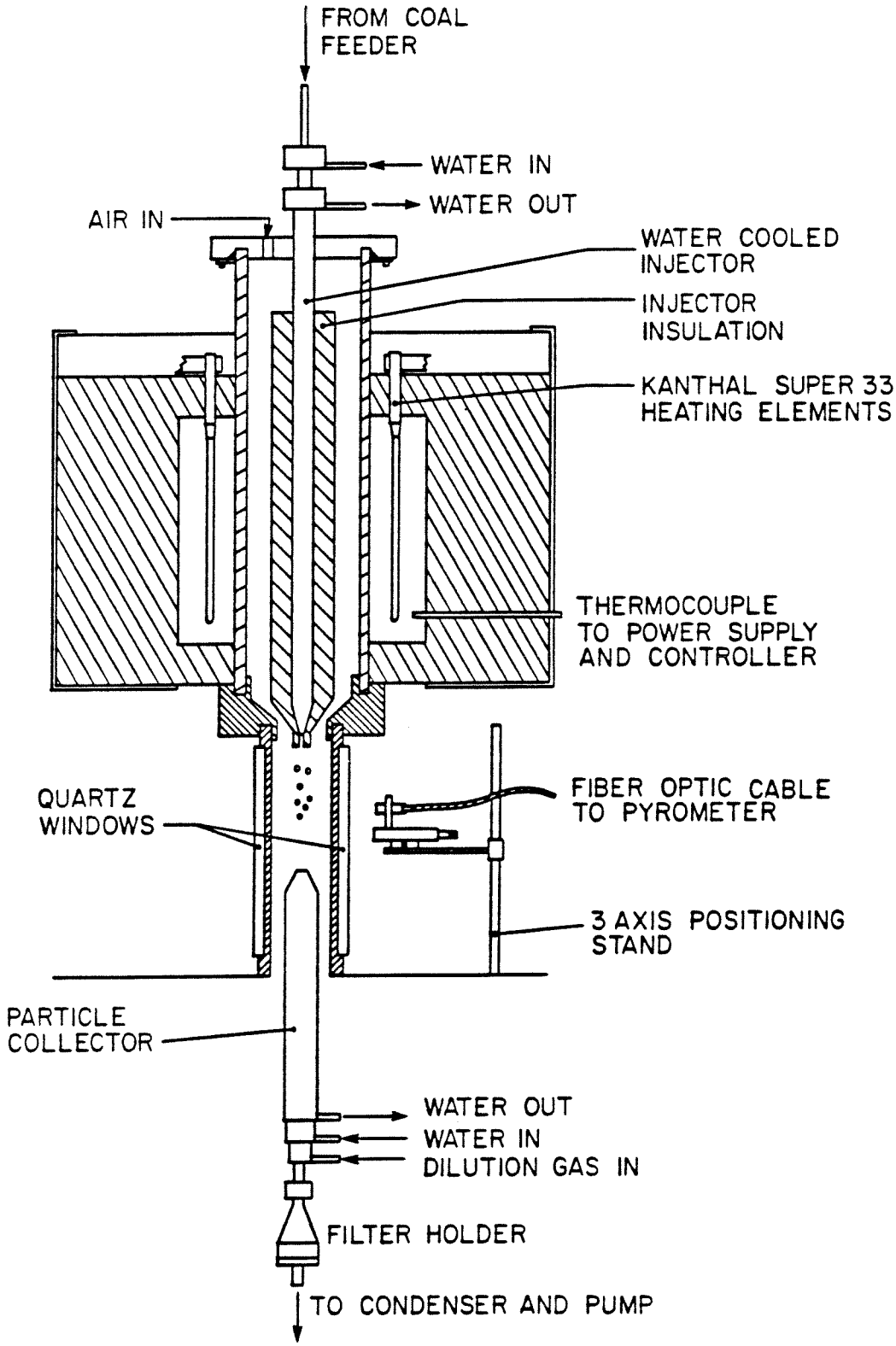

Figure AIV.1 Schematic of the high temperature reactor.

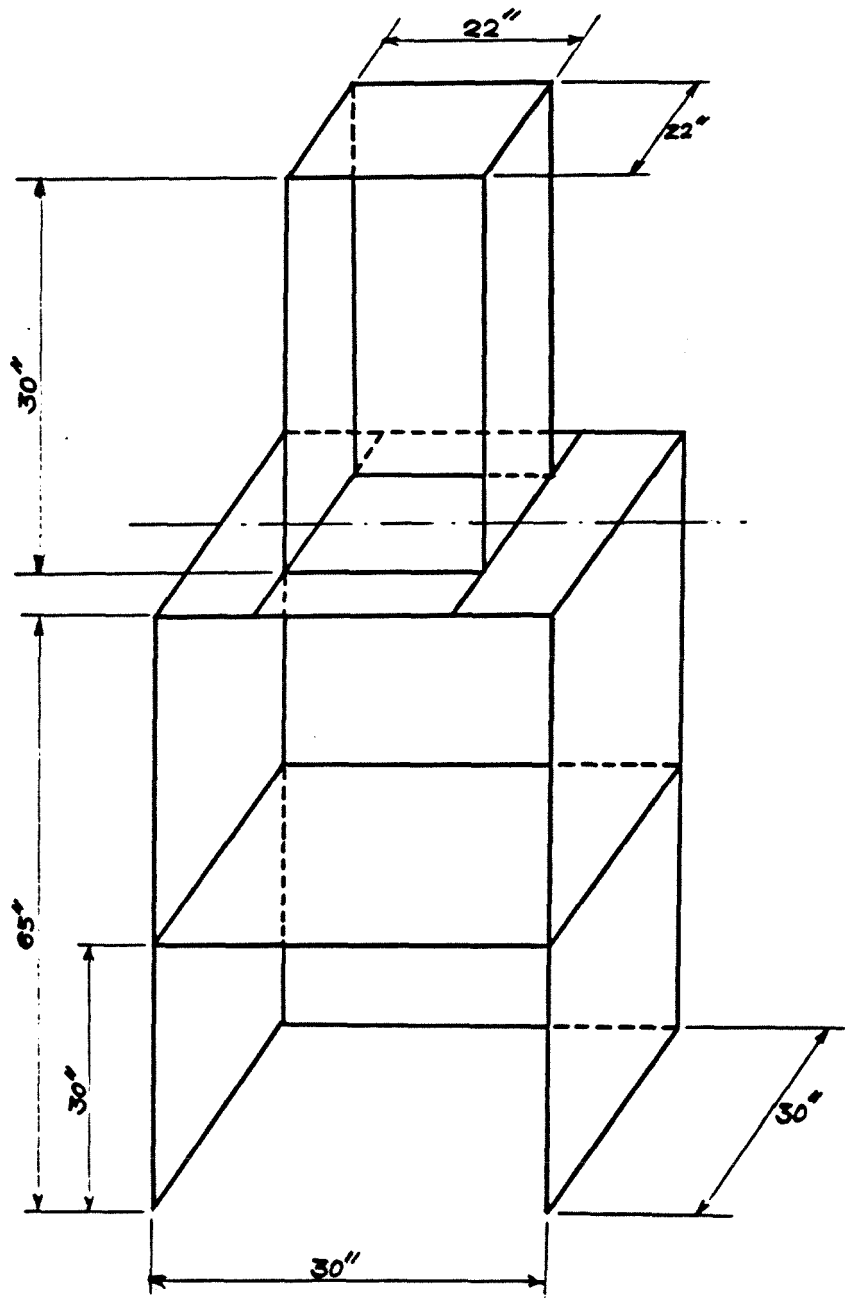

Figure AIV.2 Structural frame for the high temperature reactor.

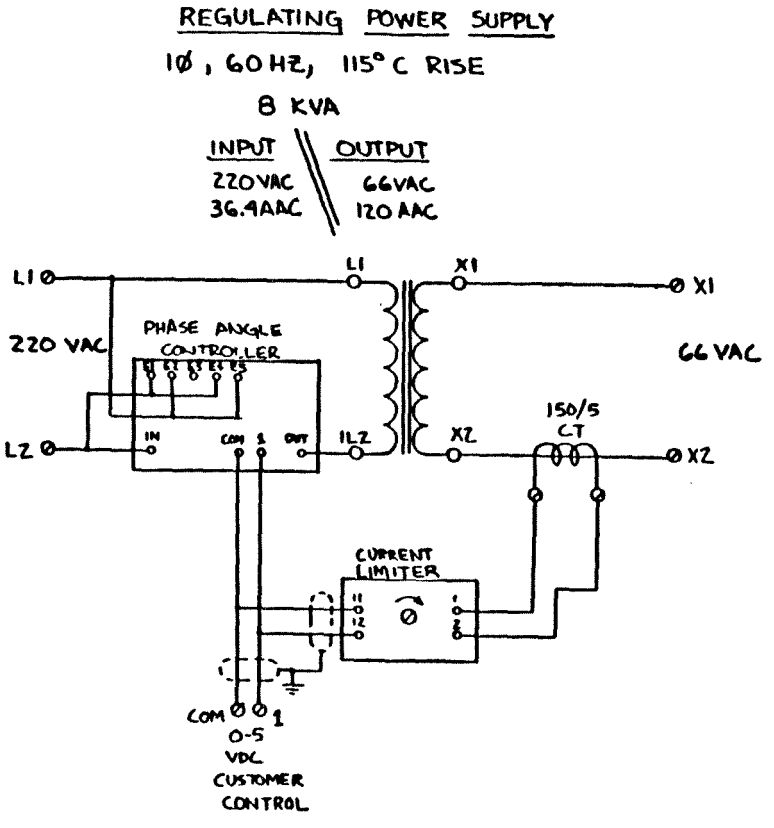

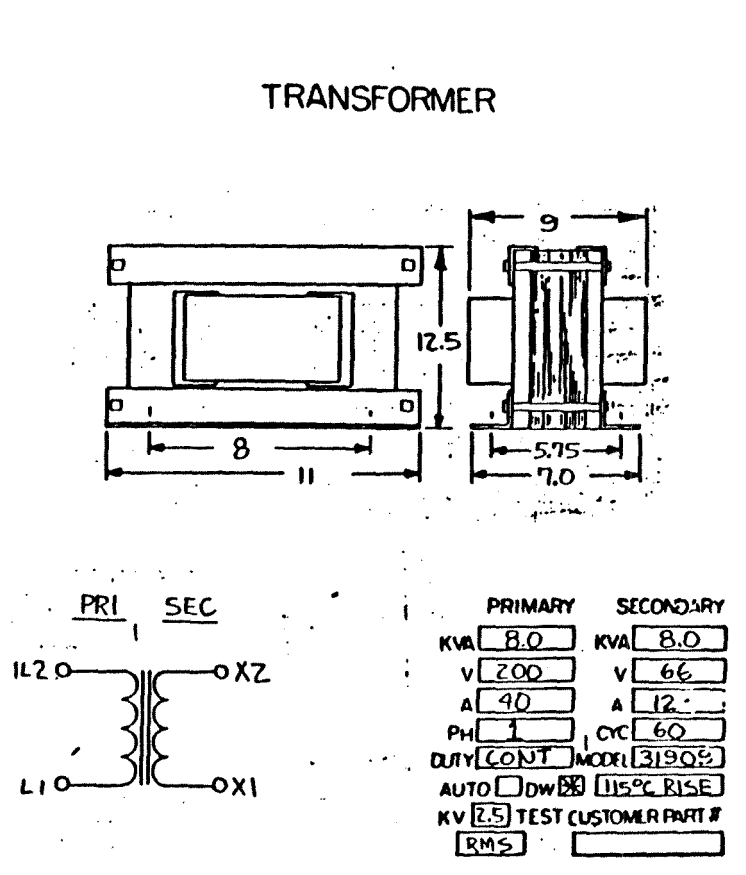

Figure AIV.3 High temperature reactor power supply schematic.

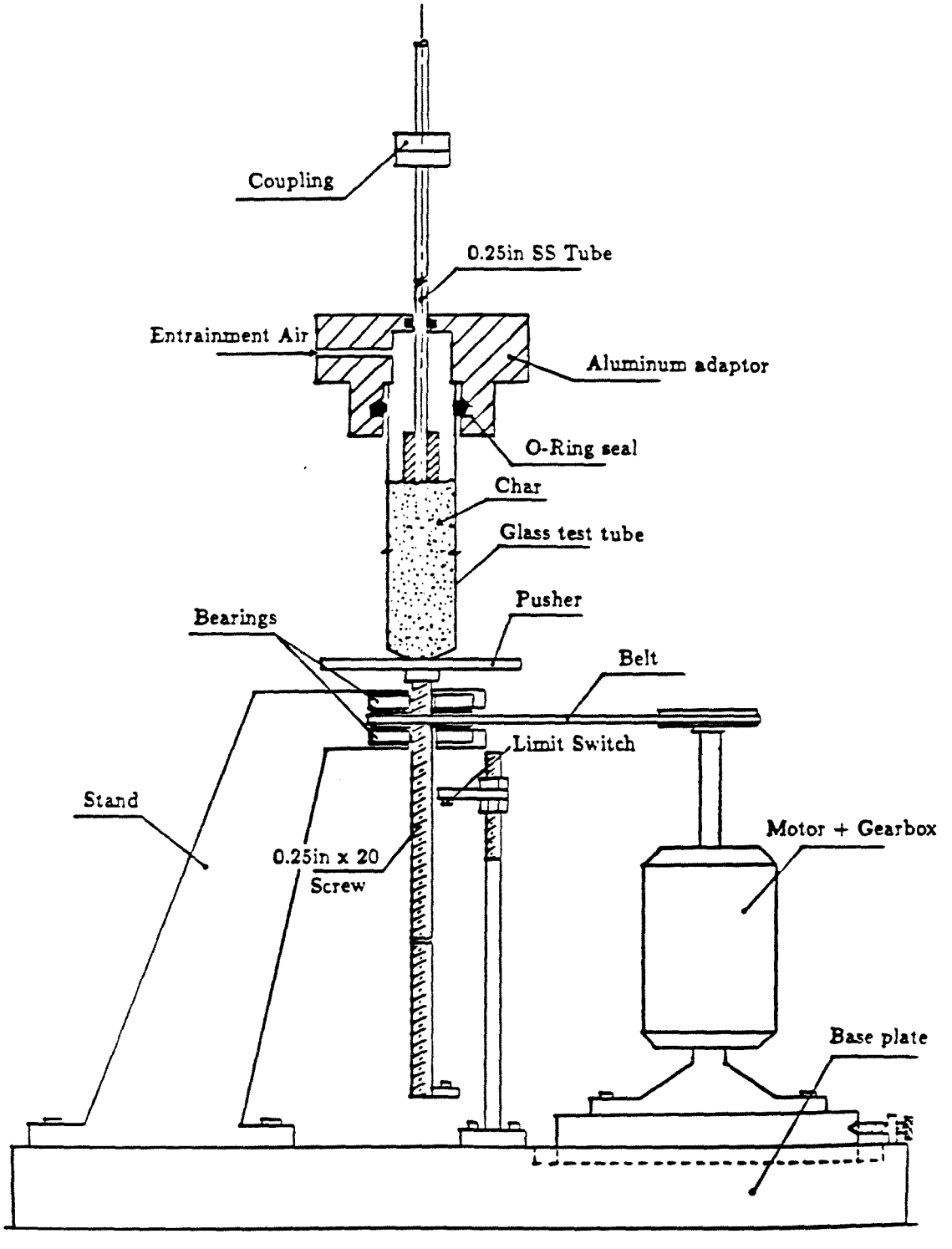

Figure AIV.4 Schematic of the char particle feeder.

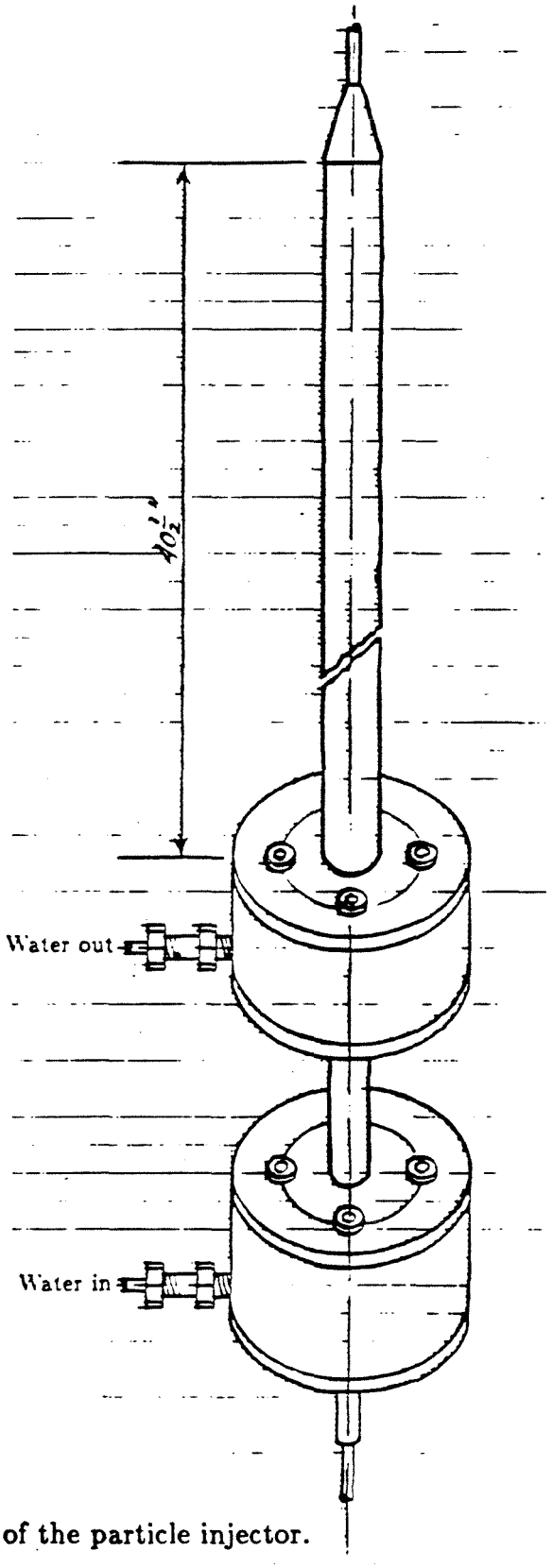

Figure AIV.5a Schematic of the particle injector.

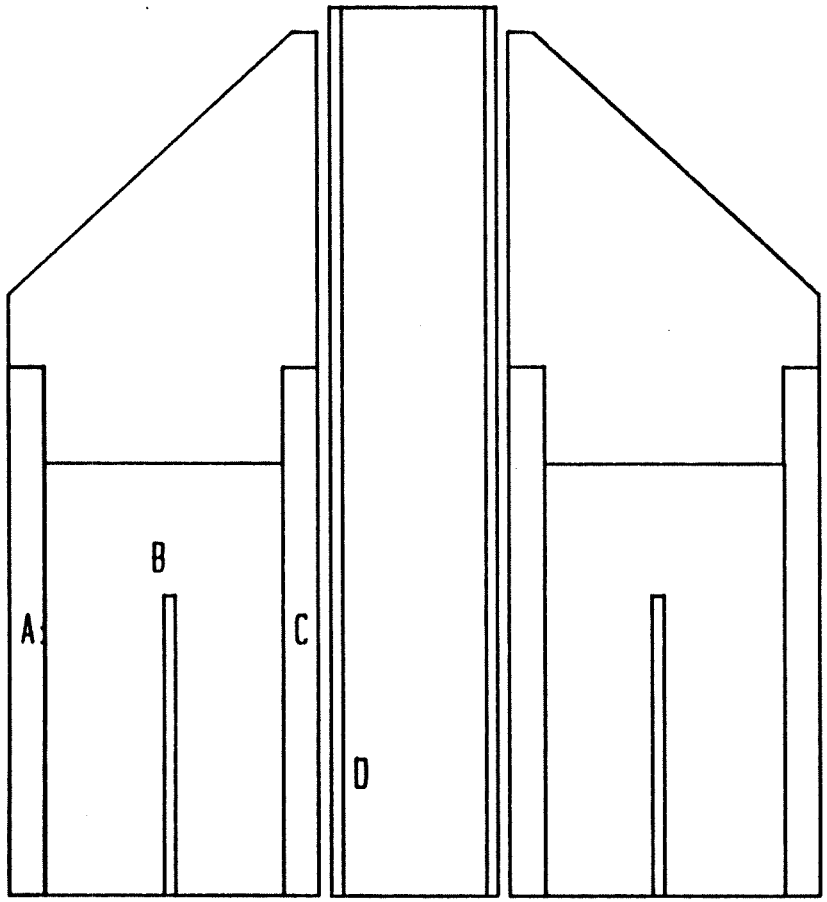

Figure AIV.5b Detail of particle injector nozzle.

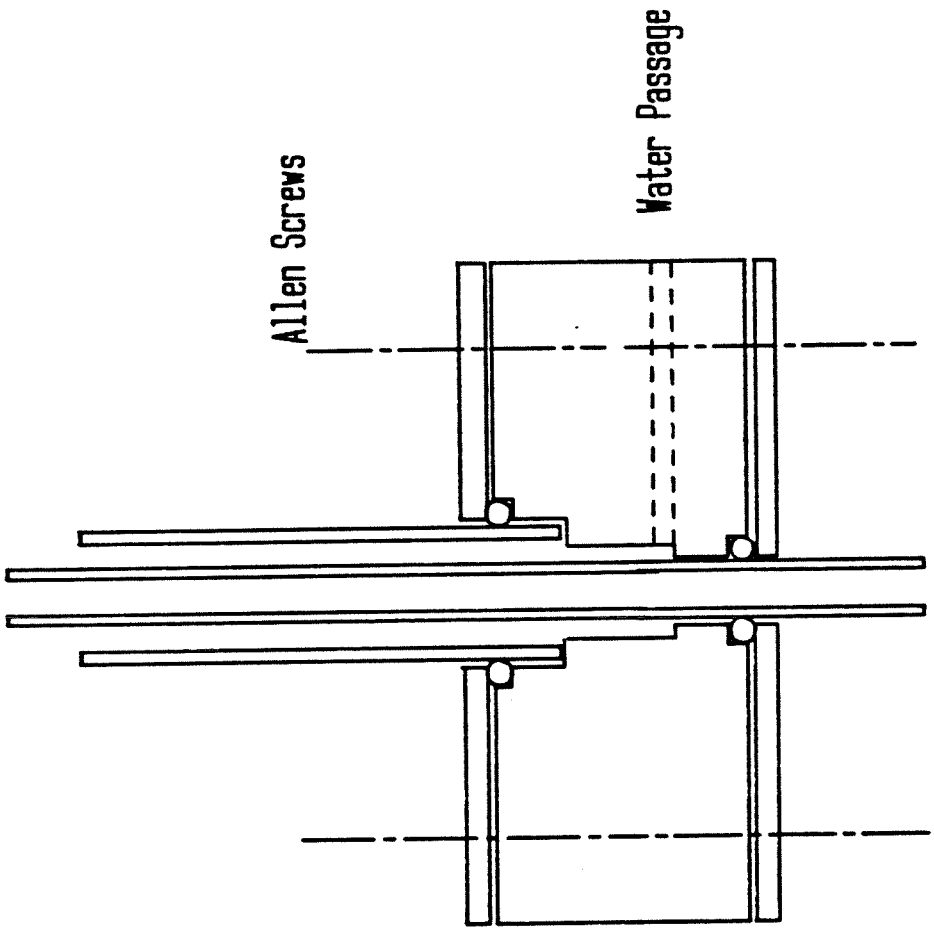

Figure AIV.5c Detail of a cooling water adaptor at injector base.

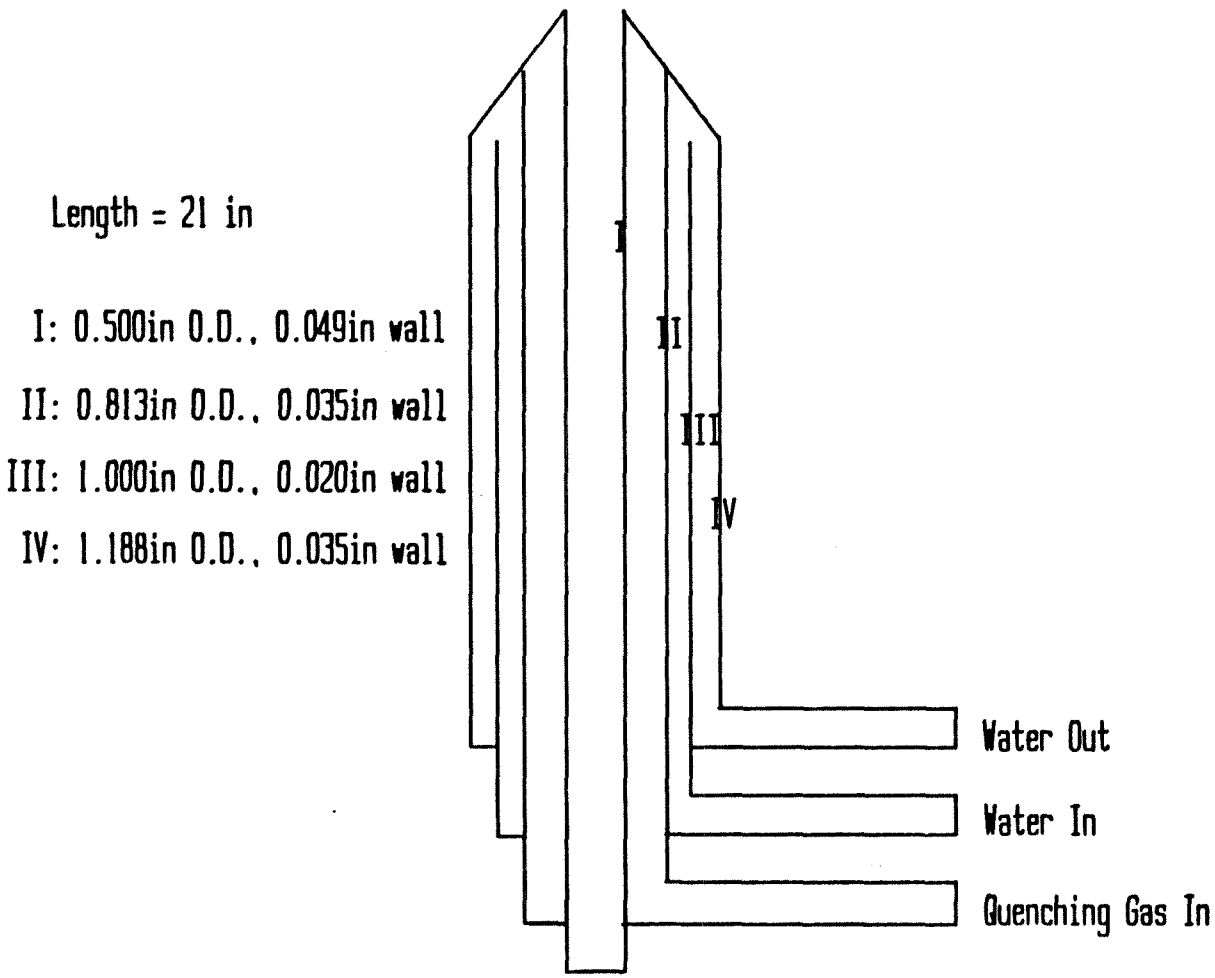

Figure AIV.6 Schematic of the char particle collector.

Appendix V

PROGRAMS FOR GAS ADSORPTION EXPERIMENTS

This Appendix gives the listings of the various computer programs used in the data acquisition and interpretation of gas adsorption data.

Two similar but distinct systems were used for the gas adsorption experiments. Both systems were used to determine BET surface areas, pore volume distributions, and densities of various char samples. Basically this involved monitoring the pressure in the sample volume as a function of time (data points every 10 seconds or so) for a period of approximately two hours. The speed of data acquisition was not important. In each system, an analog pressure signal (0-5V) from the pressure transducer was first digitized and then stored in the computer.

The first system used a DASCON1 data acquisition board manufactured by Metrabyte Corporation, Taunton, MA 02780. It was driven by a Zenith 150 series PC. The other system used a Zenith 148 series PC to drive a DT2801-A board made by Data Translation Inc., Marlborough, MA 01752. The specifications of both boards are given in Table AV.1.

Software programs provided by the respective manufacturers were modified to adapt them to the existing hardware. The modified driver programs for the DASCON1 and DT2801-A boards are RT2.BAS and GETBET.BAS, respectively. Once the raw data are obtained, further manipulation is carried out according to the scheme shown in Figure AV.1. The relevant program listings follow.

	DT2801-A	DASCON1
A/D Inputs	16SE/8DI	4SE/4DI
A/D Resolution	12-bits	12-bits
Voltage Input	±10V	±2V
Prog. Gain	1,2,4,8	No
A/D Throughput	27.5kHz	30Hz
D/A Channels	2	2
D/A Resolution	12-bits	12-bit
D/A Throughput	33kHz	30Hz
Digital I/O	16 lines	12 lines
Screw panel	DT707	STA01
DMA	Yes	No
Prog. Clock	Yes	Yes
Ext. Trigger	Yes	Yes

Table AV.1 Specifications of the Data Acquisition Boards.

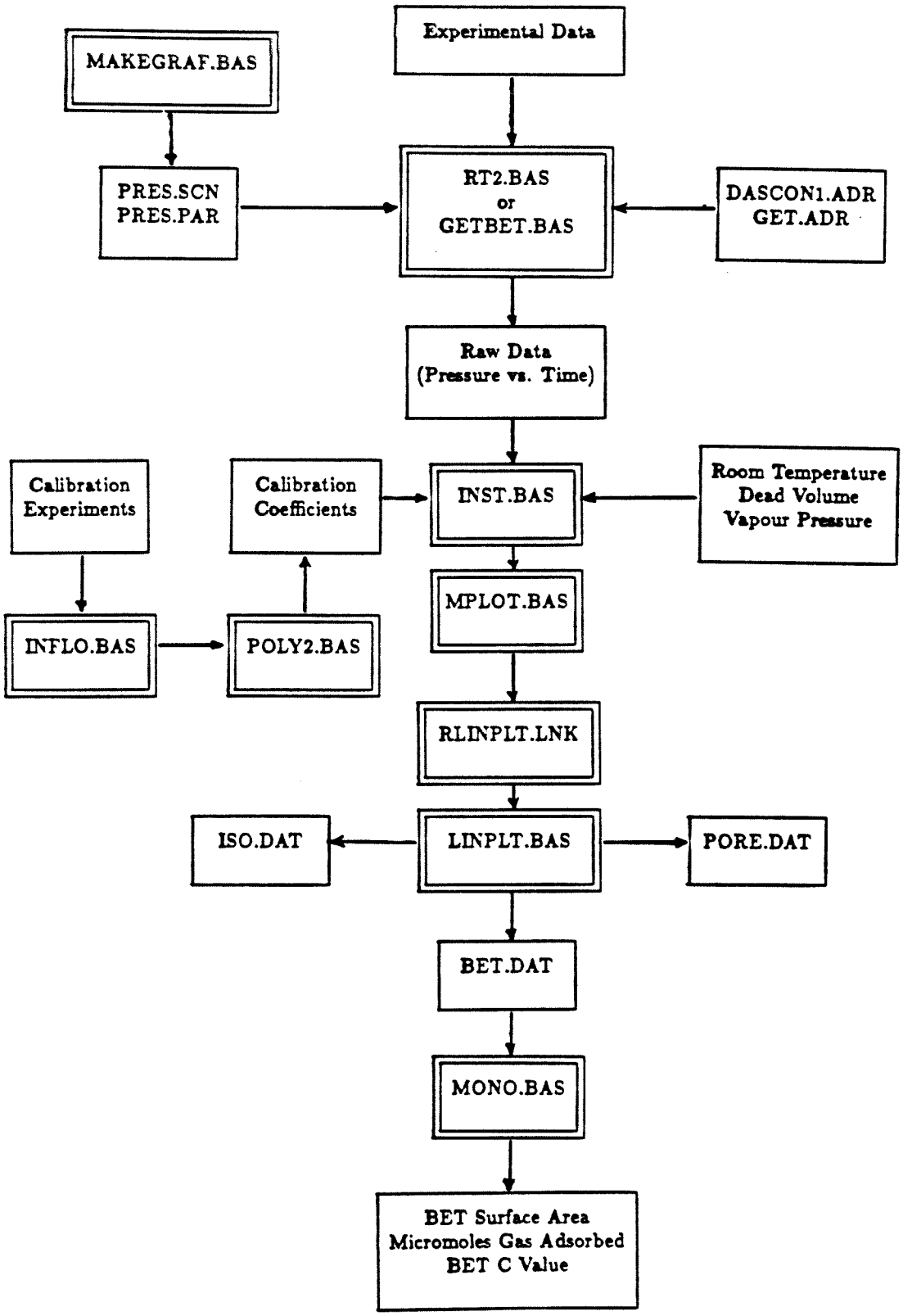

Figure AV.1 Flow Diagram for the analysis of gas adsorption experiments.

AV.1 RT2.BAS

```
10 '          REAL TIME PLOTTING AND LOGGING PROGRAM
20 '
30 'This program drives the METRABYTE DASCON1 data acquisition system. Note
40 'that the DEF SEG values occuring here had to be changed to accomodate
50 'the ZENITH 152 PC. This program allows the user to select which A/D
60 'are to be displayed for real-time plotting on the screen. The user
70 'may also store data from each channel in user-specified files.
80 'The program requires a *.SCN file plus a *.PAR file which are created
90 'by MAKEGRAF.BAS. It also requires the presence of LINPLT.BAS, RLINPLT.LNK
100 'DASCON1.ADR and DASCON1.BIN.
110 '
120 CLEAR, 32768!
130 N = 6 * 60 * 5          'size of storage arrays.
140 '
150 KEY OFF
160 TRUE = 1:FAL = 0
170 CLS:SCREEN 0,0,0
180 PRINT "       ———— REAL TIME ANALOG I/O PLOT ————
190 LOCATE 5,1
200 INPUT "ENTER SCREEN FILE AS [dsk:] filename (no extension)  ";FILX$
210 IF FILX$ = "" THEN 170
220 LOCATE 8,1
230 DIM C%(4)
240 PRINT "       ———— CHANNEL(S) TO BE DISPLAYED ————
250 PRINT
260 INPUT "              CHANNEL 0 (Yes or No) " ;CH0$
270 IF MID$(CH0$,1,1)="Y" THEN C%(0)=TRUE ELSE C%(0)=FAL
280 INPUT "              CHANNEL 1 (Yes or No) " ;CH1$
290 IF MID$(CH1$,1,1)="Y" THEN C%(1)=TRUE ELSE C%(1)=FAL
300 INPUT "              CHANNEL 2 (Yes or No) " ;CH2$
310 IF MID$(CH2$,1,1)="Y" THEN C%(2)=TRUE ELSE C%(2)=FAL
320 INPUT "              CHANNEL 3 (Yes or No) " ;CH3$
330 IF MID$(CH3$,1,1)="Y" THEN C%(3)=TRUE ELSE C%(3)=FAL
340 LOCATE 16,1:PRINT SPACE$(78);:LOCATE 16,1
350 INPUT "ENTER SCAN RATE IN SECONDS [1 to 3600]  ";SCANRATE%
360 IF SCANRATE% < 1 OR SCANRATE% > 3600 THEN 340
370 '
380 'Setup the display and load the display program and scale parameters.
390 '
400 DEF SEG = &H2000
410 BLOAD "DASCON1.BIN",0
420 DASCON1 = 0
430 DIM DIO%(8)                          'data array ANALOG I/O
440 MD% = 0                             'free scan mode 4 channels
450 OPEN "I",#1,"DASCON1.ADR":INPUT #1,BASADD%:CLOSE #1 'base address
460 CH% = 0                             'not used in mode 0
```

```
470 '
480 'Load the screen display and set the parameters for data scaling
490 '
500 CLS:SCREEN 2
510 DEF SEG = &HB800                        'graphics display segment
520 BLOAD FILX$+".SCN"                      '.SCN is the screen display
530 DEF SEG
540 OPEN FILX$+".PAR" AS #1 LEN=30          'parameter file for .SCN
550 FIELD #1,15 AS PARX$, 15 AS PARY$       'single prescion fields
560 GET #1,1
570 SX = CVS(PARX$):SY = CVS(PARY$)         'scale factors
580 GET #1,2
590 DX = CVS(PARX$):DY = CVS(PARY$)         'slope variables for axis
600 GET #1,3
610 X2 = CVS(PARX$):Y2 = CVS(PARY$)         'X,Y maximum values on graph
620 GET #1,4
630 X1 = CVS(PARX$):Y1 = CVS(PARY$)         'X,Y minimum values on graph
640 GET #1,5
650 QX = CVS(PARX$):QY = CVS(PARY$)         'X,Y screen scale factor
660 GET #1,6
670 OX = CVS(PARX$):OY = CVS(PARY$)         'graph starting point
680 GET #1,7
690 XA = CVS(PARX$):YA = CVS(PARY$)         'data positional scale factors
700 GET #1,8
710 XE = CVS(PARX$):YE = CVS(PARY$)         'scale x,y resolution
720 CLOSE #1
740 '
750 'This is the section where the data is scanned and plotted for each
760 'channel.  The display sets a different graphic character for each
770 'channel. This is added to the screen on line 23.
780 '
800 DIM OUT0%(N) , TIME%(N) , OUT1%(N) , OUT2%(N) , OUT3%(N)
810 STIME$ = TIME$:SDATE$ = DATE$           'start time/date
820 LOCATE 23,10:PRINT "START TIME IS ";STIME$;"  START DATE IS ";SDATE$;
830 LOCATE 25,1:PRINT SPACE$(78);:LOCATE 25,1
840 PRINT "F1 = SAVE SCREEN      F2 = END";
850 ON KEY(1) GOSUB 1200
860 ON KEY(2) GOSUB 1580
870 KEY(1) ON:KEY(2) ON
880 '
890 'One second delay loop
900 '
910 DEF SEG = SG
920 XAXIS =0
930 GOTO 1000
950 FOR SECDLY% = 1 TO SCANRATE%
960 TEMT$=RIGHT$(TIME$,2)
970 IF RIGHT$(TIME$,2)=TEMT$ THEN GOTO 970
980 NEXT SECDLY%
```

```
990 '
1000 DEF SEG = &H2000
1010 CALL DASCON1 (MD%, CH%, DIO%(0), DIO%(8), BASADD%)
1020 FOR I = 0 TO 3
1030 IF C%(I) = FALSE THEN 1110
1040 PS = 1
1050 X = XA + SX * XAXIS *SCANRATE%
1060 Y = YA - SY * DIO%(I)
1070 IF X < 9 OR Y < 9 THEN PS = 0
1080 IF X > 271 OR Y > 151 THEN PS = 0
1090 IF PS = 0 THEN 1110
1100 CIRCLE (QX*X+OX,QY*Y+OY),I
1110 NEXT I
1120 XAXIS = XAXIS + 1
1130 IF XAXIS = 32766 THEN GOTO 1580
1140 TIME%(XAXIS) = (XAXIS - 1) * SCANRATE%
1150 OUT0%(XAXIS) = DIO%(0)
1160 OUT1%(XAXIS) = DIO%(1)
1170 OUT2%(XAXIS) = DIO%(2)
1180 OUT3%(XAXIS) = DIO%(3)
1190 GOTO 950
1200 LOCATE 25,1:PRINT SPACE$(78);:LOCATE 25,1
1210 INPUT ;"ENTER SCREEN NAME AS [dsk:] filename (no extension) - ";SFLX$
1220 OPEN SFLX$+".PAR" AS #1 LEN=30
1230 FIELD #1,15 AS PARX$,15 AS PARY$
1240 FOR XX%=1 TO 14:LSET PARX$ ="XXX":LSET PARY$ ="YYY"
1245 PUT #1,XX%:NEXT XX%: CLOSE #1
1250 OPEN SFLX$+".PAR" AS #1 LEN=30
1260 FIELD #1,15 AS PARX$,15 AS PARY$
1270 LSET PARX$ = MKS$(SX)
1280 LSET PARY$ = MKS$(SY)
1290 PUT #1,1
1300 LSET PARX$ = MKS$(DX)
1310 LSET PARY$ = MKS$(DY)
1320 PUT #1,2
1330 LSET PARX$ = MKS$(X2)
1340 LSET PARY$ = MKS$(Y2)
1350 PUT #1,3
1360 LSET PARX$ = MKS$(X1)
1370 LSET PARY$ = MKS$(X2)
1380 PUT #1,4
1390 LSET PARX$ = MKS$(QX)
1400 LSET PARY$ = MKS$(QY)
1410 PUT #1,5
1420 LSET PARX$ = MKS$(OX)
1430 PUT #1,6
1440 LSET PARX$ = MKS$(XA)
1450 LSET PARY$ = MKS$(YA)
1460 PUT #1,7
```

```
1470 XE = 1/ABS(X2-X1):LSET PARX$ = MKS$(XE)
1480 XE = 1/ABS(Y2-Y1):LSET PARY$ = MKS$(YE)
1490 PUT #1,8
1500 CLOSE #1
1510 LOCATE 25,1:PRINT SPACE$(78);:LOCATE 25,1
1520 DEF SEG = &HB800                    'screen buffer
1530 BSAVE SFLX$+".SCN",0,&H4000         '16 k buffer
1540 DEF SEG
1550 PRINT "FILE ";SFLX$;"SAVED  HIT ANY KEY TO GO ON";:LOCATE 20,1
1560 KX$ = INKEY:IF KX$ = "" THEN 1560
1570 RETURN 1580
1580 LOCATE 25,1:PRINT SPACE$(78);:LOCATE 25,1
1590 PRINT "       TERMINATED AT  ";TIME$;" ON  ";DATE$;:LOCATE 23,1
1595 '
1597 'This is the part of the program which stores the data on disk.
1598 'Note that channel 3 is automatically stored.
1599 '
1600 KEY(1) OFF:KEY(2) OFF
1610 CLS:SCREEN 0,0,0
1620 LOCATE 1,1
1630 INPUT "Should output from channel 0 be stored on disk  : ";RESP$
1640 IF RESP$ = "n" GOTO 1840
1650 LOCATE 3,1
1660 INPUT "Enter name of storage data file [dsk:]filename.dat";FILDAT0$
1670 OPEN FILDAT0$ AS #1 LEN = 30
1680 FIELD #1, 15 AS X$, 15 AS Y$
1690 LOCATE 5,1
1700 INPUT "Line, Dot or No plot mode (L,D,N) ? ";A$
1710 IF A$="L" OR A$="l" THEN M=1:GOTO 1750
1720 IF A$="N" OR A$="n" THEN M=2:GOTO 1750
1730 IF A$="D" OR A$="d" THEN M=0:GOTO 1750
1740 LOCATE 11,1:PRINT"RE-ENTER":LOCATE 9,1:PRINT SPC(79):GOTO 1690
1750 CLS:LOCATE 12,24:PRINT"STORING DATA ON DISK"
1760 LSET X$ = MKS$(XAXIS):LSET Y$=MKS$(M)
1770 PUT #1,1
1780 FOR I=2 TO XAXIS+1
1790 LSET X$=MKS$(TIME%(I-1)):LSET Y$=MKS$(OUT0%(I-1))
1800 PUT #1,I
1810 NEXT I
1820 CLOSE #1
1830 CLS
1840 LOCATE 3,1
1850 INPUT "Should output from channel 1 be stored on disk.  " ;RESP$
1860 IF RESP$ = "n" GOTO 2060
1870 LOCATE 5,1
1880 INPUT "Enter name of storage data file [dsk:]filename.dat";FILDAT1$
1890 OPEN FILDAT1$ AS #1 LEN = 30
1900 FIELD #1, 15 AS X$, 15 AS Y$
1910 LOCATE 7,1
```

```
1920 INPUT "Line, Dot or No plot mode (L,D,N) ? ";A$
1930 IF A$="L" OR A$="l" THEN M=1:GOTO 1970
1940 IF A$="N" OR A$="n" THEN M=2:GOTO 1970
1950 IF A$="D" OR A$="d" THEN M=0:GOTO 1970
1960 LOCATE 11,1:PRINT"RE-ENTER":LOCATE 9,1:PRINT SPC(79):GOTO 1910
1970 CLS:LOCATE 12,24:PRINT"STORING DATA ON DISK"
1980 LSET X$ = MKS$(XAXIS):LSET Y$=MKS$(M)
1990 PUT #1,1
2000 FOR I=2 TO XAXIS+1
2010 LSET X$=MKS$(TIME%(I-1)):LSET Y$=MKS$(OUT1%(I-1))
2020 PUT #1,I
2030 NEXT I
2040 CLOSE #1
2050 CLS
2060 LOCATE 5,1
2070 INPUT "Should output from channel 2 be stored on disk.  " ;RESP$
2080 IF RESP$ = "n" GOTO 2290
2090 LOCATE 7,1
2100 INPUT "Enter name of storage data file [dsk:]filename.dat";FILDAT1$
2110 OPEN FILDAT1$ AS #1 LEN = 30
2120 FIELD #1, 15 AS X$, 15 AS Y$
2130 LOCATE 9,1
2140 INPUT "Line, Dot or No plot mode (L,D,N) ? ";A$
2150 IF A$="L" OR A$="l" THEN M=1:GOTO 2190
2160 IF A$="N" OR A$="n" THEN M=2:GOTO 2190
2170 IF A$="D" OR A$="d" THEN M=0:GOTO 2190
2180 LOCATE 11,1:PRINT"RE-ENTER":LOCATE 9,1:PRINT SPC(79):GOTO 2140
2190 CLS:LOCATE 12,24:PRINT"STORING DATA ON DISK"
2200 LSET X$ = MKS$(XAXIS):LSET Y$=MKS$(M)
2210 PUT #1,1
2220 FOR I = 2 TO XAXIS+1
2230 LSET X$=MKS$(TIME%(I-1)): LSET Y$=MKS$(OUT2%(I-1))
2240 PUT #1,I
2250 NEXT I
2260 CLOSE #1
2270 CLS
2280 LOCATE 9,1
2290 PRINT "Output from channel 3 will be stored on disk. "
2300 LOCATE 10,1
2310 INPUT "Enter name of storage data file [dsk:]filename.dat";FILDAT1$
2320 OPEN FILDAT1$ AS #1 LEN = 30
2330 FIELD #1, 15 AS X$, 15 AS Y$
2340 INPUT "Line, Dot or No plot mode (L,D,N) ? ";A$
2350 IF A$="L" OR A$="l" THEN M=1:GOTO 2390
2360 IF A$="N" OR A$="n" THEN M=2:GOTO 2390
2370 IF A$="D" OR A$="d" THEN M=0:GOTO 2390
2380 LOCATE 11,1:PRINT"RE-ENTER":LOCATE 9,1:PRINT SPC(79):GOTO 2340
2390 CLS:LOCATE 12,24:PRINT"STORING DATA ON DISK"
2400 LSET X$ = MKS$(XAXIS):LSET Y$=MKS$(M)
```

```
2410 PUT #1,1
2420 FOR I=2 TO XAXIS+1
2430 LSET X$=MKS$(TIME%(I-1)):LSET Y$=MKS$(OUT3%(I-1))
2440 PUT #1,I
2450 NEXT I
2460 CLOSE #1
2470 CLS:LOCATE 12,28:PRINT"DONE":LOCATE 25,1
2480 END
```

AV.2 GETBET.BAS

```
10 '      SLOW REAL TIME PLOTTING AND LOGGING PROGRAM
20 '                FEBRUARY 20 1986
30 '
40 'This program drives the DATA TRANSLATION board DT 2801-A on the
50 'Zenith 148 system. It is used to obtain data from the SETRA Digital
60 'Pressure Gage for gas adsorption measurements. It plots the data
70 'points (pressure as a function of time) in real time on screen using
80 'MAKEGRAF.BAS which makes PRES.SCN and PRES.PAR. It acquires data
90 'from 8 A/D channels by sequentially scanning them. Data from selected
100 'channels can be stored in user defined files.
110 '
120 '
130  CLEAR, 32768!
140  N = 360    'size of storage array for actual input data.
150  '
160  GAIN(0)=1: GAIN(1)=2: GAIN(2)=4: GAIN(3)=8
170  ADSCHANNEL=0: ADECHANNEL=7
180  NCONVERSIONS#=8
190  '
200  INPUT "A/D GAIN (TYPE 0,1,2 OR 3)";ADGAIN
210  IF ADGAIN < 0 THEN GOTO 200
220  IF ADGAIN > 3 THEN GOTO 200
230  '
240  KEY OFF
250  TRUE=1: FAL=0
260  CLS:SCREEN 0,0,0
270  PRINT "        ———— REAL TIME ANALOG I/O PLOT ————
280  LOCATE 5,1
290  INPUT "ENTER SCREEN DISPLAY FILE [dsk:] filename (no extension)  ";FILX$
300  IF FILX$ = "" THEN 260
310  LOCATE 8,1
320  DIM C%(8)
330  PRINT "        ———— CHANNEL(S) TO BE DISPLAYED ————
340  PRINT
350  INPUT "              CHANNEL 0 (Yes or No) " ;CH0$
360  IF MID$(CH0$,1,1)="Y" THEN C%(0)=TRUE ELSE C%(0)=FAL
370  INPUT "              CHANNEL 1 (Yes or No) " ;CH1$
380  IF MID$(CH1$,1,1)="Y" THEN C%(1)=TRUE ELSE C%(1)=FAL
390  INPUT "              CHANNEL 2 (Yes or No) " ;CH2$
400  IF MID$(CH2$,1,1)="Y" THEN C%(2)=TRUE ELSE C%(2)=FAL
410  INPUT "              CHANNEL 3 (Yes or No) " ;CH3$
420  IF MID$(CH3$,1,1)="Y" THEN C%(3)=TRUE ELSE C%(3)=FAL
430  INPUT "              CHANNEL 4 (Yes or No) " ;CH4$
440  IF MID$(CH4$,1,1)="Y" THEN C%(4)=TRUE ELSE C%(4)=FAL
450  INPUT "              CHANNEL 5 (Yes or No) " ;CH5$
460  IF MID$(CH5$,1,1)="Y" THEN C%(5)=TRUE ELSE C%(5)=FAL
```

```
470  INPUT "              CHANNEL 6 (Yes or No) " ;CH6$
480  IF MID$(CH6$,1,1)="Y" THEN C%(6)=TRUE ELSE C%(6)=FAL
490  INPUT "              CHANNEL 7 (Yes or No) " ;CH7$
500  IF MID$(CH7$,1,1)="Y" THEN C%(7)=TRUE ELSE C%(7)=FAL
510  LOCATE 20,1:PRINT SPACE$(78);:LOCATE 20,1
520  INPUT "ENTER SCAN RATE IN SECONDS [1 to 3600]  ";SCANRATE%
530  IF SCANRATE% < 1 OR SCANRATE% > 3600 THEN 510
540  '
550  'Setup the display and load the display program and scale parameters.
560  '
570  DEF SEG = &H2000
580  OPEN "I",#1,"GET.ADR":INPUT #1,BASADD%:CLOSE #1 'boards base address
590  '
600  'Load the screen display and set the parameters for data scaling
610  '
620  CLS:SCREEN 2
630  DEF SEG = &HB800                    'graphics display segment
640  BLOAD FILX$+".SCN"                   '.SCN is the screen display
650  DEF SEG
660  OPEN FILX$+".PAR" AS #1 LEN=30        'parameter file for .SCN
670  FIELD #1,15 AS PARX$, 15 AS PARY$     'single prescion fields
680  GET #1,1
690  SX = CVS(PARX$):SY = CVS(PARY$)       'scale factors
700  GET #1,2
710  DX = CVS(PARX$):DY = CVS(PARY$)       'slope variables for axis
720  GET #1,3
730  X2 = CVS(PARX$):Y2 = CVS(PARY$)       'X,Y maximum values on graph
740  GET #1,4
750  X1 = CVS(PARX$):Y1 = CVS(PARY$)       'X,Y minimum values on graph
760  GET #1,5
770  QX = CVS(PARX$):QY = CVS(PARY$)       'X,Y screen scale factor
780  GET #1,6
790  OX = CVS(PARX$):OY = CVS(PARY$)       'graph starting point
800  GET #1,7
810  XA = CVS(PARX$):YA = CVS(PARY$)       'data positional scale factors
820  GET #1,8
830  XE = CVS(PARX$):YE = CVS(PARY$)       'scale x,y resolution
840  CLOSE #1
850  '
860  '
870  'This is the section where the data is scanned and plotted for each
880  'channel. The display sets a different graphic character for each
890  'channel. This is added to the screen on line 23.
900  '
910  '
920  DIM OUT0%(N) , TIME%(N) , OUT1%(N) , OUT2%(N) , OUT3%(N)
930  DIM OUT4%(N),OUT5%(N),OUT6%(N),OUT7%(N),ADH%(8),ADL%(8)
940  STIME$ = TIME$:SDATE$ = DATE$         'start time/date
950  LOCATE 23,10:PRINT "START TIME IS  ";STIME$;" START DATE IS  ";SDATE$;
```

```
960  LOCATE 25,1:PRINT SPACE$(78);:LOCATE 25,1
970  PRINT "F1 = SAVE SCREEN      F2 = END";
980  ON KEY(1) GOSUB 1370
990  ON KEY(2) GOSUB 1760
1000  KEY(1) ON:KEY(2) ON
1010  '
1020  'One second delay loop
1030  '
1040  DEF SEG = SG
1050  XAXIS =0
1060  GOTO 1130
1070  'Start loop :
1080  FOR SECDLY% = 1 TO SCANRATE%
1090  TEMT$=RIGHT$(TIME$,2)
1100  IF RIGHT$(TIME$,2)=TEMT$ THEN GOTO 1100
1110  NEXT SECDLY%
1120  '
1130  DEF SEG = &H2000
1140  GOSUB 3570
1150  FOR I = 0 TO 7
1160    IF C%(I) = FAL THEN 1240
1170    PS = 1
1180    X = XA + SX * XAXIS * SCANRATE%
1190    Y = YA - SY * (ADL%(I+1)+ ADH%(I+1) * 256)
1200    IF X < 9 OR Y < 9 THEN PS = 0
1210    IF X > 271 OR Y > 151 THEN PS = 0
1220    IF PS = 0 THEN 1240
1230    CIRCLE (QX* X+OX,QY* Y+OY),I
1240  NEXT I
1250  XAXIS = XAXIS + 1
1260  IF XAXIS = 32766 THEN GOTO 1760
1270  TIME%(XAXIS) = (XAXIS - 1) * SCANRATE%
1280  OUT0%(XAXIS) = ADL%(1)+ADH%(1)* 256
1290  OUT1%(XAXIS) = ADL%(2)+ADH%(2)* 256
1300  OUT2%(XAXIS) = ADL%(3)+ADH%(3)* 256
1310  OUT3%(XAXIS) = ADL%(4)+ADH%(4)* 256
1320  OUT4%(XAXIS) = ADL%(5)+ADH%(5)* 256
1330  OUT5%(XAXIS) = ADL%(6)+ADH%(6)* 256
1340  OUT6%(XAXIS) = ADL%(7)+ADH%(7)* 256
1350  OUT7%(XAXIS) = ADL%(8)+ADH%(8)* 256
1360  GOTO 1080
1370  LOCATE 25,1:PRINT SPACE$(78);:LOCATE 25,1
1380  INPUT ;"ENTER SCREEN NAME AS [dsk:] filename (no ext.) -- ";SFLX$
1390  OPEN SFLX$+".PAR" AS #1 LEN=30
1400  FIELD #1,15 AS PARX$,15 AS PARY$
1410  FOR XX%=1 TO 14: LSET PARX$="XXX"
1420  LSET PARY$="YYY": PUT #1,XX%: NEXT XX%: CLOSE #1
1430  OPEN SFLX$+".PAR" AS #1 LEN=30
1440  FIELD #1,15 AS PARX$,15 AS PARY$
```

```
1450  LSET PARX$ = MKS$(SX)
1460  LSET PARY$ = MKS$(SY)
1470  PUT #1,1
1480  LSET PARX$ = MKS$(DX)
1490  LSET PARY$ = MKS$(DY)
1500  PUT #1,2
1510  LSET PARX$ = MKS$(X2)
1520  LSET PARY$ = MKS$(Y2)
1530  PUT #1,3
1540  LSET PARX$ = MKS$(X1)
1550  LSET PARY$ = MKS$(X2)
1560  PUT #1,4
1570  LSET PARX$ = MKS$(QX)
1580  LSET PARY$ = MKS$(QY)
1590  PUT #1,5
1600  LSET PARX$ = MKS$(OX)
1610  PUT #1,6
1620  LSET PARX$ = MKS$(XA)
1630  LSET PARY$ = MKS$(YA)
1640  PUT #1,7
1650  XE = 1/ABS(X2-X1):LSET PARX$ = MKS$(XE)
1660  XE = 1/ABS(Y2-Y1):LSET PARY$ = MKS$(YE)
1670  PUT #1,8
1680  CLOSE #1
1690  LOCATE 25,1:PRINT SPACE$(78);:LOCATE 25,1
1700  DEF SEG = &HB800                    'screen buffer
1710  BSAVE SFLX$+".SCN",0,&H4000         '16 k buffer
1720  DEF SEG
1730  PRINT "FILE ";SFLX$;" SAVED  HIT ANY KEY TO GO ON";:LOCATE 20,1
1740  KX$ = INKEY$:IF KX$ = "" THEN 1740
1750  RETURN 1760
1760  LOCATE 25,1:PRINT SPACE$(78);:LOCATE 25,1
1770  PRINT "       TERMINATED AT  ";TIME$;"  ON  ";DATE$;:LOCATE 23,1
1780  KEY(1) OFF:KEY(2) OFF
1790  CLS:SCREEN 0,0,0
1800  LOCATE 1,1
1810  INPUT "Should output from channel 0 be stored on disk  " ;RESP$
1820  IF RESP$ = "n" GOTO 2020
1830  LOCATE 3,1
1840  INPUT "Enter name of storage data file [dsk:]filename.dat";FILDAT0$
1850  OPEN FILDAT0$ AS #1 LEN = 30
1860  FIELD #1, 15 AS X$, 15 AS Y$
1870  LOCATE 5,1
1880  INPUT "Line, Dot or No plot mode (L,D,N)  ";A$
1890  IF A$="L" OR A$="l" THEN M=1:GOTO 1930
1900  IF A$="N" OR A$="n" THEN M=2:GOTO 1930
1910  IF A$="D" OR A$="d" THEN M=0:GOTO 1930
1920  LOCATE 11,1:PRINT"RE-ENTER":LOCATE 9,1:PRINT SPC(79):GOTO 1870
1930  CLS:LOCATE 12,24:PRINT"STORING DATA ON DISK"
```

```
1940  LSET X$ = MKS$(XAXIS):LSET Y$=MKS$(M)
1950  PUT #1,1
1960  FOR I=2 TO XAXIS+1
1970  LSET X$=MKS$(TIME%(I−1)):LSET Y$=MKS$(OUT0%(I−1))
1980  PUT #1,I
1990  NEXT I
2000  CLOSE #1
2010  CLS
2020  LOCATE 3,1
2030  INPUT "Should output from channel 1 be stored on disk.  " ;RESP$
2040  IF RESP$ = "n" GOTO 2240
2050  LOCATE 5,1
2060  INPUT "Enter name of storage data file [dsk:]file.dat";FILDAT1$
2070  OPEN FILDAT1$ AS #1 LEN = 30
2080  FIELD #1, 15 AS X$, 15 AS Y$
2090  LOCATE 7,1
2100  INPUT "Line, Dot or No plot mode (L,D,N)  ";A$
2110  IF A$="L" OR A$="l" THEN M=1:GOTO 2150
2120  IF A$="N" OR A$="n" THEN M=2:GOTO 2150
2130  IF A$="D" OR A$="d" THEN M=0:GOTO 2150
2140  LOCATE 11,1:PRINT"RE−ENTER":LOCATE 9,1:PRINT SPC(79):GOTO 2090
2150  CLS:LOCATE 12,24:PRINT"STORING DATA ON DISK"
2160  LSET X$ = MKS$(XAXIS):LSET Y$=MKS$(M)
2170  PUT #1,1
2180  FOR I=2 TO XAXIS+1
2190  LSET X$=MKS$(TIME%(I−1)):LSET Y$=MKS$(OUT1%(I−1))
2200  PUT #1,I
2210  NEXT I
2220  CLOSE #1
2230  CLS
2240  LOCATE 5,1
2250  INPUT "Should output from channel 2 be stored on disk.  " ;RESP$
2260  IF RESP$ = "n" GOTO 2460
2270  LOCATE 7,1
2280  INPUT "Enter name of storage data file [dsk:]file.dat";FILDAT2$
2290  OPEN FILDAT2$ AS #1 LEN = 30
2300  FIELD #1, 15 AS X$, 15 AS Y$
2310  LOCATE 9,1
2320  INPUT "Line, Dot or No plot mode (L,D,N)  ";A$
2330  IF A$="L" OR A$="l" THEN M=1:GOTO 2370
2340  IF A$="N" OR A$="n" THEN M=2:GOTO 2370
2350  IF A$="D" OR A$="d" THEN M=0:GOTO 2370
2360  LOCATE 11,1:PRINT"RE−ENTER":LOCATE 9,1:PRINT SPC(79):GOTO 2090
2370  CLS:LOCATE 12,24:PRINT"STORING DATA ON DISK"
2380  LSET X$ = MKS$(XAXIS):LSET Y$=MKS$(M)
2390  PUT #1,1
2400  FOR I = 2 TO XAXIS+1
2410  LSET X$=MKS$(TIME%(I−1)): LSET Y$=MKS$(OUT2%(I−1))
2420  PUT #1,I
```

```
2430  NEXT I
2440  CLOSE #1
2450  CLS
2460  LOCATE 7,1
2470  INPUT "Should output from channel 3 be stored on disk. " ;RESP$
2480  IF RESP$ = "n" GOTO 2660
2490  LOCATE 11,1
2500  INPUT "Enter name of storage data file [dsk:]file.dat";FILDAT3$
2510  OPEN FILDAT3$ AS #1 LEN = 30
2520  FIELD #1, 15 AS X$, 15 AS Y$
2530  INPUT "Line, Dot or No plot mode (L,D,N)  ";A$
2540  IF A$="L" OR A$="l" THEN M=1:GOTO 2580
2550  IF A$="N" OR A$="n" THEN M=2:GOTO 2580
2560  IF A$="D" OR A$="d" THEN M=0:GOTO 2580
2570  LOCATE 11,1:PRINT"RE-ENTER":LOCATE 9,1:PRINT SPC(79):GOTO 2090
2580  CLS:LOCATE 12,24:PRINT"STORING DATA ON DISK"
2590  LSET X$ = MKS$(XAXIS):LSET Y$=MKS$(M)
2600  PUT #1,1
2610  FOR I=2 TO XAXIS+1
2620  LSET X$=MKS$(TIME%(I-1)):LSET Y$=MKS$(OUT3%(I-1))
2630  PUT #1,I
2640  NEXT I
2650  CLOSE #1  : CLS
2660  LOCATE 9,1
2670  INPUT "Should output from channel 4 be stored on disk  : ";RESP$
2680  IF RESP$ = "n" GOTO 2880
2690  LOCATE 11,1
2700  INPUT "Enter name of storage data file [dsk:]file.dat";FILDAT4$
2710  OPEN FILDAT4$ AS #1 LEN = 30
2720  FIELD #1, 15 AS X$, 15 AS Y$
2730  LOCATE 13,1
2740  INPUT "Line, Dot or No plot mode (L,D,N)  ";A$
2750  IF A$="L" OR A$="l" THEN M=1:GOTO 2790
2760  IF A$="N" OR A$="n" THEN M=2:GOTO 2790
2770  IF A$="D" OR A$="d" THEN M=0:GOTO 2790
2780  LOCATE 11,1:PRINT"RE-ENTER":LOCATE 9,1:PRINT SPC(79):GOTO 2730
2790  CLS:LOCATE 12,24:PRINT"STORING DATA ON DISK"
2800  LSET X$ = MKS$(XAXIS):LSET Y$=MKS$(M)
2810  PUT #1,1
2820  FOR I=2 TO XAXIS+1
2830  LSET X$=MKS$(TIME%(I-1)):LSET Y$=MKS$(OUT0%(I-1))
2840  PUT #1,I
2850  NEXT I
2860  CLOSE #1
2870  CLS
2880  LOCATE 11,1
2890  INPUT "Should output from channel 5 be stored on disk.  " ;RESP$
2900  IF RESP$ = "n" GOTO 3100
2910  LOCATE 13,1
```

```
2920  INPUT "Enter name of storage data file [dsk:]file.dat";FILDAT5$
2930  OPEN FILDAT5$ AS #1 LEN = 30
2940  FIELD #1, 15 AS X$, 15 AS Y$
2950  LOCATE 15,1
2960  INPUT "Line, Dot or No plot mode (L,D,N)  ";A$
2970  IF A$="L" OR A$="l" THEN M=1:GOTO 3010
2980  IF A$="N" OR A$="n" THEN M=2:GOTO 3010
2990  IF A$="D" OR A$="d" THEN M=0:GOTO 3010
3000  LOCATE 11,1:PRINT"RE-ENTER":LOCATE 9,1:PRINT SPC(79):GOTO 2950
3010  CLS:LOCATE 12,24:PRINT"STORING DATA ON DISK"
3020  LSET X$ = MKS$(XAXIS):LSET Y$=MKS$(M)
3030  PUT #1,1
3040  FOR I=2 TO XAXIS+1
3050  LSET X$=MKS$(TIME%(I-1)):LSET Y$=MKS$(OUT1%(I-1))
3060  PUT #1,I
3070  NEXT I
3080  CLOSE #1
3090  CLS
3100  LOCATE 13,1
3110  INPUT "Should output from channel 6 be stored on disk.  " ;RESP$
3120  IF RESP$ = "n" GOTO 3310
3130  LOCATE 15,1
3140  INPUT "Enter name of storage data file [dsk:]file.dat";FILDAT6$
3150  OPEN FILDAT6$ AS #1 LEN = 30
3160  FIELD #1, 15 AS X$, 15 AS Y$
3170  LOCATE 17,1
3180  INPUT "Line, Dot or No plot mode (L,D,N)  ";A$
3190  IF A$="L" OR A$="l" THEN M=1:GOTO 3230
3200  IF A$="N" OR A$="n" THEN M=2:GOTO 3230
3210  IF A$="D" OR A$="d" THEN M=0:GOTO 3230
3220  LOCATE 11,1:PRINT"RE-ENTER":LOCATE 9,1:PRINT SPC(79):GOTO 2950
3230  CLS:LOCATE 12,24:PRINT"STORING DATA ON DISK"
3240  LSET X$ = MKS$(XAXIS):LSET Y$=MKS$(M)
3250  PUT #1,1
3260  FOR I = 2 TO XAXIS+1
3270  LSET X$=MKS$(TIME%(I-1)): LSET Y$=MKS$(OUT2%(I-1))
3280  PUT #1,I
3290  NEXT I
3300  CLOSE #1
3310  LOCATE 15,1
3320  INPUT "Should output from channel 7 be stored on disk. ";RESP$
3330  IF RESP$ = "n" GOTO 3510
3340  LOCATE 17,1
3350  INPUT "Enter name of storage data file [dsk:]file.dat";FILDAT7$
3360  OPEN FILDAT7$ AS #1 LEN = 30
3370  FIELD #1, 15 AS X$, 15 AS Y$
3380  INPUT "Line, Dot or No plot mode (L,D,N)  ";A$
3390  IF A$="L" OR A$="l" THEN M=1:GOTO 3430
3400  IF A$="N" OR A$="n" THEN M=2:GOTO 3430
```

```
3410  IF A$="D" OR A$="d" THEN M=0:GOTO 3430
3420  LOCATE 11,1:PRINT"RE-ENTER":LOCATE 9,1:PRINT SPC(79):GOTO 2950
3430  CLS:LOCATE 12,24:PRINT"STORING DATA ON DISK"
3440  LSET X$ = MKS$(XAXIS):LSET Y$=MKS$(M)
3450  PUT #1,1
3460  FOR I=2 TO XAXIS+1
3470  LSET X$=MKS$(TIME%(I-1)):LSET Y$=MKS$(OUT3%(I-1))
3480  PUT #1,I
3490  NEXT I
3500  CLOSE #1
3510  CLS:LOCATE 12,28:PRINT"DONE":LOCATE 25,1
3520  END
3530  'The following part of the program reads the board. The board is
3540  'set up for SE BIPOLAR operation.
3550  'Define constants for the board.
3560  '
3570   BASE.ADDRESS=&H2EC
3580   COMMAND.REGISTER=BASE.ADDRESS+1
3590   STATUS.REGISTER=BASE.ADDRESS+1
3600   DATA.REGISTER=BASE.ADDRESS
3610   COMMAND.WAIT=&H4
3620   WRITE.WAIT=&H2
3630   READ.WAIT=&H5
3640   CCLEAR=&H1
3650   CCLOCK=&H3
3660   CSAD=&HD
3670   CRAD=&HE
3680   CSTOP=&HF
3690   PERIOD#=40000!
3700   BASE.FACTOR#=4096
3710   BASE.CHANNELS=8
3720   NCONVERSIONS#=8
3730   GAIN(0)=1: GAIN(1)=2: GAIN(2)=4: GAIN(3)=8
3735   '
3740   'Stop and clear the DT2801-A board.
3750   '
3760   OUT COMMAND.REGISTER, CSTOP
3770   TEMP = INP(DATA.REGISTER)
3780   WAIT STATUS.REGISTER, COMMAND.WAIT
3790   OUT COMMAND.REGISTER, CCLEAR
3800   '
3810   'Set clock rate.
3820   '
3830   WAIT STATUS.REGISTER, COMMAND.WAIT
3840   OUT COMMAND.REGISTER, CCLOCK
3850   '
3860   PERIODH =INT(PERIOD#/256)
3870   PERIODL =PERIOD# - PERIODH* 256
3880   WAIT STATUS.REGISTER, WRITE.WAIT, WRITE.WAIT
```

```
3890  OUT DATA.REGISTER, PERIODL
3900  WAIT STATUS.REGISTER, WRITE.WAIT, WRITE.WAIT
3910  OUT DATA.REGISTER, PERIODH
3920  WAIT STATUS.REGISTER, COMMAND.WAIT
3930  OUT COMMAND.REGISTER, CSAD
3940  WAIT STATUS.REGISTER, WRITE.WAIT, WRITE.WAIT
3950  OUT DATA.REGISTER, ADGAIN
3960  WAIT STATUS.REGISTER, WRITE.WAIT, WRITE.WAIT
3970  OUT DATA.REGISTER, ADSCHANNEL
3980  WAIT STATUS.REGISTER, WRITE.WAIT, WRITE.WAIT
3990  OUT DATA.REGISTER, ADECHANNEL
4000  '
4010  NUMBERH = INT(NCONVERSIONS#/256)
4020  NUMBERL = NCONVERSIONS# – NUMBERH* 256
4030  '
4040  WAIT STATUS.REGISTER, WRITE.WAIT, WRITE.WAIT
4050  OUT DATA.REGISTER, NUMBERL
4060  WAIT STATUS.REGISTER, WRITE.WAIT, WRITE.WAIT
4070  OUT DATA.REGISTER, NUMBERH
4080  WAIT STATUS.REGISTER, COMMAND.WAIT
4090  OUT COMMAND.REGISTER, CRAD
4100  '
4110  FOR LOOP = 1 TO NCONVERSIONS#
4120   WAIT STATUS.REGISTER, READ.WAIT
4130   ADL%(LOOP) = INP(DATA.REGISTER)
4140   WAIT STATUS.REGISTER, READ.WAIT
4150   ADH%(LOOP) = INP(DATA.REGISTER)
4160  NEXT LOOP
4170  '
4180  WAIT STATUS.REGISTER, COMMAND.WAIT
4190  STATUS = INP(STATUS.REGISTER)
4200  IF (STATUS AND &H80) THEN GOTO 4230
4210  RETURN
4220  RETURN
4230  'Board Error.
4240  PRINT
4250  PRINT "Error"
4260  RETURN
4270  END
```

AV.3 INST.BAS

```
10 '            CREATE ADSORPTION INFORMATION FILES
20 '
30 'This program is used to invert the raw data (pressure versus time) of adsorption.
40 'It calculates the isotherm, the BET, and pore volume distribution
50 'plots. The required inputs are the raw data file, the run number (#),
60 'the temperature during the run, the dead volume, room temperature
70 'and the coefficients of the polynomial fit to the flow rate (POLY2.BAS on INFLO.BAS).
80 'Outputs are: the isotherm file (iso#.dat), BET file (bet#.dat), and the pore size
90 'distribution file (pore#.dat).
100 '
110 '
120 PGH(0)=.5 : PGH(1)=1 : PGH(2)=2 : PGH(3)=4
130 N = 1500          'size of the arrays
140 '
150 CLS:SCREEN 0,0,0:KEY OFF
160 LOCATE 1,1
170 INPUT "What was the gain "; GAIN#
180 IF GAIN#<0 OR GAIN#>3 GOTO 160
190 FACTOR=PGH(GAIN#)
200 LOCATE 3,1
210 INPUT "Enter name of data file to be read as [dsk:]file.dat";FILOLD$
220 LOCATE 5,1
230 PRINT "The new data files will be sent to drive b: "
240 LOCATE 7,1
250 INPUT "Enter run number of this experiment ";RUNNUM$
260 FILNEW1$ = "b:iso"+RUNNUM$+".dat"
270 FILNEW2$ = "b:bet"+RUNNUM$+".dat"
280 FILNEW3$ = "b:pore"+RUNNUM$+".dat"
290 DIM X(N) , Y(N) , COEF(6) ,Z(N)
300 LOCATE 9,1
310 PRINT "Reading data..."
320 OPEN FILOLD$ AS #1 LEN = 30
330 FIELD #1, 15 AS X$, 15 AS Y$
340 GET #1,1
350 NPTS = CVS(X$)
360 M = CVS(Y$)
370 FOR I = 1 TO NPTS
380 GET #1,I+1
390 X(I) = CVS(X$)
400 Y(I) = CVS(Y$)
410 NEXT I
420 CLOSE #1
430 LOCATE 11,1
440 PRINT "Smoothing data..."
450 FOR K = 1 TO NPTS
460 Z(K) = Y(K)
```

```
470 NEXT K
480 '
490 'Smooth the data by using appropriate weights of local points.
500 '
510 NMOD = NPTS − 2
520 FOR N = 3 TO NMOD
530 Y(N) = (−3*Z(N−2)+12*Z(N−1)+17*Z(N)+12*Z(N+1)−3*Z(N+2))/35
540 NEXT N
550 '
560 'Now that the data is smoothed, calculate the isotherm.
570 '
580 LOCATE 13,1
590 INPUT "Enter initial temperature in k " ; TEMP1
600 LOCATE 14,1
610 INPUT "Enter final temperature in k " ; TEMP2
620 LOCATE 15,1
630 INPUT "Enter total effective volume in ml " ; VOL
640 LOCATE 16,1
650 INPUT "What was the vapor pressure of adsorbate ";PFIN
660 LOCATE 17,1
670 '
680 'Read coefficients for instantaneous flow rate as a function of pressure:
690 '
700 INPUT "Enter first rate coefficient ";COEF(1)
710 INPUT "Enter second coefficient";COEF(2)
720 INPUT "Enter third coefficient ";COEF(3)
730 INPUT "Enter fourth coefficient ";COEF(4)
740 INPUT "Enter fifth coefficient ";COEF(5)
750 INPUT "Enter sixth coefficient ";COEF(6)
760 CLS
770 LOCATE 13,1
780 PRINT "Computing Isotherm..."
790 '
800 'Pressure = bits/4096*20psi*0.01934torr/psi
810 '
820 P0 = Y(1)/(3.96017*FACTOR)
830 DVOL=32.96
840 '
850 'The initial amount of gas is that in the dead volume at t=0.
860 '
870 TOTMOL=P0*DVOL*16.0364/TEMP1
880 TIME = X(2)−X(1)
890 FOR I = 2 TO NPTS
900 P = Y(I)/(3.96017*FACTOR)
910 Q = COEF(6)
920 FOR CNT% = 5 TO 1 STEP − 1
930 Q = Q * P + COEF(CNT%)
940 NEXT CNT%
950 '
```

```
960 TEMP = TEMP1 + (TEMP2−TEMP1)*(X(I)−X(0))/(X(NPTS)−X(0))
970 TOTMOL=TOTMOL + Q * TIME
980 ADSMOL=TOTMOL−P*VOL*16.0364/TEMP
990 X(I) = P
1000 Y(I) = ADSMOL
1010 NEXT I
1020 X(1)=P0 : Y(1)=0
1030 LOCATE 19,1
1040 PRINT "Creating data files:"
1050 OPEN FILNEW1$ AS #1 LEN = 30
1060 FIELD #1, 15 AS X$, 15 AS Y$
1070 LSET X$ = MKS$(NPTS) : LSET Y$ = MKS$(M)
1080 PUT #1,1
1090 FOR I = 1 TO NPTS
1100 LSET X$ = MKS$(X(I)) : LSET Y$ = MKS$(Y(I))
1110 PUT #1,I+1
1120 NEXT I
1130 CLOSE #1
1140 PRINT FILNEW1$
1150 '
1160 'Now create a BET file.
1170 '
1180 OPEN FILNEW1$ AS #2 LEN = 30
1190 FIELD #2, 15 AS X$, 15 AS Y$
1200 GET #2,1
1210 NPTS = CVS(X$)
1220 M = CVS(Y$)
1230 NNEW = 1
1240 FOR I = 1 TO NPTS
1250 GET #2, I+1
1260 X(NNEW) = CVS(X$)
1270 Y(NNEW) = CVS(Y$)
1280 PHI=.31*PFIN
1290 PLO=.04*PFIN
1300 IF X(NNEW) > PHI OR X(NNEW) = PHI GOTO 1330
1310 IF X(NNEW) > PLO OR X(NNEW) = PLO THEN NNEW = NNEW + 1
1320 NEXT I
1330 CLOSE #2
1340 OPEN FILNEW2$ AS #1 LEN = 30
1350 FIELD #1, 15 AS X$ , 15 AS Y$
1360 LSET X$ = MKS$(NNEW) : LSET Y$ = MKS$(M)
1370 PUT #1,1
1380 FOR I = 1 TO NNEW
1390 X(I) = X(I)/PFIN
1400 Y(I) = X(I)/(Y(I)*(1−X(I)))*1000000!
1410 LSET X$ = MKS$(X(I))
1420 LSET Y$ = MKS$(Y(I))
1430 PUT #1,I+1
1440 NEXT I
```

```
1450 CLOSE #1
1460 PRINT FILNEW2$
1470 '
1480 'Now create volume distribution file.
1490 '
1500 OPEN FILNEW1$ AS #1 LEN = 30
1510 FIELD #1, 15 AS X$, 15 AS Y$
1520 GET #1,1
1530 NPTS = CVS(X$)
1540 M = CVS(Y$)
1550 NNEW = 1
1560 FOR N =  1 TO NPTS
1570 GET #1, N+1
1580 X(NNEW) = CVS(X$)
1590 Y(NNEW) = CVS(Y$)
1600 HIEND = .92*PFIN
1610 LOEND = .5*PFIN
1620 IF X(NNEW) > HIEND OR X(NNEW)=HIEND GOTO 1650
1630 IF X(NNEW) > LOEND OR X(NNEW)=LOEND THEN NNEW=NNEW+1
1640 NEXT N
1650 CLOSE #1
1660 OPEN FILNEW3$ AS #2 LEN = 30
1670 FIELD #2, 15 AS X$, 15 AS Y$
1680 LSET X$ = MKS$(NNEW) : LSET Y$ =  MKS$(M)
1690 PUT #2,1
1700 FOR J = 1 TO NNEW
1710 Z(J) = Y(J)
1720 NEXT J
1730 NLAST = NNEW − 2
1740 Y(1)=0:X(1)=0:Y(2)=0:X(2)=0
1750 Y(NLAST+2)=0:X(NLAST+2)=0:Y(NLAST+1)=0:X(NLAST+1)=0
1760 FOR I=3 TO NLAST
1770 ARG = X(I)/PFIN
1780 IF ARG < 0 OR ARG = 0 THEN GOTO 1930
1790 DEN = −1*LOG(ARG)
1800 '
1810 'This routine uses the method developed by Yan and Zhang.
1820 '
1830 'Surface Tension nitrogen = 8.5 dynes/cm, v = 34.65 cm^3/gmole.
1840 '
1850 PRAD = 1.018E−07/DEN
1860 'For freon, gamma = 18 dynes/cm, v=73.15cm^3/gmole,T=282 K.
1870 'PRAD = 1.123E−07/DEN
1880 X(I) = LOG(PRAD)/2.303 + 6
1890 Y(I) = (Z(I−2)−8*Z(I−1)+8*Z(I+1)−Z(I+2))*3.465E−05/(12*(X(I)−X(I−1)))
1900 LSET X$ = MKS$(X(I))
1910 LSET Y$ = MKS$(Y(I))
1920 PUT #2, I−1
1930 NEXT I
```

```
1940 CLOSE #2
1950 PRINT FILNEW3$
1960 SCREEN 0,0,0
1970 DIM FL$(1)
1980 '
1990 'User has the option to plot isotherm or BET file immediately.
2000 '
2010 INPUT "Do you wish to plot the isotherm ";ANS$
2020 IF ANS$="y" OR ANS$="Y" THEN FL$(1)=FILNEW1$ ELSE GOTO 2060
2030 YLBL$= "Micromoles "
2040 XLBL$= "Pressure  (torr)"
2050 GOTO 2100
2060 INPUT "Do you wish to see the BET plot "; ANS$
2070 IF ANS$="y" OR ANS$="Y" THEN FL$(1)=FILNEW2$  ELSE GOTO 2370
2080 YLBL$= "BET plot"
2090 XLBL$= "Rel. Pres.  (P/P0)"
2100 PRINT "Working...."
2110 NOF = 1
2120 '
2130 'This part of the program sets the parameters required for plotting
2140 'the data.
2150 '
2160 OPEN "RLINPLT.LNK" AS #1 LEN = 30
2170 FIELD #1, 30 AS RFLD$
2180 FOR I = 1 TO 21:LSET RFLF$ = "XXXXXXXXX":PUT #1,I:NEXT I:CLOSE #1
2190 OPEN "RLINPLT.LNK" AS #1 LEN = 30
2200 FIELD #1, 30 AS RFLD$
2210 GET #1,1
2220 LSET RFLD$ = MKI$(NOF)
2230 PUT #1,1
2240 GET #1,2
2250 LSET RFLD$ = YLBL$
2260 PUT #1,2
2270 GET #1,3
2280 LSET RFLD$ = XLBL$
2290 PUT #1,3
2300 FOR I = 1 TO NOF
2310 GET #1,I+3
2320 LSET RFLD$ = FL$(I)
2330 PUT #1,I+3
2340 NEXT I
2350 CLOSE #1
2360 CHAIN "LINPLT.BAS"
2370 END
```

AV.4 INFLO.BAS

```
10 '          INSTANTANEOUS ORIFICE FLOW PROGRAM
20 '
30 'This program computes the instantaneous flow rate for given
40 'pressure and temperature of the system.
50 'Input data file is the raw data for the blank run.
60 'Output file is user named containing flow rate in micromoles/s
70 'versus downstream pressure in torr.
80 '
90  PGH(0)=.5 :  PGH(1)=1 : PGH(2)=2 : PGH(3)=4
100 N = 1500          'size of the arrays
110 '
120 CLS:SCREEN 0,0,0:KEY OFF
130 LOCATE 3,1
140 INPUT "What was the gain "; GAIN#
150 FACTOR = PGH(GAIN#)
160 LOCATE 5,1
170 INPUT "Enter data to be differentiated as [dsk:]file.dat  ";FILOLD$
180 LOCATE 7,1
190 INPUT "Enter name of output file as [dsk:]filename.dat    ";FILNEW$
200 DIM X(N) , Y(N) , Z(N)
210 LOCATE 9,1
220 INPUT "What was the temperature during calibration ";TEMP
230 LOCATE 11,1
240 PRINT "Reading old file..."
250 OPEN FILOLD$ AS #1 LEN = 30
260 FIELD #1, 15 AS X$, 15 AS Y$
270 GET #1,1
280 NPTS = CVS(X$)
290 M = CVS(Y$)
300 FOR I = 1 TO NPTS
310 GET #1,I+1
320 X(I) = CVS(X$)
330 Z(I) = CVS(Y$)
340 NEXT I
350 CLOSE #1
360 '
370 LOCATE 13.1
380 PRINT "Computing modifications..."
390 DEN = 12*(X(3)-X(2))*FACTOR
400 NEND = NPTS - 2
410 '
420 FOR I = 3 TO NEND
430 '
440 'For 5 micron with nitrogen, vol. = 40.00 cc. For micromoles/sec,
450 'and psia gage, const. = 20 psi/10volt*51.7149 torr/psia *30.4 ml
460 '/82.05 ml atm/gmol k /760torr/atm *10e6 micromoles/mole =12.701
```

```
470 '
480 Y(I) = (Z(I-2)-8*Z(I-1)+8*Z(I+1)-Z(I+2))*160.5655*30.4/(DEN*TEMP*40!)
490 '
500 'Conversion factor for millibar gage is 3.96017
510 '
520 X(I) = Z(I)/(3.96017*FACTOR)
530 NEXT I
540 NTOT=NPTS-5
550 LOCATE 15,1
560 PRINT "Writing new file..."
570 OPEN FILNEW$ AS #1 LEN = 30
580 FIELD #1, 15 AS X$, 15 AS Y$
590 LSET X$ = MKS$(NTOT) : LSET Y$ = MKS$(M)
600 NEND=NEND-1
610 PUT #1,1
620 FOR I = 3 TO NEND
630 LSET X$ = MKS$(X(I)) : LSET Y$ = MKS$(Y(I))
640 PUT #1,I-1
650 NEXT I
660 CLOSE #1
670 LOCATE 17,1
680 PRINT "Done."
690 LOCATE 24,1
700 END
```

AV.5 MONO.BAS

```
10 '        MONOLAYER COVERAGE CALCULATION PROGRAM
20 '
30 'This program calculates the BET surface area and 'C' value from the
40 'BET data file. The data are fit with a straight line using a modified
50 'form of POLY2.BAS. The slope and intercept of this line are used to
60 'calculate the desired quantities. Input is the BET file, output is
70 'to the screen. The values are, respectively: intercept, slope, surface
80 'area (assuming nitrogen), micromoles at monolayer coverage, 'C' value
90 'and sum of residuals.
100 'The polynomial fit is described in more detail in POLY2.BAS.
110 '
120 SCREEN 0,0,0:KEY OFF:CLS:LOCATE 25,1:PRINT"POLYNOM";
130 DIM COEF(6), MTX(6,7), SM(10), RT(6)
140 '
150 'The data points are read from the input file.
160 '
170 NP= 2000
180 LOCATE 2,1
190 INPUT "Enter name of file to be read as [dsk:]filename.dat ";FILOLD$
200 DIM X(NP) , Y(NP)
210 OPEN FILOLD$ AS #1 LEN = 30
220 FIELD #1, 15 AS X$, 15 AS Y$
230 GET #1,1
240 N = CVS(X$)
250 DUM = CVS(Y$)
260 FOR I = 1 TO N
270 GET #1,I+1
280 X(I) = CVS(X$)
290 Y(I) = CVS(Y$)
300 PRINT I,X(I),Y(I)
310 NEXT I
320 CLOSE #1
330 '
340 'This is the regression part of the program.
350 '
360 CLS:LOCATE 25,1:PRINT"POLYNOM — PERFORMING LINEAR REGRESSION";
370 ORD = 1
380 LOCATE 10,20:PRINT"WAIT — REGRESSION ANALYSIS IN PROGRESS"
390 FOR I=1 TO 2*ORD
400 SM(I)=0
410 NEXT I
420 FOR I = 1 TO ORD+1
430 RT(I)=0
440 NEXT I
450 FOR PNT = 1 TO N
460 FOR I= 1 TO ORD*2
```

```
470 SM(I)=SM(I) + X(PNT)^ I
480 NEXT I
490 FOR I = 1 TO ORD+1
500 IF I=1 THEN RT(I)=RT(I) + Y(PNT)
510 IF I<>1 THEN RT(I) = RT(I) + Y(PNT)*(X(PNT)^ (I-1))
520 NEXT I
530 NEXT PNT
540 MTX(1,1)=N
550 FOR I=1 TO ORD+1
560 MTX(I,ORD+2)=RT(I)
570 FOR J=1 TO ORD+1
580 IF I+J<>2 THEN MTX(I,J)=SM(I+J-2)
590 NEXT J
600 NEXT I
610 FOR K = 1 TO ORD
620 KTMP=K+1
630 L=K
640 FOR I=KTMP TO ORD+1
650 IF ABS(MTX(I,K))>ABS(MTX(L,K)) THEN L=I
660 NEXT I
670 IF L=K THEN GOTO 730
680 FOR J=K TO ORD+2
690 TMP=MTX(K,J)
700 MTX(K,J)=MTX(L,J)
710 MTX(L,J)=TMP
720 NEXT J
730 FOR I= KTMP TO ORD+1
740 FTR = MTX(I,K)/MTX(K,K)
750 FOR J= KTMP TO ORD+2
760 MTX(I,J)=MTX(I,J) - FTR * MTX(K,J)
770 NEXT J
780 NEXT I
790 NEXT K
800 COEF(ORD+1) = MTX(ORD+1,ORD+2)/MTX(ORD+1,ORD+1)
810 I=ORD
820 ITMP= I+1
830 TOT = 0
840 FOR J= ITMP TO ORD+1
850 TOT=TOT + MTX(I,J)*COEF(J)
860 NEXT J
870 COEF(I)=(MTX(I,ORD+2)-TOT)/MTX(I,I)
880 I=I-1
890 IF I>=1 THEN GOTO 820
900 '
910 'Display data.
920 '
930 CLS:LOCATE 1,1
940 FOR I=1 TO ORD+1
950 PRINT"COEF(";I;") = ";COEF(I)
```

```
960 NEXT I
970 RECIP = 1/(COEF(1)+COEF(2))
980 AREA  = 16.2 * 6022 * RECIP
990 NM= RECIP
1000 C=COEF(2)/COEF(1) + 1
1010 RESID = 0
1020 FOR I =1 TO N
1030 RESID = RESID +ABS(Y(I)−COEF(2)*X(I)−COEF(1))
1040 NEXT I
1050 PRINT AREA,RECIP,C,RESID
1060 END
```

AV.6 POLY2.BAS

```
10 '        FIFTH-ORDER LEAST-SQUARES POLYNOMIAL FIT PROGRAM
20 '
30 '
40 'This program evaluates the coefficients C1—6 for the polynomial
50 'approximation:-
60 '
70 '  Y = C1 + C2*X  +  C3*X^ 2  +  C4*X^ 3  +  C5*X^ 4  +  C6*X^ 5
80 '
90 'such that the sum of the squares of the errors between the actual
100 'value of Y and the polynomial value of Y for all data points entered
110 'is minimised (i.e. curve fitting).
120 'This approximation is useful for linearising transducer outputs.
130 'e.g. flowmeters, thermocouples, tacho-generators etc.. The transducer
140 'output is obtained from the A/D converter (suitably scaled if required)
150 'as variable X and the linearized output from the transducer e.g. flow,
160 'temperature, velocity etc. is calculated as variable Y. The coefficients
170 'C1—6 are calculated from a set of Y,X data or calibration points.
180 'Type RUN(CR) to run the program. The prompts are self explanatory.
190 'The data are assumed to be X,Y in the file. The program then proceeds to perform
200 'a regression analysis to calculate the coefficients of the polynomial.
210 'You are prompted to select the order required, up to 5th. order. Usually
220 '5th. order is the best option unless you want to experiment with trying
230 'a lower order. After the analysis is finished, the coefficients are
240 'displayed and you can check the conformance by inputting various values
250 'of X and seeing how accurate Y is. If you wish, before exiting the
260 'program, you can run the regression at another order on the same data
270 'to see how good the conformance is with a different order polynomial.
280 '
290 'Once the coefficients are evaluated the polynomial can be inserted
300 'into your programs as a subroutine. The neatest way is to use a loop to
310 'evaluate it as follows:-
320 '
330 '    xxx00 Y = COEF(1)
340 '    xxx10 FOR CNT% = 5 TO 1 STEP — 1
350 '    xxx20 Y = Y + COEF(CNT% + 1) * X ^  CNT%
360 '    xxx30 NEXT CNT%
370 '    xxx40 RETURN
380 '
390 '
400 '—— START - INITIALIZATION SECTION ————————————————
410  SCREEN 0,0,0:KEY OFF:CLS:LOCATE 25,1:PRINT"POLYNOM";
420  DIM COEF(6), MTX(6,7), SM(10), RT(6)
430  '— DATA POINT ENTRY ————————————————————————
440  CLS:LOCATE 25,1:PRINT"POLYNOM - DATA FILE ENTRY";
450  NP= 2000
460  LOCATE 2,1
```

```
470 INPUT "Enter name of file to be read as [dsk:]filename.dat ";FILOLD$
480 DIM X(NP) , Y(NP)
490 OPEN FILOLD$ AS #1 LEN = 30
500 FIELD #1, 15 AS X$, 15 AS Y$
510 GET #1,1
520 N = CVS(X$)
530 DUM = CVS(Y$)
540 FOR I = 1 TO N
550 GET #1,I+1
560 X(I) = CVS(X$)
570 Y(I) = CVS(Y$)
580 PRINT I,X(I),Y(I)
590 NEXT I
600 CLOSE #1
610 '—— PERFORM LINEAR REGRESSION ————————————————
620 CLS:LOCATE 25,1:PRINT"POLYNOM - PERFORMING LINEAR REGRESSION";
630 LOCATE 2,1:INPUT"ORDER OF ANALYSIS REQUIRED (0—5)? ",ORD
640 IF ORD <0 OR ORD>5 THEN GOTO 630
650 LOCATE 10,20:PRINT"WAIT - REGRESSION ANALYSIS IN PROGRESS"
660 FOR I=1 TO 2*ORD
670 SM(I)=0
680 NEXT I
690 FOR I = 1 TO ORD+1
700 RT(I)=0
710 NEXT I
720 FOR PNT = 1 TO N
730 FOR I= 1 TO ORD*2
740 SM(I)=SM(I) + X(PNT)^ I
750 NEXT I
760 FOR I = 1 TO ORD+1
770 IF I=1 THEN RT(I)=RT(I) + Y(PNT)
780 IF I<>1 THEN RT(I) = RT(I) + Y(PNT)*(X(PNT)^ (I—1))
790 NEXT I
800 NEXT PNT
810 MTX(1,1)=N
820 FOR I=1 TO ORD+1
830 MTX(I,ORD+2)=RT(I)
840 FOR J=1 TO ORD+1
850 IF I+J<>2 THEN MTX(I,J)=SM(I+J—2)
860 NEXT J
870 NEXT I
880 FOR K = 1 TO ORD
890 KTMP=K+1
900 L=K
910 FOR I=KTMP TO ORD+1
920 IF ABS(MTX(I,K))>ABS(MTX(L,K)) THEN L=I
930 NEXT I
940 IF L=K THEN GOTO 1000
950 FOR J=K TO ORD+2
```

```
960 TMP=MTX(K,J)
970 MTX(K,J)=MTX(L,J)
980 MTX(L,J)=TMP
990 NEXT J
1000 FOR I= KTMP TO ORD+1
1010 FTR = MTX(I,K)/MTX(K,K)
1020 FOR J= KTMP TO ORD+2
1030 MTX(I,J)=MTX(I,J) - FTR * MTX(K,J)
1040 NEXT J
1050 NEXT I
1060 NEXT K
1070 COEF(ORD+1) = MTX(ORD+1,ORD+2)/MTX(ORD+1,ORD+1)
1080 I=ORD
1090 ITMP= I+1
1100 TOT = 0
1110 FOR J= ITMP TO ORD+1
1120 TOT=TOT + MTX(I,J)*COEF(J)
1130 NEXT J
1140 COEF(I)=(MTX(I,ORD+2) - TOT)/MTX(I,I)
1150 I=I-1
1160 IF I>=1 THEN GOTO 1090
1170 '—— DISPLAY COEFFICIENTS ————————————————
1180 CLS:LOCATE 1,1
1190 FOR I=1 TO ORD+1
1200 PRINT"COEF(";I;") = ";COEF(I)
1210 NEXT I
1220 RESID = 0
1230 FOR I = 1 TO NPTS
1240 P = X(I)
1250 Q = COEF(6)
1260 FOR CNT% = 5 TO 1 STEP - 1
1270 Q = Q * P + COEF(CNT%)
1280 NEXT CNT%
1290 RESID = RESID + ABS( Y(I) - Q )
1300 NEXT I
1310 PRINT RESID
1320 '—— TEST FIT ————————————————————————
1330 LOCATE 25,1:PRINT SPC(79):LOCATE 25,1:PRINT"POLYNOM - TEST FIT";
1340 LOCATE 9,1:PRINT"TEST CONFORMANCE":PRINT"————————"
1350 LOCATE 12,1: PRINT SPC(79)
1360 LOCATE 12,1:INPUT "X VALUE (type Q to quit)? ",A$
1370 IF A$="Q" OR A$="q" THEN GOTO 1470
1380 X=VAL(A$)
1390 Y = COEF(1)
1400 FOR CNT%= 5 TO 1 STEP - 1
1410 Y = Y + COEF(CNT%+1) * X^ CNT%
1420 NEXT CNT%
1430 LOCATE 14,1: PRINT SPC(79)
1440 LOCATE 14,1:PRINT"Calculated Y (output) = ";Y;"  for X (input) = ";X
```

```
1450 GOTO 1360
1460 LOCATE 14,1: PRINT SPC(79)
1470 LOCATE 14,1:INPUT "TRY DIFFERENT REGRESSION ORDER (Y/N)? ",A$
1480 IF A$="y" OR A$="Y" THEN GOTO 1500
1490 LOCATE 25,1:PRINT SPC(79):LOCATE 20,1:END
1500 ERASE SM, MTX, RT, COEF
1510 DIM COEF(6), MTX(6,7), SM(10), RT(6)
1520 GOTO 610
1530 END
```

AV.7 MPLOT.BAS

```
10 '      PROGRAM TO MAKE/READ A LINEAR PLOT CONTROL FILE
20 '
30 '
40 'This routine allows the user to make or read a plot control file and
50 'execute it if desired. This program links the program LINPLT.BAS and
60 'runs the program. The LINPLT.BAS program uses the file called RLINPLT.BAS
70 'as a control file. The RLINPLT.BAS control file contains:
80 '
90 '        A. THE NUMBER OF FILES TO BE PLOTTED
100 '       B. THE 'X' AXIS LABLE [ 30 CHARACTERS LONG ]
110 '       C. THE 'Y' AXIS LABEL [ 20 CHARACTERS LONG ]
120 '       D. FILES TO BE PLOTTED (n records following )
130 '
140 SCREEN 0,0,0:CLS:KEY OFF
150 DIM FL$(15)
160 PRINT TAB(20) ;"MAKE / READ A LINEAR PLOT FILE"
170 PRINT
180 PRINT "Do you wish to (R)ead or (M)ake a plot file ";
190 R$ = INKEY$: IF R$ = "" THEN 190
200 IF R$="R" THEN 220 ELSE IF R$="M" OR R$="m" THEN 500 ELSE CLS
210 GOTO 160
220 OPEN "RLINPLT.LNK" AS #1 LEN=30
230 FIELD #1, 30 AS RFLD$
240 GET #1,1
250 NOF = CVI(RFLD$)
260 GET #1,2
270 YLBL$ = RFLD$
280 GET #1,3
290 XLBL$ = RFLD$
300 FOR I = 1 TO NOF
310 GET #1,I+3
320 FL$(I) = RFLD$
330 NEXT I
340 CLOSE #1
350 CLS
360 PRINT TAB(20);" READ A LINEAR PLOT CONTROL FILE"
370 LOCATE 3,1
380 PRINT "NUMBER OF DATA FILES TO BE PLOTTED [15 max] = ";NOF
390 LOCATE 5,1
400 PRINT "X – AXIS LABEL     [ 30 characters maximum ]: ";XLBL$
410 LOCATE 7,1
420 PRINT "Y – AXIS LABEL     [ 16 characters maximum ]: ";YLBL$
430 LOCATE 9,1
440 FOR I%= 1 TO NOF
450 LOCATE 9+I%–1,1
460 PRINT "DATA FILE NAME ";
```

```
470 PRINT USING "##";I%;:PRINT "[DSK:] FILENAME.EXT ";FL$(I%);
480 NEXT I%
490 GOTO 880
500 CLS
510 PRINT TAB(20);"  MAKE A LINEAR PLOT FILE "
520 LOCATE 3,1
530 INPUT "NUMBER OF DATA FILES TO BE PLOTTED [15 MAX] = ",NOF
540 IF NOF <1 OR NOF >15 THEN LOCATE 3,1:PRINT SPACE$(78);:GOTO 520
550 LOCATE 5,1
560 INPUT "ENTER 'X' AXIS LABEL [30 characters maximum]: ",XLBL$
570 LOCATE 7,1
580 INPUT "ENTER 'Y' AXIS LABEL [16 characters maximum]: ",YLBL$
590 LOCATE 9,1
600 FOR I%= 1 TO NOF
610 LOCATE 9+I%-1,1
620 PRINT "DATA FILE NAME  ';
630 PRINT USING "##";I%;:PRINT "  [DSK:] FILENAME.EXT     ";
640 INPUT;FL$(I%)
650 IF FL$(I%) ="" THEN LOCATE 9+I%-1,1:PRINT SPACE$(78);:LOCATE 9+I%-1,1
660 GOTO 630
670 NEXT I%
680 OPEN "RLINPLT.LNK" AS #1 LEN = 30
690 FIELD #1, 30 AS RFLD$
700 FOR I = 1 TO 21:LSET RFLF$ = "XXXXXXX":PUT #1,I:NEXT I:CLOSE #1
710 OPEN "RLINPLT.LNK" AS #1 LEN = 30
720 FIELD #1, 30 AS RFLD$
730 GET #1,1
740 LSET RFLD$ = MKI$(NOF)
750 PUT #1,1
760 GET #1,2
770 LSET RFLD$ = YLBL$
780 PUT #1,2
790 GET #1,3
800 LSET RFLD$ = XLBL$
810 PUT #1,3
820 FOR I = 1 TO NOF
830 GET #1,I+3
840 LSET RFLD$ = FL$(I)
850 PUT #1,I+3
860 NEXT I
870 CLOSE #1
880 LOCATE 25,1:PRINT SPACE$(70);:LOCATE 25,1
890 INPUT;"UPDATE ENTRY  Nof, X axis,Y axis, File#, Exit, Plot  ";ERC$
900 ERC$=LEFT$(ERC$,1)
910 IF ERC$ = "N" OR ERC$ = "n" THEN 1010
920 IF ERC$ = "X" OR ERC$ = "x" THEN 1050
930 IF ERC$ = "Y" OR ERC$ = "y" THEN 1090
940 IF ERC$ = "F" OR ERC$ = "f" THEN 1130
950 IF ERC$ = "E" OR ERC$ = "e" THEN CLS:NEW:END
```

```
960 IF ERC$ <>"P" OR ERC$ <>"p" THEN 990
970 GOTO 880
980 CLS
990 CHAIN "LINPLT.BAS"
1000 '
1010 LOCATE 3,1:PRINT SPACE$(78);:LOCATE 3,1
1020 INPUT "NUMBER OF DATA FILES TO BE PLOTTED [15 MAX] = ",NOF
1030 IF NOF < 1 THEN 1010 ELSE IF NOF > 15 THEN 1010
1040 GOTO 680
1050 LOCATE 5,1:PRINT SPACE$(78);:LOCATE 5,1
1060 INPUT "ENTER 'X' AXIS LABEL [30 characters maximum]: ",XLBL$
1070 IF LEN(XLBL$) > 30 THEN 1050
1080 GOTO 680
1090 LOCATE 7,1:PRINT SPACE$(78);:LOCATE 7,1
1100 INPUT "ENTER 'Y' AXIS LABEL [16 characters maximum]: ",YLBL$
1110 IF LEN(YLBL$) >16 THEN 1090
1120 GOTO 680
1130 LOCATE 25,1:PRINT SPACE$(78);:LOCATE 25,1
1140 INPUT;"ENTER FILE NUMBER TO BE CHANGED = ",NFC
1150 IF NFC > NOF THEN 1130 ELSE IF NFC > 15 THEN 1130
1160 LOCATE 8+NFC,1:PRINT SPACE$(79);:LOCATE 8+NFC,1
1165 PRINT "DATA FILE NAME ";
1170 PRINT USING "##";NFC;:PRINT " [DSK:] FILENAME.EXT  ";
1180 INPUT;FILX$:IF FILX$="" THEN 1160 ELSE FL$(NFC)=FILX$
1190 GOTO 680
1200 END
```

AV.8 LINPLT.BAS

```
10 '              LINEAR PLOT PROGRAM
20 '
30 '
40 'This program will plot from one to 15 data files with the same scale
50 'factors for all the files. The program also has a save screen command
60 'which allows the user to save the resultant plot for future reference.
70 'The  program  also allows the user to  chain an additional set of data
80 'files to be plotted on the already data files shown.  Printing of the
90 'screen is done by entering the option as directed, then SHFT PrtSc key.
100 'The user must have the graftrax option active.
110 '
120 'This section is where the starting graph coordinates and screen scale
130 'ratio is set. OX,OY = starting point of graph. QX,QY = screen scale x:y.
140 '
150 KEY OFF:SCREEN 0,0,0
160 OX=70:OY=0:QX=1.8:QY=.9000001
170 DIM X(100),Y(100),F$(15)
180 CLS:LOCATE 12,30:COLOR 31,0,0:PRINT "COMPUTING GRAPHICS FILES";
190 '
200 'This is the main link to the plotting program.  The file RLINPLT.LNK
210 'has the file name and disk of the file(s) to be plotted.
220 '
230 OPEN "RLINPLT.LNK" AS #1 LEN = 30
240 FIELD #1, 30 AS RLNK$
250 GET #1,1
260 NF = CVI(RLNK$)
270 GET #1,2
280 YLB$ = RLNK$
290 GET #1,3
300 XLB$ = RLNK$
310 IP = 1
320 FOR I = 1 TO NF
330 GET #1,I+3
340 F$(IP) = RLNK$
350 IP = IP + 1
360 NEXT I
370 CLOSE
380 '
390 'This loop scans the data files and sets the X,Y Max/Min values so
400 'all the data files are on the same scale.
410 '
420 X1=0
430 X2=0
440 Y1=0
450 Y2=0
460 FOR I=1 TO NF
```

```
470 IC=0
480 OPEN F$(I) AS #1 LEN=30
490 FIELD #1, 15 AS XVAL$, 15 AS YVAL$
500 GET #1,1
510 NI=CVS(XVAL$)
520 FOR J=1 TO NI
530 IC=IC+1
540 GET #1,IC+1
550 A=CVS(XVAL$)
560 B=CVS(YVAL$)
570 IF A<X1 THEN X1=A
580 IF A>X2 THEN X2=A
590 IF B<Y1 THEN Y1=B
600 IF B>Y2 THEN Y2=B
610 NEXT J
620 CLOSE #1
630 NEXT I
640 '
650 'This section establishes the actual scale factors used to plot the
660 'data as the files are read. These values are also the same values saved
670 'on the disk when a Save command is executed.
680 '
690 CLS:COLOR 7,0,0:SCREEN 2
700 DX= ABS(CINT((X2-X1)/25+.5))
710 DY = ABS(CINT(((Y2-Y1)/25)+.5))
720 SX=260 / (X2-X1)
730 SY=140 /(Y2-Y1)
740 '
750 'This section locates the Axis x,y and plots them out with the small
760 'tick marks identifing the scale. The axis labels are also printed.
770 '
780 '
790 IF Y2<=0 THEN YA=10:GOTO 830
800 IF Y1=>0 THEN YA=150:GOTO 830
810 YA=10 + SY * Y2
820 '
830 'Set the range limits
840 '
850 IF X2 <= 0 THEN XA=270:GOTO 880
860 IF X1 => 0 THEN XA=10:GOTO 880
870 XA=10 - SX * X1
880 FOR YLBL = 1 TO 16
890 LOCATE 2+YLBL,6:PRINT MID$(YLB$,YLBL,1);
900 NEXT YLBL
910 LOCATE 1,1:PRINT USING "#.##^^^^";Y2;
920 LOCATE 19,1:PRINT USING "#.##^^^^";Y1;
930 LOCATE 20,10:PRINT USING "#.##^^^^";X1;
940 LOCATE 20,68:PRINT USING "#.##^^^^";X2;
950 PSET (QX*0+OX,QY*0+OY)
```

```
960 LINE-(QX*279+OX,QY*0+OY)
970 LINE-(QX*279+OX,QY*159+OY)
980 LINE-(QX*0+OX,QY*159+OY)
990 LINE-(QX*0+OX,QY*0+OY)
1000 LINE (QX*XA+OX,QY*10+OY)-(QX*XA+OX,QY*150+OY)
1010 LINE (QX*10+OX,QY*YA+OY)-(QX*270+OX,QY*YA+OY)
1020 '
1030 'Mark the x axis ticks.
1040 '
1050 K=0
1060 B=YA-2
1070 C=YA+2
1080 K=K+1
1090 A=DX * K
1100 AA=XA+SX*A
1110 IF AA>271 GOTO 1140
1120 LINE (QX*AA+OX,QY*B+OY)-(QX*AA+OX,QY*C+OY)
1130 GOTO 1080
1140 K=0
1150 K=K+1
1160 A=DX*K
1170 AA=XA-SX*A
1180 IF AA<9 GOTO 1240
1190 LINE (QX*AA+OX,QY*B+OY)-(QX*AA+OX,QY*C+OY)
1200 GOTO 1150
1210 '
1220 'Mark the y axis ticks.
1230 '
1240 K=0
1250 A=XA-2
1260 C=XA+2
1270 K=K+1
1280 B=DY*K
1290 BB=YA-SY*B
1300 IF BB<9 GOTO 1330
1310 LINE (QX*A+OX,QY*BB+OY)-(QX*C+OX,QY*BB+OY)
1320 GOTO 1270
1330 K=0
1340 K=K+1
1350 B=DY*K
1360 BB=YA+SY*B
1370 IF BB>151 GOTO 1400
1380 LINE (QX*A+OX,QY*BB+OY)-(QX*C+OX,QY*BB+OY)
1390 GOTO 1340
1400 LOCATE 22,1
1410 PRINT "   X TICK=";INT(DX);"  Y TICK=";INT(DY);"  File#1 is ";F$(1)
1420 LOCATE 20,22:PRINT XLB$;:LOCATE 22,1
1430 '
1440 'This section recalls all the files and plots them one by one.
```

```
1450 '
1460 FOR I=1 TO NF
1470 IC=0
1480 JC=0
1490 OPEN F$(I) AS #1 LEN=30
1500 FIELD #1, 15 AS XVAL$, 15 AS YVAL$
1510 GET #1,1
1520 NI = CVS(XVAL$):DOT = CVS(YVAL$)
1530 FOR J=1 TO 100
1540 IC=IC+1
1550 GET #1,IC+1
1560 X(J)=CVS(XVAL$)
1570 Y(J)=CVS(YVAL$)
1580 IF J = 1 AND IC = 1 THEN XIN = X(J):YIN = Y(J):GOTO 1600
1590 IF J = 100 THEN XTMP = X(J): YTMP = Y(J)
1600 IF IC =NI GOTO 1620
1610 NEXT J
1620 FOR J=1 TO 100
1630 JC=JC+1
1640 PS = 0
1650 IF J = 1 AND JC=1 THEN XTMP=XIN:YTMP = YIN:GOTO 1680
1660 IF J = 1 THEN GOTO 1680
1670 XTMP = X(J−1):YTMP=Y(J−1)
1680 AA = XA +SX * X(J)
1690 AT = XA + SX * XTMP
1700 BB = YA −SY * Y(J)
1710 BT = YA − SY * YTMP
1720 IF AA < 9 OR BB < 9 THEN PS = 1
1730 IF AA > 271 OR BB > 151 THEN PS = 1
1740 IF PS GOTO 1810
1750 IF INT(DOT + .5) = 2 THEN GOTO 1810 'No plot
1760 IF INT(DOT+.5)=0 THEN GOTO 1790 'Dot plot
1770 LINE (QX*AT+OX,QY*BT+OY) − (QX*AA+OX,QY*BB+OY) 'Line plot
1780 CIRCLE (QX*AA+OX, QY*BB+OY),2 :GOTO 1810
1790 IDOT = I
1800 CIRCLE (QX*AA+OX,QY*BB+OY),IDOT
1810 IF JC=NI GOTO 1840
1820 NEXT J
1830 GOTO 1530
1840 CLOSE #1
1850 NEXT I
1860 '
1870 'This is the conversational part of the program where the user may
1880 'save the plot/graph or add more data or print plot/graph.
1890 '
1900 LOCATE 24,1:INPUT ;"ENTER OPTION Save, Make plot, Exit ";OPTX$
1910 IF OPTX$="S" OR OPTX$="s" THEN 1970
1920 IF OPTX$="M" OR OPTX$="m" THEN 2110
1930 IF OPTX$="E" OR OPTX$="e" THEN LOCATE 24,1:PRINT SPACE$(78);
```

```
1940 LOCATE 23,1:END
1950 LOCATE 24,1:PRINT SPC(79):LOCATE 24,1:GOTO 1900
1960 '
1970 'Save screen routine.
1980 '
1990 LOCATE 25,1:PRINT SPACE$(78);:LOCATE 25,1
2000 INPUT ;"ENTER [DSK:] filename (NO EXTENSION)  ";FIL$
2010 OPEN FIL$+".PAR" AS #1 LEN=30
2020 GOSUB 2170
2030 LOCATE 24,1:PRINT SPACE$(78);:LOCATE 25,1:PRINT SPACE$(78);:LOCATE 23,1
2040 DEF SEG =&HB800
2050 BSAVE FIL$+".SCN",0,&H4000
2060 DEF SEG
2070 LOCATE 25,1:PRINT "FILE ";CHR$(34);FIL$ ;CHR$(34);" SAVED ";
2080 LOCATE 23,1:END
2090 LOCATE 24,1:PRINT SPACE$(78);:LOCATE 23,1
2100 END
2110 LOCATE 24,1:PRINT SPACE$(78);:LOCATE 24,1
2120 FLX$="mplot.bas"
2130 LOCATE 24,1:PRINT SPACE$(78);:LOCATE 24,1
2140 GOSUB 2160
2150 GOTO 2440
2160 OPEN "CHAINDAT.PAR" AS #1 LEN = 30
2170 FIELD #1, 15 AS XPAR$,15 AS YPAR$
2180 LSET XPAR$ = MKS$(SX)
2190 LSET YPAR$ = MKS$(SY)
2200 PUT #1,1
2210 LSET XPAR$ = MKS$(DX)
2220 LSET YPAR$ = MKS$(DY)
2230 PUT #1,2
2240 LSET XPAR$ = MKS$(X2)
2250 LSET YPAR$ = MKS$(Y2)
2260 PUT #1,3
2270 LSET XPAR$ = MKS$(X1)
2280 LSET YPAR$ = MKS$(Y1)
2290 PUT #1,4
2300 LSET XPAR$ = MKS$(QX)
2310 LSET YPAR$ = MKS$(QY)
2320 PUT #1,5
2330 LSET XPAR$ = MKS$(OX)
2340 LSET YPAR$ = MKS$(OY)
2350 PUT #1,6
2360 LSET XPAR$ = MKS$(XA)
2370 LSET YPAR$ = MKS$(YA)
2380 PUT #1,7
2390 XE = 1/ABS(X2-X1):LSET XPAR$ = MKS$(XE)
2400 YE = 1/ABS(Y2-Y1):LSET YPAR$ = MKS$(YE)
2410 PUT #1,8
2420 CLOSE #1
```

```
2430 RETURN
2440 CHAIN FLX$
2450 END
```

AV.9 MAKEGRAF.BAS

```
10 '          MAKE A LINEAR X,Y GRAPH
20 '
30 '
40 'This program allows the user to make an x,y linear graph on the
50 'graphics monitor with the x and y axis labeled. The graph is generated
60 'via LINPLT.BAS program which calls file RLINPLT.LNK. The RLINPLT.LNK
70 'file has the x and y labels and the data file which this program makes.
80 '
90 CLS:KEY OFF
100 XLOOP = 0
110 GOTO 580
120 OPEN "RLINPLT.LNK" AS #1 LEN = 30
130 FIELD #1,30 AS RFLD$
140 GET #1,1
150 LSET RFLD$ = MKI$(1)
160 PUT #1,1
170 GET #1,2
180 LSET RFLD$ = YLBL$
190 PUT #1,2
200 GET #1,3
210 LSET RFLD$ = XLBL$
220 PUT #1,3
230 GET #1,4
240 LSET RFLD$ = FILX$
250 PUT #1,4
260 CLOSE #1
270 OPEN FILX$ AS #1 LEN = 30
280 FIELD #1,15 AS X$,15 AS Y$
290 FOR I = 1 TO 14:LSET X$ = "XXX":LSET Y$ ="YYY":PUT #1,I:
    NEXT I:CLOSE #1
300 OPEN FILX$ AS #1 LEN = 30
310 FIELD #1,15 AS X$,15 AS Y$
320 GET #1,1
330 LSET X$ = MKS$(2):LSET Y$ = MKS$(2)
340 PUT #1,1
350 GET #1,2
360 LSET X$ = MKS$(XMAX):LSET Y$ = MKS$(YMAX)
370 PUT #1,2
380 GET #1,3
390 LSET X$ = MKS$(XMIN):LSET Y$ = MKS$(YMIN)
400 PUT #1,3
410 LOCATE 25,1
420 PRINT SPACE$(78);:LOCATE 25,1
430 PRINT "ENTER OPTION  Plot, End ";
440 YN$ = INKEY$: IF YN$ ="" THEN 440
450 IF YN$ ="E" OR YN$ = "e" THEN CLS:NEW:END
```

```
460 IF YN$ ="P" OR YN$ = "p" THEN CLOSE #1:CHAIN "LINPLT.BAS" ELSE 410
470 LOCATE 25,1:PRINT SPACE$(78);:LOCATE 25,1:XLOOP = 1
480 INPUT;"ENTER FIELD CHANGE XMAX, XMIN, YMAX, YMIN, XLAB, YLAB,
    FILE, RUN :",EF$
490 IF EF$ = "XMAX" OR EF$ = "xmax" THEN 580
500 IF EF$ = "YMAX" OR EF$ = "ymax" THEN 640
510 IF EF$ = "XMIN" OR EF$ = "xmin" THEN 610
520 IF EF$ = "YMIN" OR EF$ = "ymin" THEN 670
530 IF EF$ = "XLAB" OR EF$ = "xlab" THEN 700
540 IF EF$ = "YLAB" OR EF$ = "ylab" THEN 730
550 IF EF$ = "FILE" OR EF$ = "file" THEN 760
560 IF EF$ = "RUN" OR EF$ = "run" THEN 120
570 GOTO 470
580 LOCATE 3,1:PRINT SPACE$(78);:LOCATE 3,1
590 INPUT ;"ENTER 'X' MAXIMUM VALUE = ",XMAX
600 IF XLOOP = 1 THEN GOTO 470 ELSE 610
610 LOCATE 4,1:PRINT SPACE$(78);:LOCATE 4,1
620 INPUT ;"ENTER 'X' MINIMUM VALUE = ",XMIN
630 IF XLOOP = 1 THEN GOTO 470 ELSE 640
640 LOCATE 6,1:PRINT SPACE$(78);:LOCATE 6,1
650 INPUT ;"ENTER 'Y' MAXIMUM VALUE = ",YMAX
660 IF XLOOP = 1 THEN GOTO 470 ELSE 670
670 LOCATE 7,1:PRINT SPACE$(78);:LOCATE 7,1
680 INPUT ;"ENTER 'Y' MINIMUM VALUE = ",YMIN
690 IF XLOOP = 1 THEN GOTO 470 ELSE 700
700 LOCATE 9,1:PRINT SPACE$(78);:LOCATE 9,1
710 INPUT ;"ENTER 'X' LABEL [30 charactr's]: ",XLBL$
720 IF XLOOP = 1 THEN GOTO 470 ELSE 730
730 LOCATE 10,1:PRINT SPACE$(78);:LOCATE 10,1
740 INPUT ;"ENTER 'Y' LABEL [16 charactr's]: ",YLBL$
750 IF XLOOP = 1 THEN GOTO 470 ELSE 760
760 LOCATE 12,1:PRINT SPACE$(78);:LOCATE 12,1
770 INPUT ;"ENTER DATA FILE NAME dsk:filename.ext — ",FILX$
780 GOTO 470
```

Appendix VI

PROGRAMS FOR POROSIMETRY EXPERIMENTS

Two short progams used in the inversion of data from the mercury porosimetry experiments are given in this Appendix.

The raw data from a porosimetry run are in the form of intrusion pressures versus intrusion volumes. This is plotted on graph paper in real-time. That data is digitized either by hand or by any other suitable means and a digitized data file is made. The program HGINV.BAS reads the digitized data file and after suitable manipulations, produces a file containing the pore volume and pore surface area distributions. The dead volume correction as provided by the porosimeter manufacturer is incorporated in the program.

The HGVOLPRT.BAS program computes the specific volumes and surface areas from the respective distribution data in the three pore size ranges corresponding to micro, transitional, and macro pores. The appropriate ranges are user defined.

AVI.1 HGINV.BAS

```
10 '          MERCURY INTRUSION INVERSION PROGRAM
20 '
30 'This program reads the digitized data file and creates a file containing
40 'r(P), dV/d(log r) and dS/d(log r). The distribution curves are plotted
50 'versus log r. The dead volume correction is included.
60 KEY OFF
70 CLS
80 'Polynomial corrections for blank volume:
90 'These coefficients are from the run performed on 2/13/87.
100 'Intrusion 0-3000 psi
110 '
120 C0=-.000762 : C1=-9.243701E-07 : C2=1.59553E-10
130 '
140 'Intrusion 3000-33000 psi
150 '
160 D0=-.002943 : D1=1.560229E-07 : D2=-1.902453E-12
170 '
180 'Extrusion 25-3000 psi
190 '
200 E0=.0015 : E1=0! : E2=0!
210 '
220 'Extrusion 3000-33000 psi
230 '
240 F0=.001016 : F1= 1.43002E-07 : F2=-4.873868E-12
250 '
260 DIM VOLLOG(NN),SURLOG(NN),DV(NN),DP(NN),P(NN),V(NN)
270 DIM R(NN),RR(NN),VRAW(NN),VCOR(NN),RAV(NN)
280 INPUT "NO.OF PRESSURE POINTS";NN
290 INPUT "NAME OF DATA FILE";N$
300 INPUT "MASS OF SAMPLE";M
310 INPUT "NAME OF OUTPUT FILE ";FIL1$
320 INPUT "Intrusion (0) or extrusion (1)";FLAG
330 IF (FLAG=0 OR FLAG=1)GOTO 340 ELSE GOTO 320
340 OPEN "I",#1,N$
350 FOR I = 1 TO NN
360  INPUT #1,P(I),VRAW(I)
370 NEXT I
380 CLOSE #1
390 IF FLAG = 1 THEN GOTO 490
400 '
410 'The first point correction is different.
420 '
430 FOR I=2 TO NN
440  IF P(I)<3000 THEN VCOR(I)=C0+P(I)*(C1+P(I)*C2)
450  IF P(I)>3000 THEN VCOR(I)=D0+P(I)*(D1+P(I)*D2)
460 NEXT I
```

```
470 VCOR(1)=0!
480 GOTO 540
490 FOR I=2 TO NN
500  IF P(I)<3000 THEN VCOR(I)=E0+P(I)*(E1+P(I)*E2)
510  IF P(I)>3000 THEN VCOR(I)=F0+P(I)*(F1+P(I)*F2)
520 NEXT I
530 VCOR(1)=.0035
540 FOR I=1 TO NN
550  V(I)=VRAW(I)−VCOR(I)
560 NEXT I
570 R(1)=106.66/(P(1)+14.7): DV(1)=V(1)/M : DP(1)=P(1)+14.7
580 RAV(1)=2*106.66/(P(1)+14.7)
590 TOTSURF=0
600 FOR I = 2 TO NN
610  R(I) = 106.66/(P(I)+14.7)
620  RAV(I)=(R(I)+R(I−1))/2
630  DV(I)=(V(I)−V(I−1))/M
640  IF DV(I)<0 THEN DV(I)=0
650  DP(I) = P(I) − P(I−1)
660  VOLLOG(I) = 2.303*P(I)*DV(I)/DP(I)
670  SURLOG(I)=VOLLOG(I)*2/RAV(I)
680  SURF=2*DV(I)*10000!/RAV(I)
690  TOTSURF=TOTSURF+SURF
700 NEXT I
710 VFIN=V(NN)/M
720 LOCATE 11,1
730 PRINT "Total volume intruded was (cc/g)" : PRINT VFIN
740 LOCATE 13,1
750 PRINT "Total surface area was (sq. cm/g)" :PRINT TOTSURF
760 LOCATE 15,1
770 PRINT "Writing new files . . . "
780 OPEN FIL1$ FOR OUTPUT AS #1
790 FOR I= 1 TO NN
800  RAV(I)=RAV(I)*10000
810  WRITE #1, RAV(I),VOLLOG(I),SURLOG(I)
820 NEXT I
830 CLOSE #1
840 LOCATE 17,1
850 PRINT "DONE."
860 END
```

AVI.2 HGVOLPRT.BAS

```
10 '          POROSIMETRY DATA PARTITIONING PROGRAM
20 '
30 'This program computes the specific volume and surface area
40 'from pore volume and pore surface distributions in three
50 'pore size ranges corresponding to external, macro, and transition
60 'pores. The ranges are defined by the user.
70 'Suggested ranges are: < 500 Å  for transitional—macro boundary and
80 '< 17600 Å  for macro—interparticle boundary (60 psi).
90 'This program also calculates a mean pore radius for each range.
100 '
110 DIM R(200), VLOG(200), SLOG(200), DVDR(200), DSDR(200)
120 DIM DELVOL(200),DELSURF(200),RVOL(200)
130 CLS
140 INPUT "What is the name of the input file ";FIL1$
150 INPUT "What is the file name you will write to ";N$
160 INPUT "Number of points in file ";NPTS
170 INPUT "Enter the radius (A) for transition—macro boundary ";R1
180 INPUT "Enter the radius (A) for macro—interparticle boundary ";R2
190 '
200 'Open pore volume distribution file (from HGINV.BAS)
210 '
220 OPEN FIL1$ FOR INPUT AS #1
230 FOR X=1 TO NPTS
240   INPUT #1,R(X),VLOG(X),SLOG(X)
250 NEXT X
260 CLOSE #1
270 '
280 'Calculate area under dV/dlog r curve to get volume.
290 'The average radius is obtained from the first moment.
300 '
310 FOR I=1 TO NPTS−1
320   DVDR(I)=VLOG(I)/R(I)
330   DELVOL(I)=.5*(DVDR(I)+DVDR(I+1))*(R(I)−R(I+1))
340   RVOL(I)=.5*(VLOG(I)+VLOG(I+1))*(R(I)−R(I+1))
350   DSDR(I)=SLOG(I)/R(I)
360   DELSURF(I)=.5*(DSDR(I)+DSDR(I+1))*(R(I)−R(I+1))
370 NEXT I
380 RTRANS=R1/2!
390 RMACRO=(R1+R2)/2!
400 RINTRP=(R2+R(1))/2!
410 EXTVOL=0:MACVOL=0:TRNVOL=0:EXTSUR=0:MACSUR=0:TRNSUR=0
420 FOR J=2 TO NPTS
430   IF R(J) > R2 THEN EXTVOL=EXTVOL+DELVOL(J)
440   IF R(J) > R2 THEN EXTSUR=EXTSUR+DELSURF(J)
450   IF R(J) < R2 AND R(J) > R1 THEN MACVOL=MACVOL+DELVOL(J)
460   IF R(J) < R2 AND R(J) > R1 THEN MACSUR=MACSUR+DELSURF(J)
```

```
470  IF R(J) < R1 THEN TRNVOL=TRNVOL+DELVOL(J)
480  IF R(J) < R1 THEN TRNSUR=TRNSUR+DELSURF(J)
490 NEXT J
500 EXTSUMRV=0: MACSUMRV=0: TRNSUMRV=0
510 FOR J=2 TO NPTS
520  IF R(J) > R2 THEN EXTSUMRV=EXTSUMRV+RVOL(J)
530  IF R(J) < R2 AND R(J) > R1 THEN MACSUMRV=MACSUMRV+RVOL(J)
540  IF R(J) < R1 THEN TRNSUMRV=TRNSUMRV+RVOL(J)
550 NEXT J
560 EXTRAV=EXTSUMRV/EXTVOL
570 MACRAV=MACSUMRV/MACVOL
580 TRNRAV=TRNSUMRV/TRNVOL
590 VOLSUM=EXTVOL+MACVOL+TRNVOL
600 SURSUM=EXTSUR+MACSUR+TRNSUR
610 OPEN N$ FOR OUTPUT AS #1
620 WRITE #1,RTRANS,TRNVOL,TRNSUR
630 WRITE #1,RMACRO,MACVOL,MACSUR
640 WRITE #1,RINTRP,EXTVOL,EXTSUR
650 PRINT RTRANS,TRNVOL,TRNSUR
660 PRINT RMACRO,MACVOL,MACSUR
670 PRINT RINTRP,EXTVOL,EXTSUR
680 PRINT
690 PRINT ,VOLSUM, SURSUM
700 PRINT
710 PRINT
720 PRINT EXTRAV,MACRAV,TRNRAV
730 CLOSE #1
740 END
```

Appendix VII

PROGRAMS FOR HIGH TEMPERATURE PYROMETRY

The programs used to acquire particle temperature data from the high temperature reactor pyrometer are given in this Appendix.

The data acquisition program is GETTEMP.BAS. It uses the DT2801-A board and an external trigger to gather the signals from the 1000nm and 800nm channels of the pyrometer. The signals are digitized and stored in the computer RAM via a DMA procedure. PYRO.BAS reads in the raw signal data and creates the actual signal data for temperature inversion. Basically, this involves separating the DMA data into their respective channels, calculating the baselines averages and finally, calculating the signal strengths above their respective baselines. MTEMP.FOR uses suitable calibration data and Planck law analysis to generate the particle temperature-time data.

Figure AVII.1 shows the sequence of steps just outlined. Program listings follow.

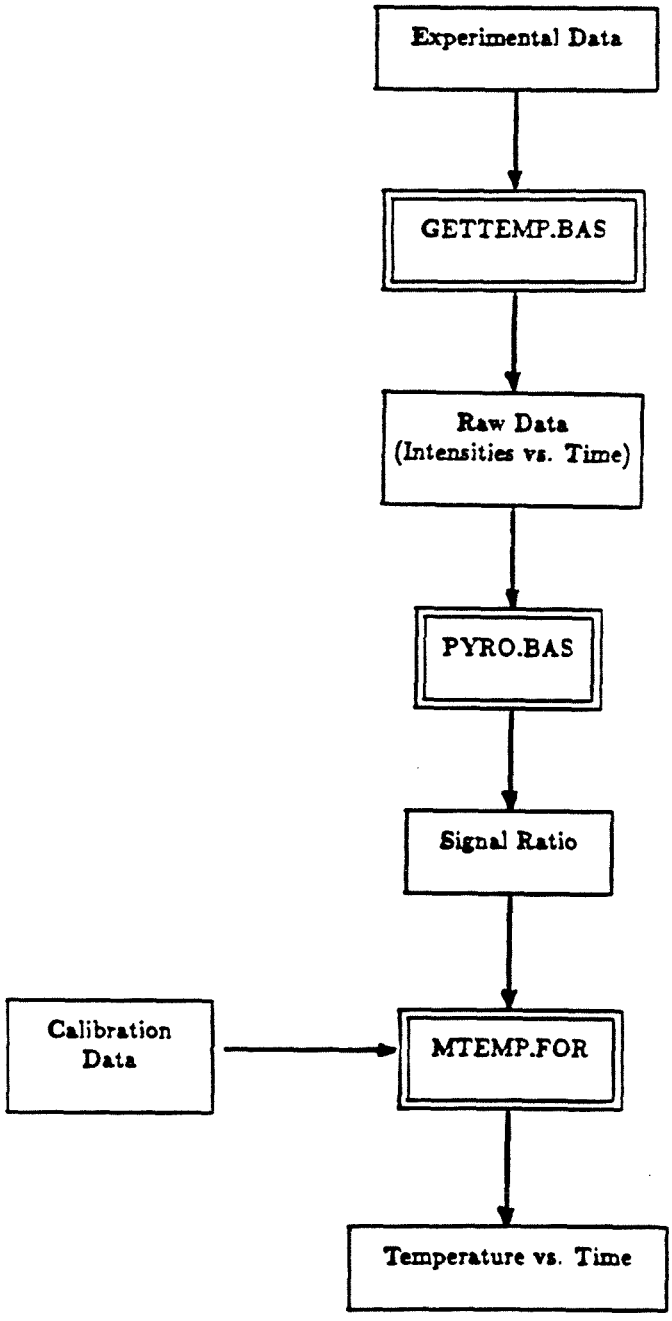

Figure AVII.1 Flow Diagram for the analysis of optical pyrometry data.

AVII.1 GETTEMP.BAS

```
10 '            DIRECT MEMORY ACCESS PROGRAM
20 '
30 '
40 '
50 'This program is used to gather pyrometry data from the high
60 'temperature reactor. Channels 0 and 1 collect the
70 'signals from wavelengths 1000 and 800 nm.
80 'It performs fast data acquisition (20kHz) by driving
90 'the DT2801-A data acquisition board (DATA TRANSLATION INC.).
100 'The system is externally triggered when the voltage on channel 0/1
110 'rises above an adjustable threshold. A fixed number points
120 '(user specified) are obtained from each channel.
130 'These data are printed sequentially on the screen, and then plotted
140 'by chaining to MPLOT.BAS, thence to LINPLT.BAS via RLINPLT.LNK.
150 'The memory allocation specifications etc. are for the Zenith 148.
160  CLEAR ,25000
170  '
180  DEFINT A-Z
190  BASE.ADDRESS = &H2EC
200  COMMAND.REGISTER = BASE.ADDRESS + 1
210  STATUS.REGISTER = BASE.ADDRESS + 1
220  DATA.REGISTER = BASE.ADDRESS
230  COMMAND.WAIT = &H4
240  WRITE.WAIT = &H2
250  READ.WAIT = &H5
260  CSTOP = &HF
270  CCLEAR = &H1
280  CERROR = &H2
290  CCLOCK = &H3
300  CSAD = &HD
310  CRAD = &HE
320  MIN.CONV = 3
330  MAX.CONV = 20000!
340  CDMA = &H10
350  DUMMY = 5
360  FREQUENCY# = 800000!
370  PERIOD# = 40
380  EXT.TRIGGER = &H80
390  '
400  'A/D parameter constants.
410  '
420  FACTOR# = 4096
430  '
440  'The memory to be used for DMA starts at memory address &HF800
450  'on memory page 0.
460  '
```

```
470 DMACHANNEL = 1
480 DMAMODE = &H45
490 BASEREG = 2
500 COUNTREG = 3
510 PAGEREG = &H83
520 DMABASEL = 0
530 DMABASEH = &H0
540 DMAPAGE = 3
550 '
560 'Check for legal Status Register.
570 '
580 STATUS = INP(STATUS.REGISTER)
590 IF NOT((STATUS AND &H70) = 0) THEN GOTO 2540
600 '
610 'Stop and clear the DT2801-A.
620 '
630 OUT  COMMAND.REGISTER, CSTOP
640 TEMP = INP(DATA.REGISTER)
650 WAIT STATUS.REGISTER,  COMMAND.WAIT
660 OUT  COMMAND.REGISTER, CCLEAR
670 COMMAND=COMMAND+EXT.TRIGGER
680 '
690 GAIN(0) = 1 : GAIN(1) = 2
700 GAIN(2) = 4 : GAIN(3) = 8
710 '
720 'Range and Offset are set for unipolar differential outputs.
730 '
740 RANGE=10 : OFFSET=0
750 CLS
760 INPUT "What is the name of the file series ";FILSER$
770 '
780 'Print out conversion rate.
790 '
800 PRINT
810 PRINT "The internal clock is set to a frequency of ";
820 PRINT USING "#####";FREQUENCY#/PERIOD#; : PRINT " Hertz."
830 '
840 'Get A/D gain.
850 '
860 PRINT "Legal values for gain are ";GAIN(0);", ";GAIN(1);
870 PRINT ", ";GAIN(2);", and ";GAIN(3);"."
880 INPUT " Gain value = ";Y
890 '
900 FOR GAIN.CODE = 0 TO 3 : IF GAIN(GAIN.CODE) = Y  THEN GOTO 950
910 NEXT GAIN.CODE
920 '
930 PRINT : PRINT " Please use legal gain value."
940 GOTO 860
950 START.CHANNEL=0 : END.CHANNEL=1
```

```
960  '
970  'Get number of conversions to do.
980  '
990  PRINT : PRINT : PRINT "          ";
1000  PRINT "Legal values for number of conversions are ";MIN.CONV;
1010  PRINT " through ";MAX.CONV;"."
1020  INPUT " Number of conversions value = ";NUM.CONV
1030  '
1040  IF (NUM.CONV >= MIN.CONV AND NUM.CONV =< MAX.CONV)
       THEN GOTO 1090
1050  '
1060  PRINT
1070  PRINT "Please use legal number of conversions value."
1080  GOTO 960
1090  '
1100  'Set up the A/D converter.
1110  'Write SET A/D PARAMETERS command.
1120  '
1130  WAIT STATUS.REGISTER,  COMMAND.WAIT
1140  OUT  COMMAND.REGISTER, CSAD
1150  '
1160  'Write A/D gain byte.
1170  '
1180  WAIT STATUS.REGISTER,  WRITE.WAIT, WRITE.WAIT
1190  OUT  DATA.REGISTER,    GAIN.CODE
1200  '
1210  'Write A/D start channel byte.
1220  '
1230  WAIT STATUS.REGISTER,  WRITE.WAIT, WRITE.WAIT
1240  OUT  DATA.REGISTER,    START.CHANNEL
1250  '
1260  'Write A/D end channel byte.
1270  '
1280  WAIT STATUS.REGISTER,  WRITE.WAIT, WRITE.WAIT
1290  OUT  DATA.REGISTER,    END.CHANNEL
1300  '
1310  'Write two bytes, dummy number of conversions.
1320  '
1330  WAIT STATUS.REGISTER,  WRITE.WAIT, WRITE.WAIT
1340  OUT  DATA.REGISTER,    DUMMY
1350  WAIT STATUS.REGISTER,  WRITE.WAIT, WRITE.WAIT
1360  OUT  DATA.REGISTER,    DUMMY
1370  '
1380  'Set internal clock rate.
1390  'Write SET CLOCK PERIOD command.
1400  '
1410  WAIT STATUS.REGISTER,  COMMAND.WAIT
1420  OUT  COMMAND.REGISTER, CCLOCK
1430  '
```

```
1440  'Write high and low bytes of PERIOD#.
1450  '
1460  PERIODH = INT(PERIOD#/256)
1470  PERIODL = PERIOD# – PERIODH * 256
1480  WAIT STATUS.REGISTER,  WRITE.WAIT, WRITE.WAIT
1490  OUT  DATA.REGISTER,   PERIODL
1500  WAIT STATUS.REGISTER,  WRITE.WAIT, WRITE.WAIT
1510  OUT  DATA.REGISTER,   PERIODH
1520  '
1530  'Set–up DMA controller
1540  '
1550  DMACOUNT  = (NUM.CONV * 2) – 1
1560  DMACOUNTH = INT(DMACOUNT/256)
1570  DMACOUNTL = DMACOUNT – DMACOUNTH * 256
1580  '
1590  OUT 11,DMAMODE           ' set DMA mode
1600  OUT 12,0                 ' clear byte flip–flop
1610  OUT BASEREG,DMABASEL     ' set DMA memory base address
1620  OUT BASEREG,DMABASEH     '
1630  OUT COUNTREG,DMACOUNTL   ' set DMA byte count
1640  OUT COUNTREG,DMACOUNTH   '
1650  OUT PAGEREG,DMAPAGE      ' set DMA memory page
1660  OUT 10,DMACHANNEL        ' enable DMA channel mask
1670  '
1680  'Check for ERROR.
1690  '
1700  WAIT STATUS.REGISTER,  COMMAND.WAIT
1710  STATUS = INP(STATUS.REGISTER)
1720  IF (STATUS AND &H80) THEN GOTO 2320
1730  '
1740  'Write READ A/D WITH DMA command.
1750  '
1760  PRINT : PRINT "        Starting conversions." : PRINT
1770  '
1780  WAIT STATUS.REGISTER,  COMMAND.WAIT
1790  OUT  COMMAND.REGISTER, CRAD + CDMA + COMMAND
1800  '
1810  'Check for ERROR.
1820  '
1830  WAIT STATUS.REGISTER,  COMMAND.WAIT
1840  STATUS = INP(STATUS.REGISTER)
1850  PRINT "TRIGGERED"
1860  IF (STATUS AND &H80) THEN GOTO 2320
1870  '
1880  'Calculate and print the A/D readings in volts.
1890  '
1900  PRINT
1910  '
1920  DEF SEG = &H3000
```

```
1930  SUFF=MAIN+97
1940  RUNNUM$=CHR$(SUFF)
1950  '
1960  FILNEW$=FILSER$+RUNNUM$+".dat"
1970  OPEN FILNEW$ AS #1 LEN=30
1980  FIELD #1, 15 AS X$, 15 AS Y$
1990  LSET X$=MKS$(NUM.CONV) : LSET Y$=MKS$(0)
2000  PUT #1,1
2010  FOR LOOP = 1 TO NUM.CONV
2020  ADDRESS = (LOOP - 1) * 2
2030  DATA.VALUE# = PEEK(ADDRESS)
2040  DATA.VALUE# = DATA.VALUE# + PEEK(ADDRESS + 1) * 256
2050  VOLTS#=((RANGE*DATA.VALUE#/FACTOR#)-OFFSET)/
       GAIN(GAIN.CODE)
2060  TIME#=(LOOP-1)*.05
2070  LSET X$ =MKS$(TIME#): LSET Y$ =MKS$(VOLTS#)
2080  PUT #1, LOOP+1
2090  PRINT "        CHANNEL "; : PRINT USING "##";CHANNEL;
2100  PRINT " = "; : PRINT USING "###.######";VOLTS#;
2110  IF CHANNEL = END.CHANNEL THEN PRINT
2120  NEXT LOOP
2130  CLOSE #1
2140  PRINT
2150  PRINT FILNEW$
2160  GOTO 2700
2170  PRINT : PRINT
2180  INPUT "         Do you want to do more conversions (Y/N)";Y$
2190  IF Y$ = "N" OR Y$ = "n" THEN GOTO 2230
2200  IF Y$ = "Y" OR Y$ = "y" THEN GOTO 760
2210  '
2220  GOSUB 2270 : GOTO 2160
2230  '
2240  PRINT : PRINT
2250  PRINT "       READ A/D WITH DMA Operation Complete"
2260  GOTO 2610
2270  '
2280  'Respond to query with 'Y' or 'N'.
2290  '
2300  PRINT : PRINT "         Please respond with 'Y' or 'N' only."
2310  RETURN
2320  '
2330  'Fatal board error.
2340  '
2350  PRINT
2360  PRINT "FATAL BOARD ERROR"
2370  PRINT "STATUS REGISTER VALUE IS ";HEX$(STATUS);" HEXIDECIMAL"
2380  PRINT : BEEP : BEEP : GOSUB 2430
2390  PRINT "ERROR REGISTER VALUES ARE:"
2400  PRINT "     BYTE 1 -   ";HEX$(ERROR1);"  HEXIDECIMAL"
```

```
2410 PRINT "     BYTE 2 –  ";HEX$(ERROR2);" HEXIDECIMAL"
2420 PRINT : GOTO 2610
2430 '
2440 'Read the Error Register.
2450 '
2460 OUT  COMMAND.REGISTER, CSTOP : TEMP = INP(DATA.REGISTER)
2470 WAIT STATUS.REGISTER, COMMAND.WAIT
2480 OUT COMMAND.REGISTER, CERROR
2490 WAIT STATUS.REGISTER, READ.WAIT
2500 ERROR1 = INP(DATA.REGISTER)
2510 WAIT STATUS.REGISTER, READ.WAIT
2520 ERROR2 = INP(DATA.REGISTER)
2530 RETURN
2540 '
2550 'Illegal Status Register.
2560 '
2570 PRINT
2580 PRINT "FATAL ERROR – ILLEGAL STATUS REGISTER VALUE"
2590 PRINT "STATUS REGISTER VALUE IS ";HEX$(STATUS);" HEXIDECIMAL"
2600 BEEP : BEEP
2610 PRINT : PRINT
2620 '
2630 INPUT "        Run program again (Y/N)";Y$
2640 IF Y$ = "Y" OR Y$ = "y" THEN RUN
2650 IF Y$ = "N" OR Y$ = "n" THEN GOTO 2690
2660 '
2670 PRINT : PRINT "        Please respond with 'Y' or 'N'."
2680 GOTO 2620
2690 '
2700 'This part of the program sets the parameters for plotting the data.
2710 '
2720 SCREEN 0,0,0:CLS:KEY OFF
2730 DIM FL$(1)
2740 NOF=1
2750 XLBL$ = "TIME"
2760 YLBL$ = "VOLTS"
2770 FL$(1)=FILNEW$
2780 OPEN "RLINPLT.LNK" AS #1 LEN = 30
2790 FIELD #1, 30 AS RFLD$
2800 FOR I = 1 TO 21:LSET RFLF$ = "XXXXXXXXX":PUT #1,I:NEXT I:CLOSE #1
2810 OPEN "RLINPLT.LNK" AS #1 LEN = 30
2820 FIELD #1, 30 AS RFLD$
2830 GET #1,1
2840 LSET RFLD$ = MKI$(NOF)
2850 PUT #1,1
2860 GET #1,2
2870 LSET RFLD$ = YLBL$
2880 PUT #1,2
2890 GET #1,3
```

```
2900  LSET RFLD$ = XLBL$
2910  PUT #1,3
2920  FOR I = 1 TO NOF
2930  GET #1,I+3
2940  LSET RFLD$ = FL$(I)
2950  PUT #1,I+3
2960  NEXT I
2970  CLOSE #1
2980  CLS
2990  CHAIN "LINPLT.BAS"
3000  '
3010  END
```

AVII.2 PYRO.BAS

```
10 '            PYROMETRY INVERSION PROGRAM
20 '
30 'This program takes the pyrometry signal file (from GETTEMP.BAS)
40 'and first separates the signals into their respective channels.
50 'It then computes the baseline average (over the last 15 points)
60 'signal in each channel. Finally, it computes the actual signal
70 '(input−average) in each channel and the ratio of the signals (rat)
80 'The output file, readable by zplot (ASCII) contains the actual
90 'signals, their ratio and also the raw signals and time.
100 'This output file is read by MTEMP.EXE (from MTEMP.FOR) to deduce
110 'the temperature from the signal ratio.
120 '
130 '
140 N = 200          'size of the arrays
150 '
160 CLS:SCREEN 0,0,0:KEY OFF
170 LOCATE 5,1
180 '
190 'Enter input file from GETTEMP.BAS
200 '
210 INPUT "Enter name of file to be modified  as [dsk:]filename.dat  ";FILOLD$
220 LOCATE 7,1
230 INPUT "Enter name of new file as [dsk:]filename.dat              ";FILNEW$
240 DIM X(N),Y(N),Y1(N),Y2(N),Y1SIG(N),Y2SIG(N),RAT(N)
250 LOCATE 9,1
260 PRINT "Reading old file..."
270 OPEN FILOLD$ AS #1 LEN = 30
280 FIELD #1, 15 AS X$, 15 AS Y$
290 GET #1,1
300 NPTS = CVS(X$)
310 M = CVS(Y$)
320 FOR I = 1 TO NPTS
330 GET #1,I+1
340 X(I) = CVS(X$)
350 Y(I) = CVS(Y$)
360 NEXT I
370 CLOSE #1
380 IC=1
390 '
400 'Separate the signals into proper channels.
410 '
420 FOR I=NPTS TO 2 STEP−2
430 Y1(IC)=Y(I)
440 Y2(IC)=Y(I−1)
450 X(IC)=(IC−1)*.1
460 IC=IC+1
```

```
470 NEXT I
480 NNEW=NPTS/2
490 '
500 'Calculate baseline average in each channel.
510 '
520 SUM1 = 0
530 SUM2 = 0
540 FOR J=1 TO 15
550 SUM1=SUM1+Y1(J)
560 SUM2=SUM2+Y2(J)
570 NEXT J
580 Y1AV=SUM1/15!
590 Y2AV=SUM2/15!
600 '
610 'Find the actual signal level in each channel and the signal ratio.
620 '
630 FOR K=1 TO NNEW
640 Y1SIG(K)=Y1(K)-Y1AV
650 Y2SIG(K)=Y2(K)-Y2AV
660 RAT(K)=Y1SIG(K)/Y2SIG(K)
670 IF RAT(K)<1! THEN RAT(K)=1!/RAT(K)
680 PRINT RAT(K)
690 NEXT K
700 PRINT "Computing modifications..."
710 '
720 'Write to output file.
730 '
740 LOCATE 13,1
750 PRINT "Writing new file..."
760 OPEN FILNEW$ FOR OUTPUT AS #1
770 FOR I = 1 TO NNEW
780 WRITE #1,X(I),Y1(I),Y2(I),Y1SIG(I),Y2SIG(I),RAT(I)
790 NEXT I
800 CLOSE #1
810 LOCATE 15,1
820 PRINT "Done."
830 KEY ON
840 LOCATE 24,1
850 END
```

AVII.3 MTEMP.FOR

```
C   This program calculates the particle temperature from the
C   high temperature pyrometry experiments. Its input is the
C   file from PYRO.BAS that has the ratio of the signals in the
C   two wavelengths. Using that ratio and a calibration factor
C   the particle temperature is calculated from a Planck law
C   analysis.
C
C
      DIMENSION X(50),Y1(50),Y2(50),Y1S(50),Y2S(50)
      DIMENSION RAT(50),TEMP(50),TIME(50)
      CHARACTER*15 OLDFILE,NEWFILE
C
      WRITE(*,10)
 10   FORMAT(1X,'ENTER OLDFILE:')
      READ(*,12)OLDFILE
 12   FORMAT(A15)
      WRITE(*,14)
 14   FORMAT(1X,'ENTER NEWFILE')
      READ(*,12)NEWFILE
      WRITE(*,16)
 16   FORMAT(1X,'ENTER RATIO')
      READ(*,*)RATIO
C
      OPEN(1,FILE=OLDFILE,STATUS='OLD',FORM='FORMATTED')
      DO 100 I=1,50
```

```
260           READ(1,*,END=101)X(I),Y1(I),Y2(I),Y1S(I),Y2S(I),RAT(I)
270    100    CONTINUE
280    101    CONTINUE
290           CLOSE(1)
300   C
310           CAL=-1.0*ALOG(RATIO/26.3114)
320   C
330           DO 200 J=1,50
340           IF (RAT(J) .EQ. 0.0)GOTO 201
350           TIME(J)=(J-1)*0.1
360           TEMP(J)=3597.0/(ALOG(RAT(J))+CAL)
370    200    CONTINUE
380    201    CONTINUE
390   C
400           OPEN(2,FILE=NEWFILE,STATUS='NEW')
410           DO 300 K=1,50
420             IF(Y1S(K) .NE. 0.0)THEN
430               WRITE(2,400)TIME(K),TEMP(K),Y1S(K),Y2S(K),RAT(K)
440             ELSE
450               CONTINUE
460             ENDIF
470    300    CONTINUE
480    400    FORMAT(5X,5G12.6)
490   C
500           CLOSE(2)
510           STOP
520           END
```

Appendix VIII

PROGRAMS FOR KINETIC PARAMETER ESTIMATION

The experimental and theoretical procedure used to get the chemical kinetic parameters at high temperatures is outlined in Figure AVIII.1. First, single particle experiments are done and individual temperature-time traces depicting the particle combustion histories are obtained. The program AD2.FOR is used for data acquisition purposes. The raw data containing the light intensity voltage values are converted to particle temperatures in the program RETEMP.FOR.

Once the experimental time histories are known, the kinetic parameter estimation program VARASH.FOR is used to determine the kinetic parameters. Individual traces are fit by polynomial functions and the polynomial coefficents are used as inputs in the VARASH program. VARASH also contains a suitable particle combustion model (VARNU.FOR, see Appendix IX) to interpret the traces. Details of the procedure are given in Chapter 4. Temperature-time traces of most of the runs are collected in Appendix XII.

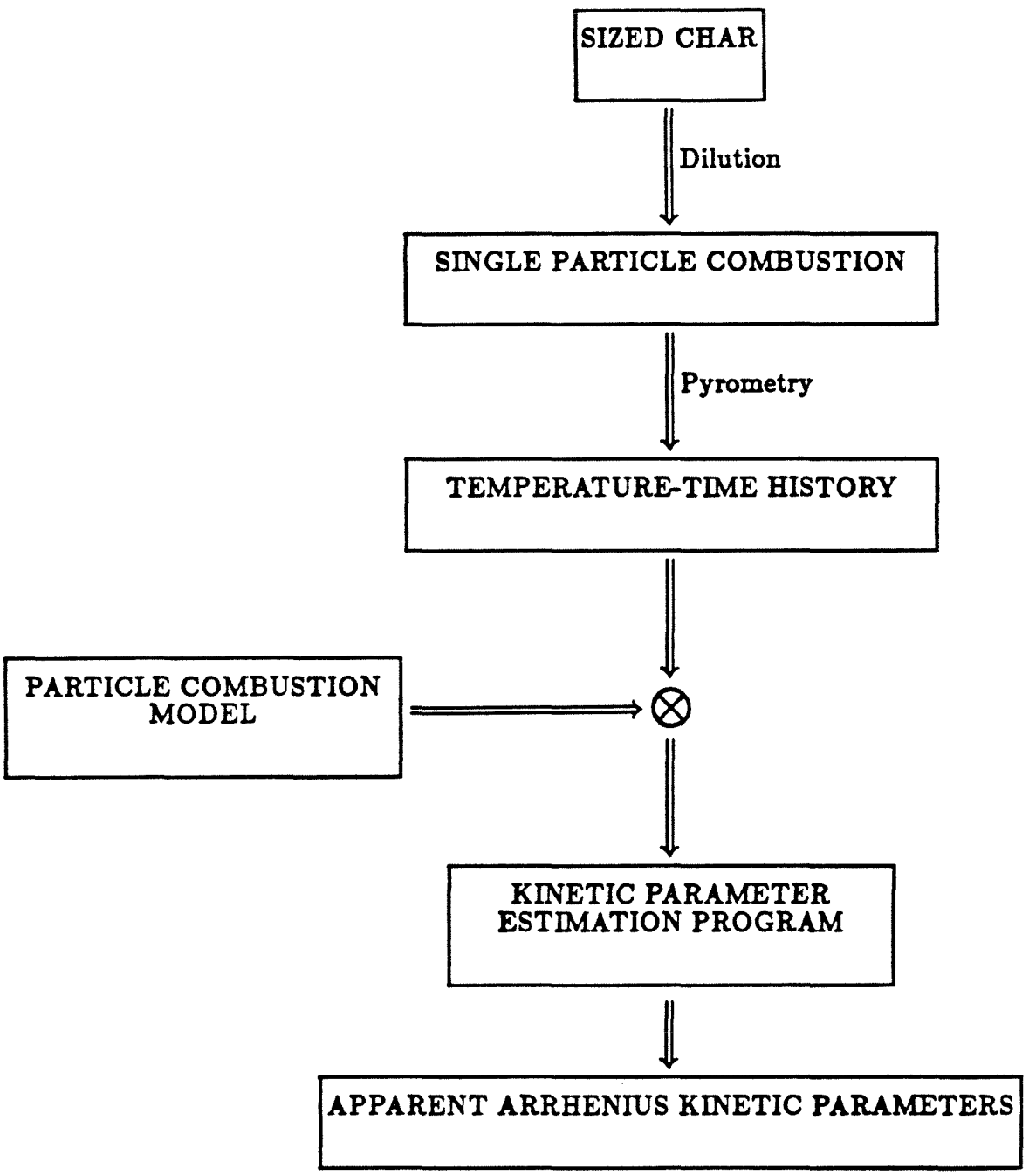

Figure AVIII.1 Flow diagram for kinetic parameter estimation.

AVIII.1 AD2.FOR

```
C
C
C       ROUTINE AD2 (data aquisition)
        DIMENSION IRAW1(1200),IRAW2(1200)
        DIMENSION X(1200),Y(1200)
        BYTE FILE(20),ANSW
        VCON = 10. / 4096.
        KMAX = 1500
        ICH1 = 2
        ICH2 = 3
        TYPE 10, ICH1, ICH2
10      FORMAT(//T10,'Dual A/D Fast Sampling Program -- ',
        1 'Sampling Channels ',I2,' & ',I2 //)
12      TYPE 15
15      FORMAT('$Enter the Number of A/D Samples to Take: ')
        ACCEPT *, KOUNT
        IF (KOUNT.LE.0 .OR. KOUNT.GT.KMAX) GOTO 12
        IDIM=KOUNT
        TYPE 30
30      FORMAT('$Enter threshold (100mv=40) : ')
        ACCEPT *,IEXC
        TYPE 35
35      FORMAT('$Enter # of baseline points: ')
        ACCEPT *,NAVG
40      TYPE 50
50      FORMAT('$Hit RETURN to start sampling:')
        ACCEPT 55, JUNK
55      FORMAT(A1)
59      ITER=0
60      CALL GTIM(TINTB)
61      CALL ADSET2(ICH1,ICH2,KOUNT,IRAW1,IRAW2)
        CALL GTIM(TINTE)
        SEC = ELAPSE(TINTB,TINTE)
        CALL FPEAK (IRAW2,IDIM,IEXC,NAVG,IAVG,ICEN,INS,INE)
        ITER=ITER+1
        TYPE 70, ITER,ICEN,IAVG
70      FORMAT(/T5,'ITERATION=',I3,5X,'PEAK AT :',I4,
     $  5X,'BASELINE SIGNAL :',I4)
        IF (ITER .EQ. 500) GO TO 222
        IF (ICEN .EQ. -1) GO TO 60
        IF (ICEN .EQ. -2) GO TO 60
        IF (ICEN .EQ. -3) GO TO 60
        TYPE 150, SEC, KOUNT
150     FORMAT(' The Elapsed Time is',F10.3,' seconds for',I5 /)
        TYPE 160, INS,INE
160     FORMAT(T5,'SIGNAL STARTS AT:',I4,5X,'SIGNAL ENDS AT:',I4)
        CALL ISTAT(KOUNT,IRAW1,AV1,SD1,SL1)
        AV1 = AV1 * VCON
        SD1 = VCON * SD1
        SL1 = SL1 * VCON
        CALL ISTAT(KOUNT,IRAW2,AV2,SD2,SL2)
        AV2 = AV2 * VCON
        SD2 = SD2 * VCON
        SL2 = SL2 * VCON
        TYPE 200, 1,AV1,SD1,SL1
        TYPE 200, 2,AV2,SD2,SL2
200     FORMAT(' For Channel',I3,' Average=',F8.4,'   St.Dev.=',
        1  F8.4,'  Slope=',F9.5,' Volts')
        DO 7 I=1,KOUNT
          Y(I) = FLOAT(VCON*IRAW1(I))
          X(I) = FLOAT(I)
 7      CONTINUE
        ISTIME = 0.0
        IMIN = 1
        IMAX = KOUNT
```

```
205     IKOUNT=IMAX-IMIN+1
C       CALL RANGES(IKOUNT,X(IMIN),Y(IMIN),XMIN,XMAX,YMIN,YMAX)
        XMIN=X(IMIN)
        XMAX=X(IMAX)
        YMIN=Y(IMIN)
        YMAX=Y(IMIN)
        IF (XMIN.EQ.1) XMIN=0.
        DO 212 I=IMIN,IMAX
          IF (Y(I).LT.YMIN) YMIN=Y(I)
          IF (Y(I).GT.YMAX) YMAX=Y(I)
212     CONTINUE
        YMIN=YMIN-0.001
        YMAX=YMAX+0.001
        CALL VSETS(YMIN,YMAX,XMIN,XMAX,0)
210     CALL VXPLOT(0,X,Y)
        ISTEP = (IMAX-IMIN+1)/100
        IF (ISTEP.LT.1) ISTEP = 1
        DO 220 I = IMIN,IMAX,ISTEP
          CALL VXADD(1,X(I),Y(I))
220     CONTINUE
        CALL VPUT(24,1)
222     TYPE 225
225     FORMAT('$Select M to magnify, S to Save, R to Repeat, ',
        1  'I to Initialize, Q to Quit: ')
        ACCEPT 226,ANSW
226     FORMAT(A1)
        IF (ANSW.EQ.'S') GOTO 240
        IF (ANSW.EQ.'I') GOTO 12
        IF (ANSW.EQ.'Q') GOTO 401
        IF (ANSW.EQ.'R') GOTO 400
        IF (ANSW.EQ.'M') GOTO 229
        GOTO 222
229     TYPE 230
230     FORMAT('$Enter IMIN,IMAX : ')
        ACCEPT *, IMIN,IMAX
        IF (IMIN.GE.IMAX .OR. IMAX.GT.KOUNT) GOTO 229
        GOTO 205
240     CALL ASKFIL(3,FILE)
        CALL ASSIGN(3,FILE)
        DO 300 I=IMIN,IMAX
          WRITE(3,333) VCON*IRAW1(I),VCON*IRAW2(I)
333       FORMAT(' ',2F8.4)
300     CONTINUE
        CLOSE (UNIT=3)
400     CALL VINIT
        GO TO 59
401     STOP
        END
```

```
C
C
      SUBROUTINE FPEAK(IBUF,IDIM,IEXC,NAVG,IAVG,ICEN,INS,INE)
C
C     THIS ROUTINE IS USED TO DETECT SIGNALS EMITTED BY BURNING
C     COAL PARTICLES AND RECORDED BY A TWO COLOR PYROMETER
C     (THE APPROXIMATE CENTER OF THE PEAK CAN ALSO BE FOUND)
C
C
C
C     METHOD: THE CENTER OF THE PEAK IS DEFINED AS THE POINT WHICH
C         GIVES THE MAXIMUM CORRELATION OF THE SIGNAL AND A WINDOW
C         OF CONSTANT VALUE.
C
C     NOTE: THIS ROUTINE ASSUMES THAT THE FIRST "NAVG" DATA POINTS
C           REPRESENT A ZERO LEVEL IN THE SIGNAL AND THAT THE PEAK
C           OCCURS "IWIN" POINTS BEFORE THE END SPECIFIED BY "IDIM"
C
C     INPUT:    IBUF-   ARRAY CONTAINING THE SIGNAL
C
C               IDIM-    LENGTH OF ARRAY
C
C     OUTPUT:   ICEN-   INDEX TO APPROXIMATE CENTER OF THE PEAK
C
C               INS-    FIRST OCCURENCE WHEN SIGNAL EXCEEDS THRESHOLD
C                      STARTING FROM THE BEGINNING OF THE SIGNAL
C
C               INE-    FIRST OCCURENCE WHEN SIGNAL EXCEEDS THRESHOLD
C                      STARTING FROM THE END OF THE SIGNAL
C     ERRORS:   ICEN-    SET TO -1 IF NO PEAK FOUND
C
C     PARAMETERS: NAVG-  # OF POINTS TO FIND AVERAGE OVER ZERO LEVEL
C                        IN SIGNAL
C
C                 IWIN-  WIDTH OF WINDOW TO FIND PEAK
C
C                 IEXC-  ABSOLUTE VALUE THE SIGNAL MUST CHANGE BY
C                        BEFORE SEARCH FOR PEAK IS MADE
C                        100mv IS 41.
C
C
      INTEGER*2  IBUF(IDIM)
C     VIRTUAL    IBUF(IDIM)
C
C     GET ZERO LEVEL FOR START OF SIGNAL
C
      AVG=0.
      DO 10 J=1,NAVG
 10   AVG=AVG+IBUF(J)
      IAVG=AVG/NAVG
C
C     FIND ENDING ZERO LEVEL
C
      AVG=0.
      DO 15 J=IDIM-NAVG+1,IDIM
 15   AVG=AVG+IBUF(J)
      IAVGE=AVG/NAVG
C
      IWIN=IDIM-NAVG*2
C
C     TWO STATEMENTS THAT SET ERROR FLAGS FOLLOW
C
      IF (IWIN .GT. 20) GO TO 19
      ICEN=-2
      RETURN
```

```
      IF (IBUF(IDIM) .LT. IEXC/2)GO TO 19
      ICEN=-3
      RETURN
C
C     FIND STARTING INDEX WHERE SIGNAL EXCEEDS THRESHOLD
C
 19   INS=1
 20   IF ( IABS(IBUF(INS)-IAVG) .GT. IEXC ) GO TO 25
      INS=INS+1
      IF ( INS .LT. IWIN )GO TO 20
      ICEN=-1                              !SET ERROR IF SIGNAL
      RETURN                               !DOESN'T EXCEED THRESHOLD
C
C     FIND ENDING INDEX WHERE SIGNAL EXCEEDS THRESHOLD
C
 25   INE=IDIM
 28   IF ( IABS(IBUF(INE)-IAVGE) .GT. IEXC ) GO TO 30
      INE=INE-1
      GO TO 28
C     INS=INS-IWIN/2
C     INE=INE+IWIN/2
      IF ( INS .LT. 1) INS=1
      IF ( INE .GT. IDIM) INE=IDIM
C
C     LOOK FOR PEAK
C
 30   XMAX=0
      DO 50 K=INS,INE
       TMAX=0
 40    TMAX=TMAX+IABS(IBUF(K)-IAVG)
      IF ( TMAX.LE.XMAX) GO TO 50
      ICEN=K
      XMAX=TMAX
 50   CONTINUE
      RETURN
      END
```

```
;
C
        .TITLE ADSET2 -- TAKES 2 SETS OF A/D READINGS
        .GLOBL ADSET2

;       FORTRAN USAGE:  CALL ADSETS(IC1,IC2,KOUNT,IAR1,IAR2)
;               ICH1 = FIRST A/D CHANNEL NUMBER (0-15 NORMALLY)
;               ICH2 = SECOND A/D CHANNEL NUMBER (0-15)
;               KOUNT = NUMBER OF READINGS TO TAKE
;               IAR1 = FIRST INTEGER ARRAY SPACE FOR RAW A/D VALUES
;               IAR2 = SECONDE INTEGER ARRAY SPACE FOR RAW A/D VALUES
;       NOTE THAT ICH1, ICH2, AND KOUNT ARE INTEGER*2 VARIABLES, AND
;        IAR1 AND IAR2 ARE INTEGER*2 ARRAYS DIMENSIONED TO AT LEAST KOUNT

CDSTAT=170400
GNCHAD=170402
ADDATA=170402

ADSET2::
        TST     (R5)+           ; IGNORE # OF ARGUMENTS
        MOV     @(R5)+,R1       ; R1 = ICH1
        MOV     @(R5)+,R2       ; R2 = ICH2
        MOV     @(R5)+,R0       ; R0 = KOUNT
        MOV     (R5)+,R3        ; R3 = ADDRESS OF IAR1
        MOV     (R5)+,R4        ; R4 = ADDRESS OF IAR2
NEXT:   MOV     R1,@#GNCHAD     ; START CONVERSION
LOOP1:  TST     @#CDSTAT        ; A/D CONVERSION DONE?
        BGE     LOOP1           ; LOOP UNTIL DONE
        MOV     @#ADDATA,(R3)+  ; SAVE RAW DATA IN IAR1
        MOV     R2,@#GNCHAD     ; START ICH2 CONVERSION
LOOP2:  TST     @#CDSTAT        ; A/D CONVERSION DONE?
        BGE     LOOP2
        MOV     @#ADDATA,(R4)+  ; SAVE RAW DATA IN IAR2
        DEC     R0              ; DECREMENT KOUNT
        BNE     NEXT            ; NEXT SAMPLE UNLESS R2=0
        RETURN                  ; ALL DONE
        .END
```

AVIII.2 RETEMP.FOR

```
C     This program calculates the ratio of the two signals
C     generated by the combustion of a char particle.
C     First the magnitudes of the two signals are computed
C     then the ratio is taken and finaly the temperature
C     is calculated.
C
C
          CHARACTER*15 INFIL,OUTFIL
          REAL*4 A1(1000),A2(1000),DA(1000),AA1(1000),AA2(1000)
          REAL*4 TIME(1000),T(1000)
C
C     Read in data from the input file.
C
          WRITE(*,2)
 2        FORMAT(2X,' ENTER INPUT DATA FILENAME :'\)
          READ(*,50)INFIL
 50       FORMAT(A15)
C
          OPEN ( 1, FILE=INFIL,FORM='FORMATTED',STATUS='OLD')
C
          DO 100 I=1,1000
            READ(1,99,END=101) A1(I),A2(I)
 100      CONTINUE
 101      CONTINUE
 99       FORMAT(1X,2F8.4)
```

```
260          DO 102 I=1,15
270            WRITE(*,99) A1(I),A2(I)
280   102    CONTINUE
290  C
300  C     Enter flag corresponding to furnace wall temperature.
310  C
320          WRITE(*,33)
330   33     FORMAT ('   ENTER FLAG : FLAG=1 FOR 10.3MV ELSE 0:'\)
340          READ(*,*)FLAG
350  C
360  C     Compute the baseline average in each channel.
370  C
380          A1SUM=0.
390          A2SUM=0.
400          DO 110       I=1,15
410             A1SUM=A1(I)+A1SUM
420             A2SUM=A2(I)+A2SUM
430   110    CONTINUE
440          A1BCK=A1SUM/15.
450          A2BCK=A2SUM/15.
460          WRITE(*,111)A1BCK,A2BCK
470   111    FORMAT(//,2X,' A1BCK = ',F8.4,3X,' A2BCK = ',F8.4)
480  C
490  C     Calculate the signal average in each channel.
500  C
510          DO 200 I=1,1000
520             AA1(I)=A1(I)-A1BCK
```

```
530            AA2(I)=A2(I)-A2BCK
540  200     CONTINUE
550 C
560 C    Compute signal ratio.
570 C
580         DO 300 I=1,1000
590            IF(AA1(I).LT.0.000001) GOTO 300
600            DA(I)=AA2(I)/AA1(I)
610  300     CONTINUE
620 C
630 C    Calculate the temperature.
640 C
650         IF(FLAG .EQ. 1.)THEN
660            DO 310 I=1,1000
670              IF(DA(I).LE.0.0)GO TO 311
680              IF(DA(I).GT.0.0)GO TO 312
690  311         T(I)=0.0
700              GO TO 310
710  312         T(I)=(3597)/(ALOG(DA(I))+1.0921929)
720  310       CONTINUE
730         ELSE
740            DO 410 I=1,1000
750              IF(DA(I).LE.0.0)GO TO 411
760              IF(DA(I).GT.0.0)GO TO 412
770  411         T(I)=0.0
780              GO TO 410
790  412         T(I)=(3597)/(ALOG(DA(I))+1.2033064)
```

```
800   410       CONTINUE
810             ENDIF
820   C
830   C     Write to output file.
840   C     Time(i) is in milliseconds, assuming 1000/0.1sec rate.
850   C
860             WRITE(*,320)
870   320       FORMAT(2X,' ENTER OUTPUT FILENAME :'\)
880             READ(*,50)OUTFIL
890             OPEN(2,FILE=OUTFIL,FORM='FORMATTED',STATUS ='NEW')
900             DO 350 I=1,1000
910                TIME(I)=0.1*I
920                WRITE (2,330)I,TIME(I),AA1(I),AA2(I),DA(I),T(I)
930   350       CONTINUE
940   330       FORMAT(1X,I4,1X,5F10.4)
950   C
960             CLOSE(1)
970             CLOSE(2)
980             GOTO 999
990   990       WRITE(*,991)
1000            GOTO 999
1010  992       WRITE(*,993)
1020            GOTO 999
1030  993       FORMAT('  ERROR DURING READ')
1040  991       FORMAT('  ERROR IN OPENING INPUT FILE')
1050  999       STOP
1060            END
```

AVIII.3 VARASH.FOR

```
10 C    This program is used to determine the apparent Arrhenius
20 C    kinetic parameters from single particle temperature-time
30 C    traces. The experiments were done in the drop-tube reactor
40 C    at high temperatures.
50 C
60 C    Since there is significant particle to particle variability
70 C    even when experimental conditions are the same, this is
80 C    attributed to variation in the particle initial size and the
90 C    particle shape. Both parameters are lumped in the initial
100 C   particle radius.
110 C
120 C   The experimental temperature trace is first fit with a fifth
130 C   order polynomial using the program POLY2.BAS. These
140 C   coefficients are inputs to this program. The average initial
150 C   particle radius, guesses for the pre-exponential factor
160 C   and activation energy, wall temperature, and oxygen partial
170 C   pressure are the other inputs.
180 C
190 C   Using the guessed kinetic parameters, the particle burning
200 C   model (asymptotic version VARNU.FOR) is run. This predicts
210 C   a temperature-time trace. The pre-exponential factor is
220 C   adjusted till the experimental and model burn times match.
230 C
240 C   Then a least squares residual is computed that represents
250 C   the difference between the model and experimental traces.
```

```
C     The above procedure is repeated with different initial
C     particle radii and activation energies. For each trace,
C     the residual is computed for many values of activation
C     energies and initial radii. That value of activation energy
C     (and the associated pre-exponential factor) and initial
C     radius is chosen which minimizes the residual.
C
C     The process is then repeated for many traces. Finally the
C     activation energy that minimizes the sum of the minimum
C     residuals of each trace is chosen as the correct parameter.
C
C-----------------------------------------------
C
C     Declarations.
C
          IMPLICIT REAL*4(A-H,O-Z)
          REAL*8 CHRONO(800),CALOR(800)
          REAL*8 TFAC,PEMMIS
          CHARACTER*15 OFIL
          DIMENSION CTIME(10),CTEMP(10),ATEMP(10),PLTEMP(10)
          DIMENSION ER(10),VARER(15),PHTEMP(10)
          INTEGER  IER,NCOUNT
          EXTERNAL QCR,VARNU
          COMMON /BIG/ EPSO,RHOC,RINIT,RFINAL,PINF,AERR,RERR,
         1  TWALL,DUM,RBAR,NCOUNT,ENG,PTS,NDEG,EPSF,ASHO,A(3)
          COMMON  /DATA/CHRONO,CALOR
          COMMON  /TI/TSTART,TEND
```

```
530          COMMON  /TF/TFAC,PEMMIS
540 C
550 C-----------------------------------------------
560 C
570 C    Parameter inputs.
580 C
590          WRITE(*,306)
600   306    FORMAT(1X,'ENTER THE OUTPUT FILE NAME:')
610          READ(*,305)OFIL
620   305    FORMAT(A15)
630          WRITE(*,310)
640   310    FORMAT(1X,'ENTER START AND END TIMES (ms):')
650          READ(*,*)TSTART,TEND
660          WRITE(*,312)
670   312    FORMAT(1X,'ENTER INIT ASH AND VOID FRACTIONS, PEMMIS:')
680          READ(*,*)ASHO,EPSO,PEMMIS
690          WRITE(*,315)
700   315    FORMAT(1X,'ENTER INITIAL RAD(mic), TWALL AND O2 P.P:')
710          READ(*,*)RINIT,TWALL,PINF
720          WRITE(*,317)
730   317    FORMAT(1X,'ENTER INIT., FINAL ACT. ENERGIES, INCREMENT:')
740          READ(*,*)E,FAE,DELE
750          WRITE(*,320)
760   320    FORMAT(1X,'ENTER THE INIT. GUESS FOR A AND THCK FACTOR:')
770          READ(*,*)GUESSA,TFAC
780          WRITE(*,325)
790   325    FORMAT(1X,'ENTER NUMBER OF COEFF.S (MAX=5):')
```

```
      READ(*,*)NDEG
      DO 340 IT=1,NDEG
       WRITE(*,330)IT
330    FORMAT(1X,'ENTER COEFF. ',I2)
       READ(*,*)A(IT)
340   CONTINUE
C
C     ASHO=0.12
C     EPSO=0.58
      RHOC=1.5
      OPEN(2,FILE=OFIL,STATUS='NEW')
C
      DELRINIT=1.0*1.0E-04
      E=E-DELE
      XACC=0.0001
      XACC2=0.025
      RINIT=RINIT*1.0E-04
      RFINAL=RINIT*(ASHO/(1.0-EPSO))**0.333333
      INDEX=(FAE-E)/DELE
C
C     Main program main loop begins.
C
      DO 370 I=1,INDEX
       E=E+DELE
       GUESS1=1.7*GUESSA
       GUESS2=3.0*GUESSA
C
```

```
1070            DUMR=RINIT
1080            X1=GUESS1
1090            X2=GUESS2
1100            CALL QCR(E,X1,DUMR,FX1)
1110            WRITE(*,*)FX1
1120            CALL QCR(E,X2,DUMR,FX2)
1130            WRITE(*,*)FX2
1140            DO 350 J=1,100
1150              GUESS3=GUESS1+(GUESS1-GUESS2)*FX1/(FX2-FX1)
1160              CALL QCR(E,GUESS3,DUMR,FX3)
1170              WRITE(*,*)FX1,FX2,FX3
1180              IF(ABS(FX3) .LE. 0.1)GOTO 365
1190              GUESS1=GUESS2
1200              GUESS2=GUESS3
1210              FX1=FX2
1220              FX2=FX3
1230   350      CONTINUE
1240   365      FREQ=GUESS3
1250            GUESSA=FREQ
1260            WRITE(*,*)FREQ
1270  C
1280            DELCHRO=(TEND-TSTART)/11.0
1290            DO 400 J=1,10
1300               DUMJ=TSTART+DELCHRO*J
1310               DO 450 K=1,800
1320                  IF (CHRONO(K) .GT. DUMJ)THEN
1330                     CTIME(J)=CHRONO(K)
```

```
1340                    CTEMP(J)=CALOR(K)
1350                    GOTO 401
1360                 ENDIF
1370  450          CONTINUE
1380  401          CONTINUE
1390  400       CONTINUE
1400 C
1410 C     The following two program blocks perform numerical
1420 C     differentiation with respect to initial radius.
1430 C
1440           RLOW=RINIT-DELRINIT
1450           CALL QCR(E,FREQ,RLOW,FUNT)
1460           DO 500 J=1,10
1470              DUMJ=TSTART+DELCHRO*J
1480              DO 550 K=1,800
1490                 IF (CHRONO(K) .GT. DUMJ)THEN
1500                    PLTEMP(J)=CALOR(K)
1510                    GOTO 501
1520                 ENDIF
1530  550          CONTINUE
1540  501          CONTINUE
1550  500       CONTINUE
1560 C
1570           RHIGH=RINIT+DELRINIT
1580           CALL QCR(E,FREQ,RHIGH,FUNT)
1590           DO 600 J=1,10
1600              DUMJ=TSTART+DELCHRO*J
```

```
1610              DO 650 K=1,800
1620                 IF (CHRONO(K) .GT. DUMJ)THEN
1630                    PHTEMP(J)=CALOR(K)
1640                    GOTO 601
1650                 ENDIF
1660  650          CONTINUE
1670  601          CONTINUE
1680  600       CONTINUE
1690 C
1700            SUMER=0.0
1710            DO 700 IL=1,10
1720 C
1730 C     Set Initial ATEMPS to 0.
1740 C
1750            ATEMP(IL)=0.0
1760            DO 710 JK=1,NDEG
1770              ATEMP(IL)=ATEMP(IL)+A(JK)*(CHRONO(IL)*1.OE-03)**(JK-1)
1780  710       CONTINUE
1790            DERIV=(PHTEMP(IL)-PLTEMP(IL))/(2.0*DELRINIT)
1800            ER(IL)= (ATEMP(IL)-CTEMP(IL))/DERIV
1810            SUMER=SUMER+ER(IL)
1820  700     CONTINUE
1830 C
1840            VARSUM=0.0
1850            ERBAR=SUMER/10.0
1860            DO 800 KL=1,10
1870             VARSUM=VARSUM+(ER(KL)-ERBAR)*(ER(KL)-ERBAR)
```

```
 800    CONTINUE
C
C     Write to file.
C
          VARER(I)=VARSUM/9.0
          WRITE(2,380)E,FREQ,VARER(I)
          WRITE(*,380)E,FREQ,VARER(I)
C
 370    CONTINUE
 380    FORMAT(1X,2F12.5,1X,1F18.12)
          CLOSE(2)
          STOP
          END
C
C-----------------------------------------------
C
C     This is the calling program for VARNU.
C
          SUBROUTINE QCR(EM,P,DUMR,FUNT)
          IMPLICIT REAL*4(A-H,O-Z)
          REAL*8 RHOP,DTWAL,TPINIT,DP,C1INF,DRINIT
          REAL*8 ASHINIT,ACEN,TTOT
          EXTERNAL VARNU
          COMMON  /BIG/ EPSO,RHOC,RINIT,RFINAL,PINF,AERR,RERR,
     1          TWALL,DUM,RBAR,NCOUNT,ENG,PTS,NDEG,EPSF,ASHO,A(3)
          COMMON  /TI/TSTART,TEND
C
```

```
      RHOP=(1.0-EPS0-ASHO)*RHOC
      DTWAL=TWALL
      TMPR=0.0
      DO 75 K=1,NDEG
           TMPR=TMPR+A(K)*(TSTART*1.0E-03)**(K-1)
75    CONTINUE
      TPINIT=TMPR
      DP=P
      C1INF=PINF
      DRINIT=DUMR*1.0D04
      ASHINIT=ASHO
      ACEN=EM
C
      CALL VARNU(RHOP,DTWAL,TPINIT,DP,
     1                  C1INF,DRINIT,ASHINIT,ACEN,TTOT)
      FUNT = TTOT-(TEND-TSTART)
      RETURN
      END
C
C-----------------------------------------------
C
      SUBROUTINE VARNU(AZ1,BZ1,CZ1,DZ1,EZ1,FZ1,GZ1,HZ1,TBURN)
C
      IMPLICIT REAL*8(A-H,O-Z)
      REAL*8  NMAX
      REAL*8  K11,K12,K13,K14,K21,K22,K23,K24
      REAL*4  TSTART,TEND
```

```
2420          DIMENSION CHRONO(800),CALOR(800)
2430 C .
2440 C
2450          EXTERNAL  EC,ECH,CPC,CPCH
2460          EXTERNAL  FLUX,ENERGY
2470          EXTERNAL  GAMMA,RTBIS,RADIUS,SOLID
2480 C
2490 C
2500          COMMON  /FIRST/T,GAM,TWALL,FP
2510          COMMON  /R/RHOC,XFAC,ACEN
2520          COMMON  /Y1S/Y1S,Y1INF
2530          COMMON  /ASH/ASHFRAC,RHOASH,ASHINIT,
2540       1           RPINIT,CPASH,AMMIS,THCK
2550          COMMON  /DATA/CHRONO,CALOR
2560          COMMON  /TI/TSTART,TEND
2570          COMMON  /TF/TFAC,PEMMIS
2580 C
2590 C    Initialization.
2600 C
2610          RHOC=AZ1
2620          TWALL=BZ1
2630          TPINIT=CZ1
2640          XFAC=DZ1
2650          C1INF=EZ1
2660          RPINIT=FZ1
2670          ASHINIT=GZ1
2680          ACEN=HZ1
```

```
2690 C
2700          RHOASH=2.5
2710          NMAX=2000
2720          ES1=1.0D-6
2730          ES2=1.0D07
2740          XACC=0.0001
2750          STEPO=0.0001
2760          DELTEMP=20
2770          WEMMIS=0.8
2780 C        PEMMIS=0.8
2790          AMMIS=0.8
2800 C
2810  3000    Y1INF=(C1INF * 32.0)/(C1INF * 32.0 +(1.0 - C1INF)*28.0)
2820          A = (1.0 / (1.0 - Y1INF)) * (Y1INF / 4.0)
2830 C
2840          TP = TPINIT
2850          RP = RPINIT
2860          C1S = C1INF
2870          TIME = 0.0
2880          DTDR = 0.0
2890          FP=0.0
2900          THCK=0.0
2910          ASHFRAC = ASHINIT
2920 C
2930 C        WRITE(*, 900) TIME, RP, TP, C1S, FP
2940   900    FORMAT(1X,5G12.4)
2950 C
```

```
2960 C    X1 and X2 are appropriate brackets for GAM.
2970 C    Typically, ES1 is O(1D-6), while ES2 is O(1D11).
2980 C
2990         IF ( TPINIT .LT. TWALL) THEN
3000                 X1 =  ( -2331.5425 + 0.3388749*TPINIT) - ES2
3010                 X2 =  ( -2331.5425 + 0.3388749*TPINIT) - ES1
3020         ELSE
3030                 X1 =  ( -2331.5425 + 0.3388749*TPINIT) + ES1
3040                 X2 =  ( -2331.5425 + 0.3388749*TPINIT) + ES2
3050         ENDIF
3060 C
3070 C    Main loop in VARNU begins.
3080 C
3090         JMAX = NMAX
3100         DO 1000 I = 1, JMAX
3110           STEP=STEPO
3120           T = TP
3130           RR = RP * 1D-04
3140           THCK=(RP**3.0+(ASHINIT*(RPINIT**3.0-RP**3.0))/0.65)**
3150      1          (1.0/3.0)-RP + 1.0D-08
3160           THCK=THCK*1.0D-04*TFAC
3170           CALL RTBIS(GAMMA,X1,X2,XACC,RR,GAM)
3180           DUMC = (1.0/(-1.0/7.0 + 8.0/(7.0*Y1S)))
3190           CALL FLUX(DUMC,RR)
3200           FP1 = -1.3333 * FP
3210           FP2 = 2.3333 * FP
3220           EP = GAM * FP
```

```
3230            CALL SOLID(RR)
3240  991       CALL RUNG(RADIUS,ENERGY,DUMC,STEP,EP,
3250       1                PEMMIS,WEMMIS,RR,RNEW,TNEW)
3260  C         IF(DABS((RNEW-RR)/RR) .LT. 0.0001)THEN
3270            IF(RNEW .LE. 0.0001)THEN
3280              TBURN=TIME
3290              GOTO 1001
3300            ENDIF
3310            RP = 1.0D4*RNEW
3320            TP = TNEW
3330            TIME = TIME + 1.0D3*STEP
3340  C
3350            CHRONO(I)=TIME+TSTART
3360            CALOR(I)=TP
3370  C
3380  C     Reducing brackets for the next call of GAM.
3390  C
3400            IF ( TP .LT. TWALL) THEN
3410                  X1 =  GAM - DABS(1000.0*GAM)
3420                  X2 =  ( -2331.5425 + 0.3388749*TP ) - ES1
3430            ELSE
3440                  X1 =  ( -2331.5425 + 0.3388749*TP ) + ES1
3450                  X2 =  GAM + DABS(1000.0*GAM)
3460            ENDIF
3470  C
3480   1000   CONTINUE
3490   1001   CONTINUE
```

```
3500          RETURN
3510          END
3520 C
3530 C    Main loop in VARNU ends.
3540 C
3550 C-------------------------------------------
3560 C
3570 C    Property values.
3580 C
3590 C    EC and ECH calculate the enthalpy of the solid in cal/g.
3600 C    Data from the Coal Data Book.
3610 C
3620          REAL*8 FUNCTION EC(D)
3630          IMPLICIT REAL*8(A-H,O-Z)
3640          COMMON  /FIRST/T,GAM,TWALL,FP
3650          CPCO = 0.024
3660          CPC1 = 6.953D-04
3670          CPC2 = -2.841D-07
3680          EC = CPCO*(D - 298) + (CPC1 / 2.0)*(D*D - 298*298)
3690       1  + (CPC2 / 3.0)*(D*D*D - 298*298*298)
3700          RETURN
3710          END
3720 C
3730          REAL*8 FUNCTION ECH(D)
3740          IMPLICIT REAL*8(A-H,O-Z)
3750          COMMON  /FIRST/T,GAM,TWALL,FP
3760          CPCHO = 0.36
```

```
3770          CPCH1 = 6.931D-05
3780          ECH = CPCHO*(D - 298) + (CPCH1 / 2.0)*(D*D - 298*298)
3790          RETURN
3800          END
3810  C
3820  C     CPC and CPCH calculate heat cap. of the solid in cal/g-K.
3830  C     Data from Coal Data Book.
3840  C
3850          REAL*8 FUNCTION CPC(D)
3860          IMPLICIT REAL*8(A-H,O-Z)
3870          COMMON  /FIRST/T,GAM,TWALL,FP
3880          CPCO = 0.024
3890          CPC1 = 6.953D-04
3900          CPC2 = -2.841D-07
3910          CPC = CPCO + CPC1 * D + CPC2 * D * D
3920          RETURN
3930          END
3940  C
3950          REAL*8 FUNCTION CPCH(D)
3960          IMPLICIT REAL*8(A-H,O-Z)
3970          COMMON  /FIRST/T,GAM,TWALL,FP
3980          CPCHO = 0.36
3990          CPCH1 = 6.931D-05
4000          CPCH = CPCHO + CPCH1 * D
4010          RETURN
4020          END
4030  C
```

```
4040 C-------------------------------------------
4050 C
4060 C    This routine finds the fraction of solid covered by ash
4070 C    (ASHFRAC). (ASHFRAC --> 1.0 as RR --> RMIN).
4080 C
4090          SUBROUTINE SOLID(RR)
4100          IMPLICIT REAL*8(A-H,O-Z)
4110          COMMON  /ASH/ASHFRAC,RHOASH,ASHINIT,
4120         1           RPINIT,CPASH,AMMIS,THCK
4130 C
4140          ASHFRAC = ASHINIT*(1.0D-4*RPINIT/RR)**3.0
4150          RETURN
4160          END
4170 C
4180 C-------------------------------------------
4190 C
4200 C    Root finder by the method of bisection for function TET.
4210 C
4220          SUBROUTINE RTBIS(TET,X1,X2,XACC,R2,XMID)
4230          IMPLICIT REAL*8(A-H,O-Z)
4240          EXTERNAL  TET
4250          COMMON  /FIRST/T,GAM,TWALL,FP
4260          PARAMETER (JMAX = 500)
4270 C
4280          CALL TET(X1,FX1,R2)
4290          CALL TET(X2,FX2,R2)
4300          IF(FX2*FX1 .GE. 0.0) PAUSE 'BRACKET ROOT IN VARNU'
```

```
4310          DX = X2 - X1
4320          DO 200 J = 1, JMAX
4330                  DX = DX * 0.5
4340                  XMID = X1 + DX
4350                  CALL TET(XMID,FMID,R2)
4360                  IF (FMID * FX1 .GT. 0.0)THEN
4370                          X1 = XMID
4380                          FX1 = FMID
4390                  ELSE
4400                          X2 = XMID
4410                          FX2 = FMID
4420                  ENDIF
4430                  IF (DABS(DX/XMID) .LT. XACC)  RETURN
4440   200    CONTINUE
4450          PAUSE 'TOO MANY BISECTIONS IN VARNU'
4460          END
4470  C
4480  C-------------------------------------------
4490  C
4500  C    Calculation of solid flux in gmC/cm^2-s.(Smith 1974)
4510  C
4520          SUBROUTINE FLUX(B,R)
4530          IMPLICIT REAL*8(A-H,O-Z)
4540          COMMON  /ASH/ASHFRAC,RHOASH,ASHINIT,
4550       1           RPINIT,CPASH,AMMIS,THCK
4560          COMMON  /FIRST/T,GAM,TWALL,FP
4570          COMMON  /R/RHOC,XFAC,ACEN
```

```
C
C    Older calculation of FP.
C
C       CASH=B-FP*R*R(1/(R+T)-1/R)/C*M02*DASH
C       FP = XFAC*DEXP( -1.0*ACEN/(1.98 * T))*CASH
C
        DASH=0.35*3.13*(T/1500.0)**1.75/2.0
        PF= XFAC*DEXP( -1.0*ACEN/(1.98 * T))
        FP=PF*B/(1.0+82.05*T*PF*R*THCK/
     1          ((R+THCK)*(32.0*DASH)))
        TEST=PF*B
        RETURN
        END
C
C-----------------------------------------------
C
C    This routine calculates the value of the integrated
C    equations from TWALL to TP based on GAM1.
C
        SUBROUTINE GAMMA(GAM1,F,R1)
        IMPLICIT REAL*8(A-H,O-Z)
        COMMON  /ASH/ASHFRAC,RHOASH,ASHINIT,
     1           RPINIT,CPASH,AMMIS,THCK
        COMMON  /FIRST/ T,GAM,TWALL,FP
        COMMON  /R/RHOC,XFAC,ACEN
        COMMON  /Y1S/Y1S,Y1INF
C
```

```
4850          CC = -3.0043D-05
4860          DASH=0.35*3.13*(T/1500.0)**1.75/2.0
4870          IF (T .LT. TWALL) THEN
4880             HH = DSQRT(DABS(-2331.5425 - GAM1)/0.3388749)
4890             IF (GAM1 .GT.-2331.5425) THEN
4900                AR1=-1.0*CC * ((DSQRT(TWALL) - DSQRT(T)) + HH/2.0 *
4910         1         (DLOG((DSQRT(TWALL) - HH)*(DSQRT(T) + HH)/
4920         2         ((DSQRT(TWALL) + HH)*(DSQRT(T) - HH)))))
4930                HM = (2331.5425 + GAM1)/0.3388749
4940                Y1S=(Y1INF+4.0/3.0)*((T-HM)/
4950         1         (TWALL-HM))**0.8095478-4.0/3.0
4960                CONC=(1.0/(-1.0/7.0 + 8.0/(7.0*Y1S)))
4970                PF=XFAC*DEXP( -1.0*ACEN/(1.98 * T))
4980                FFP=PF*CONC/(1.0+82.05*T*PF*R1*THCK/
4990         1                    ((R1+THCK)*(32.0*DASH)))
5000                F = AR1-R1* FFP
5010             ELSE
5020                AR2=-1.0*CC*((DSQRT(TWALL)-DSQRT(T))-HH*
5030         1         (DATAN(DSQRT(TWALL)/HH)-DATAN(DSQRT(T)/HH)))
5040                HM = (2331.5425 + GAM1)/0.3388749
5050                Y1S=(Y1INF+4.0/3.0)*((T-HM)/(TWALL-HM))**
5060         1           0.8095478-4.0/3.0
5070                CONC=(1.0/(-1.0/7.0 + 8.0/(7.0*Y1S)))
5080                PF=XFAC*DEXP( -1.0*ACEN/(1.98 * T))
5090                FFP=PF*CONC/(1.0+82.05*T*PF*R1*THCK/
5100         1                    ((R1+THCK)*(32.0*DASH)))
5110                F = AR2-R1* FFP
```

```
5120            ENDIF
5130          ELSE
5140            FF = DSQRT(DABS(2331.5425 + GAM1)/0.3388749)
5150            IF (GAM1 .LT.-2331.5425) THEN
5160              AR3 = CC*((DSQRT(T)-DSQRT(TWALL))-FF*
5170         1          (DATAN(DSQRT(T)/FF)-DATAN(DSQRT(TWALL)/FF)))
5180              C3 = (2331.5425 + GAM1)/0.3388749
5190              Y1S=(Y1INF+4.0/3.0)*((T-C3)/(TWALL-C3))**
5200         1          0.8095478-4.0/3.0
5210              CONC=(1.0/(-1.0/7.0 + 8.0/(7.0*Y1S)))
5220              PF=XFAC*DEXP( -1.0*ACEN/(1.98 * T))
5230              FFP=PF*CONC/(1.0+82.05*T*PF*R1*THCK/
5240         1                   ((R1+THCK)*(32.0*DASH)))
5250              F = AR3-R1* FFP
5260            ELSE
5270              AR4 = CC * ((DSQRT(T) - DSQRT(TWALL)) + FF/2.0 *
5280         1          (DLOG((DSQRT(T) - FF)*(DSQRT(TWALL) + FF)/
5290         2          ((DSQRT(T) + FF)*(DSQRT(TWALL) - FF)))))
5300              C3 = (2331.5425 + GAM1)/0.3388749
5310              Y1S=(Y1INF+4.0/3.0)*((T-C3)/(TWALL-C3))**
5320         1          0.8095478-4.0/3.0
5330              CONC=(1.0/(-1.0/7.0 + 8.0/(7.0*Y1S)))
5340              PF=XFAC*DEXP( -1.0*ACEN/(1.98 * T))
5350              FFP=PF*CONC/(1.0+82.05*T*PF*R1*THCK/
5360         1                   ((R1+THCK)*(32.0*DASH)))
5370              F = AR4-R1* FFP
5380            ENDIF
```

```
5390          ENDIF
5400          RETURN
5410          END
5420  C
5430  C-----------------------------------------------
5440  C
5450  C     Energy balance.
5460  C
5470          SUBROUTINE ENERGY(EP,PEMMIS,WEMMIS,RR,DUM2,ANST)
5480          IMPLICIT REAL*8(A-H,O-Z)
5490          EXTERNAL  CPC,EC,CPCH,ECH
5500          COMMON  /FIRST/ T,GAM,TWALL,FP
5510          COMMON  /R/RHOC,XFAC,ACEN
5520          COMMON  /ASH/ASHFRAC,RHOASH,ASHINIT,
5530       1           RPINIT,CPASH,AMMIS,THCK
5540  C
5550  C     Note that RHOC=1.5*(1-ASHINIT-EPSINIT)=Apparent density
5560  C
5570          SIG = 1.595D-12
5580          IF (DUM2 .LT. 1350) THEN
5590                  CPSOL= CPC(DUM2)
5600                  VAL = EC(DUM2)
5610          ELSE
5620                  CPSOL= CPCH(DUM2)
5630                  VAL = ECH(DUM2)
5640          ENDIF
5650          CPASH = 0.183 + 0.111D-3*T
```

```
5660          ANST=3.0*(RR+THCK)*(RR+THCK)*(FP*VAL-EP-SIG*
5670         1    (PEMMIS*DUM2**4-WEMMIS*TWALL**4))/
5680         2    (RR*RR*RR*(CPSOL*RHOC + CPASH*RHOASH*
5690         3    (ASHINIT+0.65*((1+THCK/RR)**3.0-1.0))))
5700          RETURN
5710          END
5720  C
5730  C-----------------------------------------------
5740  C
5750  C     Fourth order Runge-Kutta method for solving
5760  C     TEST1 and TEST2 for each time step.
5770  C
5780          SUBROUTINE RUNG(TEST1,TEST2,DUMC,STEP,EP,
5790         1                      PEMMIS,WEMMIS,RR,RNEW,TNEW)
5800          IMPLICIT REAL*8(A-H,O-Z)
5810          REAL*8 K11,K12,K13,K14,K21,K22,K23,K24
5820          EXTERNAL TEST1,TEST2,ENERGY,RADIUS
5830          COMMON  /FIRST/ T,GAM,TWALL,FP
5840          COMMON  /R/RHOC,XFAC,ACEN
5850  C
5860          DUM1=RR
5870          DUM2=T
5880          CALL TEST1(DUMC,DUM1,DUM2,DRDT)
5890          CALL TEST2(EP,PEMMIS,WEMMIS,DUM1,DUM2,DTDT)
5900          K11=DRDT
5910          K21=DTDT
5920          DUM1 = RR + K11*STEP/2.0
```

```
5930          DUM2 = T + K21*STEP/2.0
5940          CALL TEST1(DUMC,DUM1,DUM2,DRDT)
5950          CALL TEST2(EP,PEMMIS,WEMMIS,DUM1,DUM2,DTDT)
5960          K12 = DRDT
5970          K22 = DTDT
5980          DUM1 = RR + K12*STEP/2.0
5990          DUM2 = T + K22*STEP/2.0
6000          CALL TEST1(DUMC,DUM1,DUM2,DRDT)
6010          CALL TEST2(EP,PEMMIS,WEMMIS,DUM1,DUM2,DTDT)
6020          K13 = DRDT
6030          K23 = DTDT
6040          DUM1 = RR + K13*STEP
6050          DUM2 = T + K23*STEP
6060          CALL TEST1(DUMC,DUM1,DUM2,DRDT)
6070          CALL TEST2(EP,PEMMIS,WEMMIS,DUM1,DUM2,DTDT)
6080          K14 = DRDT
6090          K24 = DTDT
6100          RNEW = RR + STEP*(K11 + 2.0*K12 + 2.0*K13 + K14)/6.0
6110          TNEW = T + STEP*(K21 + 2.0*K22 + 2.0*K23 + K24)/6.0
6120          RETURN
6130          END
6140  C
6150  C-----------------------------------------------
6160  C
6170  C     Mass balance.
6180  C
6190          SUBROUTINE RADIUS(B,DUM1,DUM2,ANS)
```

```
      IMPLICIT REAL*8(A-H,O-Z)
      COMMON  /FIRST/ T,GAM,TWALL,FP
      COMMON  /R/RHOC,XFAC,ACEN
      COMMON  /ASH/ASHFRAC,RHOASH,ASHINIT,
     1          RPINIT,CPASH,AMMIS,THCK
C
C    Note that RHOC=1.5*(1-ASHINIT-EPSINIT)=Apparent density
C
      DASH=0.35*3.13*(DUM2/1500.0)**1.75/2.0
      PF= XFAC*DEXP( -1.0*ACEN/(1.98 * DUM2))
      FFP=PF*B/(1.0+82.05*DUM2*PF*DUM1*THCK
     1             /((DUM1+THCK)*(32.0*DASH)))
      ANS =-1.0*FFP/RHOC
      RETURN
      END
C
C-----------------------------------------------
```

Appendix IX

NUMERICAL MODELS

Program listings of various numerical models are gathered in this Appendix. Every effort has been made to document the programs with generous comments whereever applicable. All programs were written in DOS FORTRAN 3.3 and run on IBM PC/AT's or clones.

IGNIT2 is the model used to determine ignition delay times for single particle combustion. The model is described in Chapter 6.

MENU and VARNU are two versions of the asymptotic model for single particles. While VARNU has been described in detail (Chapter 7), MENU differs from it only in the way the presence of ash is accounted for. While VARNU treats the ash as a diffusion layer around the particle, MENU treats ash as forming patches on the particle. The ash patches prevent reactant access to portions of the particle they cover.

3VOIDS is the general single particle combustion program described in Chapter 7. It describes the internal morphology with three different sized voids. It uses linear kinetics. This model is extended to include power law kinetics in PCONC. A similar extension to include Langmuir-Hinschelwood kinetics was done in another program that is not listed here for reasons of space.

An example of the discrete approach to modelling char combustion is CENMOD21 (Chapter 8).

AIX.1 IGNIT2.FOR

```
 10         PROGRAM IGNIT2
 20 C
 30         IMPLICIT REAL*4(A-H,O-Z)
 40         CHARACTER*15 IFILE
 50         DIMENSION RADMIC(100),ARAT(100)
 60         COMMON  /S/S(100)
 70         COMMON  /R/RAD(100)
 80         COMMON  /A/A1,A2,A3,A4
 90         COMMON  /CS/A11,B11
100         EXTERNAL SUM,FUNT
110 C
120         WRITE(*,7)
130  7      FORMAT(1X,'ENTER PART.RAD (cm), DOD (cm):')
140         READ(*,*)RP,DOD
150         WRITE(*,8)
160  8      FORMAT(1X,'ENTER E,ARR,CMAX,CMIN:')
170         READ(*,*)E,ARR,CMAX,CMIN
180         WRITE(*,9)
190  9      FORMAT(1X,'ENTER ETA,RHOAP,EPS,TS:')
200         READ(*,*)ETA,RHOAP,EPS,TS
210         WRITE(*,11)
220  11     FORMAT(1X, 'ENTER THE DATA FILENAME')
230         READ(*,12)IFILE
240  12     FORMAT(A15)
250 C
```

```
260         SBET=3500000
270 C       RHOAP=0.5
280         DELH=2340*4.187
290 C       CSURF=0.15
300         B11=LOG(CMAX/CMIN)/RP
310         A11=CMAX
320         A1=ETA*ARR*EXP(-E/(1.98*TS))*SBET*DOD*RHOAP*DELH
330 C
340         CPCARB=1.880
350         TC=1200
360         A2=2.0*RHOAP*DOD*CPCARB*(TS-TC)
370 C
380         SIG=5.667E-012
390         EMMS=0.25
400         TINF=1150
410         TWALL=1250
420 C       EPS=0.75
430         CCARB=10.0E-02
440         CAIR=0.0891E-02
450         CEFF=CCARB*(1.0-EPS)**2.0 + CAIR*(EPS**2.0)
460 C
470 C       Alternate values for CCARB: 57.4(1000K);60.2(1300K);
480 C                           0.71(3300K);5.9(300K)
490 C
500         TFILM=(TS+TINF)/2.0
510         RADP=RP
520         A3=SIG*EMMS*(TS**4-TWALL**4) + CAIR*(TS-TINF)/RADP
```

```
C
C       EPS1=0.03
C       EPS2=0.60
C       EPS3=0.12
C       DBULK=3.13*(TFILM/1500)**1.75
C       PORER2=1.0E-07
C       PORER3=25E-07
C       DK2=9700*PORER2*SQRT(TS/32.0)
C       DK3=9700*PORER3*SQRT(TS/32.0)
C       DEFF2=1.0/(1.0/DBULK + 1.0/DK2)
C       DEFF3=1.0/(1.0/DBULK + 1.0/DK3)
C       DEFF=0.5*(EPS1*DBULK + EPS2*DEFF2 + EPS3*DEFF3)
        ALPHAEFF=CEFF/(RHOAP*CPCARB)
        A4=2.0*CEFF*(TS-TC)/SQRT(ALPHAEFF)
C
        DO 50 I=1,100
          S(I)=0.0
 50     CONTINUE
C
        OPEN(2,FILE=IFILE,STATUS='NEW')
        XACC=0.001
        GAP=RP/99.0
C
        DO 300 I=2,99
C
          GUESSL=1.0E-10
          GUESSH=100000
```

```
800           RAD(I)=(I-1)*GAP
810 C
820           R=RAD(I)
830           CALL FUNT(I,GAP,RADP,GUESSL,FX1,R)
840           CALL FUNT(I,GAP,RADP,GUESSH,FX2,R)
850           IF(FX2*FX1 .GE. 0.0) PAUSE 'BRACKET ROOT IN MAIN'
860           DX = GUESSH-GUESSL
870           DO 200 J = 1, 500
880                DX = DX * 0.5
890                ANSW = GUESSL + DX
900                CALL FUNT(I,GAP,RADP,ANSW,FMID,R)
910                IF (FMID * FX1 .GT. 0.0)THEN
920                       GUESSL = ANSW
930                       FX1 = FMID
940                ELSE
950                       GUESSH = ANSW
960                       FX2 = FMID
970                ENDIF
980              IF (ABS(DX/ANSW) .LT. XACC)  GOTO 111
990   200      CONTINUE
1000           PAUSE 'TOO MANY BISECTIONS IN MAIN'
1010  111      S(I)=ANSW
1020           WRITE(*,*)I,RAD(I),S(I)
1030  300    CONTINUE
1040 C
1050          TAU=0.0
1060          DO 400 I=2,99
```

```
1070            RADMIC(I)=RAD(I)*1E04
1080            ARAT(I)=RAD(I)**2/RAD(99)**2
1090            TAU=TAU + GAP/S(I)
1100            WRITE(2,*)TAU,RADMIC(I),S(I),ARAT(I)
1110   400    CONTINUE
1120          WRITE(*,*)TAU
1130  C
1140          CLOSE(2)
1150          STOP
1160          END
1170  C
1180  C-------------------------------------------------------
1190  C
1200          SUBROUTINE FUNT(I,GAP,RADP,X,FX,R)
1210          IMPLICIT REAL*4(A-H,O-Z)
1220          COMMON  /A/A1,A2,A3,A4
1230          COMMON  /CS/A11,B11
1240          EXTERNAL SUM
1250  C
1260          CALL SUM(I,GAP,X,ANS,RADP)
1270          DUMSUM=ANS
1280          FX=A2*R*X*RADP/(SQRT(RADP**2-R**2))+
1290        1       (A3-A1*A11*EXP(-B11*R))*2.0*(RADP**2) ·
1300        2       *(1.0-SQRT(1.0-(R/RADP)**2))+A4*DUMSUM
1310          RETURN
1320          END
1330  C
```

```
1340 C-------------------------------------------------------
1350 C
1360         SUBROUTINE SUM(I,GAP,X,ANS,RADP)
1370         IMPLICIT REAL*4(A-H,O-Z)
1380         COMMON  /S/S(100)
1390         COMMON  /R/RAD(100)
1400 C
1410         ANS=0.0
1420         DO 100 J=2,I
1430           IF(I.EQ.2)THEN
1440                SUM1=GAP/X
1450           ELSE
1460                SUM1=0.0
1470                DO 200 K=J,I-1
1480                    SUM1=SUM1+GAP/S(K)
1490  200           CONTINUE
1500                SUM1=SUM1+GAP/X
1510           ENDIF
1520         ANS=ANS+(RADP/(SQRT(RADP**2-RAD(J)**2)))*
1530        1       ((RAD(J)*GAP)/(SQRT(SUM1)))
1540  100    CONTINUE
1550         RETURN
1560         END
1570 C
1580 C-------------------------------------------------------
```

AIX.2 MENU.FOR

```
 10 C    This program simulates the combustion of a single solid
 20 C    carbon particle with no internal structure. The particle
 30 C    is assumed to be isothermal.
 40 C    The gas phase is assumed to be in a quasi-steady state
 50 C    relative to the solid for a given time step. The
 60 C    reaction at the solid is 2C + 02 ---> 2C0 and in the gas
 70 C    phase the oxidation is assumed to be far enough from the
 80 C    particle so as to have no effect on it. The gas phase
 90 C    equations include the Stefan flow term. Gas phase property
100 C    values are calculated using the kinetic theory of gases.
110 C    The integral equations are then solved analytically.
120 C
130 C    Ash is assumed to be distributed uniformly inside the
140 C    particle, initially. However, as the particle burns, its
150 C    radius shrinks and the ash fraction in the particle
160 C    increases as only the  carbon burns. It is assumed that
170 C    at each step, the fraction of ash covering the surface is
180 C    the same as the ash volume fraction in the particle. The
190 C    presence of ash affects the access of oxygen to the
200 C    particle (blockage effect), the effective
210 C    emmissivity of the particle (since ash has an emissivity
220 C    different from carbon), and the thermal inertia
230 C    of the particle (assuming some heat capacity for ash).
240 C    These effects have been taken into account.
250 C
```

```
C-----------------------------------------
C
C    Declarations.
C
C
      IMPLICIT REAL*8(A-H,O-Z)
      REAL*8  NMAX
      REAL*8  K11,K12,K13,K14,K21,K22,K23,K24
      CHARACTER*15 IFILE
      CHARACTER*1 QRESP
C
C
      EXTERNAL RHOG,DIFF,EC,ECH,CPC,CPCH
      EXTERNAL RLAMB,EOX,ECO,FLUX,MFRC,ENERGY
      EXTERNAL GAMMA,RTBIS,RADIUS,SOLID
C
C
      COMMON T,GAM,TWALL,FP
      COMMON /R/RHOC,XFAC,ACEN
      COMMON /Y1S/Y1S,Y1INF
      COMMON /ASH/ASHFRAC,RHOASH,ASHINIT,RPINIT,CPASH,AMMIS
C
C-----------------------------------------
C
C    Interactive program parameter inputs.
C
C
```

```
C
      WRITE(*,9)
   9  FORMAT(1x,'WANT TO READ THE MENU.INP FILE (Y OR N)?')
      READ(*,8)QRESP
   8  FORMAT(A1)
      IF((QRESP .EQ. 'y') .OR. (QRESP .EQ .'Y'))GOTO 2000
C
      OPEN(1,FILE='MENU.INP',STATUS='NEW')

      WRITE(*,10)
  10  FORMAT(1x,'ENTER PARTICLE AND ASH DENSITIES IN G/CC')
      READ(*,*)RHOC,RHOASH
      WRITE(1,*)RHOC,RHOASH

      WRITE(*,11)
  11  FORMAT(1x,'ENTER WALL AND INIT. PARTICLE TEMPS. IN K')
      READ(*,*)TWALL,TPINIT
      WRITE(1,*)TWALL,TPINIT

      WRITE(*,12)
  12  FORMAT(1x,'ENTER THE INITIAL ASH VOLUME FRACTION')
      READ(*,*)ASHINIT
      WRITE(1,*)ASHINIT

      WRITE(*,13)
  13  FORMAT(1x,'ENTER THE INIT. PART. RADIUS IN MICRONS')
      READ(*,*)RPINIT
```

```
800         WRITE(1,*)RPINIT
810
820         WRITE(*,14)
830   14    FORMAT(1x,'ENTER THE O2 PART. PRES. IN THE AMBIENT')
840         READ(*,*)C1INF
850         WRITE(1,*)C1INF
860
870         WRITE(*,15)
880   15    FORMAT(1x,'ENTER THE WALL, CARBON AND ASH EMMISIVITIES')
890         READ(*,*)WEMMIS,PEMMIS,AMMIS
900         WRITE(1,*)WEMMIS,PEMMIS,AMMIS
910
920         WRITE(*,16)
930   16    FORMAT( 1x,'ENTER THE MAXIMUM TEMPERATURE INCREMENT')
940         READ(*,*)DELTEMP
950         WRITE(1,*)DELTEMP
960
970         WRITE(*,17)
980   17    FORMAT( 1x,'ENTER FACTOR XFAC, ACEN AND TIMESTEP')
990         READ(*,*)XFAC,ACEN,STEPO
1000        WRITE(1,*)XFAC,ACEN,STEPO
1010
1020        WRITE(*,18)
1030  18    FORMAT(1X,'ENTER ES1,ES2,XACC (0 < ES1 << ES2) ')
1040        READ(*,*)ES1,ES2,XACC
1050        WRITE(1,*)ES1,ES2,XACC
1060
```

```
1070          WRITE(*,19)
1080    19    FORMAT( 1x,'ENTER THE NUMBER OF TIMESTEPS')
1090          READ(*,*)NMAX
1100          WRITE(1,*)NMAX
1110
1120          WRITE(*,21)
1130    21    FORMAT( 1x,'WRITE OUTPUT FILENAME (NOT MENU.INP !)')
1140          READ(*,22)IFILE
1150    22    FORMAT(A15)
1160
1170          CLOSE(1)
1180          GOTO 3000
1190
1200    2000  OPEN(1,FILE='MENU.INP',STATUS='OLD')
1210          READ(1,*)RHOC,RHOASH,TWALL,TPINIT,ASHINIT,RPINIT,C1INF,
1220         1 WEMMIS,PEMMIS,AMMIS,DELTEMP,XFAC,ACEN,STEPO,ES1,ES2,
1230         2 XACC,NMAX
1240          CLOSE(1)
1250
1260          WRITE(*,30)RHOC,RHOASH
1270    30    FORMAT(1x,'1. PARTICLE AND ASH DENSITIES IN G/CC:
1280         1       ',F8.4,3X,F8.4,/)
1290
1300          WRITE(*,31)TWALL,TPINIT
1310    31    FORMAT(1x,'2. WALL AND INIT. PART. TEMPS.IN K: ',
1320         1     F10.4,3X,F10.4,/)
1330
```

```
1340        WRITE(*,32)ASHINIT
1350  32    FORMAT(1x,'3. THE INIT. ASH VOLUME FRACTION: ',F8.4,/)
1360
1370        WRITE(*,33)RPINIT
1380  33    FORMAT(1x,'4. THE INIT. PART. RAD. IN MICRONS: ',F8.4,/)
1390
1400        WRITE(*,34)C1INF
1410  34    FORMAT(1x,'5. THE O2 PART. PRES. (AMBIENT): ',F8.4,/)
1420
1430        WRITE(*,35)WEMMIS,PEMMIS,AMMIS
1440  35    FORMAT(1x,'6. THE WALL, CARBON AND ASH EMMISIVITIES: ',
1450     1      F6.4,3X,F6.4,3X,F6.4,/)
1460
1470        WRITE(*,36)DELTEMP
1480  36    FORMAT( 1x,'7. THE MAXIMUM TEMP. INCREMENT: ',F8.2,/)
1490
1500        WRITE(*,37)XFAC,ACEN,STEPO
1510  37    FORMAT( 1x,'8. THE FACTOR XFAC, ACEN AND TIMESTEP: ',
1520     1      F8.4,3X,F10.4,3X,F8.6,/)
1530
1540        WRITE(*,38)ES1,ES2,XACC
1550  38    FORMAT(1X,'9. ES1,ES2,XACC (0 < ES1 << ES2): ',
1560     1      E9.4,3X,E9.4,3X,E9.4,/)
1570
1580        WRITE(*,39)NMAX
1590  39    FORMAT( 1x,'10. THE NUMBER OF TIMESTEPS: ',F10.2,/)
1600
```

```
1610          WRITE(*,41)
1620    41    FORMAT( 1x,'WRITE OUTPUT FILENAME (NOT MENU.INP !)')
1630          READ(*,42)IFILE
1640    42    FORMAT(A15)
1650
1660    1990  WRITE(*,43)
1670    43    FORMAT(1X, 'WRITE ENTRY NO. TO BE ALTERED (0 TO RUN)')
1680          READ(*,*)NALT
1690          IF(NALT .EQ. 0)GOTO 2500
1700          IF(NALT .EQ. 1)GOTO 2010
1710          IF(NALT .EQ. 2)GOTO 2020
1720          IF(NALT .EQ. 3)GOTO 2030
1730          IF(NALT .EQ. 4)GOTO 2040
1740          IF(NALT .EQ. 5)GOTO 2050
1750          IF(NALT .EQ. 6)GOTO 2060
1760          IF(NALT .EQ. 7)GOTO 2070
1770          IF(NALT .EQ. 8)GOTO 2080
1780          IF(NALT .EQ. 9)GOTO 2090
1790          IF(NALT .EQ. 10)GOTO 2100
1800          GOTO 1990
1810
1820    2010  WRITE(*,10)
1830          READ(*,*)RHOC,RHOASH
1840          GOTO 1990
1850
1860    2020  WRITE(*,11)
1870          READ(*,*)TWALL,TPINIT
```

```
1880          GOTO 1990
1890
1900    2030  WRITE(*,12)
1910          READ(*,*)ASHINIT
1920          GOTO 1990
1930
1940    2040  WRITE(*,13)
1950          READ(*,*)RPINIT
1960          GOTO 1990
1970
1980    2050  WRITE(*,14)
1990          READ(*,*)C1INF
2000          GOTO 1990
2010
2020    2060  WRITE(*,15)
2030          READ(*,*)WEMMIS,PEMMIS,AMMIS
2040          GOTO 1990
2050
2060    2070  WRITE(*,16)
2070          READ(*,*)DELTEMP
2080          GOTO 1990
2090
2100    2080  WRITE(*,17)
2110          READ(*,*)XFAC,ACEN,STEPO
2120          GOTO 1990
2130
2140    2090  WRITE(*,18)
```

```
2150          READ(*,*)ES1,ES2,XACC
2160          GOTO 1990
2170
2180    2100  WRITE(*,19)
2190          READ(*,*)NMAX
2200          GOTO 1990
2210
2220    2500  OPEN(1,FILE='MENU.INP',STATUS='NEW')
2230          WRITE(1,*)RHOC,RHOASH,TWALL,TPINIT,ASHINIT,RPINIT,C1INF,
2240         1 WEMMIS,PEMMIS,AMMIS,DELTEMP,XFAC,ACEN,STEPO,ES1,ES2,
2250         2 XACC,NMAX
2260          CLOSE(1)
2270  C
2280  C---------------------------------------
2290  C---------------------------------------
2300  C
2310  C     Main program.
2320  C
2330  C     After initialization, the main loop begins. Timestep
2340  C     (STEP) is set to its original value. Radii are converted
2350  C     to centimeters for the actual calculation but are written
2360  C     out in microns. GAM is found by the method of bisection.
2370  C     The coupled gas and solid phase equations are solved to
2380  C     get GAM. Flux is calculated based on a reaction rate by
2390  C     Smith. Property values in the gas phase are functions of
2400  C     temperature. DUMC is the mole fraction of O2 at the
2410  C     external surface of the particle. X1, X2 are initial
```

```
2420 C     guesses for GAM and XACC is the error tolerance. DTDR is
2430 C     the temperature gradient at the surface.
2440 C
2450 C     Subroutine SOLID calculates the ash coverage of the
2460 C     particle. The reaction takes place on that portion of the
2470 C     solid that is free of ash. Ash is assumed to be at the
2480 C     same temperature as the rest of the particle.
2490 C
2500 C     Subroutine RUNG solves the coupled equations of mass and
2510 C     energy for a given time step. If the temperature change
2520 C     in the time step is larger than DELTEMP, the time step is
2530 C     halved and the process is repeated.
2540 C
2550 C     Every tenth data point is written to file and screen.
2560 C
2570 C
2580 C   Initialization.
2590 C
2600 C
2610  3000  Y1INF=(C1INF*32.0)/(C1INF*32.0+(1.0-C1INF)*28.0)
2620        A = (1.0 / (1.0 - Y1INF)) * (Y1INF / 4.0)
2630 C
2640        TP = TPINIT
2650        RP = RPINIT
2660        C1S = C1INF
2670        TIME = 0.0
2680        DTDR = 0.0
```

```
2690          FP=0.0
2700          ASHFRAC = ASHINIT
2710  C
2720          OPEN(2,FILE=IFILE,STATUS='NEW')
2730          WRITE(2, 900) TIME, RP, TP, C1S, FP
2740          WRITE(*, 900) TIME, RP, TP, C1S, FP
2750   900    FORMAT(1X,5G12.4)
2760  C
2770  C     X1 and X2 are appropriate brackets for GAM.
2780  C     Typically, ES1 is O(1D-6), while ES2 is O(1D11).
2790  C
2800          IF ( TPINIT .LT. TWALL) THEN
2810                  X1=( -2331.5425 + 0.3388749*TPINIT) - ES2
2820                  X2=( -2331.5425 + 0.3388749*TPINIT) - ES1
2830          ELSE
2840                 X1=( -2331.5425 + 0.3388749*TPINIT) + ES1
2850                 X2=( -2331.5425 + 0.3388749*TPINIT) + ES2
2860          ENDIF
2870  C
2880  C     Main loop begins.
2890  C
2900          JMAX = NMAX
2910          DO 1000 I = 1, JMAX
2920             STEP=STEPO
2930             T = TP
2940             RR = RP* 1D-04
2950             CALL RTBIS(GAMMA,X1,X2,XACC,RR,GAM)
```

```
2960            DUMC = (1.0/(-1.0/7.0 + 8.0/(7.0*Y1S)))
2970            CALL FLUX(DUMC)
2980            FP1 = -1.3333 * FP
2990            FP2 = 2.3333 * FP
3000            EP = GAM * FP
3010            DTDR=-1.OD-4*(EP-FP1*EOX(T)-FP2*ECO(T))/RLAMB(T)
3020            CALL SOLID(RR)
3030  991       CALL RUNG(RADIUS,ENERGY,DUMC,STEP,EP,PEMMIS,WEMMIS,
3040       1      RR,RNEW,TNEW)
3050            DELR=(RR-RNEW)/RR
3060            IF((ASHFRAC .GE. 1.0).OR.(DELR .LT. 0.00001))GOTO 1001
3070            IF(ABS(TNEW - TP) .GT. DELTEMP)THEN
3080                STEP = STEP/2.0
3090                GOTO 991
3100            ENDIF
3110            RP = 1.OD4*RNEW
3120            TP = TNEW
3130            TIME = TIME + 1.OD3*STEP
3140 C
3150 C     Writing to file.
3160 C
3170            IF(MOD(I,10) .EQ. 0)THEN
3180            WRITE(2, 900) TIME, RP, TP, DUMC ,FP
3190            WRITE(*, 900) TIME, RP, TP, DUMC ,FP
3200            ENDIF
3210 C
3220 C     Reducing the brackets for the next call of GAM.
```

```
C
          IF ( TP .LT. TWALL) THEN
               X1 =  GAM - DABS(1000.0*GAM)
               X2 =  ( -2331.5425 + 0.3388749*TP ) - ES1
          ELSE
               X1 =  ( -2331.5425 + 0.3388749*TP ) + ES1
               X2 =  GAM + DABS(1000.0*GAM)
          ENDIF
C
 1000  CONTINUE
 1001  CLOSE(2)
       STOP
       END
C
C    Main loop and main program end.
C
C-----------------------------------------
C-----------------------------------------
C
C    Property values.
C
C
C    Gas diffusivity is calculated for an N2-O2 system over a
C    range of 300K to 3000K. Units are cm^2/s.
C
       REAL*8 FUNCTION DIFF(D)
       IMPLICIT REAL*8(A-H,O-Z)
```

```
      COMMON T,GAM,TWALL,FP
      DIFF0 = -0.099
      DIFF1 = 6.910D-04
      DIFF2 = 1.070D-06
      DIFF3 = -6.04D-11
      DIFF = DIFF0 + DIFF1*D + DIFF2*(D*D) + DIFF3*(D*D*D)
      RETURN
      END
C
C     Gas density is found using the ideal gas law in g/cc.
C     Average molecular weight for air is taken as 29.0.
C
      REAL*8 FUNCTION RHOG(D)
      IMPLICIT REAL*8(A-H,O-Z)
      COMMON T,GAM,TWALL,FP
      RHOG =  29.0/(82.05*D)
      RETURN
      END
C
C     Gas thermal conductivity coeffs. are in W/m-K for D in K.
C     Data from Eckert (300K to 2500K). RLAMB is converted
C     to cal/cm-K.
C
      REAL*8 FUNCTION RLAMB(D)
      IMPLICIT REAL*8(A-H,O-Z)
      REAL*8 LG0,LG1,LG2,LG3,D
      COMMON T,GAM,TWALL,FP
```

```
3770          LGO = -1.333D-03
3780          LG1 =  1.036D-04
3790          LG2 = -4.715D-08
3800          LG3 =  1.341D-11
3810          RLAMB=(1.0/418.0)*(LGO+LG1*D+LG2*(D*D)+LG3*(D*D*D))
3820          RETURN
3830          END
3840  C
3850  C     The enthalpies for the gases are in cal/mol for D in K.
3860  C     Ref state = 0 at 298K (except CO); Data from Smith and
3870  C     VanNess (298K to 2500K). Heat capacities are assumed
3880  C     to be constant to obtain reasonable integrable forms.
3890  C
3900          REAL*8 FUNCTION EOX(D)
3910          IMPLICIT REAL*8(A-H,O-Z)
3920          COMMON T,GAM,TWALL,FP
3930          CPOXO = 7.16
3940          CPOX1 = 0.001
3950          CPOX2 = -40000.0
3960          EOX = (CPOXO*(D - 298) + (CPOX1 / 2.0)*(D*D - 298*298)
3970         1        + CPOX2*(1.0/D - 1.0/298)) / 32.0
3980          RETURN
3990          END
4000  C
4010          REAL*8 FUNCTION ECO(D)
4020          IMPLICIT REAL*8(A-H,O-Z)
4030          COMMON T,GAM,TWALL,FP
```

```
4040          CPCO0 = 6.79
4050          CPCO1 = 0.00098
4060          CPCO2 = -11000.0
4070          DELH = -26416.0
4080          ECO=(DELH+CPCO0*(D-298)+(CPCO1/2.0)*(D*D-298*298)
4090         1        + CPCO2*(1.0/D-1.0/298))/28.0
4100          RETURN
4110          END
4120  C
4130          REAL*8 FUNCTION EN(D)
4140          IMPLICIT REAL*8(A-H,O-Z)
4150          COMMON T,GAM,TWALL,FP
4160          CPNO = 6.83
4170          CPN1 = 0.0009
4180          CPN2 = -12000.0
4190          EN = (CPNO*(D - 298) + (CPN1 / 2.0)*(D*D - 298*298)
4200         1        + CPN2*(1.0/D - 1.0/298))/ 28.0
4210          RETURN
4220          END
4230  C
4240  C     EC and ECH calculate the enthalpy of the solid in cal/g.
4250  C     Data from coal data book.
4260  C
4270          REAL*8 FUNCTION EC(D)
4280          IMPLICIT REAL*8(A-H,O-Z)
4290          COMMON T,GAM,TWALL,FP
4300          CPCO = 0.024
```

```
4310          CPC1 = 6.953D-04
4320          CPC2 = -2.841D-07
4330          EC = CPC0*(D - 298) + (CPC1 / 2.0)*(D*D - 298*298)
4340         1       + (CPC2 / 3.0)*(D*D*D - 298*298*298)
4350          RETURN
4360          END
4370  C
4380  C
4390          REAL*8 FUNCTION ECH(D)
4400          IMPLICIT REAL*8(A-H,O-Z)
4410          COMMON T,GAM,TWALL,FP
4420          CPCH0 = 0.36
4430          CPCH1 = 6.931D-05
4440          ECH = CPCH0*(D - 298) + (CPCH1 / 2.0)*(D*D - 298*298)
4450          RETURN
4460          END
4470  C
4480  C     CPC and CPCH calculate the heat capacity of the solid in
4490  C     cal/g-K.  Data from coal data book.
4500  C
4510          REAL*8 FUNCTION CPC(D)
4520          IMPLICIT REAL*8(A-H,O-Z)
4530          COMMON T,GAM,TWALL,FP
4540          CPC0 = 0.024
4550          CPC1 = 6.953D-04
4560          CPC2 = -2.841D-07
4570          CPC = CPC0 + CPC1 * D + CPC2 * D * D
```

```
4580          RETURN
4590          END
4600  C
4610          REAL*8 FUNCTION CPCH(D)
4620          IMPLICIT REAL*8(A-H,O-Z)
4630          COMMON T,GAM,TWALL,FP
4640          CPCHO = 0.36
4650          CPCH1 = 6.931D-05
4660          CPCH = CPCHO + CPCH1 * D
4670          RETURN
4680          END
4690  C
4700  C---------------------------------------
4710  C
4720  C     This routine calculates the fraction of solid covered by
4730  C     ash (ASHFRAC). (ASHFRAC --> 1.0 as RR --> RMIN)
4740  C
4750          SUBROUTINE SOLID(RR)
4760          IMPLICIT REAL*8(A-H,O-Z)
4770          COMMON /ASH/ASHFRAC,RHOASH,ASHINIT,RPINIT,CPASH,AMMIS
4780  C
4790          ASHFRAC = ASHINIT*(1.0D-4*RPINIT/RR)**3.0
4800          RETURN
4810          END
4820  C
4830  C---------------------------------------
4840  C
```

```
4850 C    Root finder by the method of bisection for function TET.
4860 C
4870        SUBROUTINE RTBIS(TET,X1,X2,XACC,R2,XMID)
4880        IMPLICIT REAL*8(A-H,O-Z)
4890        EXTERNAL  TET
4900        COMMON         T,GAM,TWALL,FP
4910        PARAMETER (JMAX = 500)
4920 C
4930        CALL TET(X1,FX1,R2)
4940        CALL TET(X2,FX2,R2)
4950        IF(FX2*FX1 .GE. 0.0) PAUSE 'BRACKET ROOT IN RTBIS'
4960        DX = X2 - X1
4970          DO 200 J = 1, JMAX
4980               DX = DX * 0.5
4990               XMID = X1 + DX
5000               CALL TET(XMID,FMID,R2)
5010               IF (FMID * FX1 .GT. 0.0)THEN
5020                     X1 = XMID
5030                     FX1 = FMID
5040               ELSE
5050                     X2 = XMID
5060                     FX2 = FMID
5070               ENDIF
5080               IF (DABS(DX/XMID) .LT. XACC)  RETURN
5090  200      CONTINUE
5100        PAUSE 'TOO MANY BISECTIONS'
5110        END
```

```
5120 C
5130 C----------------------------------------
5140 C
5150 C    Calculation of solid flux in gmc/cm^2-s.(Smith 1974)
5160 C
5170         SUBROUTINE FLUX(B)
5180         IMPLICIT REAL*8(A-H,O-Z)
5190         COMMON /ASH/ASHFRAC,RHOASH,ASHINIT,RPINIT,CPASH,AMMIS
5200         COMMON T,GAM,TWALL,FP
5210         COMMON /R/RHOC,XFAC,ACEN
5220 C
5230         FP=(1.0-ASHFRAC)*XFAC*9.3*DEXP(-ACEN/(1.98*T))*B
5240         RETURN
5250         END
5260 C
5270 C----------------------------------------
5280 C
5290 C       This routine calculates the value of the fully
5300 C       integrated equations from TWALL to TP based on GAM1.
5310 C
5320         SUBROUTINE GAMMA(GAM1,F,R1)
5330         IMPLICIT REAL*8(A-H,O-Z)
5340         COMMON T, GAM, TWALL,FP
5350         COMMON /R/RHOC,XFAC,ACEN
5360         COMMON /Y1S/Y1S,Y1INF
5370 C
5380         CC = -3.0043D-05
```

```
      IF (T .LT. TWALL) THEN
             HH = DSQRT(DABS(-2331.5425 - GAM1)/0.3388749)
      IF (GAM1 .GT.-2331.5425) THEN
            AR1=-1.0*CC*((DSQRT(TWALL) - DSQRT(T))+HH/2.0*
     1           (DLOG((DSQRT(TWALL) - HH)*(DSQRT(T) + HH)/
     2                ((DSQRT(TWALL) + HH)*(DSQRT(T) - HH)))))
            HM = (2331.5425 + GAM1)/0.3388749
        Y1S=(Y1INF+4.0/3.0)*((T-HM)/(TWALL-HM))**0.8095478-4.0/3.0
            F = AR1-R1* XFAC*9.3*DEXP(-ACEN/(1.98*T))*
     1              (1.0/(-1.0/7.0 + 8.0/(7.0*Y1S)))
      ELSE
            AR2 = -1.0*CC*((DSQRT(TWALL)-DSQRT(T))-HH*
     1           (DATAN(DSQRT(TWALL)/HH)-DATAN(DSQRT(T)/HH)))
            HM = (2331.5425 + GAM1)/0.3388749
        Y1S=(Y1INF+4.0/3.0)*((T-HM)/(TWALL-HM))**0.8095478-4.0/3.0
            F = AR2-R1* XFAC*9.3*DEXP(-ACEN/(1.98*T))*
     1          (1.0/(-1.0/7.0 + 8.0/(7.0*Y1S)))
      ENDIF
      ELSE
            FF = DSQRT(DABS(2331.5425 + GAM1)/0.3388749)
      IF (GAM1 .LT.-2331.5425) THEN
             AR3 = CC*((DSQRT(T)-DSQRT(TWALL))-FF*
     1           (DATAN(DSQRT(T)/FF)-DATAN(DSQRT(TWALL)/FF)))
            C3 = (2331.5425 + GAM1)/0.3388749
        Y1S=(Y1INF+4.0/3.0)*((T-C3)/(TWALL-C3))**0.8095478-4.0/3.0
            F = AR3-R1* XFAC*9.3*DEXP(-ACEN/(1.98*T))*
     1              (1.0/(-1.0/7.0 + 8.0/(7.0*Y1S)))
```

```
5660         ELSE
5670                 AR4 = CC * ((DSQRT(T) - DSQRT(TWALL)) + FF/2.0 *
5680        1                (DLOG((DSQRT(T) - FF)*(DSQRT(TWALL) + FF)/
5690        2                     ((DSQRT(T) + FF)*(DSQRT(TWALL) - FF)))))
5700                 C3 = (2331.5425 + GAM1)/0.3388749
5710         Y1S=(Y1INF+4.0/3.0)*((T-C3)/(TWALL-C3))**0.8095478-4.0/3.0
5720                      F = AR4-R1* XFAC*9.3*DEXP(-ACEN/(1.98*T))*
5730        1                   (1.0/(-1.0/7.0 + 8.0/(7.0*Y1S)))
5740         ENDIF
5750         ENDIF
5760         RETURN
5770         END
5780 C
5790 C----------------------------------------
5800 C
5810 C    Energy equation.
5820 C
5830         SUBROUTINE ENERGY(EP,PEMMIS,WEMMIS,RR,DUM2,ANST)
5840         IMPLICIT REAL*8(A-H,O-Z)
5850         EXTERNAL  CPC,EC,CPCH,ECH
5860         COMMON T, GAM, TWALL,FP
5870         COMMON /R/RHOC,XFAC,ACEN
5880         COMMON /ASH/ASHFRAC,RHOASH,ASHINIT,RPINIT,CPASH,AMMIS
5890 C
5900         SIG = 1.595D-12
5910         IF (DUM2 .LT. 1350) THEN
5920                 CPSOL= CPC(DUM2)
```

```
5930                VAL = EC(DUM2)
5940          ELSE
5950                CPSOL= CPCH(DUM2)
5960                VAL = ECH(DUM2)
5970          ENDIF
5980          CPASH = 0.183 + 0.111D-3*T
5990          ANST=3.0*RR*RR*(FP*VAL - EP - SIG* ((ASHFRAC*AMMIS+
6000         1      (1.0-ASHFRAC)*PEMMIS)*DUM2**4-WEMMIS*TWALL**4))/
6010         2         (RHOC*RR*RR*RR*CPSOL+
6020         3       CPASH*RHOASH*ASHINIT*((1.0D-4*RPINIT)**3.0))
6030          RETURN
6040          END
6050  C
6060  C----------------------------------------
6070  C
6080  C     Fourth order Runge-Kutta method for solving TEST1 and
6090  C     TEST2 for one time step.
6100  C
6110          SUBROUTINE RUNG(TEST1,TEST2,DUMC,STEP,EP,
6120         1                    PEMMIS,WEMMIS,RR,RNEW,TNEW)
6130          IMPLICIT REAL*8(A-H,O-Z)
6140          REAL*8 K11,K12,K13,K14,K21,K22,K23,K24
6150          EXTERNAL TEST1,TEST2,ENERGY,RADIUS
6160          COMMON T, GAM, TWALL,FP
6170          COMMON /R/RHOC,XFAC,ACEN
6180  C
6190          DUM1=RR
```

```
6200        DUM2=T
6210        CALL TEST1(DUMC,DUM1,DUM2,DRDT)
6220        CALL TEST2(EP,PEMMIS,WEMMIS,DUM1,DUM2,DTDT)
6230        K11=DRDT
6240        K21=DTDT
6250        DUM1 = RR + K11*STEP/2.0
6260        DUM2 = T + K21*STEP/2.0
6270        CALL TEST1(DUMC,DUM1,DUM2,DRDT)
6280        CALL TEST2(EP,PEMMIS,WEMMIS,DUM1,DUM2,DTDT)
6290        K12 = DRDT
6300        K22 = DTDT
6310        DUM1 = RR + K12*STEP/2.0
6320        DUM2 = T + K22*STEP/2.0
6330        CALL TEST1(DUMC,DUM1,DUM2,DRDT)
6340        CALL TEST2(EP,PEMMIS,WEMMIS,DUM1,DUM2,DTDT)
6350        K13 = DRDT
6360        K23 = DTDT
6370        DUM1 = RR + K13*STEP
6380        DUM2 = T + K23*STEP
6390        CALL TEST1(DUMC,DUM1,DUM2,DRDT)
6400        CALL TEST2(EP,PEMMIS,WEMMIS,DUM1,DUM2,DTDT)
6410        K14 = DRDT
6420        K24 = DTDT
6430        RNEW = RR + STEP*(K11 + 2.0*K12 + 2.0*K13 + K14)/6.0
6440        TNEW = T + STEP*(K21 + 2.0*K22 + 2.0*K23 + K24)/6.0
6450        RETURN
6460        END
```

```
6470 C
6480 C-----------------------------------------
6490 C
6500 C    Particle mass balance.
6510 C
6520        SUBROUTINE RADIUS(B,DUM1,DUM2,ANS)
6530        IMPLICIT REAL*8(A-H,O-Z)
6540        COMMON T, GAM, TWALL,FP
6550        COMMON /R/RHOC,XFAC,ACEN
6560        COMMON /ASH/ASHFRAC,RHOASH,ASHINIT,RPINIT,CPASH,AMMIS
6570 C
6580        ANS=((-1.0*(XFAC*9.3*DEXP(-ACEN/(1.98 * DUM2))* B))*
6590       1     (1.0-ASHFRAC))/((RHOASH*ASHFRAC + RHOC*(1.0-ASHFRAC))
6600       2     +((RHOC -RHOASH)*ASHINIT*((1.0D-4*RPINIT)**3.0)/
6610       3     (DUM1**3.0)))
6620        RETURN
6630        END
6640 C
6650 C-----------------------------------------
```

AIX.3 VARNU.FOR

```
C     This program simulates the combustion of a single solid
C     carbon particle with no internal structure. The particle is
C     assumed to be isothermal.
C     The gas phase is assumed to be in a quasi-steady state
C     relative to the solid for a given time step. The hetero
C     reaction at the solid is 2C + O2 ---> 2CO and in the gas
C     phase the oxidation is assumed to be far enough from the
C     particle so as to have no effect on it. The gas phase
C     equations include the Stefan flow term. Gas phase properties
C     are calculated using the kinetic theory of gases. The
C     integral equations are then solved analytically.
C
C     Ash is assumed to be distributed uniformly inside the
C     particle, initially. However, as the particle burns, the
C     carbon shrinks and the ash fraction in the particle rises.
C     It is assumed that none of the ash is lost; it accumulates
C     on the carbon surface. The ash layer affects the access of
C     oxygen to the particle (blockage effect), the effective
C     emmissivity of the particle (since ash has an emissivity
C     different from carbon), and the thermal inertia
C     of the particle (assuming some heat capacity for ash).
C     These effects have been taken into account.
C
C-----------------------------------------
C
```

```
260 C    Declarations.
270 C
280 C
290          IMPLICIT REAL*8(A-H,O-Z)
300          REAL*8  NMAX
310          REAL*8  K11,K12,K13,K14,K21,K22,K23,K24
320          CHARACTER*15 IFILE
330          CHARACTER*1  QRESP
340 C
350          EXTERNAL  EC,ECH,CPC,CPCH
360          EXTERNAL  FLUX,ENERGY
370          EXTERNAL  GAMMA,RTBIS,RADIUS,SOLID
380 C
390 C
400          COMMON  /FIRST/T,GAM,TWALL,FP
410          COMMON  /R/RHOC,XFAC,ACEN
420          COMMON  /Y1S/Y1S,Y1INF
430          COMMON  /ASH/ASHFRAC,RHOASH,ASHINIT,
440       1          RPINIT,CPASH,AMMIS,THCK
450          COMMON  /TF/TFAC,PEMMIS
460 C
470 C-----------------------------------------
480 C
490 C    Interactive program parameter inputs.
500 C
510 C
520          WRITE(*,9)
```

```
530   9     FORMAT(1X,'WANT TO READ THE VARNU.INP FILE (Y OR N)?')
540         READ(*,8)QRESP
550   8     FORMAT(A1)
560         IF((QRESP .EQ. 'y') .OR. (QRESP .EQ .'Y'))GOTO 2000
570
580         OPEN(1,FILE='VARNU.INP',STATUS='NEW')
590
600         WRITE(*,10)
610   10    FORMAT(1X,'ENTER VOID FRC. AND THICKNESS FACTOR')
620         READ(*,*)EPSO,TFAC
630         WRITE(1,*)EPSO,TFAC
640
650         WRITE(*,11)
660   11    FORMAT(1X,'ENTER WALL AND INIT. PART. TEMPS. IN K')
670         READ(*,*)TWALL,TPINIT
680         WRITE(1,*)TWALL,TPINIT
690
700         WRITE(*,12)
710   12    FORMAT(1X,'ENTER THE INITIAL ASH VOLUME FRACTION')
720         READ(*,*)ASHO
730         WRITE(1,*)ASHO
740
750         WRITE(*,13)
760   13    FORMAT(1X,'ENTER THE INIT. PART. RADIUS IN MICRONS')
770         READ(*,*)RINIT
780         WRITE(1,*)RINIT
790
```

```
      WRITE(*,14)
14    FORMAT(1X,'ENTER THE O2 PART. PRES. IN THE AMBIENT')
      READ(*,*)PINF
      WRITE(1,*)PINF

      WRITE(*,15)
15    FORMAT(1X,'INPUT WALL, CARBON AND ASH EMMISIVITIES')
      READ(*,*)WEMMIS,PEMMIS,AMMIS
      WRITE(1,*)WEMMIS,PEMMIS,AMMIS

      WRITE(*,16)
16    FORMAT(1X,'ENTER THE MAXIMUM TEMPERATURE INCREMENT')
      READ(*,*)DELTEMP
      WRITE(1,*)DELTEMP

      WRITE(*,17)
17    FORMAT(1X,'ENTER XFAC, ACEN AND TIMESTEP')
      READ(*,*)XFAC,ACEN,STEPO
      WRITE(1,*)XFAC,ACEN,STEPO

      WRITE(*,18)
18    FORMAT(1X,'ENTER ES1,ES2,XACC (0 < ES1 << ES2) ')
      READ(*,*)ES1,ES2,XACC
      WRITE(1,*)ES1,ES2,XACC

      WRITE(*,19)
19    FORMAT(1X,'ENTER THE NUMBER OF TIMESTEPS')
```

```
1070          READ(*,*)NMAX
1080          WRITE(1,*)NMAX
1090
1100          WRITE(*,21)
1110    21    FORMAT(1X,'ENTER THE OUTPUT FILENAME (NOT VARNU.INP!)')
1120          READ(*,22)IFILE
1130    22    FORMAT(A15)
1140
1150          CLOSE(1)
1160          GOTO 3000
1170
1180    2000  OPEN(1,FILE='VARNU.INP',STATUS='OLD')
1190          READ(1,*)EPSO,TFAC,TWALL,TPINIT,ASHO,RINIT,PINF,WEMMIS,
1200         1  PEMMIS,AMMIS,DELTEMP,XFAC,ACEN,STEPO,ES1,ES2,XACC,NMAX
1210          CLOSE(1)
1220
1230          WRITE(*,30)EPSO,TFAC
1240    30    FORMAT(1X,'1. PARTICLE VOID FRAC. AND TFAC:
1250         1  ',F8.4,3X,F8.4,/)
1260
1270          WRITE(*,31)TWALL,TPINIT
1280    31    FORMAT(1X,'2. WALL AND INIT. PART. TEMPS. IN K: ',
1290         1    F10.4,3X,F10.4,/)
1300
1310          WRITE(*,32)ASHO
1320    32    FORMAT(1X,'3. THE INIT. ASH VOLUME FRACTION: ',F8.4,/)
1330
```

```
1340          WRITE(*,33)RINIT
1350    33    FORMAT(1X,'4. THE INIT. PART. RADIUS IN MIC.: ',F8.4,/)
1360
1370          WRITE(*,34)PINF
1380    34    FORMAT(1X,'5. THE O2 PART. PRES. (AMBIENT): ',F8.4,/)
1390
1400          WRITE(*,35)WEMMIS,PEMMIS,AMMIS
1410    35    FORMAT(1X,'6. THE WALL, CARBON AND ASH EMMISIVITIES: ',
1420         1      F6.4,3X,F6.4,3X,F6.4,/)
1430
1440          WRITE(*,36)DELTEMP
1450    36    FORMAT(1X,'7. THE MAXIMUM TEMP. INCREMENT: ',F8.2,/)
1460
1470          WRITE(*,37)XFAC,ACEN,STEPO
1480    37    FORMAT(1X,'8. THE FACTOR XFAC, ACEN AND TIMESTEP: ',
1490         1      F8.4,3X,F12.2,2X,F8.6,/)
1500
1510          WRITE(*,38)ES1,ES2,XACC
1520    38    FORMAT(1X,'9. ES1,ES2,XACC (0 < ES1 << ES2): ',
1530         1      E9.4,3X,E9.4,3X,E9.4,/)
1540
1550          WRITE(*,39)NMAX
1560    39    FORMAT(1X,'10. THE NUMBER OF TIMESTEPS: ',F10.2,/)
1570
1580          WRITE(*,41)
1590    41    FORMAT(1X,'ENTER THE OUTPUT FILENAME (NOT VARNU.INP!)')
1600          READ(*,42)IFILE
```

```
1610  42     FORMAT(A15)
1620
1630  1990   WRITE(*,43)
1640  43     FORMAT(1X, 'ENTRY NO. TO BE ALTERED (0 TO RUN)')
1650         READ(*,*)NALT
1660         IF(NALT .EQ. 0)GOTO 2500
1670         IF(NALT .EQ. 1)GOTO 2010
1680         IF(NALT .EQ. 2)GOTO 2020
1690         IF(NALT .EQ. 3)GOTO 2030
1700         IF(NALT .EQ. 4)GOTO 2040
1710         IF(NALT .EQ. 5)GOTO 2050
1720         IF(NALT .EQ. 6)GOTO 2060
1730         IF(NALT .EQ. 7)GOTO 2070
1740         IF(NALT .EQ. 8)GOTO 2080
1750         IF(NALT .EQ. 9)GOTO 2090
1760         IF(NALT .EQ. 10)GOTO 2100
1770         GOTO 1990
1780
1790  2010   WRITE(*,10)
1800         READ(*,*)EPSO,TFAC
1810         GOTO 1990
1820
1830  2020   WRITE(*,11)
1840         READ(*,*)TWALL,TPINIT
1850         GOTO 1990
1860
1870  2030   WRITE(*,12)
```

```
1880          READ(*,*)ASHO
1890          GOTO 1990
1900
1910    2040  WRITE(*,13)
1920          READ(*,*)RINIT
1930          GOTO 1990
1940
1950    2050  WRITE(*,14)
1960          READ(*,*)PINF
1970          GOTO 1990
1980
1990    2060  WRITE(*,15)
2000          READ(*,*)WEMMIS,PEMMIS,AMMIS
2010          GOTO 1990
2020
2030    2070  WRITE(*,16)
2040          READ(*,*)DELTEMP
2050          GOTO 1990
2060
2070    2080  WRITE(*,17)
2080          READ(*,*)XFAC,ACEN,STEPO
2090          GOTO 1990
2100
2110    2090  WRITE(*,18)
2120          READ(*,*)ES1,ES2,XACC
2130          GOTO 1990
2140
```

```
2150  2100   WRITE(*,19)
2160         READ(*,*)NMAX
2170         GOTO 1990
2180 .
2190  2500   OPEN(1,FILE='VARNU.INP',STATUS='NEW')
2200         WRITE(1,*)EPSO,TFAC,TWALL,TPINIT,ASHO,RINIT,PINF,WEMMIS,
2210       1  PEMMIS,AMMIS,DELTEMP,XFAC,ACEN,STEPO,ES1,ES2,XACC,NMAX
2220         CLOSE(1)
2230 C
2240 C-----------------------------------------------
2250 C
2260 C    Main program.
2270 C
2280 C    After initialization, the main loop begins. STEP (timestep)
2290 C    is set to its original value. Radii are converted to cms.
2300 C    for actual calculation but are written out in microns. GAM
2310 C    is found by bisection. The coupled gas and solid phase
2320 C    equations are solved to get GAM. Flux is calculated based on
2330 C    a reaction rate by Smith. Property values in the gas phase
2340 C    are functions of temperature. DUMC is the mole fraction of
2350 C    O2 at the external surface of the particle. X1, X2 are
2360 C    initial guesses for GAM and XACC is the error tolerance.
2370 C    DTDR is the temperature gradient at the surface.
2380 C
2390 C    Subroutine SOLID finds the ash fraction of the particle.
2400 C    Ash is assumed to be at the same temperature as the rest
2410 C    of the particle.
```

```
C
C     Subroutine RUNG solves the coupled equations of mass and
C     energy for a given time step. If the temperature change in
C     a time step is larger than DELTEMP, the time step is halved
C     and the process is repeated.
C
C     Every tenth data point is written to file and screen.
C
C
C     Initialization.
C
          RHOC=1.5*(1-ASHO-EPSO)
          C1INF=PINF
          RPINIT=RINIT
          ASHINIT=ASHO
C
          RHOASH=2.0
C
C         NMAX=2000
C         ES1=1.0D-6
C         ES2=1.0D07
C         XACC=0.0001
C         STEPO=0.0001
C         DELTEMP=20
C         WEMMIS=0.8
C         PEMMIS=0.8
C         AMMIS=0.8
```

```
2690 C
2700  3000   Y1INF=(C1INF*32.0)/(C1INF * 32.0 +(1.0 - C1INF )*28.0)
2710         A = (1.0 / (1.0 - Y1INF)) * (Y1INF / 4.0)
2720 C
2730         TP = TPINIT
2740         RP = RPINIT
2750         C1S = C1INF
2760         TIME = 0.0
2770         DTDR = 0.0
2780         FP=0.0
2790         THCK=0.0
2800         ASHFRAC = ASHINIT
2810
2820         OPEN(2,FILE=IFILE,STATUS='NEW')
2830         WRITE(*, 900) TIME, RP, TP, C1S, FP
2840         WRITE(2, 900) TIME, RP, TP, C1S, FP
2850  900    FORMAT(1X,5G12.4)
2860 C
2870 C    X1 and X2 are appropriate brackets for GAM.
2880 C    Typically, ES1 is O(1D-6), while ES2 is O(1D11).
2890 C
2900         IF ( TPINIT .LT. TWALL) THEN
2910                X1 =  ( -2331.5425 + 0.3388749*TPINIT) - ES2
2920                X2 =  ( -2331.5425 + 0.3388749*TPINIT) - ES1
2930         ELSE
2940                X1 =  ( -2331.5425 + 0.3388749*TPINIT) + ES1
2950                X2 =  ( -2331.5425 + 0.3388749*TPINIT) + ES2
```

```
2960          ENDIF
2970  C
2980  C     Main loop begins.
2990  C
3000          JMAX = NMAX
3010          DO 1000 I = 1, JMAX
3020            STEP=STEPO
3030            T = TP
3040            RR = RP * 1D-04
3050            THCK=(RP**3.0+(ASHINIT*(RPINIT**3.0-RP**3.0))/
3060       1          0.65)**(1.0/3.0)-RP + 1.0D-08
3070            THCK=THCK*1.0D-04*TFAC
3080            CALL RTBIS(GAMMA,X1,X2,XACC,RR,GAM)
3090            DUMC = (1.0/(-1.0/7.0 + 8.0/(7.0*Y1S)))
3100            CALL FLUX(DUMC,RR)
3110            FP1 = -1.3333 * FP
3120            FP2 = 2.3333 * FP
3130            EP = GAM * FP
3140            CALL SOLID(RR)
3150  991       CALL RUNG(RADIUS,ENERGY,DUMC,STEP,EP,
3160       1                      PEMMIS,WEMMIS,RR,RNEW,TNEW)
3170            IF(RNEW .LE. 0.0001)THEN
3180               TBURN=TIME
3190               GOTO 1001
3200            ENDIF
3210            RP = 1.0D4*RNEW
3220            TP = TNEW
```

```
3230            TIME = TIME + 1.0D3*STEP
3240 C
3250 C    Writing to file.
3260 C
3270            IF(MOD(I,10) .EQ. 0)THEN
3280                WRITE(*, 900) TIME, RP, TP, DUMC ,FP
3290                WRITE(2, 900) TIME, RP, TP, DUMC ,FP
3300            ENDIF
3310 C
3320 C    Reducing the brackets for the next call of GAM.
3330 C
3340            IF ( TP .LT. TWALL) THEN
3350                  X1 =  GAM - DABS(1000.0*GAM)
3360                  X2 =  ( -2331.5425 + 0.3388749*TP ) - ES1
3370            ELSE
3380                  X1 =  ( -2331.5425 + 0.3388749*TP ) + ES1
3390                  X2 =  GAM + DABS(1000.0*GAM)
3400            ENDIF
3410 C
3420  1000    CONTINUE
3430  1001    CONTINUE
3440          CLOSE(2)
3450          END
3460 C
3470 C    Main loop and main program end.
3480 C
3490 C-----------------------------------------
```

```
3500 C-----------------------------------------
3510 C
3520 C    Property values.
3530 C
3540 C    EC and ECH calculate the enthalpy of the solid in cal/g.
3550 C    Data from coal data book.
3560 C
3570          REAL*8 FUNCTION EC(D)
3580          IMPLICIT REAL*8(A-H,O-Z)
3590          COMMON  /FIRST/T,GAM,TWALL,FP
3600          CPC0 = 0.024
3610          CPC1 = 6.953D-04
3620          CPC2 = -2.841D-07
3630          EC = CPC0*(D - 298) + (CPC1 / 2.0)*(D*D - 298*298)
3640      1   + (CPC2 / 3.0)*(D*D*D - 298*298*298)
3650          RETURN
3660          END
3670 C
3680 C
3690          REAL*8 FUNCTION ECH(D)
3700          IMPLICIT REAL*8(A-H,O-Z)
3710          COMMON  /FIRST/T,GAM,TWALL,FP
3720          CPCH0 = 0.36
3730          CPCH1 = 6.931D-05
3740          ECH = CPCH0*(D - 298) + (CPCH1 / 2.0)*(D*D - 298*298)
3750          RETURN
3760          END
```

```
C
C    CPC and CPCH calculate the heat capacity of the solid in
C    cal/g-K.  Data from coal data book.
C
         REAL*8 FUNCTION CPC(D)
         IMPLICIT REAL*8(A-H,O-Z)
         COMMON  /FIRST/T,GAM,TWALL,FP
         CPCO = 0.024
         CPC1 = 6.953D-04
         CPC2 = -2.841D-07
         CPC = CPCO + CPC1 * D + CPC2 * D * D
         RETURN
         END
C
         REAL*8 FUNCTION CPCH(D)
         IMPLICIT REAL*8(A-H,O-Z)
         COMMON  /FIRST/T,GAM,TWALL,FP
         CPCHO = 0.36
         CPCH1 = 6.931D-05
         CPCH = CPCHO + CPCH1 * D
         RETURN
         END
C
C-------------------------------------------------
C
C    This routine calculates the fraction of ash in the solid.
C    (ASHFRAC). (ASHFRAC --> 1.0 as RR --> RMIN)
```

```
4040 C
4050          SUBROUTINE SOLID(RR)
4060          IMPLICIT REAL*8(A-H,O-Z)
4070          COMMON  /ASH/ASHFRAC,RHOASH,ASHINIT,
4080         1          RPINIT,CPASH,AMMIS,THCK
4090 C
4100          ASHFRAC = ASHINIT*(1.OD-4*RPINIT/RR)**3.0
4110          RETURN
4120          END
4130 C
4140 C-----------------------------------------------
4150 C
4160 C    Root finder by the method of bisection for function TET.
4170 C
4180          SUBROUTINE RTBIS(TET,X1,X2,XACC,R2,XMID)
4190          IMPLICIT REAL*8(A-H,O-Z)
4200          EXTERNAL  TET
4210          COMMON  /FIRST/T,GAM,TWALL,FP
4220          PARAMETER (JMAX = 500)
4230 C
4240          CALL TET(X1,FX1,R2)
4250          CALL TET(X2,FX2,R2)
4260          IF(FX2*FX1 .GE. 0.0) PAUSE 'BRACKET ROOT IN MENU'
4270          DX = X2 - X1
4280          DO 200 J = 1, JMAX
4290                  DX = DX * 0.5
4300                  XMID = X1 + DX
```

```
4310                    CALL TET(XMID,FMID,R2)
4320                    IF (FMID * FX1 .GT. 0.0)THEN
4330                            X1 = XMID
4340                            FX1 = FMID
4350                    ELSE
4360                            X2 = XMID
4370                            FX2 = FMID
4380                    ENDIF
4390                    IF (DABS(DX/XMID) .LT. XACC)  RETURN
4400   200      CONTINUE
4410            PAUSE 'TOO MANY BISECTIONS IN MENU'
4420            END
4430   C
4440   C-------------------------------------------------
4450   C
4460   C     Calculation of solid flux in gmc/cm^2-s.(Smith 1974)
4470   C
4480            SUBROUTINE FLUX(B,R)
4490            IMPLICIT REAL*8(A-H,O-Z)
4500            COMMON  /ASH/ASHFRAC,RHOASH,ASHINIT,
4510         1          RPINIT,CPASH,AMMIS,THCK
4520            COMMON  /FIRST/T,GAM,TWALL,FP
4530            COMMON  /R/RHOC,XFAC,ACEN
4540   C
4550   C     Older approach to calculate FP.
4560   C
4570   C        CASH=B-FP*R*R(1/(R+T)-1/R)/C*MO2*DASH
```

```
4580 C       FP = XFAC*DEXP( -1.0*ACEN/(1.98 * T))*CASH
4590 C
4600         DASH=0.35*3.13*(T/1500.0)**1.75/2.0
4610         PF= XFAC*DEXP( -1.0*ACEN/(1.98 * T))
4620         FP=PF*B/(1.0+82.05*T*PF*R*THCK/
4630        1         ((R+THCK)*(32.0*DASH)))
4640         TEST=PF*B
4650         RETURN
4660         END
4670 C
4680 C-------------------------------------------------
4690 C
4700 C    This routine calculates the value of the fully integrated
4710 C    equations from TWALL to TP based on GAM1.
4720 C
4730         SUBROUTINE GAMMA(GAM1,F,R1)
4740         IMPLICIT REAL*8(A-H,O-Z)
4750         COMMON  /ASH/ASHFRAC,RHOASH,ASHINIT,
4760        1          RPINIT,CPASH,AMMIS,THCK
4770         COMMON  /FIRST/ T,GAM,TWALL,FP
4780         COMMON  /R/RHOC,XFAC,ACEN
4790         COMMON  /Y1S/Y1S,Y1INF
4800 C
4810         CC = -3.0043D-05
4820         DASH=0.35*3.13*(T/1500.0)**1.75/2.0
4830         IF (T .LT. TWALL) THEN
4840            HH = DSQRT(DABS(-2331.5425 - GAM1)/0.3388749)
```

```
4850            IF (GAM1 .GT.-2331.5425) THEN
4860              AR1=-1.0*CC*((DSQRT(TWALL) - DSQRT(T)) + HH/2.0 *
4870     1              (DLOG((DSQRT(TWALL) - HH)*(DSQRT(T) + HH)/
4880     2              ((DSQRT(TWALL) + HH)*(DSQRT(T) - HH)))))
4890              HM = (2331.5425 + GAM1)/0.3388749
4900              Y1S= (Y1INF+4.0/3.0)*((T-HM)/(TWALL-HM))**
4910     1             0.8095478-4.0/3.0
4920              CONC=(1.0/(-1.0/7.0 + 8.0/(7.0*Y1S)))
4930              PF= XFAC*DEXP( -1.0*ACEN/(1.98 * T))
4940              FFP=PF*CONC/(1.0+82.05*T*PF*R1*THCK/
4950     1            ((R1+THCK)*(32.0*DASH)))
4960              F=AR1-R1* FFP
4970            ELSE
4980              AR2 = -1.0*CC*((DSQRT(TWALL)-DSQRT(T))-HH*
4990     1             (DATAN(DSQRT(TWALL)/HH)-DATAN(DSQRT(T)/HH)))
5000              HM = (2331.5425 + GAM1)/0.3388749
5010              Y1S= (Y1INF+4.0/3.0)*((T-HM)/(TWALL-HM))**
5020     1             0.8095478-4.0/3.0
5030              CONC=(1.0/(-1.0/7.0 + 8.0/(7.0*Y1S)))
5040              PF= XFAC*DEXP( -1.0*ACEN/(1.98 * T))
5050              FFP=PF*CONC/(1.0+82.05*T*PF*R1*THCK/
5060     1            ((R1+THCK)*(32.0*DASH)))
5070              F = AR2-R1* FFP
5080            ENDIF
5090          ELSE
5100            FF = DSQRT(DABS(2331.5425 + GAM1)/0.3388749)
5110            IF (GAM1 .LT.-2331.5425) THEN
```

```
5120              AR3 = CC*((DSQRT(T)-DSQRT(TWALL))-FF*
5130       1           (DATAN(DSQRT(T)/FF)-DATAN(DSQRT(TWALL)/FF)))
5140              C3 = (2331.5425 + GAM1)/0.3388749
5150              Y1S=(Y1INF+4.0/3.0)*((T-C3)/(TWALL-C3))**
5160       1           0.8095478-4.0/3.0
5170              CONC=(1.0/(-1.0/7.0 + 8.0/(7.0*Y1S)))
5180              PF= XFAC*DEXP( -1.0*ACEN/(1.98 * T))
5190              FFP=PF*CONC/(1.0+82.05*T*PF*R1*THCK/
5200       1           ((R1+THCK)*(32.0*DASH)))
5210              F = AR3-R1* FFP
5220            ELSE
5230              AR4 = CC * ((DSQRT(T) - DSQRT(TWALL)) + FF/2.0 *
5240       1           (DLOG((DSQRT(T) - FF)*(DSQRT(TWALL) + FF)/
5250       2           ((DSQRT(T) + FF)*(DSQRT(TWALL) - FF)))))
5260              C3 = (2331.5425 + GAM1)/0.3388749
5270              Y1S=(Y1INF+4.0/3.0)*((T-C3)/(TWALL-C3))**
5280       1           0.8095478-4.0/3.0
5290              CONC=(1.0/(-1.0/7.0 + 8.0/(7.0*Y1S)))
5300              PF= XFAC*DEXP( -1.0*ACEN/(1.98 * T))
5310              FFP=PF*CONC/(1.0+82.05*T*PF*R1*THCK/
5320       1           ((R1+THCK)*(32.0*DASH)))
5330              F = AR4-R1* FFP
5340            ENDIF
5350          ENDIF
5360          RETURN
5370          END
5380  C
```

```
5390 C-----------------------------------------------
5400 C
5410 C    Energy balance.
5420 C
5430          SUBROUTINE ENERGY(EP,PEMMIS,WEMMIS,RR,DUM2,ANST)
5440          IMPLICIT REAL*8(A-H,O-Z)
5450          EXTERNAL  CPC,EC,CPCH,ECH
5460          COMMON  /FIRST/ T,GAM,TWALL,FP
5470          COMMON  /R/RHOC,XFAC,ACEN
5480          COMMON  /ASH/ASHFRAC,RHOASH,ASHINIT,
5490       1          RPINIT,CPASH,AMMIS,THCK
5500 C
5510 C    Note that RHOC=1.5*(1-ASHINIT-EPSINIT) = Apparent density
5520 C
5530          SIG = 1.595D-12
5540          IF (DUM2 .LT. 1350) THEN
5550                  CPSOL= CPC(DUM2)
5560                  VAL = EC(DUM2)
5570          ELSE
5580                  CPSOL= CPCH(DUM2)
5590                  VAL = ECH(DUM2)
5600          ENDIF
5610          CPASH = 0.183 + 0.111D-3*T
5620          ANST=3.0*(RR+THCK)*(RR+THCK)*(FP*VAL-EP-SIG*
5630       1    (PEMMIS*DUM2**4-WEMMIS*TWALL**4))/
5640       2    (RR*RR*RR*(CPSOL*RHOC + CPASH*RHOASH*
5650       3    (ASHINIT+0.65*((1+THCK/RR)**3.0-1.0))))
```

```
5660          RETURN
5670          END
5680  C
5690  C-----------------------------------------------
5700  C
5710  C     Fourth order Runge-Kutta method for solving TEST1 and
5720  C     TEST2 for one time step.
5730  C
5740          SUBROUTINE RUNG(TEST1,TEST2,DUMC,STEP,EP,
5750         1                    PEMMIS,WEMMIS,RR,RNEW,TNEW)
5760          IMPLICIT REAL*8(A-H,O-Z)
5770          REAL*8 K11,K12,K13,K14,K21,K22,K23,K24
5780          EXTERNAL TEST1,TEST2,ENERGY,RADIUS
5790          COMMON  /FIRST/ T,GAM,TWALL,FP
5800          COMMON  /R/RHOC,XFAC,ACEN
5810  C
5820          DUM1=RR
5830          DUM2=T
5840          CALL TEST1(DUMC,DUM1,DUM2,DRDT)
5850          CALL TEST2(EP,PEMMIS,WEMMIS,DUM1,DUM2,DTDT)
5860          K11=DRDT
5870          K21=DTDT
5880          DUM1 = RR + K11*STEP/2.0
5890          DUM2 = T + K21*STEP/2.0
5900          CALL TEST1(DUMC,DUM1,DUM2,DRDT)
5910          CALL TEST2(EP,PEMMIS,WEMMIS,DUM1,DUM2,DTDT)
5920          K12 = DRDT
```

```
5930          K22 = DTDT
5940          DUM1 = RR + K12*STEP/2.0
5950          DUM2 = T + K22*STEP/2.0
5960          CALL TEST1(DUMC,DUM1,DUM2,DRDT)
5970          CALL TEST2(EP,PEMMIS,WEMMIS,DUM1,DUM2,DTDT)
5980          K13 = DRDT
5990          K23 = DTDT
6000          DUM1 = RR + K13*STEP
6010          DUM2 = T + K23*STEP
6020          CALL TEST1(DUMC,DUM1,DUM2,DRDT)
6030          CALL TEST2(EP,PEMMIS,WEMMIS,DUM1,DUM2,DTDT)
6040          K14 = DRDT
6050          K24 = DTDT
6060          RNEW = RR + STEP*(K11 + 2.0*K12 + 2.0*K13 + K14)/6.0
6070          TNEW = T + STEP*(K21 + 2.0*K22 + 2.0*K23 + K24)/6.0
6080          RETURN
6090          END
6100 C
6110 C-----------------------------------------------
6120 C
6130 C    Mass balance.
6140 C
6150          SUBROUTINE RADIUS(B,DUM1,DUM2,ANS)
6160          IMPLICIT REAL*8(A-H,O-Z)
6170          COMMON  /FIRST/ T,GAM,TWALL,FP
6180          COMMON  /R/RHOC,XFAC,ACEN
6190          COMMON  /ASH/ASHFRAC,RHOASH,ASHINIT,
```

```
6200      1          RPINIT,CPASH,AMMIS,THCK
6210 C
6220 C    Note that RHOC=1.5*(1-ASHINIT-EPSINIT) = Apparent density
6230 C
6240         DASH=0.35*3.13*(DUM2/1500.0)**1.75/2.0
6250         PF= XFAC*DEXP( -1.0*ACEN/(1.98 * DUM2))
6260         FFP=PF*B/(1.0+82.05*DUM2*PF*DUM1*THCK
6270      1              /((DUM1+THCK)*(32.0*DASH)))
6280         ANS = -1.0*FFP/RHOC
6290         RETURN
6300         END
6310 C
6320 C-------------------------------------------------
```

AIX.4 3VOIDS.FOR

```
10 C    This program simulates the combustion of a single porous
20 C    carbon particle. The particle is assumed to be isothermal
30 C    internally. It has spherical voids distributed inside.
40 C    Three sizes of voids corresponding to macro, transition
50 C    and micro pores are used to describe the internal structure.
60 C
70 C    As combustion proceeds, the local recession, which is a
80 C    function of the local oxygen concentration and the particle
90 C    temperature is computed at 50 fixed points within the
100 C   particle. This local recession, Q, determines the local
110 C   voidfraction and the local surface area at any radial
120 C   location. The bulk diffusion coefficient is used throughout.
130 C   It is modified to account for the local void fraction
140 C   according to the Satterfield relation. The diffusion
150 C   equation is solved inside the particle to determine the
160 C   oxygen profile inside the particle. The boundary conditions
170 C   are zero gradient at the particle center and known surface
180 C   concentration determined by solving the gas phase equations.
190 C
200 C   The particle radius changes in two ways. Until the
210 C   external void fraction reaches the user-set value, radius
```

```
220 C     changes due to reaction. However, once the external void
230 C     fraction reaches the critical value, that portion of the
240 C     solid in which the void fraction exceeds or equals the
250 C     the critical value is shed. The particle temperature is
260 C     determined by an overall energy balance including radiation
270 C     conduction and convection terms.
280 C
290 C     The gas phase is assumed to be quasi-steady relative to the
300 C     solid for a given time step. The heterogenous reaction
310 C     at the solid is 2C + O2 ---> 2CO and in the gas phase,
320 C     the CO oxidation is assumed to be far enough from the
330 C     particle so as to have no thermal effect on the particle.
340 C     The gas phase equations include the Stefan flow term.
350 C     Gas phase properties are calculated using kinetic theory
360 C     of gases. The integral equations are solved analytically.
370 C
380 C     The reaction rate is assumed to be linear with respect to
390 C     the surface oxygen concentration.
400 C
410 C     No attempt has been made to simulate the presence of ash in
420 C     this version.
430 C
440 C-----------------------------------------------
```

```
450 C
460 C    Declarations.
470 C
480         IMPLICIT REAL*8(A-H,O-Z)
490         CHARACTER*15 IFILE
500         CHARACTER*1  QRESP
510 C
520         DIMENSION WK(54)
530 C
540 C
550         EXTERNAL EC,ECH,CPC,CPCH,RLAMB,EOX,ECO
560         EXTERNAL RTBIS,GAMMA,RUNG,PROF,RADIUS,ENERGY,QUE
570         EXTERNAL STROBE,RTBISOL,RUNGSOL,EQN1,EQN2
580         EXTERNAL QCR
590 C
600 C
610         COMMON  T,TWALL
620         COMMON  /R/RHOC,FRAC,RPINIT
630         COMMON  /SOL/VOID1,EPS1,DLAMB1,EPSOUT,EPSOLD,FSHED,
640        1          EPSCRIT,VOID2,EPS2,DLAMB2,VOID3,EPS3,DLAMB3
650         COMMON  /MISC/C,XLOW,AO,BO,XFAC,ACEN
660         COMMON  /ARR/X(50),R(50),Y1(50),Y2(50)
670         COMMON  /CS/CSTAR,TAU,XACC,SURFSUM
```

```
      COMMON  /QS/Q(4,50),DQDR(4,50),QINT,QBAR,QCRIT
      COMMON  /AQ/AQ(50),ADQDR(50)
      COMMON  /Y1/Y1S,Y1INF
C
C
C-----------------------------------------------
C
C     Interactive program parameter inputs.
C
C
        WRITE(*,9)
 9      FORMAT(1x,'WANT TO READ THE 3VOIDS.INP FILE (Y OR N)?')
        READ(*,8)QRESP
 8      FORMAT(A1)
        IF((QRESP .EQ. 'y') .OR. (QRESP .EQ .'Y'))GOTO 2000

        WRITE(*,10)
 10     FORMAT(1x,'ENTER SOLID DENSITY IN G/CC')
        READ(*,*)RHOC

        WRITE(*,11)
 11     FORMAT(1x,'ENTER WALL AND INIT. PARTICLE TEMPS. IN K')
        READ(*,*)TWALL,TPINIT
```

```
910
920         WRITE(*,12)
930   12    FORMAT(1x,'ENTER THE CRITICAL VOLUME FRACTION')
940         READ(*,*)EPSCRIT
950
960         WRITE(*,13)
970   13    FORMAT(1x,'INIT. PART., VOID RADII(mu) AND VOIDFRACTS
980        1  (BIG --> SMALL)')
990         READ(*,*)RPINIT,VOID1,VOID2,VOID3,EPS1,EPS2,EPS3
1000
1010        WRITE(*,14)
1020  14    FORMAT(1x,'ENTER THE O2 PARTIAL PRES. IN THE AMBIENT')
1030        READ(*,*)C1INF
1040
1050        WRITE(*,15)
1060  15    FORMAT(1x,'ENTER THE WALL AND CARBON EMMISIVITIES')
1070        READ(*,*)WEMMIS,PEMMIS
1080
1090        WRITE(*,16)
1100  16    FORMAT( 1x,'ENTER FRAC AND SWITCH(1:1 VOID;0:2/3 VOIDS)')
1110        READ(*,*)FRAC,SWITCH
1120
1130        WRITE(*,17)
```

```
1140   17    FORMAT( 1x,'ENTER FACTOR XFAC, ACEN AND TIMESTEP')
1150         READ(*,*)XFAC,ACEN,STEPO
1160
1170         WRITE(*,18)
1180   18    FORMAT(1X,'ENTER ES1,ES2,XACC (0 < ES1 << ES2) ')
1190         READ(*,*)ES1,ES2,XACC
1200
1210         WRITE(*,19)
1220   19    FORMAT( 1x,'ENTER THE NO. OF TIMESTEPS, TAU AND CSTAR')
1230         READ(*,*)NMAX,TAU,CSTAR
1240
1250         WRITE(*,21)
1260   21    FORMAT( 1x,'ENTER THE OUTPUT FILENAME (NOT *.INP !)')
1270         READ(*,22)IFILE
1280   22    FORMAT(A15)
1290
1300         GOTO 2500
1310
1320   2000  OPEN(1,FILE='3VOIDS.INP',STATUS='OLD')
1330         READ(1,*,END=129)RHOC,TWALL,TPINIT,EPSCRIT,RPINIT,VOID1,
1340        1 VOID2,VOID3,EPS1,EPS2,EPS3,C1INF,WEMMIS,PEMMIS,FRAC,
1350        2 SWITCH,XFAC,ACEN,STEPO,ES1,ES2,XACC,NMAX,TAU,CSTAR
1360         CLOSE(1)
```

```
1370
1380  129   WRITE(*,30)RHOC
1390  30    FORMAT(1x,'1. SOLID  DENSITY IN G/CC:
1400       1        ',F8.4,/)
1410
1420        WRITE(*,31)TWALL,TPINIT
1430  31    FORMAT(1x,'2. WALL AND INIT. PARTICLE TEMPS. IN K: ',
1440       1    F10.4,3X,F10.4,/)
1450
1460        WRITE(*,32)EPSCRIT
1470  32    FORMAT(1x,'3. THE CRITICAL VOLUME FRACTION: ',F8.4,/)
1480
1490        WRITE(*,33)RPINIT,VOID1,VOID2,VOID3,EPS1,EPS2,EPS3
1500  33    FORMAT(1x,'4. INIT. PART.,VOID RADII(mu) AND VOIDFRAC.:'
1510       1 ,/7G10.4,/)
1520
1530        WRITE(*,34)C1INF
1540  34    FORMAT(1x,'5. THE O2 PART. PRES. (AMBIENT):',F8.4,/)
1550
1560        WRITE(*,35)WEMMIS,PEMMIS
1570  35    FORMAT(1x,'6. THE WALL AND CARBON EMMISIVITIES: ',
1580       1      F6.4,3X,F6.4,/)
1590
```

```
1600          WRITE(*,36)FRAC,SWITCH
1610    36    FORMAT( 1x,'7. FRAC AND SWITCH: ',2F8.2,/)
1620
1630          WRITE(*,37)XFAC,ACEN,STEPO
1640    37    FORMAT( 1x,'8. THE FACTOR XFAC, ACEN AND TIMESTEP: ',
1650       1       F9.4,3X,F10.2,2X,F8.6,/)
1660
1670          WRITE(*,38)ES1,ES2,XACC
1680    38    FORMAT(1X,'9. ES1,ES2,XACC (0 < ES1 << ES2): ',
1690       1       E9.4,3X,E9.4,3X,E9.4,/)
1700
1710          WRITE(*,39)NMAX,TAU,CSTAR
1720    39    FORMAT( 1x,'10. THE NO. OF STEPS, TAU, CSTAR:
1730       1          ',I8,2X,2F12.4,/)
1740
1750          WRITE(*,41)
1760    41    FORMAT( 1x,'ENTER THE OUTPUT FILENAME (NOT *.INP !)')
1770          READ(*,42)IFILE
1780    42    FORMAT(A15)
1790
1800    1990  WRITE(*,43)
1810    43    FORMAT(1X, 'ENTER # OF ENTRY TO BE ALTERED (0 TO RUN)')
1820          READ(*,*)NALT
```

```
1830          IF(NALT .EQ. 0)GOTO 2500
1840          IF(NALT .EQ. 1)GOTO 2010
1850          IF(NALT .EQ. 2)GOTO 2020
1860          IF(NALT .EQ. 3)GOTO 2030
1870          IF(NALT .EQ. 4)GOTO 2040
1880          IF(NALT .EQ. 5)GOTO 2050
1890          IF(NALT .EQ. 6)GOTO 2060
1900          IF(NALT .EQ. 7)GOTO 2070
1910          IF(NALT .EQ. 8)GOTO 2080
1920          IF(NALT .EQ. 9)GOTO 2090
1930          IF(NALT .EQ. 10)GOTO 2100
1940          GOTO 1990
1950
1960    2010  WRITE(*,10)
1970          READ(*,*)RHOC
1980          GOTO 1990
1990
2000    2020  WRITE(*,11)
2010          READ(*,*)TWALL,TPINIT
2020          GOTO 1990
2030
2040    2030  WRITE(*,12)
2050          READ(*,*)EPSCRIT
```

```
2060          GOTO 1990
2070
2080    2040  WRITE(*,13)
2090          READ(*,*)RPINIT,VOID1,VOID2,VOID3,EPS1,EPS2,EPS3
2100          GOTO 1990
2110
2120    2050  WRITE(*,14)
2130          READ(*,*)C1INF
2140          GOTO 1990
2150
2160    2060  WRITE(*,15)
2170          READ(*,*)WEMMIS,PEMMIS
2180          GOTO 1990
2190
2200    2070  WRITE(*,16)
2210          READ(*,*)FRAC,SWITCH
2220          GOTO 1990
2230
2240    2080  WRITE(*,17)
2250          READ(*,*)XFAC,ACEN,STEPO
2260          GOTO 1990
2270
2280    2090  WRITE(*,18)
```

```
      READ(*,*)ES1,ES2,XACC
      GOTO 1990

 2100 WRITE(*,19)
      READ(*,*)NMAX,TAU,CSTAR
      GOTO 1990

 2500 OPEN(1,FILE='3VOIDS.INP',STATUS='NEW')
      WRITE(1,*)RHOC,TWALL,TPINIT,EPSCRIT,RPINIT,VOID1,VOID2,
     1 VOID3,EPS1,EPS2,EPS3,C1INF,WEMMIS,PEMMIS,FRAC,
     2 SWITCH,XFAC,ACEN,STEPO,ES1,ES2,XACC,NMAX,TAU,CSTAR
      CLOSE(1)
C
C-----------------------------------------------
C-----------------------------------------------
C
C   Main Program.
C
C     After initialisation of various parameters, the main
C     loop begins. C1INF and Y1INF are the mole and mass
C     fractions of oxygen far from the particle. A is used
C     to calculate the mass fractions of the other species.
C     EPSCRIT is the critical voidfraction at which shedding
```

```
2520 C     starts. QINT is the interval between the 50 fixed
2530 C     points where Q's are calculated.
2540 C
2550 C     The porosity in the solid is characterized by the
2560 C     three parameters EPS, VOID and DLAMB for each void size.
2570 C     The porosity is obtained by polydisperse spherical voids
2580 C     whose initial sizes are VOID1, VOID2 and VOID3 microns.
2590 C     The initial void fractions are EPS1, EPS2 and EPS3
2600 C     respectively. From the EPS's and VOID's, the DLAMB's
2610 C     (the number densities of the voids (#/vol)) are obtained.
2620 C     DLAMB's remain constant thereafter.
2630 C
2640 C     Factors of 1D4 or 1D-4 occur in converting from cms. to
2650 C     microns and back.
2660 C
2670 C     RTBIS is called to calculate the carbon flux from the
2680 C     solid. It calls GAMMA which in turn calls SOLID. SOLID
2690 C     solves for the oxygen concentration profile inside the
2700 C     particle using EQN1 and EQN2. It uses a scaling method
2710 C     to solve the two-point boundary value problem for the
2720 C     profile.
2730 C
2740 C     The routine RUNG uses a fourth order Runge-Kutta scheme
```

```
2750 C     to solve the simultaneous equations for particle radius
2760 C     and temperature. It calls ENERGY and RADIUS. The latter
2770 C     calls SOLID and QUE to actually calculate DR/DT. The
2780 C     routine QUE calculates the recession at points inside
2790 C     the particle and checks to see if the critical recession
2800 C     (calculated from EPSCRIT) is reached at the surface.
2810 C
2820 C     The concentration  profiles in the particle are written
2830 C     into a file called PRO.DAT at every 20th step.
2840 C
2850 C     After a profile has been calculated, PLACE is called.
2860 C     This routine rearranges the R's such that more points
2870 C     are put in the region where the profile has steeper
2880 C     gradients.
2890 C
2900 C     The reaction rate expression is from Smith's paper (1974).
2910 C     It is based on the external surface area.
2920 C     XFAC multiplies the pre-exponential factor and can be
2930 C     adjusted.
2940 C
2950 C     RATE=XFAC*305*DEXP(-ACEN/(1.98*T))*CONC  [G/CM^2-S]
2960 C
2970 C
```

```
2980 C     Initialization.
2990 C
3000 C     Initially equally spaces R's
3010 C
3020        DO 153 I=1,50
3030          FIX=I-1
3040          R(I)=FIX*RPINIT/49.0
3050  153   CONTINUE
3060 C
3070        DO 156 L=1,50
3080          AQ(L)=0.0
3090          ADQDR(L)=0.0
3100  156   CONTINUE
3110 C
3120        Y1INF=(C1INF*32.0)/(C1INF * 32.0 +(1.0 - C1INF )*28.0)
3130        A = (1.0 / (1.0 - Y1INF)) * (Y1INF / 4.0)
3140 C
3150        FP=0.0
3160        TIME = 0.0
3170        DTDR = 0.0
3180        FLAG=1.0
3190        CONV=0.0
3200        QINT=RPINIT/49.0
```

```
3210          T = TPINIT
3220          TPOLD=TPINIT
3230          RP = RPINIT
3240          ROLD=RPINIT*1.OD-04
3250          C1S = C1INF
3260          Y1OLD=Y1INF
3270          Y1S=Y1INF
3280  C
3290          DLAMB3=-1.O*DLOG(1.O-EPS3)/(4.2*VOID3*VOID3*VOID3)
3300          DLAMB2=(-1.O*DLOG(1.O-EPS3-EPS2)-DLAMB3*
3310         1          (4.2*VOID3*VOID3*VOID3))
3320         2          /(4.2*VOID2*VOID2*VOID2)
3330          DLAMB1=(-1.O*DLOG(1.O-EPS3-EPS2-EPS1)-DLAMB3*4.2*VOID3**3
3340         1       -DLAMB2*4.2*VOID2**3)/(4.2*VOID1**3)
3350          EPS=1.O-DEXP((-4.2*DLAMB1*(VOID1)**3)+(-4.2*DLAMB2*
3360         1       (VOID2)**3)+(-4.2*DLAMB3*(VOID3)**3))
3370          SURF=((1.O-EPS)*12.6*(DLAMB1*VOID1**2
3380         1    + DLAMB2*VOID2**2 + DLAMB3*VOID3**2))/((1.O-EPS)*RHOC)
3390          EPSOLD=EPS
3400          EPSOUT=EPS
3410          EPSINIT=EPS
3420  C
3430  C
```

```
3440          OPEN(2,FILE=IFILE,STATUS='NEW',FORM='FORMATTED')
3450          OPEN(3,FILE='PRO.DAT',STATUS='NEW',FORM='FORMATTED')
3460          WRITE(2, 900)TIME,CONV,RP,T,C1S,FP,SURF,EPSOLD,EPSOUT
3470          WRITE(*, 900)TIME,CONV,RP,T,C1S,FP,SURF,EPSOLD,EPSOUT
3480   900    FORMAT(1X,3F9.4,1X,F7.2,1X,2F8.6,1X,F6.2,1X,
3490         1        F6.4,1X,F6.4)
3500  C
3510  C      X1 and X2 are appropriate brackets for GAM.
3520  C      Typically, ES1 is O(1D-6), while ES2 is O(1D11).
3530  C
3540          IF ( TPINIT .LT. TWALL) THEN
3550                X1 =  ( -2331.5425 + 0.3388749*TPINIT) - ES2
3560                X2 =  ( -2331.5425 + 0.3388749*TPINIT) - ES1
3570          ELSE
3580               X1 =  ( -2331.5425 + 0.3388749*TPINIT) + ES1
3590               X2 =  ( -2331.5425 + 0.3388749*TPINIT) + ES2
3600          ENDIF
3610  C
3620  C     Calculation of QCRIT.
3630  C
3640          IF(SWITCH .EQ. 1)THEN
3650          QCRIT=(-1.0*DLOG(1.0-EPSCRIT)/(DLAMB1*4.2))**.33-VOID1
3660          ELSE
```

```
3670          GUESS1=(-1.0*DLOG(1.0-EPSCRIT)/(DLAMB1*4.2))**.33-VOID1
3680          GUESS2=0.0
3690          CALL RTBISOL(QCR,GUESS2,GUESS1,XACC,RSLT)
3700          QCRIT=RSLT
3710          ENDIF
3720          WRITE(*,*)QCRIT
3730  C
3740  C     Main loop begins.
3750  C
3760          DO 1000 I = 1, NMAX
3770            SWIT=0.0
3780            STEP=STEPO
3790            RR = RP* 1.0D-04
3800            CALL RTBIS(GAMMA,X1,X2,XACC,STEP,PEMMIS,WEMMIS,RR,RNEW,
3810       1         TNEW,FP,ANSW,SWIT)
3820            FP1 = -1.3333 * FP
3830            FP2 = 2.3333 * FP
3840            EPF=ANSW*FP
3850  C         DTDR = -1.0D-4*(EPF-FP1*EOX(T)-FP2*ECO(T))/RLAMB(T)
3860            DUMC= (1.0/(-1.0/7.0 + 8.0/(7.0*Y1S)))
3870            RBAR=(ROLD+RNEW)/2.0
3880            FSHED=0.333*(1.0-EPSOUT)*RHOC*
3890       1         (ROLD**3.0-RNEW**3.0)/(STEP*RBAR**2.0)
```

```
3900            ROLD=RNEW
3910            RP = 1.0D4*RNEW
3920            CONV=1.0-((RP/RPINIT)**3.0)*((1.0-EPSOLD)/(1.0-EPSINIT))
3930            SURF=SURFSUM*1.0D-12/(4.2*RNEW**3.0*(1.0-EPSOLD)*RHOC)
3940            T = TNEW
3950            TIME = TIME + 1.0D3*STEP
3960            TPOLD=T
3970 C
3980 C      Writing profiles to PRO.DAT
3990 C
4000            IF(MOD(I,20) .EQ. 0)THEN
4010               DO 148 LI=1,50
4020                  WRITE(3,147)R(LI),Y1(LI)
4030    148        CONTINUE
4040            ENDIF
4050    147     FORMAT(5X,2G12.4)
4060 C
4070 C      Writing results to DATA file.
4080 C
4090            IF(MOD(I,10) .EQ. 0)THEN
4100             WRITE(2,900)TIME,CONV,RP,T,DUMC,FP,SURF,EPSOLD,EPSOUT
4110             WRITE(*,900)TIME,CONV,RP,T,DUMC,FP,SURF,EPSOLD,EPSOUT
4120            ENDIF
```

```
4130 C
4140 C     Equispacing R's
4150 C
4160          DO 157 KI=1,50
4170             FIX=KI-1
4180             R(KI)=FIX*RP/49.0
4190  157     CONTINUE
4200 C
4210          DO 158 LI=1,50
4220             AQ(LI)=Q(4,LI)
4230             ADQDR(LI)=DQDR(4,LI)
4240  158     CONTINUE
4250 C
4260 C      Reducing brackets for next call of ANS.
4270 C
4280          IF ( T .LT. TWALL) THEN
4290                X1 =  ANSW - DABS(10.0*ANSW)
4300                X2 =  ( -2331.5425 + 0.3388749*T ) - ES1
4310          ELSE
4320                X1 =  ( -2331.5425 + 0.3388749*T ) + ES1
4330                X2 =  ANSW + DABS(10.0*ANSW)
4340          ENDIF
4350 C
```

```
C      Program exit condition.
C
        IF((EPSOLD .GE. EPSCRIT) .OR.
     1        (R(50) .LE. 0.0))GOTO 1001
C
 1000  CONTINUE
C
 1001  CLOSE(2)
       CLOSE(3)
       CONTINUE
       STOP
       END
C
C    Main loop and main program end.
C
C
C-----------------------------------------------
C-----------------------------------------------
C
C    Property subprograms.
C
C    RLAMB:gas thermal conductivity (cal/cm-K) [300-2500K]
C          from Eckert. The COEFFS are in W/m-K for D in K
```

```
4590 C          Form NOT used here.
4600 C     EOX  :oxygen enthalpy (cal/gmol). Ref. state is 0.0 at
4610 C          298K. Valid for 298-2500K. Heat capacities assumed
4620 C          constant. From Smith and VanNess. Form NOT used.
4630 C     ECO  :CO enthalpy. As above except ref. state.
4640 C     EC   :Carbon enthalpy (cal/g) [LT 1350K](COAL DATA BOOK)
4650 C     ECH  :Carbon enthalpy (cal/g) [GE 1350K](COAL DATA BOOK)
4660 C     CPC  :Carbon heat cap. (cal/g-K) [LT 1350K](COAL DATA BOOK)
4670 C     CPCH :Carbon heat cap. (cal/g-K) [GE 1350K](COAL DATA BOOK)
4680 C
4690 C
4700         REAL*8 FUNCTION RLAMB(D)
4710         IMPLICIT REAL*8(A-H,O-Z)
4720         REAL*8 LGO,LG1,LG2,LG3
4730         LGO = -1.333D-03
4740         LG1 =  1.036D-04
4750         LG2 = -4.715D-08
4760         LG3 =  1.341D-11
4770         RLAMB = (1.0/418.0)*(LGO+LG1*D+LG2*(D*D)+LG3*(D*D*D))
4780         RETURN
4790         END
4800 C
4810 C
```

```
      REAL*8 FUNCTION EOX(D)
      IMPLICIT REAL*8(A-H,O-Z)
      CPOXO = 7.16
      CPOX1 = 0.001
      CPOX2 = -40000.0
      EOX = (CPOXO*(D - 298) + (CPOX1 / 2.0)*(D*D - 298*298)
     1       + CPOX2*(1.0/D - 1.0/298)) / 32.0
      RETURN
      END
C
C
      REAL*8 FUNCTION ECO(D)
      IMPLICIT REAL*8(A-H,O-Z)
      CPCOO = 6.79
      CPCO1 = 0.00098
      CPCO2 = -11000.0
      DELH = -26416.0
      ECO = (DELH+CPCOO*(D-298)+(CPCO1/2.0)*(D*D-298*298)
     1       + CPCO2*(1.0/D - 1.0/298))/ 28.0
      RETURN
      END
C
C
```

```
5050          REAL*8 FUNCTION EC(D)
5060          IMPLICIT REAL*8(A-H,O-Z)
5070          CPCO = 0.024
5080          CPC1 = 6.953D-04
5090          CPC2 = -2.841D-07
5100          EC = CPCO*(D - 298) + (CPC1 / 2.0)*(D*D - 298*298)
5110         1        + (CPC2 / 3.0)*(D*D*D - 298*298*298)
5120          RETURN
5130          END
5140  C
5150          REAL*8 FUNCTION ECH(D)
5160          IMPLICIT REAL*8(A-H,O-Z)
5170          CPCHO = 0.36
5180          CPCH1 = 6.931D-05
5190          ECH = CPCHO*(D - 298) + (CPCH1 / 2.0)*(D*D - 298*298)
5200          RETURN
5210          END
5220  C
5230  C
5240          REAL*8 FUNCTION CPC(D)
5250          IMPLICIT REAL*8(A-H,O-Z)
5260          CPCO = 0.024
5270          CPC1 = 6.953D-04
```

```
5280          CPC2 = -2.841D-07
5290          CPC = CPC0 + CPC1 * D + CPC2 * D * D
5300          RETURN
5310          END
5320  C
5330          REAL*8 FUNCTION CPCH(D)
5340          IMPLICIT REAL*8(A-H,O-Z)
5350          CPCH0 = 0.36
5360          CPCH1 = 6.931D-05
5370          CPCH = CPCH0 + CPCH1 * D
5380          RETURN
5390          END
5400  C
5410  C-----------------------------------------------
5420  C
5430          SUBROUTINE RTBISOL(TET,X1,X2,XACC,XMID)
5440          IMPLICIT REAL*8(A-H,O-Z)
5450          EXTERNAL  TET
5460          PARAMETER (JMAX = 500)
5470  C
5480          CALL TET(X1,FX1)
5490          CALL TET(X2,FX2)
5500          IF(FX2*FX1.GE.0)PAUSE 'ROOT MUST BE BRACKETED IN RTBISOL'
```

```
5510         DX=X2-X1
5520         DO 200 J = 1, JMAX
5530               DX = DX * 0.5
5540               XMID = X1 + DX
5550               CALL TET(XMID,FMID)
5560               IF (FMID * FX1 .GT. 0.0)THEN
5570                     X1 = XMID
5580                     FX1 = FMID
5590               ELSE
5600                     X2 = XMID
5610                     FX2 = FMID
5620               ENDIF
5630               IF (DABS(DX) .LT. XACC)  RETURN
5640   200   CONTINUE
5650         PAUSE 'TOO MANY BISECTIONS IN RTBISOL'
5660         END
5670  C
5680  C---------------------------------------------
5690  C
5700         SUBROUTINE QCR(P,FUNT)
5710         IMPLICIT REAL*8(A-H,O-Z)
5720         COMMON  /SOL/VOID1,EPS1,DLAMB1,EPSOUT,EPSOLD,FSHED,
5730        1          EPSCRIT,VOID2,EPS2,DLAMB2,VOID3,EPS3,DLAMB3
```

```
C
      FUNT=DLAMB1*(VOID1+P)**3+DLAMB2*(VOID2+P)**3+DLAMB3*
     1      (VOID3+P)**3 + DLOG(1.0-EPSCRIT)/4.2
      RETURN
      END
C
C
C-----------------------------------------------
C
C
      SUBROUTINE PROF(ITER,RPIN,T,BETA)
      IMPLICIT REAL*8(A-H,O-Z)
      EXTERNAL STROBE,RTBISOL,RUNGSOL,EQN1,EQN2
      COMMON  /ARR/X(50),R(50),Y1(50),Y2(50)
      COMMON  /MISC/C,XLOW,AO,BO,XFAC,ACEN
C
C
      AO=0.0
      BO=R(50)
      RP=RPIN*1.0D4
      Y1INIT=1.0
      Y2INIT=0.0
      CALL STROBE(T,Y1INIT,Y2INIT,ANS)
```

```
5970          FACTOR=BETA/Y1(50)
5980          DO 181 I=1,50
5990             Y1(I)=FACTOR*Y1(I)
6000             Y2(I)=FACTOR*Y2(I)
6010             X(I)=R(I)
6020   181    CONTINUE
6030          RETURN
6040          END
6050  C
6060  C-----------------------------------------------
6070  C
6080          SUBROUTINE STROBE(T,Y1INIT,Y2INIT,SHOT)
6090          IMPLICIT REAL*8(A-H,O-Z)
6100          EXTERNAL RTBISOL,RUNGSOL,EQN1,EQN2
6110          EXTERNAL DCADRE,IFLSQ
6120          COMMON  /ARR/X(50),R(50),Y1(50),Y2(50)
6130  C
6140          Y1(1)=Y1INIT
6150          Y2(1)=Y2INIT
6160          DO 600 I=1,49
6170           RINIT=R(I)
6180           Y1INIT=Y1(I)
6190           Y2INIT=Y2(I)
```

```
6200          H=R(I+1)-R(I)
6210          CALL RUNGSOL(T,EQN1,EQN2,RINIT,Y1INIT,Y2INIT,H,ANS,ANSP)
6220          Y1(I+1)=ANS
6230          Y2(I+1)=ANSP
6240   600    CONTINUE
6250          SHOT=Y1(50)
6260          RETURN
6270          END
6280  C
6290  C-----------------------------------------------
6300  C
6310          SUBROUTINE RUNGSOL(T,TST1,TST2,RINIT,
6320         1   Y1INIT,Y2INIT,H,ANS,ANSP)
6330          IMPLICIT REAL*8(A-H,O-Z)
6340          REAL*8 K11,K12,K13,K14,K21,K22,K23,K24
6350          EXTERNAL TST1,TST2,EQN1,EQN2,DCADRE,IFLSQ
6360  C
6370          XP=RINIT
6380          DUM1=Y1INIT
6390          DUM2=Y2INIT
6400          CALL TST1(DUM1,DUM2,DY1DT)
6410          CALL TST2(T,XP,DUM1,DUM2,DY2DT)
6420          K11=DY1DT
```

```
6430        K21=DY2DT
6440        XP=XP+H/2.0
6450        DUM1 = Y1INIT+ K11*H/2.0
6460        DUM2 = Y2INIT + K21*H/2.0
6470        CALL TST1(DUM1,DUM2,DY1DT)
6480        CALL TST2(T,XP,DUM1,DUM2,DY2DT)
6490        K12 = DY1DT
6500        K22 = DY2DT
6510        DUM1 = Y1INIT + K12*H/2.0
6520        DUM2 = Y2INIT + K22*H/2.0
6530        CALL TST1(DUM1,DUM2,DY1DT)
6540        CALL TST2(T,XP,DUM1,DUM2,DY2DT)
6550        K13 = DY1DT
6560        K23 = DY2DT
6570        XP=XP+H/2.0
6580        DUM1 = Y1INIT + K13*H
6590        DUM2 = Y2INIT + K23*H
6600        CALL TST1(DUM1,DUM2,DY1DT)
6610        CALL TST2(T,XP,DUM1,DUM2,DY2DT)
6620        K14 = DY1DT
6630        K24 = DY2DT
6640        ANS = Y1INIT + H*(K11 + 2.0*K12 + 2.0*K13 + K14)/6.0
6650        ANSP = Y2INIT + H*(K21 + 2.0*K22 + 2.0*K23 + K24)/6.0
```

```
      RETURN
      END
C
C-----------------------------------------------
C
C     DY1DT is in molfrac/mu.
C
      SUBROUTINE EQN1(DUM1,DUM2,DY1DT)
      IMPLICIT REAL*8(A-H,O-Z)
C
      DY1DT = DUM2
      RETURN
      END
C
C-----------------------------------------------
C
      SUBROUTINE EQN2(T,XP,DUM1,DUM2,DY2DT)
      IMPLICIT REAL*8(A-H,O-Z)
      COMMON  /MISC/C,XLOW,AO,BO,XFAC,ACEN
      COMMON  /SOL/VOID1,EPS1,DLAMB1,EPSOUT,EPSOLD,FSHED,
     1        EPSCRIT,VOID2,EPS2,DLAMB2,VOID3,EPS3,DLAMB3
      COMMON  /QS/Q(4,50),DQDR(4,50),QINT,QBAR,QCRIT
      COMMON  /CS/CSTAR,TAU,XACC,SURFSUM
```

```
      COMMON  /R/RHOC,FRAC,RPINIT
C
      KL=INT(XP/QINT)+1
      QBARL=Q(4,KL)+((XP-(KL-1)*QINT)/QINT)*(Q(4,KL+1)-Q(4,KL))
      DQBARL=DQDR(4,KL)+((XP-(KL-1)*QINT)/QINT)*(DQDR(4,KL+1)-
     1              DQDR(4,KL))
      EPS=1.0-DEXP((-DLAMB1*4.2*(VOID1+QBARL)**3)+(-DLAMB2*4.2*
     1      (VOID2+QBARL)**3)+(-DLAMB3*4.2*(VOID3+QBARL)**3))
      SQ=(1.0-EPS)*12.6*(DLAMB1*(VOID1+QBARL)**2
     1    + DLAMB2*(VOID2+QBARL)**2 + DLAMB3*(VOID3+QBARL)**2)
      FREQ=305.0
      DIFF=3.13*(T/1500.0)**1.75
      E=ACEN/1.98
      RHOG=1.0/(82.05*T)
      C1=TAU*FREQ*XFAC/(24.0*DIFF*RHOG)
      IF(XP .GT. CSTAR)THEN
          DY2DT = C1*DEXP(-E/T)*SQ*1D-04*DUM1/EPS-2.0*DUM2/XP
     1              -SQ*DQBARL*DUM2/EPS
      ELSE
          DY2DT = C1*DEXP(-E/T)*SQ*1D-04*DUM1/EPS-
     1              SQ*DQBARL*DUM2/EPS
      ENDIF
      RETURN
```

```
      END
C
C-----------------------------------------------
C
      SUBROUTINE QUE(T,DELT,DRDT,ITER,FP)
      IMPLICIT REAL*8(A-H,O-Z)
      DIMENSION Y1BAR(50),Y2BAR(50)
      COMMON  /ARR/X(50),R(50),Y1(50),Y2(50)
      COMMON  /MISC/C,XLOW,AO,BO,XFAC,ACEN
      COMMON  /SOL/VOID1,EPS1,DLAMB1,EPSOUT,EPSOLD,FSHED,
     1        EPSCRIT,VOID2,EPS2,DLAMB2,VOID3,EPS3,DLAMB3
      COMMON  /QS/Q(4,50),DQDR(4,50),QINT,QBAR,QCRIT
      COMMON  /R/RHOC,FRAC,RPINIT
      COMMON  /CS/CSTAR,TAU,XACC,SURFSUM
      COMMON  /AQ/AQ(50),ADQDR(50)
C
      FREQ=305.0
      E=ACEN/1.98
      C2=FREQ*XFAC/RHOC
      RXN = C2*DEXP(-E/T)*1.0D04
C
C   Q's are in microns for the above expression of reaction
C   The inner J-loop finds the position of Q(I) just below
```

```
7350 C   R(J). Y1BAR and Y2BAR are the interpolated values of
7360 C   mass fraction and its gradients at the fixed locations
7370 C   where Q's are calculated.
7380 C
7390         Y1BAR(1)=Y1(1)
7400         Y2BAR(1)=Y2(1)
7410         DO 300 I=2,50
7420          DIST = QINT*(I-1)
7430          DO 350 J=1,49
7440           IF((R(J).LT.DIST).AND.(R(J+1).GE.DIST))THEN
7450             Y1BAR(I)=Y1(J)+((DIST-R(J))/(R(J+1)-R(J)))*
7460      1              (Y1(J+1)-Y1(J))
7470             Y2BAR(I)=Y2(J)+((DIST-R(J))/(R(J+1)-R(J)))*
7480      1              (Y2(J+1)-Y2(J))
7490           ELSEIF (DIST .GT. R(50)) THEN
7500             Y1BAR(I)=Y1(50)
7510             Y2BAR(I)=Y2(50)
7520           ENDIF
7530    350   CONTINUE
7540    300  CONTINUE
7550 C
7560         Q(ITER,1)=AQ(1)+DELT*RXN*Y1BAR(1)
7570         DQDR(ITER,1)=ADQDR(1)+DELT*RXN*Y2BAR(1)
```

```
7580          DO 310 I=2,50
7590           Q(ITER,I)=AQ(I)+DELT*RXN*Y1BAR(I)
7600           DQDR(ITER,I)=ADQDR(I)+DELT*RXN*Y2BAR(I)
7610    750    IF((Q(ITER,I).GE.QCRIT).AND.(Q(ITER,I-1).LT.QCRIT))THEN
7620            RCRIT=QINT*(I-2)+((QCRIT-Q(ITER,I-1))/(Q(ITER,I)-
7630       1         Q(ITER,I-1)))*QINT
7640            DQDT=RXN*Y1AVG
7650            DRDT=-1D-04*(R(50)-RCRIT)/DELT
7660            FLAG=0.0
7670            GOTO 940
7680           ENDIF
7690    310   CONTINUE
7700  C
7710          KL=INT(R(50)/QINT)+1
7720          IF(KL .EQ. 50) THEN
7730            QBAR=Q(ITER,50)
7740            DQDRP=DQDR(ITER,50)
7750          ELSE
7760            QBAR=Q(ITER,KL)+((R(50)-(KL-1)*QINT)/QINT)*(Q(ITER,KL+1)
7770       1         -Q(ITER,KL))
7780             DQDRP=DQDR(ITER,KL)+((R(50)-(KL-1)*QINT)/QINT)*
7790       1           (DQDR(ITER,KL+1)-DQDR(ITER,KL))
7800          ENDIF
```

```
7810          QLAST=AQ(KL)+((R(50)-(KL-1)*QINT)/QINT)*(AQ(KL+1)
7820         1         -AQ(KL))
7830          DRDT=-1D-04*(QBAR-QLAST)/DELT
7840          FLAG=1.0
7850  C
7860  C     Flux (fp) is  calculated using mole fraction gradient
7870  C     at the surface Y2(50), diffusivity, and stoichiometric
7880  C     coefficient 24.0 [gm/cm^2-s]. The expression for
7890  C     diffusivity is from Field's book.
7900  C
7910    940   IF(FLAG .EQ. 1.0)THEN
7920            IF (R(50) .EQ. RPINIT)THEN
7930               QBAR=Q(ITER,50)
7940            ELSE
7950               KL=INT(R(50)/QINT)+1
7960               QBAR=Q(ITER,KL)+((R(50)-(KL-1)*QINT)/QINT)*
7970         1            (Q(ITER,KL+1)-Q(ITER,KL))
7980            ENDIF
7990            EPSOUT=1.0-DEXP((-4.2*DLAMB1*(VOID1+QBAR)**3)+
8000         1          (-4.2*DLAMB2* (VOID2+QBAR)**3)+(-4.2*DLAMB3*
8010         2          (VOID3+QBAR)**3))
8020          ELSE
8030            KL=INT(R(50)/QINT)+1
```

```
8040            QSUP=Q(ITER,KL)+((R(50)-(KL-1)*QINT)/QINT)*
8050       1          (Q(ITER,KL+1) -Q(ITER,KL))
8060            EPSSUP=1.0-DEXP((-4.2*DLAMB1*(VOID1+QSUP)**3)+
8070       1           (-4.2*DLAMB2* (VOID2+QSUP)**3)+(-4.2*DLAMB3*
8080       2           (VOID3+QSUP)**3))
8090            EPSOUT=(EPSCRIT+EPSSUP)/2.0
8100          ENDIF
8110  C
8120          SUM=0.0
8130          VOLSUM=0.0
8140          SURFSUM=0.0
8150          KL=INT(R(50)/QINT)+1
8160          DO 560 I=2,KL
8170            QSHELL=(Q(ITER,I)+Q(ITER,I-1))/2.0
8180            AQSHELL=(AQ(I)+AQ(I-1))/2.0
8190            EPSSHELL=1.0-DEXP((-4.2*DLAMB1*(VOID1+QSHELL)**3)+
8200       1             (-4.2*DLAMB2* (VOID2+QSHELL)**3)+(-4.2*DLAMB3*
8210       2             (VOID3+QSHELL)**3))
8220            SQSHELL=(1.0-EPSSHELL)*12.6*(DLAMB1*(VOID1+QSHELL)**2
8230       1           + DLAMB2*(VOID2+QSHELL)**2 +
8240       2             DLAMB3*(VOID3+QSHELL)**2)
8250            ROUT=QINT*(I-1)
8260            RIN =QINT*(I-2)
```

```
8270          FPSHELL=4.2*(ROUT**3.0-RIN**3.0)*SQSHELL*
8280     1            (QSHELL-AQSHELL)
8290          SURFSUM=SURFSUM+4.2*(ROUT**3.0-RIN**3.0)*SQSHELL
8300          SUM=SUM+FPSHELL
8310          IF(QSHELL .LT. QCRIT)THEN
8320            VOLSUM=VOLSUM+EPSSHELL*(4.2*(ROUT**3.0-RIN**3.0))
8330          ENDIF
8340   560  CONTINUE
8350        QR50=Q(ITER,KL)+0.5*(((R(50)-(KL-1)*QINT)/QINT)*
8360     1       (Q(ITER,KL+1)-Q(ITER,KL)))
8370        AQR50=AQ(KL)+0.5*(((R(50)-(KL-1)*QINT)/QINT)*(AQ(KL+1)
8380     1                  -AQ(KL)))
8390        EPSR50=1.0-DEXP((-4.2*DLAMB1*(VOID1+QR50)**3)+
8400     1          (-4.2*DLAMB2* (VOID2+QR50)**3)+(-4.2*DLAMB3*
8410     2          (VOID3+QR50)**3))
8420        SQR50=(1.0-EPSR50)*12.6*(DLAMB1*(VOID1+QR50)**2
8430     1        +DLAMB2*(VOID2+QR50)**2+DLAMB3*(VOID3+QR50)**2)
8440        FPQ50=4.2*(R(50)**3.0-(QINT*(KL-1))**3.0)*
8450     1          SQR50*(QR50-AQR50)
8460        VOLR50=EPSR50*(R(50)**3.0-(QINT*(KL-1))**3.0)*4.2
8470        SURFSUM=SURFSUM+SQR50*(R(50)**3.0-
8480     1          (QINT*(KL-1))**3.0)*4.2
8490        EPSOLD=(VOLSUM+VOLR50)/(4.2*R(50)**3.0)
```

```
8500          FP=(SUM+FPQ50)*RHOC*1.0D-04/(DELT*12.6*R(50)**2.0)
8510          RETURN
8520          END
8530  C
8540  C-------------------------------------------------
8550  C
8560  C     This routine uses the method of bisection to find the
8570  C     root of the function described by TET. X1 and X2 are the
8580  C     bounds of the root and must be input into the routine.
8590  C     When the relative accuracy specified by XACC is reached,
8600  C     the root is returned as XMID.
8610  C
8620  C
8630            SUBROUTINE RTBIS(TET,X1,X2,XACC,STEP,PEMMIS,WEMMIS,R2,
8640           1       RNEW,TNEW,FP,XMID,SWIT)
8650            IMPLICIT REAL*8(A-H,O-Z)
8660            EXTERNAL TET
8670            EXTERNAL EC,ECH,CPC,CPCH,RLAMB,EOX,ECO
8680            EXTERNAL GAMMA,RUNG,PROF,RADIUS,ENERGY,QUE
8690            EXTERNAL STROBE,RTBISOL,RUNGSOL,EQN1,EQN2
8700            COMMON  T,TWALL
8710            PARAMETER (JMAX = 500)
8720  C
```

```
      DXACC=XACC
      CALL TET(X1,FX1,R2,STEP,PEMMIS,WEMMIS,RNEW,TNEW,FP,SWIT)
      CALL TET(X2,FX2,R2,STEP,PEMMIS,WEMMIS,RNEW,TNEW,FP,SWIT)
      IF(FX2*FX1 .GE. 0.0)PAUSE 'YOU BRACKET ROOT IN RTBIS'
      DX = X2 - X1
      DO 200 J = 1, JMAX
            DX = DX * 0.5
            XMID = X1 + DX
            CALL TET(XMID,FMID,R2,STEP,PEMMIS,WEMMIS,
     1                                  RNEW,TNEW,FP,SWIT)
            IF (FMID * FX1 .GT. 0.0)THEN
                  X1 = XMID
                  FX1 = FMID
            ELSE
                  X2 = XMID
                  FX2 = FMID
            ENDIF
            IF (DABS(DX/XMID) .LT. 0.05)SWIT=1.0
            IF (DABS(DX/XMID) .LT. DXACC)  RETURN
  200 CONTINUE
      PAUSE 'TOO MANY BISECTIONS IN RTBIS'
      END
C
```

```
8960 C-----------------------------------------------
8970 C
8980       SUBROUTINE GAMMA(GAM1,F,R1,STEP,PEMMIS,WEMMIS,RNEW,
8990      1          TNEW,FP,SWIT)
9000       IMPLICIT REAL*8(A-H,O-Z)
9010       EXTERNAL  EC,ECH,CPC,CPCH,RLAMB,EOX,ECO
9020       EXTERNAL  RUNG,PROF,RADIUS,ENERGY,QUE
9030       EXTERNAL  STROBE,RTBISOL,RUNGSOL,EQN1,EQN2
9040       COMMON  T, TWALL
9050       COMMON  /Y1/Y1S,Y1INF
9060 C
9070       CC = -3.0043D-05
9080       C3 = (2331.5425 + GAM1)/0.3388749
9090       Y1S=(Y1INF+4.0/3.0)*((T-C3)/(TWALL-C3))**
9100      1      0.8095478-4.0/3.0
9110       C1SURF= (1.0/(-1.0/7.0 + 8.0/(7.0*Y1S)))
9120       CALL RUNG(RADIUS,ENERGY,C1SURF,STEP,PEMMIS,WEMMIS,
9130      1        GAM1,R1,RNEW,TNEW,FP,SWIT)
9140 C
9150       IF (T .LT. TWALL) THEN
9160          HH = DSQRT(DABS(-2331.5425 - GAM1)/0.3388749)
9170        IF (GAM1 .GT.-2331.5425) THEN
9180          AR1 = -1.0*CC*((DSQRT(TWALL)-DSQRT(T))+HH/2.0*
```

```
9190      1          (DLOG((DSQRT(TWALL) - HH)*(DSQRT(T) + HH)/
9200      2          ((DSQRT(TWALL) + HH)*(DSQRT(T) - HH)))))
9210            F = AR1-R1* FP
9220          ELSE
9230            AR2 = -1.0*CC*((DSQRT(TWALL)-DSQRT(T))-HH*
9240      1           (DATAN(DSQRT(TWALL)/HH)-DATAN(DSQRT(T)/HH)))
9250            F = AR2-R1* FP
9260          ENDIF
9270        ELSE
9280                FF = DSQRT(DABS(2331.5425 + GAM1)/0.3388749)
9290          IF (GAM1 .LT.-2331.5425) THEN
9300            AR3 = CC*((DSQRT(T)-DSQRT(TWALL))-FF*
9310      1          (DATAN(DSQRT(T)/FF)-DATAN(DSQRT(TWALL)/FF)))
9320            F = AR3-R1* FP
9330          ELSE
9340            AR4 = CC * ((DSQRT(T) - DSQRT(TWALL)) + FF/2.0 *
9350      1          (DLOG((DSQRT(T) - FF)*(DSQRT(TWALL) + FF)/
9360      2          ((DSQRT(T) + FF)*(DSQRT(TWALL) - FF)))))
9370            F = AR4-R1* FP
9380          ENDIF
9390        ENDIF
9400        RETURN
9410        END
```

```
9420 C
9430 C-----------------------------------------------
9440 C
9450       SUBROUTINE ENERGY(EP,PEMMIS,WEMMIS,RR,DUM2,ANST)
9460       IMPLICIT REAL*8(A-H,O-Z)
9470       EXTERNAL  EC,ECH,CPC,CPCH,RLAMB,EOX,ECO
9480       COMMON    T,TWALL
9490       COMMON    /R/RHOC,FRAC,RPINIT
9500       COMMON   /SOL/VOID1,EPS1,DLAMB1,EPSOUT,EPSOLD,FSHED,
9510      1          EPSCRIT,VOID2,EPS2,DLAMB2,VOID3,EPS3,DLAMB3
9520 C
9530       SIG = 1.595D-12
9540       IF (DUM2 .LT. 1350) THEN
9550             CPSOL= CPC(DUM2)
9560             VAL = EC(DUM2)
9570       ELSE
9580             CPSOL= CPCH(DUM2)
9590             VAL = ECH(DUM2)
9600       ENDIF
9610       ANST=(3.0/(1.0-EPSOLD))*((FP+(1.0-FRAC)*FSHED)*
9620      1      VAL-EP-SIG* (PEMMIS*DUM2**4-WEMMIS*TWALL**4))
9630      2      /(RR*RHOC*CPSOL)
9640       RETURN
```

```
9650        END
9660 C
9670 C-----------------------------------------------
9680 C
9690 C    This routine solves the coupled equations TEST1 and
9700 C    TEST2 for one time step. It is a standard first order
9710 C    Runge Kutta algorithm.
9720 C
9730        SUBROUTINE RUNG(TEST1,TEST2,DUMC,STEP,PEMMIS,WEMMIS,
9740       1                GAM1,RR,RNEW,TNEW,FP,SWIT)
9750        IMPLICIT REAL*8(A-H,O-Z)
9760        REAL*8 K11,K12,K13,K14,K21,K22,K23,K24
9770        EXTERNAL  TEST1,TEST2
9780        EXTERNAL  EC,ECH,CPC,CPCH,RLAMB,EOX,ECO
9790        EXTERNAL  PROF,RADIUS,ENERGY,QUE
9800        EXTERNAL  STROBE,RTBISOL,RUNGSOL,EQN1,EQN2
9810        COMMON  T,TWALL
9820        COMMON  /ARR/X(50),R(50),Y1(50),Y2(50)
9830        COMMON  /SOL/VOID1,EPS1,DLAMB1,EPSOUT,EPSOLD,FSHED,
9840       1             VOID2,EPS2,DLAMB2,VOID3,EPS3,DLAMB3
9850        COMMON  /R/RHOC,FRAC,RPINIT
9860        COMMON  /CS/CSTAR,TAU,XACC,SURFSUM
9870 C
```

```
      IF(SWIT .EQ. 0.0)THEN
          ITER=4
          CALL PROF(ITER,R1,T,DUMC)
          DIFF=3.13*(T/1500)**1.75
          FP=1.0D04*Y2(50)*DIFF*EPSOUT*24.0/(TAU*82.05*T)
          RETURN
      ENDIF
      DUM1=RR
      DUM2=T
      ITER=4
      CALL PROF(ITER,DUM1,DUM2,DUMC)
      CALL TEST1(STEP,DUM2,ITER,DRDT,FP)
      EP=FP*GAM1
      CALL TEST2(EP,PEMMIS,WEMMIS,DUM1,DUM2,DTDT)
      K11=DRDT
      K21=DTDT
      RNEW = RR + STEP*K11
      TNEW = T + STEP*K21
      RETURN
      END
C
C-----------------------------------------------
C
```

```
10110         SUBROUTINE RADIUS(TMSTP,DUM2,ITER,ANS,FP)
10120         IMPLICIT REAL*8(A-H,O-Z)
10130         EXTERNAL QUE
10140 C
10150         CALL QUE(DUM2,TMSTP,DRDT,ITER,FP)
10160         ANS=DRDT
10170         RETURN
10180         END
10190 C
10200 C-----------------------------------------------
```

AIX.5 PCONC.FOR

```
C     This program simulates the combustion of a single porous
C     carbon particle. The particle is assumed to be isothermal
C     internally. It has spherical voids distributed inside.
C     Three sizes of voids corresponding to macro, transition
C     and micro pores are used to describe the internal
C     structure.
C
C     The reaction rate has a nonlinear dependence on the oxygen
C     concentration at the particle surface. This function is
C     a  m-th power expression where m can be varied between 0
C     and 1. For small values of m, the problem becomes very
C     stiff and concentration is zero inside of the particle
C     except in a thin outer shell. Thus the asymptotic model
C     MENU can be used for those cases with proper reaction
C     rate expressions.
C
C     As combustion proceeds, the local recession, which is a
C     function of the local oxygen concentration and the particle
C     temperature is computed at 50 fixed points within the
C     particle. This local recession, Q, determines the local
C     void fraction and the local surface area at any radial
```

```
220 C     location. The bulk diffusion coefficient is used throughout.
230 C     It is modified to account for the local void fraction
240 C     according to the Satterfield relation. The diffusion
250 C     equation is solved inside the particle to determine the
260 C     oxygen profile inside the particle. The boundary conditions
270 C     are zero gradient at the particle center and known surface
280 C     concentration determined by solving the gas phase equations.
290 C
300 C     The particle radius changes in two ways. Until the
310 C     external void fraction reaches the user-set value, radius
320 C     changes due to reaction. However, once the external void
330 C     fraction reaches the critical value, that portion of the
340 C     solid in which the void fraction exceeds or equals the
350 C     the critical value is shed. The particle temperature is
360 C     determined by an overall energy balance including radiation
370 C     conduction and convection terms.
380 C
390 C     The gas phase is assumed to be quasi-steady relative to the
400 C     solid for a given time step. The heterogenous reaction
410 C     at the solid is 2C + O2 ---> 2CO and in the gas phase,
420 C     the CO oxidation is assumed to be far enough from the
430 C     particle so as to have no thermal effect on the particle.
440 C     The gas phase equations include the Stefan flow term.
```

```
C    Gas phase properties are calculated using kinetic theory
C    of gases. The integral equations are solved analytically.
C
C    No attempt has been made to simulate the presence of ash in
C    this version.
C
C-----------------------------------------------
C
C    Declarations.
C
      IMPLICIT REAL*8(A-H,O-Z)
      CHARACTER*15 IFILE
      CHARACTER*1 QRESP
C
      DIMENSION WK(54)
C
      EXTERNAL  EC,ECH,CPC,CPCH,RLAMB,EOX,ECO
      EXTERNAL  GAMMA,PROF,RADIUS,ENERGY,QUE
      EXTERNAL  STROBE,RTBISOL,EQN1,EQN2
      EXTERNAL  QCR,SHOOT
C
      COMMON  T,TWALL
      COMMON  /R/RHOC,FRAC,RPINIT
```

```
      COMMON  /SOL/VOID1,EPS1,DLAMB1,EPSOUT,EPSOLD,FSHED,
     1          EPSCRIT,VOID2,EPS2,DLAMB2,VOID3,EPS3,DLAMB3
      COMMON  /MISC/C,XLOW,AO,BO,XFAC,ACEN
      COMMON  /ARR/X(50),R(50),Y1(50),Y2(50)
      COMMON  /CS/CSTAR,TAU,XACC,SURFSUM
      COMMON  /QS/Q(4,50),DQDR(4,50),QINT,QBAR,QCRIT
      COMMON  /AQ/AQ(50),ADQDR(50)
      COMMON  /Y1/Y1S,Y1INF
      COMMON  /POW/POW
C
C-----------------------------------------------
C
C     Interactive program parameter inputs.
C
C
      WRITE(*,9)
   9  FORMAT(1x,'WANT TO READ THE PCONC.INP FILE (Y OR N)?')
      READ(*,8)QRESP
   8  FORMAT(A1)
      IF((QRESP .EQ. 'y') .OR. (QRESP .EQ .'Y'))GOTO 2000
C
      WRITE(*,10)
  10  FORMAT(1x,'ENTER SOLID DENSITY IN G/CC')
```

```
      READ(*,*)RHOC

      WRITE(*,11)
11    FORMAT(1x,'ENTER WALL AND INIT. PART. TEMPS IN K')
      READ(*,*)TWALL,TPINIT

      WRITE(*,12)
12    FORMAT(1x,'ENTER THE CRITICAL VOLUME FRACTION')
      READ(*,*)EPSCRIT

      WRITE(*,13)
13    FORMAT(1x,'INIT PART., VOID RADII(mu) AND VOIDFRACTIONS
     1  (BIG --> SMALL)')
      READ(*,*)RPINIT,VOID1,VOID2,VOID3,EPS1,EPS2,EPS3

      WRITE(*,14)
14    FORMAT(1x,'ENTER THE O2 PART. PRES. IN THE AMBIENT')
      READ(*,*)C1INF

      WRITE(*,15)
15    FORMAT(1x,'ENTER THE WALL AND CARBON EMMISIVITIES')
      READ(*,*)WEMMIS,PEMMIS
```

```
1140          WRITE(*,16)
1150    16    FORMAT( 1x,'ENTER FRAC ,POW ')
1160          READ(*,*)FRAC,POW
1170
1180          WRITE(*,17)
1190    17    FORMAT( 1x,'ENTER XFAC, ACEN AND TIMESTEP')
1200          READ(*,*)XFAC,ACEN,STEPO
1210
1220          WRITE(*,18)
1230    18    FORMAT(1X,'ENTER ES1,ES2,XACC (0 < ES1 << ES2) ')
1240          READ(*,*)ES1,ES2,XACC
1250
1260          WRITE(*,19)
1270    19    FORMAT( 1x,'ENTER THE NO. OF TIMESTEPS, TAU AND CSTAR')
1280          READ(*,*)NMAX,TAU,CSTAR
1290
1300          WRITE(*,21)
1310    21    FORMAT( 1x,'ENTER THE OUTPUT FILENAME (NOT *.INP !)')
1320          READ(*,22)IFILE
1330    22    FORMAT(A15)
1340
1350          GOTO 2500
1360
```

```
2000  OPEN(1,FILE='PCONC.INP',STATUS='OLD')
      READ(1,*,END=129)RHOC,TWALL,TPINIT,EPSCRIT,RPINIT,VOID1,
     1    VOID2,VOID3,EPS1,EPS2,EPS3,C1INF,WEMMIS,PEMMIS,FRAC,
     2    POW,XFAC,ACEN,STEPO,ES1,ES2,XACC,NMAX,TAU,CSTAR
      CLOSE(1)


129   WRITE(*,30)RHOC
30    FORMAT(1x,'1. SOLID  DENSITY IN G/CC:
     1       ',F8.4,/)

      WRITE(*,31)TWALL,TPINIT
31    FORMAT(1x,'2. WALL AND INIT. PARTICLE TEMPS. IN K: ',
     1    F10.4,3X,F10.4,/)

      WRITE(*,32)EPSCRIT
32    FORMAT(1x,'3. THE CRITICAL VOLUME FRACTION: ',F8.4,/)

      WRITE(*,33)RPINIT,VOID1,VOID2,VOID3,EPS1,EPS2,EPS3
33    FORMAT(1x,'4. INIT. PART., VOID RADII(mu) AND VOIDFRAC.:'
     1 ,/7G10.4,/)

      WRITE(*,34)C1INF
```

```
1600   34    FORMAT(1x,'5. THE 02 PART. PRES. (AMBIENT): ',F8.4,/)
1610
1620         WRITE(*,35)WEMMIS,PEMMIS
1630   35    FORMAT(1x,'6. THE WALL AND CARBON EMMISIVITIES: ',
1640        1      F6.4,3X,F6.4,/)
1650
1660         WRITE(*,36)FRAC,POW
1670   36    FORMAT( 1x,'7. FRAC ,POW : ',F8.2,2X,E9.4,/)
1680
1690         WRITE(*,37)XFAC,ACEN,STEPO
1700   37    FORMAT( 1x,'8. THE FACTOR XFAC, ACEN AND TIMESTEP: ',
1710        1      F10.4,3X,F10.2,3X,F8.6,/)
1720
1730         WRITE(*,38)ES1,ES2,XACC
1740   38    FORMAT(1X,'9. ES1,ES2,XACC (0 < ES1 << ES2): ',
1750        1      E9.4,3X,E9.4,3X,E9.4,/)
1760
1770         WRITE(*,39)NMAX,TAU,CSTAR
1780   39    FORMAT(1x,'10. NO. OF STEPS, TAU, CSTAR:',I8,2X,2F12.4,/)
1790
1800         WRITE(*,41)
1810   41    FORMAT( 1x,'ENTER THE OUTPUT FILENAME (EXCEPT *.INP !)')
1820         READ(*,42)IFILE
```

```
1830   42     FORMAT(A15)
1840
1850   1990   WRITE(*,43)
1860   43     FORMAT(1X, 'ENTRY NO. TO BE ALTERED (0 TO RUN)')
1870          READ(*,*)NALT
1880          IF(NALT .EQ. 0)GOTO 2500
1890          IF(NALT .EQ. 1)GOTO 2010
1900          IF(NALT .EQ. 2)GOTO 2020
1910          IF(NALT .EQ. 3)GOTO 2030
1920          IF(NALT .EQ. 4)GOTO 2040
1930          IF(NALT .EQ. 5)GOTO 2050
1940          IF(NALT .EQ. 6)GOTO 2060
1950          IF(NALT .EQ. 7)GOTO 2070
1960          IF(NALT .EQ. 8)GOTO 2080
1970          IF(NALT .EQ. 9)GOTO 2090
1980          IF(NALT .EQ. 10)GOTO 2100
1990          GOTO 1990
2000
2010   2010   WRITE(*,10)
2020          READ(*,*)RHOC
2030          GOTO 1990
2040
2050   2020   WRITE(*,11)
```

```
2060          READ(*,*)TWALL,TPINIT
2070          GOTO 1990
2080
2090    2030  WRITE(*,12)
2100          READ(*,*)EPSCRIT
2110          GOTO 1990
2120
2130    2040  WRITE(*,13)
2140          READ(*,*)RPINIT,VOID1,VOID2,VOID3,EPS1,EPS2,EPS3
2150          GOTO 1990
2160
2170    2050  WRITE(*,14)
2180          READ(*,*)C1INF
2190          GOTO 1990
2200
2210    2060  WRITE(*,15)
2220          READ(*,*)WEMMIS,PEMMIS
2230          GOTO 1990
2240
2250    2070  WRITE(*,16)
2260          READ(*,*)FRAC,POW
2270          GOTO 1990
2280
```

```
2080  WRITE(*,17)
      READ(*,*)XFAC,ACEN,STEPO
      GOTO 1990

2090  WRITE(*,18)
      READ(*,*)ES1,ES2,XACC
      GOTO 1990

2100  WRITE(*,19)
      READ(*,*)NMAX,TAU,CSTAR
      GOTO 1990

2500  OPEN(1,FILE='PCONC.INP',STATUS='NEW')
      WRITE(1,*)RHOC,TWALL,TPINIT,EPSCRIT,RPINIT,VOID1,VOID2,
     1   VOID3,EPS1,EPS2,EPS3,C1INF,WEMMIS,PEMMIS,FRAC,
     2   POW,XFAC,ACEN,STEPO,ES1,ES2,XACC,NMAX,TAU,CSTAR
        CLOSE(1)
C
C-----------------------------------------------
C-----------------------------------------------
C
C    Main Program.
C
```

```
2520 C     After initialization of various parameters, the main
2530 C     loop begins. C1INF and Y1INF are the mole and mass
2540 C     fractions of oxygen far from the particle. A is used
2550 C     to calculate the mass fractions of the other species.
2560 C     EPSCRIT is the critical void fraction at which shedding
2570 C     starts. QINT is the interval between the 50 fixed
2580 C     points where Q's are calculated.
2590 C
2600 C     The porosity in the solid is characterized by the
2610 C     three parameters EPS, VOID and DLAMB for each void size.
2620 C     The porosity is obtained by polydisperse spherical voids
2630 C     whose initial sizes are VOID1, VOID2 and VOID3 microns.
2640 C     The initial void fractions are EPS1, EPS2 and EPS3
2650 C     respectively. From the EPS's and VOID's, the DLAMB's (the
2660 C     number densities of the voids (#/vol)) are obtained.
2670 C     DLAMB's remain constant thereafter.
2680 C
2690 C     Factors of 1D4 or 1D-4 occur in converting from cms. to
2700 C     microns and back.
2710 C
2720 C     RTBIS is called to calculate the carbon flux from the
2730 C     solid. It calls GAMMA which in turn calls SOLID. SOLID
2740 C     solves for the oxygen concentration profile inside the
```

```
2750 C    particle using EQN1 and EQN2. It uses a shooting method
2760 C    to solve the two-point boundary value problem for the
2770 C    profile.
2780 C
2790 C    The routine RUNG uses a fourth order Runge-Kutta scheme
2800 C    to solve the simultaneous equations for particle radius
2810 C    and temperature. It calls ENERGY and RADIUS. The latter
2820 C    calls SOLID and QUE to actually calculate DR/DT. The
2830 C    routine QUE calculates the recession at points inside
2840 C    the particle and checks to see if the critical recession
2850 C    (calculated from EPSCRIT) is reached at the surface.
2860 C
2870 C    The concentration  profiles in the particle are written
2880 C    into a file called PRO.DAT at every 20th step.
2890 C
2900 C    After a profile has been calculated, PLACE is called.
2910 C    This routine rearranges the R's such that more points
2920 C    are put in the region where the profile has steeper
2930 C    gradients.
2940 C
2950 C    The reaction rate expression is from Smith's paper (1974).
2960 C    It is based on the external surface area.
2970 C    XFAC multiplies the pre-exponential factor and can be
```

```
2980 C     adjusted. The concentration is raised to the m-th power.
2990 C
3000 C     RATE = XFAC*305*DEXP(-ACEN/(1.98*T))*CONC**m   [G/CM^2-S]
3010 C
3020 C     Initialization.
3030 C
3040 C     Initially equally spaces R's
3050 C
3060 C
3070          DO 153 I=1,50
3080            FIX=I-1
3090            R(I)=FIX*RPINIT/49.0
3100   153    CONTINUE
3110 C
3120          DO 156 L=1,50
3130            AQ(L)=0.0
3140            ADQDR(L)=0.0
3150   156    CONTINUE
3160 C
3170          Y1INF=(C1INF*32.0)/(C1INF*32.0+(1.0-C1INF)*28.0)
3180          A = (1.0 / (1.0 - Y1INF)) * (Y1INF / 4.0)
3190 C
3200          FP=0.0
```

```
3210          TIME = 0.0
3220          DTDR = 0.0
3230          FLAG=1.0
3240          CONV=0.0
3250          LIE=1
3260          QINT=RPINIT/49.0
3270          T = TPINIT
3280          TPOLD=TPINIT
3290          RP = RPINIT
3300          ROLD=RPINIT*1.0D-04
3310          C1S = C1INF
3320          Y1OLD=Y1INF
3330          Y1S=Y1INF
3340  C
3350          DLAMB3=-1.0*DLOG(1.0-EPS3)/(4.2*VOID3*VOID3*VOID3)
3360          DLAMB2=(-1.0*DLOG(1.0-EPS3-EPS2)-DLAMB3*
3370         1        (4.2*VOID3*VOID3*VOID3)) /(4.2*VOID2*VOID2*VOID2)
3380          DLAMB1=(-1.0*DLOG(1.0-EPS3-EPS2-EPS1)-DLAMB3*4.2*VOID3**3
3390         1       -DLAMB2*4.2*VOID2**3)/(4.2*VOID1**3)
3400          EPS=1.0-DEXP((-4.2*DLAMB1*(VOID1)**3)+(-4.2*DLAMB2*
3410         1       (VOID2)**3)+(-4.2*DLAMB3*(VOID3)**3))
3420          SURF=((1.0-EPS)*12.6*(DLAMB1*VOID1**2
3430         1        +DLAMB2*VOID2**2+DLAMB3*VOID3**2))/(RHOC*(1.0-EPS))
```

```
3440          EPSOLD=EPS
3450          EPSOUT=EPS
3460          EPSINIT=EPS
3470  C
3480  C
3490          OPEN(2,FILE=IFILE,STATUS='NEW',FORM='FORMATTED')
3500          OPEN(3,FILE='PRO.DAT',STATUS='NEW',FORM='FORMATTED')
3510          WRITE(2,900)TIME,CONV,RP,T,C1S,FP,SURF,EPSOLD,EPSOUT
3520          WRITE(*,900)TIME,CONV,RP,T,C1S,FP,SURF,EPSOLD,EPSOUT
3530   900    FORMAT(1X,3F9.4,1X,F7.2,1X,2F8.6,1X,F6.2,1X,
3540       1         F6.4,1X,F6.4)
3550  C
3560  C     X1 and X2 are appropriate brackets for GAM.
3570  C     Typically, ES1 is O(1D-6), while ES2 is O(1D11).
3580  C
3590          IF ( TPINIT .LT. TWALL) THEN
3600                X1 =  ( -2331.5425 + 0.3388749*TPINIT) - ES2
3610                X2 =  ( -2331.5425 + 0.3388749*TPINIT) - ES1
3620          ELSE
3630               X1 =  ( -2331.5425 + 0.3388749*TPINIT) + ES1
3640               X2 =  ( -2331.5425 + 0.3388749*TPINIT) + ES2
3650          ENDIF
3660  C
```

```
C     Calculation of QCRIT.
C
        GUESS1=(-1.0*DLOG(1.0-EPSCRIT)/(DLAMB1*4.2))**.33-VOID1
        GUESS2=0.0
        CALL RTBISOL(QCR,GUESS2,GUESS1,XACC,RSLT)
        QCRIT=RSLT
C
C
C     Main loop begins.
C
C
        DO 1000 I = 1, NMAX
         SWIT=0.0
         STEP=STEP0
         RR = RP * 1.0D-04
C
C     RTBIS merged here.
C
         DXACC=XACC
         CALL GAMMA(X1,FX1,RR,STEP,PEMMIS,WEMMIS,
     1             RNEW,TNEW,FP,SWIT)
         CALL GAMMA(X2,FX2,RR,STEP,PEMMIS,WEMMIS,
     1             RNEW,TNEW,FP,SWIT)
```

```
3900          IF(FX2*FX1 .GE. 0.0) PAUSE 'BRACKET ROOT IN MAIN'
3910          DX = X2 - X1
3920          DO 200 J = 1, 500
3930               DX = DX * 0.5
3940               ANSW = X1 + DX
3950               CALL GAMMA(ANSW,FMID,RR,STEP,PEMMIS,WEMMIS,
3960         1                                   RNEW,TNEW,FP,SWIT)
3970               IF (FMID * FX1 .GT. 0.0)THEN
3980                    X1 = ANSW
3990                    FX1 = FMID
4000               ELSE
4010                    X2 = ANSW
4020                    FX2 = FMID
4030               ENDIF
4040               IF (DABS(DX/ANSW) .LT. 0.20)SWIT=1.0
4050               IF (DABS(DX/ANSW) .LT. DXACC)  GOTO 111
4060   200    CONTINUE
4070          PAUSE 'TOO MANY BISECTIONS IN MAIN'
4080  C
4090  C
4100   111    FP1 = -1.3333 * FP
4110          FP2 = 2.3333 * FP
4120          EPF=ANSW*FP
```

```
C       DTDR=-1.0D-4*(EPF-FP1*EOX(T)-FP2*ECO(T))/RLAMB(T)
        DUMC= (1.0/(-1.0/7.0 + 8.0/(7.0*Y1S)))
        RBAR=(ROLD+RNEW)/2.0
        FSHED=0.333*(1.0-EPSOUT)*RHOC*
     1          (ROLD**3.0-RNEW**3.0)/(STEP*RBAR**2.0)
        ROLD=RNEW
        RP = 1.0D4*RNEW
        CONV=1.0-((RP/RPINIT)**3.0)*((1.0-EPSOLD)/(1.0-EPSINIT))
        SURF=SURFSUM*1.0D-12/(4.2*RNEW**3.0*(1.0-EPSOLD)*RHOC)
        T = TNEW
        TIME = TIME + 1.0D3*STEP
        TPOLD=T
C
C    Writing profiles to PRO.DAT
C
C       IF(MOD(I,10) .EQ. 0)THEN
          DO 148 LI=1,50
            WRITE(3,147)R(LI),Y1(LI)
  148     CONTINUE
C       ENDIF
  147   FORMAT(5X,2G12.4)
C
C    Writing results to data file.
```

```
4360 C
4370          WRITE(2,900)TIME,CONV,RP,T,DUMC,FP,SURF,EPSOLD,EPSOUT
4380          WRITE(*,900)TIME,CONV,RP,T,DUMC,FP,SURF,EPSOLD,EPSOUT
4390 C
4400 C     Equispacing R's
4410 C
4420          DO 157 KI=1,50
4430             FIX=KI-1
4440             R(KI)=FIX*RP/49.0
4450  157     CONTINUE
4460 C
4470          DO 158 LI=1,50
4480             AQ(LI)=Q(4,LI)
4490             ADQDR(LI)=DQDR(4,LI)
4500  158     CONTINUE
4510 C
4520 C     Reducing brackets for next call of ANS.
4530 C
4540          IF ( T .LT. TWALL) THEN
4550               X1 =  ANSW - DABS(4.0*ANSW)
4560               X2 =  ( -2331.5425 + 0.3388749*T ) - ES1
4570          ELSE
4580               X1 =  ( -2331.5425 + 0.3388749*T ) + ES1
```

```
4590                X2 =  ANSW + DABS(4.0*ANSW)
4600           ENDIF
4610 C
4620 C    Program exit condition.
4630 C
4640           IF((EPSOLD .GE. EPSCRIT) .OR.
4650       1        (R(50) .LE. 0.0))GOTO 1001
4660 C
4670  1000  CONTINUE
4680 C
4690  1001  CLOSE(2)
4700        CLOSE(3)
4710        CONTINUE
4720        STOP
4730        END
4740 C
4750 C    Main loop and main program end.
4760 C
4770 C-----------------------------------------------
4780 C-----------------------------------------------
4790 C
4800 C    Property subprograms.
4810 C
```

```
4820 C    RLAMB:gas thermal conductivity (cal/cm-K) [300-2500K]
4830 C          from Eckert. The COEFFS are in W/m-K for D in K
4840 C          Form NOT used here.
4850 C    EOX  :oxygen enthalpy (cal/gmol). Ref. state is 0.0 at
4860 C          298K. Valid for 298-2500K. Heat capacities assumed
4870 C          constant. From Smith and VanNess. Form NOT used.
4880 C    ECO  :CO enthalpy. As above except ref. state.
4890 C    EC   :Carbon enthalpy (cal/g) [LT 1350K](COAL DATA BOOK)
4900 C    ECH  :Carbon enthalpy (cal/g) [GE 1350K](COAL DATA BOOK)
4910 C    CPC  :Carbon heat cap. (cal/g-K) [LT 1350K](COAL DATA BOOK)
4920 C    CPCH :Carbon heat cap. (cal/g-K) [GE 1350K](COAL DATA BOOK)
4930 C
4940 C
4950        REAL*8 FUNCTION RLAMB(D)
4960        IMPLICIT REAL*8(A-H,O-Z)
4970        REAL*8 LG0,LG1,LG2,LG3
4980        LG0 = -1.333D-03
4990        LG1 =  1.036D-04
5000        LG2 = -4.715D-08
5010        LG3 =  1.341D-11
5020        RLAMB = (1.0/418.0)*(LG0+LG1*D+LG2*(D*D)+LG3*(D*D*D))
5030        RETURN
5040        END
```

```
5050 C
5060 C
5070        REAL*8 FUNCTION EOX(D)
5080        IMPLICIT REAL*8(A-H,O-Z)
5090        CPOXO = 7.16
5100        CPOX1 = 0.001
5110        CPOX2 = -40000.0
5120        EOX = (CPOXO*(D - 298) + (CPOX1 / 2.0)*(D*D - 298*298)
5130       1       + CPOX2*(1.0/D - 1.0/298)) / 32.0
5140        RETURN
5150        END
5160 C
5170 C
5180        REAL*8 FUNCTION ECO(D)
5190        IMPLICIT REAL*8(A-H,O-Z)
5200        CPCOO = 6.79
5210        CPCO1 = 0.00098
5220        CPCO2 = -11000.0
5230        DELH = -26416.0
5240        ECO = (DELH+CPCOO*(D-298)+(CPCO1/2.0)*(D*D-298*298)
5250       1       + CPCO2*(1.0/D - 1.0/298))/ 28.0
5260        RETURN
5270        END
```

```
5280 C
5290 C
5300        REAL*8 FUNCTION EC(D)
5310        IMPLICIT REAL*8(A-H,O-Z)
5320        CPCO = 0.024
5330        CPC1 = 6.953D-04
5340        CPC2 = -2.841D-07
5350        EC = CPCO*(D - 298) + (CPC1 / 2.0)*(D*D - 298*298)
5360       1       + (CPC2 / 3.0)*(D*D*D - 298*298*298)
5370        RETURN
5380        END
5390 C
5400        REAL*8 FUNCTION ECH(D)
5410        IMPLICIT REAL*8(A-H,O-Z)
5420        CPCHO = 0.36
5430        CPCH1 = 6.931D-05
5440        ECH = CPCHO*(D - 298) + (CPCH1 / 2.0)*(D*D - 298*298)
5450        RETURN
5460        END
5470 C
5480 C
5490        REAL*8 FUNCTION CPC(D)
5500        IMPLICIT REAL*8(A-H,O-Z)
```

```
5510          CPCO = 0.024
5520          CPC1 = 6.953D-04
5530          CPC2 = -2.841D-07
5540          CPC = CPCO + CPC1 * D + CPC2 * D * D
5550          RETURN
5560          END
5570  C
5580          REAL*8 FUNCTION CPCH(D)
5590          IMPLICIT REAL*8(A-H,O-Z)
5600          CPCHO = 0.36
5610          CPCH1 = 6.931D-05
5620          CPCH = CPCHO + CPCH1 * D
5630          RETURN
5640          END
5650  C
5660  C---------------------------------------------
5670  C
5680          SUBROUTINE RTBISOL(TET,X1,X2,XACC,XMID)
5690          IMPLICIT REAL*8(A-H,O-Z)
5700          EXTERNAL  TET
5710          PARAMETER (JMAX = 500)
5720  C
5730          CALL TET(X1,FX1)
```

```
5740          CALL TET(X2,FX2)
5750          IF(FX2*FX1 .GE. 0.0) PAUSE 'BRACKET ROOT IN RTBISOL'
5760          DX=X2-X1
5770          DO 200 J = 1, JMAX
5780                DX = DX * 0.5
5790                XMID = X1 + DX
5800                CALL TET(XMID,FMID)
5810                IF (FMID * FX1 .GT. 0.0)THEN
5820                      X1 = XMID
5830                      FX1 = FMID
5840                ELSE
5850                      X2 = XMID
5860                      FX2 = FMID
5870                ENDIF
5880                IF (DABS(DX) .LT. XACC)  RETURN
5890   200    CONTINUE
5900          PAUSE 'TOO MANY BISECTIONS IN RTBISOL'
5910          END
5920  C
5930  C---------------------------------------------
5940  C
5950          SUBROUTINE QCR(P,FUNT)
5960          IMPLICIT REAL*8(A-H,O-Z)
```

```
5970          COMMON  /SOL/VOID1,EPS1,DLAMB1,EPSOUT,EPSOLD,FSHED,
5980         1          EPSCRIT,VOID2,EPS2,DLAMB2,VOID3,EPS3,DLAMB3
5990  C
6000          FUNT=DLAMB1*(VOID1+P)**3+DLAMB2*(VOID2+P)**3+
6010         1      DLAMB3*(VOID3+P)**3 + DLOG(1.0-EPSCRIT)/4.2
6020          RETURN
6030          END
6040  C
6050  C
6060  C-----------------------------------------------
6070  C
6080  C
6090          SUBROUTINE PROF(LIE,ITER,RPIN,T,BETA)
6100          IMPLICIT REAL*8(A-H,O-Z)
6110          EXTERNAL SHOOT,STROBE,RTBISOL,EQN1,EQN2
6120          COMMON  /ARR/X(50),R(50),Y1(50),Y2(50)
6130          COMMON  /MISC/C,XLOW,AO,BO,XFAC,ACEN
6140          COMMON  /JW/JWARN
6150  C
6160  C
6170          RSTART=R(LIE)
6180          BO=R(50)
6190          Y1BASE=BETA
```

```
6200          ALPHAB=1.OD-04
6210          ALPHAA=0.0
6220          GRADO=0.0
6230          CALL SHOOT(T,GRADO,ALPHAA,ALPHAB,Y1BASE,RSTART,LIE)
6240          IF(Y1(1) .GE. 1.OD-10)RETURN
6250  C
6260          DO 201 J=1,10
6270          DO 101 I=1,49
6280          IF ((Y1(I).LT.1.OD-10) .AND. (Y1(I+1).GE.1.OD-10))THEN
6290             RSTART=R(I)
6300             LIE=I
6310             Y1BASE=BETA
6320             ALPHAB=Y1(LIE+1)+1.OD-07
6330             ALPHAA=0.0
6340             GRADO=0.0
6350             CALL SHOOT(T,GRADO,ALPHAA,ALPHAB,Y1BASE,RSTART,LIE)
6360             IF(JWARN .NE. 100) RETURN
6370          ENDIF
6380    101   CONTINUE
6390    201   CONTINUE
6400          RETURN
6410          END
6420  C
```

```
6430 C-----------------------------------------------
6440 C
6450       SUBROUTINE SHOOT(T,GRADO,ALPHAA,ALPHAB,Y1BASE,RSTART,LIE)
6460       IMPLICIT REAL*8(A-H,O-Z)
6470       EXTERNAL STROBE,EQN1,EQN2,RTBISOL
6480       COMMON  /JW/JWARN
6490 C
6500       Y1INIT=ALPHAA
6510       Y2INIT=GRADO
6520       CALL STROBE(T,Y1INIT,Y2INIT,RSTART,LIE,ANS)
6530       VOUTA=ANS
6540       Y1INIT=ALPHAB
6550       Y2INIT=GRADO
6560       CALL STROBE(T,Y1INIT,Y2INIT,RSTART,LIE,ANS)
6570       VOUTB=ANS
6580       TOLR=0.0001
6590       DO 100 J=1,100
6600         JWARN=J
6610         ALP=ALPHAA+(ALPHAB-ALPHAA)*(Y1BASE-VOUTA)/(VOUTB-VOUTA)
6620         Y1INIT=ALP
6630         Y2INIT=GRADO
6640         CALL STROBE(T,Y1INIT,Y2INIT,RSTART,LIE,ANS)
6650         VALOUT=ANS
```

```
6660            IF(DABS((VALOUT-Y1BASE)/Y1BASE) .LT. TOLR)THEN
6670              GOTO 201
6680            ELSEIF(VALOUT .GT. Y1BASE)THEN
6690              ALPHAB=ALP
6700              VOUTB=VALOUT
6710              GOTO 199
6720            ELSEIF(VALOUT .LT. Y1BASE)THEN
6730              ALPHAA=ALP
6740              VOUTA=VALOUT
6750              GOTO 199
6760            ENDIF
6770    199     CONTINUE
6780    100   CONTINUE
6790    201   RETURN
6800          END
6810  C
6820  C-----------------------------------------------
6830  C
6840          SUBROUTINE STROBE(T,Y1INIT,Y2INIT,RSTART,LIE,SHOT)
6850          IMPLICIT REAL*8(A-H,O-Z)
6860          REAL*8 K11,K12,K13,K14,K21,K22,K23,K24
6870          EXTERNAL RTBISOL,EQN1,EQN2
6880          COMMON /ARR/X(50),R(50),Y1(50),Y2(50)
```

```
6890 C
6900          IF(RSTART .EQ. 0.0)THEN
6910            Y1(1)=Y1INIT
6920            Y2(1)=Y2INIT
6930            L=2
6940          ELSE
6950            DO 200 J=1,LIE
6960             Y1(J)=0.0
6970             Y2(J)=0.0
6980   200       CONTINUE
6990            Y1(LIE+1)=Y1INIT
7000            Y2(LIE+1)=Y2INIT
7010            L=LIE+2
7020          ENDIF
7030          DO 600 I=L,50
7040            RINIT=R(I-1)
7050            Y1INIT=Y1(I-1)
7060            Y2INIT=Y2(I-1)
7070            H=R(I)-R(I-1)
7080 C
7090 C     Following is the old RUNGSOL routine now absorbed here.
7100 C
7110            XP=RINIT
```

```
7120            DUM1=Y1INIT
7130            DUM2=Y2INIT
7140            CALL EQN1(DUM1,DUM2,DY1DT)
7150            CALL EQN2(T,XP,DUM1,DUM2,DY2DT)
7160            K11=DY1DT
7170            K21=DY2DT
7180            XP=XP+H/2.0
7190            DUM1 = Y1INIT+ K11*H/2.0
7200            DUM2 = Y2INIT + K21*H/2.0
7210            CALL EQN1(DUM1,DUM2,DY1DT)
7220            CALL EQN2(T,XP,DUM1,DUM2,DY2DT)
7230            K12 = DY1DT
7240            K22 = DY2DT
7250            DUM1 = Y1INIT + K12*H/2.0
7260            DUM2 = Y2INIT + K22*H/2.0
7270            CALL EQN1(DUM1,DUM2,DY1DT)
7280            CALL EQN2(T,XP,DUM1,DUM2,DY2DT)
7290            K13 = DY1DT
7300            K23 = DY2DT
7310            XP=XP+H/2.0
7320            DUM1 = Y1INIT + K13*H
7330            DUM2 = Y2INIT + K23*H
7340            CALL EQN1(DUM1,DUM2,DY1DT)
```

```
7350            CALL EQN2(T,XP,DUM1,DUM2,DY2DT)
7360            K14 = DY1DT
7370            K24 = DY2DT
7380            ANS = Y1INIT + H*(K11 + 2.0*K12 + 2.0*K13 + K14)/6.0
7390            ANSP = Y2INIT + H*(K21 + 2.0*K22 + 2.0*K23 + K24)/6.0
7400 C
7410            Y1(I)=ANS
7420            Y2(I)=ANSP
7430  600     CONTINUE
7440          SHOT=Y1(50)
7450          RETURN
7460          END
7470 C
7480 C-----------------------------------------------
7490 C
7500 C     DY1DT is in molfrac/micron.
7510 C
7520          SUBROUTINE EQN1(DUM1,DUM2,DY1DT)
7530          IMPLICIT REAL*8(A-H,O-Z)
7540 C
7550          DY1DT = DUM2
7560          RETURN
7570          END
```

```
7580 C
7590 C-----------------------------------------------
7600 C
7610       SUBROUTINE EQN2(T,XP,DUM1,DUM2,DY2DT)
7620       IMPLICIT REAL*8(A-H,O-Z)
7630       COMMON  /MISC/C,XLOW,AO,BO,XFAC,ACEN
7640       COMMON  /SOL/VOID1,EPS1,DLAMB1,EPSOUT,EPSOLD,FSHED,
7650      1          EPSCRIT,VOID2,EPS2,DLAMB2,VOID3,EPS3,DLAMB3
7660       COMMON  /QS/Q(4,50),DQDR(4,50),QINT,QBAR,QCRIT
7670       COMMON  /CS/CSTAR,TAU,XACC,SURFSUM
7680       COMMON  /R/RHOC,FRAC,RPINIT
7690       COMMON  /POW/POW
7700 C
7710       KL=INT(XP/QINT)+1
7720       QBARL=Q(4,KL)+((XP-(KL-1)*QINT)/QINT)*(Q(4,KL+1)-Q(4,KL))
7730       DQBARL=DQDR(4,KL)+((XP-(KL-1)*QINT)/QINT)*(DQDR(4,KL+1)-
7740      1            DQDR(4,KL))
7750       EPS=1.0-DEXP((-DLAMB1*4.2*(VOID1+QBARL)**3)+(-DLAMB2*4.2*
7760      1      (VOID2+QBARL)**3)+(-DLAMB3*4.2*(VOID3+QBARL)**3))
7770       SQ=(1.0-EPS)*12.6*(DLAMB1*(VOID1+QBARL)**2
7780      1      +DLAMB2*(VOID2+QBARL)**2 + DLAMB3*(VOID3+QBARL)**2)
7790       FREQ=305.0
7800       DIFF=3.13*(T/1500.0)**1.75
```

```
7810          E=ACEN/1.98
7820          RHOG=1.0/(82.05*T)
7830          C1=TAU*FREQ*XFAC/(24.0*DIFF*RHOG)
7840          IF(XP .GT. CSTAR)THEN
7850             DY2DT = C1*DEXP(-E/T)*SQ*1D-04*DUM1**POW/EPS
7860         1           -2.0*DUM2/XP-SQ*DQBARL*DUM2/EPS
7870          ELSE
7880             DY2DT = C1*DEXP(-E/T)*SQ*1D-04*DUM1**POW/EPS
7890         1           -SQ*DQBARL*DUM2/EPS
7900          ENDIF
7910          RETURN
7920          END
7930  C
7940  C-----------------------------------------------
7950  C
7960          SUBROUTINE QUE(T,DELT,DRDT,ITER,FP)
7970          IMPLICIT REAL*8(A-H,O-Z)
7980          DIMENSION Y1BAR(50),Y2BAR(50)
7990          COMMON  /ARR/X(50),R(50),Y1(50),Y2(50)
8000          COMMON  /MISC/C,XLOW,AO,BO,XFAC,ACEN
8010          COMMON  /SOL/VOID1,EPS1,DLAMB1,EPSOUT,EPSOLD,FSHED,
8020         1          EPSCRIT,VOID2,EPS2,DLAMB2,VOID3,EPS3,DLAMB3
8030          COMMON  /QS/Q(4,50),DQDR(4,50),QINT,QBAR,QCRIT
```

```
8040          COMMON  /R/RHOC,FRAC,RPINIT
8050          COMMON  /CS/CSTAR,TAU,XACC,SURFSUM
8060          COMMON  /AQ/AQ(50),ADQDR(50)
8070          COMMON  /POW/POW
8080  C
8090          FREQ=305.0
8100          E=ACEN/1.98
8110          C2=FREQ*XFAC/RHOC
8120          RXN = C2*DEXP(-E/T)*1.0D04
8130  C
8140  C     Q's are in microns for the above expression of RXN.
8150  C     The inner J-loop finds the position of Q(I) just below
8160  C     R(J). Y1BAR and Y2BAR are the interpolated values of
8170  C     mass fraction and its gradient at the fixed locations
8180  C     where Q's are calculated.
8190  C
8200            Y1BAR(1)=Y1(1)
8210            Y2BAR(1)=Y2(1)
8220            DO 300 I=2,50
8230               DIST = QINT*(I-1)
8240               DO 350 J=1,49
8250               IF((R(J).LT.DIST).AND.(R(J+1).GE.DIST))THEN
8260                  Y1BAR(I)=Y1(J)+((DIST-R(J))/
```

```
8270      1                (R(J+1)-R(J)))*(Y1(J+1)-Y1(J))
8280             Y2BAR(I)=Y2(J)+((DIST-R(J))/
8290      1                (R(J+1)-R(J)))*(Y2(J+1)-Y2(J))
8300           ELSEIF (DIST .GT. R(50)) THEN
8310              Y1BAR(I)=Y1(50)
8320              Y2BAR(I)=Y2(50)
8330           ENDIF
8340   350     CONTINUE
8350   300  CONTINUE
8360 C
8370        IF(Y1BAR(1) .EQ. 0)THEN
8380           Q(ITER,1)=AQ(1)
8390           DQDR(ITER,1)=ADQDR(1)
8400        ELSE
8410           Q(ITER,1)=AQ(1)+DELT*RXN*Y1BAR(1)**POW
8420           DQDR(ITER,1)=ADQDR(1)+DELT*RXN*Y2BAR(1)*
8430      1        POW*Y1BAR(1)**(POW-1.0)
8440        ENDIF
8450 C
8460        DO 310 I=2,50
8470           IF(Y1BAR(I) .EQ. 0)THEN
8480              Q(ITER,I)=AQ(I)
8490              DQDR(ITER,I)=ADQDR(I)
```

```
8500            ELSE
8510               Q(ITER,I)=AQ(I)+DELT*RXN*Y1BAR(I)**POW
8520               DQDR(ITER,I)=ADQDR(I)+DELT*RXN*Y2BAR(I)*
8530      1          POW*Y1BAR(I)**(POW-1.0)
8540            ENDIF
8550 C
8560          IF((Q(ITER,I).GE.QCRIT).AND.(Q(ITER,I-1).LT.QCRIT))THEN
8570            RCRIT=QINT*(I-2)+((QCRIT-Q(ITER,I-1))/(Q(ITER,I)-
8580      1                              Q(ITER,I-1)))*QINT
8590            DRDT=-1D-04*(R(50)-RCRIT)/DELT
8600            FLAG=0.0
8610            GOTO 940
8620          ENDIF
8630   310    CONTINUE
8640 C
8650          KL=INT(R(50)/QINT)+1
8660          IF(KL .EQ. 50) THEN
8670            QBAR=Q(ITER,50)
8680            DQDRP=DQDR(ITER,50)
8690          ELSE
8700            QBAR=Q(ITER,KL)+((R(50)-(KL-1)*QINT)/QINT)*(Q(ITER,KL+1)
8710      1        -Q(ITER,KL))
8720            DQDRP=DQDR(ITER,KL)+((R(50)-(KL-1)*QINT)/QINT)*
```

```
8730      1          (DQDR(ITER,KL+1)-DQDR(ITER,KL))
8740        ENDIF
8750        QLAST=AQ(KL)+((R(50)-(KL-1)*QINT)/QINT)*(AQ(KL+1)
8760      1       -AQ(KL))
8770        DRDT=-1D-04*(QBAR-QLAST)/DELT
8780        FLAG=1.0
8790 C
8800 C    Flux (FP) is calculated using mole fraction gradient
8810 C    at the surface Y2(50), diffusivity, and stoichiometric
8820 C    coefficient 24.0 [gm/cm^2-s].
8830 C    The expression for diffusivity is from FIELD's book.
8840 C
8850   940  IF(FLAG .EQ. 1.0)THEN
8860          IF (R(50) .EQ. RPINIT)THEN
8870             QBAR=Q(ITER,50)
8880          ELSE
8890             KL=INT(R(50)/QINT)+1
8900             QBAR=Q(ITER,KL)+((R(50)-(KL-1)*QINT)/QINT)*
8910      1           (Q(ITER,KL+1)-Q(ITER,KL))
8920          ENDIF
8930          EPSOUT=1.0-DEXP((-4.2*DLAMB1*(VOID1+QBAR)**3)+
8940      1          (-4.2*DLAMB2* (VOID2+QBAR)**3)+
8950      2          (-4.2*DLAMB3*(VOID3+QBAR)**3))
```

```
8960          ELSE
8970            KL=INT(R(50)/QINT)+1
8980            QSUP=Q(ITER,KL)+((R(50)-(KL-1)*QINT)/QINT)*
8990         1        (Q(ITER,KL+1)-Q(ITER,KL))
9000            EPSSUP=1.0-DEXP((-4.2*DLAMB1*(VOID1+QSUP)**3)+
9010         1          (-4.2*DLAMB2*(VOID2+QSUP)**3)+
9020         2          (-4.2*DLAMB3*(VOID3+QSUP)**3))
9030            EPSOUT=(EPSCRIT+EPSSUP)/2.0
9040          ENDIF
9050  C
9060          SUM=0.0
9070          VOLSUM=0.0
9080          SURFSUM=0.0
9090          KL=INT(R(50)/QINT)+1
9100          DO 560 I=2,KL
9110            QSHELL=(Q(ITER,I)+Q(ITER,I-1))/2.0
9120            AQSHELL=(AQ(I)+AQ(I-1))/2.0
9130            EPSSHELL=1.0-DEXP((-4.2*DLAMB1*(VOID1+QSHELL)**3)+
9140         1            (-4.2*DLAMB2*(VOID2+QSHELL)**3)+
9150         2            (-4.2*DLAMB3*(VOID3+QSHELL)**3))
9160            SQSHELL=(1.0-EPSSHELL)*12.6*(DLAMB1*(VOID1+QSHELL)**2
9170         1       +DLAMB2*(VOID2+QSHELL)**2+DLAMB3*(VOID3+QSHELL)**2)
9180            ROUT=QINT*(I-1)
```

```
9190          RIN =QINT*(I-2)
9200          FPSHELL=4.2*(ROUT**3.0-RIN**3.0)*SQSHELL*
9210     1             (QSHELL-AQSHELL)
9220          SURFSUM=SURFSUM+4.2*(ROUT**3.0-RIN**3.0)*SQSHELL
9230          SUM=SUM+FPSHELL
9240          IF(QSHELL .LT. QCRIT)THEN
9250            VOLSUM=VOLSUM+EPSSHELL*(4.2*(ROUT**3.0-RIN**3.0))
9260          ENDIF
9270   560  CONTINUE
9280        QR50=Q(ITER,KL)+0.5*(((R(50)-(KL-1)*QINT)/QINT)*
9290     1      (Q(ITER,KL+1)-Q(ITER,KL)))
9300        AQR50=AQ(KL)+0.5*(((R(50)-(KL-1)*QINT)/QINT)*(AQ(KL+1)
9310     1                -AQ(KL)))
9320        EPSR50=1.0-DEXP((-4.2*DLAMB1*(VOID1+QR50)**3)+
9330     1         (-4.2*DLAMB2*(VOID2+QR50)**3)+
9340     2         (-4.2*DLAMB3*(VOID3+QR50)**3))
9350        SQR50=(1.0-EPSR50)*12.6*(DLAMB1*(VOID1+QR50)**2
9360     1      +DLAMB2*(VOID2+QR50)**2+DLAMB3*(VOID3+QR50)**2)
9370        FPQ50=4.2*(R(50)**3.0-(QINT*(KL-1))**3.0)*
9380     1       SQR50*(QR50-AQR50)
9390        VOLR50=EPSR50*(R(50)**3.0-(QINT*(KL-1))**3.0)*4.2
9400        SURFSUM=SURFSUM+SQR50*(R(50)**3.0-(QINT*(KL-1))**3.0)*4.2
9410        EPSOLD=(VOLSUM+VOLR50)/(4.2*R(50)**3.0)
```

```
9420          FP=(SUM+FPQ50)*RHOC*1.0D-04/(DELT*12.6*R(50)**2.0)
9430          RETURN
9440          END
9450  C
9460  C-----------------------------------------------
9470  C
9480          SUBROUTINE GAMMA(GAM1,F,R1,STEP,PEMMIS,WEMMIS,RNEW,TNEW,
9490         1                 FP,SWIT)
9500          IMPLICIT REAL*8(A-H,O-Z)
9510          REAL*8 K11,K12,K13,K14,K21,K22,K23,K24
9520          EXTERNAL  EC,ECH,CPC,CPCH,RLAMB,EOX,ECO
9530          EXTERNAL  PROF,RADIUS,ENERGY,QUE,SHOOT
9540          EXTERNAL  STROBE,RTBISOL,EQN1,EQN2
9550          COMMON  T,TWALL
9560          COMMON  /MISC/C,XLOW,AO,BO,XFAC,ACEN
9570          COMMON  /ARR/X(50),R(50),Y1(50),Y2(50)
9580          COMMON  /SOL/VOID1,EPS1,DLAMB1,EPSOUT,EPSOLD,FSHED,
9590         1          EPSCRIT,VOID2,EPS2,DLAMB2,VOID3,EPS3,DLAMB3
9600          COMMON  /R/RHOC,FRAC,RPINIT
9610          COMMON  /CS/CSTAR,TAU,XACC,SURFSUM
9620          COMMON  /Y1/Y1S,Y1INF
9630  C
9640          CC = -3.0043D-05
```

```
9650          C3 = (2331.5425 + GAM1)/0.3388749
9660          Y1S=(Y1INF+4.0/3.0)*((T-C3)/(TWALL-C3))**0.8095478-4.0/3.0
9670          C1SURF= (1.0/(-1.0/7.0 + 8.0/(7.0*Y1S)))
9680          IF(C1SURF .LT. 0.0)THEN
9690              F=1.0
9700              RETURN
9710          ENDIF
9720  C
9730  C     RUNG merged here.
9740  C
9750          LIE=1
9760          IF(SWIT .EQ. 0.0)THEN
9770               ITER=4
9780               CALL PROF(LIE,ITER,R1,T,C1SURF)
9790               DIFF=3.13*(T/1500)**1.75
9800               FP=1.0D04*Y2(50)*DIFF*EPSOUT*24.0/(TAU*82.05*T)
9810               GO TO 111
9820          ENDIF
9830          DUM1=R1
9840          DUM2=T
9850          ITER=4
9860          CALL PROF(LIE,ITER,DUM1,DUM2,C1SURF)
9870          CALL RADIUS(STEP,DUM2,ITER,DRDT,FP)
```

```
9880          EP=FP*GAM1
9890          CALL ENERGY(EP,PEMMIS,WEMMIS,DUM1,DUM2,DTDT)
9900          K11=DRDT
9910          K21=DTDT
9920          RNEW = R1 + STEP*K11
9930          TNEW = T + STEP*K21
9940  C
9950  C
9960   111    IF (T .LT. TWALL) THEN
9970           HH = DSQRT(DABS(-2331.5425 - GAM1)/0.3388749)
9980           IF (GAM1 .GT.-2331.5425) THEN
9990             AR1 = -1.0*CC * ((DSQRT(TWALL) - DSQRT(T)) + HH/2.0 *
10000       1          (DLOG((DSQRT(TWALL) - HH)*(DSQRT(T) + HH)/
10010       2          ((DSQRT(TWALL) + HH)*(DSQRT(T) - HH)))))
10020            F = AR1-R1* FP
10030          ELSE
10040            AR2 = -1.0*CC*((DSQRT(TWALL)-DSQRT(T))-HH*
10050       1          (DATAN(DSQRT(TWALL)/HH)-DATAN(DSQRT(T)/HH)))
10060            F = AR2-R1* FP
10070          ENDIF
10080         ELSE
10090           FF = DSQRT(DABS(2331.5425 + GAM1)/0.3388749)
10100           IF (GAM1 .LT.-2331.5425) THEN
```

```
10110            AR3 = CC*((DSQRT(T)-DSQRT(TWALL))-FF*
10120       1          (DATAN(DSQRT(T)/FF)-DATAN(DSQRT(TWALL)/FF)))
10130            F = AR3-R1* FP
10140          ELSE
10150            AR4 = CC * ((DSQRT(T) - DSQRT(TWALL)) + FF/2.0 *
10160       1          (DLOG((DSQRT(T) - FF)*(DSQRT(TWALL) + FF)/
10170       2          ((DSQRT(T) + FF)*(DSQRT(TWALL) - FF)))))
10180            F = AR4-R1* FP
10190          ENDIF
10200        ENDIF
10210        RETURN
10220        END
10230 C
10240 C-----------------------------------------------
10250 C
10260        SUBROUTINE ENERGY(EP,PEMMIS,WEMMIS,RR,DUM2,ANST)
10270        IMPLICIT REAL*8(A-H,O-Z)
10280        EXTERNAL EC,ECH,CPC,CPCH,RLAMB,EOX,ECO
10290        COMMON  T,TWALL
10300        COMMON  /R/RHOC,FRAC,RPINIT
10310        COMMON  /SOL/VOID1,EPS1,DLAMB1,EPSOUT,EPSOLD,FSHED,
10320       1          EPSCRIT,VOID2,EPS2,DLAMB2,VOID3,EPS3,DLAMB3
10330 C
```

```
10340         SIG = 1.595D-12
10350         IF (DUM2 .LT. 1350) THEN
10360                 CPSOL= CPC(DUM2)
10370                 VAL = EC(DUM2)
10380         ELSE
10390                 CPSOL= CPCH(DUM2)
10400                 VAL = ECH(DUM2)
10410         ENDIF
10420         ANST=(3.0/(1.0-EPSOLD))*((FP+(1.0-FRAC)*FSHED)*VAL-EP-SIG*
10430        1 (PEMMIS*DUM2**4-WEMMIS*TWALL**4))/(RR*RHOC*CPSOL)
10440         RETURN
10450         END
10460 C
10470 C-----------------------------------------------
10480 C
10490         SUBROUTINE RADIUS(TMSTP,DUM2,ITER,ANS,FP)
10500         IMPLICIT REAL*8(A-H,O-Z)
10510         EXTERNAL QUE
10520 C
10530         CALL QUE(DUM2,TMSTP,DRDT,ITER,FP)
10540         ANS=DRDT
10550         RETURN
10560         END
```

```
10570 C
10580 C-----------------------------------------------
```

AIX.6 CENMOD21.FOR

```
10 C    This program describes the growth of the internal structure
20 C    of a char particle containing polydisperse spherical voids
30 C    randomly distributed in it. It is a phenomenological model
40 C    and does not consider actual effects of chemical kinetics,
50 C    temperature and diffusion. Instead it simulates the burning
60 C    of the char particle. The focus is on how the pores grow,
70 C    coalesce etc. ultimately fragmenting the particle at high
80 C    conversions.
90 C
100 C   The voids are randomly distributed in the particle. Their
110 C   sizes are also randomly selected. Once the void centers
120 C   fixed, they remain unchanged. Only void size can grow by
130 C   reaction. Clearly, due to the random placement, voids may
140 C   intersect each other and might have access to the outside.
150 C   Two voids intersect if the sum of their radii is less than
160 C   their center separation. Similarly, a void is connected to
170 C   the outside if its center lies closer to the particle
180 C   surface than its radius.
190 C
200 C   Reaction is simulated by allowing those voids that are
210 C   either directly or indirectly (via other voids) connected
```

```
220 C     to the outside to grow a certain amount in each time
230 C     step. The external surface is also assumed to reduce in
240 C     each time step. In this program diffusion is not taken
250 C     into account and thus voids grow the same amount no matter
260 C     where they are present as long as they have access to the
270 C     outside. However, diffusion can be simulated by allowing
280 C     the growth parameter to be a function of radius.
290 C
300 C     Thus, after many time steps, the particle void fraction
310 C     will reach large values and the particle may fragment.
320 C     The user sets both the growth parameter and the number
330 C     of time steps.
340 C
350 C     This discrete model keeps track of the connectivity of
360 C     individual voids. It computes the void fraction at each
370 C     time step and calculates conversion. Other parameters
380 C     of interest are the number fraction of voids connected
390 C     to the outside, and the number fraction of voids in the
400 C     largest void cluster.
410 C
420 C-----------------------------------------------
430 C
440 C     Declarations.
```

```
C
$LARGE C(ND1,3),VC(ND,3),PC1(ID1,3),PC(ID,3)
$LARGE RVX(ND1),RVY(ND1),RVZ(ND1),RPX(ID1),RPY(ID1),RPZ(ID1)
$LARGE VOID(ND),VDIA(ND),VDIAM(ND1),ICON(ND,ND),MAT(ND,ND)
C
      PARAMETER (ND1=430,NDIM=1290,ID1=3200,IDIM=9600,NCON=151)
      PARAMETER (ND=220,ID=2000,NDEL=50)
C
      REAL RVX(ND1),RVY(ND1),RVZ(ND1),RVA(ND1)
      REAL RPX(ID1),RPY(ID1),RPZ(ID1)
      REAL C(ND1,3),VC(ND,3),RS,VS,DIST1,RC
      REAL DIST2,Q,IN,OUT,PC1(ID1,3),PC(ID,3)
      REAL Q1,Q2,COUNTIN,COUNTOUT,RCOUNTOUT,RTOTAL,RTOT
      REAL DIST,RSO,VDIAO,QCONV,CCOUNT,VOID(ND),XLARGE
      REAL VDIA(ND),VDIAM(ND1),VOIDF(NCON),CONV(NCON)
      REAL SUMX,SUMY,SUMZ,SUMM,SUMR,RADGY,USED(ID)
      REAL CMASSX,CMASSY,CMASSZ,DCON(NCON)
      REAL CF,RLN,XLN,Q3,RNDEL
      REAL RTO(NDEL),RSOLID(NDEL),RBIG(NDEL)
      REAL RSMALL(NDEL),RMEAN(NDEL),RRATIO(NDEL)
C
      INTEGER ICON(ND,ND),ICLUSTER,IDCON(1,ND),MOUT,NOUT
      INTEGER MAT(ND,ND),IMAP(1,ND),LICLU
```

```
680 C
690       REAL*8 DSEED1,DSEED2,DSEED3,DSEED4,DSEED5,DSEED6
700       REAL*8 DSEED7
710 C
720 C
730       OPEN(9,FILE='FOR.DAT',STATUS='NEW')
740       OPEN(8,FILE='MOD.DAT',STATUS='NEW')
750       OPEN(7,FILE='RAD.DAT',STATUS='NEW')
760 C
770       WRITE(*,89)
780  89   FORMAT(3X,'ENTER THE VALUES OF DSEEDS 1-6 like xxxx.DX')
790       READ(*,*)DSEED1,DSEED2,DSEED3,DSEED4,DSEED5,DSEED6
800       WRITE(*,88)
810  88   FORMAT(3X,'ENTER THE VALUE OF DSEED7')
820       READ(*,*)DSEED7
830 C
840       RSO=25.0
850       VDIAO=5.0
860       QCONV=0.05
870       VS=VDIAO-2.0*QCONV
880       RC=RSO+VDIAO/2.0
890       RS=25.0+QCONV
900 C
```

```
C     Random number generation for void centers. Separate
C     strings for x,y and z coordinates.
C
      I1=ND1
      I2=NDIM
      CALL GGUBS(DSEED1,ND1,RVX)
      CALL GGUBS(DSEED2,ND1,RVY)
      CALL GGUBS(DSEED3,ND1,RVZ)
C
C     Creating the void centers in the cube.
C
      DO 200 J=1,ND1
         C(J,1)=RVX(J)*RC*2.0
         C(J,2)=RVY(J)*RC*2.0
         C(J,3)=RVZ(J)*RC*2.0
  200 CONTINUE
C
C     Random number generation for probe points.
C
      I3=ID1
      I4=IDIM
      CALL GGUBS(DSEED4,ID1,RPX)
      CALL GGUBS(DSEED5,ID1,RPY)
```

```
      CALL GGUBS(DSEED6,ID1,RPZ)
C
C     Creating probe centers in the cube.
C
      DO 700 J1=1,ID1
         PC1(J1,1)=RPX(J1)*RSO*2.0+VDIAO/2.0
         PC1(J1,2)=RPY(J1)*RSO*2.0+VDIAO/2.0
         PC1(J1,3)=RPZ(J1)*RSO*2.0+VDIAO/2.0
700   CONTINUE
C
C     Setting the initial diameters of the voids.
C
      CALL GGUBS(DSEED7,ND1,RVA)
      DO 91 I31=1,I1
         VDIAM(I31)=VDIAO*RVA(I31)
91    CONTINUE
C
C     Ordering the void centers in the sphere. Since this
C     does not change, this part is outside the main loop.
C
      OUT=0.0
      IN=0.0
      INC=0
```

```
1370        INC1=0
1380        DO 300 J10=1,I1
1390         Q=SQRT((C(J10,1)-RC)**2+(C(J10,2)-RC)**2+
1400       1   (C(J10,3)-RC)**2)
1410         IF(Q.GT.(VDIAM(J10)/2.0+RS))THEN
1420           OUT=OUT+1
1430         ELSE
1440           IN=IN+1
1450           INC=INC+1
1460           INC1=INC1+1
1470           VC(INC,1)=C(J10,1)
1480           VC(INC,2)=C(J10,2)
1490           VC(INC,3)=C(J10,3)
1500           VDIA(INC)=VDIAM(J10)
1510         ENDIF
1520   300   CONTINUE
1530        WRITE (*,11)INC
1540   11   FORMAT(10X,I4)
1550 C
1560 C     Ordering the probe centers in the original sphere.
1570 C
1580        DO 334 M1=1,ID
1590           USED(M1)=0.0
```

```
1600   334  CONTINUE
1610        IPIN=0
1620        IPIN1=0
1630        DO 800 J9=1,ID1
1640         Q1=SQRT((PC1(J9,1)-RC)**2+(PC1(J9,2)-RC)**2+
1650       1           (PC1(J9,3)-RC)**2)
1660         IF(Q1 .LE. RSO)THEN
1670           IPIN=IPIN+1
1680           IPIN1=IPIN1+1
1690           PC(IPIN,1)=PC1(J9,1)
1700           PC(IPIN,2)=PC1(J9,2)
1710           PC(IPIN,3)=PC1(J9,3)
1720         ELSE
1730           CONTINUE
1740         ENDIF
1750   800  CONTINUE
1760 C
1770 C     Initialisation.
1780 C
1790        DO 333 M=1,NCON
1800           VOIDF(M)=0.0
1810           CONV(M)=0.0
1820   333  CONTINUE
```

```
1830 C
1840 C    Main loop starts here.
1850 C
1860       DO 5000 I17=1,NCON
1870         RS=RS-QCONV
1880         VS=VS+2.0*QCONV
1890         DO 801 J9=1,IPIN
1900           Q2=SQRT((PC(J9,1)-RC)**2+(PC(J9,2)-RC)**2+
1910      1      (PC(J9,3)-RC)**2)
1920           IF(Q2 .GT. RS)THEN
1930             USED(J9)=1.0
1940             IPIN1=IPIN1-1
1950           ELSE
1960             CONTINUE
1970           ENDIF
1980  801    CONTINUE
1990 C
2000 C    Initialization for connectivity matrix.
2010 C
2020         DO 2000 JCON=1,INC
2030            DO 2000 KCON=1,INC
2040               IF(JCON .EQ. KCON)THEN
2050                  ICON(JCON,KCON)=1
```

```
2060                ELSE
2070                   ICON(JCON,KCON)=0
2080                ENDIF
2090   2000   CONTINUE
2100          WRITE(*,12)INC
2110   12     FORMAT(10X,I4)
2120  C
2130  C     Internal connectivity calculation.
2140  C
2150          DO 3000 JCON=1,INC
2160             DO 3000 KCON=1,INC
2170                DIST1=SQRT((VC(JCON,1)-VC(KCON,1))**2+
2180       1              (VC(JCON,2)-VC(KCON,2))**2
2190       2              +(VC(JCON,3)-VC(KCON,3))**2)
2200                IF(DIST1 .LT. (VDIA(JCON)+VDIA(KCON))/2.0)THEN
2210                ICON(JCON,KCON)=1
2220             ELSE
2230                CONTINUE
2240             ENDIF
2250   3000   CONTINUE
2260  C
2270  C     External connectivity calculation.
2280  C
```

```
      IN3=INC+1
      DO 4000 JCON=1,INC
         DIST2=SQRT((VC(JCON,1)-RC)**2+(VC(JCON,2)-RC)**2
     1           +(VC(JCON,3)-RC)**2)
         IF(ABS(RS-DIST2) .LT. VDIA(JCON)/2.0)THEN
               ICON(JCON,IN3)=1
         ELSE
               ICON(JCON,IN3)=0
         ENDIF
 4000  CONTINUE
C
C    Initializing the diagonal of the connectivity matrix ICON.
C
      DO 400 JCON=1,INC
         ICON(JCON,JCON)=0
 400  CONTINUE
C
C    Writing to screen.
C
      WRITE(*,998)RS,VS
 998  FORMAT(5X,'RS=',1PE10.3,5X,'VS=',1PE10.3/)
C
C    Calculating connected clusters and those connected to
```

```
2520 C     the outside. Results in MAT(ICLUSTER,KCON).
2530 C
2540         DO 2010 JX=1,INC
2550            DO 2010 KX=1,IN3
2560               MAT(JX,KX)=0
2570   2010  CONTINUE
2580         ICLUSTER=1
2590         DO 50 JCON=1,INC
2600           IF(ICON(JCON,JCON) .EQ. 0)THEN
2610               ICLUSTER=ICLUSTER+1
2620               DO 60 KCON=1,INC
2630                  IDCON(1,KCON)=ICON(JCON,KCON)
2640   60             CONTINUE
2650   10             DO 70 KCON=1,INC
2660                  IF((ICON(KCON,KCON).EQ.0).AND.
2670        1            (IDCON(1,KCON).EQ.1))THEN
2680                     DO 80 KCON1=1,INC
2690                        IF((IDCON(1,KCON1).EQ.1).OR.
2700        1                  (ICON(KCON,KCON1) .EQ. 1))THEN
2710                           IDCON(1,KCON1)=1
2720                        ELSE
2730                           IDCON(1,KCON1)=0
2740                        ENDIF
```

```
2750  80                CONTINUE
2760                    ICON(KCON,KCON)=ICLUSTER
2770                    MAT(ICLUSTER,KCON)=1
2780                    IF(ICON(KCON,IN3) .EQ. 1)THEN
2790                       MAT(ICLUSTER,IN3)=1
2800                       MOUT=1
2810                    ELSE
2820                       MOUT=0
2830                    ENDIF
2840                    IF(KCON .NE. JCON)THEN
2850 C                     WRITE(*,1)ICLUSTER,KCON,MOUT
2860                    ELSE
2870                       CONTINUE
2880                    ENDIF
2890                    GOTO 10
2900                 ELSE
2910                    CONTINUE
2920                 ENDIF
2930  70            CONTINUE
2940                ICON(JCON,JCON)=ICLUSTER
2950                MAT(ICLUSTER,JCON)=1
2960                IF(ICON(JCON,IN3) .EQ. 1)THEN
2970                   MAT(ICLUSTER,IN3)=1
```

```
2980                  NOUT=1
2990               ELSE
3000                  NOUT=0
3010               ENDIF
3020 C             WRITE(*,2)ICLUSTER,JCON,NOUT
3030            ELSE
3040               CONTINUE
3050            ENDIF
3060   50    CONTINUE
3070 C
3080 C    Calculating the number of clusters, number of clusters
3090 C    connected to the outside, number of voids in the largest
3100 C    cluster, number of voids connected to the outside.
3110 C
3120         XLARGE=0.0
3130         LICLU=0
3140         KOUNT=0
3150         DO 705 ICLU=2,ICLUSTER
3160            IF(MAT(ICLU,IN3) .EQ. 1)THEN
3170               DO 710 KCON=1,INC
3180               IF(MAT(ICLU,KCON) .EQ. 1)THEN
3190                  KOUNT=KOUNT+1
3200               ELSE
```

```
3210                  CONTINUE
3220                ENDIF
3230  710           CONTINUE
3240              ELSE
3250                CONTINUE
3260              ENDIF
3270  705       CONTINUE
3280            KOUNT1=KOUNT
3290            DO 36 ICLU=2,ICLUSTER
3300              VOID(ICLU)=0.0
3310  36        CONTINUE
3320            ICLUSTER1=ICLUSTER-1
3330            CCOUNT=1.0
3340            DO 37 ICLU=2,ICLUSTER
3350              IF(MAT(ICLU,IN3) .EQ. 1)THEN
3360                CCOUNT=CCOUNT+1.0
3370              ELSE
3380                CONTINUE
3390              ENDIF
3400              DO 38 KCON=1,INC
3410                IF(MAT(ICLU,KCON) .EQ. 1)THEN
3420                    VOID(ICLU)=VOID(ICLU)+1.0
3430                ELSE
```

```
3440                  CONTINUE
3450               ENDIF
3460   38        CONTINUE
3470             IF(VOID(ICLU) .GT. XLARGE)THEN
3480               XLARGE=VOID(ICLU)
3490               LICLU=ICLU
3500             ELSE
3510               CONTINUE
3520             ENDIF
3530   37      CONTINUE
3540           XLN=ALOG(XLARGE)
3550  C
3560  C
3570  C
3580           CMASSX=0.0
3590           CMASSY=0.0
3600           CMASSZ=0.0
3610           RADGY=0.0
3620           DO 49 KCON=1,ND
3630             IMAP(1,KCON)=0
3640   49      CONTINUE
3650           DO 51 KCON=1,INC
3660             IMAP(1,KCON)=MAT(LICLU,KCON)
```

```
3670   51    CONTINUE
3680  C
3690  C     Calculating the center of mass of the largest cluster.
3700  C
3710          SUMX=0.0
3720          SUMY=0.0
3730          SUMZ=0.0
3740          SUMM=0.0
3750          DO 52 KCON=1,INC
3760            IF(IMAP(1,KCON) .EQ. 1)THEN
3770               SUMX=SUMX+((VDIA(KCON))**3)*VC(KCON,1)
3780               SUMY=SUMY+((VDIA(KCON))**3)*VC(KCON,2)
3790               SUMZ=SUMZ+((VDIA(KCON))**3)*VC(KCON,3)
3800               SUMM=SUMM+VDIA(KCON)**3
3810            ELSE
3820               CONTINUE
3830            ENDIF
3840   52    CONTINUE
3850          CMASSX=SUMX/SUMM
3860          CMASSY=SUMY/SUMM
3870          CMASSZ=SUMZ/SUMM
3880  C
3890  C     Finding the radius of gyration of the largest cluster.
```

```
3900 C
3910         SUMR=0.0
3920         DO 53 KCON=1,INC
3930           IF(IMAP(1,KCON) .EQ. 1)THEN
3940              SUMR=SUMR+(((VC(KCON,1)-CMASSX)**2)+
3950      1            ((VC(KCON,2)-CMASSY)**2)
3960      2            +((VC(KCON,3)-CMASSZ)**2))*(VDIA(KCON)**3)
3970           ELSE
3980              CONTINUE
3990           ENDIF
4000   53    CONTINUE
4010         RADGY=SQRT(SUMR/SUMM)
4020         RLN=ALOG(RADGY)
4030 C
4040 C    Writing to file.
4050 C
4060         WRITE(9,1007)ICLUSTER1,CCOUNT,XLARGE,RADGY,KOUNT1,SUMM
4070   1007  FORMAT(5X,'NO. OF CLUSTERS=',I5/
4080      1  5X,'NO.OF CLUSTERS CONNECTED TO THE OUTSIDE=',E10.4/
4090      2  5X,'NO. OF VOIDS IN THE LARGEST CLUSTER=',E10.4/
4100      3  5X,'RADIUS OF GYRATION OF THE LARGEST CLUSTER=',E10.4/
4110      4  5X,'NO. OF VOIDS CONNECTED TO THE OUTSIDE=',I5/
4120      5  5X,'NONOVERLAP VOL. OF THE LARGEST CLUSTER=',E10.4)
```

```
      WRITE(9,1008)CMASSX,CMASSY,CMASSZ
 1008 FORMAT(5X,'CMASSX=',E10.4,2X,'CMASSY=',
     1    E10.4,2X,'CMASSZ=',E10.4/)
C
C    Finding the probe points that are outside all the voids.
C
      DO 61 I=1,NDEL
        RSOLID(I)=0.0
        RTO(I)=0.0
        RMEAN(I)=0.0
 61   CONTINUE
      RNDEL=NDEL
      DO 62 IP=1,IPIN
        DO 63 I=1,NDEL
          RBIG(I)=RS-((I-1)*RS/RNDEL)
          RSMALL(I)=RS-(I*RS/RNDEL)
          RMEAN(I)=(RBIG(I)+RSMALL(I))/2.0
          Q3=SQRT((PC(IP,1)-RC)**2+(PC(IP,2)-RC)**2+
     1              (PC(IP,3)-RC)**2)
          IF(Q3 .LE. RS)THEN
            IF((Q3.LE.RBIG(I)).AND.(Q3.GT.RSMALL(I)))THEN
              RTO(I)=RTO(I)+1.0
            ELSE
```

```
4360                        CONTINUE
4370                    ENDIF
4380                ELSE
4390                    CONTINUE
4400                ENDIF
4410  63          CONTINUE
4420  62        CONTINUE
4430            COUNTIN=0.0
4440            COUNTOUT=0.0
4450            RCOUNTOUT=0.0
4460            RTOTAL=IPIN1
4470            RTOT=INC1
4480            DO 900 IP=1,IPIN
4490                IF(USED(IP) .EQ. 0.0)THEN
4500                    DO 90 I=1,NDEL
4510                        Q3=SQRT((PC(IP,1)-RC)**2+(PC(IP,2)-RC)**2+
4520       1                      (PC(IP,3)-RC)**2)
4530                        IF((Q3.LE.RBIG(I)).AND.
4540       1                                  (Q3.GT.RSMALL(I)))THEN
4550                            DO 13 MC=1,INC
4560                               DIST=SQRT((VC(MC,1)-PC(IP,1))**2+
4570       1                           (VC(MC,2)-PC(IP,2))**2+
4580       2                           (VC(MC,3)-PC(IP,3))**2)
```

```
4590                                IF(DIST .GE. VDIA(MC)/2.0)THEN
4600                                    COUNTOUT=COUNTOUT+1.0
4610                                ELSE
4620                                    COUNTIN=COUNTIN+1.0
4630                                    USED(IP)=1.0
4640                                ENDIF
4650  13                          CONTINUE
4660 C                           WRITE(*,*)COUNTOUT,COUNTIN
4670                             IF(COUNTIN .EQ. 0)THEN
4680                                RSOLID(I)=RSOLID(I)+1.0
4690                             ELSE
4700                                CONTINUE
4710                             ENDIF
4720                         ELSE
4730                             CONTINUE
4740                         ENDIF
4750  90                 CONTINUE
4760                     COUNTOUT=0.0
4770                     COUNTIN=0.0
4780                 ELSE
4790                     CONTINUE
4800                 ENDIF
4810  900    CONTINUE
```

```
4820          RCOUNTOUT=0.0
4830          I16=I17-1
4840          DO 92 I=1,NDEL
4850             RCOUNTOUT=RCOUNTOUT+RSOLID(I)
4860             IF(RTO(I) .NE. 0.0)THEN
4870                RRATIO(I)=RSOLID(I)/RTO(I)
4880             ELSE
4890                RRATIO(I)=1.0
4900             ENDIF
4910             IF((I16 .EQ. 0) .OR. (I16 .GE. 10))THEN
4920                IF(MOD(I16,10) .EQ. 0)THEN
4930                   WRITE(7,93)RMEAN(I),RRATIO(I)
4940    93             FORMAT(5X,E10.4,5X,E10.4)
4950                ELSE
4960                   CONTINUE
4970                ENDIF
4980             ELSE
4990                CONTINUE
5000             ENDIF
5010    92    CONTINUE
5020  C       WRITE(*,*)RCOUNTOUT,RTOT,RTOTAL
5030          CF=XLARGE/RTOT
5040  C
```

```
5050 C     Calculate and write void fraction and conversion.
5060 C
5070         I12=I17-5
5080         VOIDF(I17)=1.0-(RCOUNTOUT/RTOTAL)
5090         CONV(I17)=1.0-((1.0-VOIDF(I17))/
5100       1           (1.0-VOIDF(1)))*((RS/RSO)**3)
5110         IF(I16 .GE. 5)THEN
5120            DCON(I17)=CONV(I17)-CONV(I12)
5130         ELSE
5140            DCON(I17)=0.0
5150         ENDIF
5160         WRITE(9,1111)I16
5170  1111   FORMAT(5X,'STEP='I5/)
5180         WRITE(9,1002)RS,VS,VOIDF(I17),INC1,
5190       1           IPIN1,ND,CONV(I17),DCON(I17)
5200  1002   FORMAT(5X,'RS=',E10.4,2X,'VS=',E10.4,2X,'VOIDF=',E10.4/
5210       1  5X,'INC1=',I5,2X,'IPIN1=',I5,2X,'ND=',I5/
5220       2  5X,'CONVERSION=',E10.4,2X,'DELTA CONVER=',E10.4///)
5230         WRITE(8,444)I16,VOIDF(I17),CONV(I17),
5240       1           DCON(I17),CF,KOUNT1,RLN,XLN
5250  444    FORMAT(1X,I4,1X,E9.4,1X,E9.4,1X,
5260       1          E9.4,1X,E9.4,1X,I4,1X,E9.4,1X,E9.4)
5270 C
```

```
5280 C    Increasing void diameters if they are connected to the
5290 C    outside.
5300 C
5310        DO 905 ICLU=2,ICLUSTER
5320           IF((MAT(ICLU,IN3) .EQ. 1))THEN
5330              DO 910 KCON=1,INC1
5340                 IF((MAT(ICLU,KCON) .EQ. 1))THEN
5350                    VDIA(KCON)=VDIA(KCON)+2.0*QCONV
5360                 ELSE
5370                    CONTINUE
5380                 ENDIF
5390  910          CONTINUE
5400           ELSE
5410              CONTINUE
5420           ENDIF
5430  905   CONTINUE
5440        IPIN1=IPIN
5450  5000 CONTINUE
5460 C
5470 C    Main loop ends.
5480 C
5490       STOP
5500       CLOSE(7)
```

```
5510        CLOSE(8)
5520        CLOSE(9)
5530        END
```

Appendix X

TGA EXPERIMENTAL CONDITIONS

This Appendix shows the details of the experimental conditions for the different sets of TGA experiments that were done. All the chars used were derived from PSOC 1451 coal. Experiments done on other chars are not reported in this thesis.

Table AX.6 shows the organization of a typical data file after the raw data have been converted to suitable form. Time, in seconds, is shown in column 1. Data points were collected everysix seconds by a computerized data acquisition system. Column 2 shows the normalized carbon mass of the sample. The normalizing factor is the carbon mass at the moment the oxidizer reaches the sample. Column 3 shows the rate of loss of carbon normalized by the instantaneous carbon mass. Sample temperature, as recorded by a thermocouple is shown in column 4. Finally, the carbon conversion is shown in the last column. Since all samples were burned until there was no further weight loss, the final mass was taken to be the mass of ash.

Table AX.1 shows two sets of similar experiments done at TGA temperatures of 800K and 1100K. In each set, two char sizes (45-53μm and 90-104μm) were used. Finally, four different pyrolysis temperatures (1000K, 1200K, 1400K, and 1600K) were used for each size and TGA temperature. The parent coal was also used. In all experiments, the total flow rate (110 cc/min) and oxygen concentration (17%) was kept constant. All chars used for experiments in Table AX.1 were made from parent coal of size 53-90μm. The experiments in Table AX.2 were exactly like those in Table AX.1, the only difference being the parent coal size. The effect of initial mass was investigated in the runs shown in Table AX.3. The behaviour of chars made from large size coal particles was investigated in the runs reported

in Table AX.4. Finally, Table AX.5 shows experiments in which only the oxygen concentration was varied.

RUN NAME	COAL SIZE	CHAR SIZE	PYROLYSIS TEMPERATURE	OXYGEN CONCENTRATION	INITIAL MASS	TGA TEMPERATURE	COMMENTS
	(μm)	(μm)	(K)	(%)	(mg)	(K)	
CAN1.DAT	53-90	45-53	1600	17	13.403	1100	(In all runs
CAN2.DAT			1400		11.328		the total flow
CAN3.DAT			1200		10.132		rate was 110cc/min)
CAN4.DAT			1000		15.234		
CAN5.DAT	45-53	—	—		17.383		
CAN11.DAT	53-90	104-125	1600	17	12.524	1100	(Total flow rate
CAN12.DAT			1400		13.306		=110 cc/min)
CAN13.DAT			1200		9.766		
CAN14.DAT			1000		12.207		
CAN15.DAT	104-125	—	—		11.914		
CAN21.DAT	53-90	45-53	1600	17	10.864	800	(Total flow rate
CAN22.DAT			1400		12.231		=110 cc/min)
CAN23.DAT			1200		13.770		
CAN24.DAT			1000		12.524		
CAN25.DAT	45-53	—	—		10.278		
CAN25A.DAT	45-53	—	—		18.164		
CAN31.DAT	53-90	104-125	1600	17	10.962	800	(Total flow rate
CAN32.DAT			1400		13.281		=110 cc/min)
CAN33.DAT			1200		10.938		
CAN34.DAT			1000		11.719		
CAN35.DAT	104-125	—	—		19.067		

Table AX.1 TGA runs on chars from PSOC 1451 53-90μm coal.

RUN NAME	COAL SIZE	CHAR SIZE	PYROLYSIS TEMPERATURE	OXYGEN CONCENTRATION	INITIAL MASS	TGA TEMPERATURE	COMMENTS
	(μm)	(μm)	(K)	(%)	(mg)	(K)	
DAN1.DAT	L.T. 45	45-53	1600	17	6.543	1100	(In all runs
DAN2.DAT			1400		5.078		the total flow
DAN3.DAT			1200		5.176		rate was 110cc/min)
DAN4.DAT			1000		5.884		
DAN5.DAT							=CAN5.DAT
DAN11.DAT	L.T. 45	104-125	1600	17	10.742	1100	(Total flow rate
DAN12.DAT			1400		10.156		=110 cc/min)
DAN13.DAT			1200		4.688		
DAN14.DAT			1000		5.005		
DAN15.DAT							=CAN15.DAT
DAN21.DAT	L.T. 45	45-53	1600	17	5.542	800	(Total flow rate
DAN22.DAT			1400		5.762		=110 cc/min)
DAN23.DAT			1200		5.151		
DAN24.DAT			1000		6.445		
DAN25.DAT							=CAN25.DAT
DAN31.DAT	L.T. 45	104-125	1600	17	5.347	800	(Total flow rate
DAN32.DAT			1400		5.151		=110 cc/min)
DAN33.DAT			1200		4.785		
DAN34.DAT			1000		4.712		
DAN35.DAT							=CAN35.DAT

Table AX.2 TGA runs on chars from PSOC 1451 <45μm coal.

RUN NAME	COAL SIZE	CHAR SIZE	PYROLYSIS TEMPERATURE	OXYGEN CONCENTRATION	INITIAL MASS	TGA TEMPERATURE	COMMENTS
	(μm)	(μm)	(K)	(%)	(mg)	(K)	
MAN1.DAT	90-125	125-147	1600	17	5.762	1100	(In all runs
MAN2.DAT					3.057		the total flow
MAN3.DAT					1.338		rate was 110cc/min)
MAN4.DAT					19.824		
MAN5.DAT					11.523		
MAN6.DAT					1.963		

Table AX.3 Effect of initial sample mass on TGA runs.

RUN NAME	COAL SIZE	CHAR SIZE	PYROLYSIS TEMPERATURE	OXYGEN CONCENTRATION	INITIAL MASS	TGA TEMPERATURE	COMMENTS
	(μm)	(μm)	(K)	(%)	(mg)	(K)	
FAN1.DAT	90-125	L.T. 53	1600	17	5.078	1100	(Flow rate=110cc/min)
FAN11.DAT		125-147			5.762		=MAN1.DAT
FAN21.DAT	90-125	L.T. 53	1600	17	5.371	800	(Flow rate=110cc/min)
FAN31.DAT		125-147			5.029		

Table AX.4 Effect of char size and TGA temperature.

RUN NAME	COAL SIZE	CHAR SIZE	PYROLYSIS TEMPERATURE	OXYGEN CONCENTRATION	INITIAL MASS	TGA TEMPERATURE	COMMENTS
	(μm)	(μm)	(K)	(%)	(mg)	(K)	
GAN1.DAT	90-125	125-147	1600	21.0	4.883	1100	(Total flow rate
GAN2.DAT				19.1	4.980		=110 cc/min)
GAN3.DAT				17.0	5.762		=MAN1.DAT
GAN4.DAT				15.3	5.273		
GAN5.DAT				11.5	5.200		
GAN6.DAT				07.6	4.980		
GAN7.DAT				81.9	5.176		
GAN8.DAT				45.5	5.249		

Table AX.5 Effect of oxygen concentration on TGA runs.

TIME	$\frac{M_c}{M_{c,i}}$	$\frac{1}{M_c}\frac{dM_c}{dt}$	SAMPLE TEMPERATURE	CARBON CONVERSION
(s)		(s^{-1})	(K)	(%)

Table AX.6 Data file format for TGA experiments.

Appendix XI

DETAILS OF

CENOSPHERE SIMULATION RUNS

The initial conditions of all the simulation runs are shown in Tables in this Appendix. The Figures that follow show the variation of the void percolation probability (P) as a function of particle void fraction (ϵ) for the different cases.

The structure of the primary data file (MOD*runname*.DAT) produced by each simulation run is shown in Table AXI.1. Number of steps, void fraction, conversion and the rate of change of conversion are shown in columns 1-4, respectively. Column 5 shows the void percolation probability. The total number of voids connected to the outside of the particle, KOUNT1, is shown in the next column. Column 7 is the natural logarithm of the radius of gyration of the largest void cluster (RLN) and the last column is the natural logarithm of the number of voids in that cluster (XLN).

Tables AXI.2 and AXI.3 show the five main sets of simulations that were done. The initial number of voids in each case was kept reasonably similar and varied from set to set. In these runs the void size initially was monodisperse. Due to the random nature of the void placement process, particles having the same number of initial voids often have different initial void fractions. Table AXI.4 shows runs in which the size of the initial voids was randomly selected in the range 0-5 units while Table AXI.5 shows the runs where the initial size of the void was either 1 or 5 units, subject to the constraint that 90% of the voids be of the smaller size.

The effect of an assumed diffusion mechanism was tested in the runs shown in Table AXI.6. In each of the relevant Tables, the parent Fortran program name is also shown. A listing of one of the programs (CENMODE21.FOR) is given in

Appendix IX. The other programs are similar.

Number of Steps, N	Void frac., ϵ	Conv., X	dX/dN	Percolation Probability	KOUNT1	RLN	XLN

Table AXI.1 Typical data file organization (MOD*run name*.DAT).

RUN NAME	NO. OF VOIDS	INITIAL VOID FRAC.	PROGRAM	COMMENTS
A1.DAT	169	0.119	CENMOD20	Initially, voids were monodisperse. Particle diameter=50 Void diameter=5 True for all runs below.
A2.DAT	162	0.111		
A3.DAT	158	0.117		
A4.DAT	169	0.112		
A5.DAT	171	0.128		
A6.DAT	167	0.116		
A7.DAT	163	0.127		
C1.DAT	67	0.0519	CENMOD20	
C2.DAT	72	0.0588		
C3.DAT	71	0.0607		
C4.DAT	69	0.0594		
C5.DAT	73	0.0569		
C6.DAT	75	0.0575		
C7.DAT	66	0.0569		
E11.DAT	51	0.0434	CENMOD20	
E12.DAT	54	0.0362		
E13.DAT	54	0.0328		
E14.DAT	55	0.0469		
E15.DAT	52	0.0359		
E16.DAT	52	0.0348		
E17.DAT	53	0.0348		
E18.DAT	53	0.0294		

Table AXI.2 Basic simulation runs. Initially monodisperse voids.

RUN NAME	NO. OF VOIDS	INITIAL VOID FRAC.	PROGRAM	COMMENTS
B1	108	0.0807	CENMOD20	Initially, voids were monodisperse. Particle diameter=50 Void diameter=5 True for all runs below.
B2	104	0.0814		
B3	110	0.0695		
B4	117	0.0665		
B5	106	0.0814		
B6	118	0.0866		
B7	120	0.0956		
B11	104	0.0845		
B12	105	0.0852		
B13	107	0.0861		
B14	107	0.0734		
B15	104	0.0826		
B16	106	0.0872		
B17	107	0.0835		
B18	104	0.0780		
D1	216	0.143	CENMOD20	
D2	216	0.161		
D3	215	0.154		
D4	212	0.139		
D5	218	0.148		
D6	214	0.152		
D7	214	0.159		
D11	215	0.147		
D12	215	0.136		
D13	216	0.148		
D14	216	0.139		
D15	212	0.139		
D16	214	0.141		
D17	216	0.168		
D18	216	0.163		

Table AXI.3 Basic simulation runs. Initially monodisperse voids.

RUN NAME	NO. OF VOIDS	INITIAL VOID FRAC.	PROGRAM	COMMENTS
B21	105	0.0225	CENMOD21	Initially, voids
B22	107	0.0260		were randomly sized
B23	107	0.0283		in the range 0–5.
B24	106	0.0206		Particle diameter=50.
B25	105	0.0233		True for all runs
B26	104	0.0274		below.
D21	120	0.0564	CENMOD21	
D22	104	0.0479		
D23	105	0.0472		
D24	107	0.0453		

Table AXI.4 Simulations with initially random sized voids.

RUN NAME	NO. OF VOIDS	INITIAL VOID FRAC.	PROGRAM	COMMENTS
G21	172	0.0192	CENMOD22	Bimodal voids:
G22	175	0.0153		90% were 5 and 10%
G23	177	0.0158		were 1 in diameter.
G24	172	0.0120		Particle diameter=50.
G25	177	0.0140		

Table AXI.5 Simulations with initially bimodal voids.

RUN NAME	NO. OF VOIDS	INITIAL VOID FRAC.	PROGRAM	COMMENTS
B1D	105	0.0833	CENMOD20D	Void diameter=5.
B2D	097	0.0646		Particle diameter=50.
B3D	101	0.0749		With diffusion.
B4D	104	0.0774		
B5D	104	0.0883		
B4N	104	0.0774	CENMOD20N	Without diffusion.
B5N	104	0.0883		

Table AXI.6 Simulations showing the effect of diffusion.

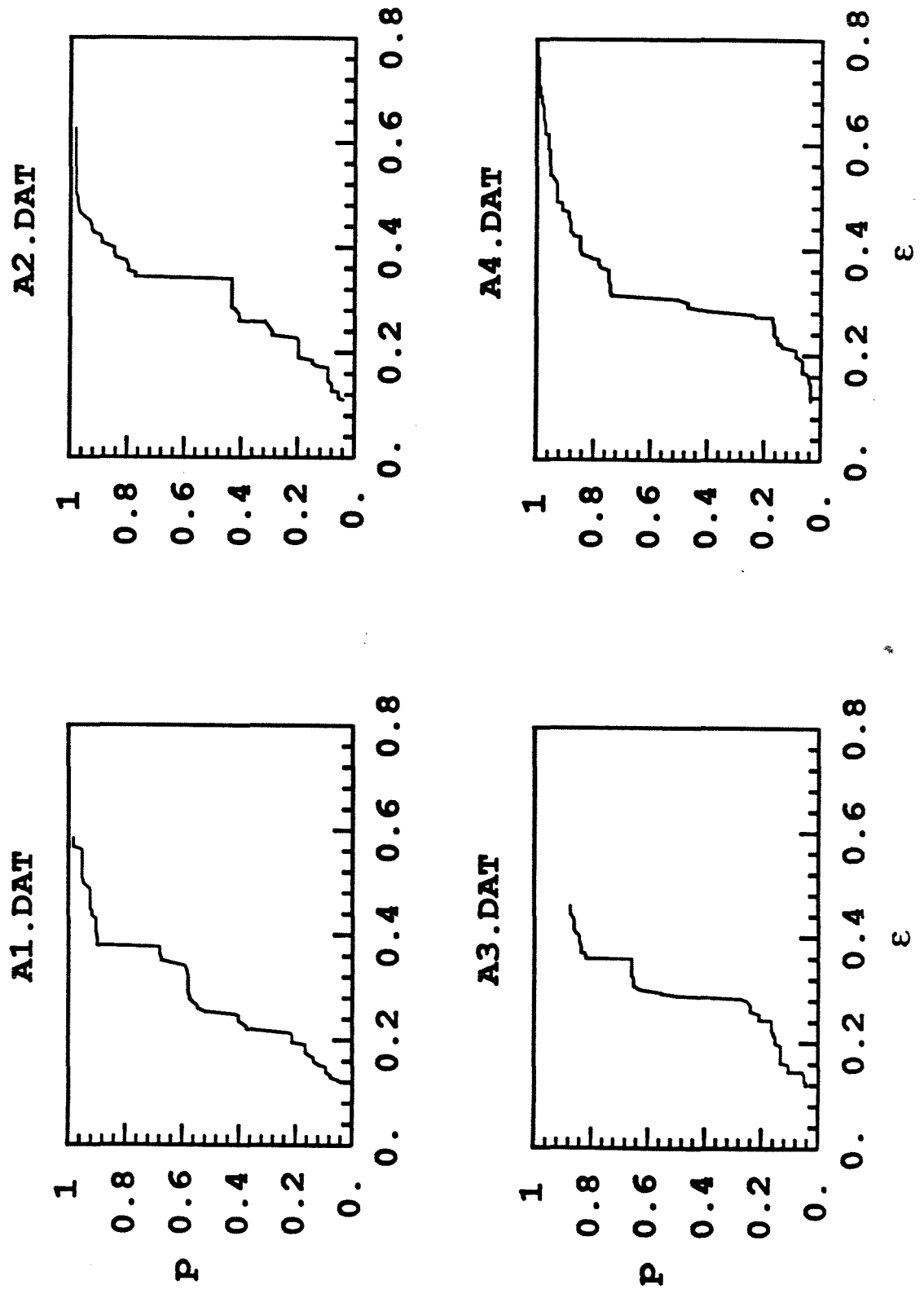
A1.DAT
A2.DAT
A3.DAT
A4.DAT
p
ε
0.
0.2
0.4
0.6
0.8
1

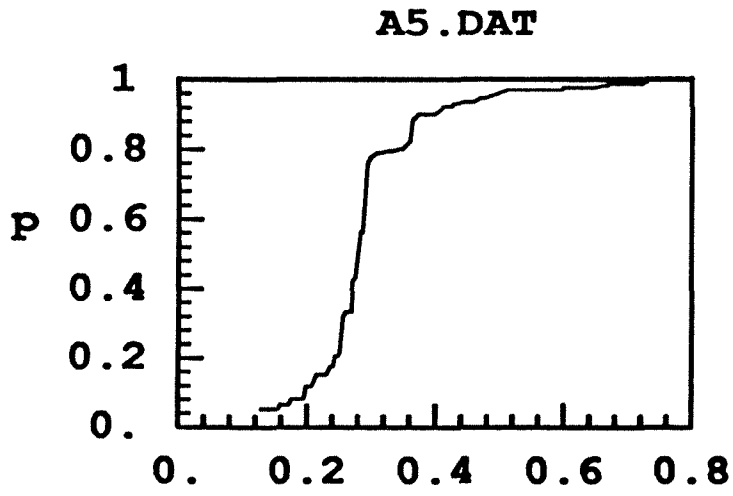
A5.DAT
1
0.8
0.6
0.4
0.2
0.
p
0.
0.2
0.4
0.6
0.8

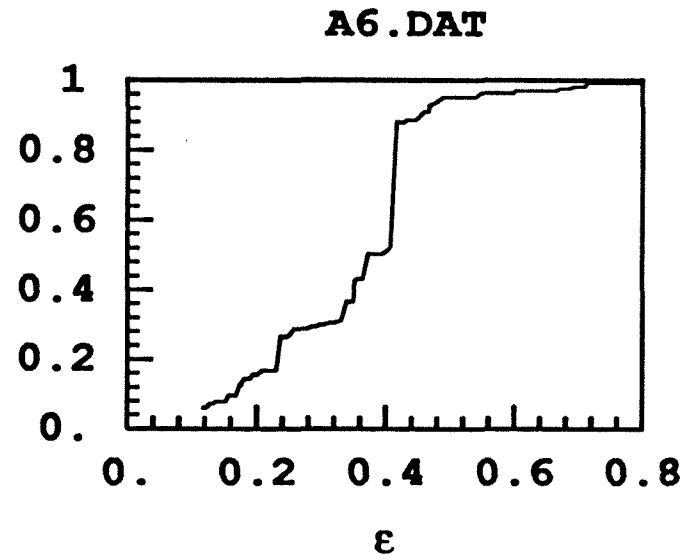
A6.DAT
1
0.8
0.6
0.4
0.2
0.
0.
0.2
0.4
0.6
0.8
ε

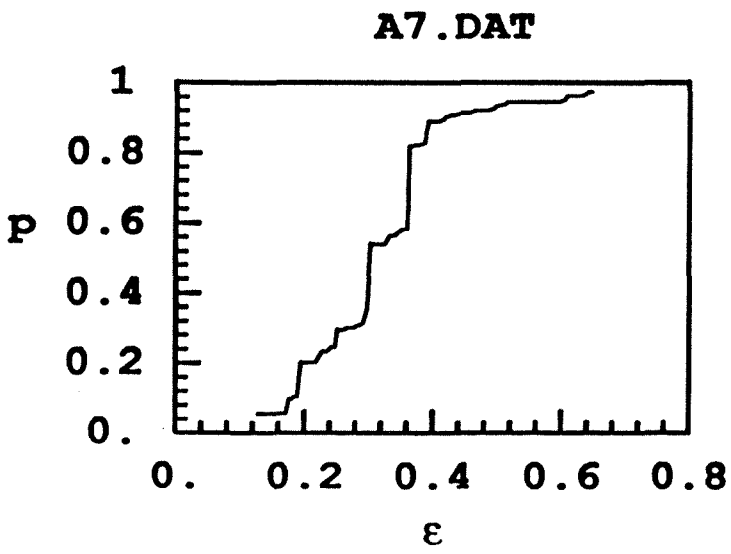
A7.DAT
1
0.8
0.6
0.4
0.2
0.
p
0.
0.2
0.4
0.6
0.8
ε

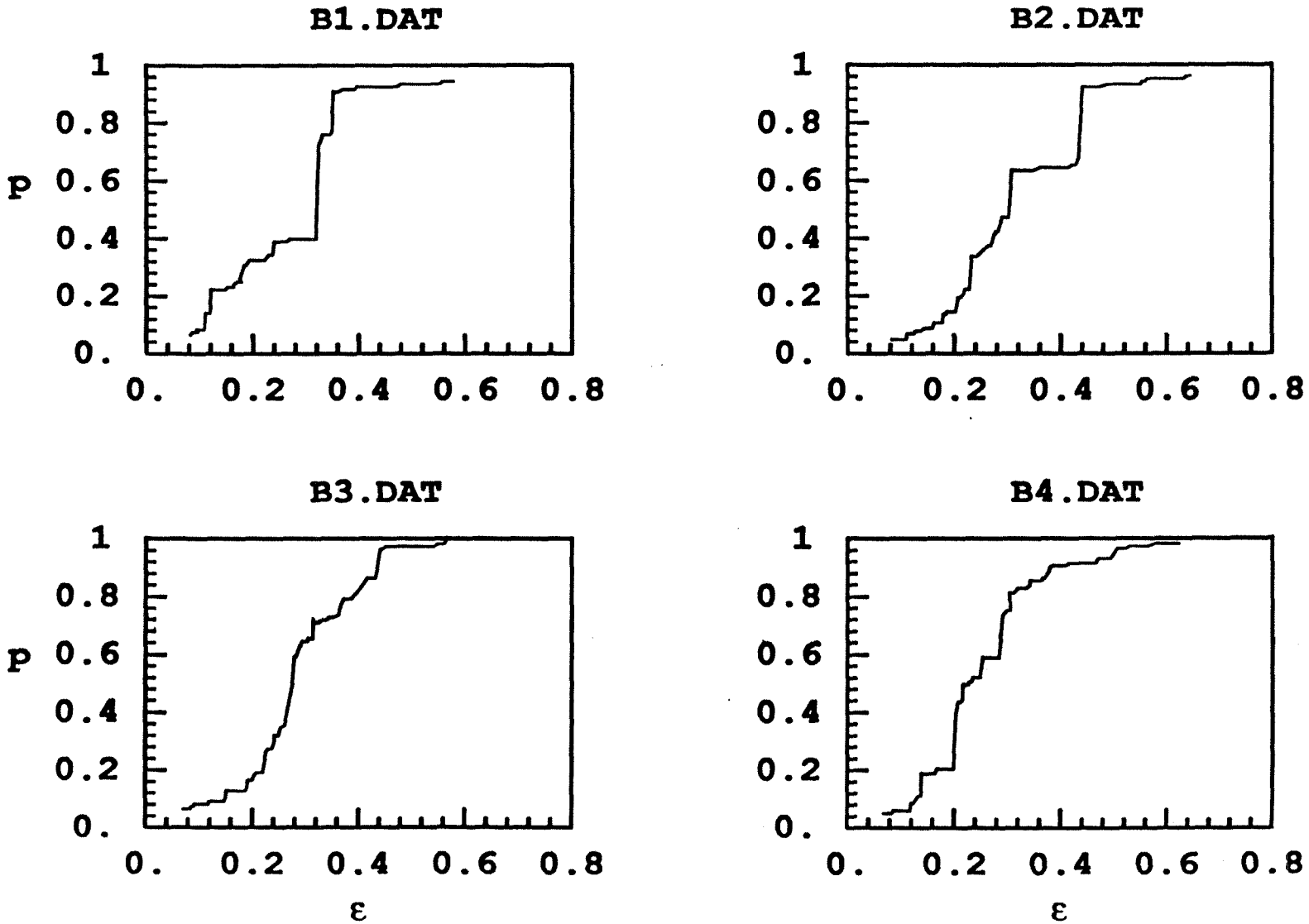
B1.DAT
B2.DAT
B3.DAT
B4.DAT
p
ε
1
0.8
0.6
0.4
0.2
0.
0.2
0.4
0.6
0.8

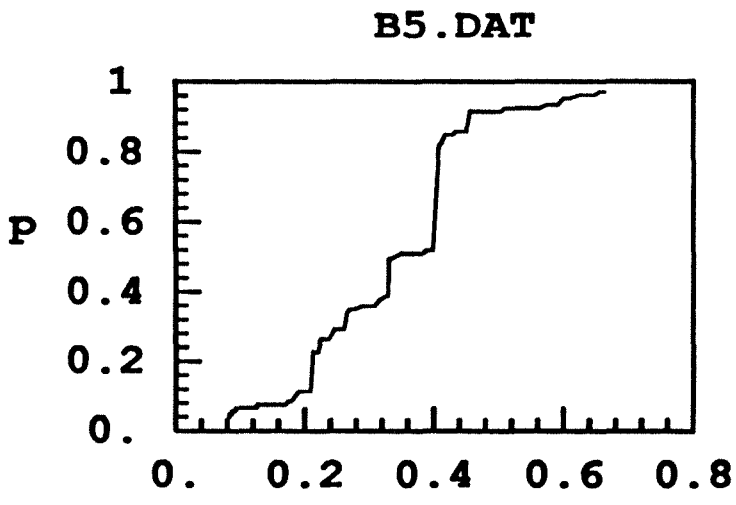
B5.DAT
p
1
0.8
0.6
0.4
0.2
0.
0.
0.2
0.4
0.6
0.8

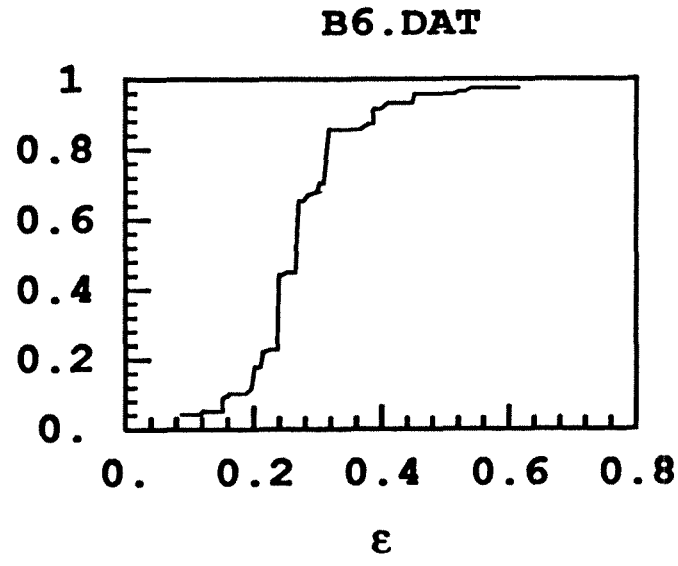
B6.DAT
1
0.8
0.6
0.4
0.2
0.
0.
0.2
0.4
0.6
0.8
ε

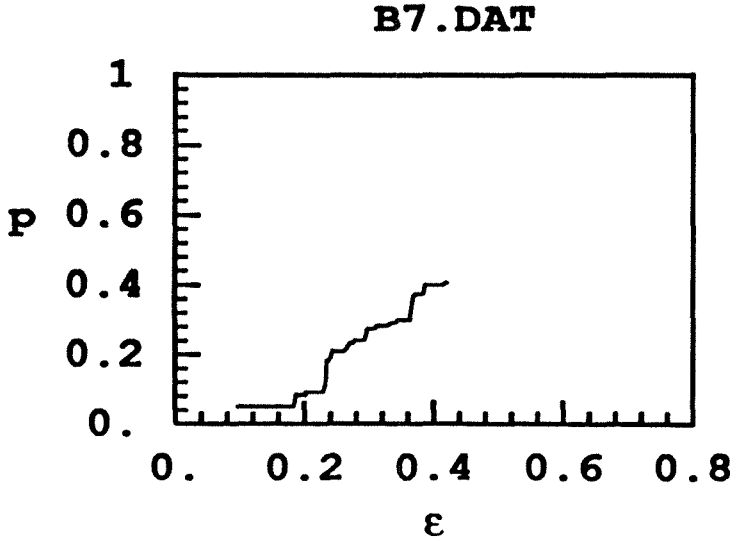
B7.DAT
p
1
0.8
0.6
0.4
0.2
0.
0.
0.2
0.4
0.6
0.8
ε

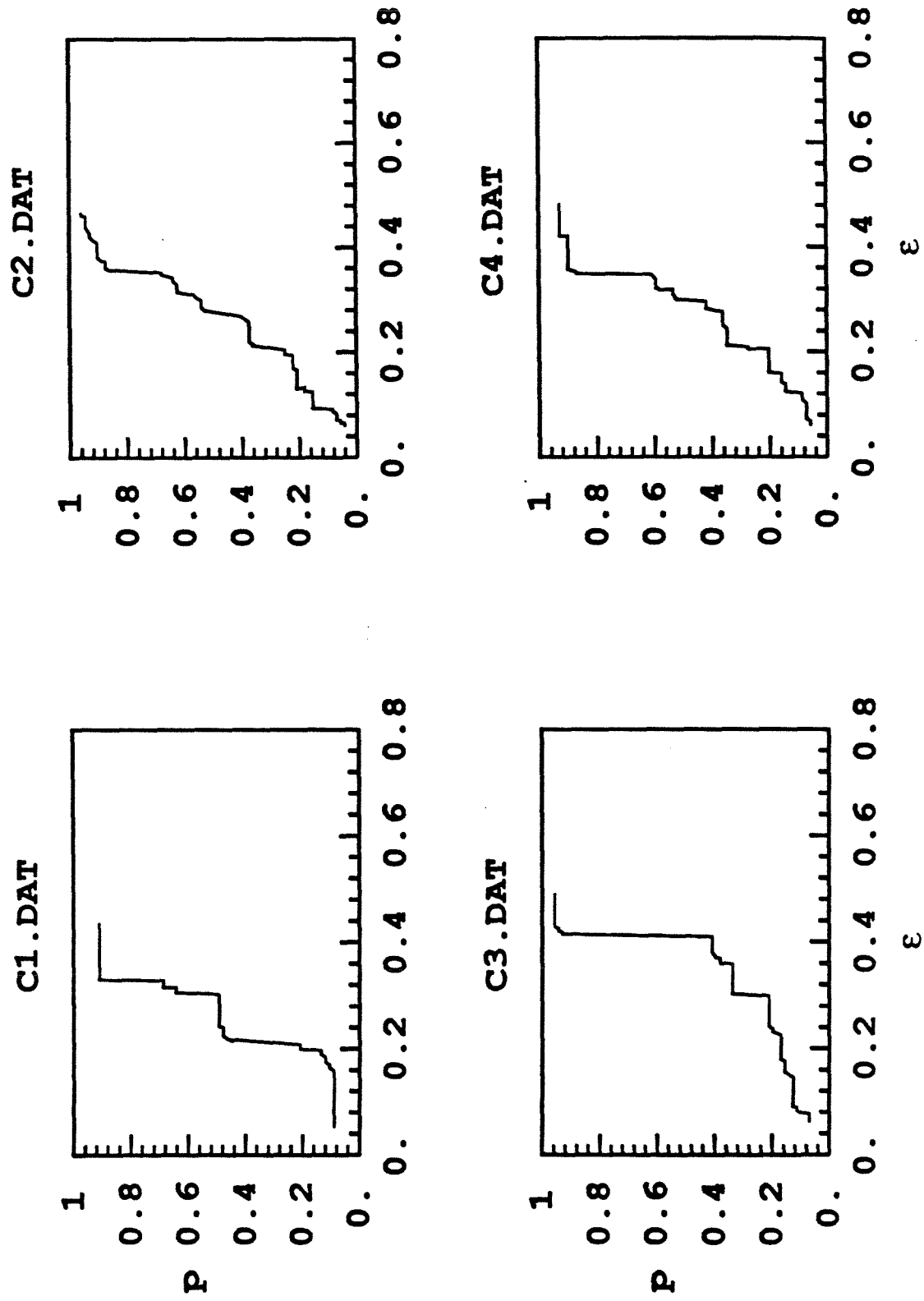
C1.DAT
C2.DAT
C3.DAT
C4.DAT
P
ε
1
0.8
0.6
0.4
0.2
0.
0.2
0.4
0.6
0.8

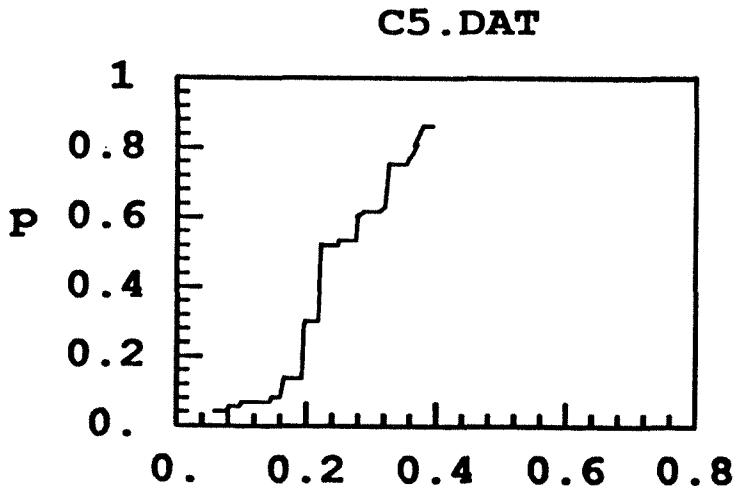
C5.DAT
1
0.8
0.6
0.4
0.2
0.
p
0.
0.2
0.4
0.6
0.8

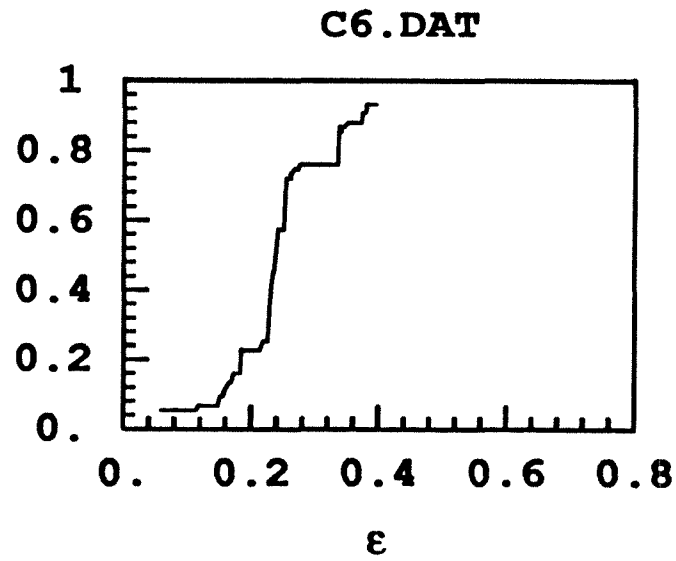
C6.DAT
1
0.8
0.6
0.4
0.2
0.
0.
0.2
0.4
0.6
0.8
ε

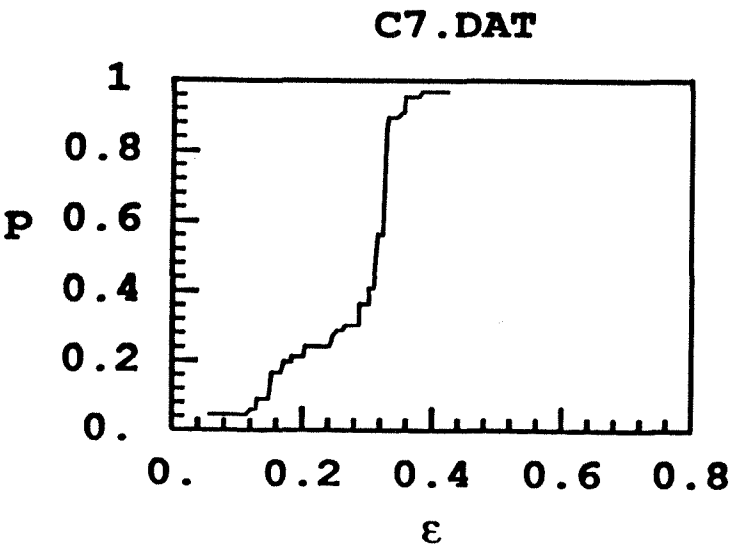
C7.DAT
1
0.8
0.6
0.4
0.2
0.
p
0.
0.2
0.4
0.6
0.8
ε

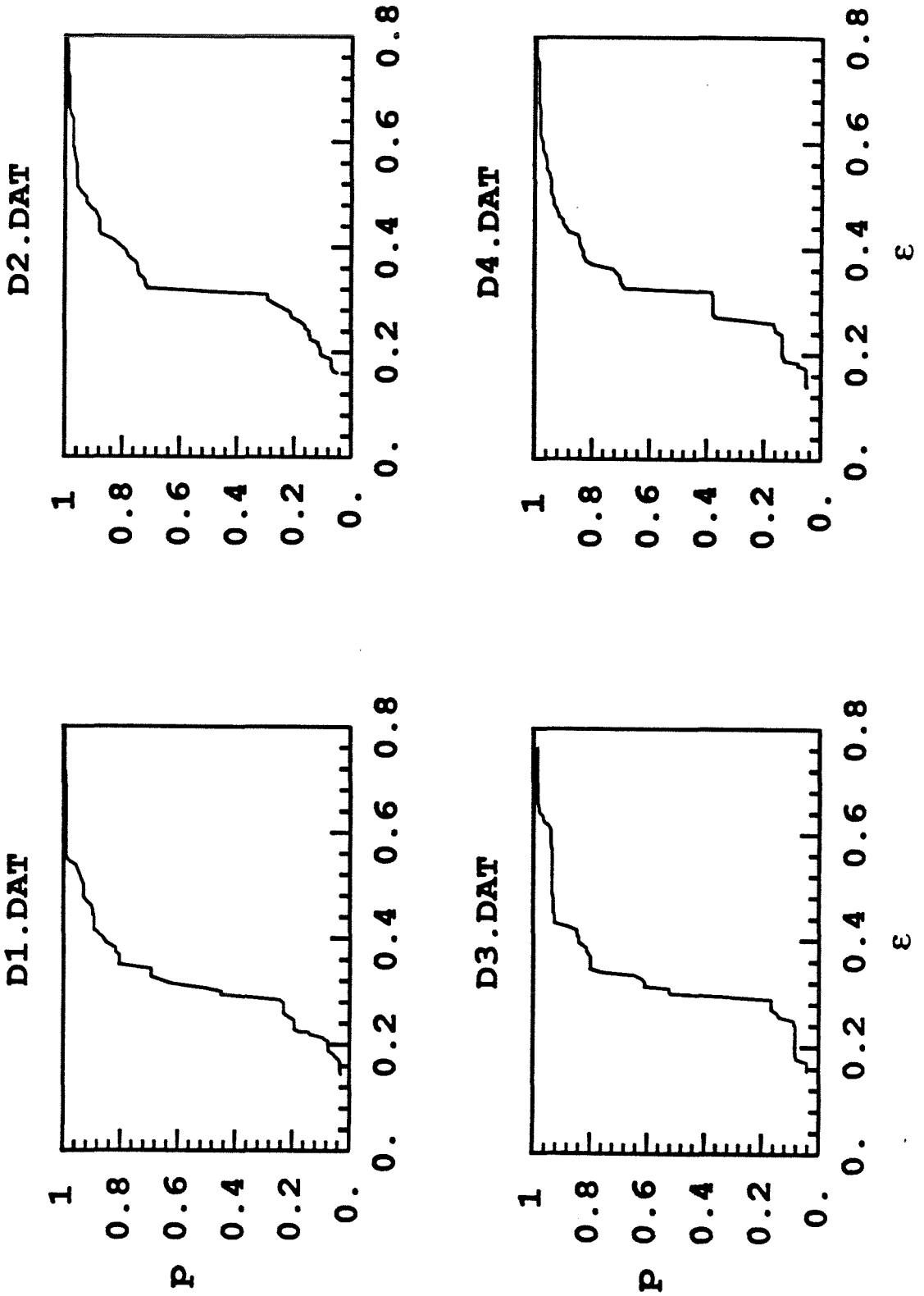
D1.DAT
D2.DAT
D3.DAT
D4.DAT
p
ε
1
0.8
0.6
0.4
0.2
0.
0.2
0.4
0.6
0.8

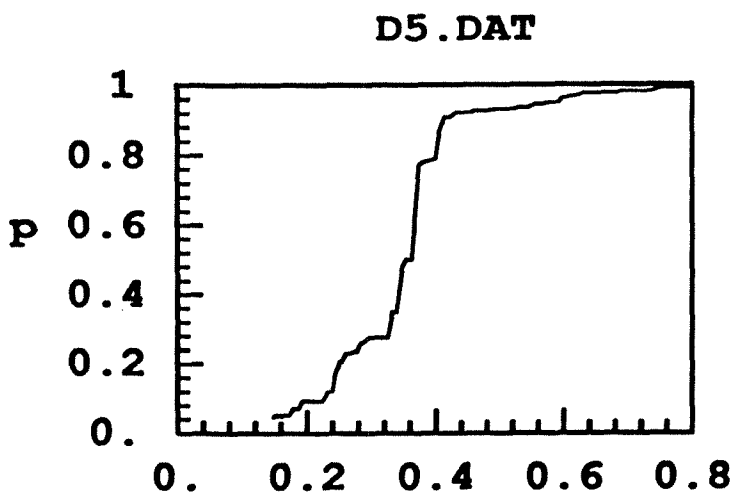
D5.DAT
p
1
0.8
0.6
0.4
0.2
0.
0.
0.2
0.4
0.6
0.8

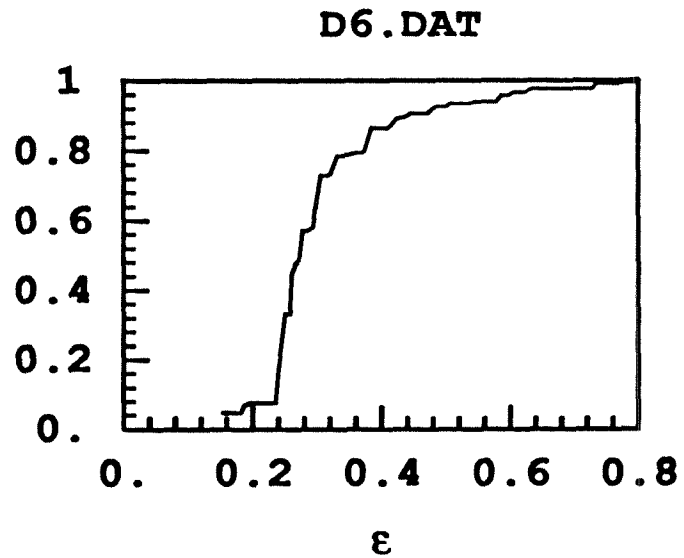
D6.DAT
1
0.8
0.6
0.4
0.2
0.
0.
0.2
0.4
0.6
0.8
ε

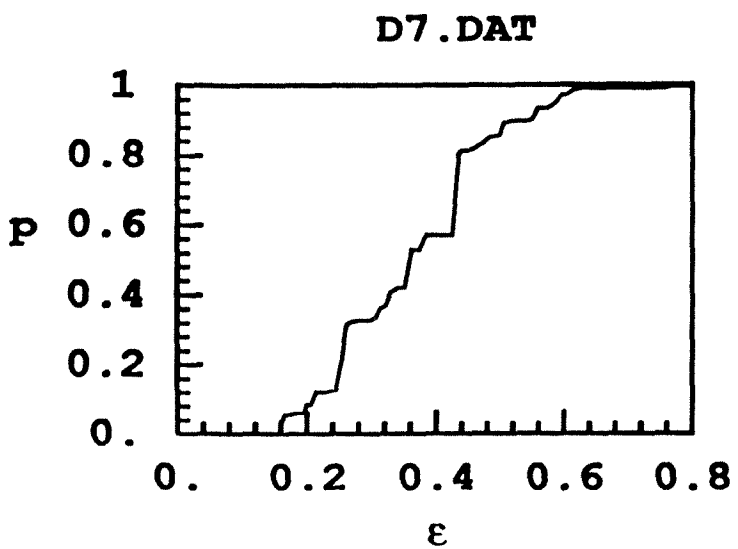
D7.DAT
p
1
0.8
0.6
0.4
0.2
0.
0.
0.2
0.4
0.6
0.8
ε

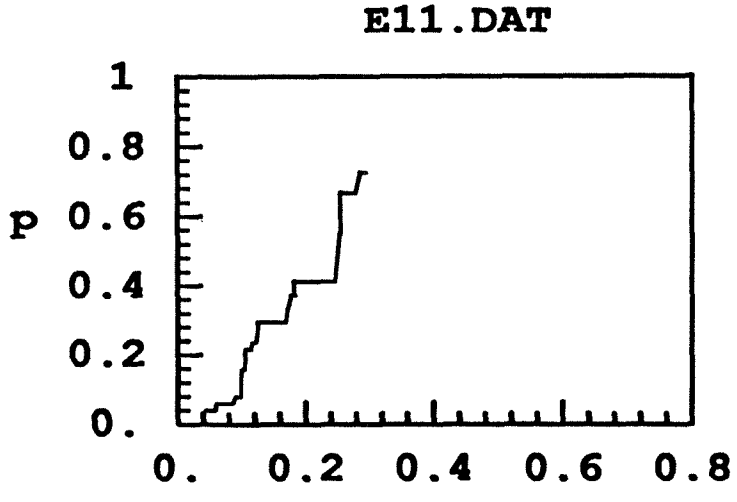
E11.DAT
p
1
0.8
0.6
0.4
0.2
0.
0.
0.2
0.4
0.6
0.8

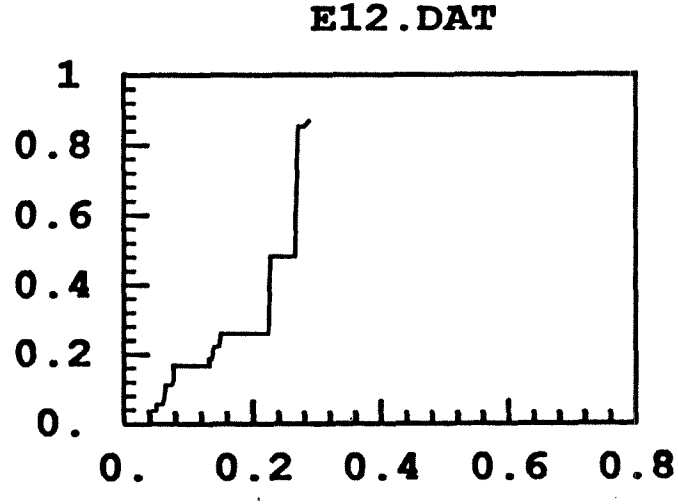
E12.DAT
1
0.8
0.6
0.4
0.2
0.
0.
0.2
0.4
0.6
0.8

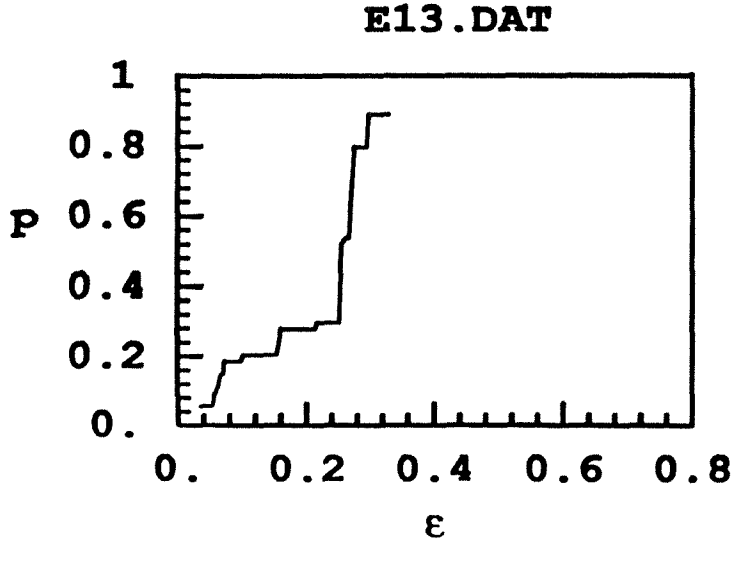
E13.DAT
p
1
0.8
0.6
0.4
0.2
0.
0.
0.2
0.4
0.6
0.8
ε

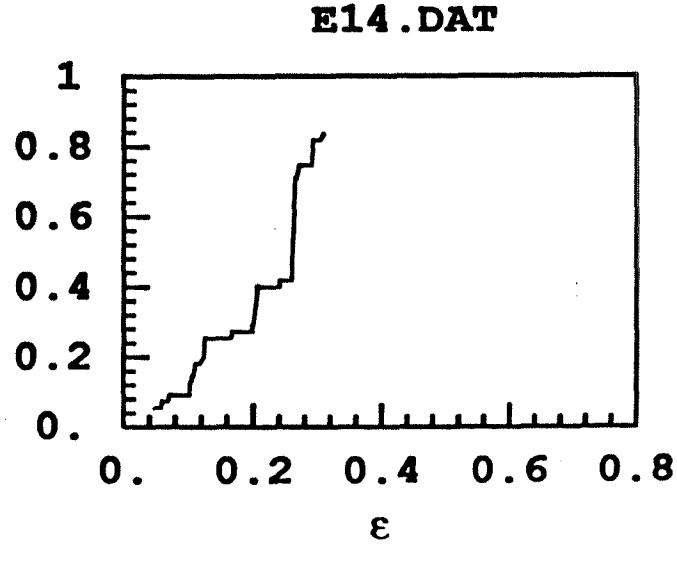
E14.DAT
1
0.8
0.6
0.4
0.2
0.
0.
0.2
0.4
0.6
0.8
ε

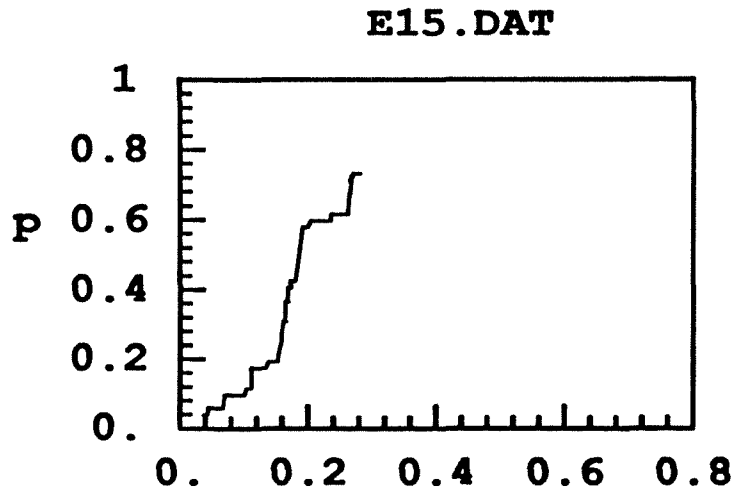
E15.DAT
p
1
0.8
0.6
0.4
0.2
0.
0.
0.2
0.4
0.6
0.8

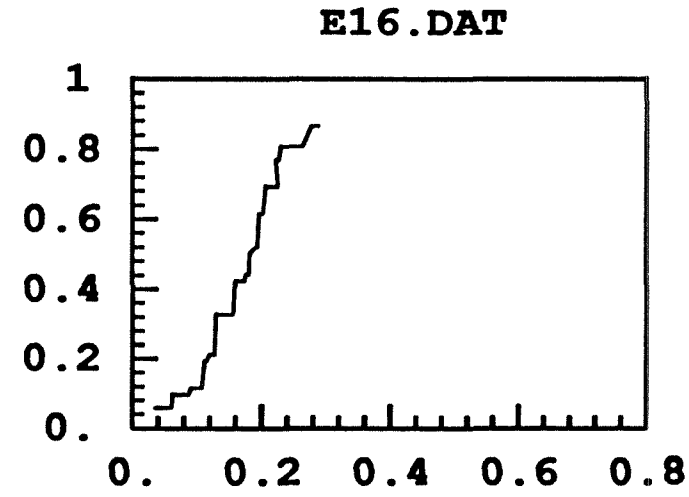
E16.DAT
1
0.8
0.6
0.4
0.2
0.
0.
0.2
0.4
0.6
0.8

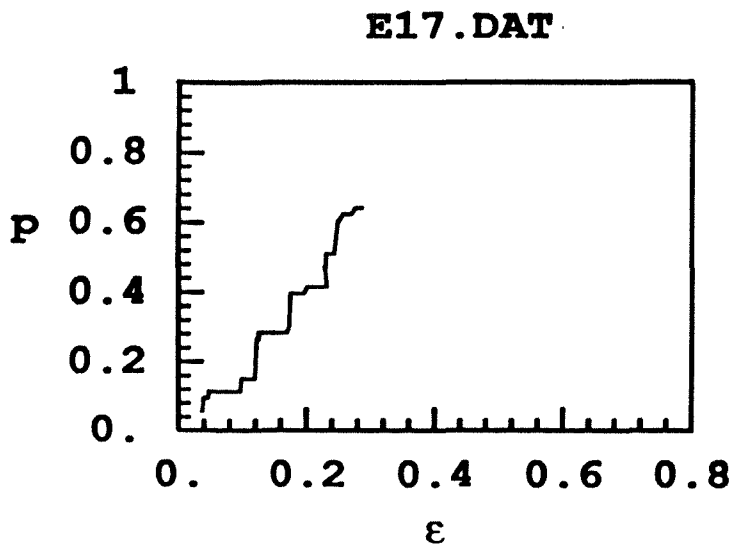
E17.DAT
p
1
0.8
0.6
0.4
0.2
0.
0.
0.2
0.4
0.6
0.8
ε

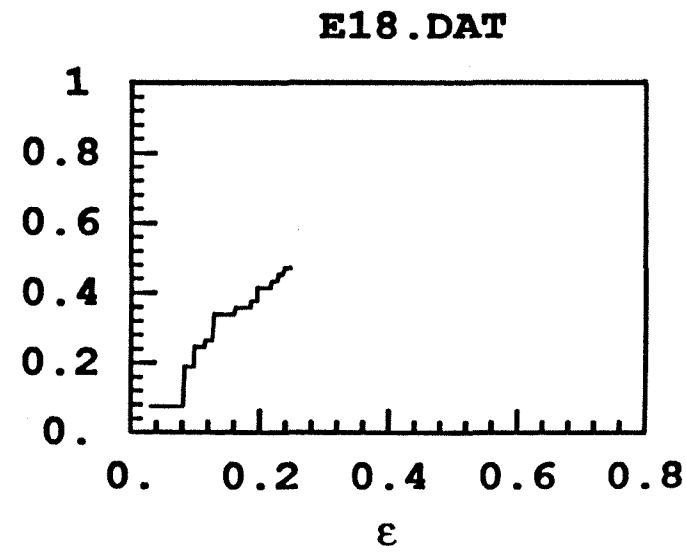
E18.DAT
1
0.8
0.6
0.4
0.2
0.
0.
0.2
0.4
0.6
0.8
ε

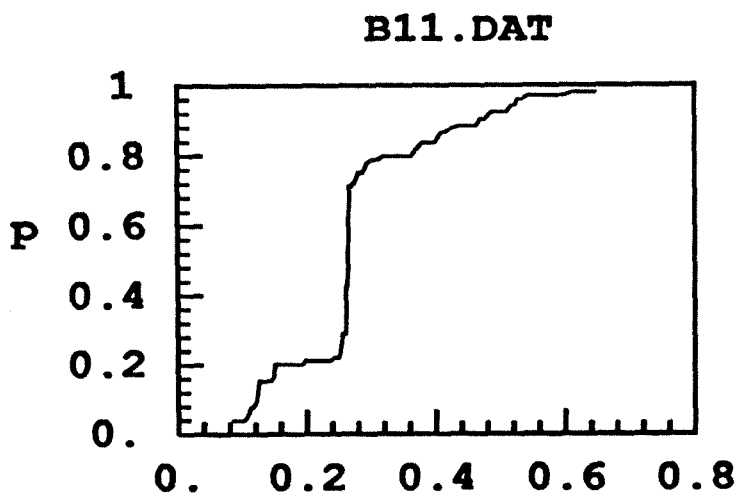
B11.DAT
p
1
0.8
0.6
0.4
0.2
0.
0.
0.2
0.4
0.6
0.8

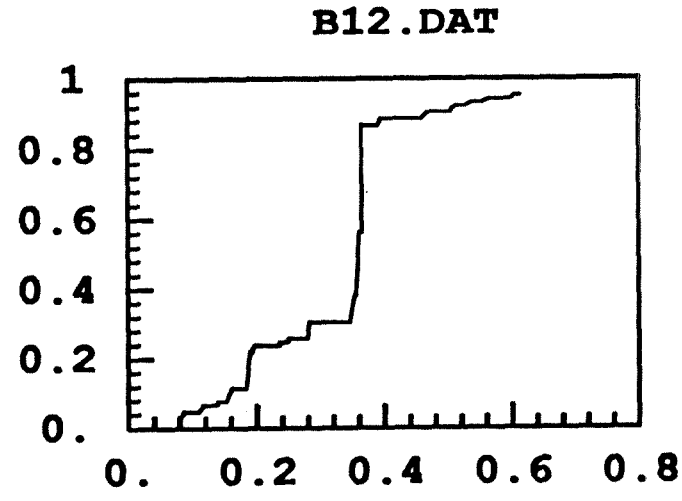
B12.DAT
1
0.8
0.6
0.4
0.2
0.
0.
0.2
0.4
0.6
0.8

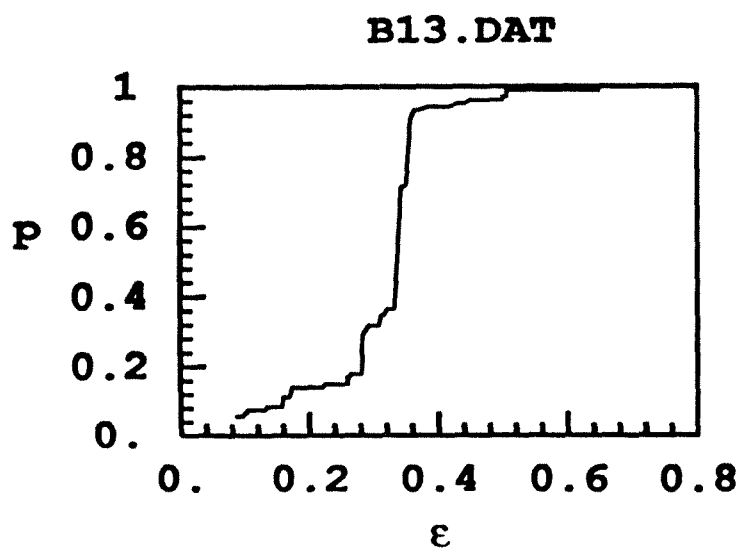
B13.DAT
p
1
0.8
0.6
0.4
0.2
0.
0.
0.2
0.4
0.6
0.8
ε

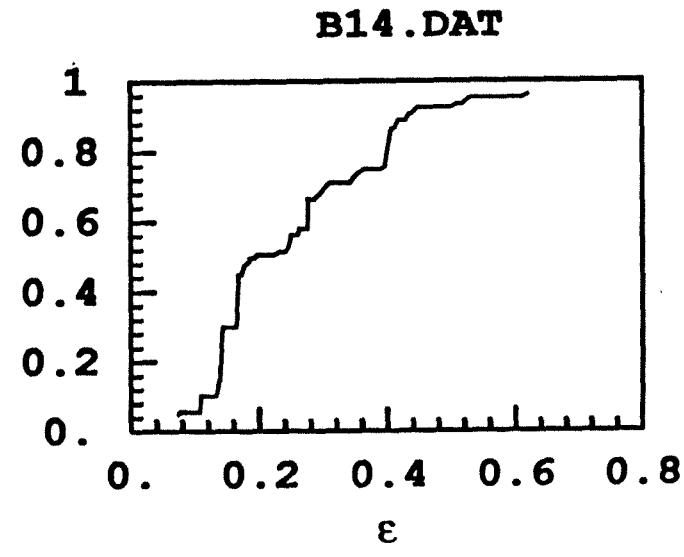
B14.DAT
1
0.8
0.6
0.4
0.2
0.
0.
0.2
0.4
0.6
0.8
ε

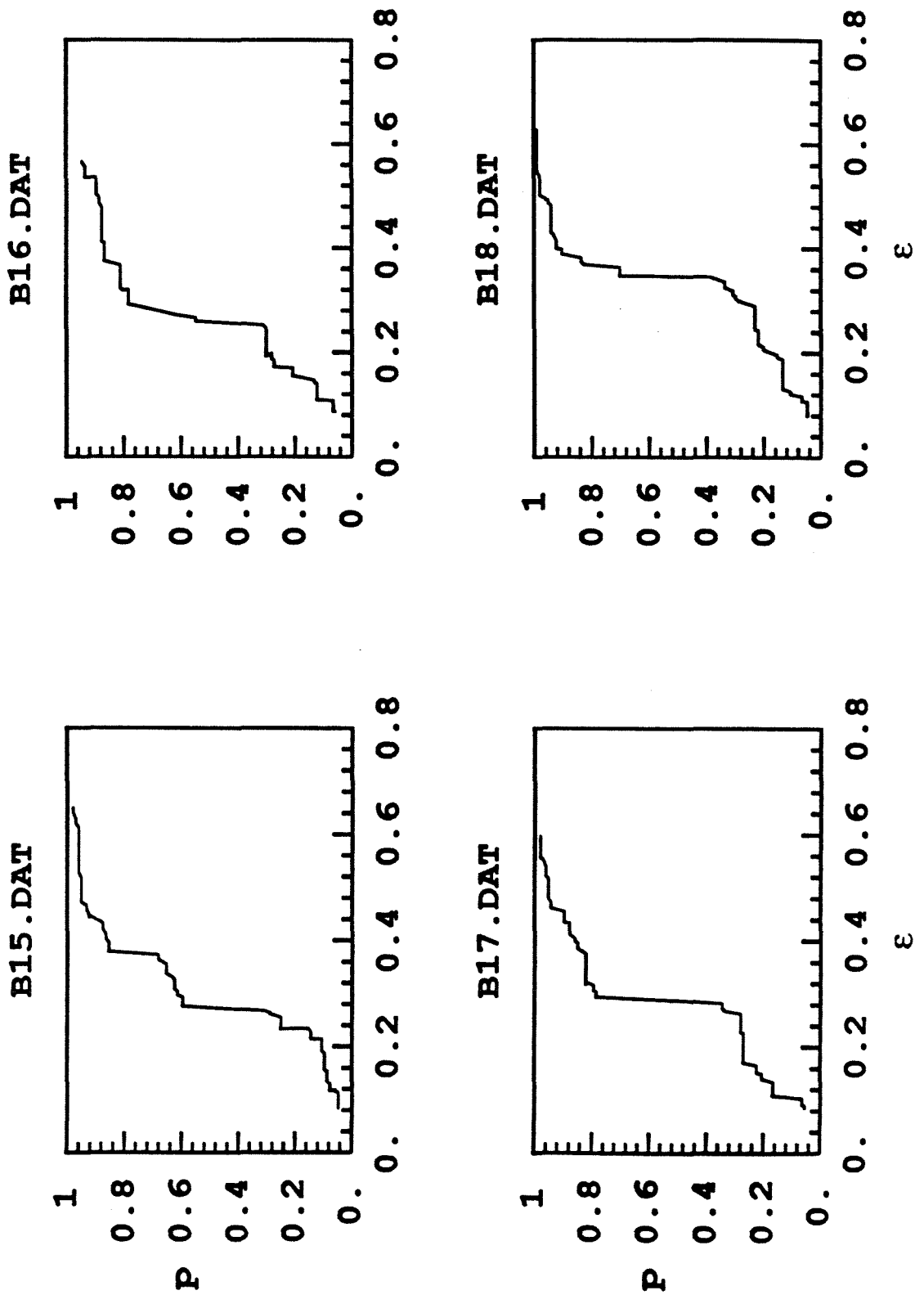
B15.DAT
B16.DAT
B17.DAT
B18.DAT
p
ε
1
0.8
0.6
0.4
0.2
0.
0.2
0.4
0.6
0.8

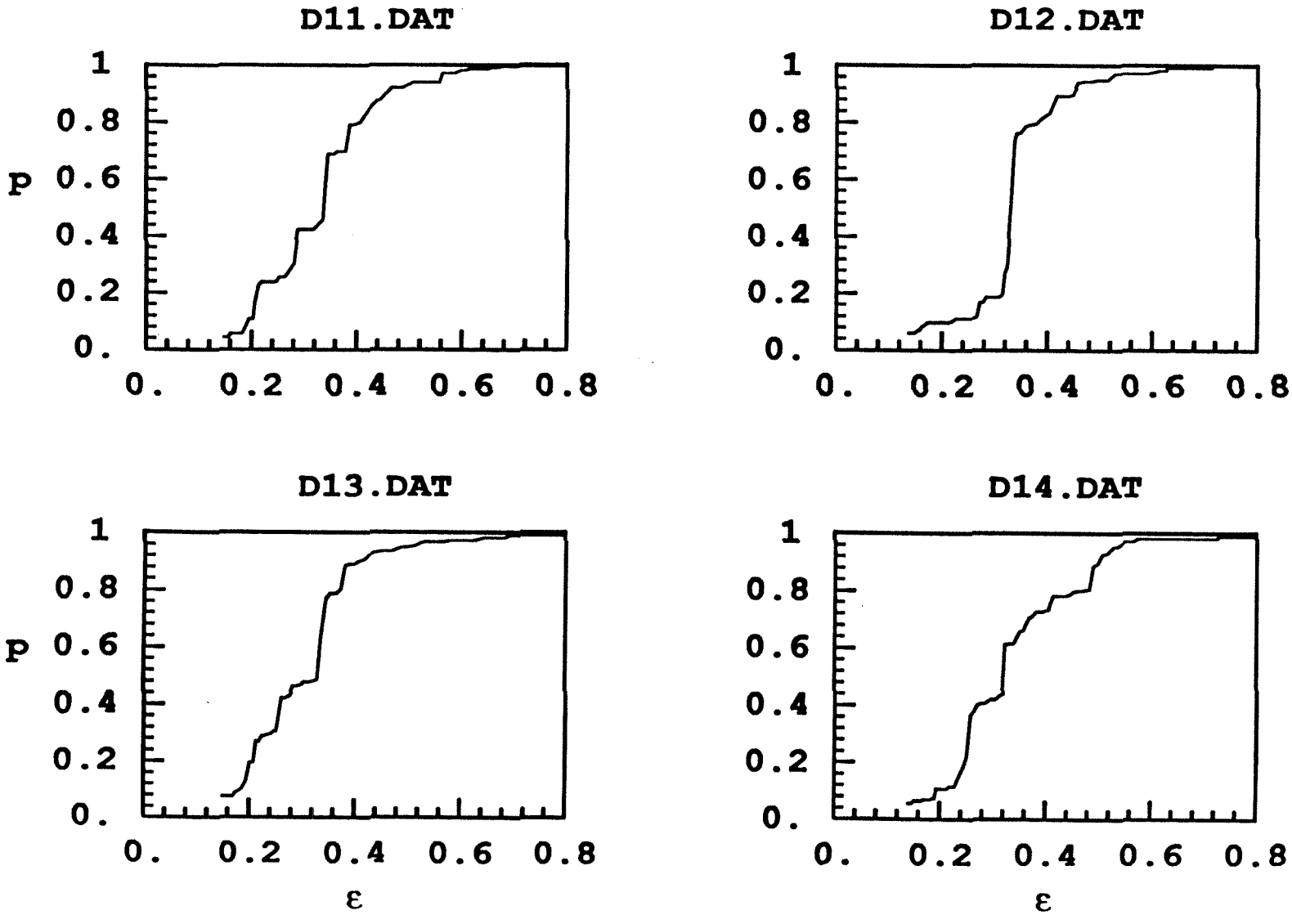
D11.DAT
D12.DAT
D13.DAT
D14.DAT
p
ε
1
0.8
0.6
0.4
0.2
0.
0.2
0.4
0.6
0.8

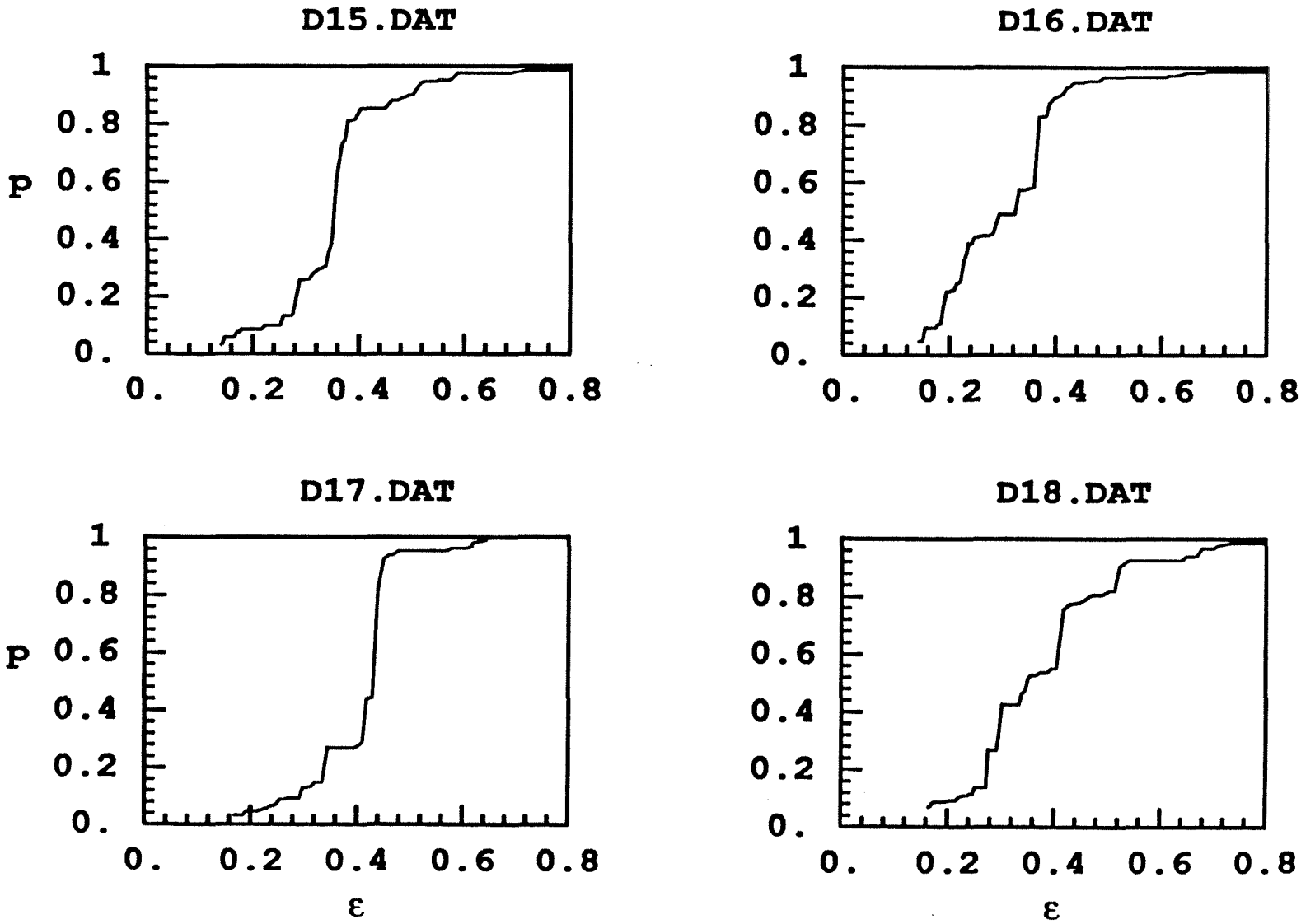
D15.DAT
D16.DAT
D17.DAT
D18.DAT
p
ε
1
0.8
0.6
0.4
0.2
0.
0.2
0.4
0.6
0.8

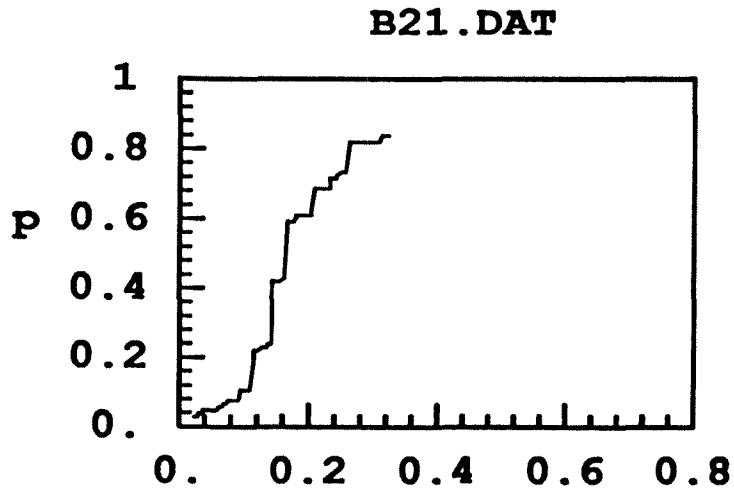
B21.DAT
p
1
0.8
0.6
0.4
0.2
0.
0.
0.2
0.4
0.6
0.8

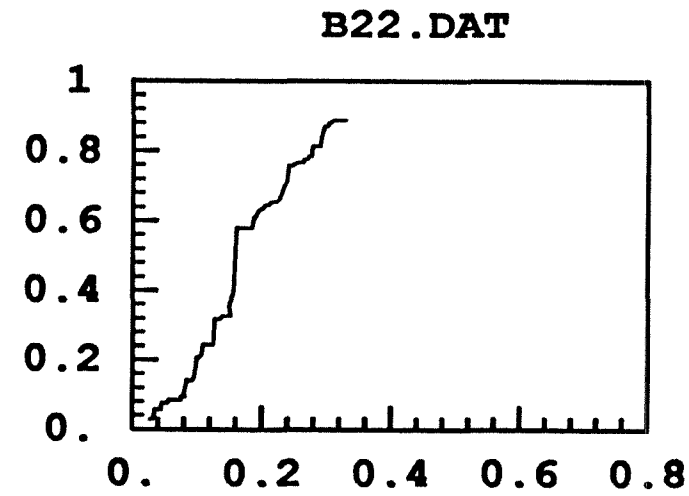
B22.DAT
1
0.8
0.6
0.4
0.2
0.
0.
0.2
0.4
0.6
0.8

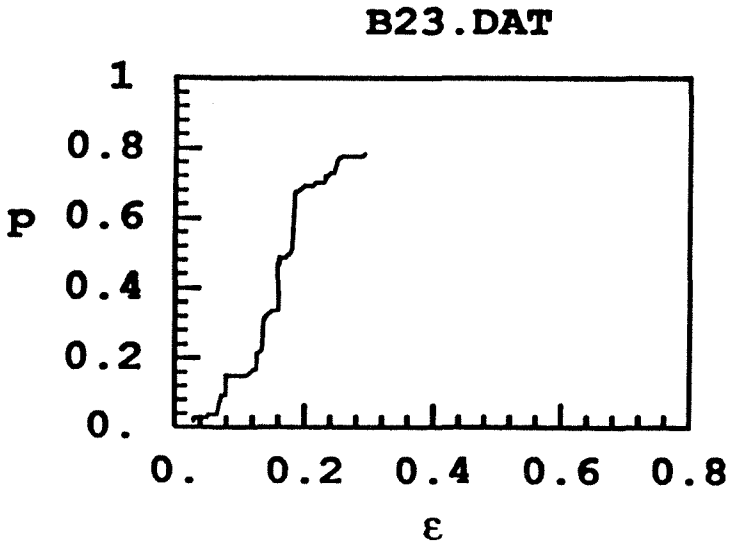
B23.DAT
p
1
0.8
0.6
0.4
0.2
0.
0.
0.2
0.4
0.6
0.8
ε

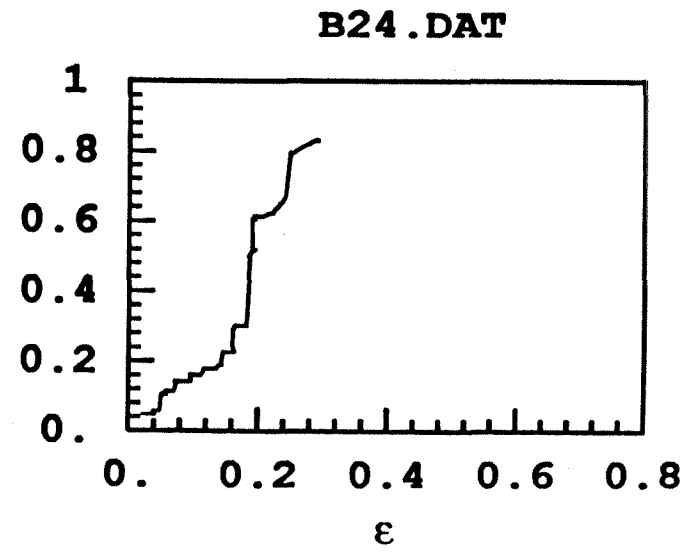
B24.DAT
1
0.8
0.6
0.4
0.2
0.
0.
0.2
0.4
0.6
0.8
ε

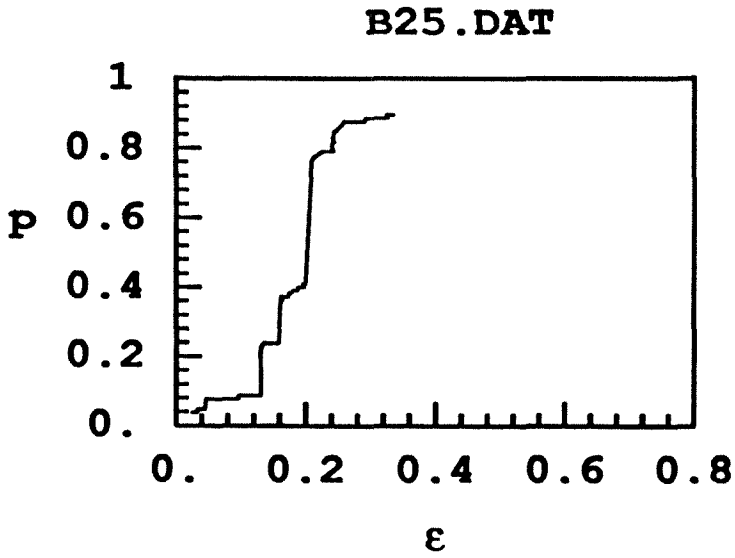
B25.DAT
1
0.8
0.6
0.4
0.2
0.
p
0.
0.2
0.4
0.6
0.8
ε

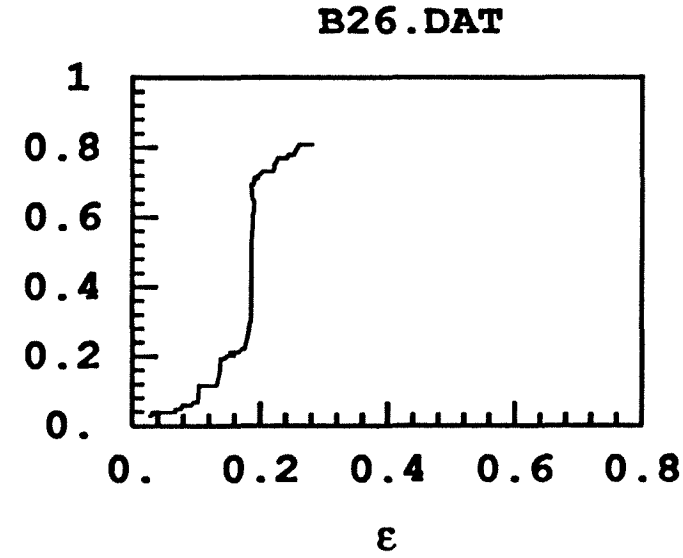
B26.DAT
1
0.8
0.6
0.4
0.2
0.
0.
0.2
0.4
0.6
0.8
ε

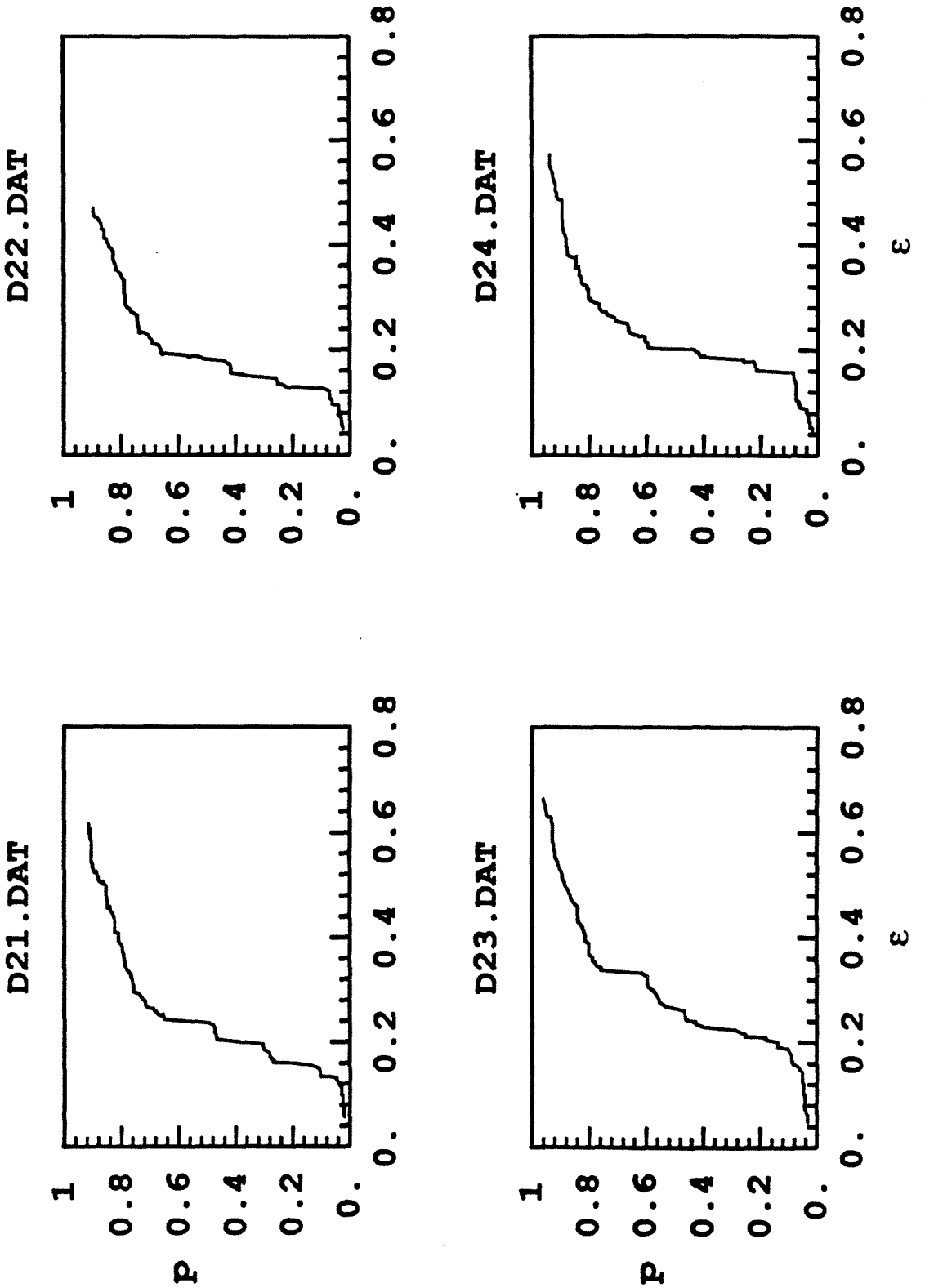
D21.DAT
D22.DAT
D23.DAT
D24.DAT
p
ε
1
0.8
0.6
0.4
0.2
0.
0.2
0.4
0.6
0.8

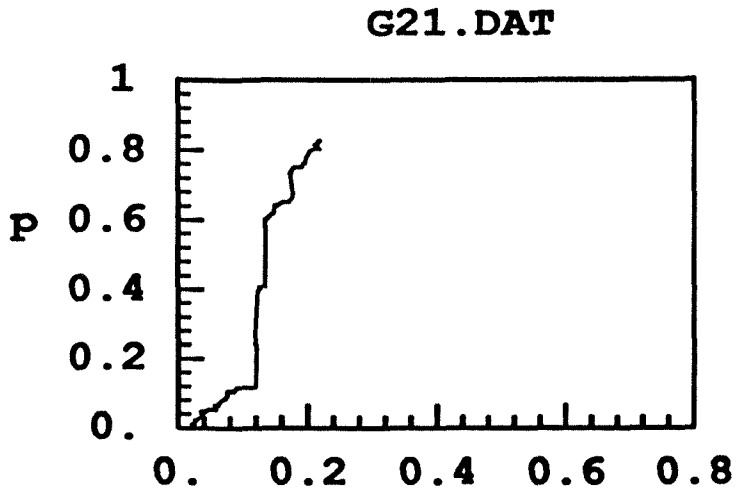
G21.DAT
p
1
0.8
0.6
0.4
0.2
0.
0.
0.2
0.4
0.6
0.8

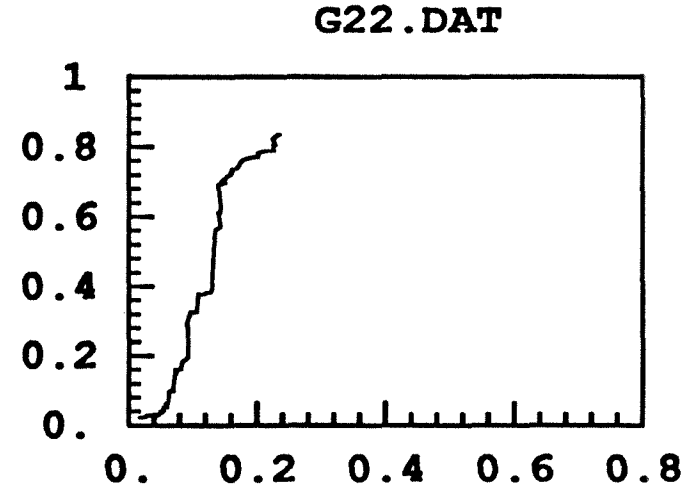
G22.DAT
1
0.8
0.6
0.4
0.2
0.
0.
0.2
0.4
0.6
0.8

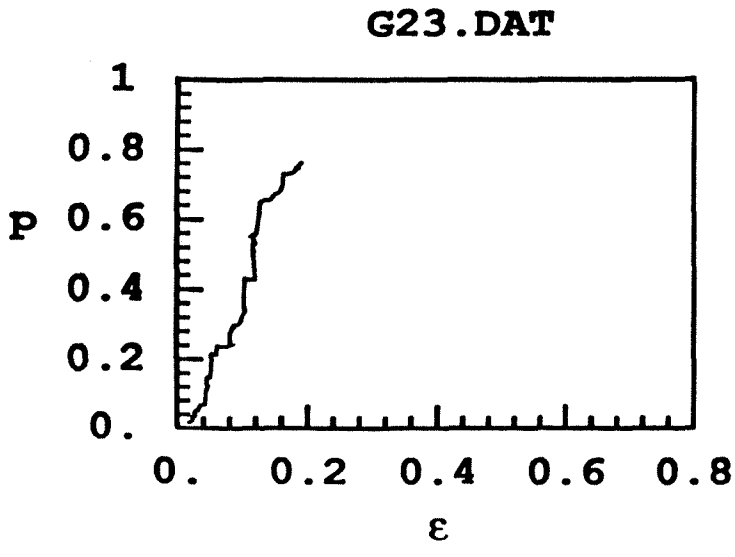
G23.DAT
p
1
0.8
0.6
0.4
0.2
0.
0.
0.2
0.4
0.6
0.8
ε

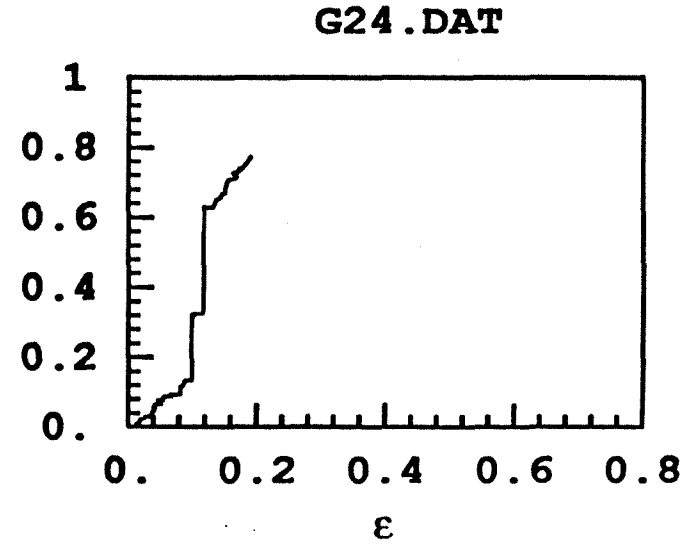
G24.DAT
1
0.8
0.6
0.4
0.2
0.
0.
0.2
0.4
0.6
0.8
ε


G25.DAT
P
1
0.8
0.6
0.4
0.2
0.
0.
0.2
0.4
0.6
0.8
ε

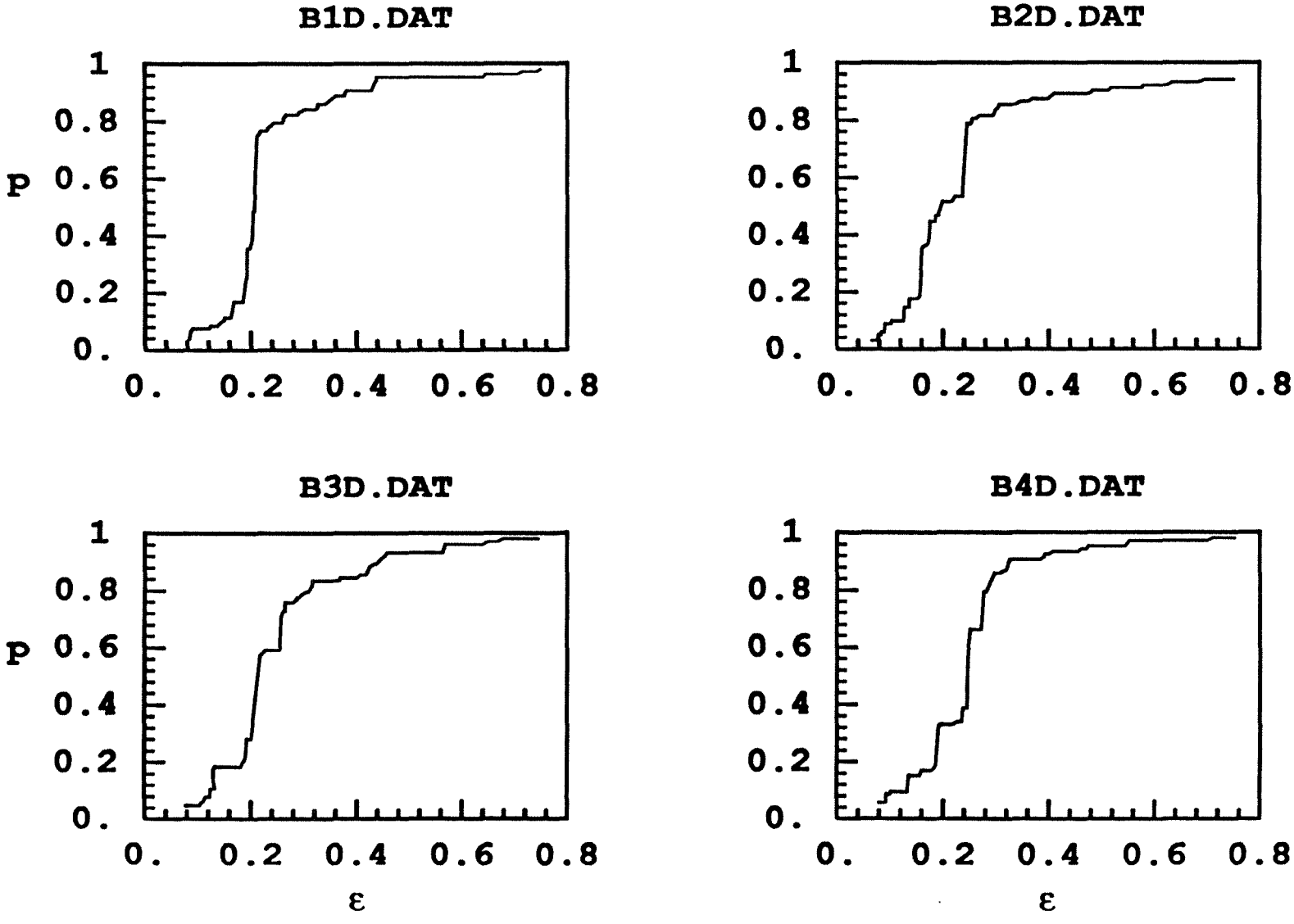
B1D.DAT
B2D.DAT
B3D.DAT
B4D.DAT
p
ε
1
0.8
0.6
0.4
0.2
0.
0.2
0.4
0.6
0.8

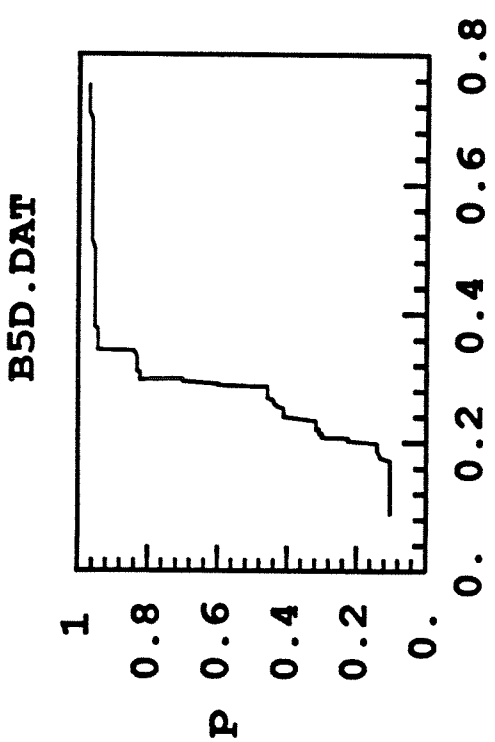
B5D.DAT
P
1
0.8
0.6
0.4
0.2
0.
0.
0.2
0.4
0.6
0.8
ε

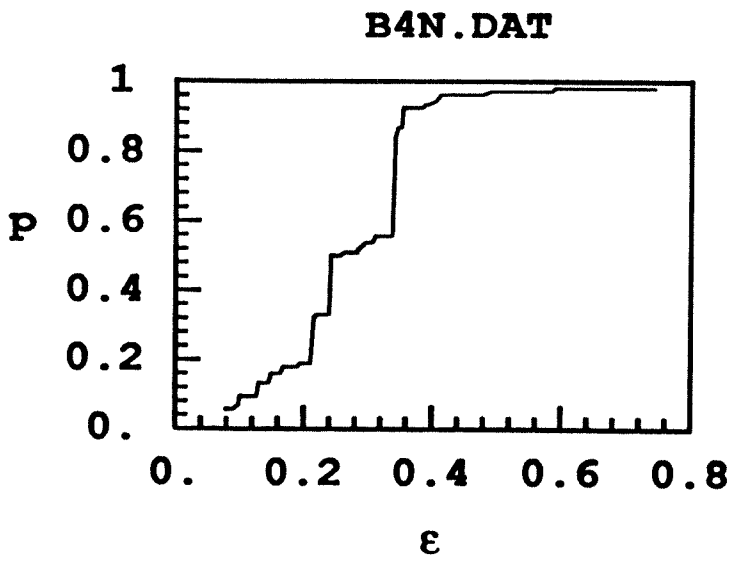
B4N.DAT
1
0.8
0.6
0.4
0.2
0.
p
0.
0.2
0.4
0.6
0.8
ε

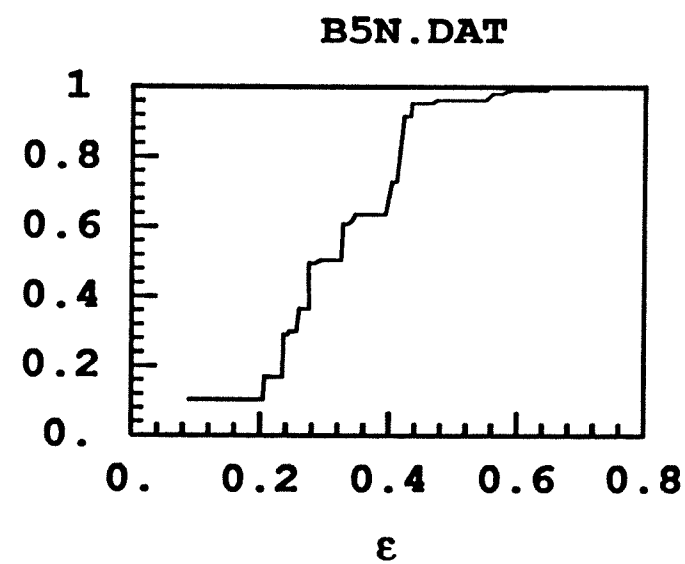
B5N.DAT
1
0.8
0.6
0.4
0.2
0.
0.
0.2
0.4
0.6
0.8
ε

Appendix XII

SINGLE PARTICLE EXPERIMENTS:

TEMPERATURE-TIME TRACES

Single particle drop-tube experiments were done under a variety of conditions. Only the temperature-time traces are shown in this Appendix. The intensity-time traces from which these were derived are not shown due to space limitations. The derived area-ratio is also not shown.

At the top of each Figure is a line that describes the conditions of that experiment. The first two words are **1451** and **1600K** indicating that the chars were derived from the bituminous PSOC 1451 coal, after pyrolysis at 1600K. The next number, e.g. **45-53** indicates the char size in microns. Following that is the value of the wall temperature in degrees Celsius. **1000W** means the wall temperature was 1000°C. Finally the particular **filename.ext** is given. The starting letter of the filename indicates whether the experiment was carried out in air or in 50% oxygen. Filenames starting with **A, P, R, X,** and **Y** denote experiments in air and those starting with **L, S, T,** and **V** are for experiments in 50% oxygen.

Two additional comments are in order. The file series starting with the letter **P** shows data from chars oxidized to 13% conversion at 500°C. This is indicated in the top header for those files. All other chars are initially unburnt. The files starting with the letters **X** and **Y** are from the same char but belong to two density classified fractions — **D** for the denser and **L** for lighter fraction. This is also indicated in their respective top headers.

Table AXII.1 shows the organization of each data file. Time, in milliseconds, is in column 1. Columns 2 and 3 show the signal intensities in Volts in the wavelength ranges centered around 800nm and 1000nm respectively. Column 4 shows

the particle temperature in degrees Kelvin. Finally, columns 5 and 6 show the area ratios (projected area of the particle along the detector line-of-sight as a function of time, divided by the initial projected area) as obtained from the 800nm and the 1000nm signals. Table AXII.2 summarizes the experimental conditions for runs in air while Table AXII.3 does the same for runs in 50% oxygen.

Figure AXII.1 is a flow diagram showing the sequence of steps involved in gathering an interpreting the data from the experiments. The various steps are discussed in Chapter 4. Figure AXII.2 shows the calibration sensitivity curve. It shows how sensitive the particle temperature is to the value of the experimentally determined calibration constant, C. The sensitivity depends on the ratio of the signals at the two wavelengths. Various curves are for different signal-ratios as shown. The subsequent Figures show the temperature-time traces of the various runs. The calibration runs are also shown in the first few Figures labelled CAL*.DAT.

Time (ms)	800nm signal	1000nm signal	Particle Temperature	Area ratio (800nm)	Area ratio (1000nm)

Table AXII.1 Data file format for single particle experiments.

RUN NAME	CHAR SIZE	WALL TEMPERATURE	COMMENTS
	(μm)	(°C)	
R16B 1,2,4, 6–10,12–14	90-104	1000	
R16S 1–14	45-53	1000	
X16B 2–7	90-104	1000	Dense particles
Y16B 1–14	90-104	1000	Light particles
P16S 1,4,5,8, 9,13,14,16,17	45-53	1000	13% B.O. at 500°C
A16S 1–16	45-53	800	

Table AXII.2 Details of single particle experiments in air. All particles were PSOC 1451 1600K char.

RUN NAME	CHAR SIZE	WALL TEMPERATURE	COMMENTS
	(μm)	(°C)	
S16B 2,6–9,11, 13,15,16,18,21	90-104	1200	
S16S 1–3,5,7–9, 12,14,16,17,20	45-53	1200	
T16B 1,4,9, 10,12	90-104	1000	
T16S 3,4,6,8, 11,13,14	45-53	1000	
L16S 1–6,8–16, 19-21	45-53	800	
V16S 1,3,4,6,8,9, 12–15,17–21	45-53	700	

Table AXII.3 Details of single particle experiments in 50% O_2. All particles were PSOC 1451 1600K char.

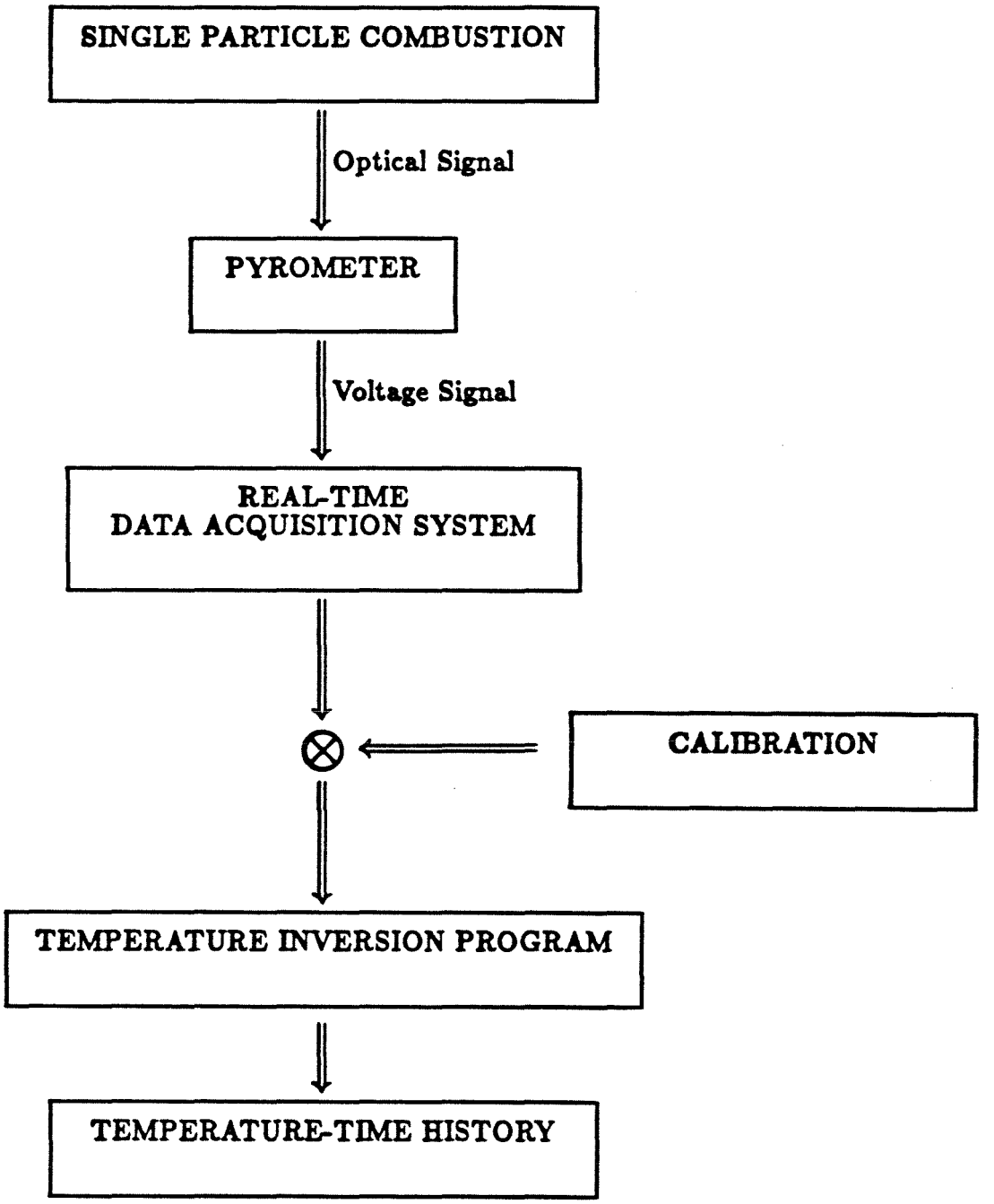

Figure XII.1 Procedure for obtaining temperature-time traces from single particle drop tube experiments.

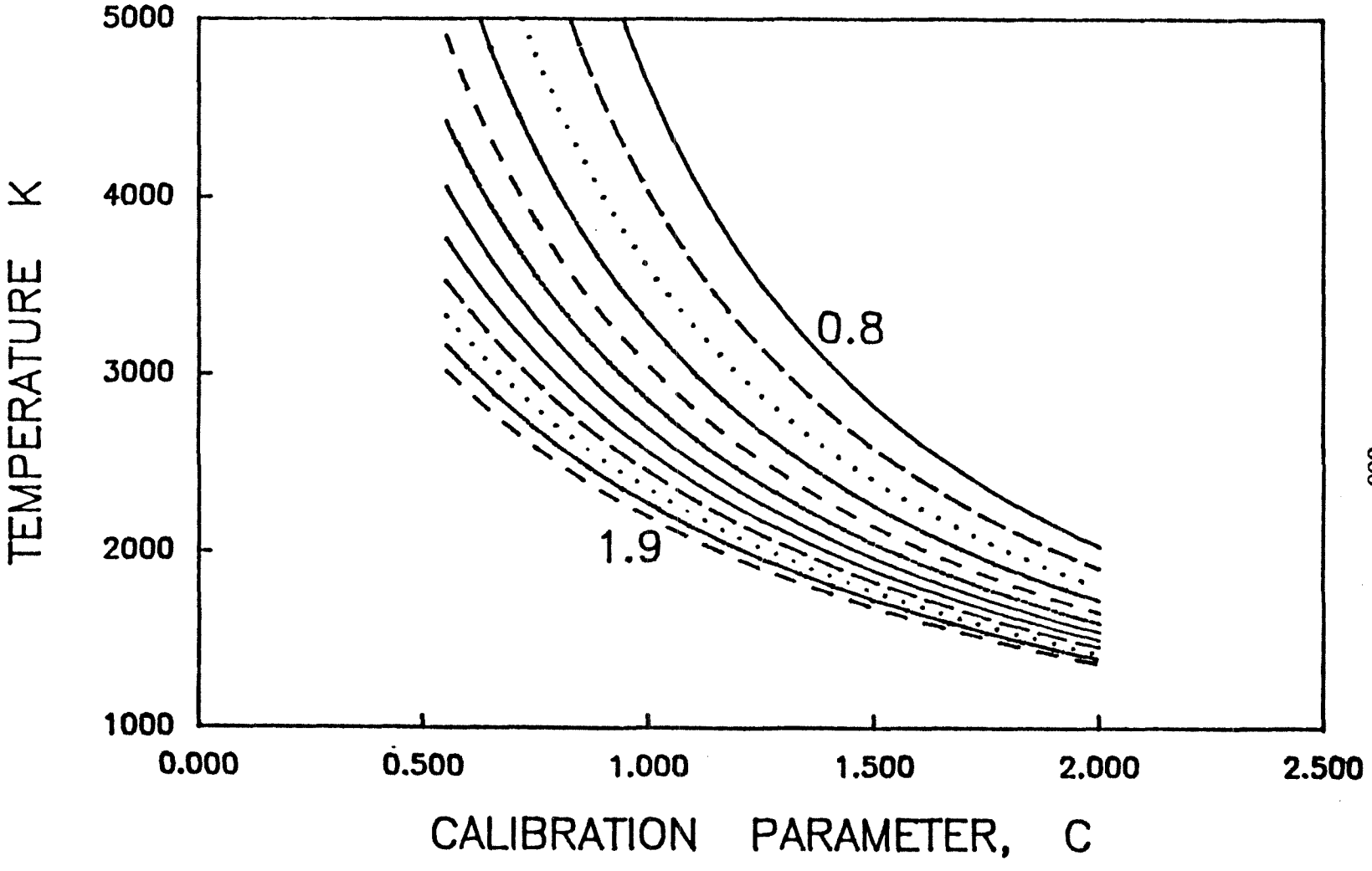

Figure XII.2 Calibration sensitivity curve for pyrometry inversion.

CALIBRATION C101.FIN

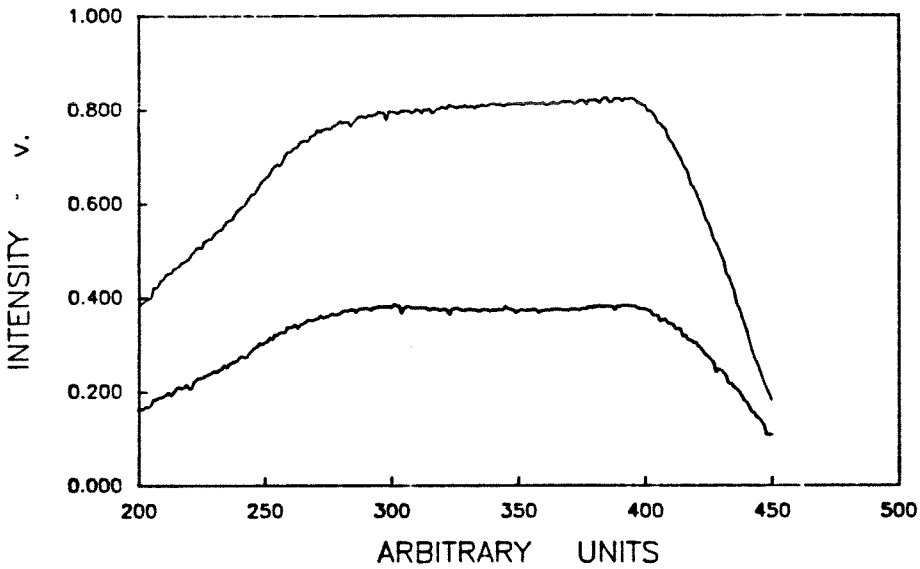

CALIBRATION C102.FIN

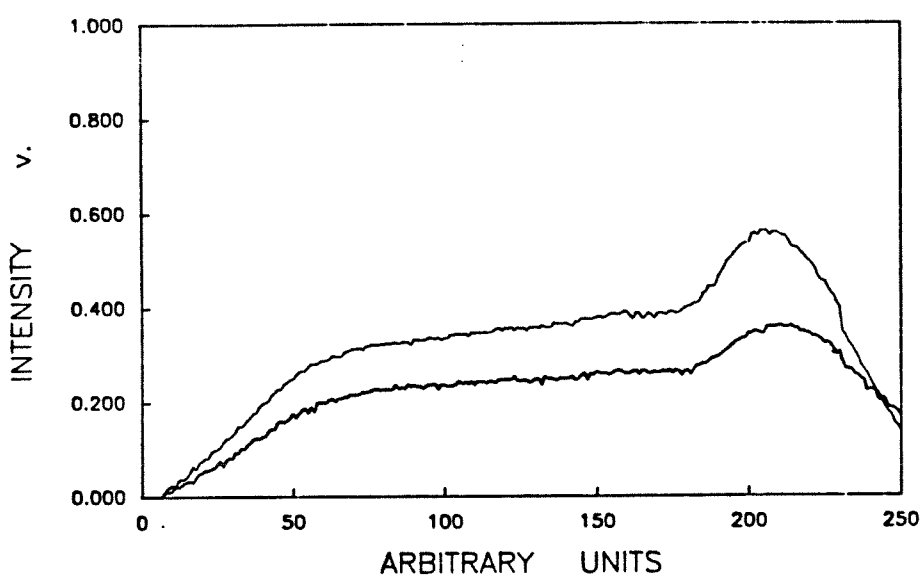

CALIBRATION C104.FIN

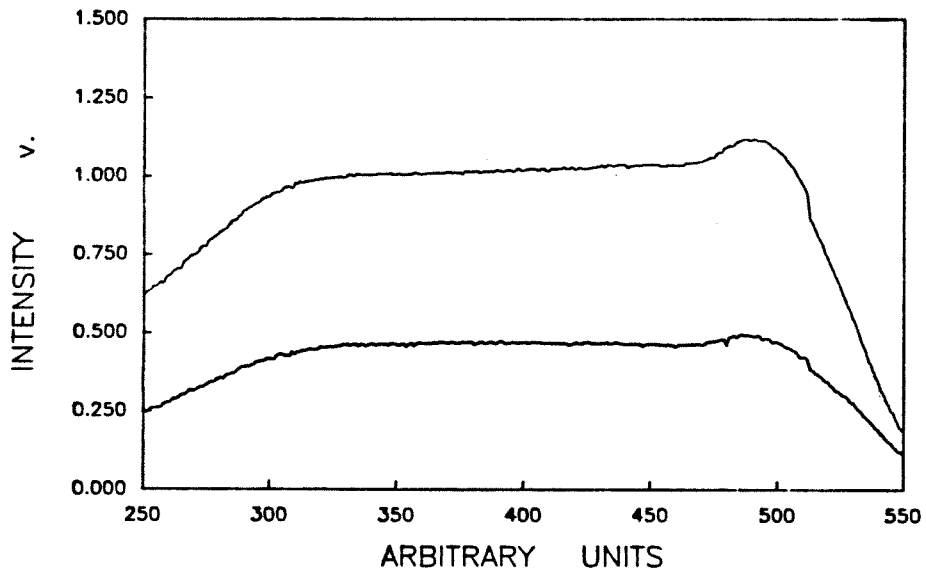

CALIBRATION C105.FIN

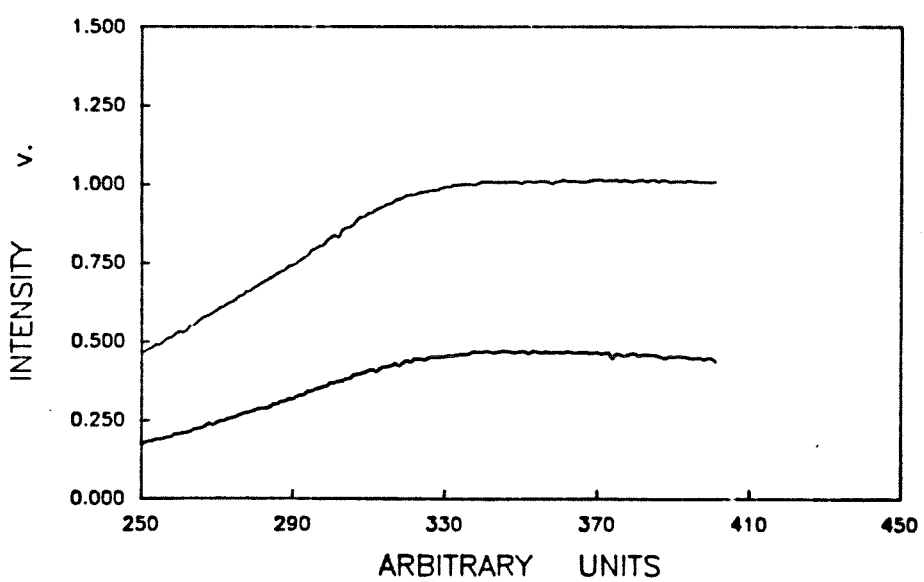

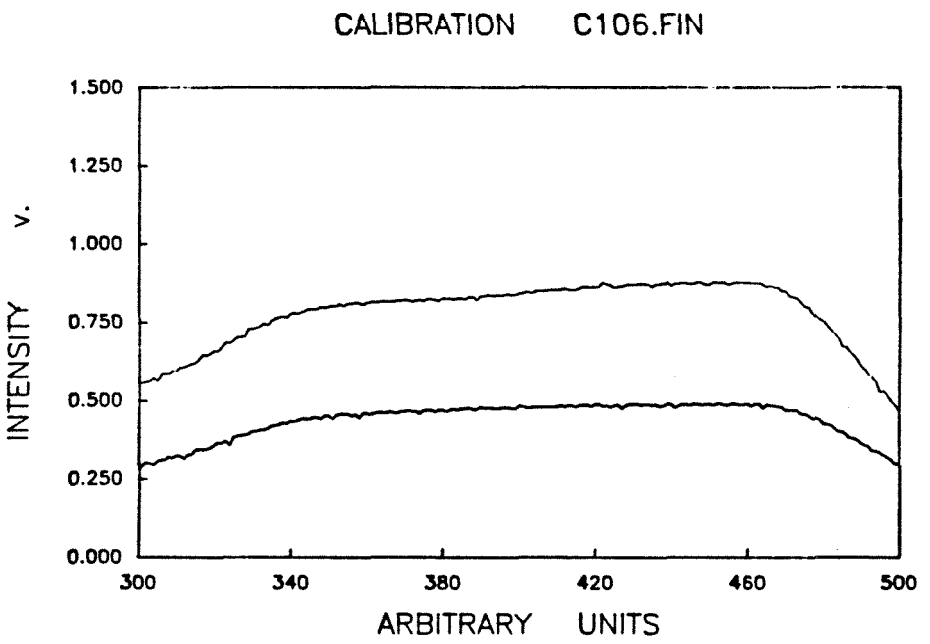
CALIBRATION C106.FIN
INTENSITY v.
1.500
1.250
1.000
0.750
0.500
0.250
0.000
300
340
380
420
460
500
ARBITRARY UNITS

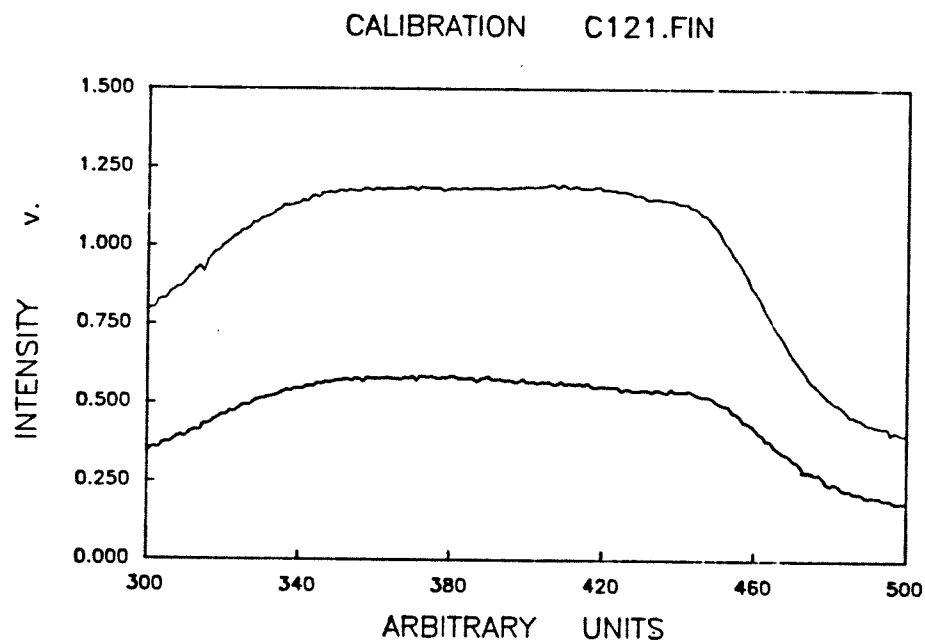
CALIBRATION C121.FIN
INTENSITY v.
1.500
1.250
1.000
0.750
0.500
0.250
0.000
300
340
380
420
460
500
ARBITRARY UNITS

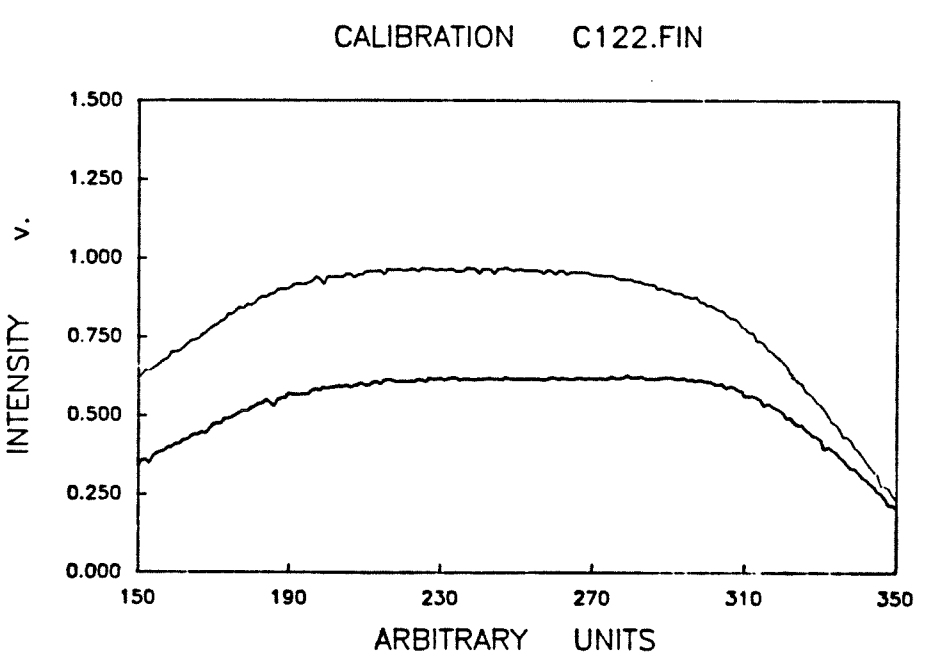
CALIBRATION C122.FIN
INTENSITY v.
1.500
1.250
1.000
0.750
0.500
0.250
0.000
150
190
230
270
310
350
ARBITRARY UNITS

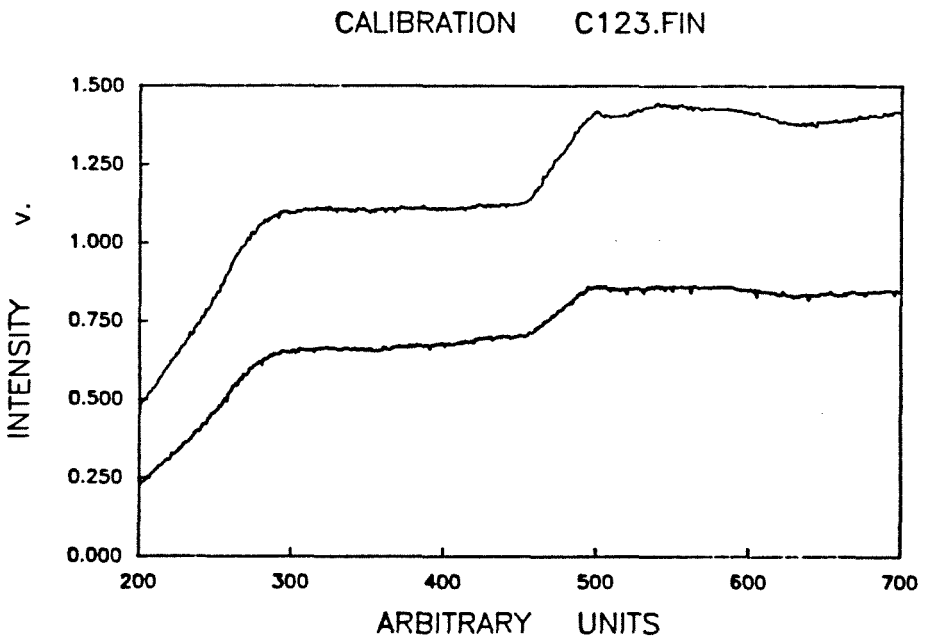
CALIBRATION C123.FIN
INTENSITY v.
1.500
1.250
1.000
0.750
0.500
0.250
0.000
200
300
400
500
600
700
ARBITRARY UNITS

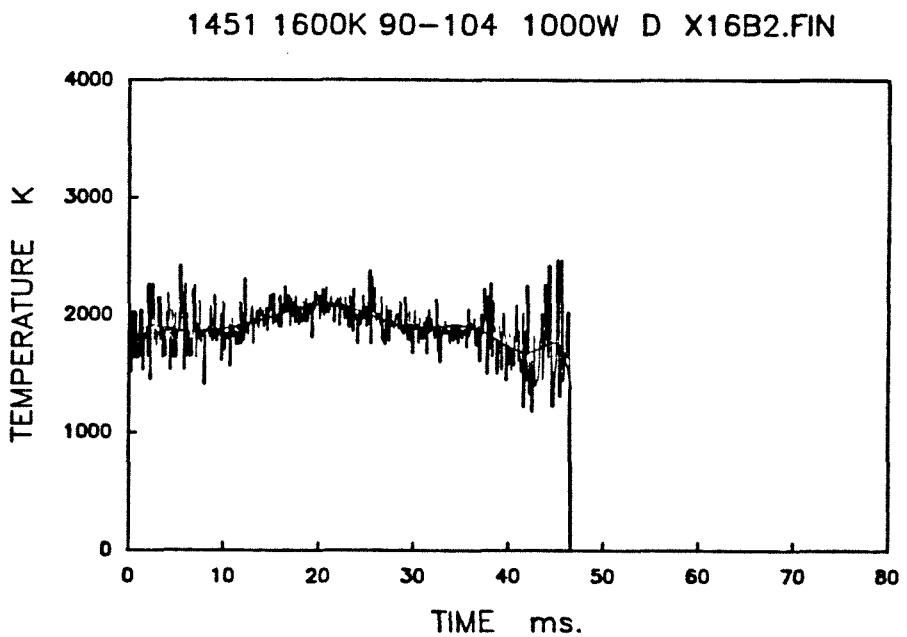
1451 1600K 90-104 1000W D X16B2.FIN
TEMPERATURE K
4000
3000
2000
1000
0
0
10
20
30
40
50
60
70
80
TIME ms.

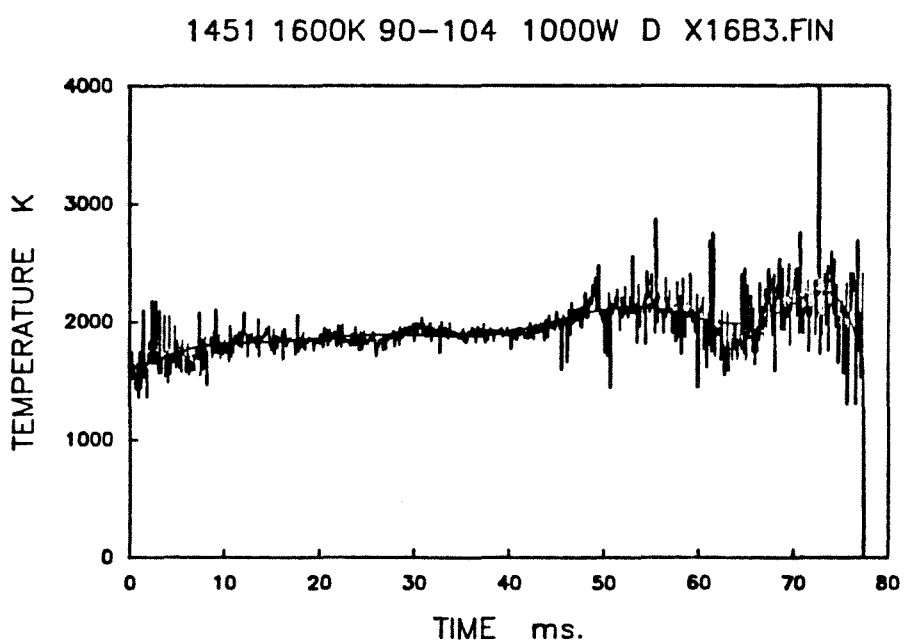
1451 1600K 90-104 1000W D X16B3.FIN
TEMPERATURE K
4000
3000
2000
1000
0
0
10
20
30
40
50
60
70
80
TIME ms.

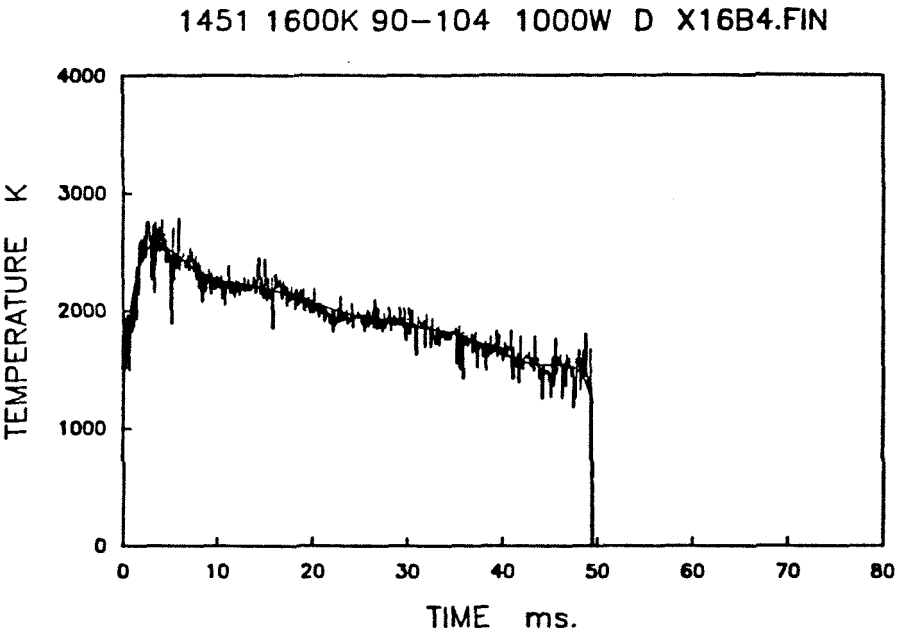
1451 1600K 90-104 1000W D X16B4.FIN
TEMPERATURE K
4000
3000
2000
1000
0
0
10
20
30
40
50
60
70
80
TIME ms.

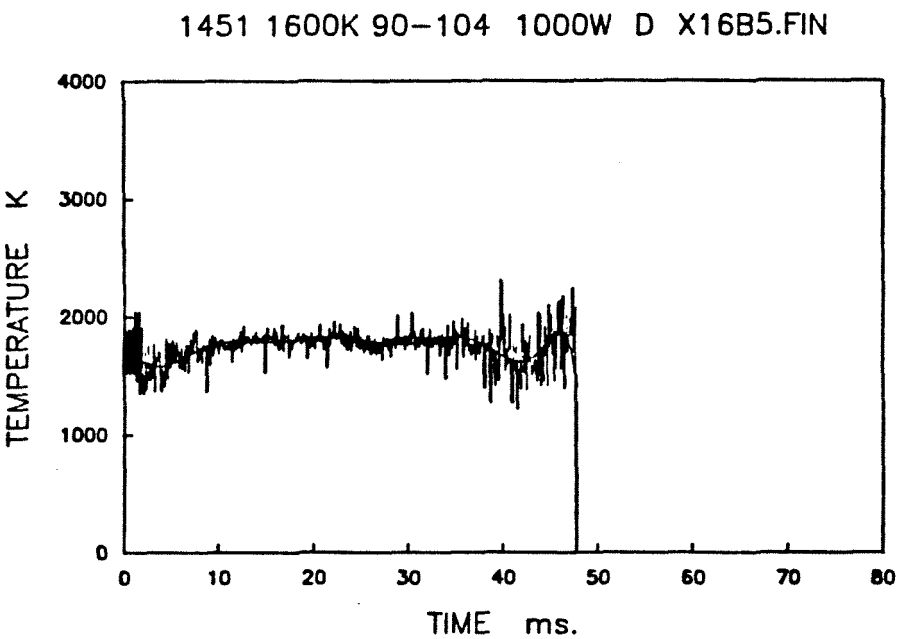
1451 1600K 90-104 1000W D X16B5.FIN
TEMPERATURE K
4000
3000
2000
1000
0
0
10
20
30
40
50
60
70
80
TIME ms.

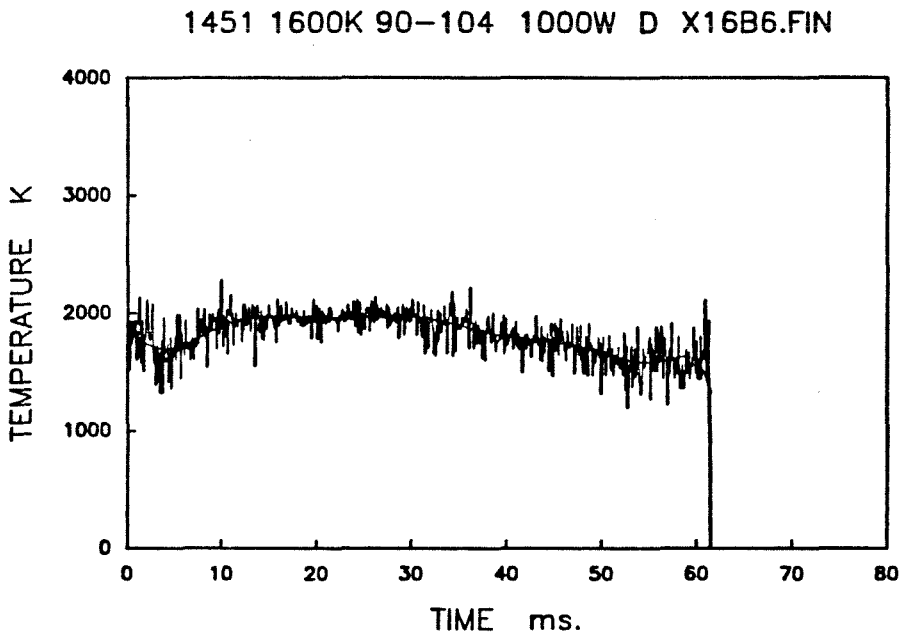
1451 1600K 90–104 1000W D X16B6.FIN
TEMPERATURE K
4000
3000
2000
1000
0
0
10
20
30
40
50
60
70
80
TIME ms.

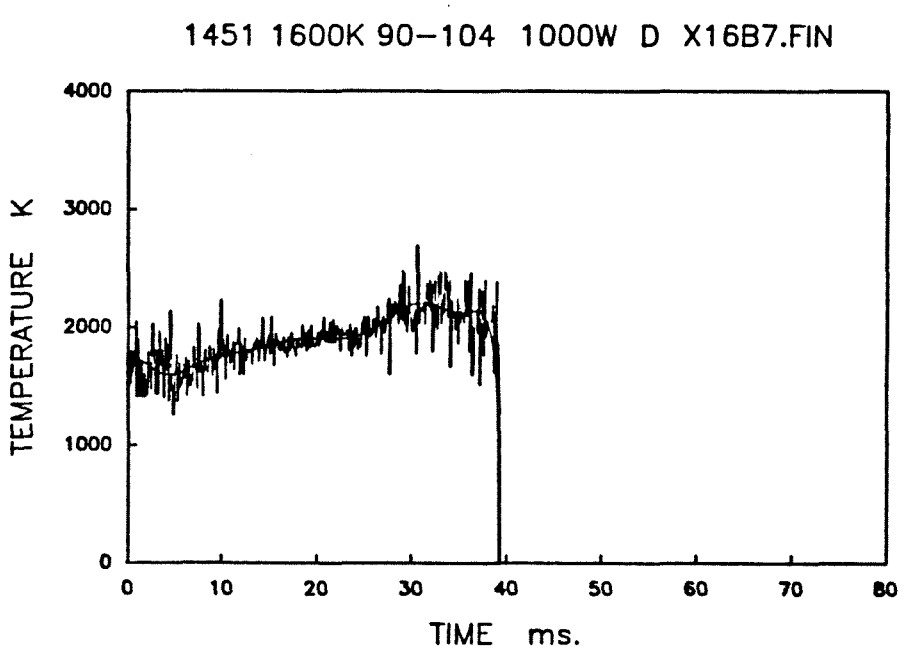
1451 1600K 90–104 1000W D X16B7.FIN
TEMPERATURE K
4000
3000
2000
1000
0
0
10
20
30
40
50
60
70
80
TIME ms.

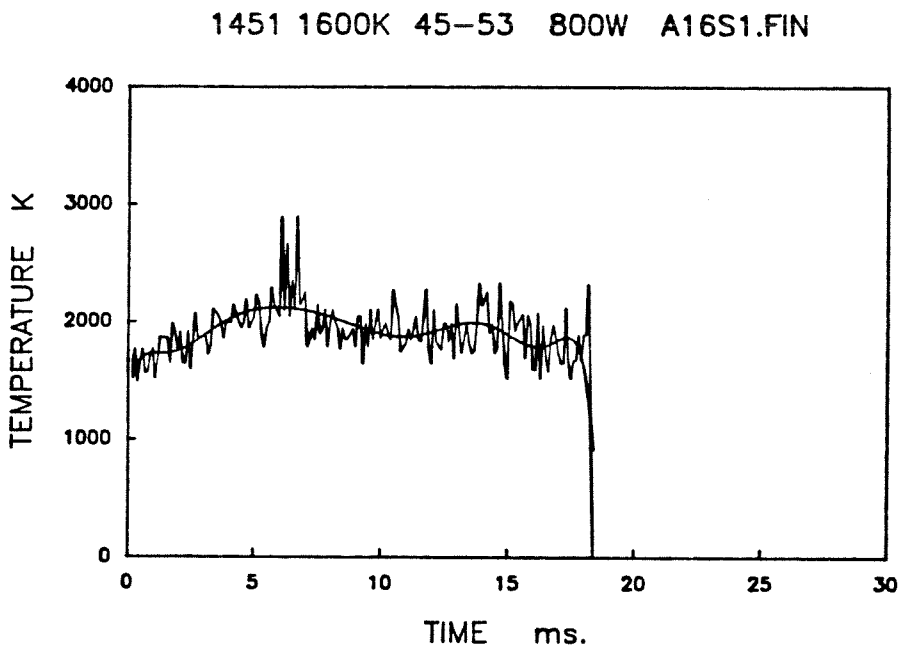
1451 1600K 45–53 800W A16S1.FIN
TEMPERATURE K
4000
3000
2000
1000
0
0
5
10
15
20
25
30
TIME ms.

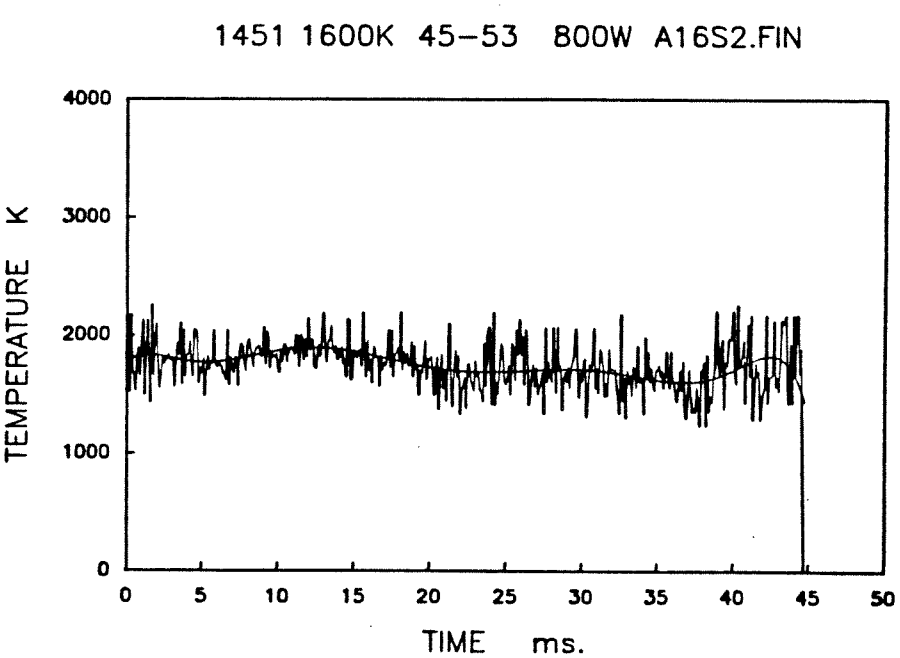
1451 1600K 45–53 800W A16S2.FIN
TEMPERATURE K
4000
3000
2000
1000
0
0
5
10
15
20
25
30
35
40
45
50
TIME ms.

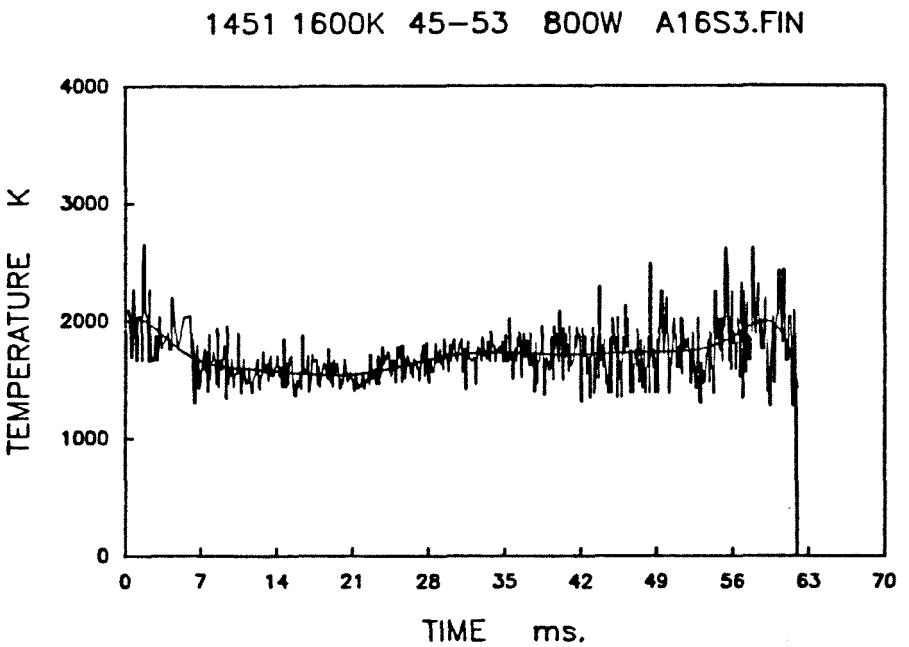
1451 1600K 45–53 800W A16S3.FIN
TEMPERATURE K
4000
3000
2000
1000
0
0 7 14 21 28 35 42 49 56 63 70
TIME ms.

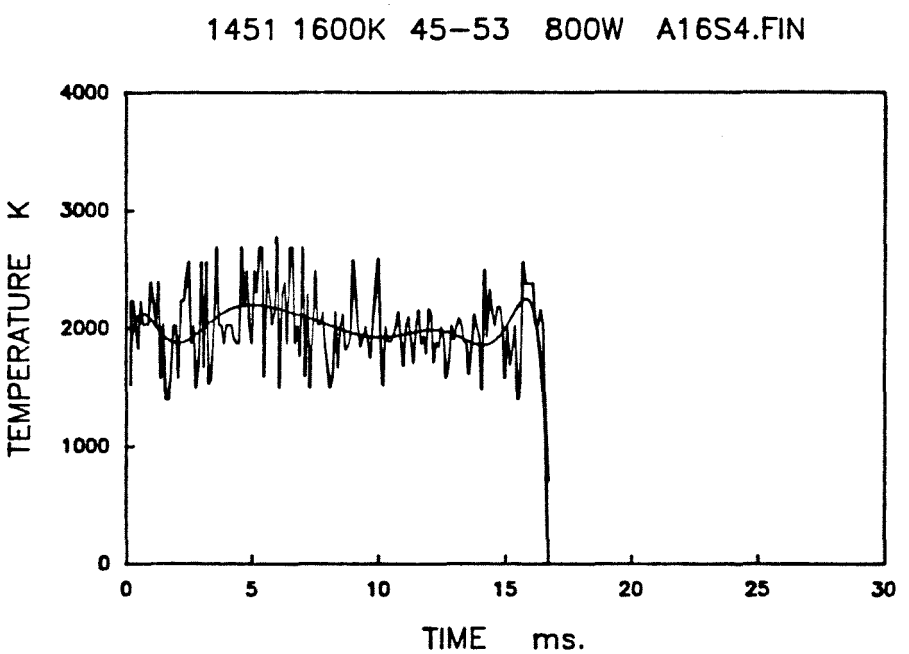
1451 1600K 45–53 800W A16S4.FIN
TEMPERATURE K
4000
3000
2000
1000
0
0 5 10 15 20 25 30
TIME ms.

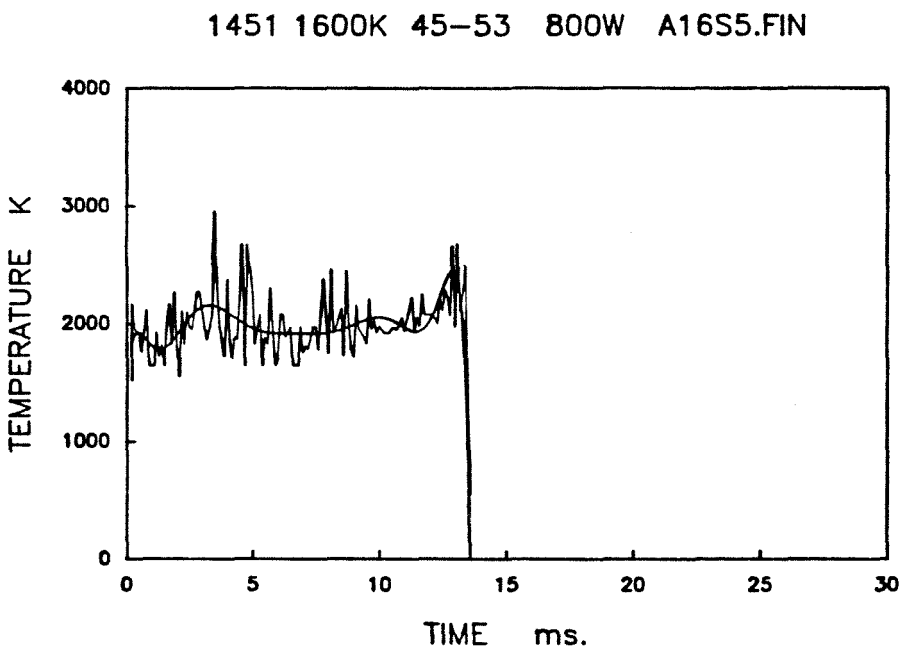
1451 1600K 45–53 800W A16S5.FIN
TEMPERATURE K
4000
3000
2000
1000
0
0
5
10
15
20
25
30
TIME ms.

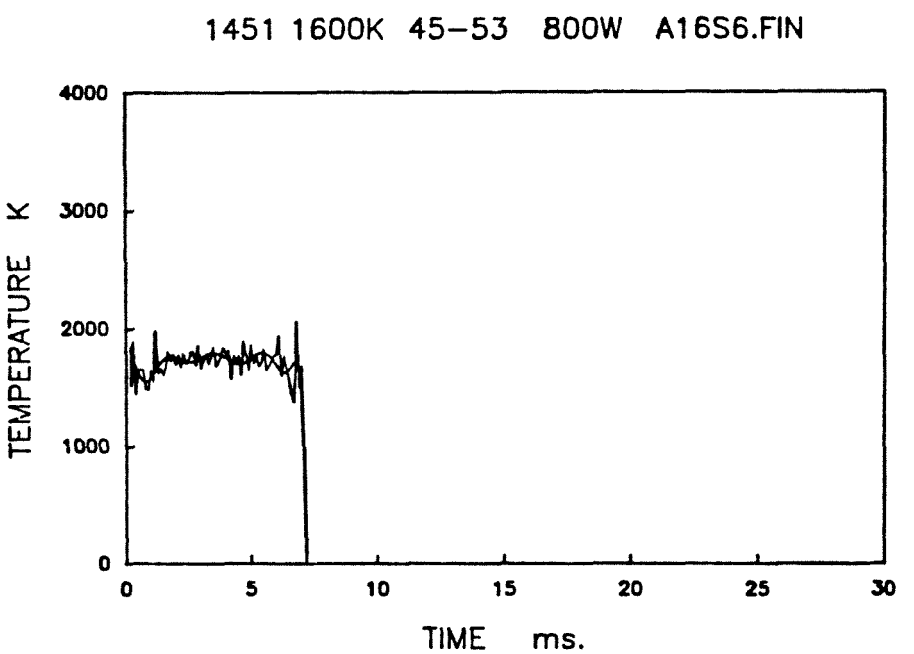
1451 1600K 45–53 800W A16S6.FIN
TEMPERATURE K
4000
3000
2000
1000
0
0
5
10
15
20
25
30
TIME ms.

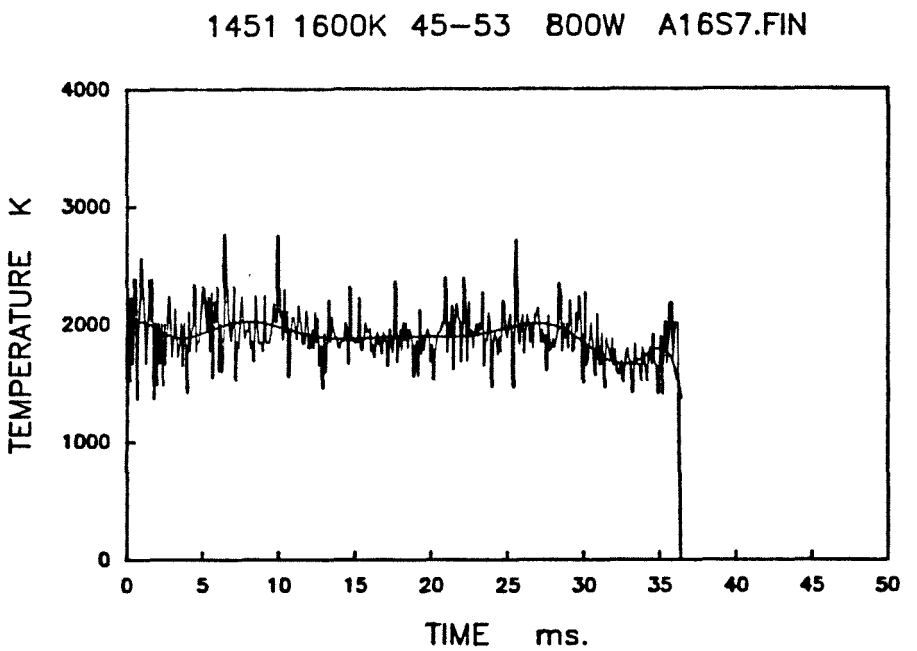
1451 1600K 45–53 800W A16S7.FIN
TEMPERATURE K
4000
3000
2000
1000
0
0 5 10 15 20 25 30 35 40 45 50
TIME ms.

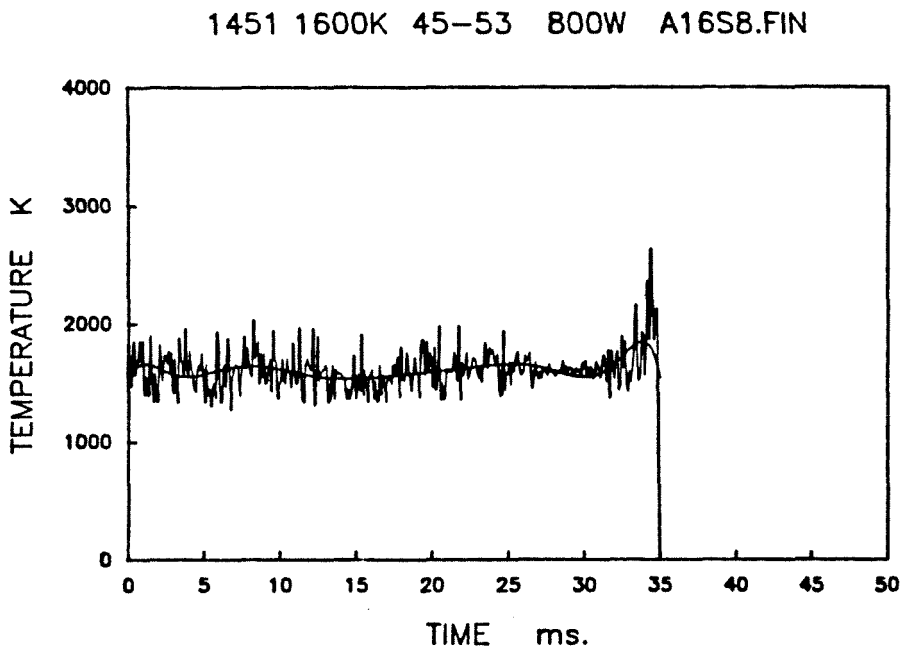
1451 1600K 45–53 800W A16S8.FIN
TEMPERATURE K
4000
3000
2000
1000
0
0 5 10 15 20 25 30 35 40 45 50
TIME ms.

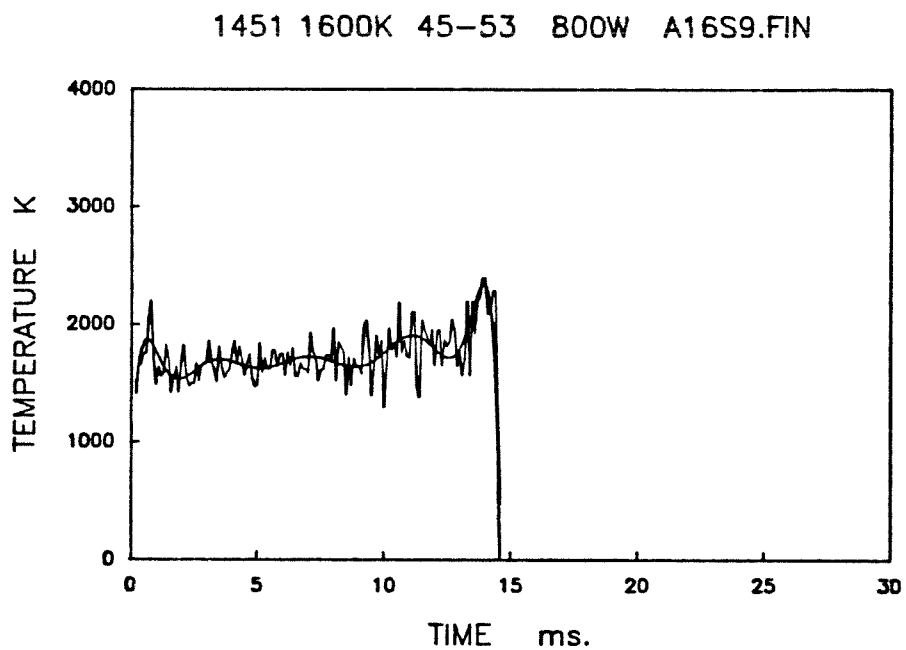
1451 1600K 45–53 800W A16S9.FIN
TEMPERATURE K
4000
3000
2000
1000
0
0
5
10
15
20
25
30
TIME ms.

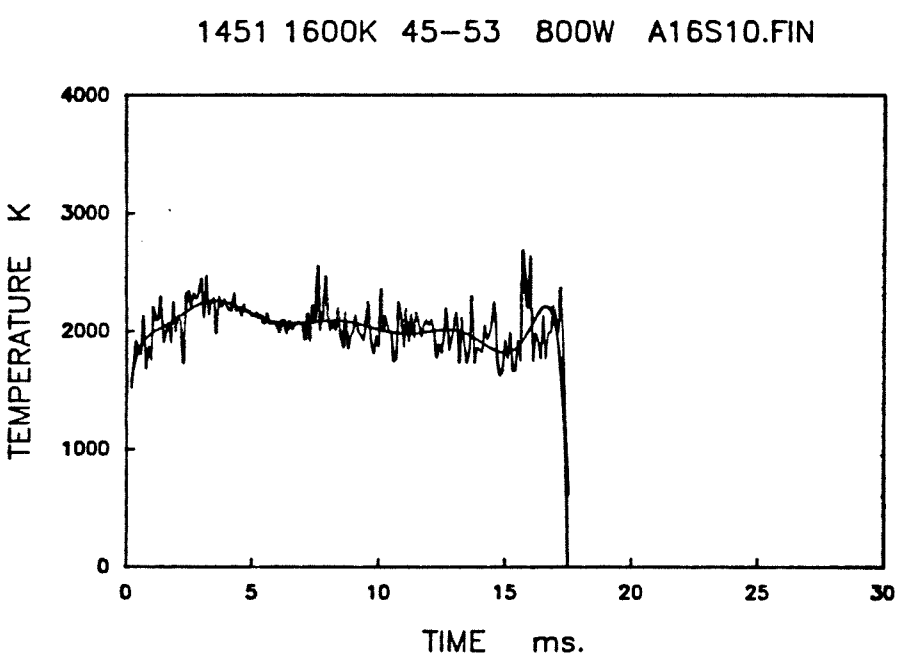
1451 1600K 45–53 800W A16S10.FIN
TEMPERATURE K
4000
3000
2000
1000
0
0
5
10
15
20
25
30
TIME ms.

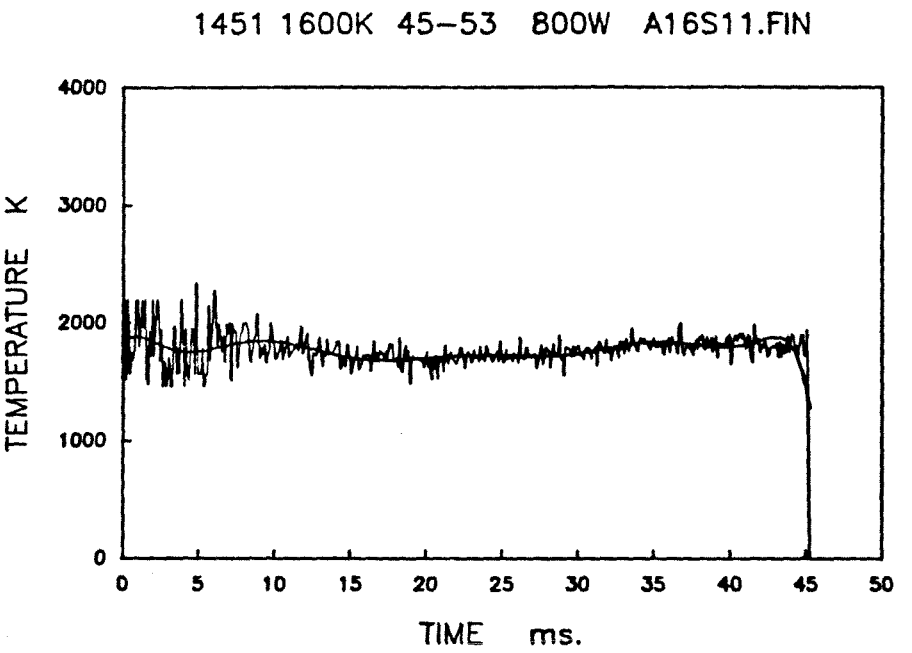
1451 1600K 45–53 800W A16S11.FIN
TEMPERATURE K
4000
3000
2000
1000
0
0 5 10 15 20 25 30 35 40 45 50
TIME ms.

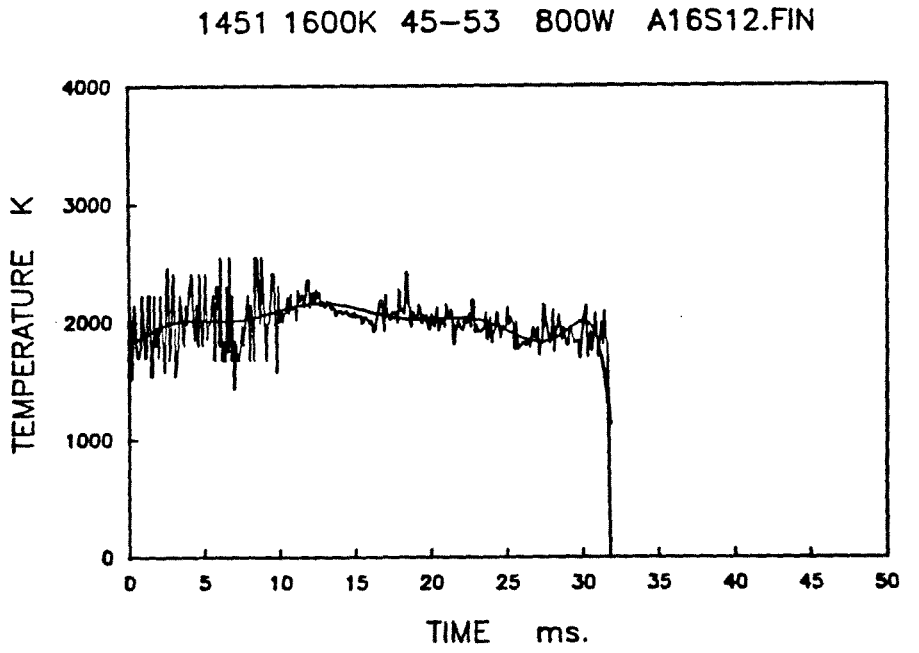
1451 1600K 45–53 800W A16S12.FIN
TEMPERATURE K
4000
3000
2000
1000
0
0 5 10 15 20 25 30 35 40 45 50
TIME ms.

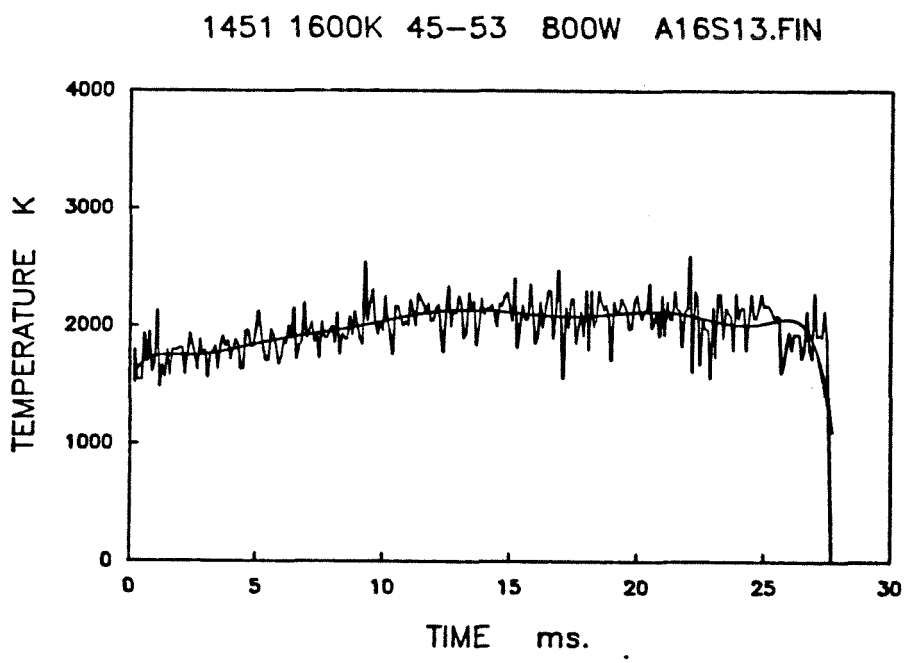
1451 1600K 45–53 800W A16S13.FIN
TEMPERATURE K
4000
3000
2000
1000
0
0
5
10
15
20
25
30
TIME ms.

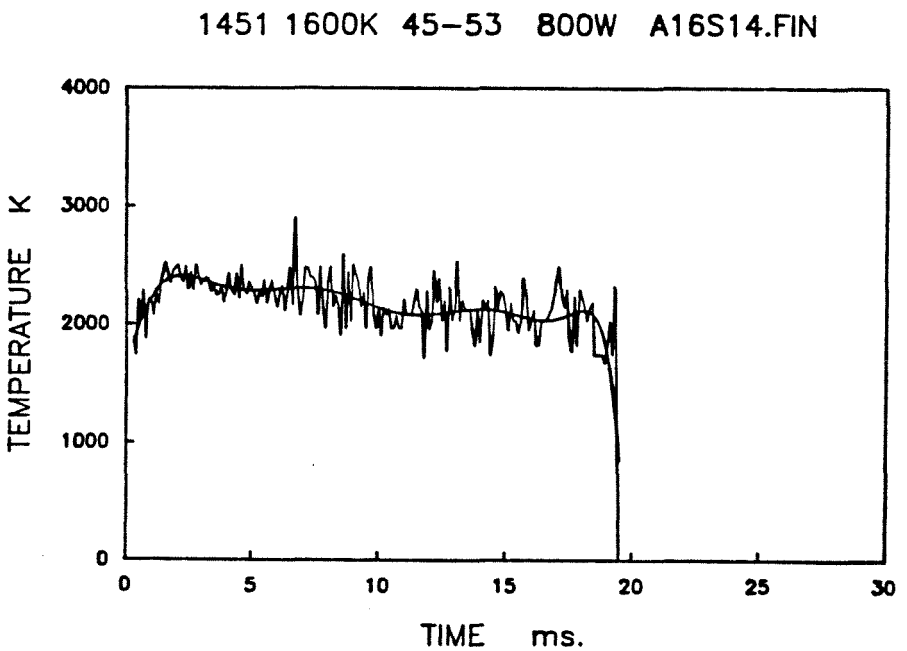
1451 1600K 45–53 800W A16S14.FIN
TEMPERATURE K
4000
3000
2000
1000
0
0
5
10
15
20
25
30
TIME ms.

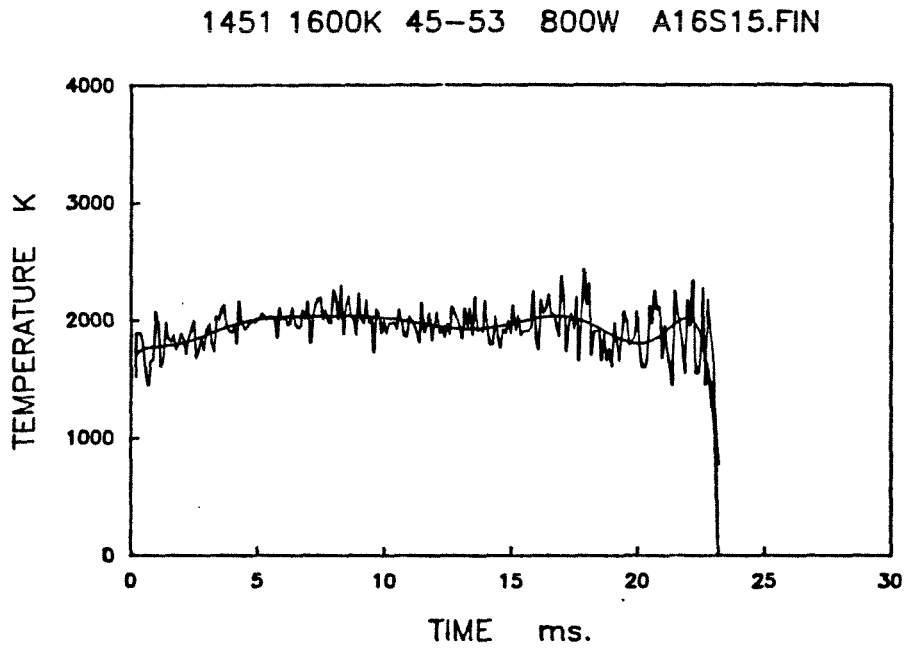
1451 1600K 45–53 800W A16S15.FIN
TEMPERATURE K
4000
3000
2000
1000
0
0
5
10
15
20
25
30
TIME ms.

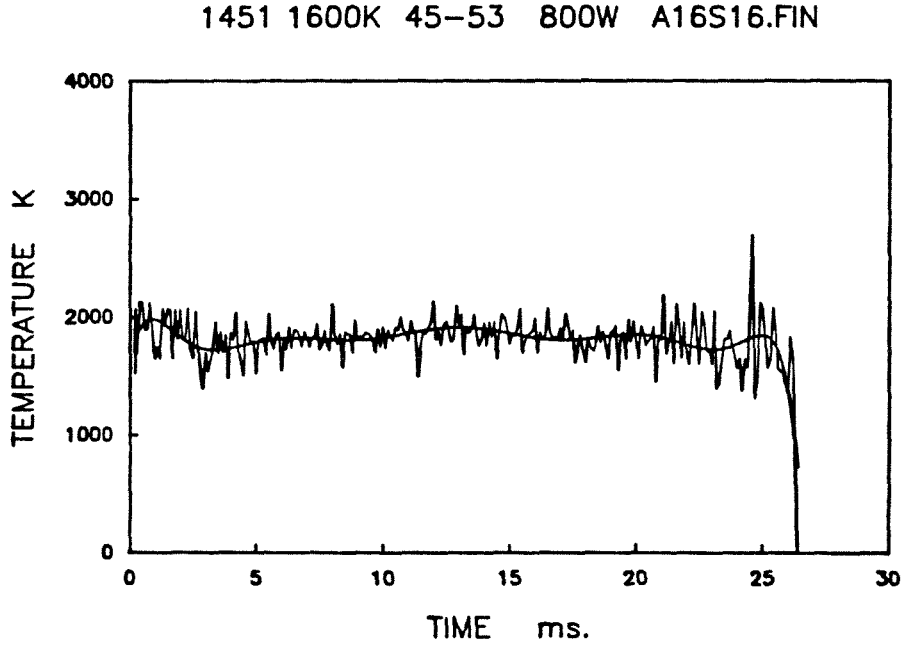
1451 1600K 45–53 800W A16S16.FIN
TEMPERATURE K
4000
3000
2000
1000
0
0
5
10
15
20
25
30
TIME ms.

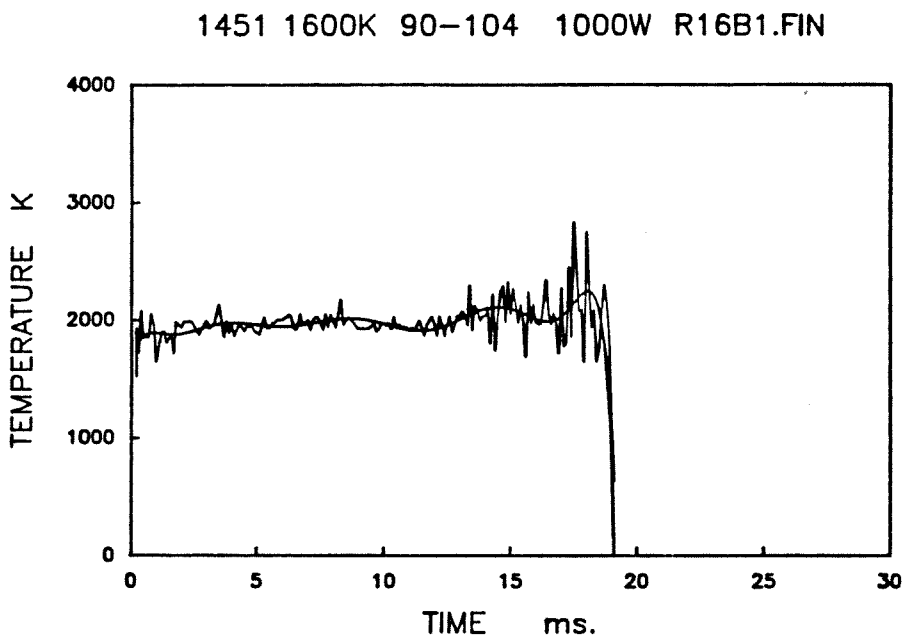
1451 1600K 90–104 1000W R16B1.FIN
TEMPERATURE K
4000
3000
2000
1000
0
0
5
10
15
20
25
30
TIME ms.

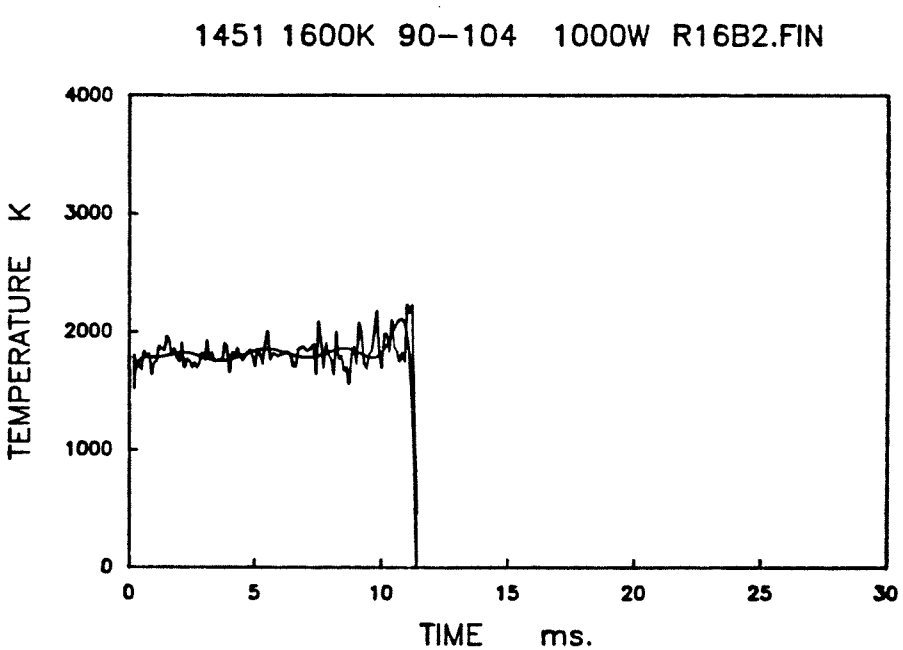
1451 1600K 90–104 1000W R16B2.FIN
TEMPERATURE K
4000
3000
2000
1000
0
0
5
10
15
20
25
30
TIME ms.

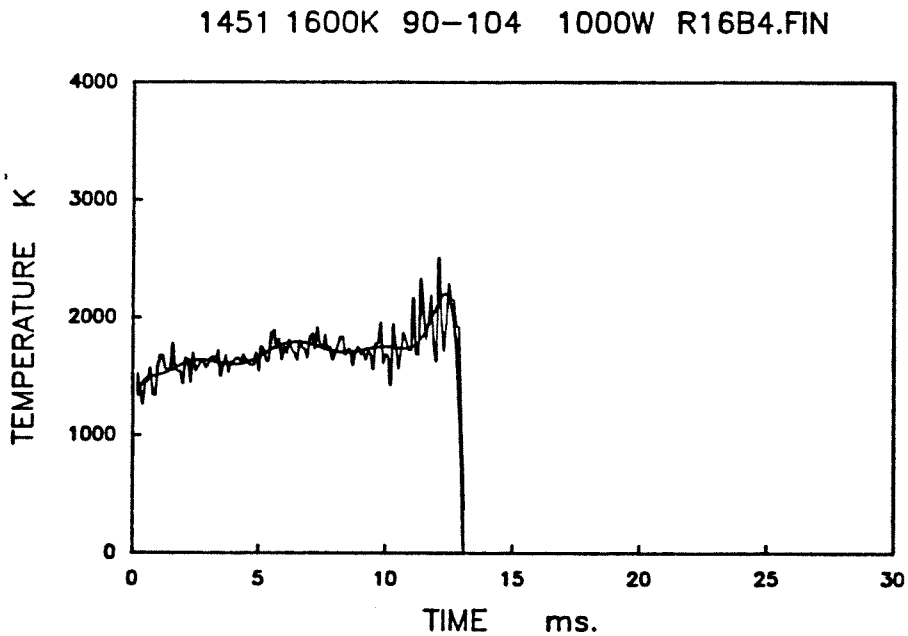
1451 1600K 90–104 1000W R16B4.FIN
TEMPERATURE K
4000
3000
2000
1000
0
0
5
10
15
20
25
30
TIME ms.

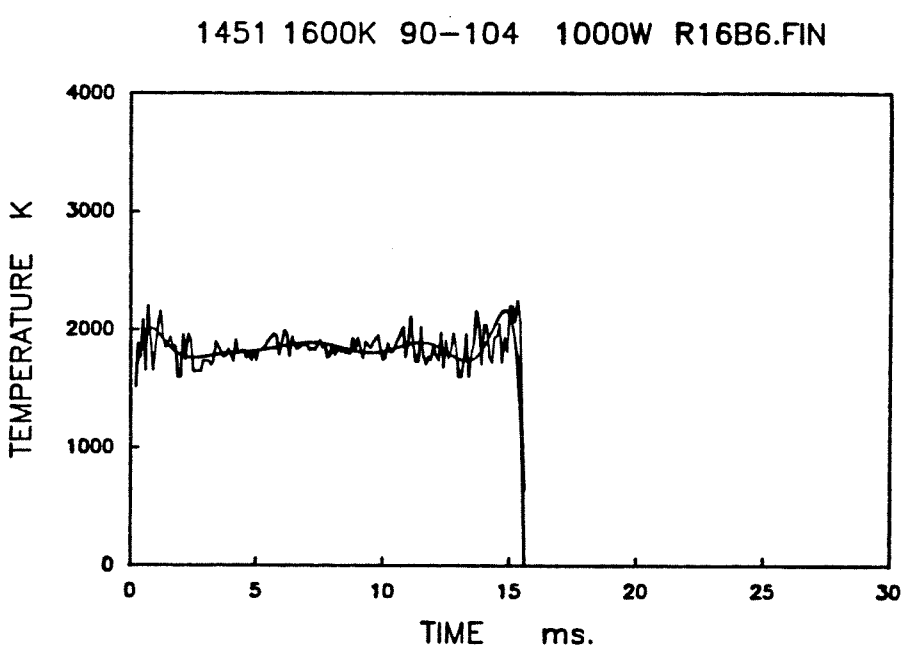
1451 1600K 90–104 1000W R16B6.FIN
TEMPERATURE K
4000
3000
2000
1000
0
0
5
10
15
20
25
30
TIME ms.

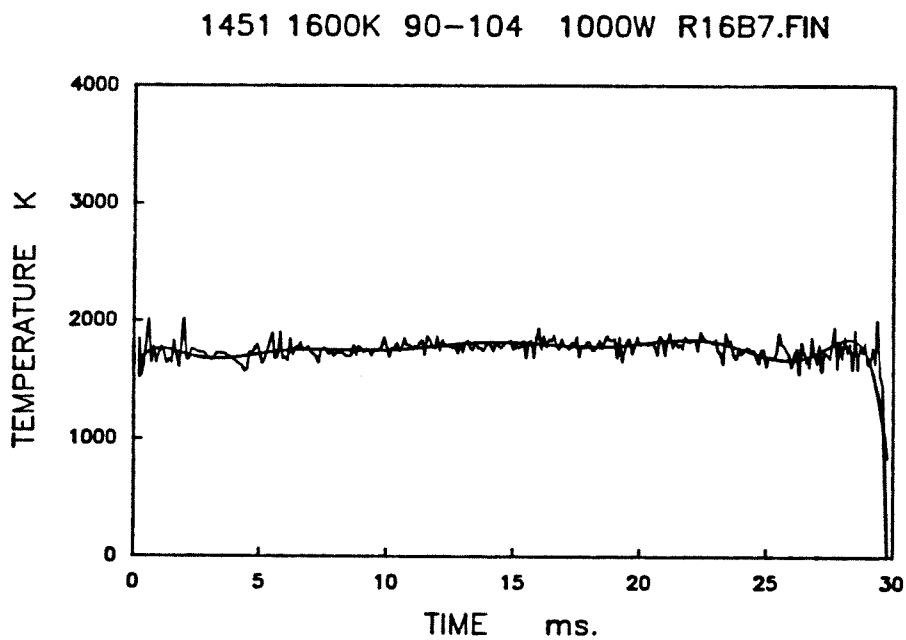
1451 1600K 90–104 1000W R16B7.FIN
TEMPERATURE K
4000
3000
2000
1000
0
0
5
10
15
20
25
30
TIME ms.

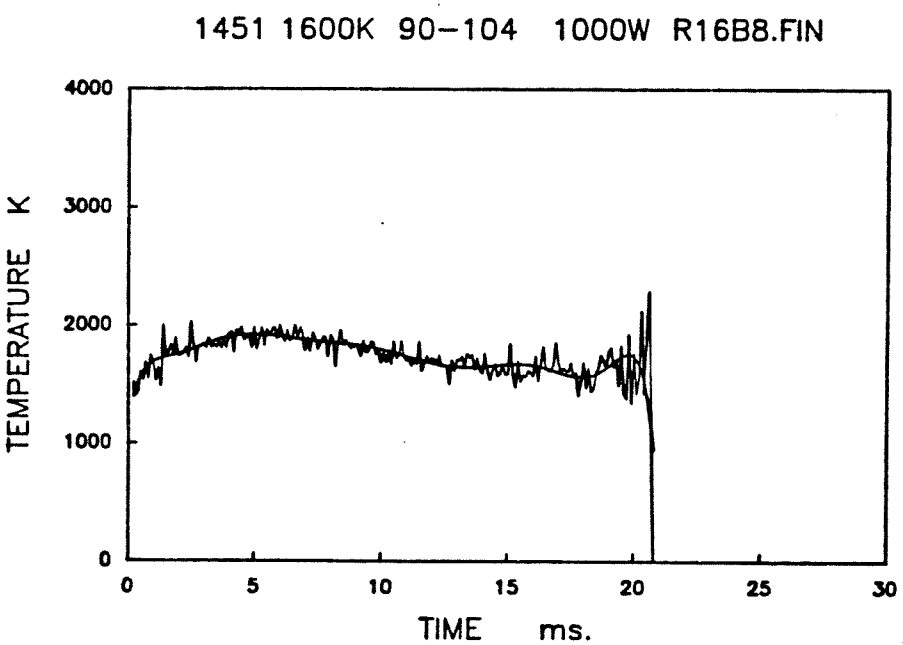
1451 1600K 90–104 1000W R16B8.FIN
TEMPERATURE K
4000
3000
2000
1000
0
0
5
10
15
20
25
30
TIME ms.

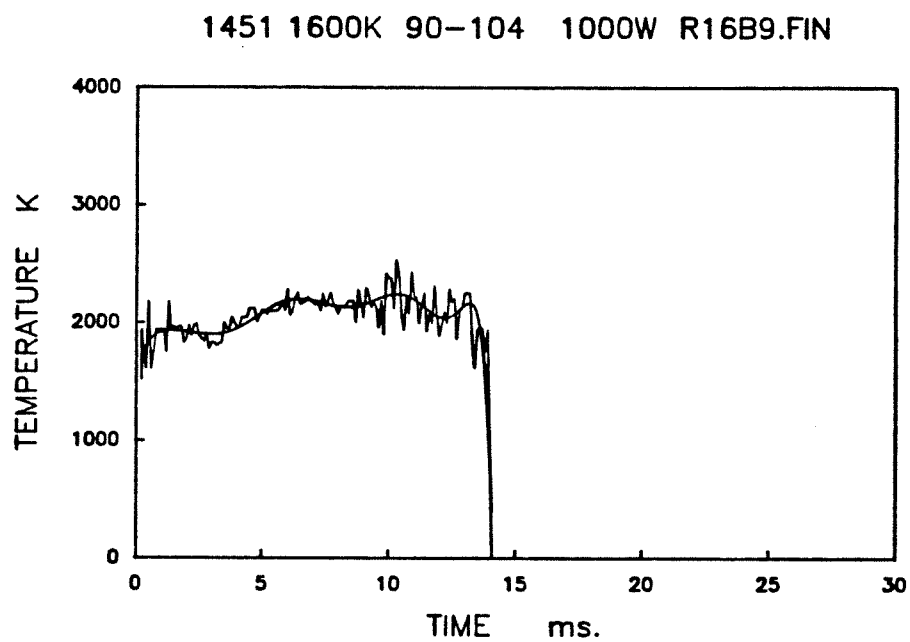
1451 1600K 90–104 1000W R16B9.FIN
TEMPERATURE K
4000
3000
2000
1000
0
0
5
10
15
20
25
30
TIME ms.

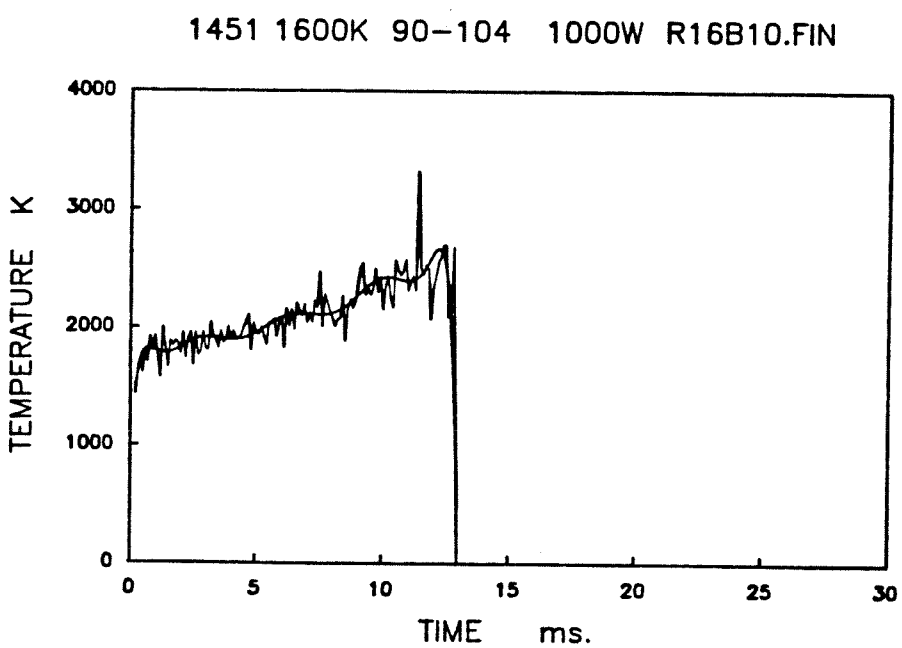
1451 1600K 90–104 1000W R16B10.FIN
TEMPERATURE K
4000
3000
2000
1000
0
0
5
10
15
20
25
30
TIME ms.

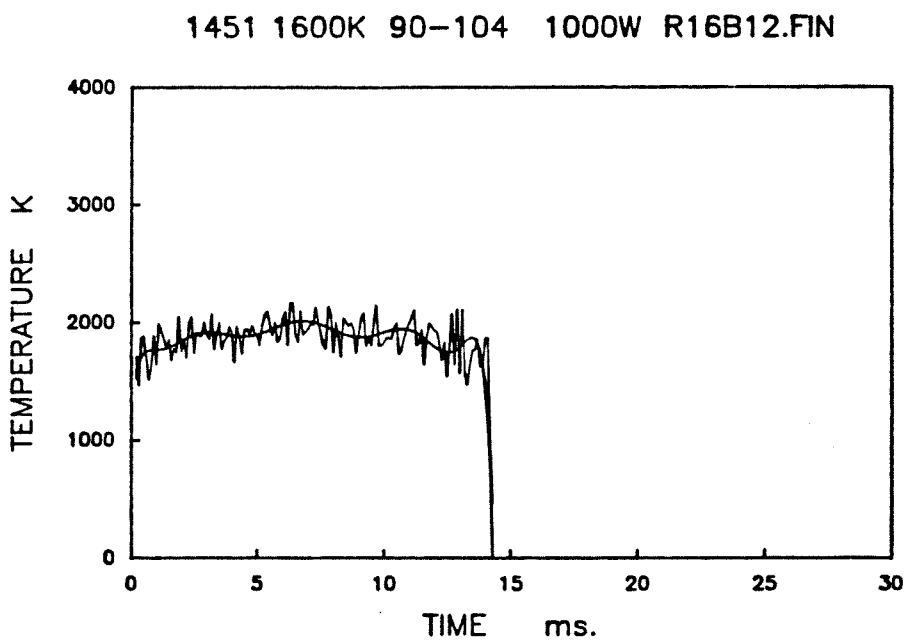
1451 1600K 90–104 1000W R16B12.FIN
TEMPERATURE K
4000
3000
2000
1000
0
0
5
10
15
20
25
30
TIME ms.

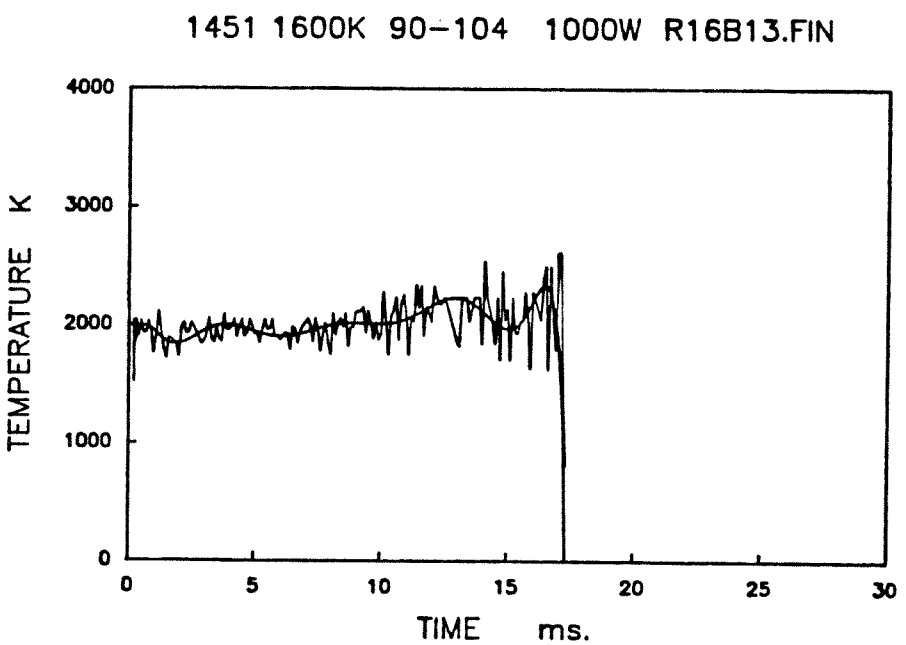
1451 1600K 90–104 1000W R16B13.FIN
TEMPERATURE K
4000
3000
2000
1000
0
0
5
10
15
20
25
30
TIME ms.

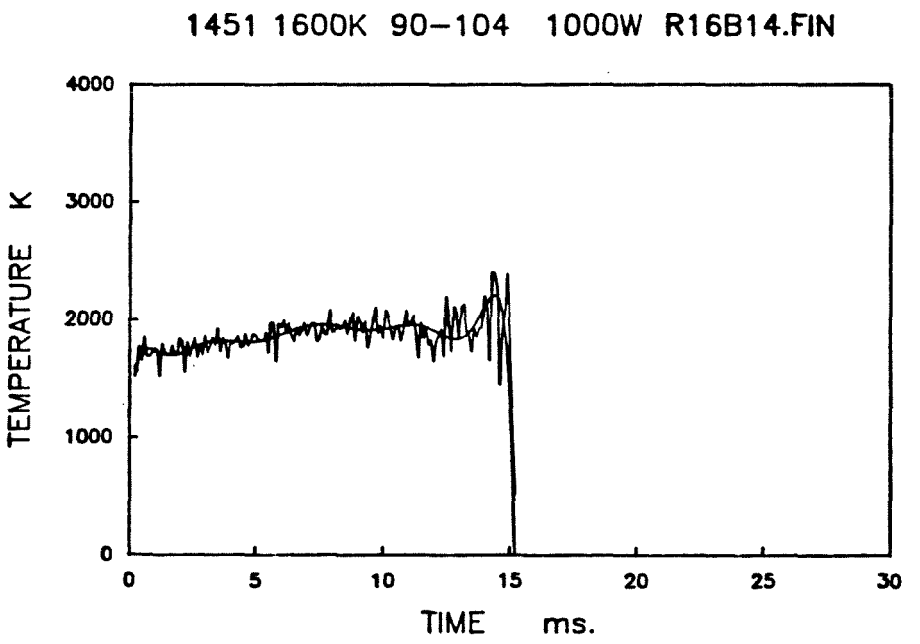
1451 1600K 90-104 1000W R16B14.FIN
TEMPERATURE K
4000
3000
2000
1000
0
0
5
10
15
20
25
30
TIME ms.

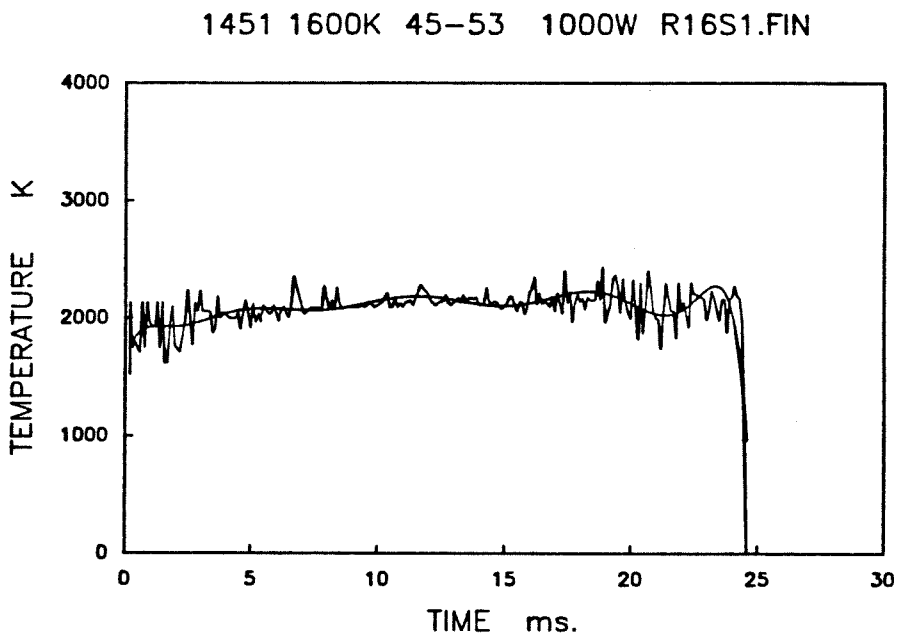
1451 1600K 45–53 1000W R16S1.FIN
TEMPERATURE K
4000
3000
2000
1000
0
0
5
10
15
20
25
30
TIME ms.

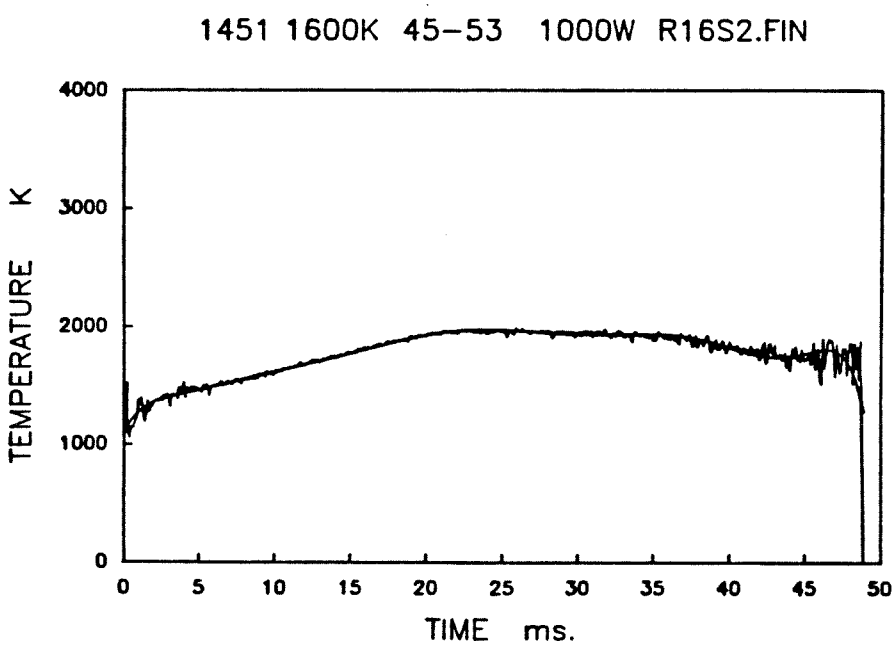
1451 1600K 45–53 1000W R16S2.FIN
TEMPERATURE K
4000
3000
2000
1000
0
0
5
10
15
20
25
30
35
40
45
50
TIME ms.

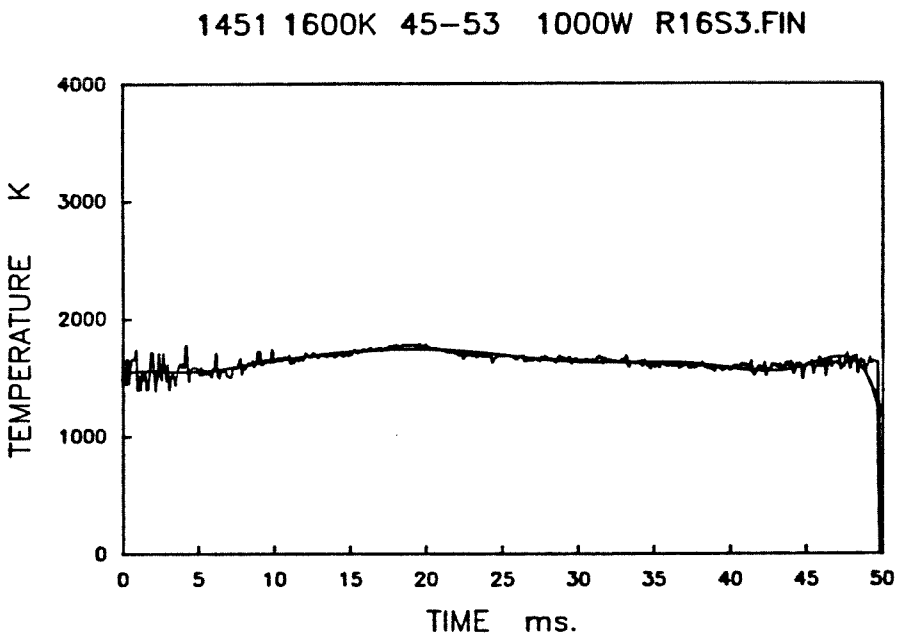
1451 1600K 45–53 1000W R16S3.FIN
TEMPERATURE K
4000
3000
2000
1000
0
0 5 10 15 20 25 30 35 40 45 50
TIME ms.

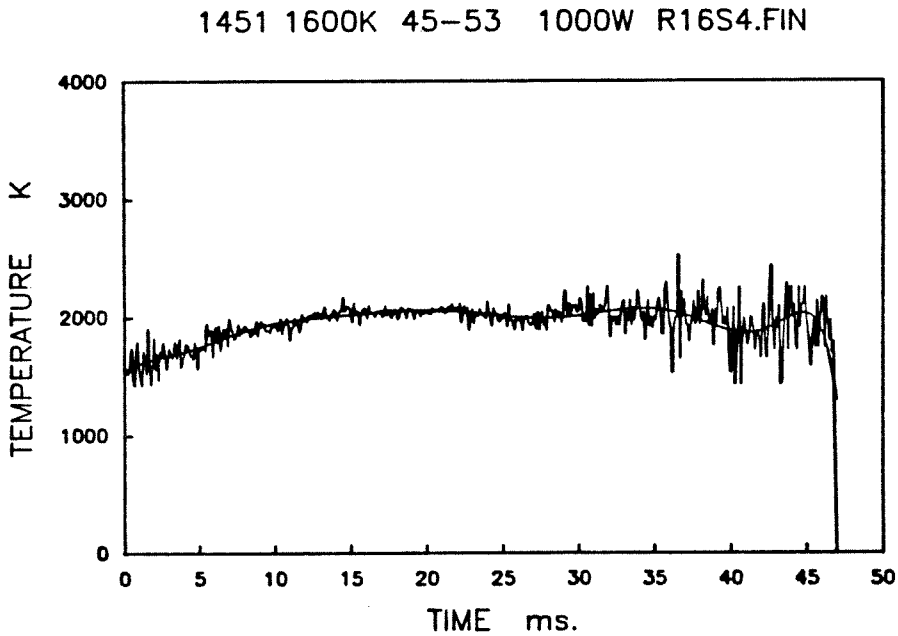
1451 1600K 45–53 1000W R16S4.FIN
TEMPERATURE K
4000
3000
2000
1000
0
0 5 10 15 20 25 30 35 40 45 50
TIME ms.

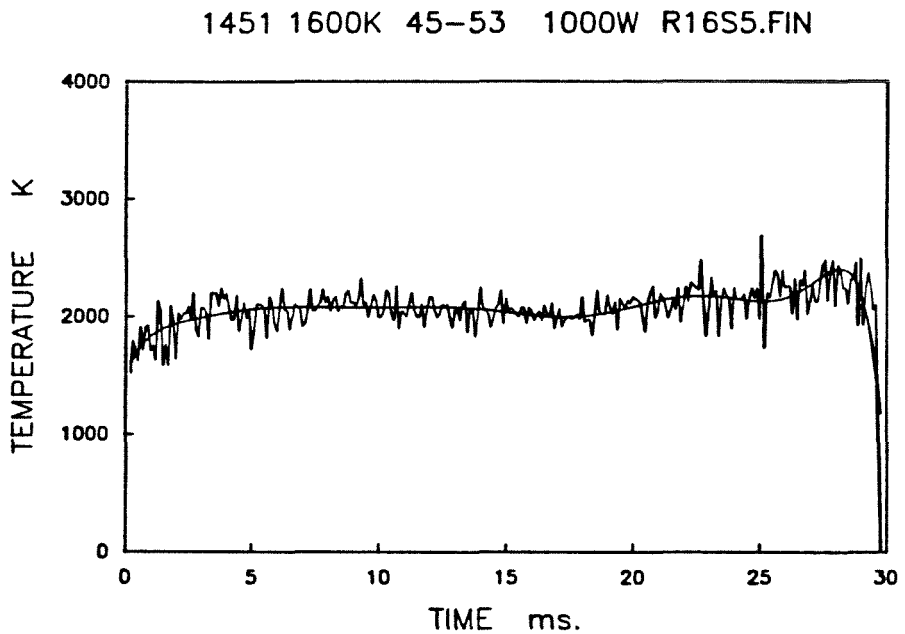
1451 1600K 45–53 1000W R16S5.FIN
TEMPERATURE K
4000
3000
2000
1000
0
0
5
10
15
20
25
30
TIME ms.

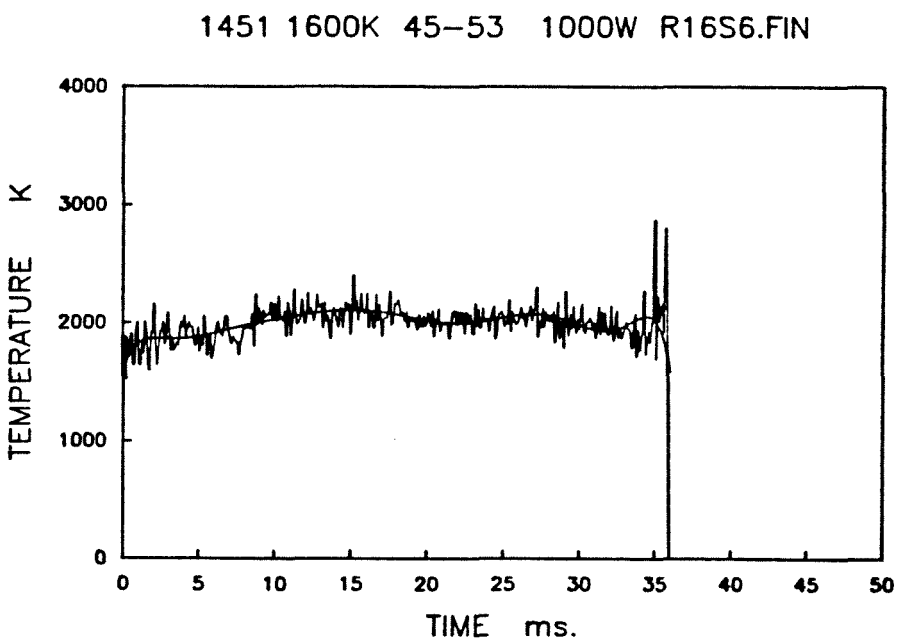
1451 1600K 45–53 1000W R16S6.FIN
TEMPERATURE K
4000
3000
2000
1000
0
0
5
10
15
20
25
30
35
40
45
50
TIME ms.

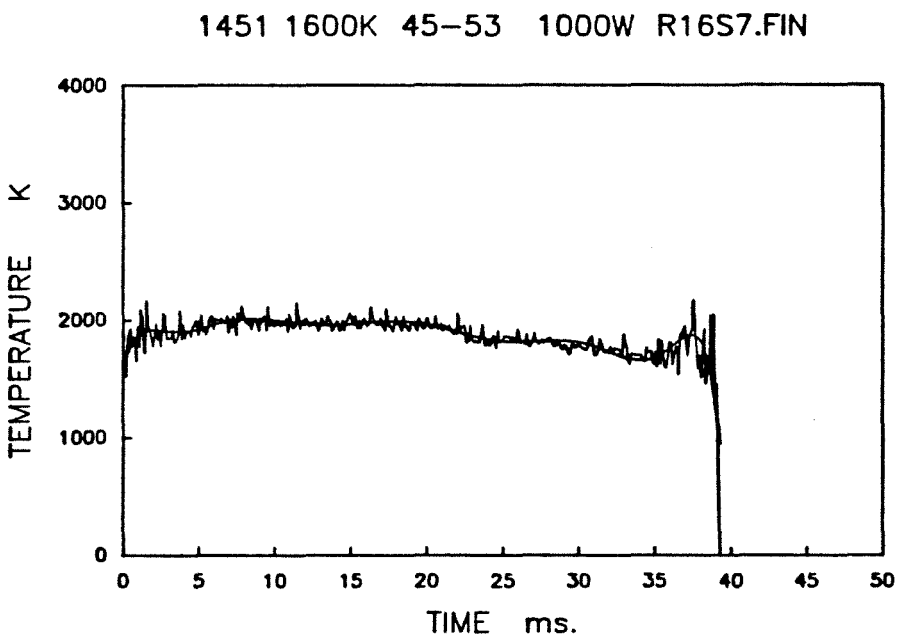
1451 1600K 45-53 1000W R16S7.FIN
TEMPERATURE K
4000
3000
2000
1000
0
0 5 10 15 20 25 30 35 40 45 50
TIME ms.

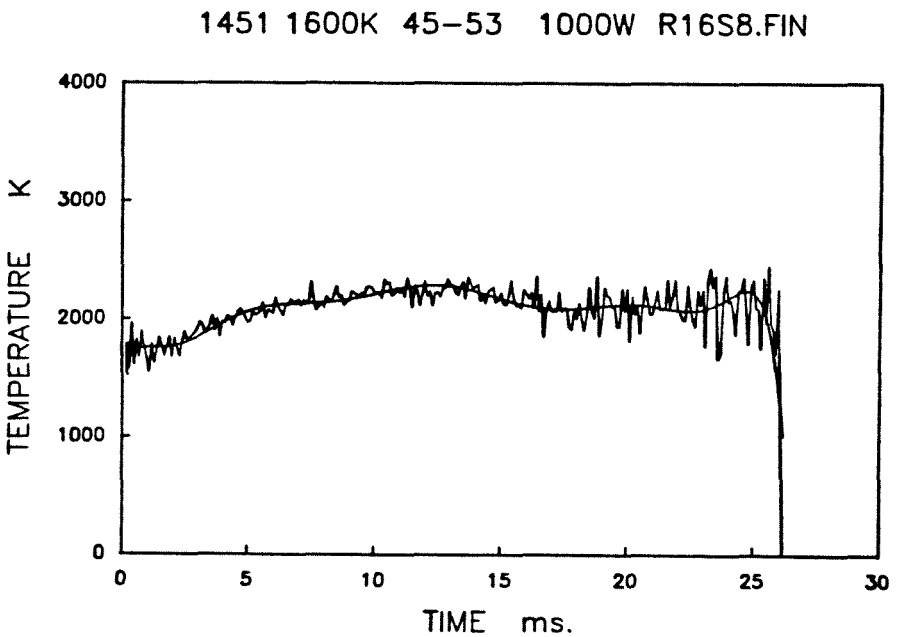
1451 1600K 45-53 1000W R16S8.FIN
TEMPERATURE K
4000
3000
2000
1000
0
0 5 10 15 20 25 30
TIME ms.

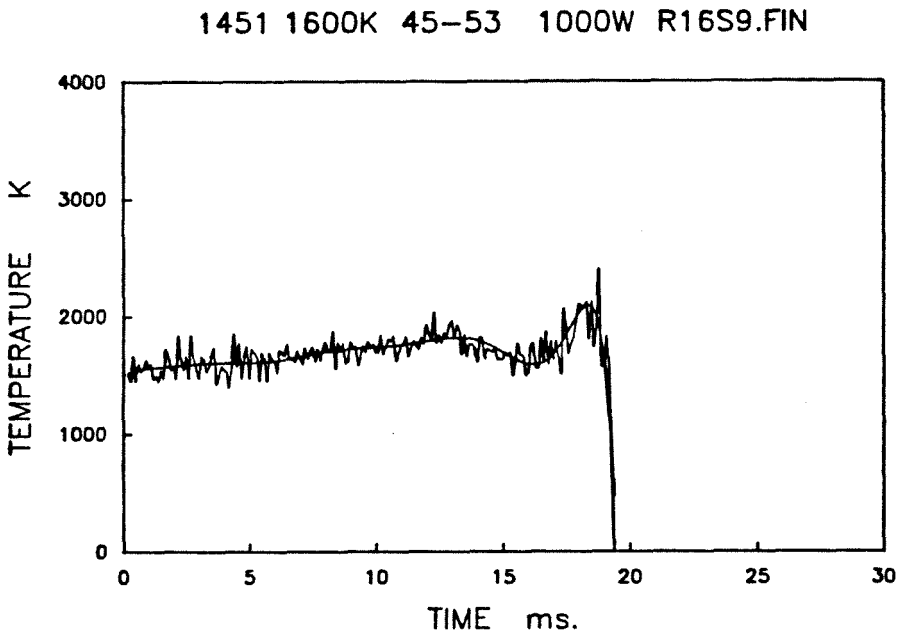
1451 1600K 45–53 1000W R16S9.FIN
TEMPERATURE K
4000
3000
2000
1000
0
0
5
10
15
20
25
30
TIME ms.

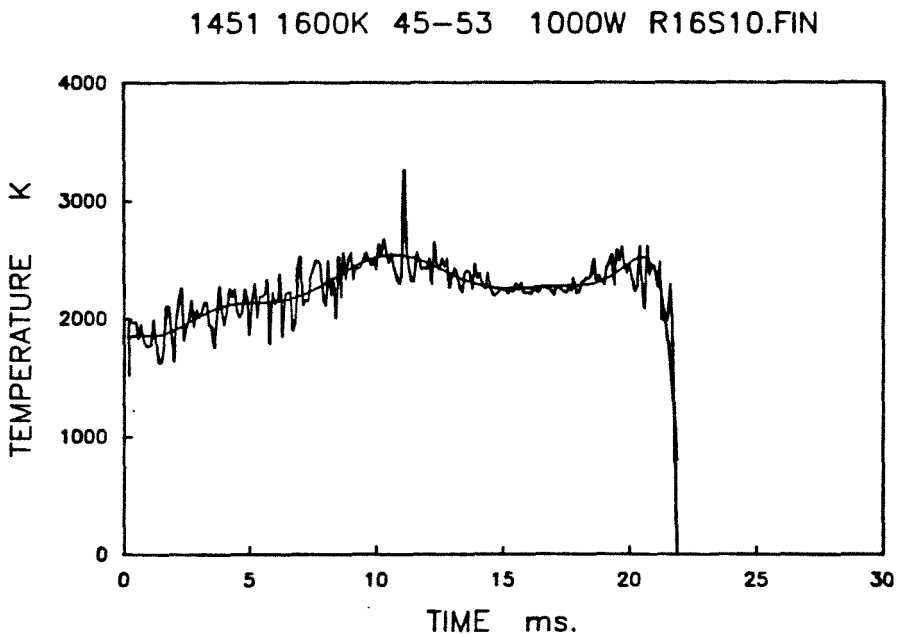
1451 1600K 45–53 1000W R16S10.FIN
TEMPERATURE K
4000
3000
2000
1000
0
0
5
10
15
20
25
30
TIME ms.

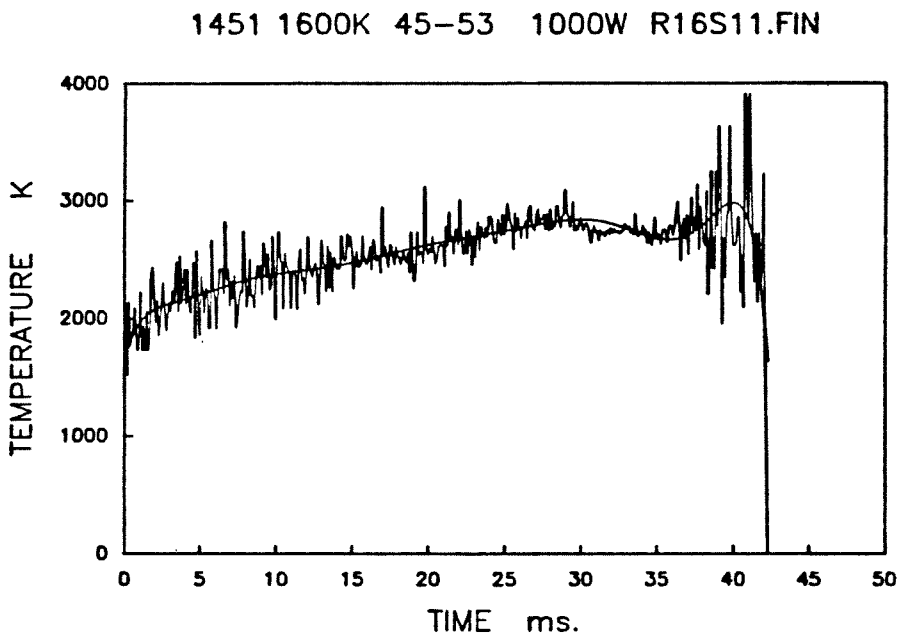
1451 1600K 45–53 1000W R16S11.FIN
TEMPERATURE K
4000
3000
2000
1000
0
0 5 10 15 20 25 30 35 40 45 50
TIME ms.

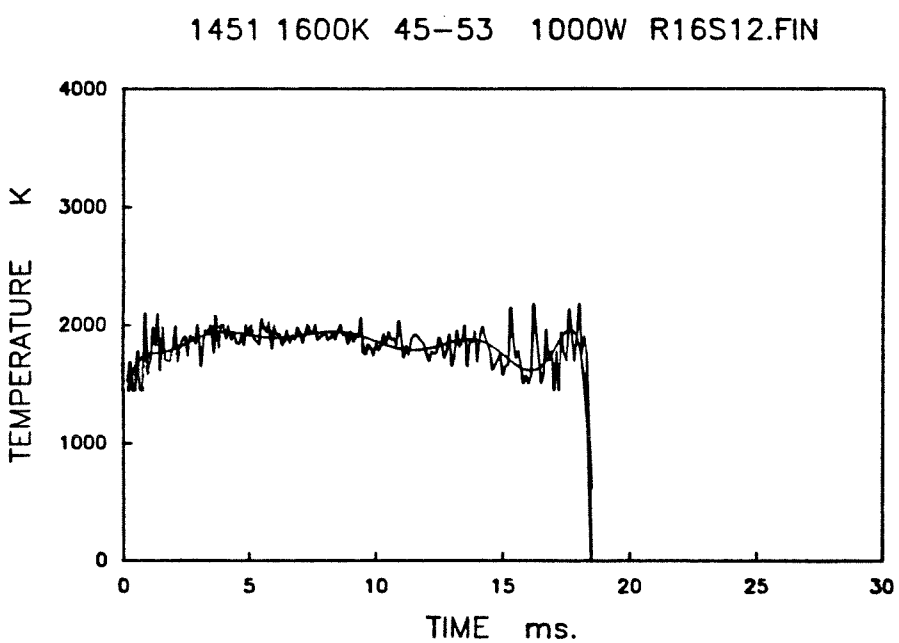
1451 1600K 45–53 1000W R16S12.FIN
TEMPERATURE K
4000
3000
2000
1000
0
0 5 10 15 20 25 30
TIME ms.

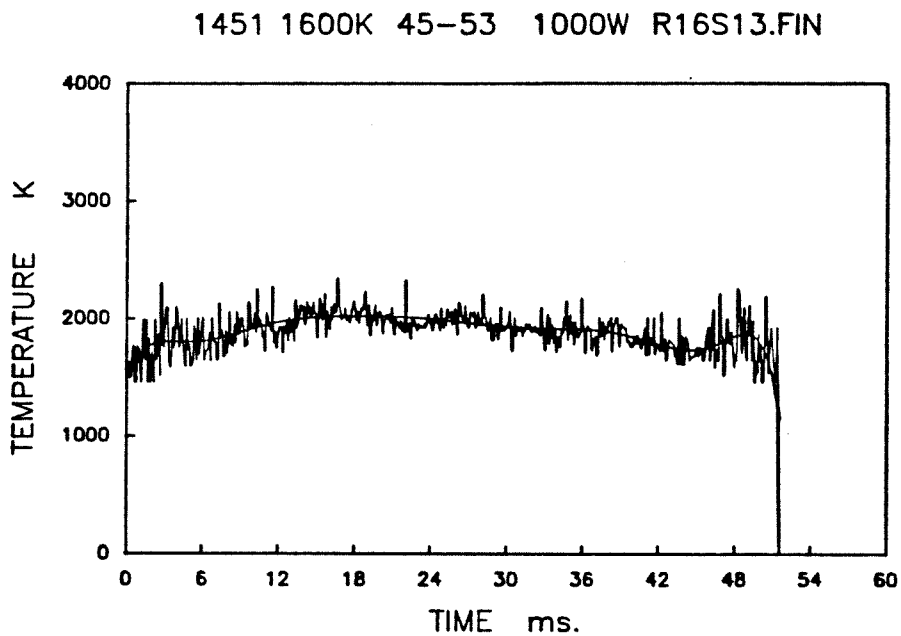
1451 1600K 45–53 1000W R16S13.FIN
TEMPERATURE K
4000
3000
2000
1000
0
0
6
12
18
24
30
36
42
48
54
60
TIME ms.

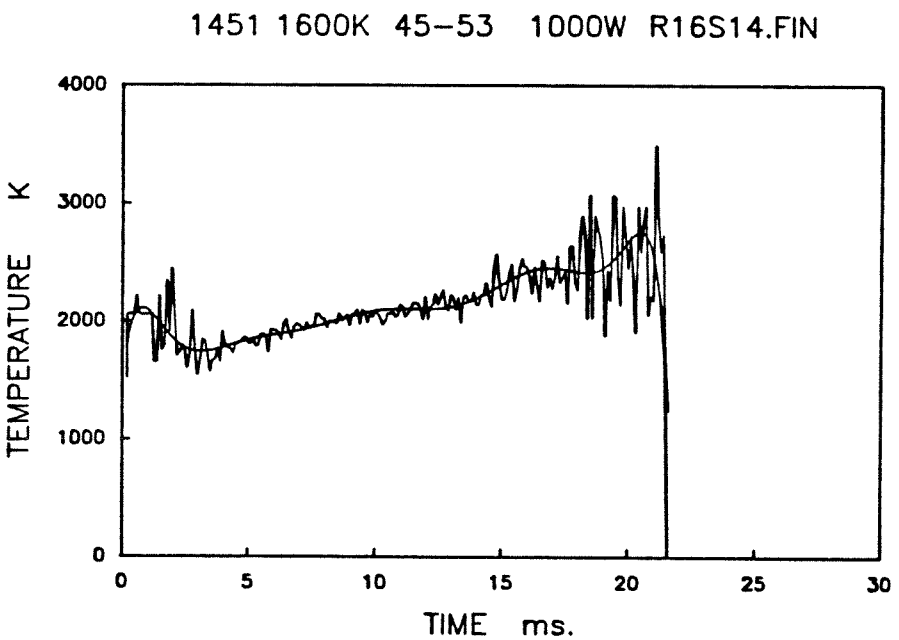
1451 1600K 45–53 1000W R16S14.FIN
TEMPERATURE K
4000
3000
2000
1000
0
0
5
10
15
20
25
30
TIME ms.

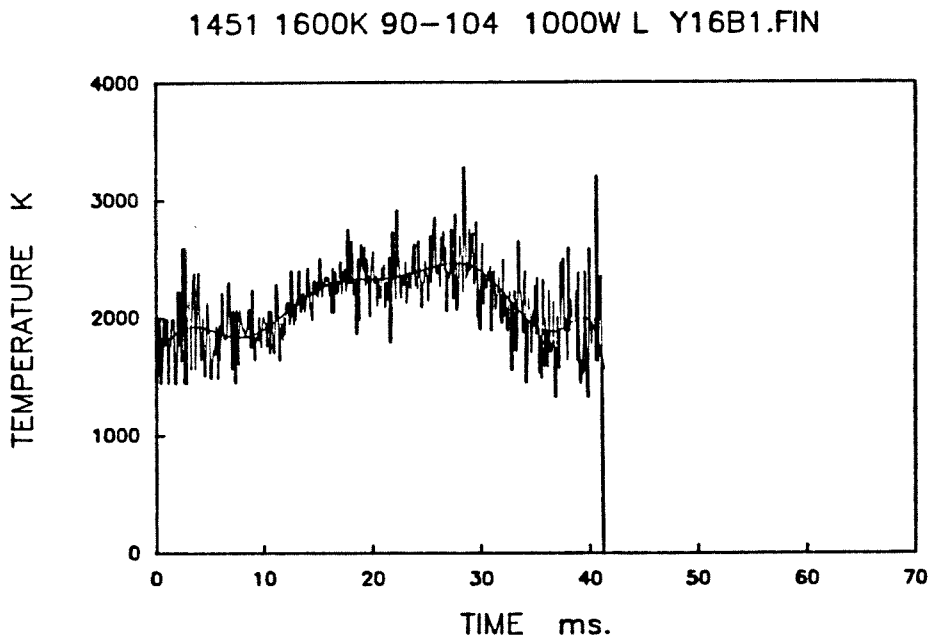
1451 1600K 90–104 1000W L Y16B1.FIN
TEMPERATURE K
4000
3000
2000
1000
0
0
10
20
30
40
50
60
70
TIME ms.

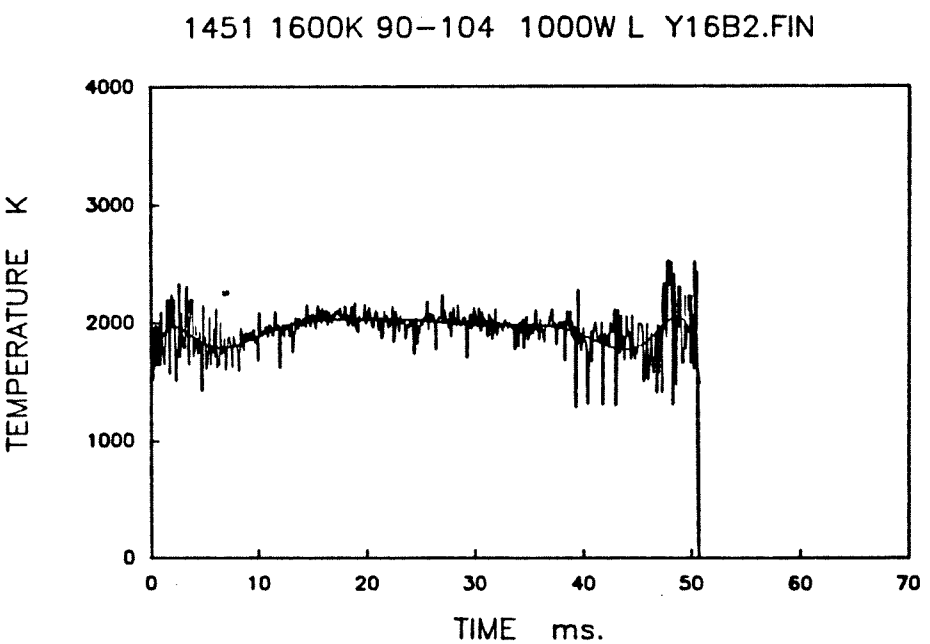
1451 1600K 90–104 1000W L Y16B2.FIN
TEMPERATURE K
4000
3000
2000
1000
0
0
10
20
30
40
50
60
70
TIME ms.

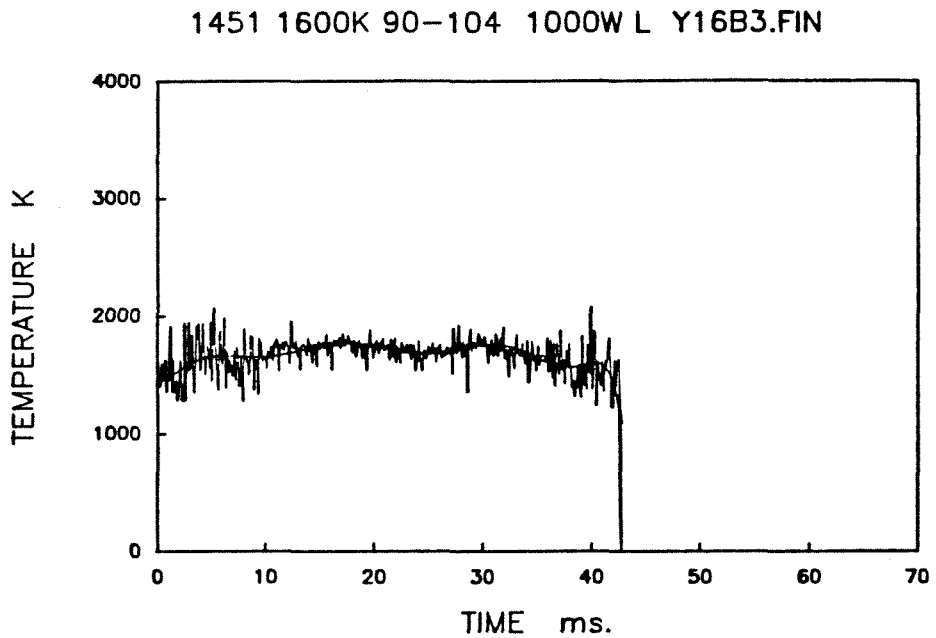
1451 1600K 90–104 1000W L Y16B3.FIN
TEMPERATURE K
4000
3000
2000
1000
0
0
10
20
30
40
50
60
70
TIME ms.

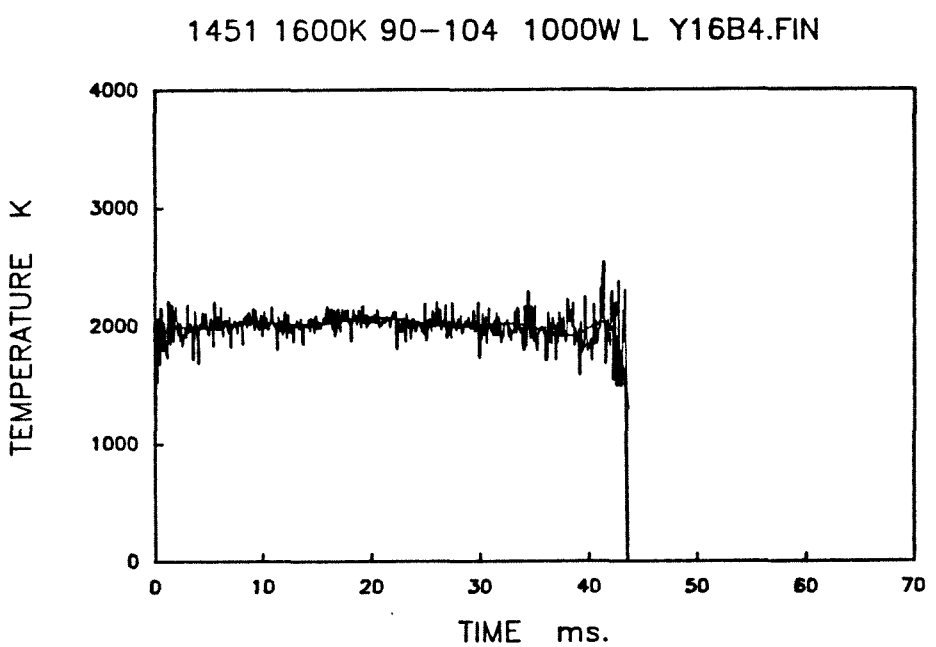
1451 1600K 90–104 1000W L Y16B4.FIN
TEMPERATURE K
4000
3000
2000
1000
0
0
10
20
30
40
50
60
70
TIME ms.

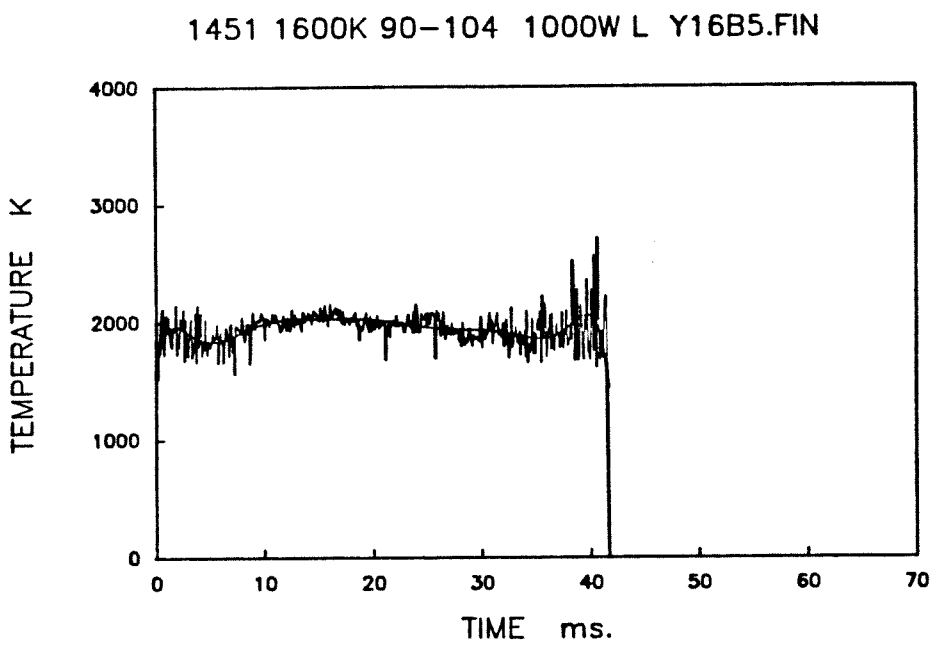
1451 1600K 90–104 1000W L Y16B5.FIN
TEMPERATURE K
4000
3000
2000
1000
0
0
10
20
30
40
50
60
70
TIME ms.

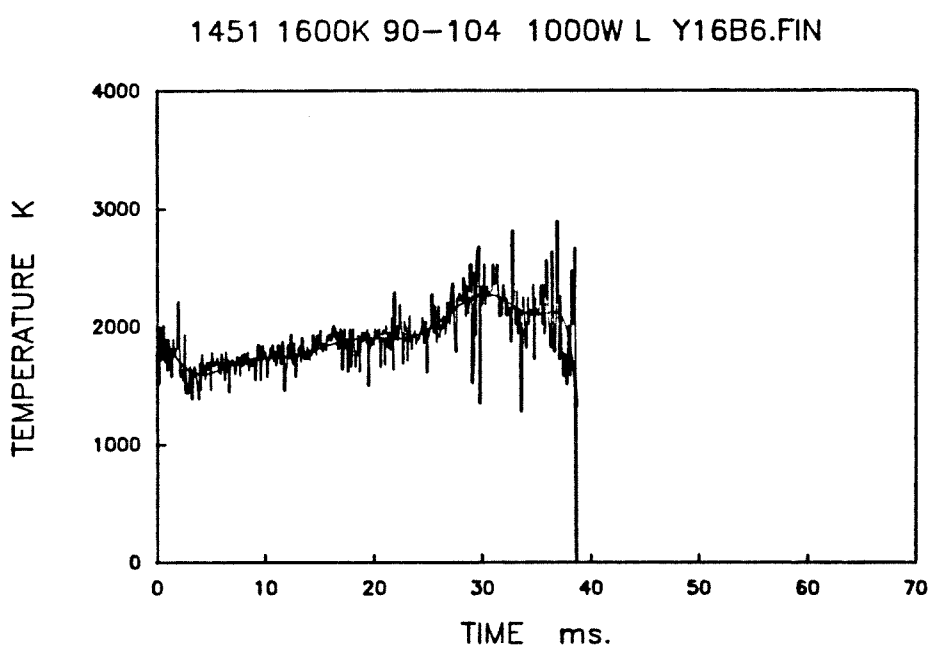
1451 1600K 90–104 1000W L Y16B6.FIN
TEMPERATURE K
4000
3000
2000
1000
0
0
10
20
30
40
50
60
70
TIME ms.

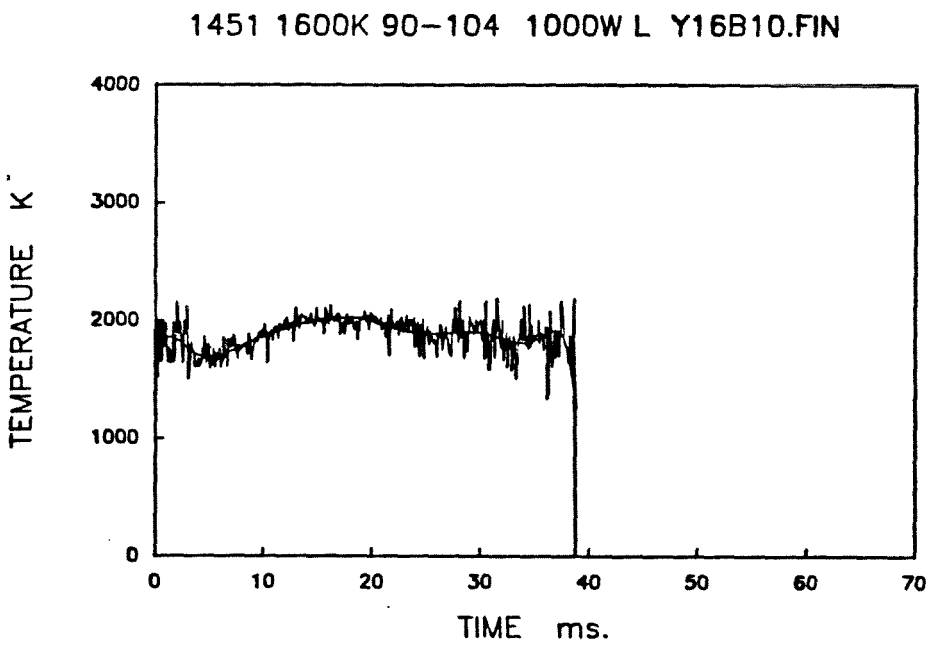
1451 1600K 90–104 1000W L Y16B10.FIN
TEMPERATURE K
4000
3000
2000
1000
0
0
10
20
30
40
50
60
70
TIME ms.

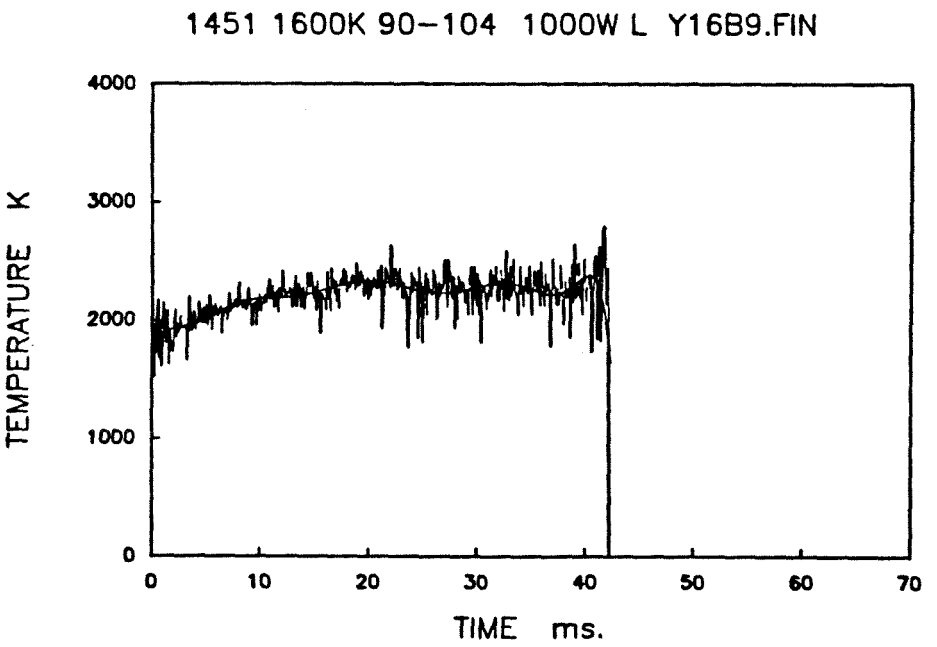
1451 1600K 90–104 1000W L Y16B9.FIN
TEMPERATURE K
4000
3000
2000
1000
0
0
10
20
30
40
50
60
70
TIME ms.

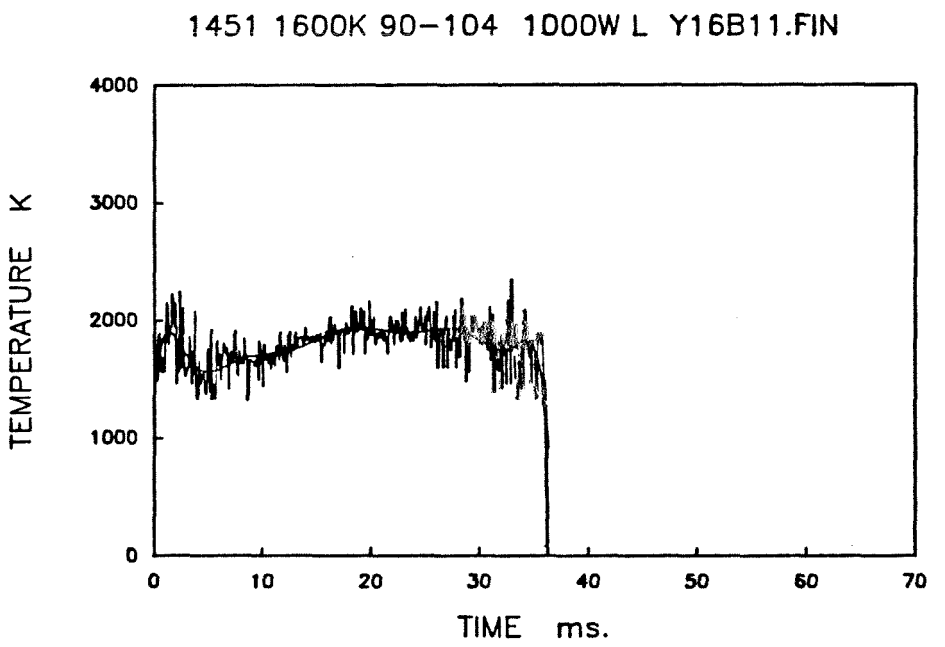
1451 1600K 90–104 1000W L Y16B11.FIN
TEMPERATURE K
4000
3000
2000
1000
0
0
10
20
30
40
50
60
70
TIME ms.

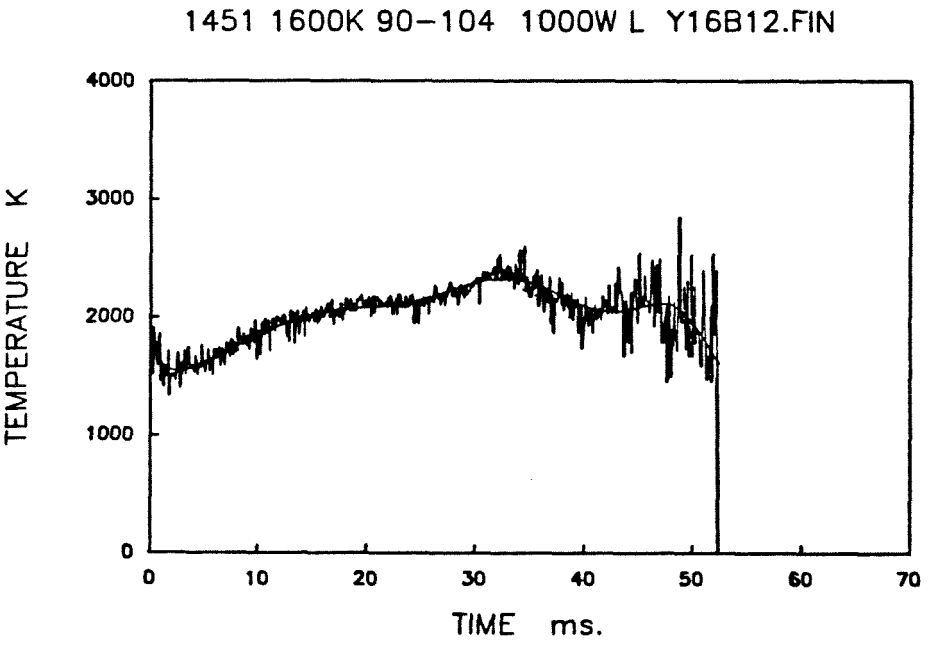
1451 1600K 90–104 1000W L Y16B12.FIN
TEMPERATURE K
4000
3000
2000
1000
0
0
10
20
30
40
50
60
70
TIME ms.

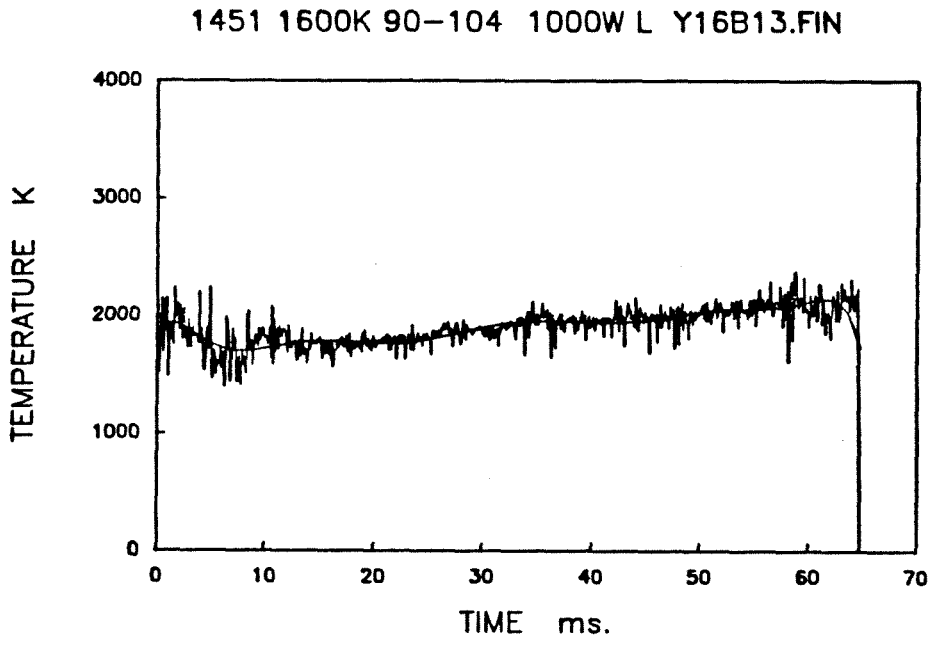
1451 1600K 90–104 1000W L Y16B13.FIN
TEMPERATURE K
4000
3000
2000
1000
0
0
10
20
30
40
50
60
70
TIME ms.

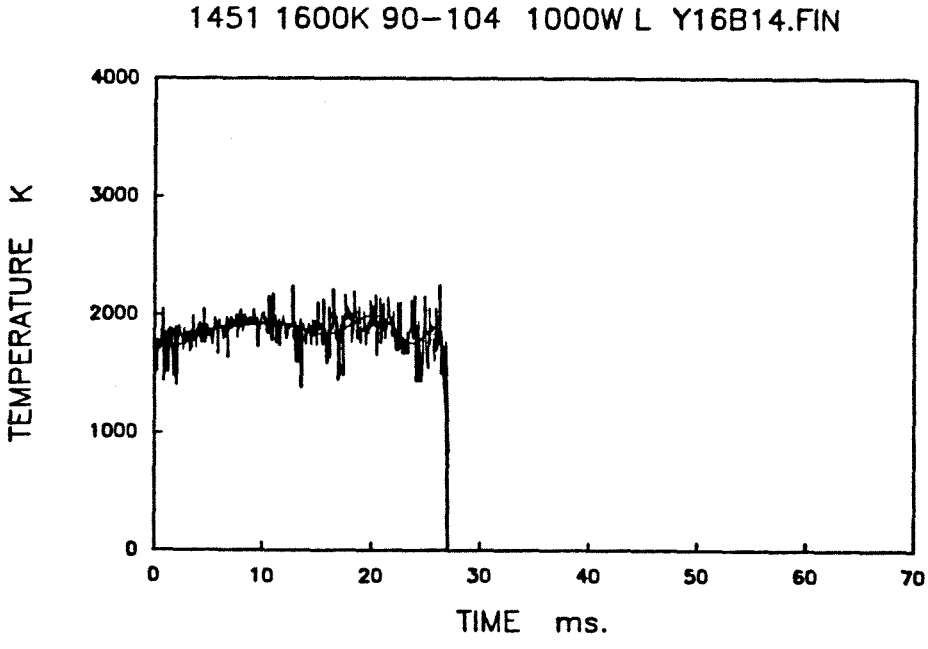
1451 1600K 90–104 1000W L Y16B14.FIN
TEMPERATURE K
4000
3000
2000
1000
0
0
10
20
30
40
50
60
70
TIME ms.

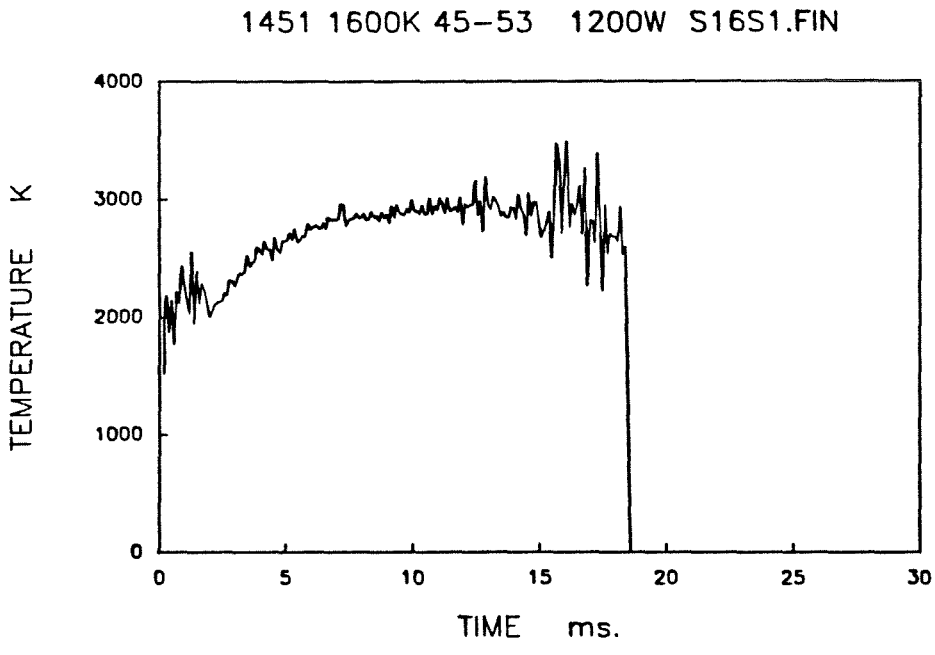
1451 1600K 45-53 1200W S16S1.FIN
TEMPERATURE K
4000
3000
2000
1000
0
0
5
10
15
20
25
30
TIME ms.

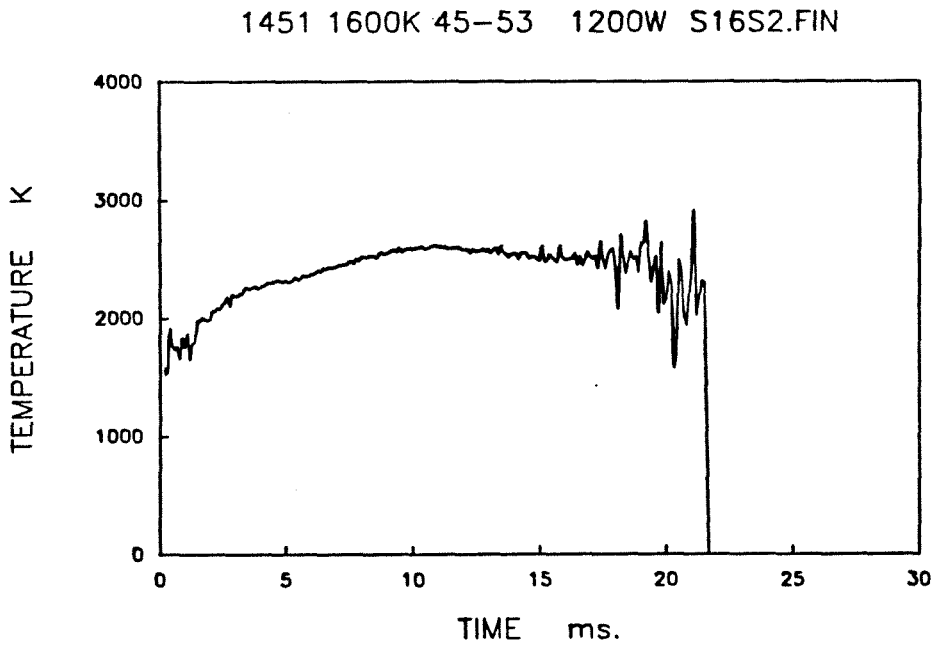
1451 1600K 45-53 1200W S16S2.FIN
TEMPERATURE K
4000
3000
2000
1000
0
0
5
10
15
20
25
30
TIME ms.

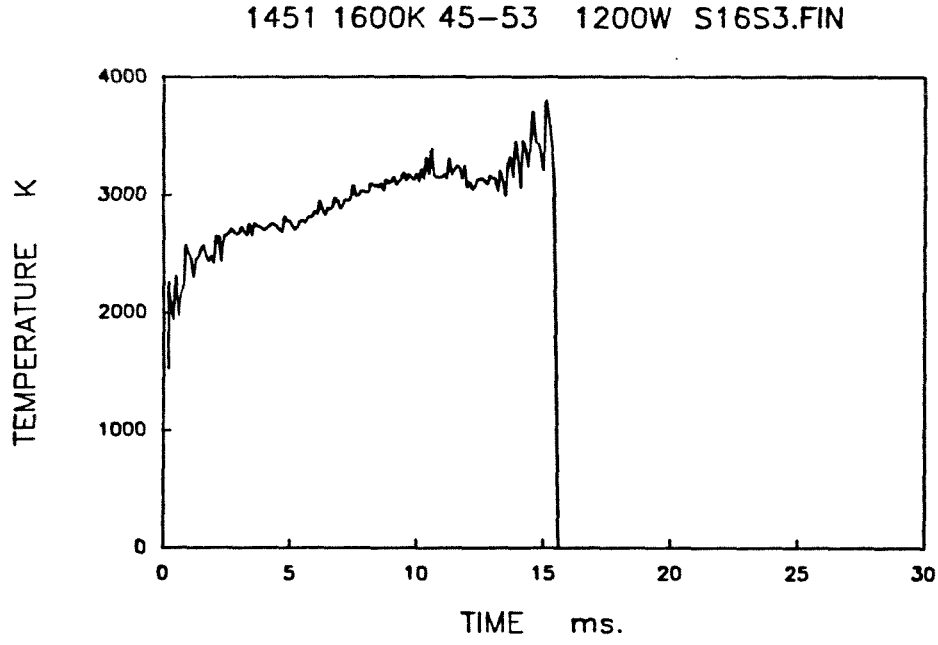
1451 1600K 45–53 1200W S16S3.FIN
TEMPERATURE K
4000
3000
2000
1000
0
0
5
10
15
20
25
30
TIME ms.

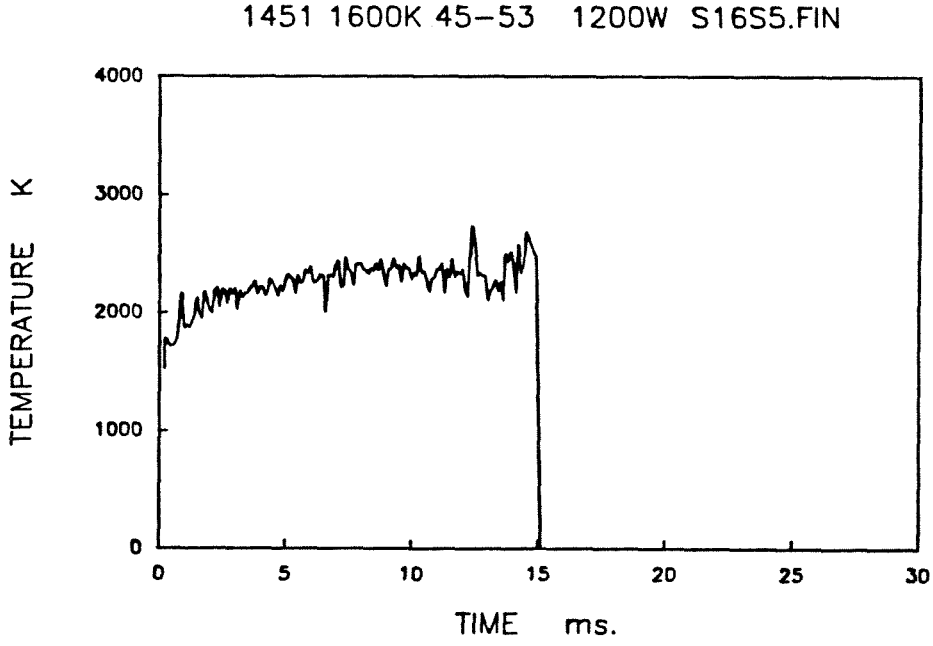
1451 1600K 45–53 1200W S16S5.FIN
TEMPERATURE K
4000
3000
2000
1000
0
0
5
10
15
20
25
30
TIME ms.

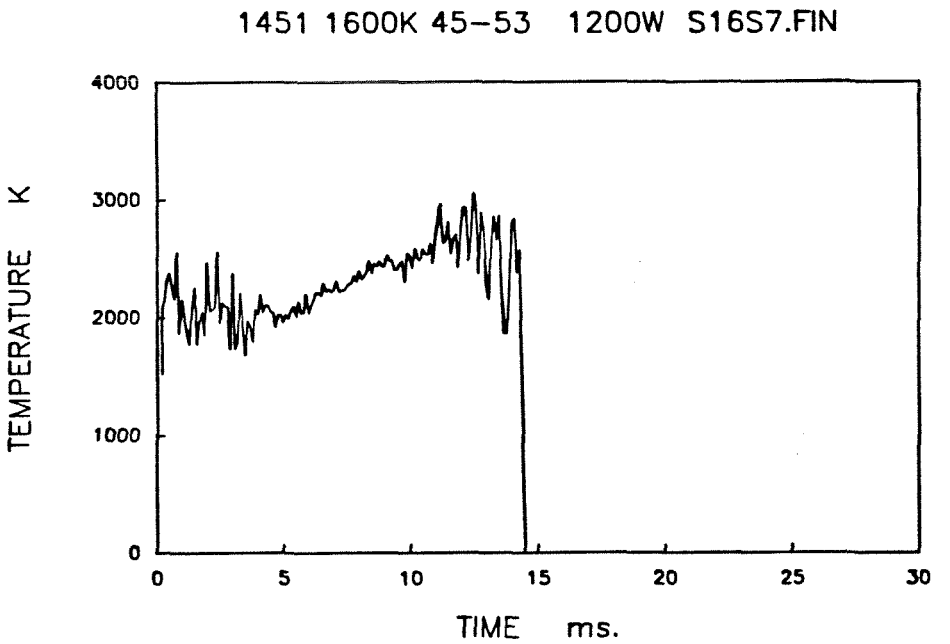
1451 1600K 45–53 1200W S16S7.FIN
TEMPERATURE K
4000
3000
2000
1000
0
0
5
10
15
20
25
30
TIME ms.

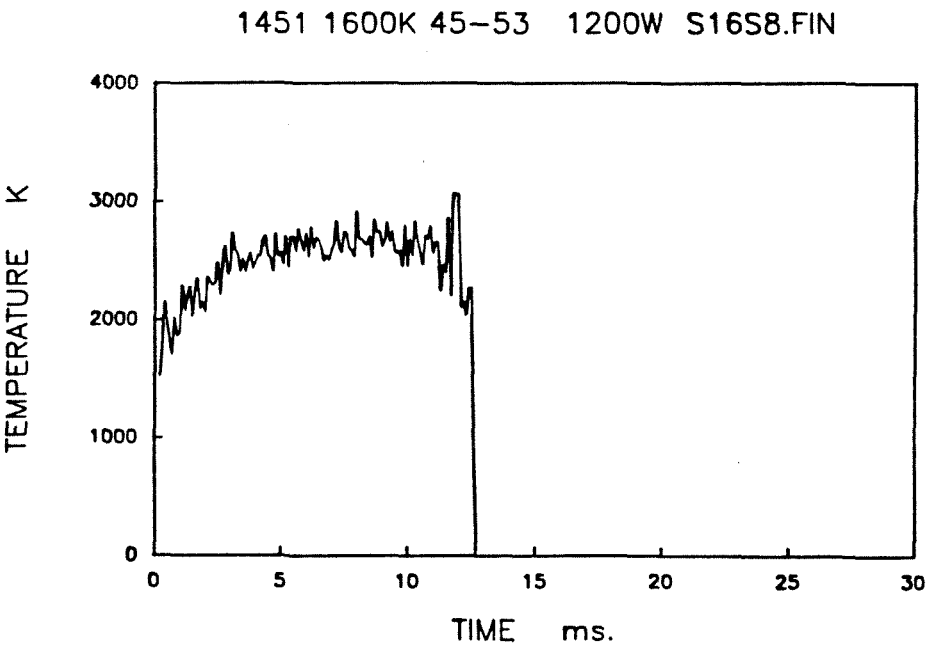
1451 1600K 45–53 1200W S16S8.FIN
TEMPERATURE K
4000
3000
2000
1000
0
0
5
10
15
20
25
30
TIME ms.

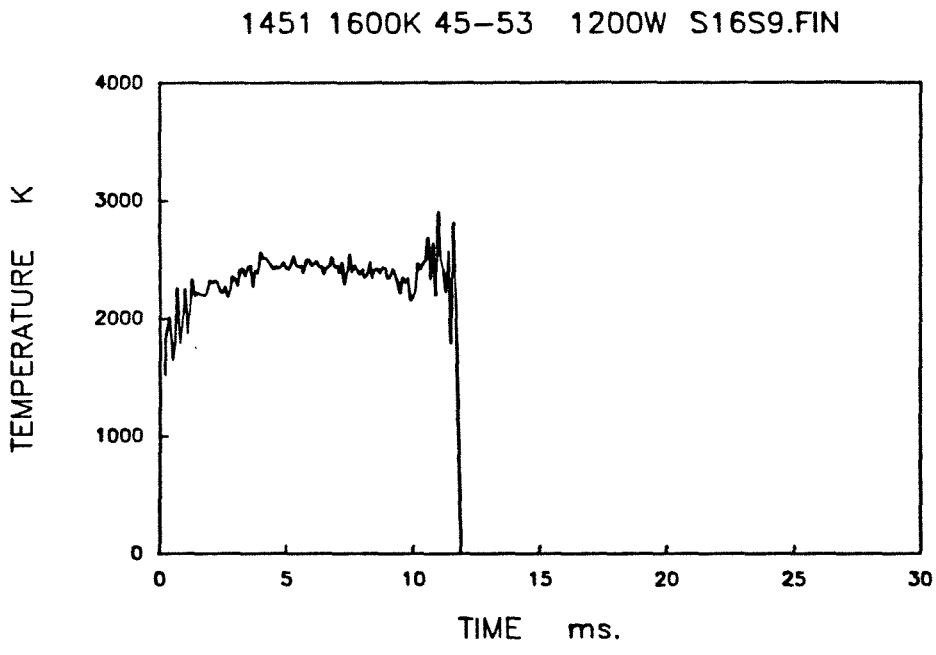
1451 1600K 45–53 1200W S16S9.FIN
TEMPERATURE K
4000
3000
2000
1000
0
0
5
10
15
20
25
30
TIME ms.

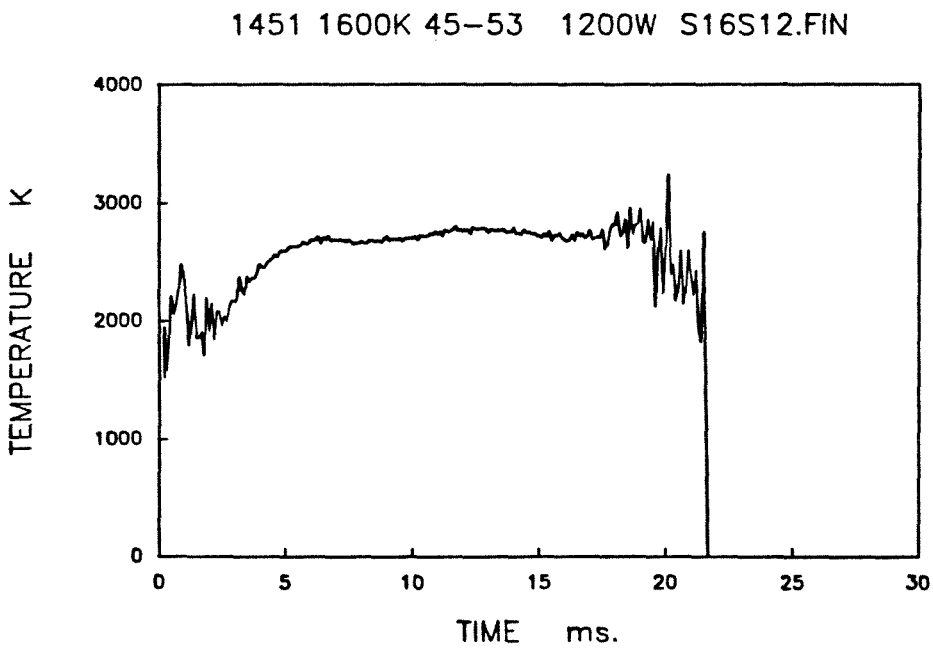
1451 1600K 45–53 1200W S16S12.FIN
TEMPERATURE K
4000
3000
2000
1000
0
0
5
10
15
20
25
30
TIME ms.

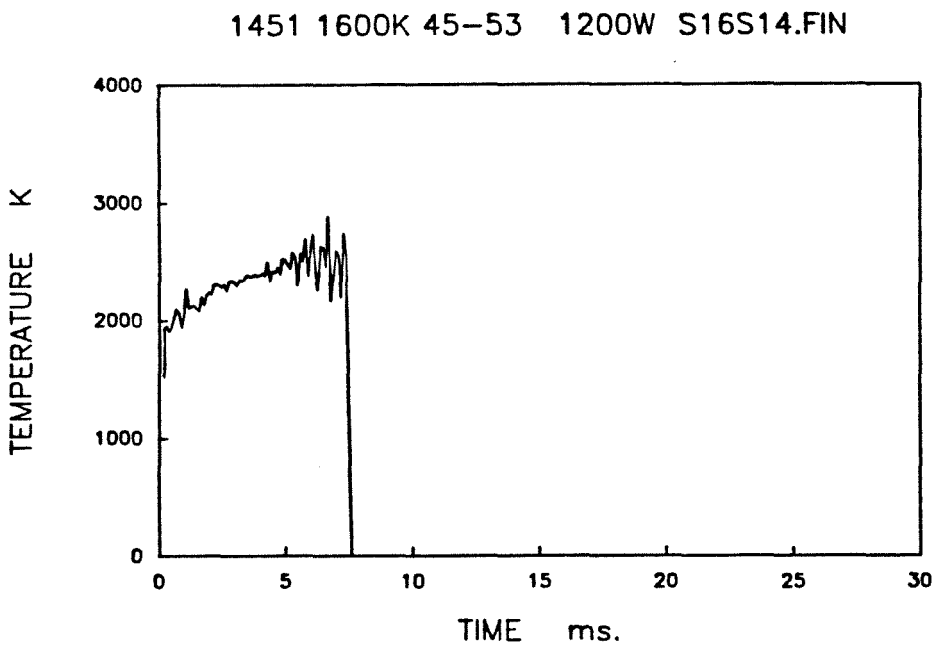
1451 1600K 45–53 1200W S16S14.FIN
TEMPERATURE K
4000
3000
2000
1000
0
0
5
10
15
20
25
30
TIME ms.

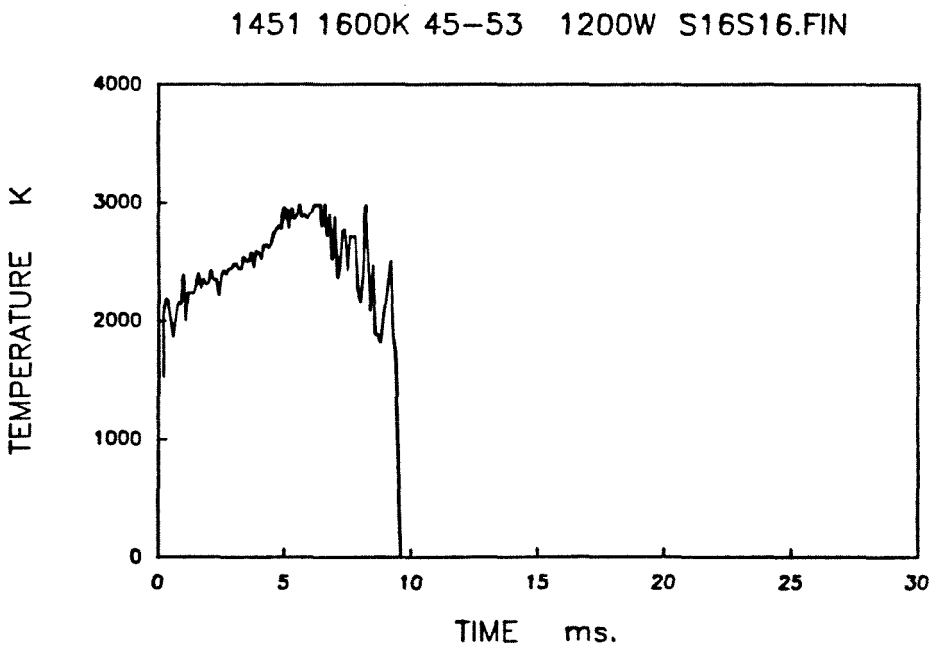
1451 1600K 45–53 1200W S16S16.FIN
TEMPERATURE K
4000
3000
2000
1000
0
0
5
10
15
20
25
30
TIME ms.

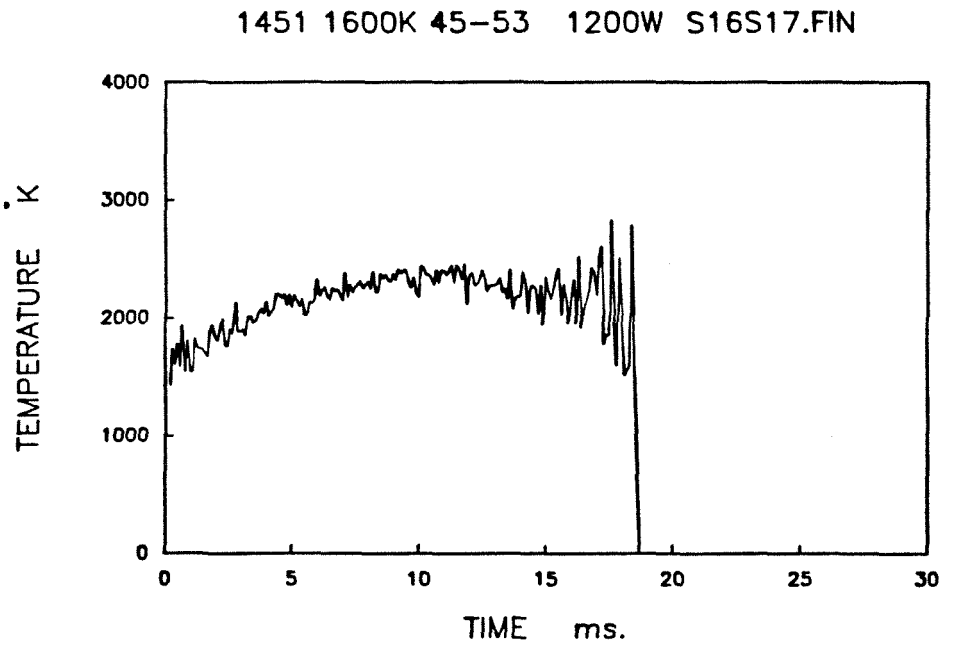
1451 1600K 45-53 1200W S16S17.FIN
TEMPERATURE K
4000
3000
2000
1000
0
0
5
10
15
20
25
30
TIME ms.

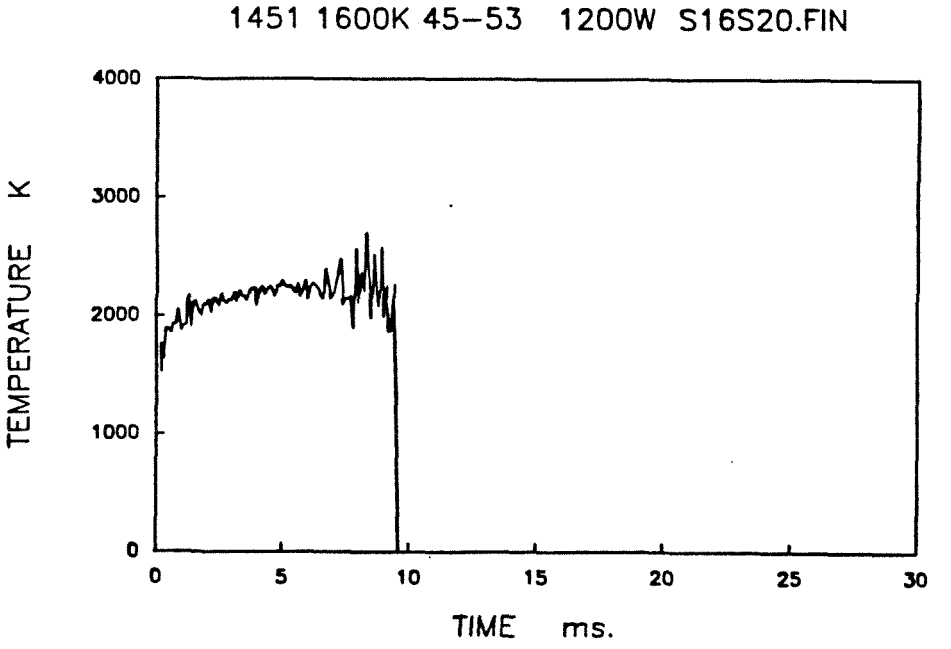
1451 1600K 45-53 1200W S16S20.FIN
TEMPERATURE K
4000
3000
2000
1000
0
0
5
10
15
20
25
30
TIME ms.

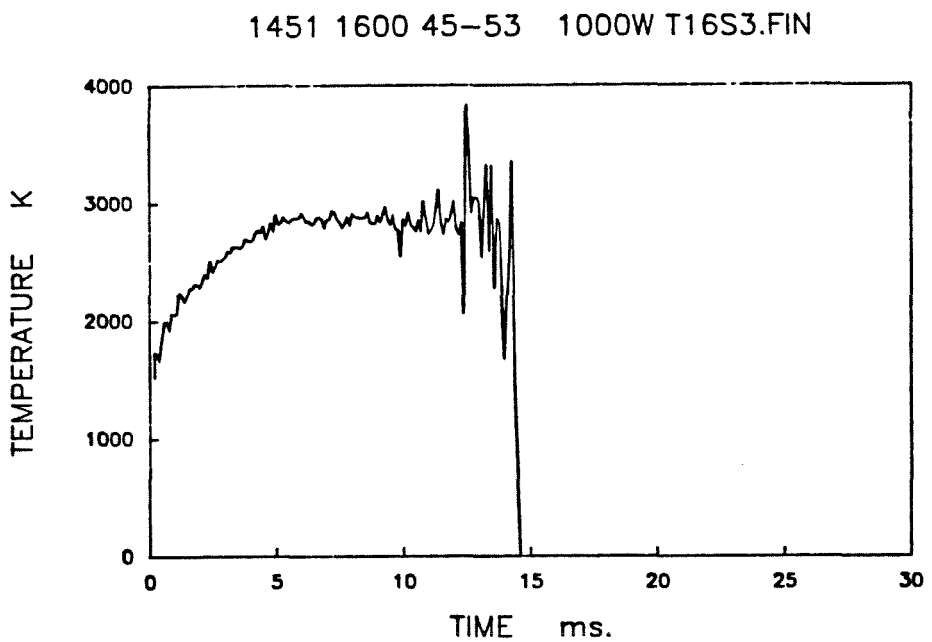
1451 1600 45–53 1000W T16S3.FIN
TEMPERATURE K
4000
3000
2000
1000
0
0
5
10
15
20
25
30
TIME ms.

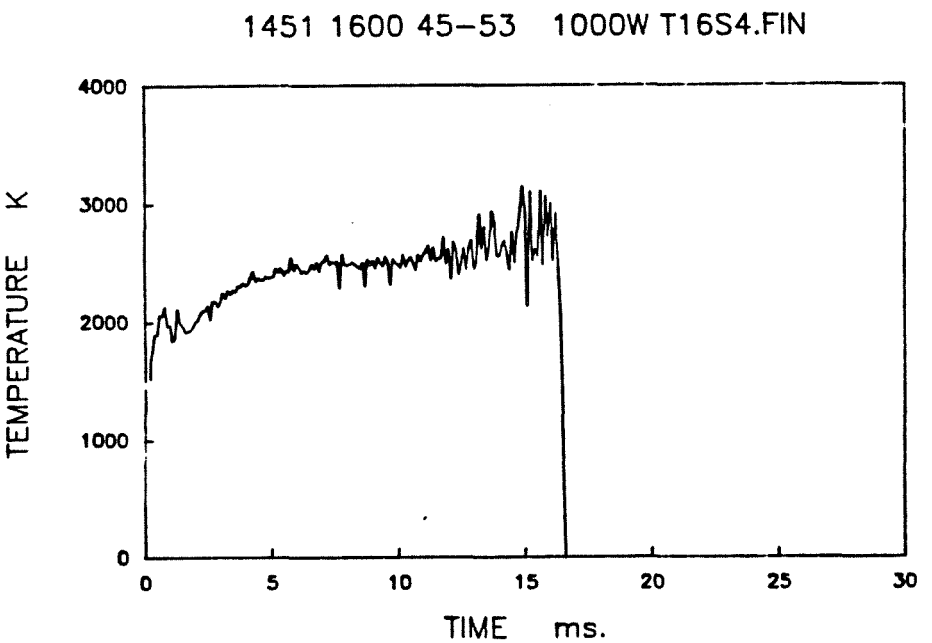
1451 1600 45–53 1000W T16S4.FIN
TEMPERATURE K
4000
3000
2000
1000
0
0
5
10
15
20
25
30
TIME ms.

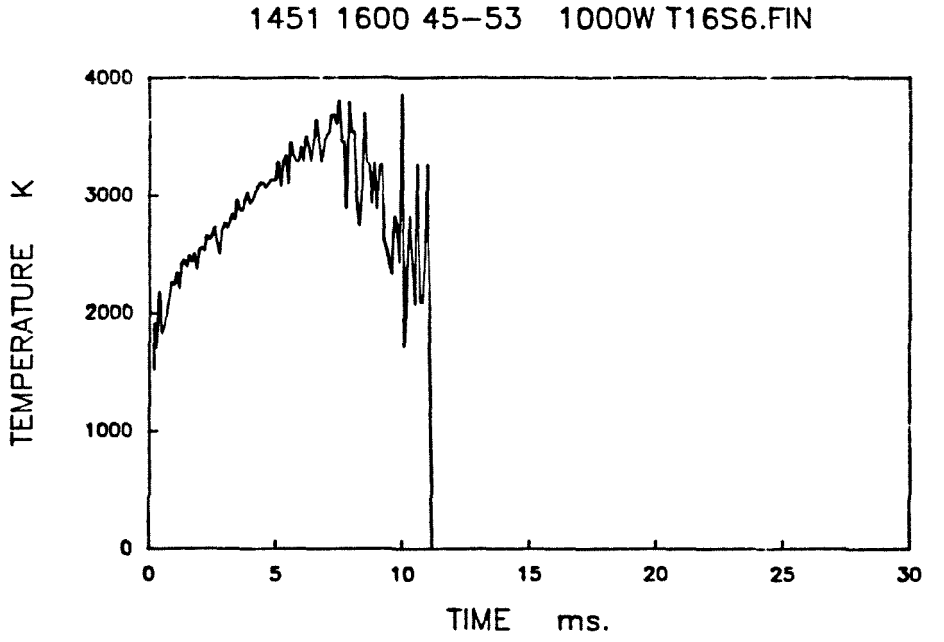
1451 1600 45–53 1000W T16S6.FIN
TEMPERATURE K
4000
3000
2000
1000
0
0
5
10
15
20
25
30
TIME ms.

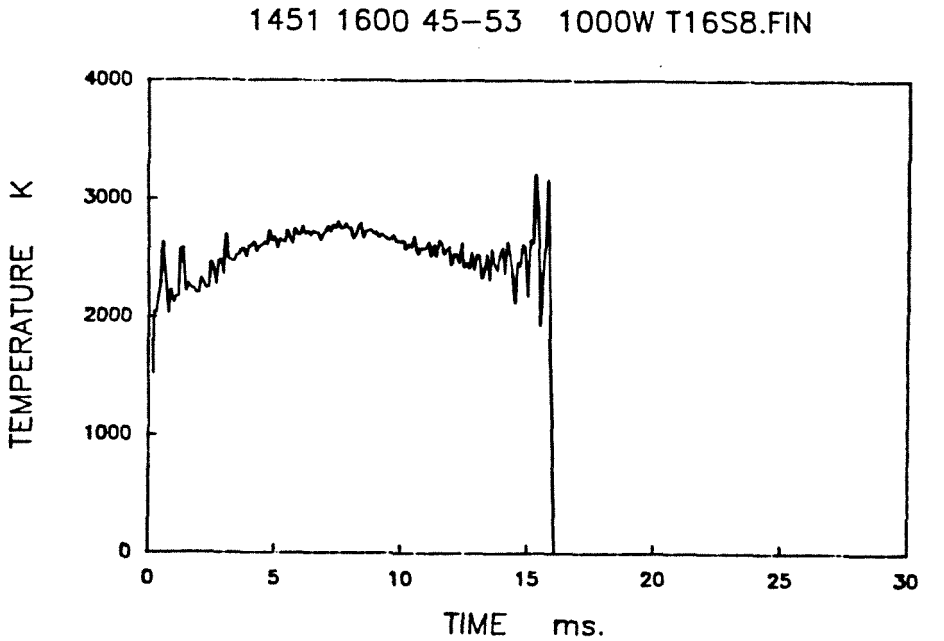
1451 1600 45–53 1000W T16S8.FIN
TEMPERATURE K
4000
3000
2000
1000
0
0
5
10
15
20
25
30
TIME ms.

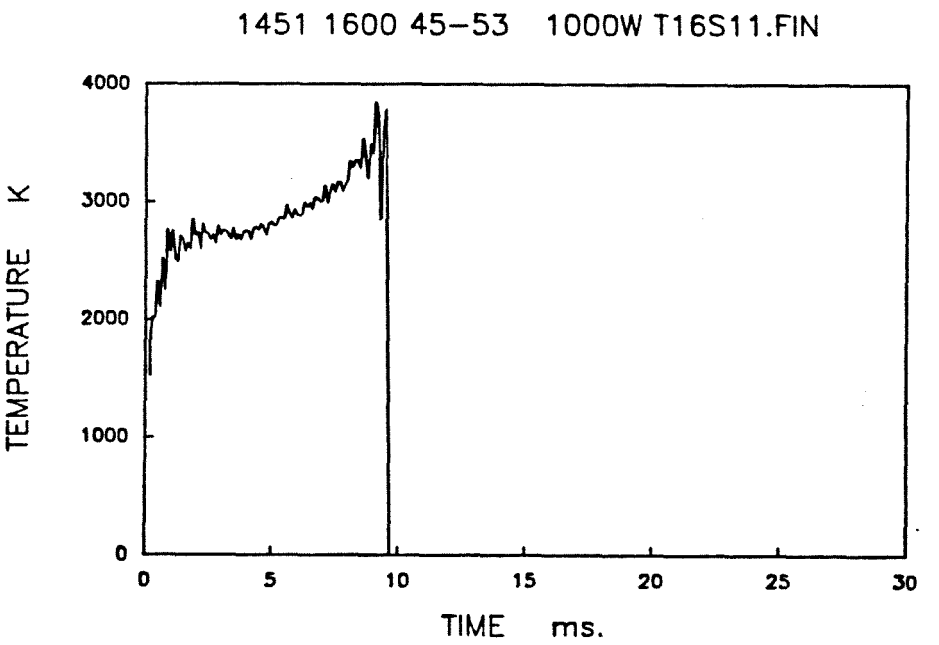
1451 1600 45–53 1000W T16S11.FIN
TEMPERATURE K
4000
3000
2000
1000
0
0
5
10
15
20
25
30
TIME ms.

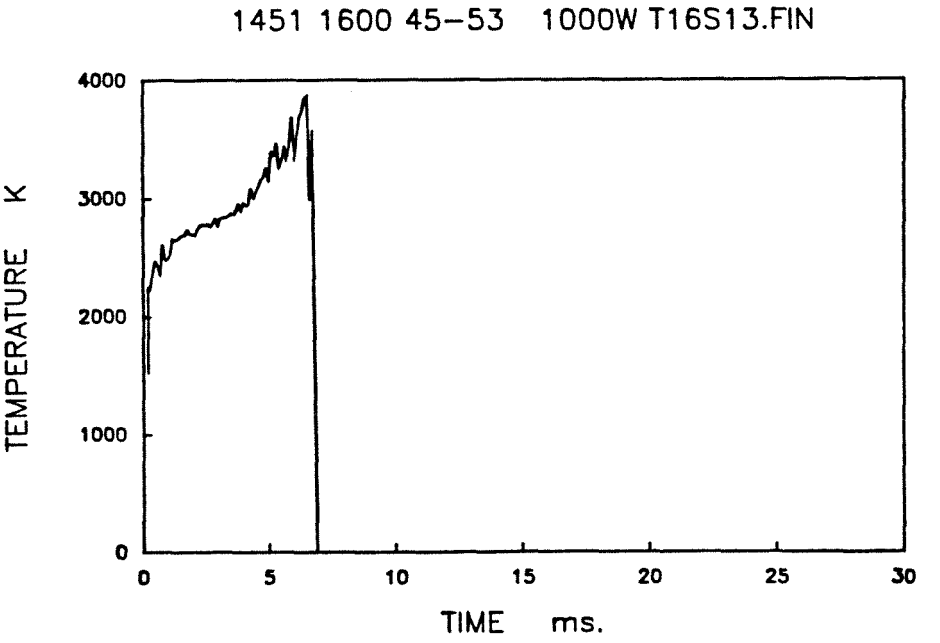
1451 1600 45–53 1000W T16S13.FIN
TEMPERATURE K
4000
3000
2000
1000
0
0
5
10
15
20
25
30
TIME ms.

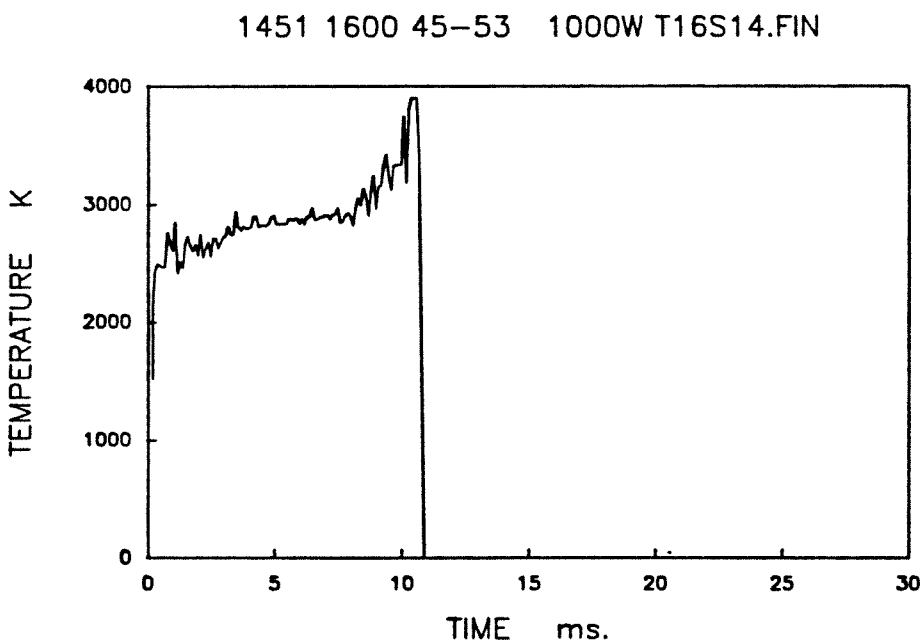
1451 1600 45–53 1000W T16S14.FIN
TEMPERATURE K
4000
3000
2000
1000
0
0
5
10
15
20
25
30
TIME ms.

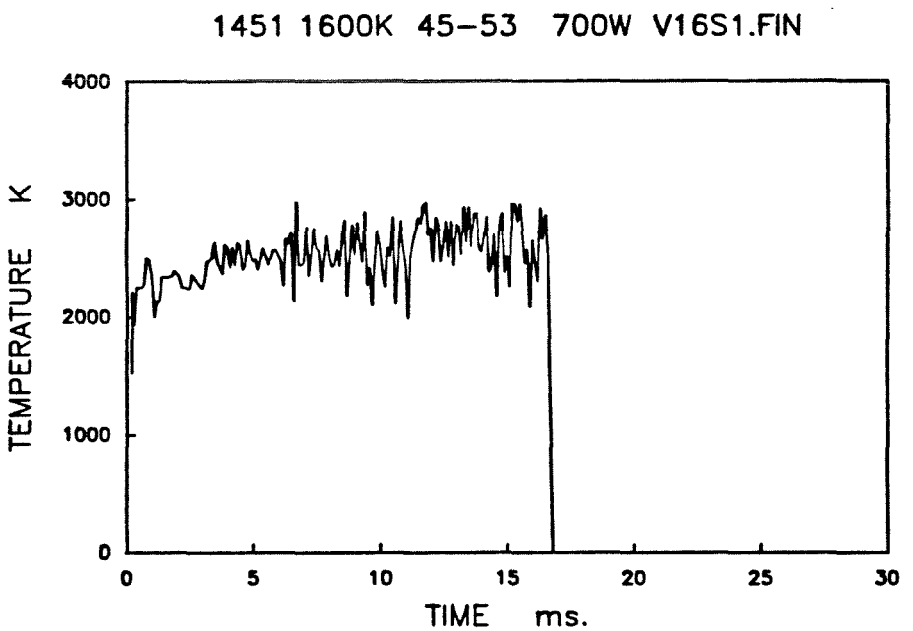
1451 1600K 45–53 700W V16S1.FIN
TEMPERATURE K
4000
3000
2000
1000
0
0
5
10
15
20
25
30
TIME ms.

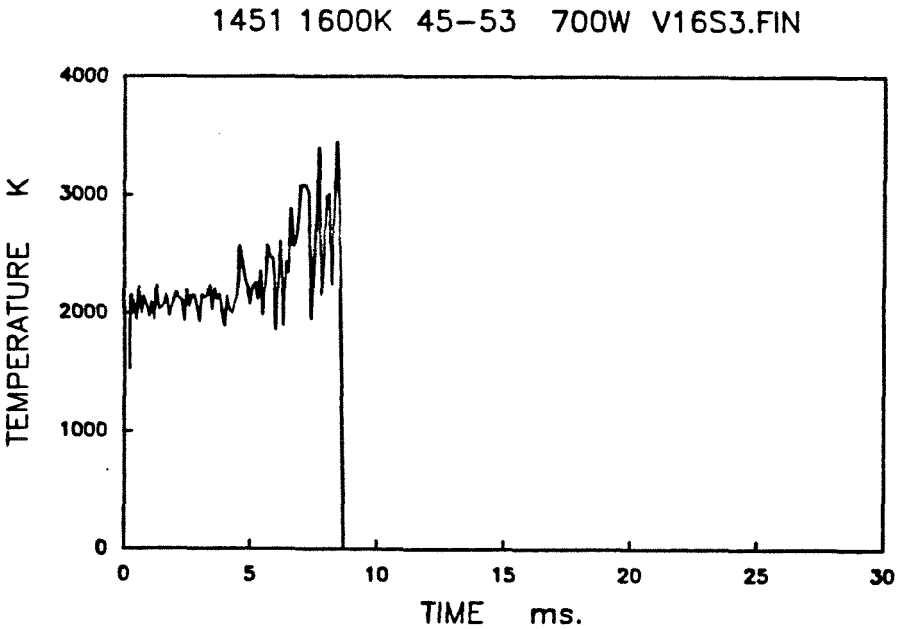
1451 1600K 45–53 700W V16S3.FIN
TEMPERATURE K
4000
3000
2000
1000
0
0
5
10
15
20
25
30
TIME ms.

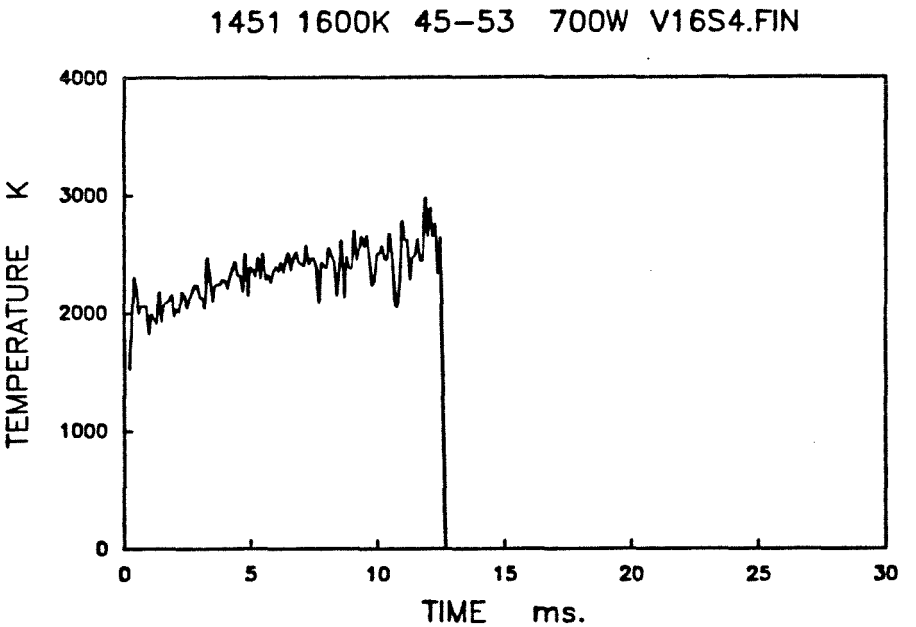
1451 1600K 45–53 700W V16S4.FIN
TEMPERATURE K
4000
3000
2000
1000
0
0
5
10
15
20
25
30
TIME ms.

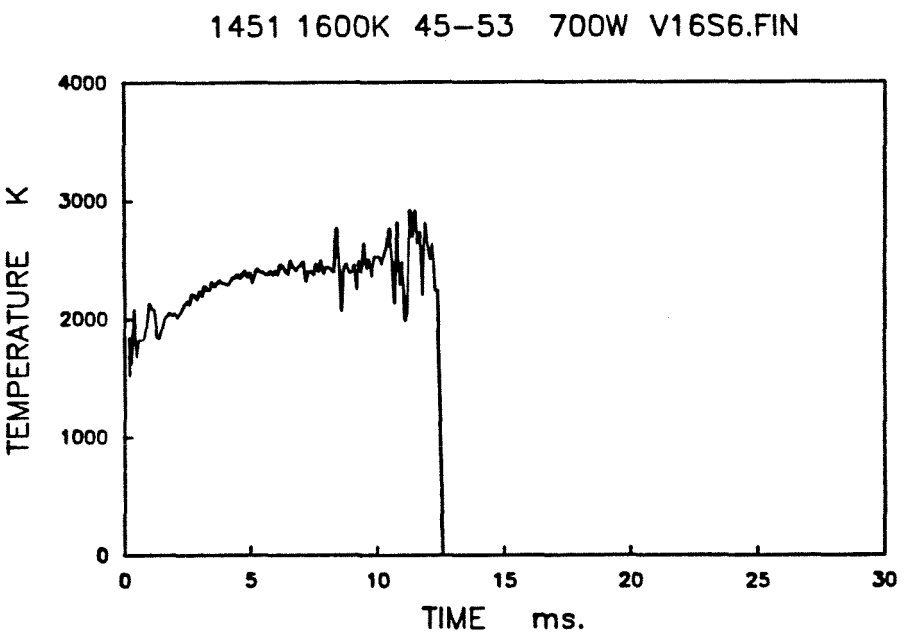
1451 1600K 45–53 700W V16S6.FIN
TEMPERATURE K
4000
3000
2000
1000
0
0
5
10
15
20
25
30
TIME ms.

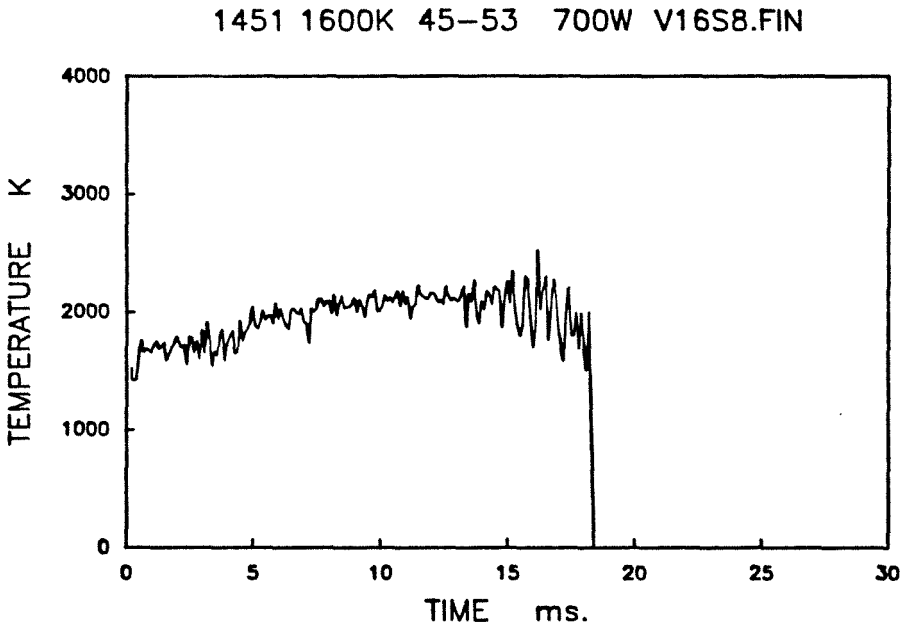
1451 1600K 45–53 700W V16S8.FIN
TEMPERATURE K
4000
3000
2000
1000
0
0
5
10
15
20
25
30
TIME ms.

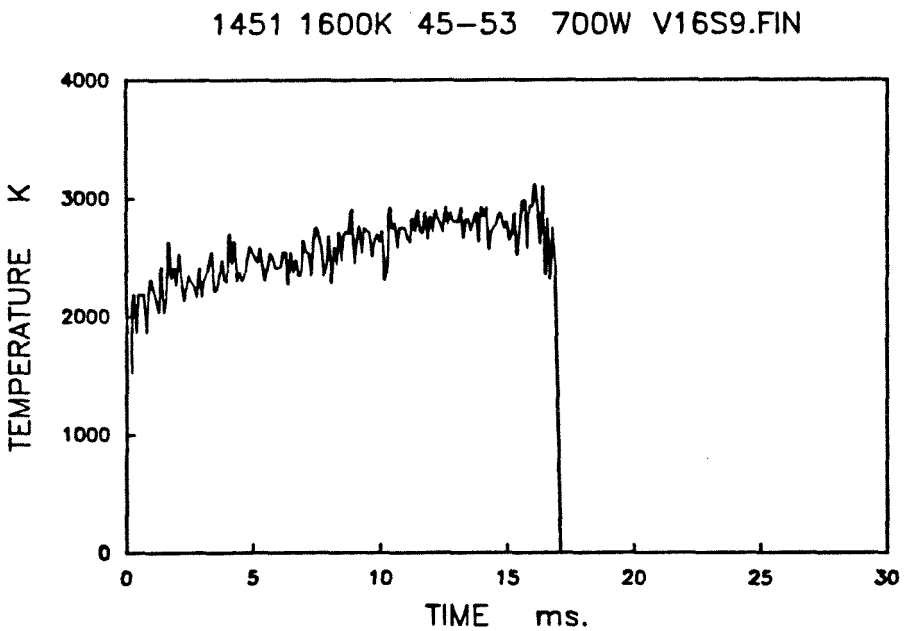
1451 1600K 45–53 700W V16S9.FIN
TEMPERATURE K
4000
3000
2000
1000
0
0
5
10
15
20
25
30
TIME ms.

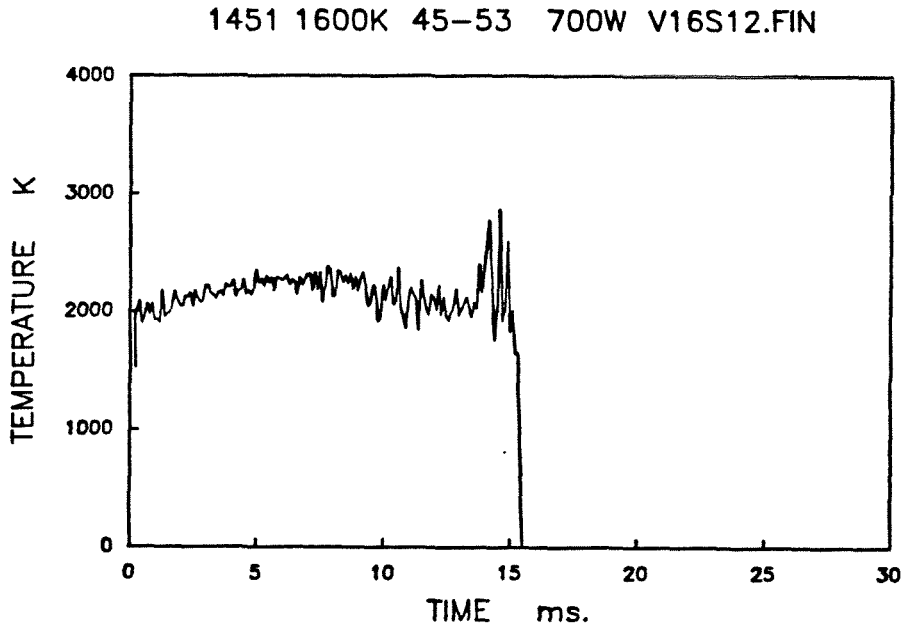
1451 1600K 45–53 700W V16S12.FIN
TEMPERATURE K
4000
3000
2000
1000
0
0
5
10
15
20
25
30
TIME ms.

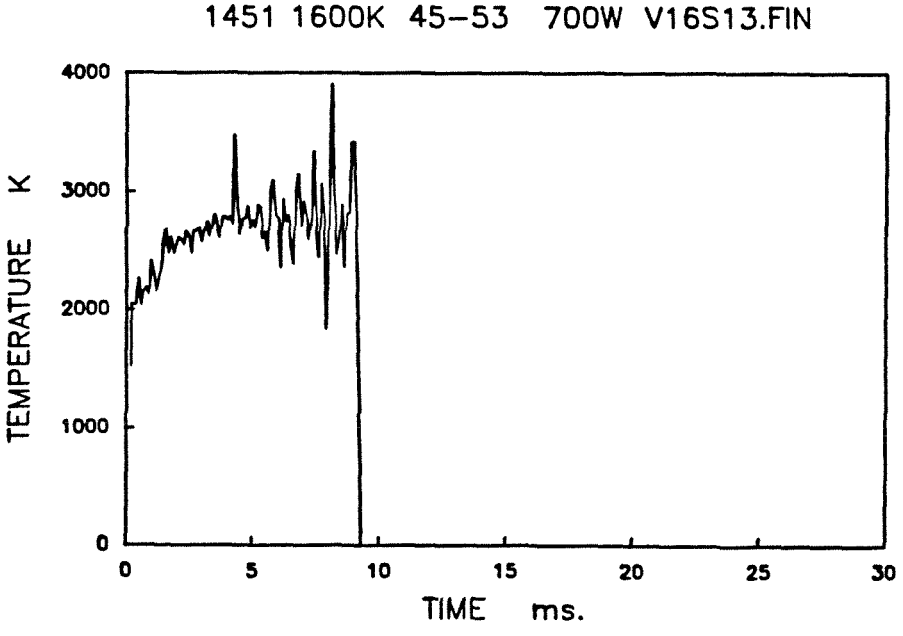
1451 1600K 45–53 700W V16S13.FIN
TEMPERATURE K
4000
3000
2000
1000
0
0
5
10
15
20
25
30
TIME ms.

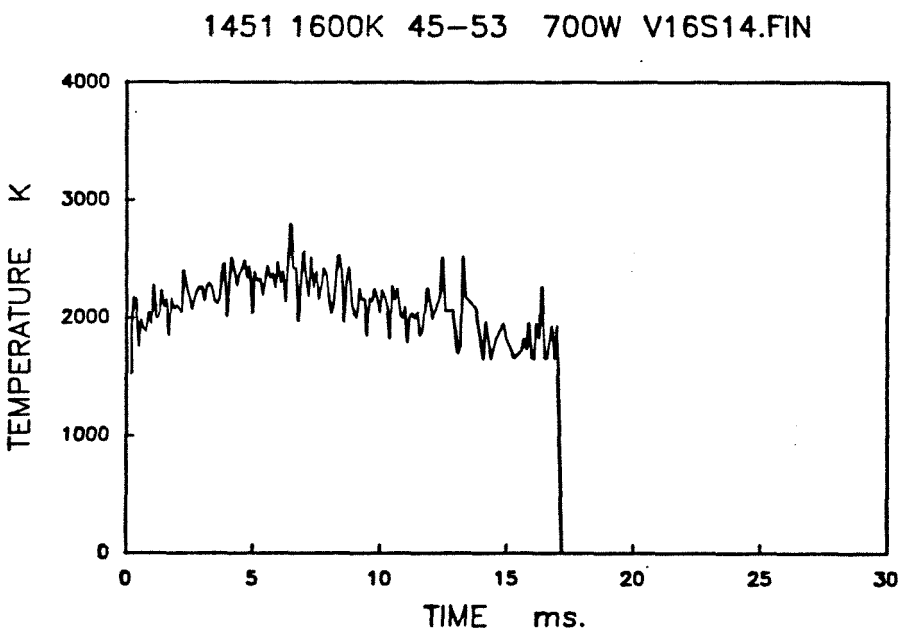
1451 1600K 45–53 700W V16S14.FIN
TEMPERATURE K
4000
3000
2000
1000
0
0
5
10
15
20
25
30
TIME ms.

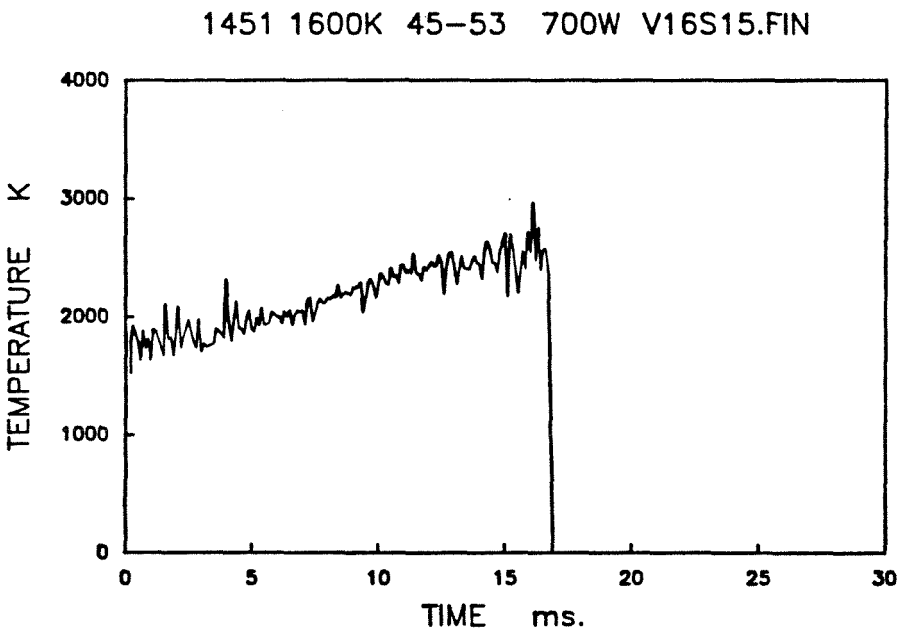
1451 1600K 45–53 700W V16S15.FIN
TEMPERATURE K
4000
3000
2000
1000
0
0
5
10
15
20
25
30
TIME ms.

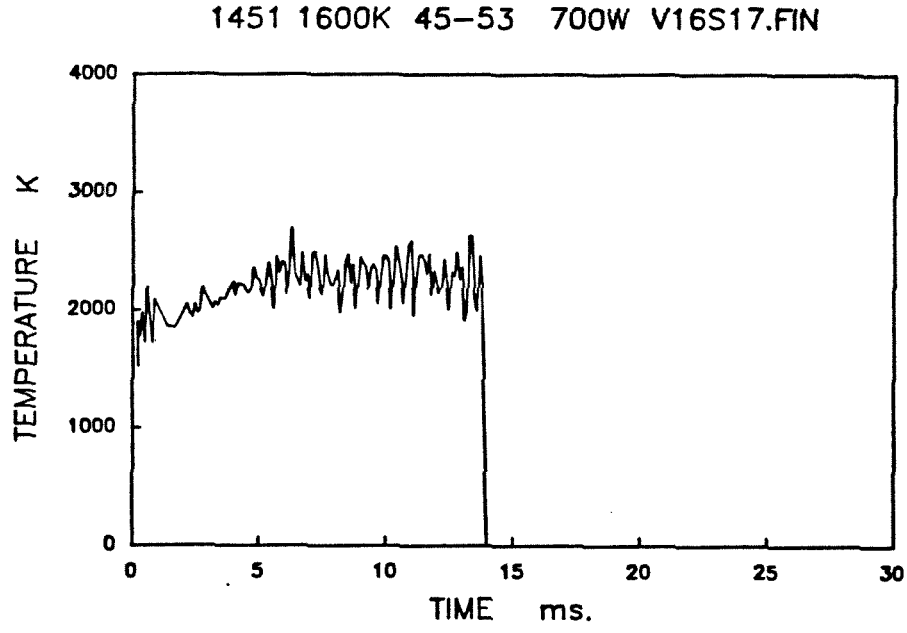
1451 1600K 45–53 700W V16S17.FIN
TEMPERATURE K
4000
3000
2000
1000
0
0
5
10
15
20
25
30
TIME ms.

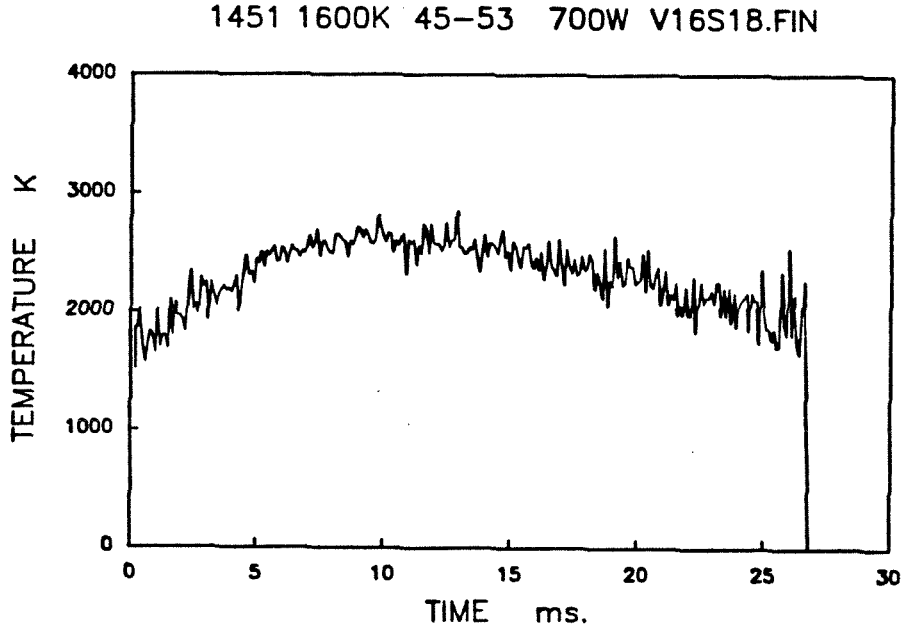
1451 1600K 45–53 700W V16S18.FIN
TEMPERATURE K
4000
3000
2000
1000
0
0
5
10
15
20
25
30
TIME ms.

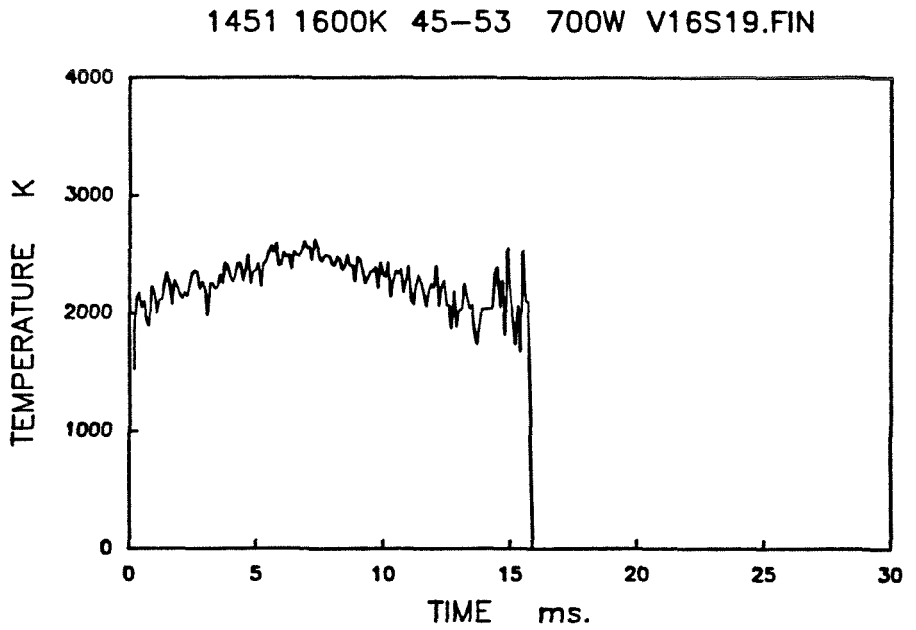
1451 1600K 45–53 700W V16S19.FIN
TEMPERATURE K
4000
3000
2000
1000
0
0
5
10
15
20
25
30
TIME ms.

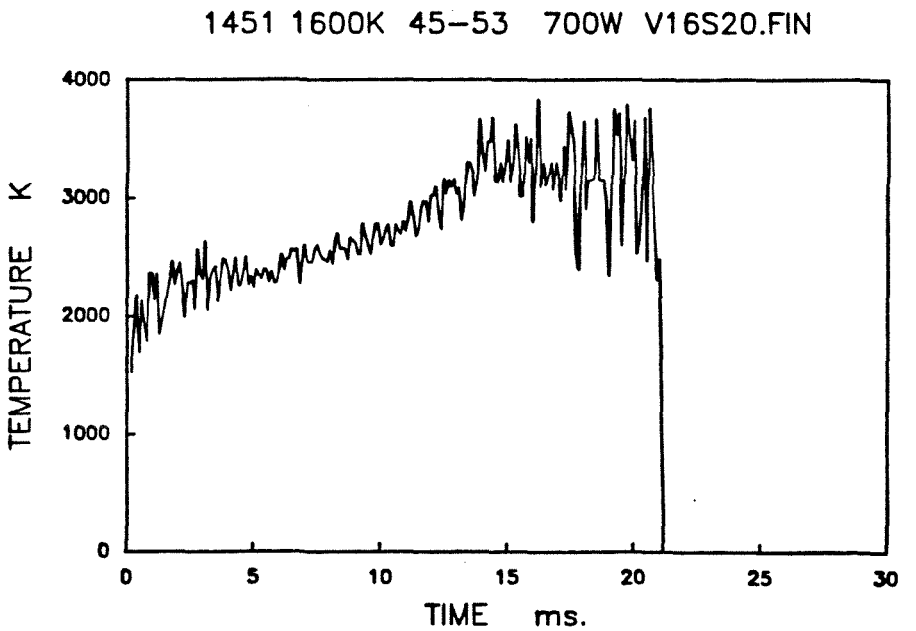
1451 1600K 45–53 700W V16S20.FIN
TEMPERATURE K
4000
3000
2000
1000
0
0
5
10
15
20
25
30
TIME ms.

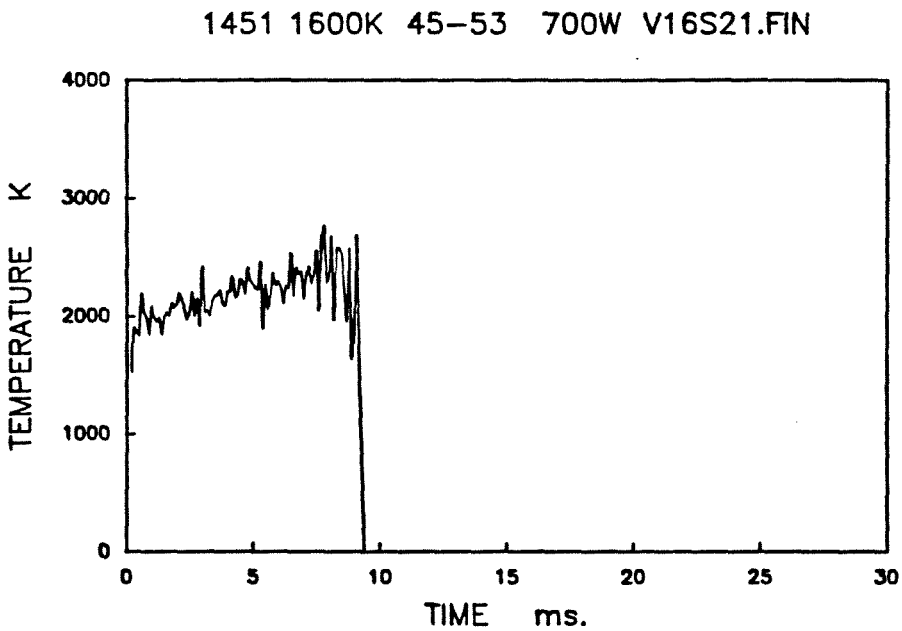
1451 1600K 45–53 700W V16S21.FIN
TEMPERATURE K
4000
3000
2000
1000
0
0
5
10
15
20
25
30
TIME ms.

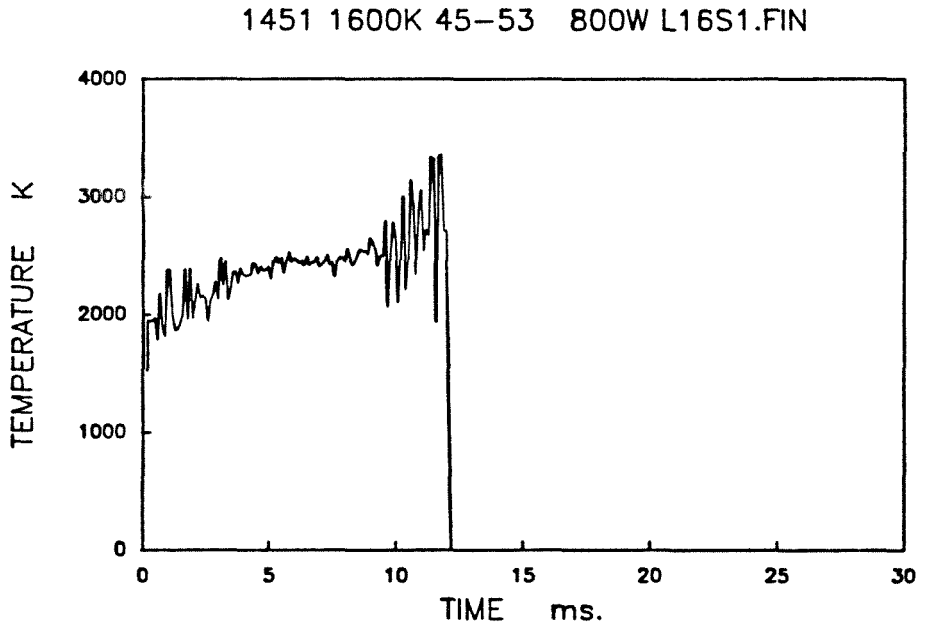
1451 1600K 45-53 800W L16S1.FIN
TEMPERATURE K
4000
3000
2000
1000
0
0
5
10
15
20
25
30
TIME ms.

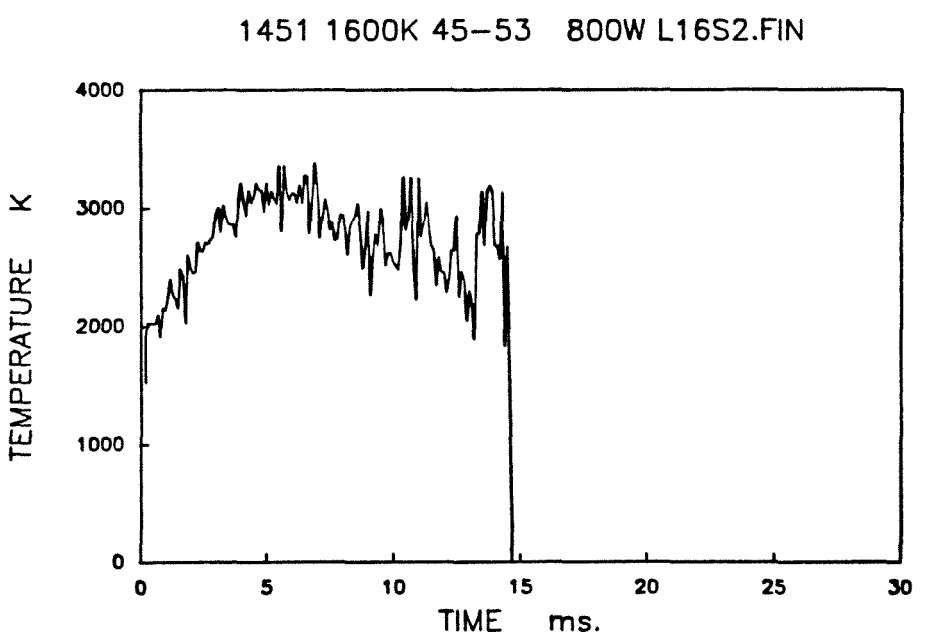
1451 1600K 45-53 800W L16S2.FIN
TEMPERATURE K
4000
3000
2000
1000
0
0
5
10
15
20
25
30
TIME ms.

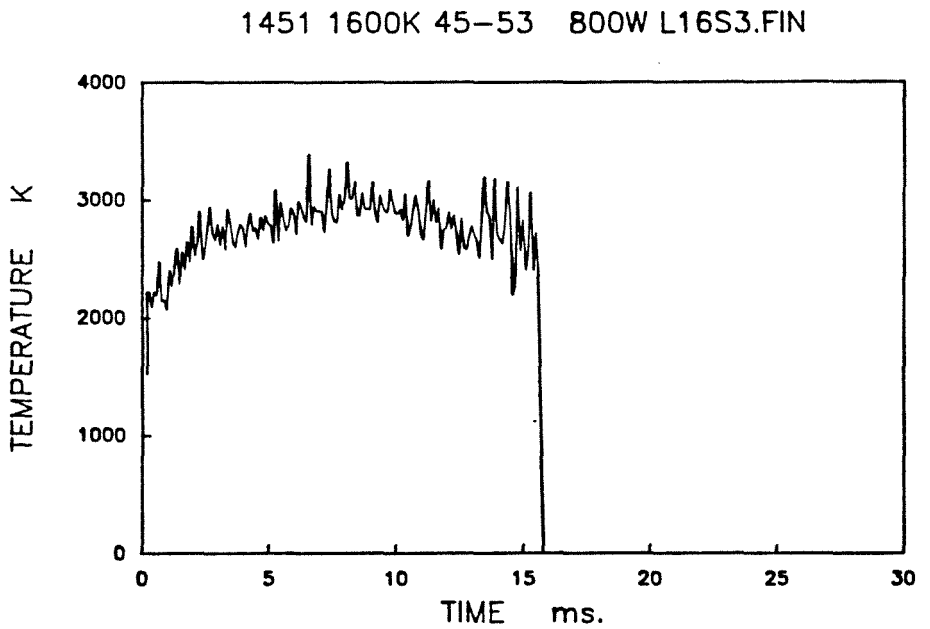
1451 1600K 45–53 800W L16S3.FIN
TEMPERATURE K
4000
3000
2000
1000
0
0
5
10
15
20
25
30
TIME ms.

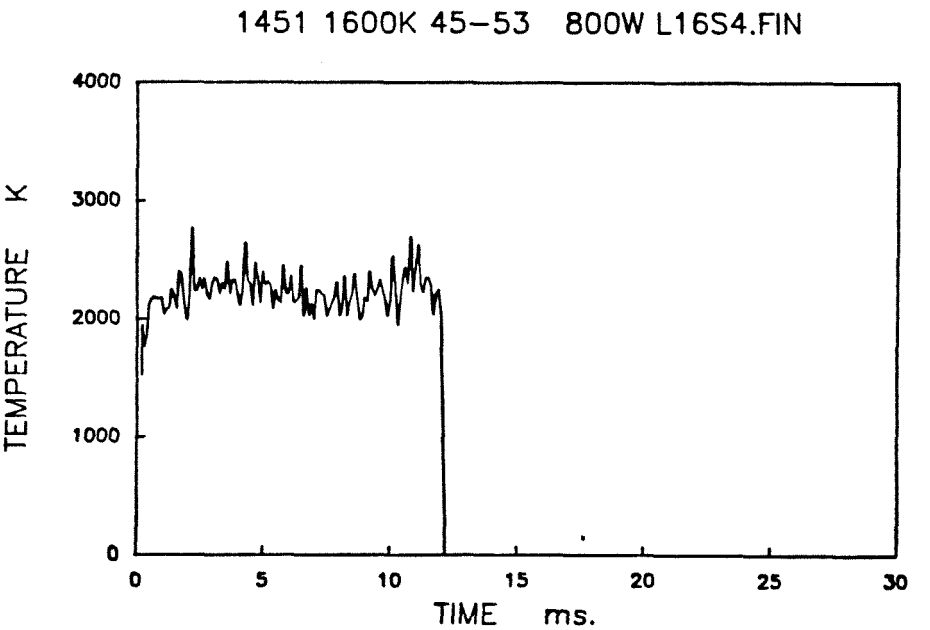
1451 1600K 45–53 800W L16S4.FIN
TEMPERATURE K
4000
3000
2000
1000
0
0
5
10
15
20
25
30
TIME ms.

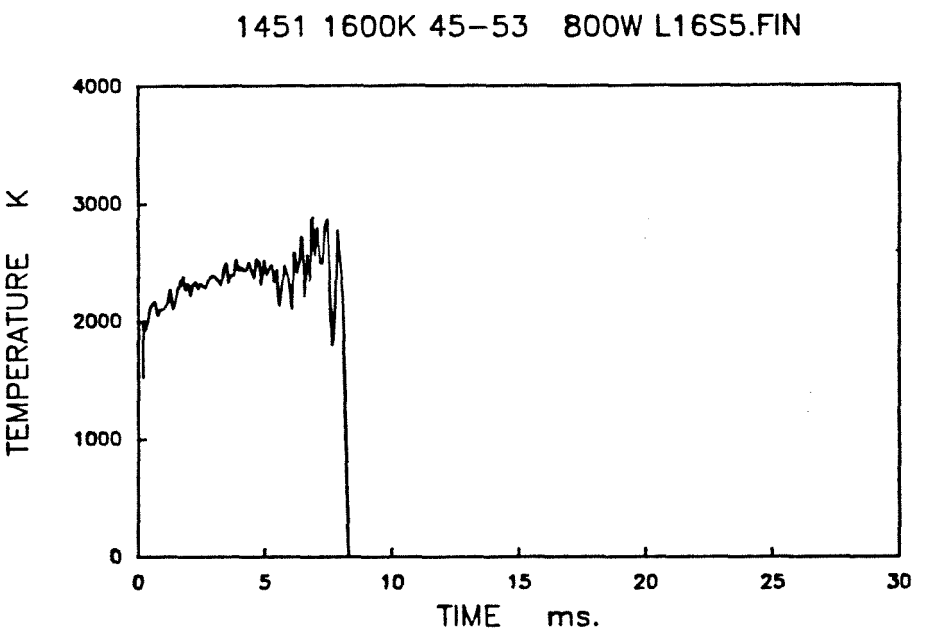
1451 1600K 45–53 800W L16S5.FIN
TEMPERATURE K
4000
3000
2000
1000
0
0
5
10
15
20
25
30
TIME ms.

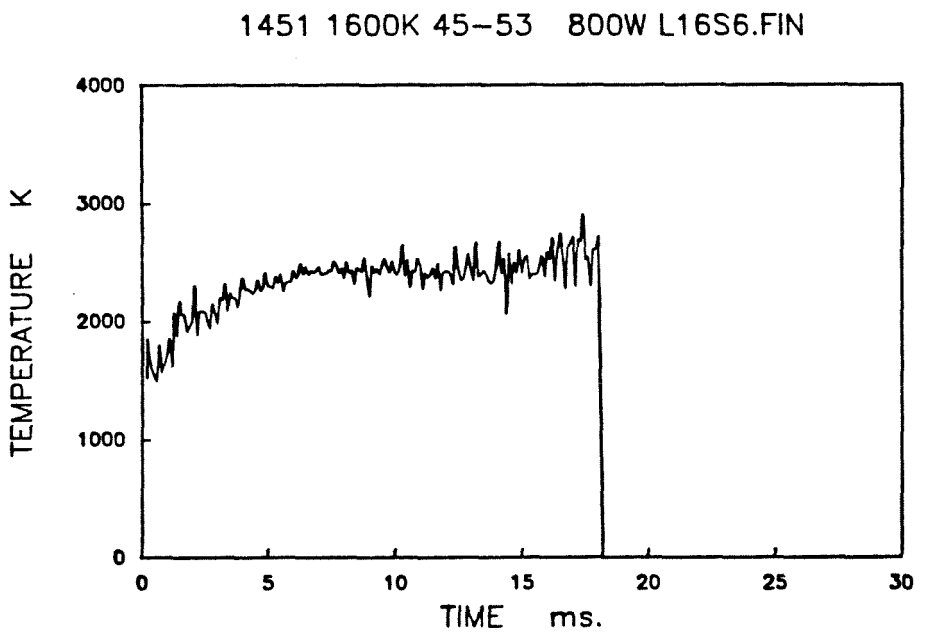
1451 1600K 45–53 800W L16S6.FIN
TEMPERATURE K
4000
3000
2000
1000
0
0
5
10
15
20
25
30
TIME ms.

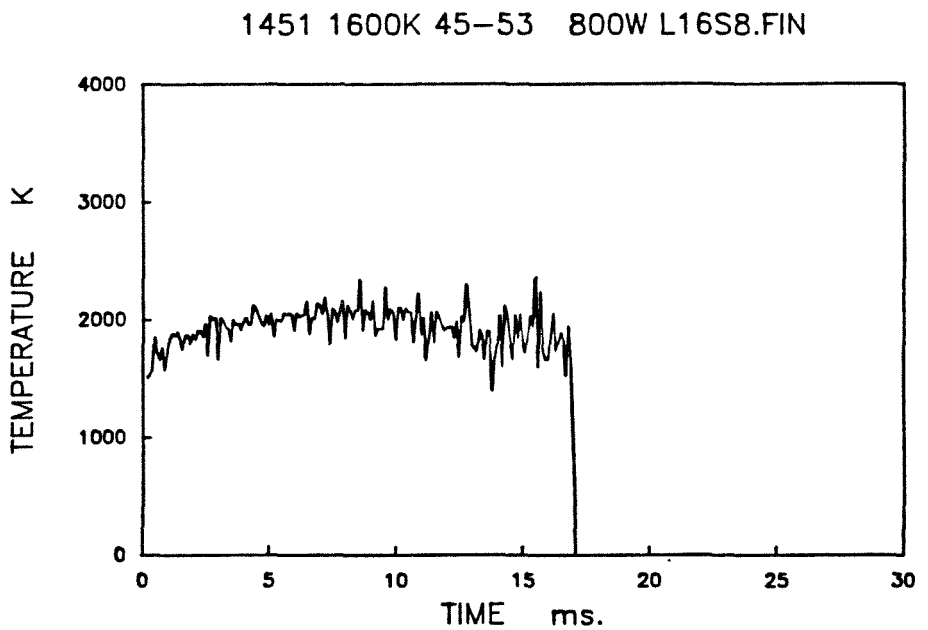
1451 1600K 45–53 800W L16S8.FIN
TEMPERATURE K
4000
3000
2000
1000
0
0
5
10
15
20
25
30
TIME ms.

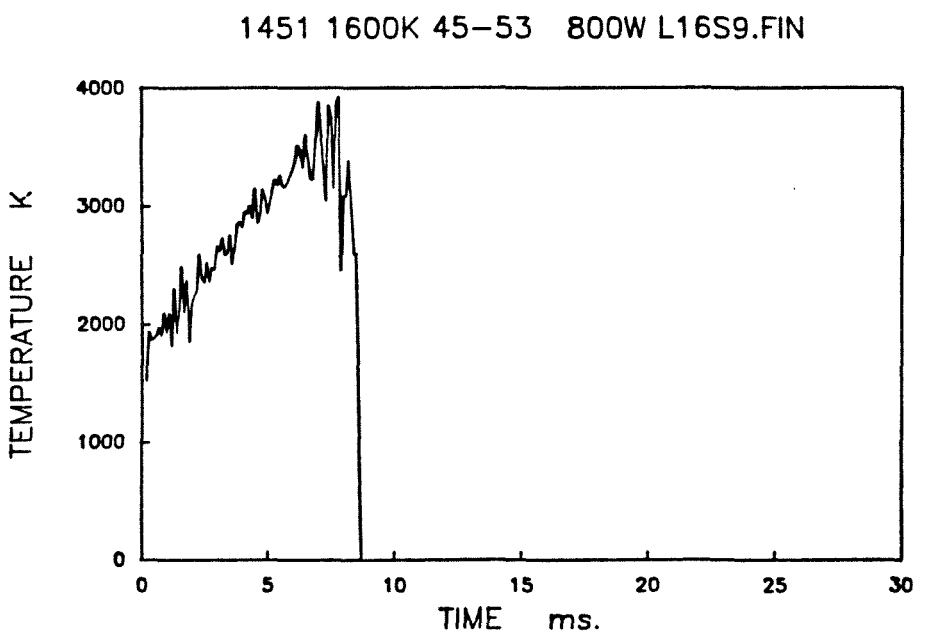
1451 1600K 45–53 800W L16S9.FIN
TEMPERATURE K
4000
3000
2000
1000
0
0
5
10
15
20
25
30
TIME ms.

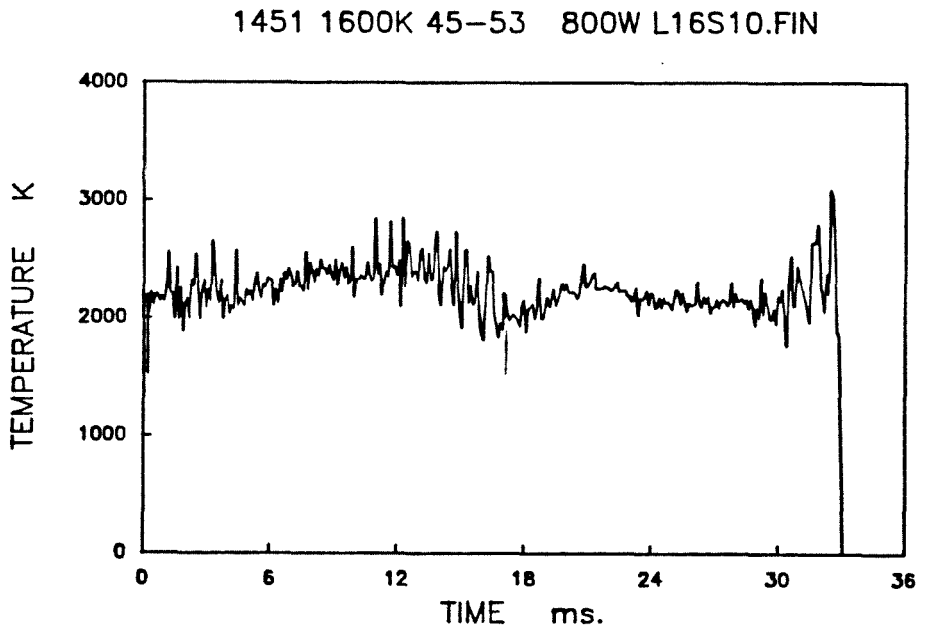
1451 1600K 45–53 800W L16S10.FIN
TEMPERATURE K
4000
3000
2000
1000
0
0
6
12
18
24
30
36
TIME ms.

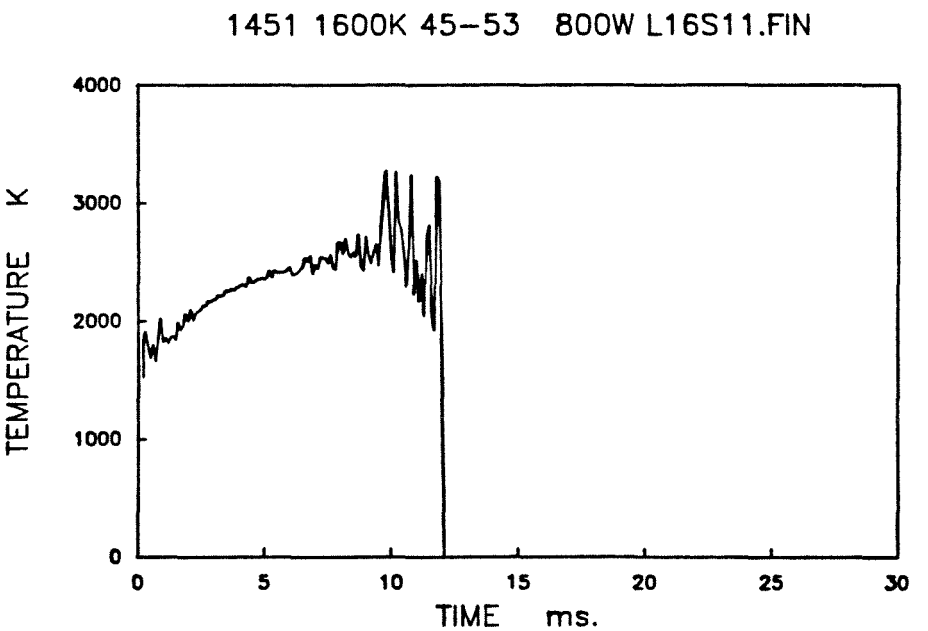
1451 1600K 45–53 800W L16S11.FIN
TEMPERATURE K
4000
3000
2000
1000
0
0
5
10
15
20
25
30
TIME ms.

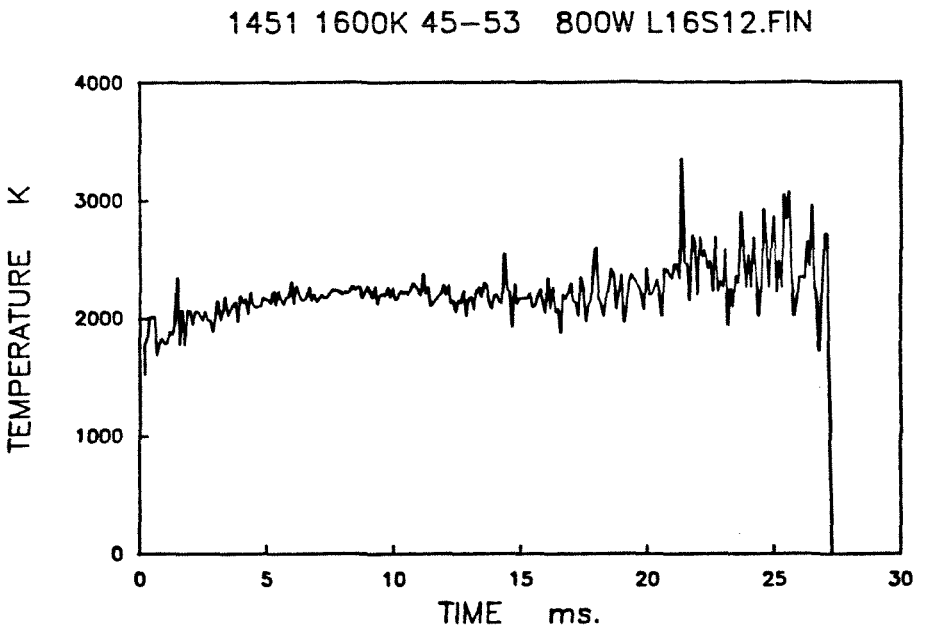
1451 1600K 45–53 800W L16S12.FIN
TEMPERATURE K
4000
3000
2000
1000
0
0
5
10
15
20
25
30
TIME ms.

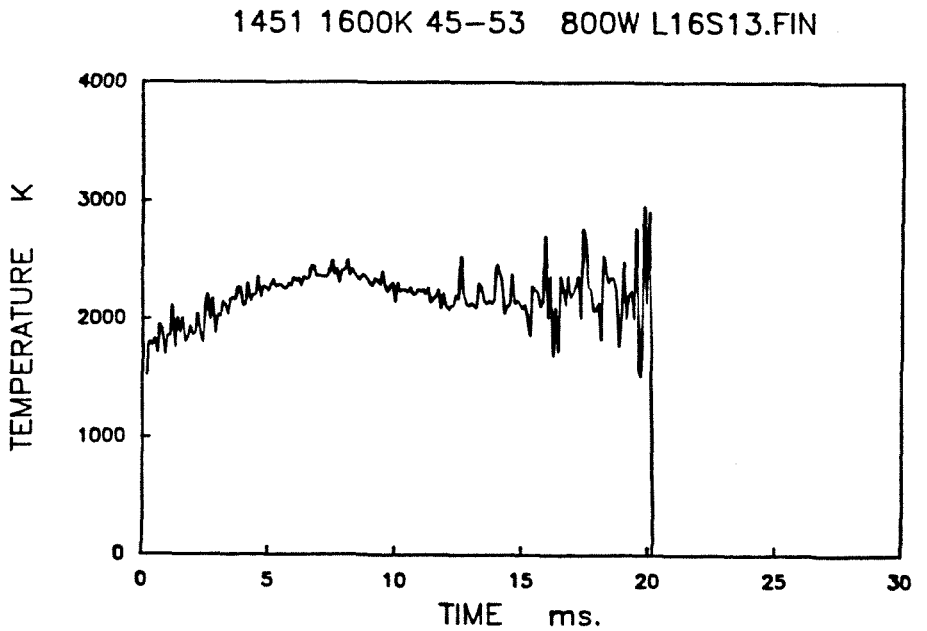
1451 1600K 45–53 800W L16S13.FIN
TEMPERATURE K
4000
3000
2000
1000
0
0
5
10
15
20
25
30
TIME ms.

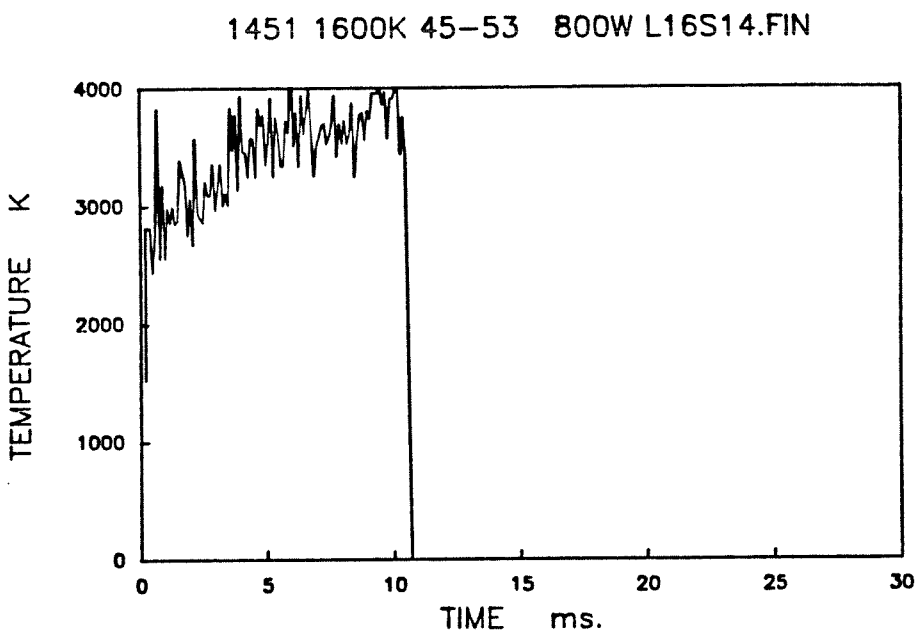
1451 1600K 45–53 800W L16S14.FIN
TEMPERATURE K
4000
3000
2000
1000
0
0
5
10
15
20
25
30
TIME ms.

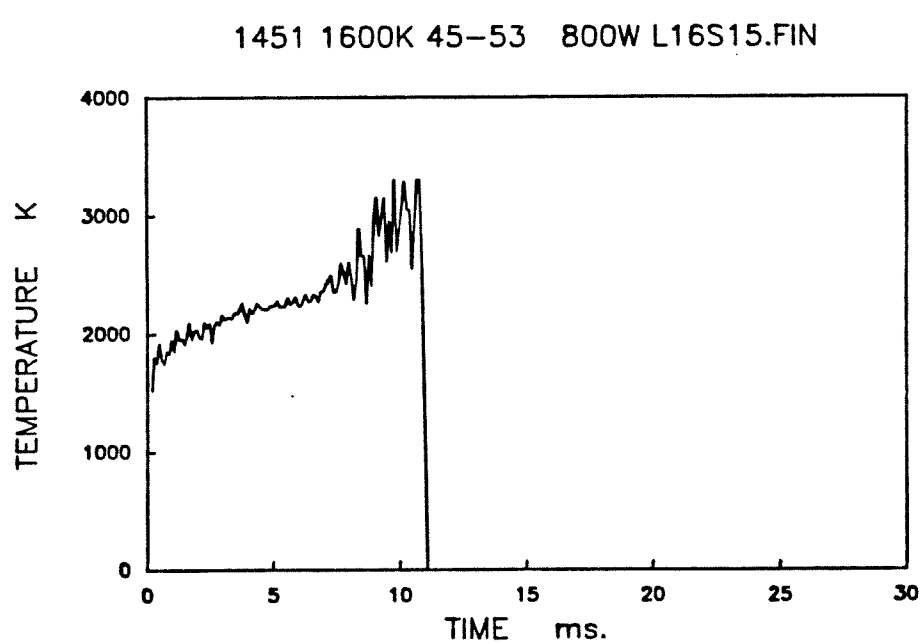
1451 1600K 45–53 800W L16S15.FIN
TEMPERATURE K
4000
3000
2000
1000
0
0
5
10
15
20
25
30
TIME ms.

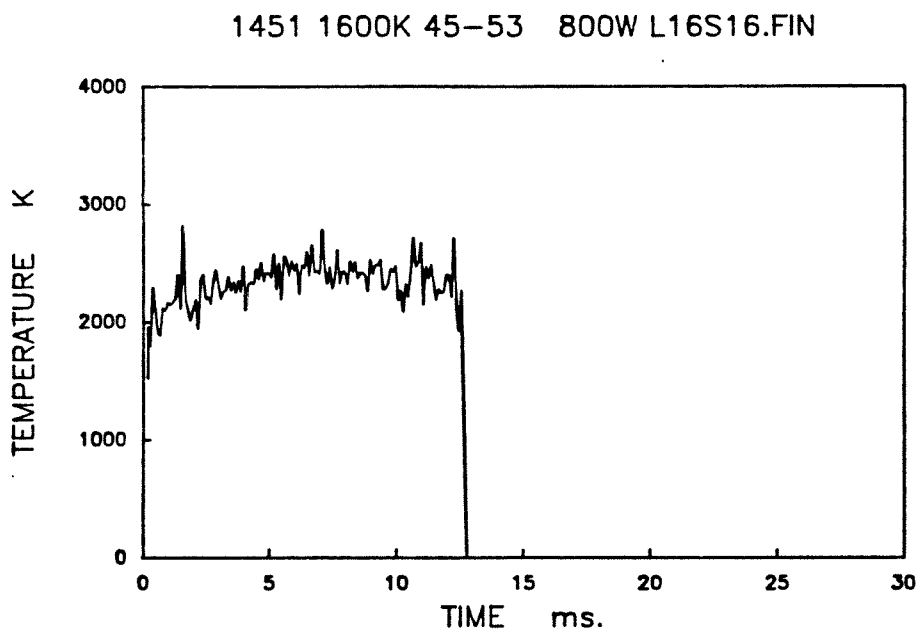
1451 1600K 45–53 800W L16S16.FIN
TEMPERATURE K
4000
3000
2000
1000
0
0
5
10
15
20
25
30
TIME ms.

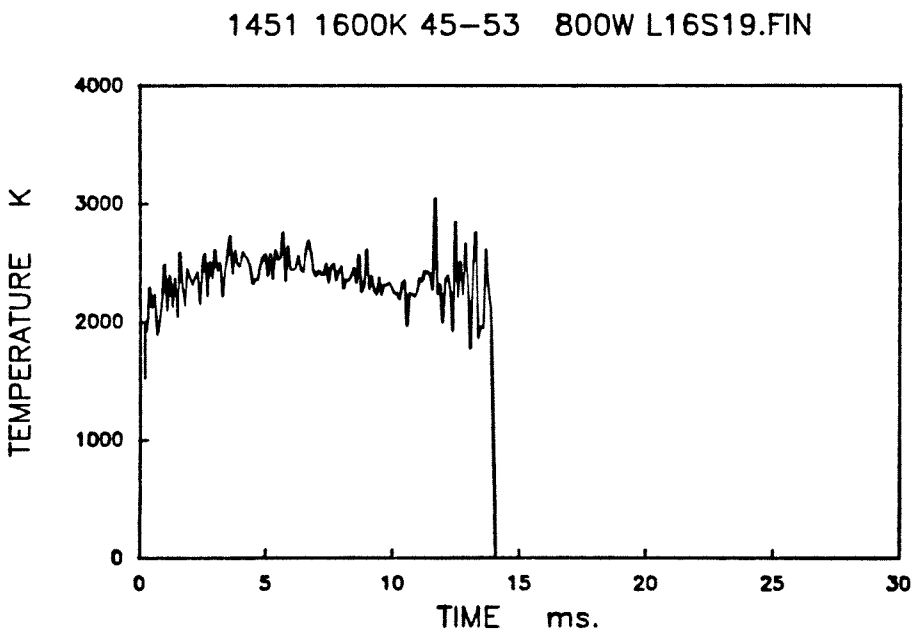
1451 1600K 45–53 800W L16S19.FIN
TEMPERATURE K
4000
3000
2000
1000
0
0
5
10
15
20
25
30
TIME ms.

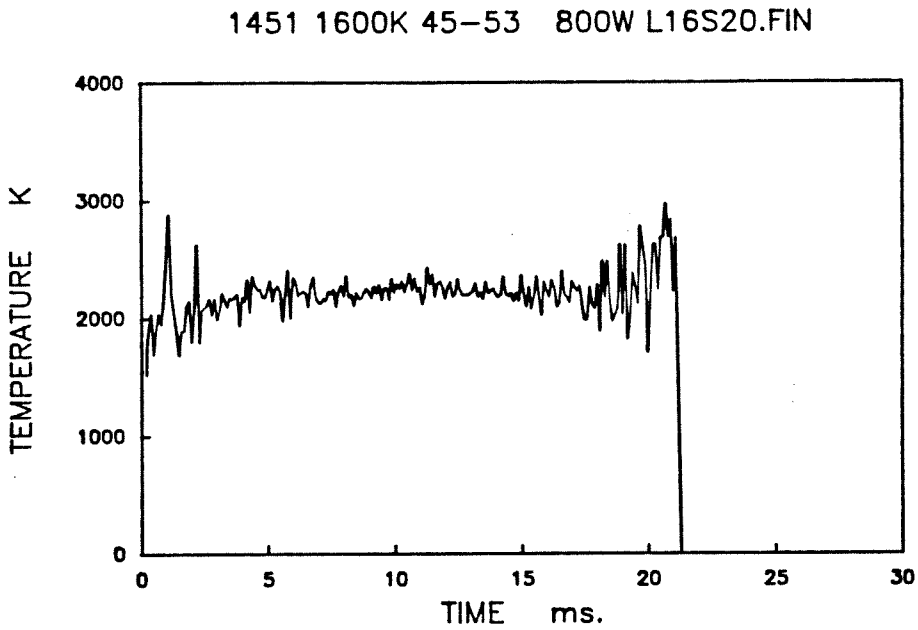
1451 1600K 45–53 800W L16S20.FIN
TEMPERATURE K
4000
3000
2000
1000
0
0
5
10
15
20
25
30
TIME ms.

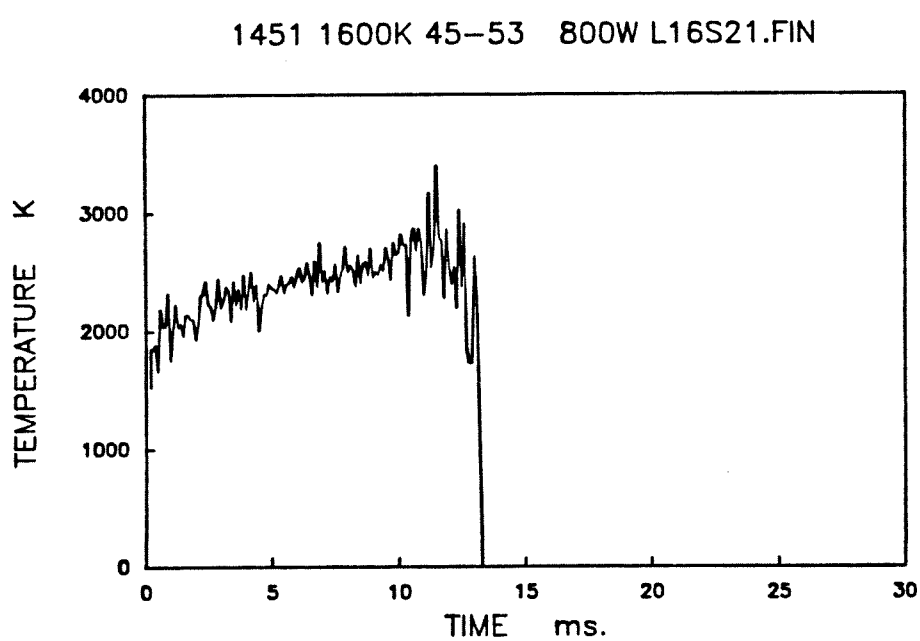
1451 1600K 45–53 800W L16S21.FIN
TEMPERATURE K
4000
3000
2000
1000
0
0
5
10
15
20
25
30
TIME ms.

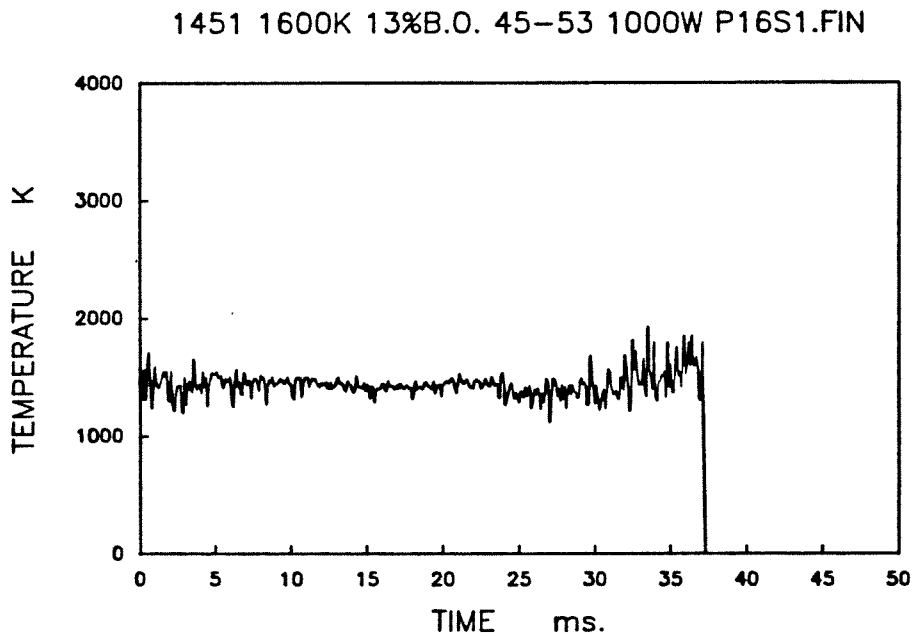
1451 1600K 13%B.O. 45–53 1000W P16S1.FIN
TEMPERATURE K
4000
3000
2000
1000
0
0
5
10
15
20
25
30
35
40
45
50
TIME ms.

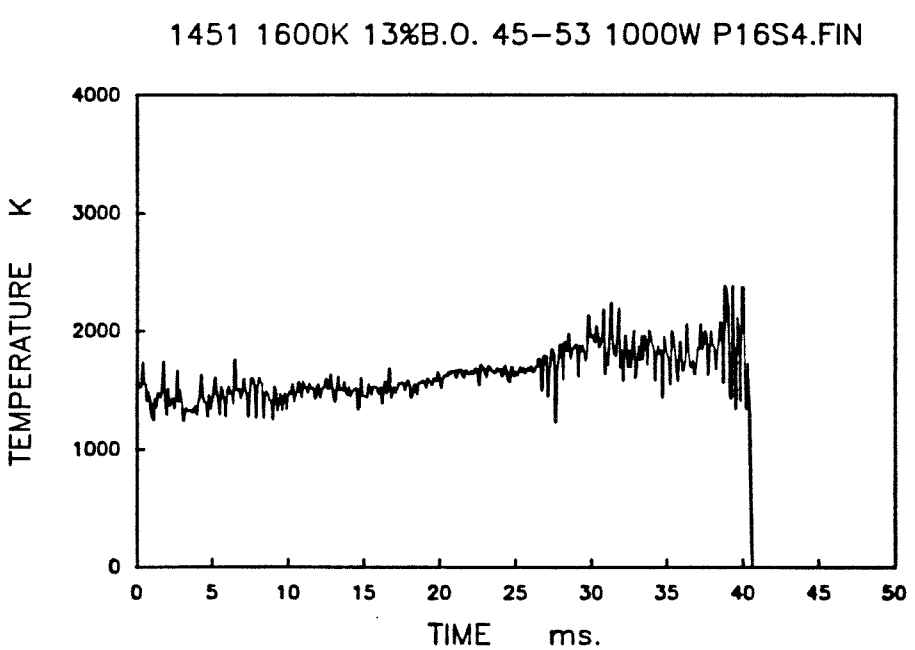
1451 1600K 13%B.O. 45–53 1000W P16S4.FIN
TEMPERATURE K
4000
3000
2000
1000
0
0
5
10
15
20
25
30
35
40
45
50
TIME ms.

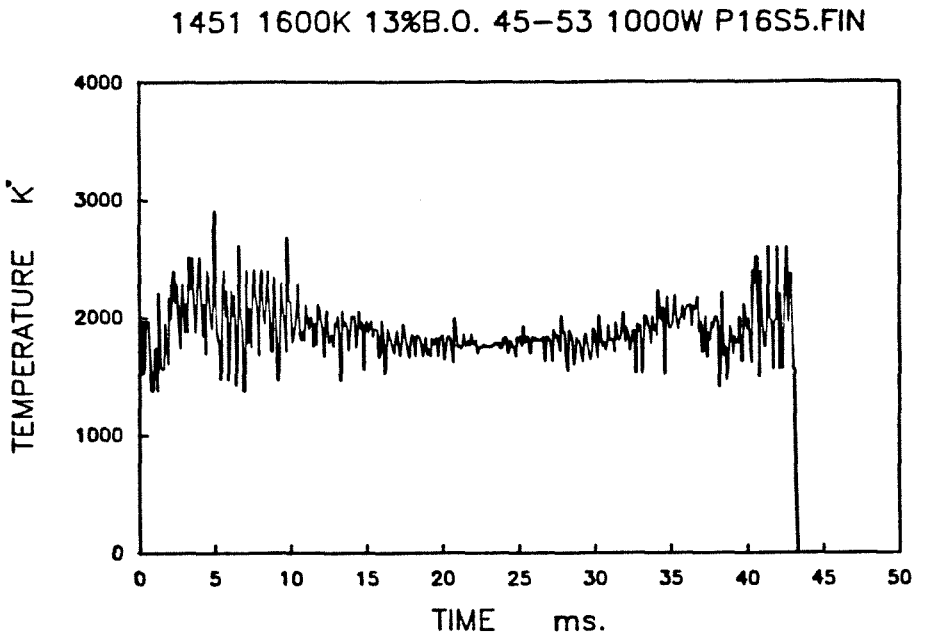
1451 1600K 13%B.O. 45–53 1000W P16S5.FIN
TEMPERATURE K
4000
3000
2000
1000
0
0
5
10
15
20
25
30
35
40
45
50
TIME ms.

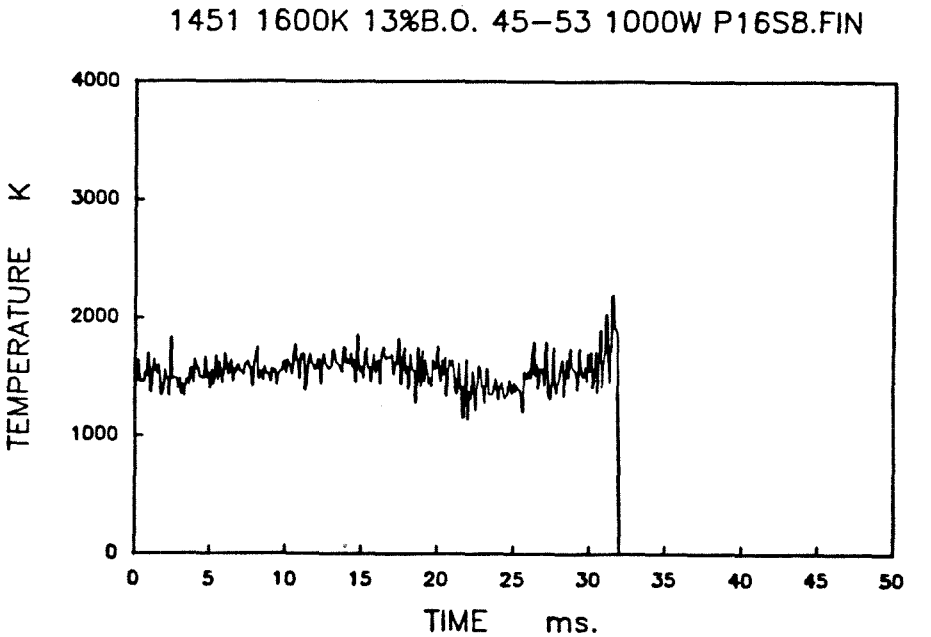
1451 1600K 13%B.O. 45–53 1000W P16S8.FIN
TEMPERATURE K
4000
3000
2000
1000
0
0
5
10
15
20
25
30
35
40
45
50
TIME ms.

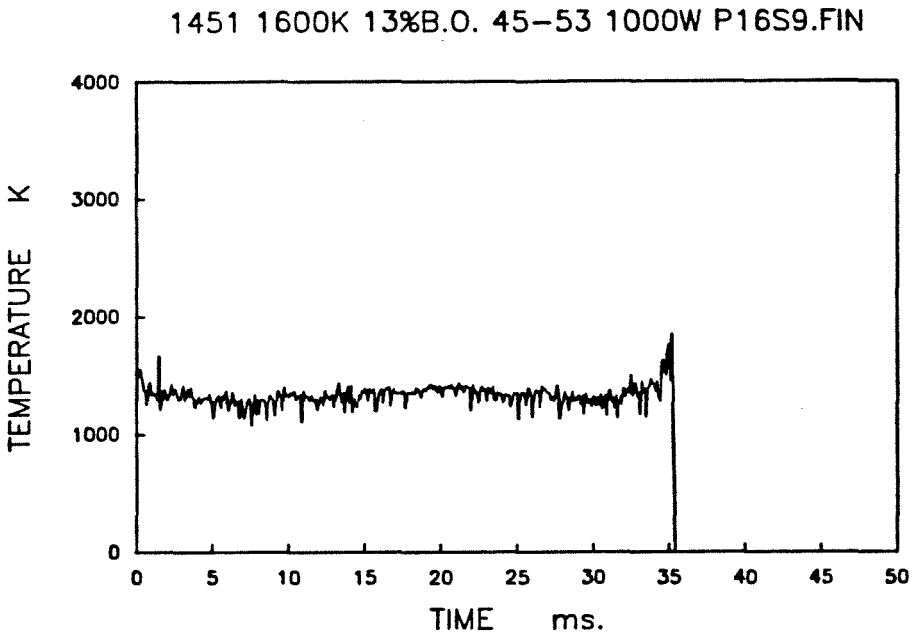
1451 1600K 13%B.O. 45–53 1000W P16S9.FIN
TEMPERATURE K
4000
3000
2000
1000
0
0
5
10
15
20
25
30
35
40
45
50
TIME ms.

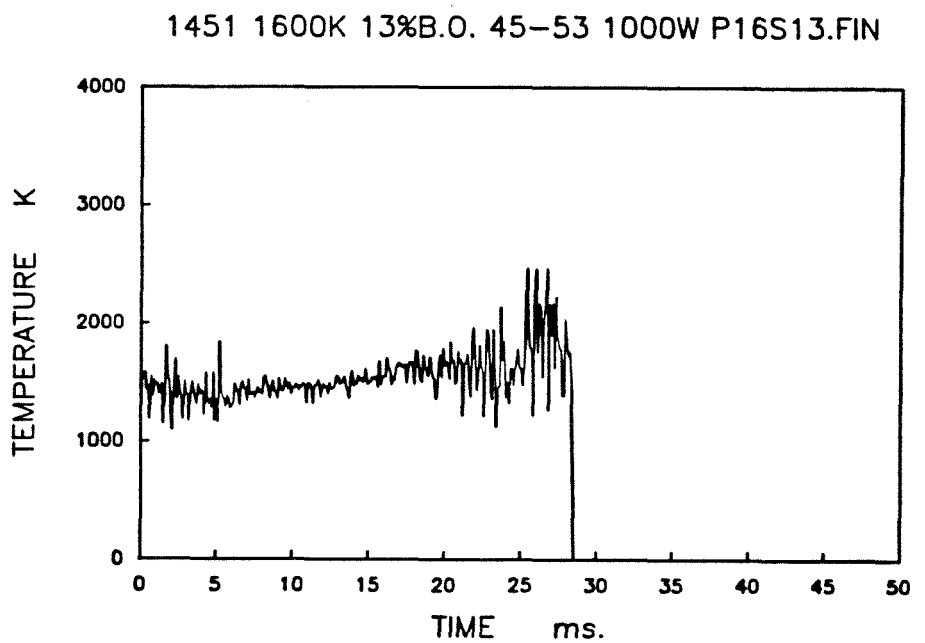
1451 1600K 13%B.O. 45–53 1000W P16S13.FIN
TEMPERATURE K
4000
3000
2000
1000
0
0
5
10
15
20
25
30
35
40
45
50
TIME ms.

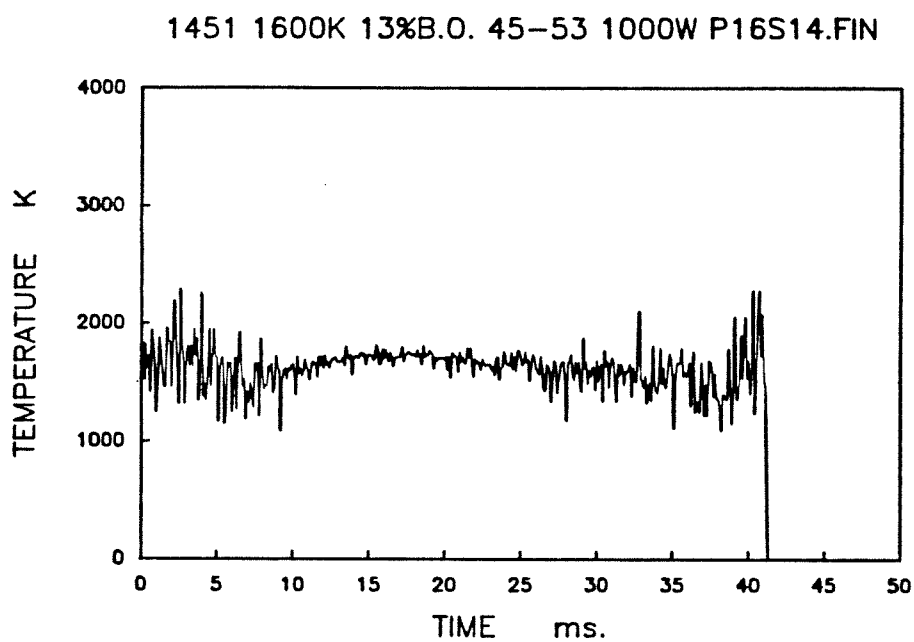
1451 1600K 13%B.O. 45–53 1000W P16S14.FIN
TEMPERATURE K
4000
3000
2000
1000
0
0
5
10
15
20
25
30
35
40
45
50
TIME ms.

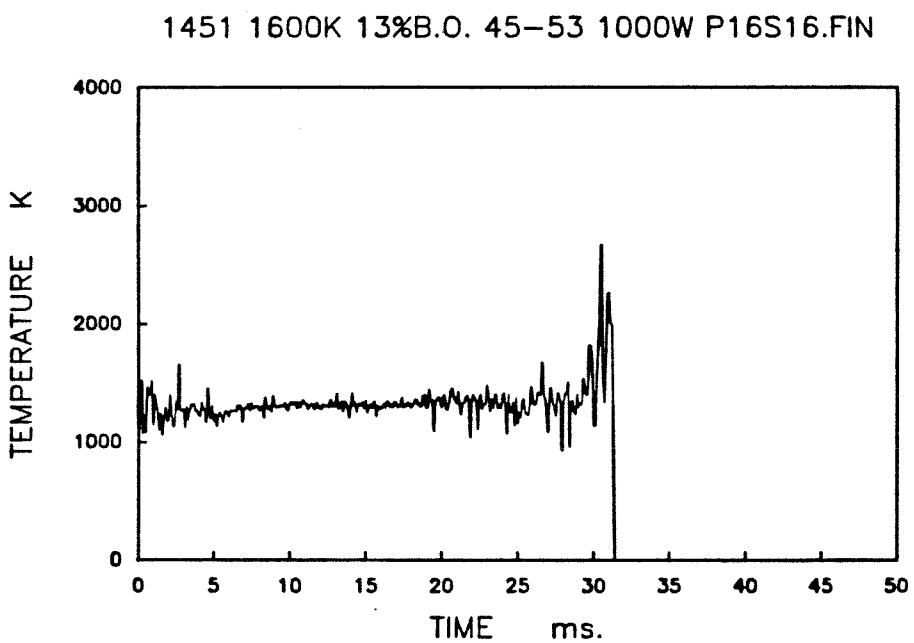
1451 1600K 13%B.O. 45–53 1000W P16S16.FIN
TEMPERATURE K
4000
3000
2000
1000
0
0
5
10
15
20
25
30
35
40
45
50
TIME ms.

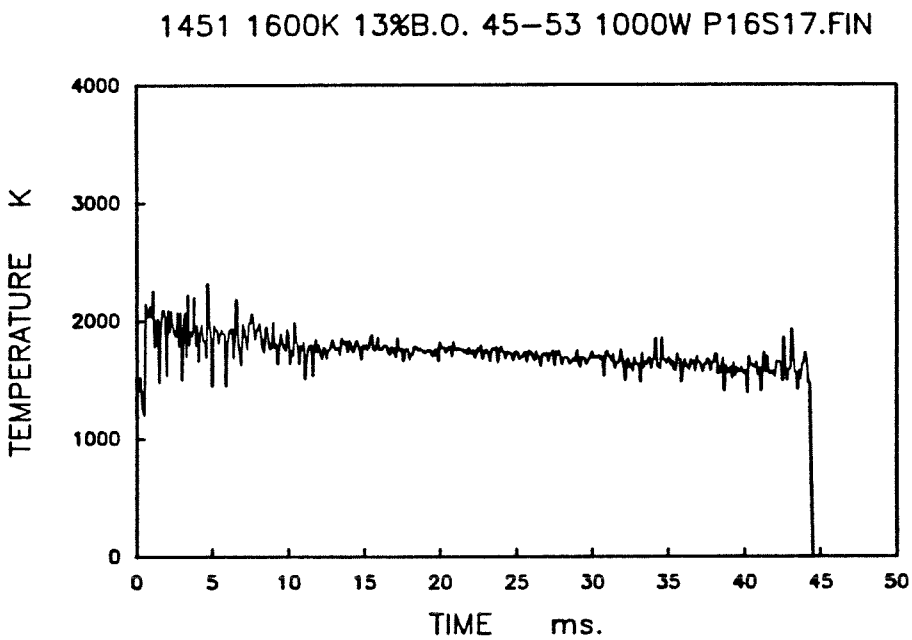
1451 1600K 13%B.O. 45–53 1000W P16S17.FIN
TEMPERATURE K
4000
3000
2000
1000
0
0
5
10
15
20
25
30
35
40
45
50
TIME ms.

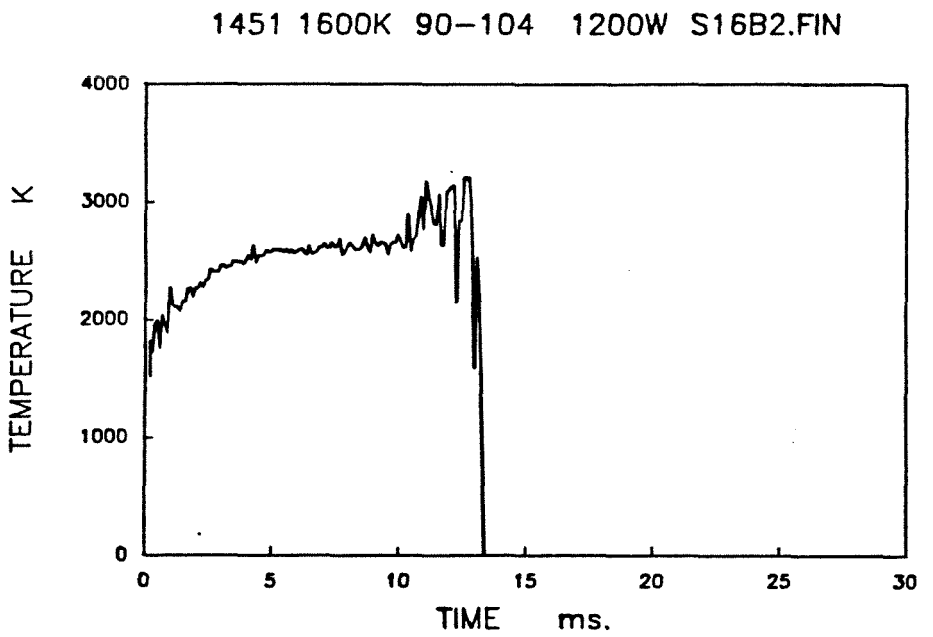
1451 1600K 90–104 1200W S16B2.FIN
TEMPERATURE K
4000
3000
2000
1000
0
0
5
10
15
20
25
30
TIME ms.

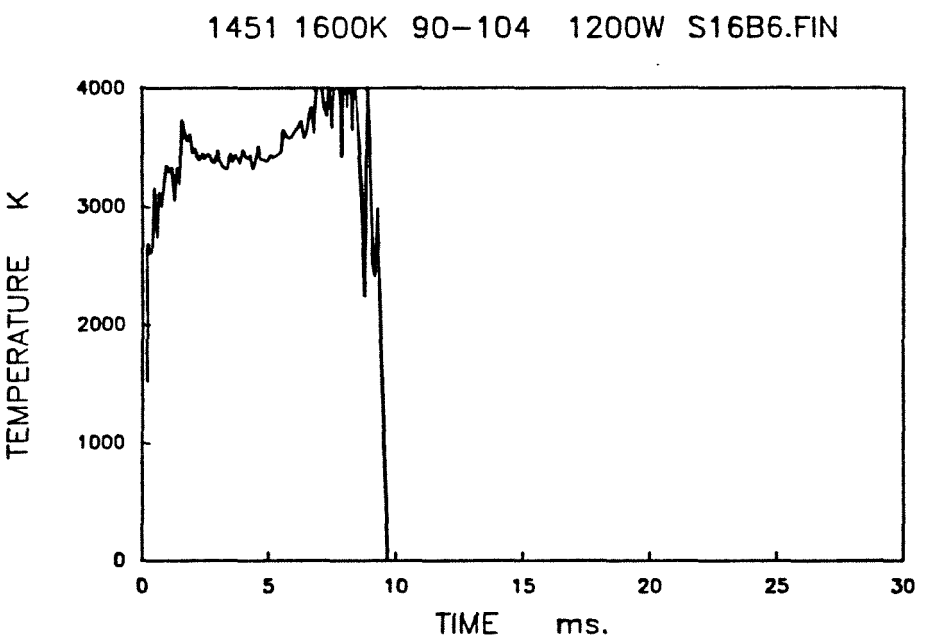
1451 1600K 90–104 1200W S16B6.FIN
TEMPERATURE K
4000
3000
2000
1000
0
0
5
10
15
20
25
30
TIME ms.

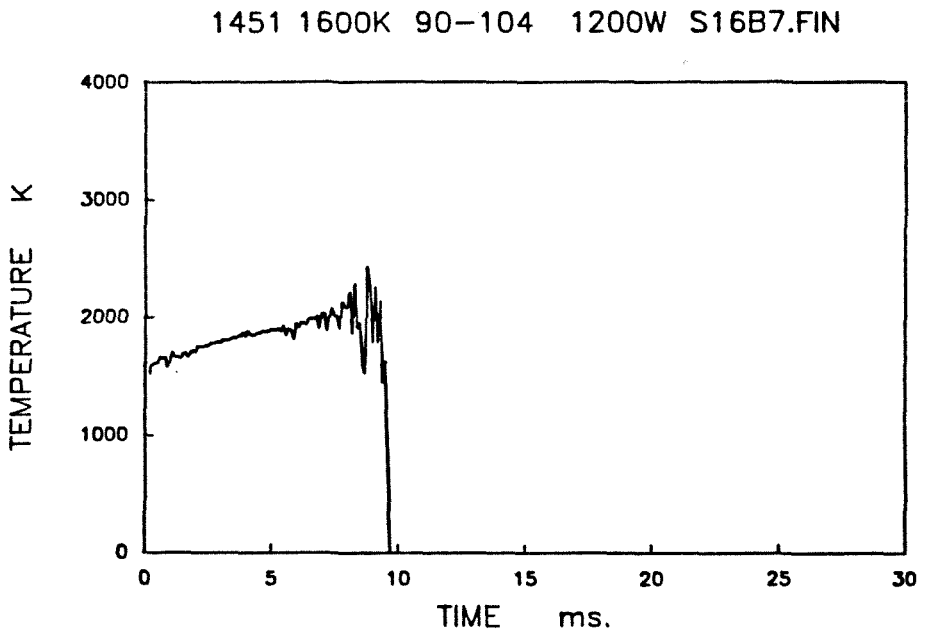
1451 1600K 90–104 1200W S16B7.FIN
TEMPERATURE K
4000
3000
2000
1000
0
0
5
10
15
20
25
30
TIME ms.

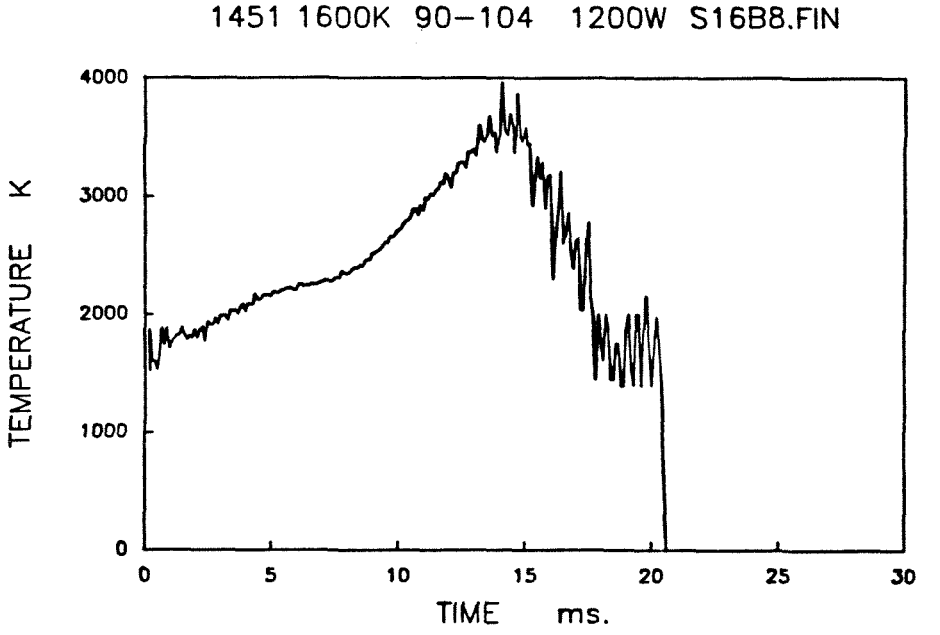
1451 1600K 90–104 1200W S16B8.FIN
TEMPERATURE K
4000
3000
2000
1000
0
0
5
10
15
20
25
30
TIME ms.

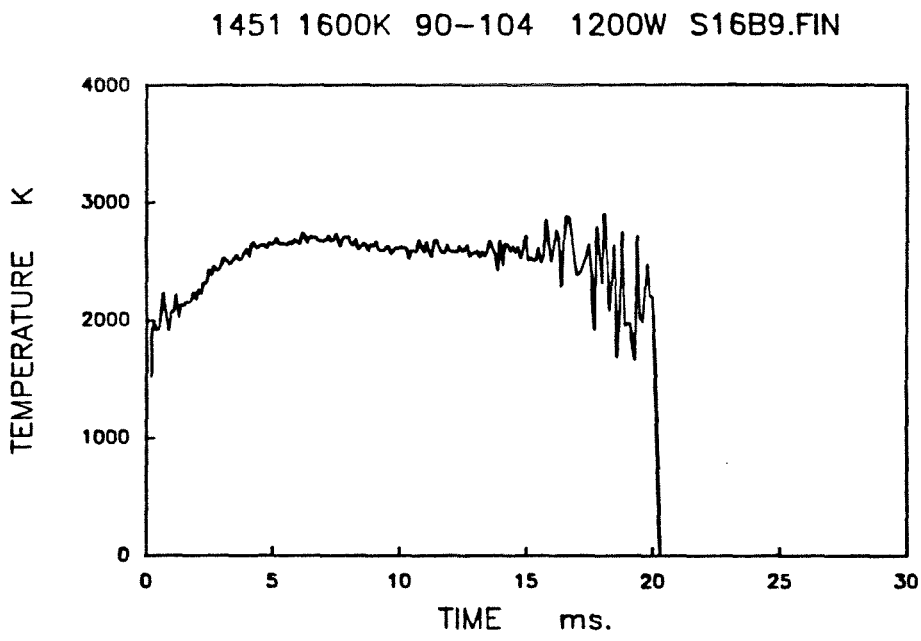
1451 1600K 90–104 1200W S16B9.FIN
TEMPERATURE K
4000
3000
2000
1000
0
0
5
10
15
20
25
30
TIME ms.

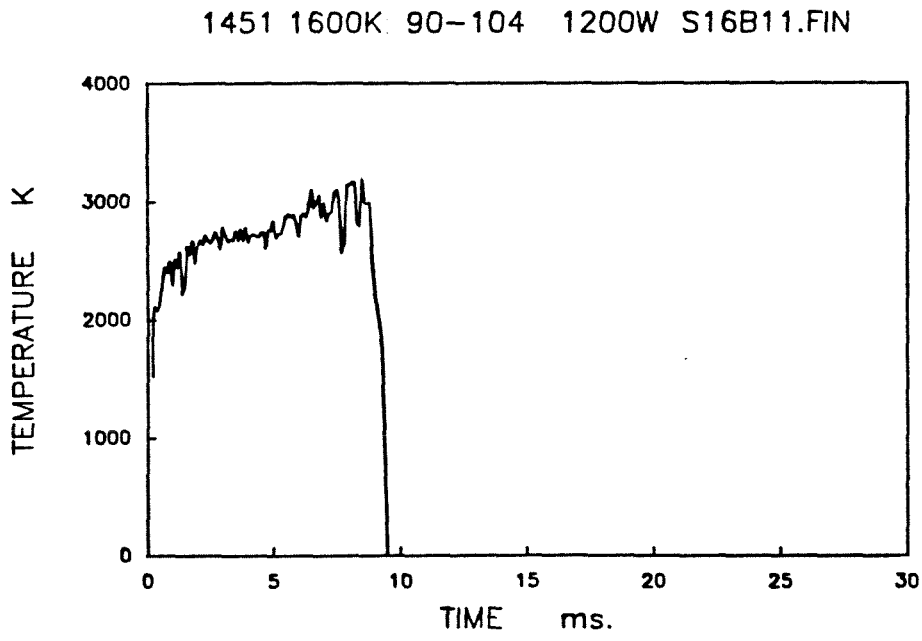
1451 1600K 90–104 1200W S16B11.FIN
TEMPERATURE K
4000
3000
2000
1000
0
0
5
10
15
20
25
30
TIME ms.

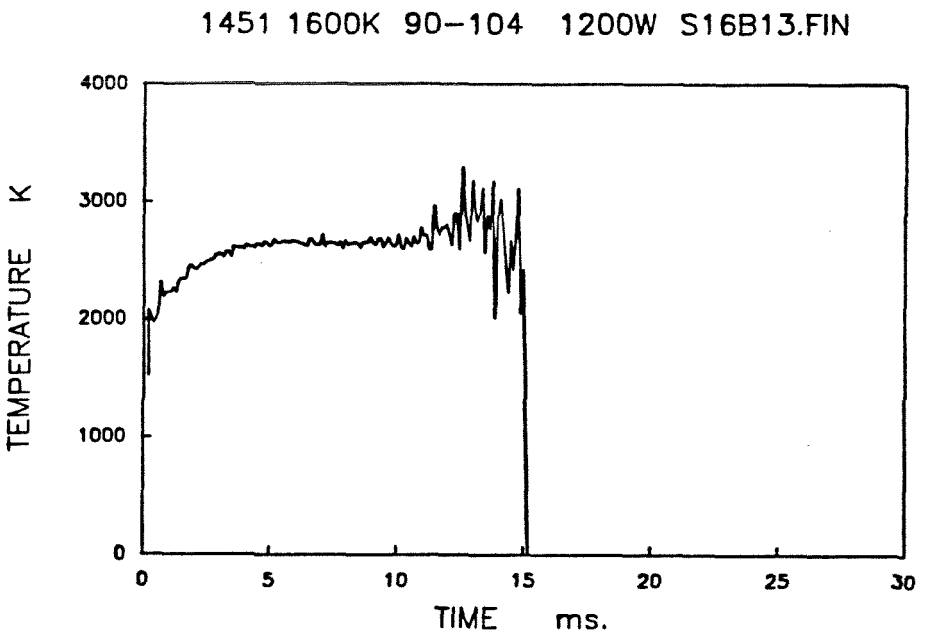
1451 1600K 90–104 1200W S16B13.FIN
TEMPERATURE K
4000
3000
2000
1000
0
0
5
10
15
20
25
30
TIME ms.

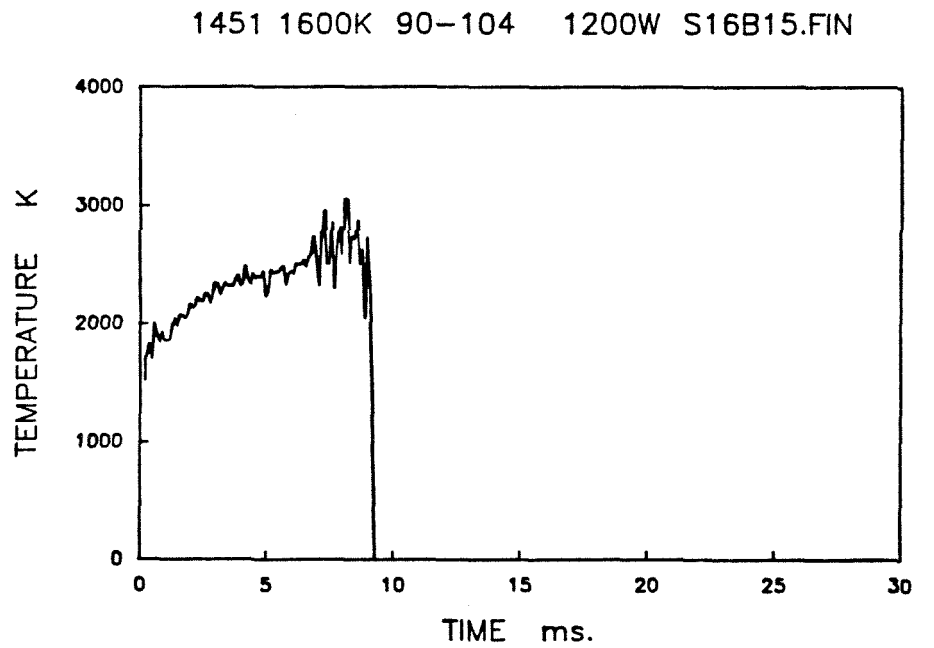
1451 1600K 90–104 1200W S16B15.FIN
TEMPERATURE K
4000
3000
2000
1000
0
0
5
10
15
20
25
30
TIME ms.

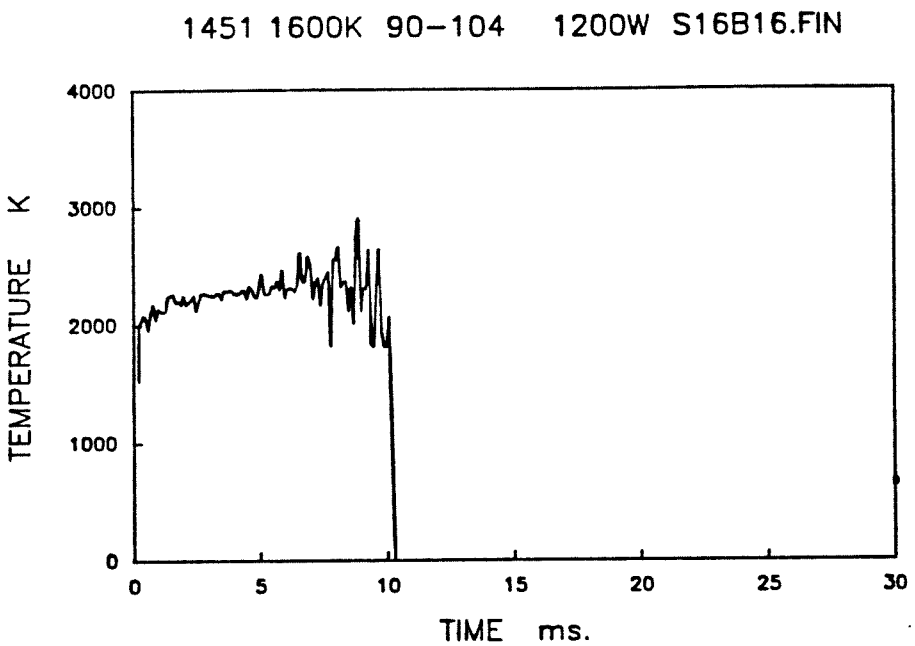
1451 1600K 90–104 1200W S16B16.FIN
TEMPERATURE K
4000
3000
2000
1000
0
0
5
10
15
20
25
30
TIME ms.

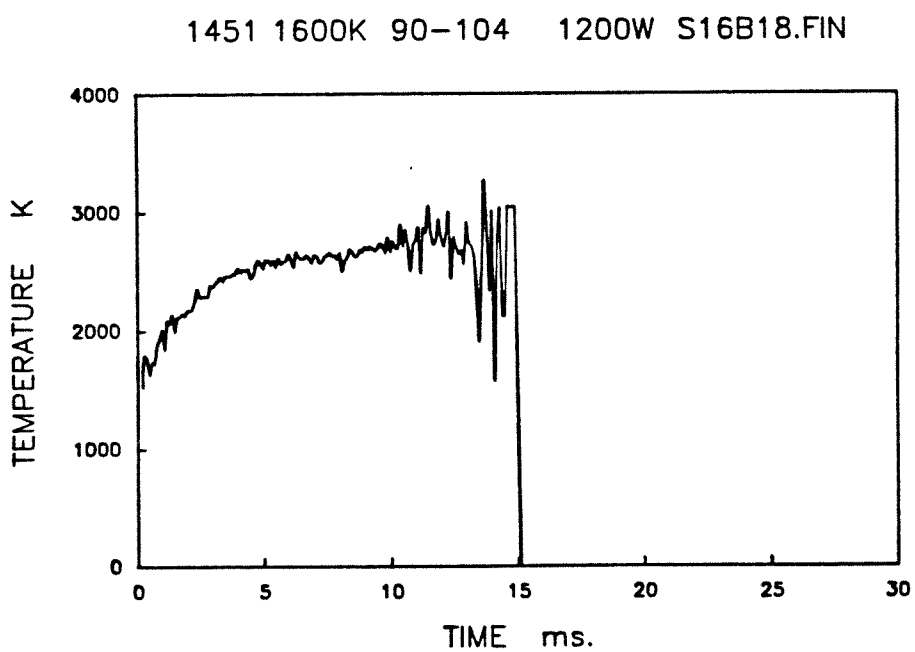
1451 1600K 90–104 1200W S16B18.FIN
TEMPERATURE K
4000
3000
2000
1000
0
0
5
10
15
20
25
30
TIME ms.

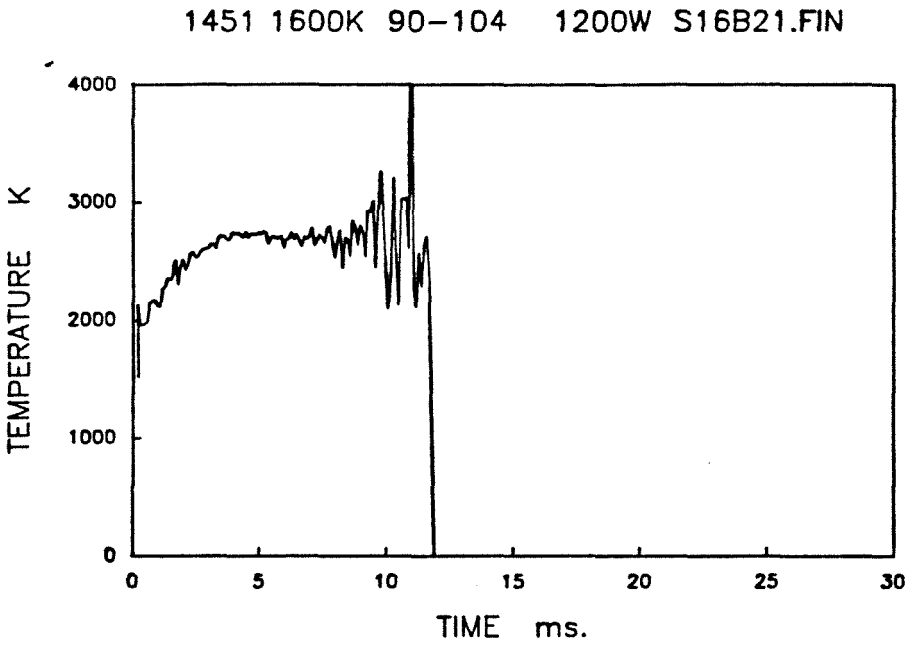
1451 1600K 90–104 1200W S16B21.FIN
TEMPERATURE K
4000
3000
2000
1000
0
0
5
10
15
20
25
30
TIME ms.

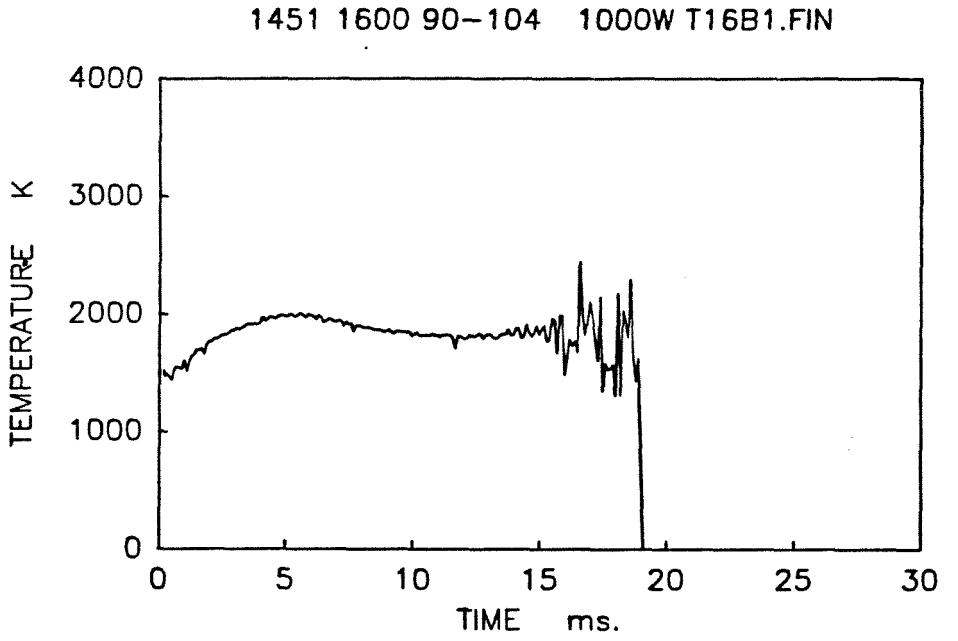
1451 1600 90–104 1000W T16B1.FIN
TEMPERATURE K
4000
3000
2000
1000
0
0
5
10
15
20
25
30
TIME ms.

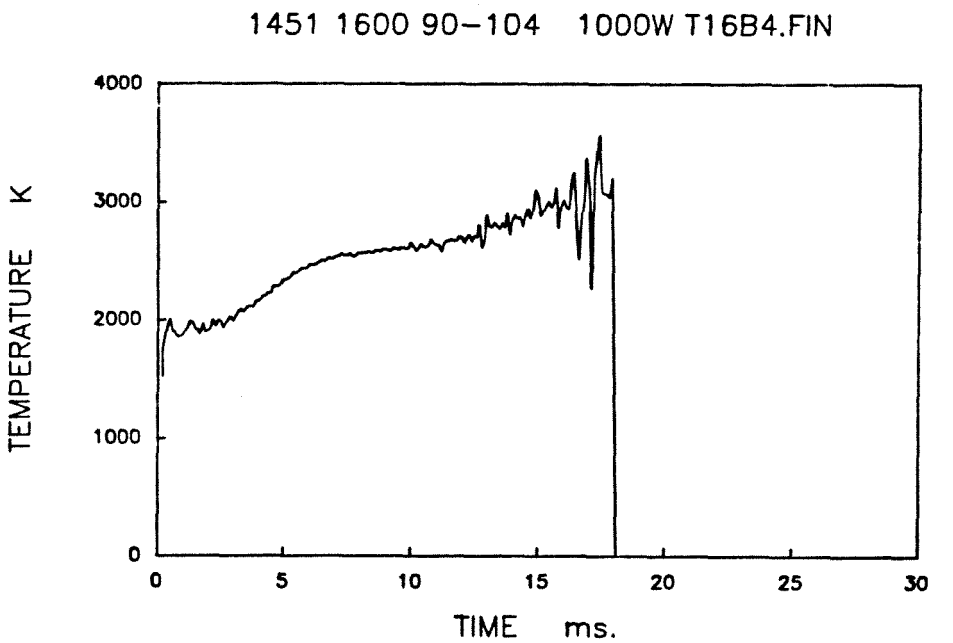
1451 1600 90–104 1000W T16B4.FIN
TEMPERATURE K
4000
3000
2000
1000
0
0
5
10
15
20
25
30
TIME ms.

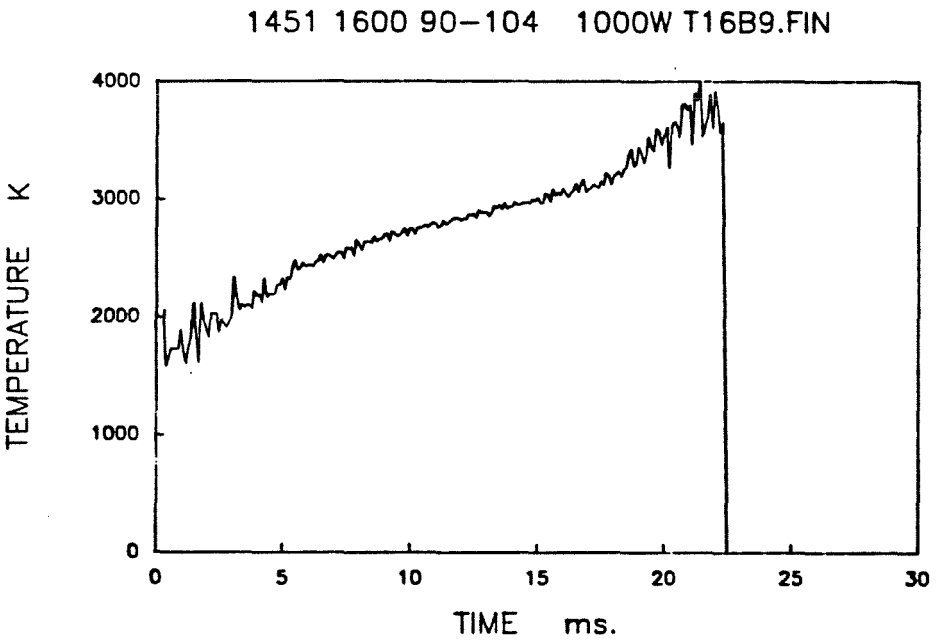
1451 1600 90–104 1000W T16B9.FIN
TEMPERATURE K
4000
3000
2000
1000
0
0
5
10
15
20
25
30
TIME ms.

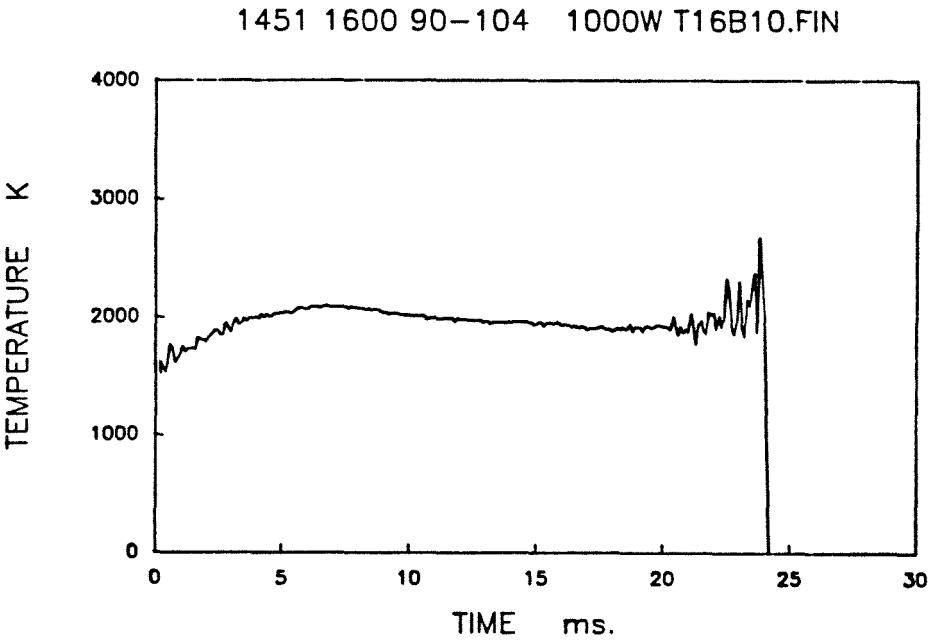
1451 1600 90–104 1000W T16B10.FIN
TEMPERATURE K
4000
3000
2000
1000
0
0
5
10
15
20
25
30
TIME ms.

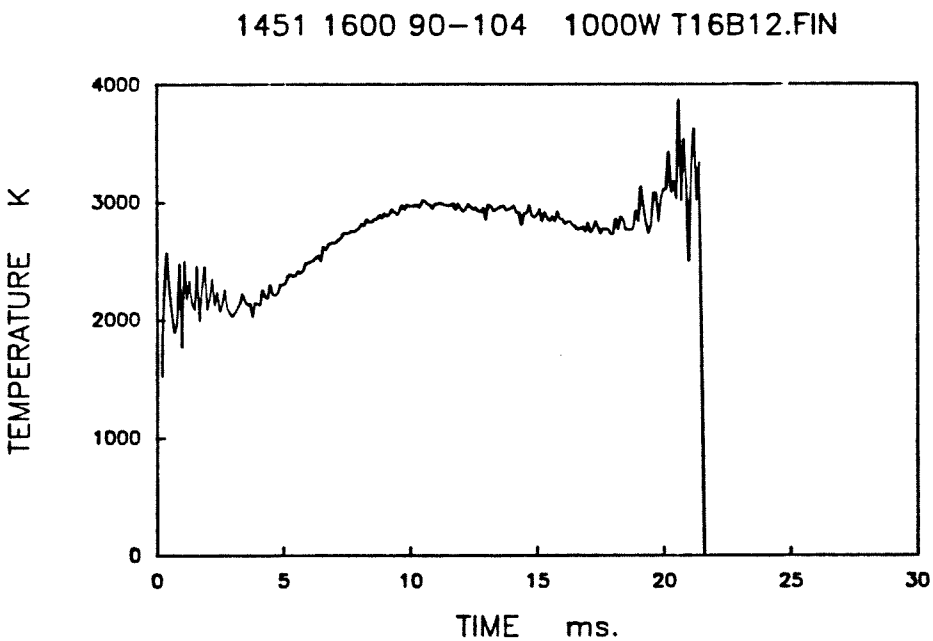
1451 1600 90–104 1000W T16B12.FIN
TEMPERATURE K
4000
3000
2000
1000
0
0
5
10
15
20
25
30
TIME ms.